AWARD NUMBER: W81XWH-18-1-0431

TITLE: Receptors in Endosomes Mediate Chronic Pain Associated with Trauma and Stress: Nonopioid Targets for Pain

PRINCIPAL INVESTIGATOR: Nigel Bunnett, PhD

CONTRACTING ORGANIZATION: New York University

REPORT DATE: OCTOBER 2021

TYPE OF REPORT: Annual Technical Progress Report

PREPARED FOR: U.S. Army Medical Research and Materiel Command
Fort Detrick, Maryland 21702-5012

DISTRIBUTION STATEMENT: Approved for Public Release;
Distribution Unlimited

The views, opinions and/or findings contained in this report are those of the author(s) and should not be construed as an official Department of the Army position, policy or decision unless so designated by other documentation.

REPORT DOCUMENTATION PAGE

Form Approved
OMB No. 0704-0188

Public reporting burden for this collection of information is estimated to average 1 hour per response, including the time for reviewing instructions, searching existing data sources, gathering and maintaining the data needed, and completing and reviewing this collection of information. Send comments regarding this burden estimate or any other aspect of this collection of information, including suggestions for reducing this burden to Department of Defense, Washington Headquarters Services, Directorate for Information Operations and Reports (0704-0188), 1215 Jefferson Davis Highway, Suite 1204, Arlington, VA 22202-4302. Respondents should be aware that notwithstanding any other provision of law, no person shall be subject to any penalty for failing to comply with a collection of information if it does not display a currently valid OMB control number. **PLEASE DO NOT RETURN YOUR FORM TO THE ABOVE ADDRESS.**

1. REPORT DATE	2. REPORT TYPE	3. DATES COVERED
OCTOBER 2021	Annual Technical Progress Report	9/1/2020 – 8/31/2021

4. TITLE AND SUBTITLE

Receptors in Endosomes Mediate Chronic Pain Associated with Trauma and Stress: Nonopioid Targets for Pain

5a. CONTRACT NUMBER
W81XWH-18-1-0431

5b. GRANT NUMBER
PR170507

5c. PROGRAM ELEMENT NUMBER

6. AUTHOR(S)

Nigel Bunnett, PhD

E-Mail: nwb2@nyu.edu

5d. PROJECT NUMBER
0011176521

5e. TASK NUMBER

5f. WORK UNIT NUMBER

7. PERFORMING ORGANIZATION NAME(S) AND ADDRESS(ES)

NEW YORK UNIVERSITY
70 Washington Square S
New York, NY 10010

8. PERFORMING ORGANIZATION REPORT NUMBER

9. SPONSORING / MONITORING AGENCY NAME(S) AND ADDRESS(ES)

U.S. Army Medical Research and Development Command
Fort Detrick, Maryland 21702-5012

10. SPONSOR/MONITOR'S ACRONYM(S)

11. SPONSOR/MONITOR'S REPORT NUMBER(S)

12. DISTRIBUTION / AVAILABILITY STATEMENT

Approved for Public Release; Distribution Unlimited

13. SUPPLEMENTARY NOTES

14. ABSTRACT The grant seeks to determine whether G protein-coupled receptors (GPCRs) in endosomes, rather than at the plasma membrane, are mediators and therapeutic targets for chronic pain. Aim 1 examines whether GPCRs in endosomes control activity of ion channels and expression of genes that induce sustained neuronal excitation. Aim 2 determines whether endosomally-targeted antagonists inhibit channel activity, gene expression and hyperexcitability of neurons. Aim 3 evaluates the therapeutic potential of endosomally-targeted GPCR antagonists in trauma- and stress-induced pain relevant to military personnel. Progress has been made in all aims. Neuropeptides (substance P, calcitonin gene-related peptide) and proteases (trypsin) stimulated GPCR endocytosis and evoked sustained signals and hyperexcitability in pain-sensing neurons. Dynamin and clathrin inhibitors suppressed endocytosis, signaling and hyperexcitability. Therapies have been developed to block endosomal signaling and evaluated in preclinical models of trauma- and stress-induced pain. Therapies include: dynamin and clathrin inhibitors; lipid-conjugated antagonists that accumulate in endosomes; antagonists encapsulated into nanoparticles that disassemble in acidic endosomes. These antagonists effectively reversed nociception in preclinical models of visceral pain, migraine pain, and nerve injury pain. They were more effective than conventional antagonists of plasma membrane GPCRs. Thus, endosomal GPCRs have been identified as major mediators and therapeutic targets for chronic pain.

15. SUBJECT TERMS Chronic pain; neuropathic pain; head injury pain; migraine pain; irritable bowel syndrome pain; G proteincoupled receptors; endosomes; analgesics.

16. SECURITY CLASSIFICATION OF:			17. LIMITATION OF ABSTRACT	18. NUMBER OF PAGES	19a. NAME OF RESPONSIBLE PERSON
a. REPORT	b. ABSTRACT	c. THIS PAGE			19b. TELEPHONE NUMBER *(include area code)*
Unclassified	Unclassified	Unclassified	Unclassified	166	USAMRMC

TABLE OF CONTENTS

	Page
1. Introduction	4
2. Keywords	4
3. Accomplishments	4-9
4. Impact	9
5. Changes/Problems	9
6. Products	10-11
7. Participants & Other Collaborating Organizations	11-12
8. Special Reporting Requirements	12
9. Appendices	12

1. INTRODUCTION

G protein-coupled receptors (GPCRs) are the largest class of transmembrane signaling proteins. They control most physiological and pathological processes, including pain, and are the target of over one third of FDA-approved drugs. GPCRs are traditionally considered to function at the plasma membrane, allowing cells to detect extracellular ligands. However, plasma membrane signaling is transient, and activated GPCRs usually undergo clathrin- and dynamin-mediated endocytosis. Endosomes were once considered merely conduits for GPCR trafficking to recycling or degradatory pathways. This grant investigates the novel concept that endosomes are a vital site for continued GPCR signaling in pain-sensing neurons that mediates sustained neuronal activity and pain. Thus, selective antagonists of endosomal GPCRs might provide superior relief from chronic pain than conventional drugs that are designed to target GPCRs at the plasma membrane. The inability of such drugs to effectively engage GPCRs in acidic endosomes might explain their lack of efficacy in clinical trials of chronic pain. The application focuses on receptors for neuropeptides (substance P [SP] neurokinin 1 receptor [NK_1R]; calcitonin gene-related peptide [CGRP] calcitonin like receptor [CLR]) and proteases (protease-activated receptor-2 [PAR_2]). These receptors have been implicated in nerve injury pain, migraine pain, and colonic pain of irritable bowel syndrome (IBS).

2. KEYWORDS

Chronic pain; neuropathic pain; head injury pain; migraine pain; irritable bowel syndrome pain; G protein-coupled receptors; endosomes; analgesics

3. ACCOMPLISHMENTS:

Goals of Project. The table indicates approved Statement of Work tasks, date of completed tasks, and percentage of tasks accomplished by those dates.

Abbreviations: GPCR, G Protein-Coupled Receptor; DRG, Dorsal Root Ganglia; PAR_2, Protease-Activated Receptor-2; NK_1R, Neurokinin 1 Receptor; CLR, Calcitonin Receptor-like Receptor; TRP, Transient Receptor Potential (ion channel); muGFP, monomeric ultrastable Green Fluorescent Protein; IBS-D, Irritable Bowel Syndrome, Diarrhea-Predominant; HC, Healthy Control; ABP, Activity-Based Probe; PTH, Post Traumatic Headache; FRET, Förster Resonance Energy Transfer; BRET, Bioluminescence Resonance Energy Transfer; RNA-Seq, RNA Sequencing

Aim 1: To determine whether GPCRs in endosomes of pain-sensing neurons control the activity of ion channels and the transcription of genes that induce sustained neuronal excitation.	**Date**	**%**
Major Task 1: Determine whether endosomal PAR_2 in DRG neurons generates compartmentalized signals that regulate channel activity and sensitization		
Subtask 1: Establish breeding colonies of PAR_2-muGFP mice.	9/29/21	100
Subtask 2: Analyze endocytosis-dependent compartmentalized signaling in DRG neurons	9/29/21	100
Subtask 3: Assess PAR_2-mediated sensitization and TRP channel activation in DRG neurons	9/29/21	75
Major Task 2: Determine whether proteases in human colon biopsy specimens activate endosomal PAR_2 in DRG neurons to generate signals that regulate channel activity and sensitization		
Subtask 1: Collect and process human colon biopsies from IBS-D (N=50) and HC (N=50) patients	9/29/21	100
Subtask 2: Determine whether proteases in human IBS-D biopsies sensitize DRG neurons and activate TRP channel through endosomal PAR_2.	9/29/21	100
Subtask 3: Profile activated serine and cysteine proteases in supernatants of IBS-D and HC biopsies using ABPs	9/29/21	50
Major Task 3: Determine whether endosomal PAR_2, NK_1R and CLR signals regulate transcription in pain-sensing neurons		
Subtask 1: Determine whether endosomal PAR_2, NK_1R and CLR signaling regulates transcription in DRG and spinal neurons	9/29/21	10

Aim 2: To determine whether endosomally-targeted antagonists inhibit endosomal GPCR signaling, channel activation, gene transcription and sustained hyperexcitability of pain-sensing neurons.		
Subtask 1: Generate small molecule tripartite PAR_2, NK_1R and CLR antagonists; generate small molecule quadripartite NK_1R and CLR antagonists; generate fluorescent probes	9/29/21	100
Major Task 1: Determine whether tripartite and quadripartite antagonists disrupt endosomal PAR_2, NK_1R and CLR signaling in HEK293 cells		
Subtask 1: Determine whether lipidated antagonists disrupt ligand/receptor interactions in endosomes	9/29/21	75
Subtask 2: Determine whether lipidated antagonists inhibit endosomal signaling of PAR_2, NK_1R and CLR in HEK293 cells	9/29/21	100
Major Task 2: Determine whether tripartite and quadripartite antagonists target PAR_2 in endosomes of DRG neurons and NK_1R and CLR in endosomes of spinal neurons, and inhibit endosomal signaling		
Subtask 1: Determine whether tripartite and quadripartite antagonists colocalize with PAR_2, NK_1R and CLR on endosomes of pain-sensing neurons	9/29/21	100
Subtask 2: Determine whether tripartite and quadripartite antagonists inhibit endosomal signaling of PAR_2, NK_1R and CLR in pain-sensing neurons	9/29/21	100
Major Task 3: Determine whether tripartite and quadripartite antagonists disrupt PAR_2-induced sensitization and transcription in DRG neurons and NK_1R- and CLR-induced sensitization and transcription in spinal neurons		
Subtask 1: Determine whether tripartite and quadripartite antagonists inhibit sensitization and TRP activation in neurons	9/29/21	75
Subtask 2: Examine whether antagonists suppress gene expression	9/29/21	25
Aim 3: To investigate the therapeutic potential of endosomally-targeted GPCR antagonists in trauma- and stress-induced pain that is relevant to disorders of military personnel and veterans.		
Major Task 1: Conduct studies in preclinical model of migraine headache to determine feasibility of using tripartite CLR antagonists for migraine pain.		
Subtask 1: Generate tripartite antagonists of PAR_2, NK_1R and CLR; generate quadripartite probes for NK_1R and CLR antagonists, similar to Aim 2 above	9/29/21	100
Subtask 2: Develop a GTN-evoked model of migraine headache pain in C57BL/6 mice	9/29/21	100
Subtask 3: Determine efficacy of tripartite or non-lipidated CLR antagonists	9/29/21	100
Major Task 2: Conduct studies in preclinical model of nerve injury pain to determine feasibility of using quadripartite NK_1R/CLR antagonists for nerve injury pain.		
Subtask 1: Develop a spared nerve injury model of neuropathic pain in C57BL/6 mice	9/29/21	100
Subtask 2: Determine efficacy of quadripartite NK_1R/CLR antagonists and non-lipidated antagonists	9/29/21	100
Major Task 3: Conduct studies in preclinical model of IBS pain to determine feasibility of using tripartite PAR_2 antagonists for post-inflammatory IBS pain.		
Subtask 1: Generate an IBS mouse model in C57BL/6 mice	9/29/21	100
Subtask 2: Training of electrophysiologist in Dr. Schmidt's laboratory by Dr. Bunnett's team on visceromotor responses following graded colorectal distention	9/29/21	75
Subtask 3: Determine efficacy of tripartite PAR_2 antagonists and non-lipidated antagonists	9/29/21	75

Research Progress

We have investigated the mechanisms by which G protein-coupled receptors (GPCRs) signal pain that is prevalent in military personnel and veterans including post-traumatic headache, nerve injury pain and irritable bowel syndrome pain. Previous drug discovery efforts, which have been largely unsuccessful, focus on targeting plasma membrane GPCRs. However, once activated GPCRs undergo endocytosis and intracellular trafficking. We investigated the hypothesis that GPCRs in endosomes (**eGPCRs**) generate sustained signals that mediate neuronal hypersensitivity and chronic pain. Thus, chronic pain results from sustained agonist release and eGPCR signaling. Antagonists designed to target plasma membrane GPCRs may not engage eGPCRs due to the acidic endosomal pH and eGPCR association with multi-protein signaling complexes. We showed antagonists designed to target eGPCRs provide more efficacious and sustained relief from chronic pain. Our major accomplishments for 2020-21 are summarized below.

a) Endosomal signaling of protease-activated receptor-2 in colonic inflammation and pain. GPCRs regulate many pathophysiological processes and are major therapeutic targets. The impact of disease on the subcellular distribution and function of GPCRs is poorly understood. We investigated trafficking and signaling of protease-activated receptor-2 (PAR_2) in colitis. To localize PAR_2 and assess redistribution during disease, we generated knockin mice expressing PAR_2 fused to monomeric ultra-stable green fluorescent protein (muGFP). PAR_2-muGFP signaled and trafficked normally. PAR_2 mRNA was detected at similar levels in *Par$_2$-mugfp* and wild-type mice, which demonstrated comparable nociceptive responses to PAR_2 agonists. Immunostaining with a GFP antibody and RNAScope® *in situ* hybridization using *F2rl1* (PAR_2) and *Gfp* probes revealed that PAR_2-muGFP was expressed in epithelial cells of the small and large intestine and in subsets of enteric and dorsal root ganglia neurons. In healthy mice, PAR_2-muGFP was prominently localized to the basolateral membrane of colonocytes (**Fig. 1**). In mice with colitis induced by dextran sodium sulphate (DSS), PAR_2-muGFP was depleted from the plasma membrane of colonocytes and redistributed to early endosomes, consistent with generation of proinflammatory proteases that activate PAR_2. PAR_2 agonists stimulated endocytosis of PAR_2 and recruitment of $G\alpha_q$, $G\alpha_i$ and β-arrestin2 to early endosomes of T84 colon carcinoma cells, assessed using bioluminescence resonance energy transfer. PAR_2 agonists increased paracellular permeability of colonic epithelial cells and evoked interleukin-8 release from segments of human colon. Knockdown of dynamin-2 (*Dnm2*), the major colonocyte isoform, and Dnm inhibition attenuated PAR_2 endocytosis, signaling complex assembly and inflammation. Thus, PAR_2 endosomal signaling sustains protease-evoked inflammation and PAR_2 in endosomes is a potential therapeutic target for colitis. This work is under revision by the *Proceedings of the National Academy of Science*.

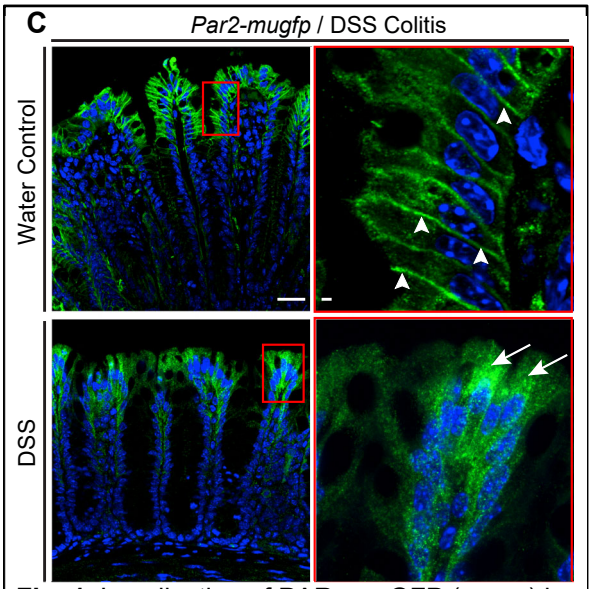


Fig. 1. Localization of PAR_2-muGFP (green) in colonocytes of control mice and mice with DSS colitis. Note marked endocytosis of PAR_2-muGFP in the inflamed colon.

b) Nanoparticle-encapsulated antagonists of protease-activated receptor-2 for the treatment of colonic pain. The observation that PAR_2 is massively internalized during intestinal inflammation and that endosomal PAR_2 signaling mediates inflammation and pain, suggests that PAR_2 in endosomes is a therapeutic target. We have previously reported the development of a nanoparticle-based strategy to selectively target eGPCRs. Nanoparticle encapsulation improves drug efficacy by enhancing the stability, tolerability, delivery and retention in diseased tissues. Nanoparticle-mediated drug delivery is especially useful for targets within endosomes because of the endosomal transport mechanisms of many nanomedicines within cells. Stimulus-responsive nanoparticles have been extensively studied for delivery of chemotherapeutic drugs to solid tumors, where extracellular acidity and protease activity can be exploited to trigger nanoparticle disassembly and cargo release. Although nanoparticles usually enter cells by endocytosis, disruption of the endosomal membrane is necessary to allow chemotherapeutic drugs to access their targets in the cytoplasm and nucleus. Less is known about the efficacy of nanoparticle delivery systems for the treatment of conditions other than cancer, such as chronic pain.

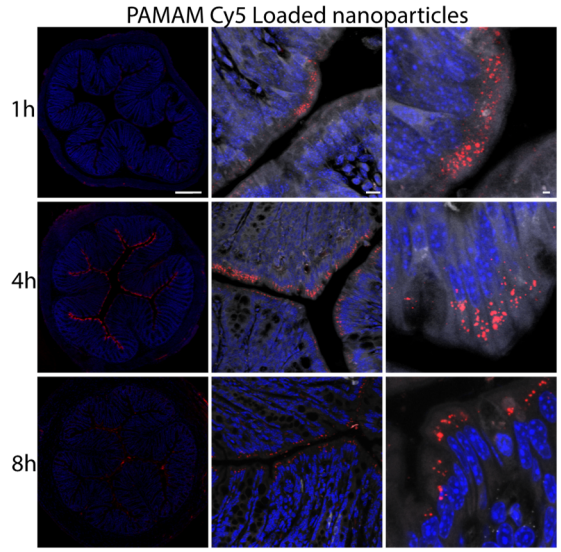


Fig. 2. Uptake of PAMAM-Chol-Cy5 nanoparticles (red) into the colonic mucosa at 1, 4 and 8 h after intracolonic delivery via enema to mice.

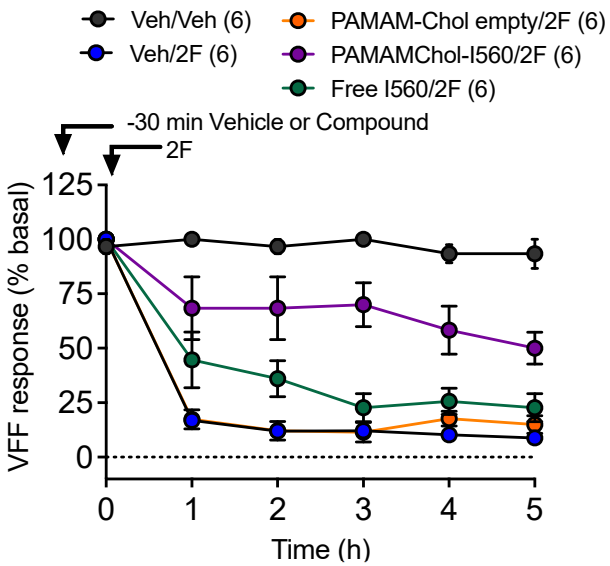


Fig. 3. Nanoparticles were injected into the mouse colon 30 min prior to intracolonic injection of PAR_2 agonist 2F. 2F caused colonic pain. PAMAM-Chol-I560 nanoparticles reversed 2F-evoked pain. (n) mouse numbers.

The realization that GPCRs signal from within endosomes to mediate pain offers an opportunity to use nanoparticles to deliver GPCR antagonists to endosomes, where the acidic microenvironment can be harnessed to stimulate cargo release. We previously reported the design of a pH-responsive, soft polymeric nanoparticle for the targeting of acidified endosomes to precisely inhibit endosomal signaling events leading to chronic pain. In chronic pain, the substance P (SP) neurokinin-1 receptor (NK_1R) redistributes from the plasma membrane to acidified endosomes, where it signals to maintain pain. Therefore, the NK_1R in endosomes provides an important target for pain relief. The pH-responsive nanoparticles entered cells by clathrin- and dynamin-dependent endocytosis and accumulated in NK_1R-containing endosomes. Following intrathecal injection into rodents, the nanoparticles, containing the FDA-approved NK_1R antagonist aprepitant, inhibited SP-induced activation of spinal neurons and thus prevent pain transmission. Treatment with the nanoparticles led to complete and persistent relief from nociceptive, inflammatory and neuropathic nociception.

We have adapted this approach to deliver antagonists of PAR_2 to endosomes of colonic cells for the treatment of colonic pain. We generated PAMAM-Cholesterol (PAMAM-Chol) nanoparticles encapsulating either the fluorophore cyanine-5 or the PAR_2 antagonist I-560. When injected into the lumen of the mouse colon *via* enema, PAMAM-Chol-Cy5 nanoparticles were detected in endosomes of colonocytes after 1-8 h (**Fig. 2**). Intracolonic injection of the PAR_2 agonist 2-Furoyl-LIGRLO-NH_2 (2F) resulted in persistent colonic pain, assessed by measuring withdrawal responses to stimulation of the abdomen with von Frey filaments (**Fig. 3**; downward deflection denotes mechanical allodynia). Pretreatment with PAMAM-Chol-I560 nanoparticles strongly inhibited PAR_2-evoked abdominal pain, whereas free I-560 or empty PAMAM-Chol nanoparticles had no effect (**Fig. 3**). We are now evaluating the efficacy of nanoparticle-encapsulated PAR_2 antagonists in preclinical models of inflammatory bowel disease and irritable bowel syndrome pain.

c) Nanoparticle-encapsulated antagonists of the neurokinin-1 receptor for the treatment of neuropathic and inflammatory pain. The design of nanoparticles that could release cargo in endosomes over days might provide long-term relief of pain. To evaluate this concept, we studied star polymer nanoparticles (nanostars) containing aprepitant, an antagonist of the SP NK_1R, for the treatment of chronic inflammatory and neuropathic pain in mice. Nanostars containing cyanine-5 slowly released cargo under acidic conditions and trafficked to endosomes of HEK-NK_1R cells, assessed by confocal imaging. The ability of nanoparticles to inhibit endosomal NK_1R signaling was examined using Bioluminescence Resonance Energy Transfer (BRET) to examine recruitment of mini-$G\alpha$ proteins and β-arrestin2 to the NK_1R in endosomes. Nanostar-aprepitant inhibited SP-evoked assembly of $NK_1R/G\alpha_{q,i}/\beta$-arrestin2 signalosomes in endosomes. These results are consistent with antagonism of the NK_1R in endosomes. Inflammatory pain was induced by intraplantar injection of complete Freund's adjuvant (CFA) to the hindpaw. The spared nerve injury (SNI) model of neuropathic pain was studied, where the tibial and peroneal branches of the sacral nerve of one hindpaw were transected, leaving the sural nerve intact. At 2 days post-CFA or 10 days post-SNI, nanoparticles or free aprepitant was injected intrathecally. Mechanical allodynia and cold allodynia were assessed by stimulation of the planter surface of the paw with von Frey filaments or a cold stimulus (acetone evaporation) respectively. Non-evoked nociception was examined using a behavioral spectrometer. In both models, nanostar-aprepitant

nanoparticles (Benzo and VBA nanoparticles) reversed withdrawal responses of the ipsilateral paw to mechanical and cold stimulation and normalized spontaneous nociceptive behavior (**Fig. 4**). Nanostar-aprepitant nanoparticles maintained analgesia for 10 h. Nanostar-aprepitant nanoparticles provided more efficacious and sustained analgesia than free aprepitant. Empty nanostars (Benzo and VBA) did not affect withdrawal responses of the contralateral hindpaw or normal behavior. Our results show that nanoparticles can be used to deliver antagonists of endosomal GPCRs that signal inflammatory and neuropathic pain. The sustained endosomal delivery of GPCR antagonists from slow-release stimulus-responsive nanoparticles offers an approach for the effective and long-lasting reversal of chronic pain. This work is being prepared for submission to *Biomaterials*.

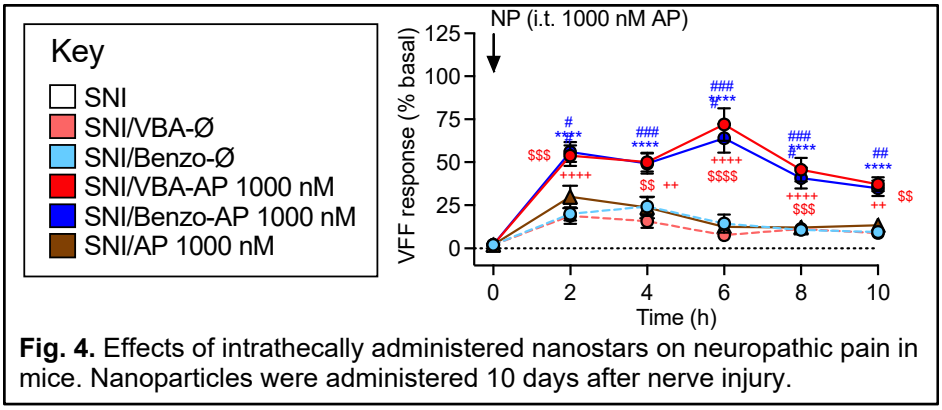


Fig. 4. Effects of intrathecally administered nanostars on neuropathic pain in mice. Nanoparticles were administered 10 days after nerve injury.

d) Endosomal signaling of calcitonin gene-related peptide in Schwann cells mediates migraine pain. The efficacy of monoclonal antibodies against calcitonin gene-related peptide (CGRP) or its receptor (calcitonin receptor-like receptor/receptor activity modifying protein-1, CLR/RAMP1) implicates peripherally-released CGRP in migraine pain. However, the site and mechanism of CGRP-evoked migraine pain remain unknown. We observed that a human Schwann cell line and primary mouse Schwann cells express mRNA and protein for CLR and RAMP1. Schwann cells in culture also expressed functional CGRP receptors. In preclinical models of migraine pain in mice, selective deletion of CGRP receptors from Schwann cells abrogated periorbital mechanical allodynia evoked by administration of CGRP, capsaicin (releases endogenous CGRP) and trinitroglycerin (provokes migraine) (**Fig. 5A**). Periorbital injection of Dyngo4a, a dynamin inhibitor, suppressed CGRP-evoked periorbital allodynia (**Fig. 5B**). Studies of cultured Schwann cells revealed that CGRP/CLR signals from endosomes to evoke cAMP-dependent formation of nitric oxide. Nitric oxide, by gating Schwann cell transient receptor potential ankyrin 1 (TRPA1) channel, releases reactive oxygen species, which in a feed-forward manner sustain nociceptor TRPA1 activation and allodynia. When encapsulated into nanoparticles that release cargo in acidified endosomes, a CLR/RAMP1 antagonist (MK-3207) provided superior inhibition of CGRP signaling and allodynia in mice compared to free MK-3207 (**Fig. 5C**). Our results reveal that neuronal/Schwann cell endosomal signaling pathway mediates nociception associated with neurogenic inflammation and explains the antimigraine effect of peripherally-acting anti-CGRP drugs. This work is under review by *Nature Communications*. Schwann cells also responded to the PAR_2 agonist, 2F; the antagonist I-560 abolished responses (**Fig. 5D**). Alexa-tagged 2F trafficked to endosomes of Schwann cells. Thus, PAR_2 might also signal from endosomes to mediate pain associated with protease activity.

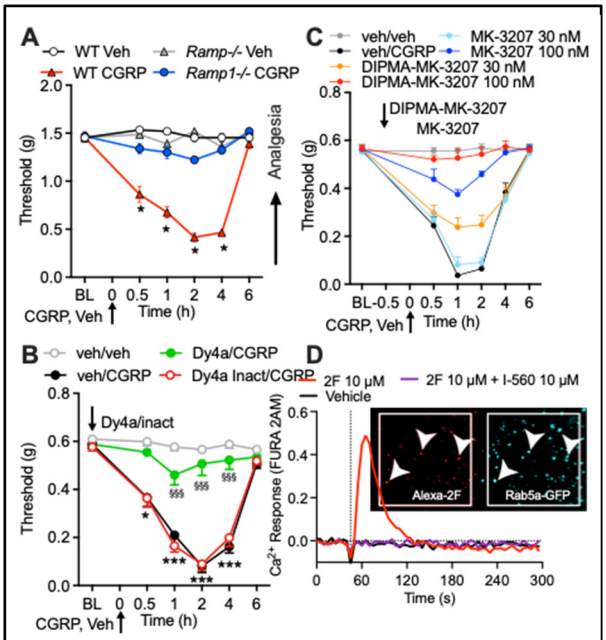


Fig. 5. A-C. Periorbital mechanical allodynia in mice after CGRP injection. **A.** RAMP1 deletion from Schwann cells abolished response. **B.** Dyngo4a (Dy4a) but not inactive analog (inact) abolished response. **C.** DIPMA-MK-3207 had greater inhibitory actions than free MK-3207. **D.** PAR_2 agonist 2F mobilized Ca^{2+} in human Schwann cells; PAR_2 antagonist I-560 abolished response. Inset shows Alexa-2F uptake into Rab5a+ve endosomes.

Training and Professional Development

The NYU Department of Molecular Pathobiology provides opportunities for mentorship, research training and professional development. Post-doctoral fellows have a faculty mentoring committee. Trainees learn laboratory skills from experienced investigators, and receive mentorship from the PI on literature reviews, experimental design, data analysis, scientific writing and presentation. They attend weekly laboratory meetings and journal

clubs, and attend symposia and seminars at NYU. A team science training program of bimonthly seminars provides training in ethical conduct of research, rigor and reproducibility, experimental design, and career development.

Dissemination of Results

The Bunnett and Schmidt laboratories meet as a group each week to evaluate progress, provide feedback on technical issues and results, arrange transfer of mice and chemical resources, and trouble-shoot problems. Technical methods specific to the project are discussed. Member of the laboratory including students, postdoctoral fellows, scientists and principal investigators attend this joint laboratory meeting.

Dr. Bunnett has presented findings at the following meetings and seminar series:

2020

- University of Arizona
- University of California, San Francisco
- New York University

Plans for Next Reporting Period

Priorities for the next reporting period include:

Analysis of the mechanisms by which GPCRs in endosomes regulate TRP channel activity at the plasma membrane and gene expression in the nucleus of neurons that sense and transmit pain.

Analysis of the mechanisms by which proteases and their receptors evoke colonic pain in mice.

4. IMPACT

Impact on principal discipline. This work has identified new targets for the treatment of chronic pain. We have discovered that painful stimuli cause the translocation of receptors from the cell surface to endosomes of neurons that sense and transmit pain. Receptors in endosomes are primarily responsible for signaling persistent pain. Drugs that target these receptors provide more effective relief from chronic pain than conventional drugs that target receptors at the surface of cells. The failure of conventional drugs in clinical trials of chronic pain may be due to their inability to inhibit receptors in endosomes.

Impact on other disciplines. GPCRs mediate many diseases beyond pain, including cardiovascular disease, inflammatory diseases and cancer. Antagonists and agonists of GPCRs represent the single largest class of drugs; more than one third of FDA-approved drugs target GPCRs. The concept that GPCRs in endosomes generate sustained signals that may underlie disease processes raises the prospect that GPCRs in endosomes might be the optimal target for the treatment of many chronic diseases.

Impact on technology transfer. The PI is a scientific founder of Endosome Therapeutics, a start-up company that seeks to develop and commercialize drugs that target endosomal GPCRs. The National Center for Advancing Translational Science (NCATS) has initiated a collaboration to develop nanoparticle-encapsulated antagonists of GPCRs for the treatment of chronic pain.

Impact on society. The development of non-opioid treatments for chronic pain has the potential to lessen the opioid crisis, which is a major cause of mortality and morbidity in the USA.

5. CHANGES/PROBLEMS

Changes in approach and reasons for change. Nothing to report.

Actual or anticipated problems or delays and actions or plans to resolve them. Nothing to report.

Changes that had a significant impact on expenditures. Nothing to report.

Significant changes in use or care of human subjects, vertebrate animals, biohazards, and/or select agents. Nothing to report.

Significant changes in use or care of human subjects. Nothing to report.

Significant changes in use or care of vertebrate animals. Nothing to report.

Significant changes in use of biohazards and/or select agents. Nothing to report.

6. PRODUCTS

Journal publications

1. Tu NH, Jensen DD, Anderson BM, Chen E, Jimenez-Vargas NN, Scheff NN, Inoue K, Tran HD, Dolan JC, Meek TA, Hollenberg MD, Liu CZ, Vanner SJ, Janal MN, Bunnett NW, Edgington-Mitchell LE & Schmidt BL. Legumain Induces Oral Cancer Pain by Biased Agonism of Protease-Activated Receptor-2. *J Neurosci* 41, 193-210, 2021. PMC7786216. https://www.ncbi.nlm.nih.gov/pubmed/33172978
2. Bhansali D, Teng SL, Lee CS, Schmidt BL, **Bunnett NW**, Leong KW. Nanotechnology for Pain Management: Current and Future Therapeutic Interventions. Nano Today. 39, 101223, 2021. https://doi.org/10.1016/j.nantod.2021.101223
3. Retamal JS, Grace MS, Dill LK, Ramirez-Garcia P, Peng S, Gondin AB, Bennetts F, Alvi S, Rajasekhar P, Almazi JG, Carbone SE, Bunnett NW, Davis TP, Veldhuis NA, Poole DP & McIntyre P. Serotonin-induced vascular permeability is mediated by transient receptor potential vanilloid 4 in the airways and upper gastrointestinal tract of mice. *Lab Invest*, 2021. PMC8047529. https://www.ncbi.nlm.nih.gov/pubmed/33859334
4. Mai QN, Shenoy P, Quach T, Retamal JS, Gondin AB, Yeatman HR, Aurelio L, Conner JW, Poole DP, Canals M, Nowell CJ, Graham B, Davis TP, Briddon SJ, Hill SJ, Porter CJH, Bunnett NW, Halls ML & Veldhuis NA. A lipid-anchored neurokinin 1 receptor antagonist prolongs pain relief by a three-pronged mechanism of action targeting the receptor at the plasma membrane and in endosomes. *J Biol Chem*, 100345, 2021. PMC7949131. https://www.ncbi.nlm.nih.gov/pubmed/33515548
5. Jimenez-Vargas NN, Yu Y, Jensen DD, Bok DD, Wisdom M, Latorre R, Lopez C, Jaramillo-Polanco JO, Degro C, Guzman-Rodriguez M, Tsang Q, Snow Z, Schmidt BL, Reed DE, Lomax AE, Margolis KG, Stein C, Bunnett NW & Vanner SJ. Agonist that activates the micro-opioid receptor in acidified microenvironments inhibits colitis pain without side effects. *Gut*, 2021. https://www.ncbi.nlm.nih.gov/pubmed/33785555
6. Gottesman-Katz L, Latorre R, Vanner S, Schmidt BL & Bunnett NW. Targeting G protein-coupled receptors for the treatment of chronic pain in the digestive system. *Gut* 70, 970-981, 2021. https://www.ncbi.nlm.nih.gov/pubmed/33272979
7. De Logu F, Marini M, Landini L, Souza Monteiro de Araujo D, Bartalucci N, Trevisan G, Bruno G, Marangoni M, Schmidt BL, Bunnett NW, Geppetti P & Nassini R. Peripheral Nerve Resident Macrophages and Schwann Cells Mediate Cancer-induced Pain. *Cancer Res*, 2021. https://www.ncbi.nlm.nih.gov/pubmed/33771895
8. Tewari D, Cook AD, Lee MC, Christensen AD, Croxford A, Becher B, Poole D, Rajasekhar P, Bunnett N, Smith JE, Hamilton JA & McMahon SB. Granulocyte-Macrophage Colony Stimulating Factor As an Indirect Mediator of Nociceptor Activation and Pain. *J Neurosci* 40, 2189-2199, 2020. PMC7083288. https://www.ncbi.nlm.nih.gov/pubmed/32019828
9. Peng S, Grace MS, Gondin AB, Retamal JS, Dill L, Darby W, Bunnett NW, Abogadie FC, Carbone SE, Tigani T, Davis TP, Poole DP, Veldhuis NA & McIntyre P. The transient receptor potential vanilloid 4 (TRPV4) ion channel mediates protease activated receptor 1 (PAR1)-induced vascular hyperpermeability. *Lab Invest* 100, 1057-1067, 2020. https://www.ncbi.nlm.nih.gov/pubmed/32341518
10. Mountford SJ, Anderson BM, Xu B, Tay ESV, Szabo M, Hoang ML, Diao J, Aurelio L, Campden RI, Lindstrom E, Sloan EK, Yates RM, Bunnett NW, Thompson PE & Edgington-Mitchell LE. Application of a Sulfoxonium Ylide Electrophile to Generate Cathepsin X-Selective Activity-Based Probes. *ACS Chem Biol* 15, 718-727, 2020. https://www.ncbi.nlm.nih.gov/pubmed/32022538
11. Jimenez-Vargas NN, Gong J, Wisdom MJ, Jensen DD, Latorre R, Hegron A, Teng S, DiCello JJ, Rajasekhar P, Veldhuis NA, Carbone SE, Yu Y, Lopez-Lopez C, Jaramillo-Polanco J, Canals M, Reed DE, Lomax AE, Schmidt BL, Leong KW, Vanner SJ, Halls ML, Bunnett NW & Poole DP. Endosomal signaling of delta opioid receptors is an endogenous mechanism and therapeutic target for relief from inflammatory pain. *Proc Natl Acad Sci U S A* 117, 15281-15292, 2020. PMC7334524. https://www.ncbi.nlm.nih.gov/pubmed/32546520

Books. Nothing to report.

Other. Nothing to report.

Websites. Bunnett Laboratory Website: https://dental.nyu.edu/faculty/molecular-pathobiology/bunnett-lab.html

Technologies and techniques. Nothing to report.

Inventions and patents. Nothing to report.

Other products. Nothing to report.

7. PARTICIPANTS AND OTHER COLLABORATING ORGANIZATIONS:

Individuals who have worked on project

NEW YORK UNIVERSITY

Name:	Nigel Bunnett, PhD
Project Role:	PI
Researcher Identifier (e.g. ORCID ID):	0000-0003-3367-0644
Nearest person month worked:	2.04 calendar
Contribution to Project:	Project conception; experimental design; interpreting results; writing manuscripts.
Funding Support:	5R01NS102722; 5R01DE026806; 5R01DK118971; 1R01DE029951; R01DK130293

Name:	Rocco Latorre, PhD
Project Role:	Assistant Research Scientist
Researcher Identifier (e.g. ORCID ID):	0000-0003-2737-8233
Nearest person month worked:	1.44 calendar
Contribution to Project:	Analysis of the role of endosomal signaling in preclinical models of pain.
Funding Support:	5R01NS102722; 5R01DK118971; 1R01DE029951

Name:	Alan Hegron, PhD
Project Role:	Postdoctoral Associate
Researcher Identifier (e.g. ORCID ID):	0000-0002-7588-9209
Nearest person month worked:	0.24 calendar
Contribution to Project:	Analysis of the pathways of endosomal signaling and gene transcription.
Funding Support:	5R01NS102722; 5R01DK118971; 1R01DE029951

Name:	Raquel Tonello, PhD
Project Role:	Assistant Research Scientist
Researcher Identifier (e.g. ORCID ID):	0000-0002-2175-9804
Nearest person month worked:	0.24 calendar
Contribution to Project:	Analysis of the pathways of endosomal signaling and gene transcription.
Funding Support:	5R01NS102722; R01DE026806 5R01DK118971; 1R01DE029951

Change in support since last reporting period

Nigel Bunnett, PhD (PI)

NEW SUPPORT

1R01DE029951-01 Bunnett/Schmidt (MPI) 9/15/2020-8/31/2024

Targeting Endosomal Receptors for Treatment of Chronic Pain

3R01DE029951-01S1 Bunnett/Schmidt (MPI) 9/01/2021-8/31/2024
Targeting Endosomal Receptors for Treatment of Chronic Pain – Research Supplement

Heptares Therapeutics Inc (Bunnett) 01/12/2021-01/11/2022
Heptares Therapeutics Contract

R01DK130293 (Bogyo) 09/21/2021-07/31/2026
Targeting bacterial proteases involved in PAR signaling to treat inflammatory bowel diseases
Role: Co-Investigator

Other organizations. Nothing to report

8. SPECIAL REPORTING REQUIREMENTS

This is a collaborative award between Dr. N.W. Bunnett (New York University) and B.L. Schmidt (New York University). Dr. Schmidt will submit his report for the 10/01/21 deadline.

9. APPENDICES

PDF of published manuscripts.

Neurobiology of Disease

Legumain Induces Oral Cancer Pain by Biased Agonism of Protease-Activated Receptor-2

Nguyen Huu Tu,[1*] Dane D. Jensen,[1,2*] Bethany M. Anderson,[3] Elyssa Chen,[1] Nestor N. Jimenez-Vargas,[4] Nicole N. Scheff,[1] Kenji Inoue,[1] Hung D. Tran,[1] John C. Dolan,[1] Tamaryn A. Meek,[5] Morley D. Hollenberg,[6] Cheng Z. Liu,[7] Stephen J. Vanner,[4] Malvin N. Janal,[8] Nigel W. Bunnett,[2] Laura E. Edgington-Mitchell,[1,3,5#] and Brian L. Schmidt[1#]

[1]Oral and Maxillofacial Surgery, Bluestone Center for Clinical Research, New York University College of Dentistry, New York, NY 10010, [2]Department of Molecular Pathobiology, New York University College of Dentistry, New York, NY 10010, [3]Biochemistry and Molecular Biology, Bio21 Institute, University of Melbourne, Parkville, VIC 3010, [4]Gastrointestinal Diseases Research Unit, Division of Gastroenterology, Queen's University, Kingston, ON K7L 3N6, Canada, [5]Drug Discovery Biology, Monash Institute of Pharmaceutical Sciences, Monash University, Parkville, VIC 3052, [6]Inflammation Research Network-Snyder Institute for Chronic Disease, Physiology and Pharmacology Department, and Medicine Department, University of Calgary Cumming School of Medicine, Calgary, AB T2N 4N1, Canada, [7]Department of Pathology, New York University Langone Health, New York, NY 10016, and [8]Department of Epidemiology and Health Promotion, New York University College of Dentistry, New York, NY 10010

Oral squamous cell carcinoma (OSCC) is one of the most painful cancers, which interferes with orofacial function including talking and eating. We report that legumain (Lgmn) cleaves protease-activated receptor-2 (PAR_2) in the acidic OSCC microenvironment to cause pain. Lgmn is a cysteine protease of late endosomes and lysosomes that can be secreted; it exhibits maximal activity in acidic environments. The role of Lgmn in PAR_2-dependent cancer pain is unknown. We studied Lgmn activation in human oral cancers and oral cancer mouse models. Lgmn was activated in OSCC patient tumors, compared with matched normal oral tissue. After intraplantar, facial or lingual injection, Lgmn evoked nociception in wild-type (WT) female mice but not in female mice lacking PAR_2 in $Na_V1.8$-positive neurons (*$Par_2Na_v1.8$*), nor in female mice treated with a Lgmn inhibitor, LI-1. Inoculation of an OSCC cell line caused mechanical and thermal hyperalgesia that was reversed by LI-1. *$Par_2Na_v1.8$* and *Lgmn* deletion attenuated mechanical allodynia in female mice with carcinogen-induced OSCC. Lgmn caused PAR_2-dependent hyperexcitability of trigeminal neurons from WT female mice. *Par_2* deletion, LI-1, and inhibitors of adenylyl cyclase or protein kinase A (PKA) prevented the effects of Lgmn. Under acidified conditions, Lgmn cleaved within the extracellular N terminus of PAR_2 at $Asn^{30}\downarrow Arg^{31}$, proximal to the canonical trypsin activation site. Lgmn activated PAR_2 by biased mechanisms in HEK293 cells to induce Ca^{2+} mobilization, cAMP formation, and PKA/protein kinase D (PKD) activation, but not β-arrestin recruitment or PAR_2 endocytosis. Thus, in the acidified OSCC microenvironment, Lgmn activates PAR_2 by biased mechanisms that evoke cancer pain.

Key words: asparaginyl endopeptidase; cancer pain; legumain; oral cancer; protease; protease-activated receptor-2

Significance Statement

Oral squamous cell carcinoma (OSCC) is one of the most painful cancers. We report that legumain (Lgmn), which exhibits maximal activity in acidic environments, cleaves protease-activated receptor-2 (PAR_2) on neurons to produce OSCC pain. Active Lgmn was elevated in OSCC patient tumors, compared with matched normal oral tissue. Lgmn evokes pain-like behavior through PAR_2. Exposure of pain-sensing neurons to Lgmn decreased the current required to generate an action potential through PAR_2. Inhibitors of adenylyl cyclase and protein kinase A (PKA) prevented the effects of Lgmn. Lgmn activated PAR_2 to induce calcium mobilization, cAMP formation, and activation of protein kinase D (PKD) and PKA, but not β-arrestin recruitment or PAR_2 endocytosis. Thus, Lgmn is a biased agonist of PAR_2 that evokes cancer pain.

Received May 16, 2020; revised Oct. 22, 2020; accepted Oct. 23, 2020.

Author contributions: N.H.T., D.D.J., B.M.A., E.C., N.N.J.-V., J.C.D., S.J.V., N.W.B., L.E.E.-M., and B.L.S. designed research; N.H.T., D.D.J., B.M.A., E.C., N.N.J.-V., N.N.S., K.I., H.D.T., T.A.M., M.D.H., C.Z.L., and L.E.E.-M. performed research; N.H.T., D.D.J., B.M.A., E.C., N.N.J.-V., T.A.M., C.Z.L., M.N.J., and L.E.E.-M. analyzed data; N.H.T., D.D.J., E.C., N.N.J.-V., J.C.D., N.W.B., L.E.E.-M., and B.L.S. wrote the paper.

*N.H.T. and D.D.J. are first authors.

#L.E.E.-M. and B.L.S. are senior authors.

This work was supported by National Institutes of Health Grants NS102722, DE026806, DK118971, and DE029951 (to N.W.B., B.L.S.) and the Department of Defense Grant W81XWH1810431 (to N.W.B., B.L.S.). L.E.E.-M. was supported by the Priority-Driven Collaborative Cancer Research Grant GNT1157171 (co-funded by Cancer Australia and Cure Cancer), a Grimwade Fellowship from the Russell and Mab Grimwade Miegunyah Fund at The University of Melbourne, and the Australian Research Council Discovery Early Career Researcher Award Fellowship DE180100418.

N.W.B. is a founding scientist of Endosome Therapeutics Inc, and research in N.W.B.'s laboratory is partly supported by Takeda Pharmaceuticals International. J.C.D. fabricates dolognawmeter assay devices through Gnatheon Scientific LLC. All other authors declare no competing financial interests.

Correspondence should be addressed to Laura E. Edgington-Mitchell at laura.edgingtonmitchell@unimelb.edu.au or Brian L. Schmidt at bls322@nyu.edu.

https://doi.org/10.1523/JNEUROSCI.1211-20.2020

Copyright © 2021 the authors

Table 1. Patient profiles

Patient #	Sex	Age	Ethnicity	Tumor location	Primary tumor stage	Nodal status
1	F	71	Hispanic	Mandibular gingiva	pT4a	pN0
2	M	57	Hispanic	Mandibular gingiva	pT2	pN2a
3	M	66	Hispanic	Floor of mouth, mandibular gingiva	pT4a	pN0
4	F	77	White/Non-Hispanic	Mandibular gingiva	pT4a	pN0
5	F	50	Asian	Tongue	pT1	pN0
6	M	93	Asian	Mandibular gingiva	pT2	pN0
7	F	81	White/Non-Hispanic	Maxillary gingiva	pT2	pN0

Introduction

Up to 90% of cancer patients endure pain; oral cancer is one of the most painful (van den Beuken-van Everdingen et al., 2007). Pain often overwhelms oral cancer patients in the final months of life; these patients suffer most while speaking, drinking, or eating, and their quality of life plummets (Connelly and Schmidt, 2004; Kolokythas et al., 2007). Oral squamous cell carcinoma (OSCC) pain worsens with disease progression and responds poorly to opioids. Development of an alternative to opioids is stymied by our poor understanding of the mechanism driving cancer pain. While the etiology of oral cancer pain is not well understood, it is known that OSCC secretes mediators that sensitize and activate nociceptors within the cancer microenvironment and generate pain. These mediators include endothelin, ATP, nerve growth factor, and proteases; proteases produce pain by cleaving protease-activated receptor-2 (PAR_2) on nociceptors (Pickering et al., 2008; Schmidt et al., 2007; Lam and Schmidt, 2010; Ye et al., 2011, 2014b; Lam et al., 2012). The proteases that activate PAR_2 in the OSCC microenvironment are unknown. Anaerobic metabolism in tumors and inflamed tissues acidifies extracellular fluid. Legumain (Lgmn; asparaginyl endopeptidase) is a cysteine protease of late endosomes and lysosomes with an acidic pH optimum. Although Lgmn has been implicated in tumor metastasis (Kembhavi et al., 1993), and patients with metastatic oral cancer report greater pain (Connelly and Schmidt, 2004), it is unknown whether Lgmn causes PAR_2-dependent cancer pain.

PAR_2 is a G-protein-coupled receptor (GPCR) expressed by nociceptors that mediates neurogenic inflammation and pain (Steinhoff et al., 2000; Vergnolle et al., 2001). Proteases activate PAR_2 through distinct mechanisms. The canonical agonists trypsin, tryptase, and kallikrein cleave within the extracellular N terminus of PAR_2, which exposes a tethered ligand that binds to and activates the cleaved receptor (Nystedt et al., 1995; Böhm et al., 1996a; Corvera et al., 1997; Angelo et al., 2006). The biased agonists cathepsin S and elastase cleave at different sites within the PAR_2 N terminus, leading to distinct pathways of PAR_2 signaling and trafficking (Ramachandran et al., 2009; Zhao et al., 2014). PAR_2 couples to signaling pathways that sensitize and activate pain-related ion channels, including the transient receptor potential vanilloid (TRPV1, TRPV4) and ankyrin (TRPA1) channels, yielding sustained sensitization of nociceptors and chronic pain (Amadesi et al., 2006; Dai et al., 2007; Zhao et al., 2015). Since PAR_2 is upstream of these pronociceptive channels, blockade of proteases and of PAR_2 is advantageous for the management of cancer pain. Therefore, there is a need to identify proteases that remain active in the acidified extracellular millieu of tumors and to determine whether they activate PAR_2 to produce pain. Some proteases known to activate PAR_2 show diminished activity under acidic conditions (Hachem et al., 2003, 2005). Moreover, proteases are often profiled in diseased tissues by measurement of protein or mRNA, not activity.

Here, we report that Lgmn is a unique activator of PAR_2. We found that Lgmn is reproducibly and robustly activated in OSCC patients and mice with OSCC. Under acidified conditions, Lgmn cleaved PAR_2 at a distinct site and activated PAR_2 by biased mechanisms, leading to hyperexcitability of nociceptors and nociceptive behavior in mice. A Lgmn inhibitor prevented OSCC pain in mice. Thus, we have identified Lgmn as a novel mediator and therapeutic target for OSCC pain.

Materials and Methods

Reagents. We used recombinant human Lgmn (440,000 ng/ml, catalog #2199-CY-010, R & D System), Lgmn substrate Z-Ala-Ala-Asn-AMC (I-1865; Bachem), DMEM and HBSS (ThermoFisher), PAR_2 agonist 2-Furoyl-LIGRLO-NH_2 and PAR_1 agonist TFLLR-NH_2 (Tocris), Lgmn-generated PAR_2 activating peptide (RSSKGR; GL Biochem), and other reagents (Sigma) unless otherwise specified.

Lgmn activation and inhibition. Lgmn was activated per manufacturer protocol. Lgmn activation was confirmed by incubating Lgmn (1 ng/µl) with Z-Ala-Ala-Asn-AMC (200 μM) in dilution buffer [250 mM NaCl, 50 mM 2-(N-morpholino) ethanesulfonic acid (MES); pH 5.0] or MES-HBSS (HBSS, 50 mM MES pH 5.0, 5.5 or 6.0). Fluorescence (excitation 340 nm, emission 460 nm) was measured every 30 s for 10 min in a Flexstation three plate reader (Molecular Devices). Lgmn (1 ng/µl) was assayed for activity in the presence of the Lgmn inhibitors QDD100531 or QDD123427 (1 pM –10 μM) and PAR_2 antagonists I-343 (10 μM) or GB88 (10 μM; Farmer, 2013; Lieu et al., 2016; Jimenez-Vargas et al., 2018). Rich Williams provided the Lgmn inhibitors. The specificity of QDD100531 was demonstrated in Ness et al. 2015 (compound 9h in Supplementary Table 1); QDD100531 showed no reactivity to other proteases including cathepsin S, cathepsin B, caspase-3, caspase-8, or USP17 (Ness et al., 2015). QDD123427 showed similar specificity (R. Williams, personal communication). GB88 exhibited specific antagonist activity against four PAR_2 agonists differing in structure and mechanism; selectivity of GB88 for PAR_2 over PAR_1 and PAR_4 was also demonstrated (Suen et al., 2012). I-343, a member of the I-191 family of full PAR_2 antagonists, inhibited inositol phosphate-1 (IP_1) generation induced by the PAR_2 agonists trypsin and 2-Furoyl-LIGRLO-NH_2, but not IP_1 accumulation induced by ATP (Farmer, 2013; Jiang et al., 2018; Jimenez-Vargas et al., 2018). For studies in mice, activated Lgmn was diluted in 50 mM MES and 250 mM NaCl, at pH 5.0 (dilution buffer) to a concentration of 300 ng/20 µl. For the *in vivo* experiments with LI-1 (10 mM, 100 µl, diluted in DMSO; Lee and Bogyo, 2010) the inhibitor was injected into the tail vein 2 h before injection of Lgmn. LI-1 was a gift from Matthew Bogyo. It is a covalent Lgmn inhibitor that exhibits >20,000-fold selectivity for Lgmn over cathepsin B, cathepsin L, and caspase-3. It has previously been shown to inhibit all Lgmn activity *in vivo* within 1 h of administration (Edgington-Mitchell et al., 2016).

OSCC patients. Patients were screened and enrolled through New York University (NYU) Oral Cancer Center after consent. Detailed demographic information (age, sex, ethnicity, cancer location, primary tumor stage, and evidence of metastasis) was collected. During surgical resection, tumor and matched normal oral mucosa specimens were collected (normal was harvested at anatomically matched contralateral site). Specimens were frozen in liquid nitrogen and maintained at −80°C. The

Committee on Human Research at NYU Langone Medical Center approved human studies.

Mice. Female C57BL/6J (#000664) and NU/J *Foxn1*^{nu} athymic mice (#002019), four to eight weeks, were from The Jackson Laboratory. Female C57BL/6J and *F2rl1*$^{-/-}$ (B6. Cg-*F2rl1*^{tm1Msl}/J) mice (#004993), four to eight weeks, from The Jackson Laboratory, were used for trigeminal ganglia (TG) dissociation. *F2rl1* conditional knock-out (KO) C57BL/6 mice were generated by genOway as described (Jimenez-Vargas et al., 2018). *Lgmn*$^{-/-}$ C57BL/6N mice were a gift from Thomas Reinheckel (Matthews et al., 2010). The NYU Institutional Animal Care and Use Committee approved mouse studies.

Analysis of total and active Lgmn in tissues. Snap frozen human and murine tissues were sonicated in 50 mM citrate pH 5.5, 0.5% CHAPS, 0.1% Triton X-100, and 4 mM DTT (10 µl/mg tissue). Solids were cleared by centrifugation and protein concentration was measured by BCA assay (Pierce). Protein was diluted in citrate buffer (50 µg/20 µl buffer), and LE28 was added from a 100× DMSO stock (1 μM final; Edgington et al., 2013). Samples were incubated at 37°C for 15 min, and the reaction was quenched with 5× sample buffer [200 mM Tris-Cl (pH 6.8), 8% SDS, 0.04% bromophenol blue, 5% β-mercaptoethanol, and 40% glycerol]. Protein was resolved on a 15% polyacrylamide gel under reducing conditions. LE28 binding was detected by scanning the gel for Cy5 fluorescence using a Typhoon 5 (GE Healthcare). Proteins were transferred to nitrocellulose membranes for immunoblotting with a goat anti-human Lgmn antibody (R & D AF2199, 1:1000 diluted in 50% Li-Cor blocking buffer and 50% PBS-T containing 0.05% Tween 20). Donkey-anti goat-HRP (1:10,000; A15999; Invitrogen) was used for detection with Clarity Western ECL Substrate (Bio-Rad). Actin (Sigma A5060) and ponceau stain were controls.

Tongue xenograft cancer model. An orthotopic xenograft tongue cancer model was created by injecting HSC-3 into the tongue (Lam et al., 2012). NU/J *Foxn1*^{nu} athymic mice were injected in the left lateral tongue under anesthesia [1×10^5 HSC-3 human tongue OSCC cells suspended in 20 µl vehicle (1:1 mixture of DMEM and Matrigel; Corning, reference #354234), or vehicle alone]. After two weeks, the resulting xenografted tumors and vehicle-injected tongues were excised and snap frozen for protein analysis as above. Goat anti-mouse Lgmn (R & D AF2058) and donkey anti-goat IR-800 (Li-Cor) were used in the immunoblot.

Paw xenograft cancer model. The plantar surface of the right hind paw of NU/J *Foxn1*^{nu} athymic mice were inoculated with 1×10^5 HSC-3 in 20 μl of DMEM and Matrigel (Ye et al., 2011, 2014a). The paw xenograft model permits measurement of mechanical and heat hypersensitivity of the paw. By 14 d after inoculation, a visible tumor developed in the paw. After measuring baseline mechanical and thermal withdrawal thresholds, HSC-3 were inoculated into the hind paw. Mechanical and thermal withdrawal were measured at post inoculation days 3, 6, 10, and 13. On post inoculation day 14, LI-1 (10 mM, 100 µl) was injected into the tail vein. Mechanical and thermal withdrawal were measured at 1, 3, 6, 12, 24, and 48 h after injection of LI-1 into the paw cancer mouse model.

4-Nitroquinoline 1-oxide (4NQO)-induced OSCC model. An OSCC mouse model was generated by exposing mice to 4NQO (100 μg/ml) in drinking water for 16 weeks (Lam et al., 2012). Functional allodynia (gnaw-time) was measured with dolognawmeters (Dolan et al., 2010). Before administration of 4NQO, mice were examined to confirm the absence of oral abnormalities. 4NQO administration and dolognawmeter training over 15 sessions overlapped; baseline gnaw-time was calculated from the final 5 sessions. Functional allodynia was measured after 28 weeks. The tongue was harvested and a 1- to 2-mm coronal section was dissected from the most clinically suspicious region, fixed in 10% neutral buffer formalin, and processed for paraffin embedding and slide preparation. Four 5-μm hematoxylin and eosin (H & E)-stained tongue sections were evaluated for OSCC. Two pathologists blinded to group identity performed histopathologic analysis. Only mice with histologically confirmed OSCC were included in the analysis of nociception.

Mechanical and thermal nociception in the hind paw. To assess mechanical nociception, mice were placed on a platform with a metal mesh floor and acclimated for 1 h. Paw withdrawal threshold was measured with von Frey filaments (Stoelting; Pickering et al., 2008). Withdrawal threshold was defined as the gram-force sufficient to elicit left hindpaw withdrawal. Withdrawal threshold for each animal was determined as the mean of three trials for each animal. Thermal hyperalgesia was measured with a paw thermal stimulator (IITC Life Sciences; Yamano et al., 2017). Mice were placed in a plastic chamber on a 25°C glass surface. A radiant heat source was focused on the left hind paw and withdrawal latency was measured as the mean of three trials taken at least 5 min apart in each mouse. The cutoff latency was established at 20 s. Lgmn (300 ng in 20 µl) or vehicle (control in 20 µl) was administered by intraplantar injection into the left hind paw under 1% isoflurane. Injections were made 1 h before the withdrawal tests (days 0, 1, and 4).

Facial mechanical nociception. Mice were placed individually in a transparent, mesh-floor, box and acclimated for 1 h every other day for two weeks. We measured withdrawal responses to mechanical stimulation of the left cheek with von Frey filaments ranging from 0.008 to 4 g-force (11 filaments in total) in ascending order (Deseure et al., 2003). We applied the von Frey filament to the cheek, defined by the area below the eye, between the nose and the ear. Each fiber was applied once; however, if the response to a von Frey filament was equivocal or the mouse was moving, the same von Frey filament was reapplied to the same area of the cheek 10 s after the first stimulus, or when the mouse stopped moving. The interval between applications of von Frey filaments of different intensities was 5 min. The facial nociception score was reported as a numerical average of the 11 responses in the following response categories: 0: no response; 1: detection, the mouse is aware of the filament that stimulates the face; the mouse turns its head slightly to the object; 2: reaction, the mouse turn its head away quickly, pulls it backward or reacts with a single face wipe; 3: escape/attack, the mouse quickly escapes from the object, attacks the object with its paw or mouth, or reacts with two facial swipes; 4: multiple facial grooming, the mouse responds to the filament simulation with more than three facial wipes continuously. Hair on the left cheek was removed before subcutaneous injections of Lgmn. The whiskers were not trimmed. Lgmn (300 ng in 20 µl) was injected subcutaneously to the left cheek under 1% isoflurane. Injections were made 1 h before the facial mechanical withdrawal test at days 0, 1, and 4.

Orofacial behavior. The dolognawmeter quantifies a behavioral index of orofacial nociception (Dolan et al., 2010). The device measures the time taken to gnaw through a dowel and is a validated index of orofacial nociception in mice with OSCC. Mice were trained for 15 training sessions in the dolognawmeter or until the coefficient of variance of the time required to gnaw was below 0.2. A baseline gnaw-time (mean of the final five training sessions) was established for each mouse. After baseline gnaw-times were determined, treatment or drug injections were initiated and the mice underwent behavioral testing. Each response was analyzed relative to the mouse's baseline. Activated Lgmn, 300 ng in 20 µl, was injected into the tongue under isoflurane. The injection was performed at days 0, 1, and 4. One hour after injection, the mice were tested with a dolognawmeter.

Quantification of Lgmn in OSCC cells. Lgmn was measured in HSC-3 and DOK cells by ELISA. HSC-3 or DOK cells (~5000/well of a 12-well plate) were cultured for 72 h (~70% confluency; Lam et al., 2012). Medium was removed, cells were washed with 5 ml PBS without Ca^{2+} and Mg^{2+}, and DMEM (500 µl) was added to each well. After 48 h, medium was collected and centrifuged (1500 rpm, 4 min, 4°C). Cells were homogenized with 100 µl of RIPA buffer/well (Thermo Scientific, product #89901). Cell lysate was collected and centrifuged (1500 rpm, 10 min, 4°C). The pellet was discarded. A RayBio Human Lgmn ELISA kit (RayBiotech, code ELH-Lgmn-1) was used for Lgmn quantification. The standard curve was generated using the following concentrations: 7000, 2800, 1120, 448, 179, 72, 29, and 0 pg/ml of Lgmn provided with the kit. The optical densities of the standards and samples were read at 450 nm wavelength using a Promega GloMax luminometer (Promega BioSystems, Model E9032). Alternatively, cells were live-labeled with LE28 (1 μM, 0.1% DMSO) for 4 h, lysed on ice in PBS containing 0.1% Triton X-100, and cleared by centrifugation. Supernatants collected overnight in serum-free media were concentrated using an Amicon Filter with a 3-kDa cutoff. Total

protein from whole-cell lysates or supernatants (~60 µg) were resolved by SDS-PAGE. Gels were scanned for Cy5 fluorescence and subject to Lgmn immunoblotting.

Lgmn immunofluorescence in cancer cells. HSC-3 and DOK cells were grown on cover slips at 37°C, 5% CO_2 for 48 h. Cells were washed with PBS and fixed in 4% paraformaldehyde at room temperature for 15 min. Cells were incubated with 3% bovine serum albumin (BSA) in PBS to block non-specific binding, then incubated with mouse monoclonal anti-Lgmn antibody (Santa Cruz Biotechnology, B-8: sc-133234, lot #A0610), 1:50, 4°C, overnight. Cells were washed in PBS and then incubated with goat anti-mouse secondary antibody conjugated to Alexa Fluor 488 (Life Technology, A11029), 1:300, room temperature for 3.5 h. Nuclei were stained with Hoechst (Thermo Scientific, product #62249, lot #RG2244203). The cover slips were mounted on slides in Fluoromount G (Electron Microscope Sciences). A laser scanning confocal microscope (LSM 700, Carl Zeiss) was used to obtain fluorescent images. The images were captured with a Zeiss Plan-Apochromat 63×/1.40 Oil DIC M27 objective lens for Lgmn signal quantification or 20× DIC objective lens for capturing the representative images. The fluorescent signal intensity of each cell was measured by a blinded researcher using NIH ImageJ. Controls included the following: (1) staining of the spleen from wild-type (WT) and $Lgmn^{-/-}$ mice; (2) preabsorption of the primary anti-Lgmn antibody with Lgmn; and (3) omission of the primary antibody. For the preabsorption negative control, the primary anti-Lgmn antibody (0.07 nM, equivalent to 1:50 dilution) was incubated in 10× higher concentration of activated Lgmn (0.7 nM) at 37°C for 48 h versus cells stained with the primary anti-Lgmn antibody, which was incubated in activated Lgmn vehicle. WT and $Lgmn^{-/-}$ mice were anesthetized with 100 mg/kg ketamine and 10 mg/kg xylazine (intraperitoneal) and transcardially perfused with 25 ml cold PBS, followed by 25 ml of 10% neutral formalin solution. The spleen was postfixed in 10% neutral formalin solution for 24 h, cryoprotected in 30% (v/v) sucrose in PBS for 2 d at 4°C, and embedded in Tissue-Tek^R optimum cutting temperature (OCT) compound (Sakura Finetek). Sections (10 µm) were processed for immunofluorescence staining.

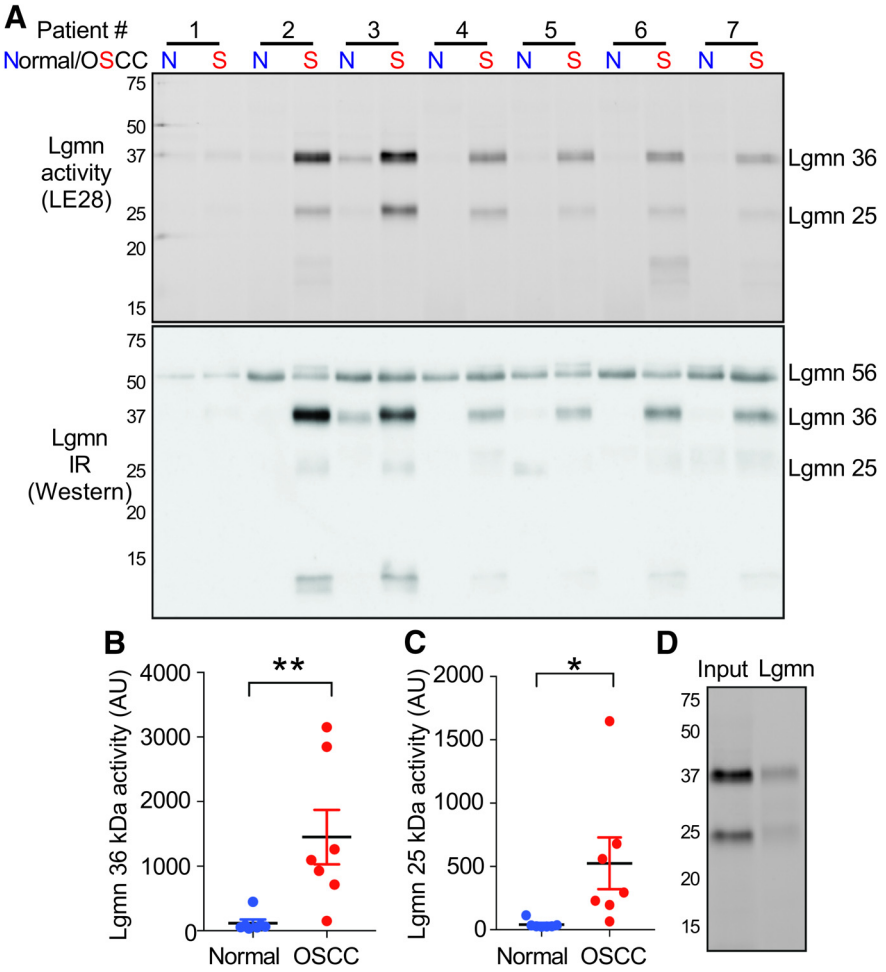


Figure 1. Lgmn activation in human OSCC. ***A***, Active Lgmn labeled by LE28 (upper panel) as shown by in-gel fluorescence and total Lgmn immunoreactivity (IR; lower panel) as shown by Western blotting in OSCC biopsies and patient-matched normal oral mucosa. The gel (upper panel) was transferred to nitrocellulose and immunoblotted for total Lgmn levels (lower panel). ***B***, Densitometry of the 36-kDa species labeled by LE28, displayed as averages for all normal and OSCC samples ($t_{(12)} = 3.124$, $^{**}p = 0.0088$, when 36-kDa Lgmn activity in matched normal oral mucosa and SCC is compared, unpaired Student's *t* test). ***C***, Densitometry of the 25-kDa species labeled by LE28, displayed as averages for all normal and OSCC samples ($t_{(12)} = 2.367$, $^{*}p = 0.0356$, when 25-kDa Lgmn activity in matched normal oral mucosa and SCC is compared, unpaired Student's *t* test). ***D***, Immunoprecipitation of LE28-labeled tumor sample with a Lgmn-specific antibody to confirm the 36- and 25-kDa species ($n = 7$).

Dissociation of TG neurons. Mice were anesthetized with isoflurane, bilateral TG were removed and neurons were enzymatically dispersed as described (Ono et al., 2015). Ganglia were cut into 8–10 segments and incubated for 30 min in collagenase and dispase (12 mg collagenase, 14 mg dispase in 3 ml HBSS). Neurons were triturated and plated onto laminin/poly-L-ornithine-coated coverslips. Neurons were cultured in Leibovitz medium containing 10% fetal calf serum, with penicillin and streptomycin for 24 h (37°C, 5% CO_2).

Electrophysiological recording. Hyperexcitability of small TG neurons (≤20 µm, <30 pF) was quantified by measuring rheobase (Scheff et al., 2018). Whole-cell patch-clamp recordings were made using Axon patch 200B amplifier (Molecular Devices). Digidata 1440A (Molecular Devices) was used for data acquisition and pulse generation. Rheobase was measured using 250 ms square pulses starting from −10 pA with steps of 10 pA until the action potential threshold was reached. The resting membrane potentials were recorded at stable conditions without current injection. Neurons with resting membrane potentials more positive than −40 mV were excluded from analysis. Input resistance was estimated from current-clamp recordings of the voltage response to 250 ms of 10 pA hyperpolarizing current. Pipette resistance was 4–5 mΩ in the following external solution: 140 mM NaCl, 5 mM KCl, 10 mM HEPES, 10 mM glucose, 1 mM $MgCl_2$, and 2 mM $CaCl_2$; pH was adjusted to 7.3–7.4 with NaOH. Pipette solution consisted of the following: 110 mM K-gluconate, 30 mM KCl, 10 mM HEPES, 1 mM $MgCl_2$, and 2 mM $CaCl_2$; pH was adjusted to 7.25 with KOH. Rheobase was measured after 10 min incubation with Lgmn (20 ng/ml in external solution, pH 5.5), Lgmn (20 ng/ml) plus LI-1 (10 µM), or Lgmn vehicle (Lgmn activation buffer pH 5.5). To study the signaling pathways of Lgmn induced hyperexcitability, perforated patch-clamp was performed to avoid dialysis of cytoplasmic constituents. Amphotericin B (240 µg/ml) was used in the pipette solution. Neurons were preincubated with GF109203X (GFX, Tocris) or PKI-tide (both 1 µM, 30 min, 37°C) before challenge with Lgmn (20 ng/ml) or Lgmn vehicle. Rheobase was measured 10 min after incubation with Lgmn or vehicle.

Cell lines. Human embryonic kidney (HEK293) cells stably expressing the human (h)PAR_2 with extracellular N-terminal FLAG and intracellular C-terminal HA11 epitopes (HEK-FLAG-PAR_2-HA cells) have been described (Böhm et al., 1996b). PAR_1 and PAR_2 were deleted from

HEK293 cells using CRISPR/Cas9 (Ungefroren et al., 2017). Cells were maintained in DMEM with 10% fetal bovine serum and hygromycin (100 µg/ml, 5% CO_2, 37°C). Dysplastic oral keratinocyte, DOK, cell number 94122104 from Sigma-Aldrich was cultured in DMEM/F12 (Invitrogen), 10% fetal bovine serum, 50 IU/ml penicillin/streptomycin and 5 µg/ml hydrocortisone. Human OSCC, HSC-3, cell number JCRB0623, was from Japanese Collection of Research Bioresources Cell Bank. HSC-3 was cultured in DMEM, 10% fetal bovine serum, and 50 IU/ml penicillin/streptomycin. DOK and HSC-3 cell lines were maintained at 37°C with 5% CO_2.

PAR_2 cleavage. A peptide corresponding to hPAR_2 amino acids 21–50 was synthesized by American Peptide Company and dissolved in water at 300 μM. The peptide was diluted to 200 μM with Lgmn activation buffer (50 mM sodium acetate, 100 mM NaCl, pH 4.5) in the presence and absence of Lgmn (200 nM; final volume 25 µl). After overnight incubation at 37°C, the reactions were quenched with 25 µl of 50% acetonitrile containing 0.1% trifluoroacetic acid (TFA). Samples (2 µl) were subject to LCMS analysis with a Shimadzu LCMS 2020 fitted with a Phenomenex Luna 3 µm C8(2) column (100 Å, 100 × 2 mm). A gradient of 0% – 60% acetonitrile over 10 min with 0.05% TFA was used for separation.

Immunofluorescence in HEK cells. HEK-FLAG-PAR_2-HA cells (45,000) were plated in eight-well ibiTreat µ-slides and incubated overnight. Cells were washed with HBSS and incubated with Lgmn (100 nM final in HBSS pH 5.5) or trypsin (10 nM final in HBSS pH 7.4; 1 h 37°C). Cells were fixed in 4% paraformaldehyde on ice for 10 min. Cells were incubated with blocking buffer [3% normal horse serum (NHS) and 0.1% saponin] for 30 min at RT. Primary antibodies in blocking buffer [rabbit anti-FLAG (1:250, Rockland) and mouse anti-HA (1:250; Ray Biotech)] were incubated overnight at 4°C. Cells were washed with PBS and secondary antibodies in blocking buffer (donkey anti-rabbit-Alexa Fluor 488 and donkey anti-mouse-Alexa Fluor 647; 1:500; ThermoFisher) were added for 1 h at RT. After washing with PBS, DAPI was added for 5 min followed by additional washing. Cells were imaged immediately on a Leica SP8 confocal microscope.

On-cell Westerns. HEK-FLAG-PAR_2-HA cells were plated on poly-D-lysine (PDL)-coated 96-well plates (30,000 cells/well) and incubated overnight. Cells were washed two times in HBSS (pH 7.4) and placed in MES-HBSS (pH 5.0) for Lgmn assays or HBSS (pH 7.4) for trypsin assays. Cells were incubated with Lgmn (1 or 10 ng/µl final concentration) in MES-HBSS (pH 5.0), trypsin (10 nM final concentration) in HBSS (pH 7.4), or vehicle (buffer control) for 30 min at 37°C. Cells were washed with HBSS and fixed with 4% paraformaldehyde in PBS for 20 min on ice. Cells were washed three times in PBS and incubated with blocking buffer (PBS + 3% NHS) for 1 h at room temperature. Cells were incubated with mouse anti-FLAG antibody (1:500, Cell Signaling) in PBS + 1% NHS overnight at 4°C. Cells were washed three times in PBS, incubated with donkey anti-mouse Alexa Fluor 790 (1:1000, A11371, ThermoFisher) in PBS + 1% NHS for 1 h at room temperature. Cells were washed 1 time in PBS and incubated with the nuclear stain SYTO 82 Orange (1 μM, ThermoFisher) in saline for 30 min. Cells were washed three times with saline and then imaged on an GE HealthcareTyphoon imaging system (GE). FLAG immunofluorescence intensity was quantified using NIH ImageJ and was normalized to nuclear fluorescent intensity to correct possible cell loss.

Measurement of intracellular Ca^{2+}. HEK-FLAG-PAR_2-HA cells were plated on PDL-coated 96-well plates (25,000 cells/well) and incubated overnight. Cells were loaded with fura-2 AM (1 μM, Cayman Chemicals) in loading buffer (150 mM NaCl, 2.6 mM KCl, 0.1 mM $CaCl_2$, 1.18 mM $MgCl_2$, 10 mM D-glucose, 10 mM HEPES, 4 mM probenecid, 0.5% BSA, pH 7.4) for 1 h at 37°C. Cells were washed 2 times in HBSS and then placed in MES-HBSS (pH 5.0, 5.5, 6.0, or 7.4) for the Lgmn assays or HBSS (pH 7.4) for trypsin assays. Fluorescence was measured with 340 or 380 nm excitation and 530 nm emission with a Flexstation three plate reader. Baseline fluorescence was measured for 45 s (Zhao et al., 2015). Cells were challenged with Lgmn (1 or 10 ng/µl final concentration) in MES-HBSS (pH 5.0, 5.5, 6.0, or 7.4), trypsin (10 nM final concentration) in HBSS (pH 7.4), or vehicle (buffer control), and fluorescence was measured for an additional 180 s. To confirm that Lgmn-induced Ca^{2+} responses were because of activation of PAR_2, cells were incubated with the PAR_2 antagonists I-343 (10 μM) or GB88 (10 μM; Farmer, 2013; Lieu et al., 2016; Jimenez-Vargas et al., 2018), the PAR_1 antagonist SCH79797 (200 nM; Ahn et al., 2000), or vehicle in HBSS + 1% DMSO for 1 h at 37°C before the Ca^{2+} assay. To confirm the requirement for protease activity, Lgmn was incubated with the Lgmn inhibitors QDD100531 (1 μM) or QDD123427 (100 nM; Ness et al., 2015) in HBSS +1% DMSO for 1 h before the Ca^{2+} assay. Cells were maintained with the inhibitors. To assess the requirement for hydrolyzis of the $Asn^{30}\downarrow Arg^{31}$ site, a mutant PAR_2 in which Asn^{30} was replaced with Ala (PAR_2-ΔN30A) was generated (Twist Biosciences, San Francisco, CA). cDNA (5 µg) encoding PAR_2-ΔN30A was expressed in HEK-PAR_2-KO cells using polyethylenimine (ratio 1:6, DNA:PEI), and cells were studied after 48 h. To assess the capacity of Lgmn or trypsin to

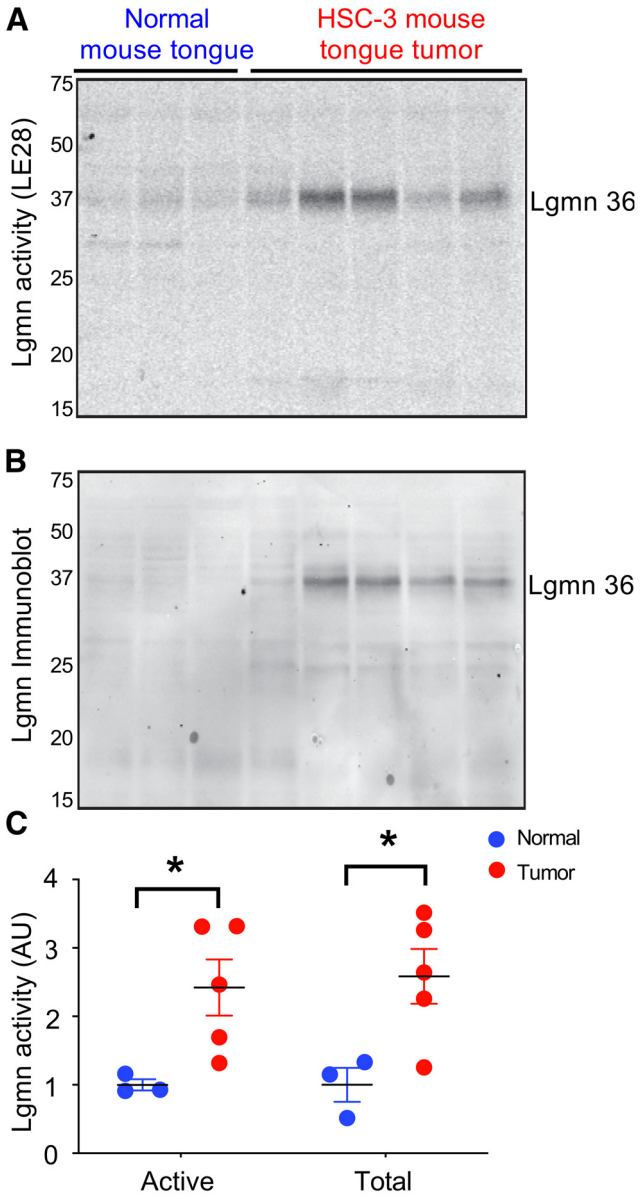


Figure 2. Lgmn in xenograft model of OSCC. ***A***, ***B***, Active Lgmn labeled by LE28 (***A***), shown by in-gel fluorescence, and total Lgmn immunoreactivity (IR; ***B***), shown by Western blotting of lysates from HSC-3 xenografts or control tongues. The gel from (***A***) was transferred to nitrocellulose and immunoblotted for total Lgmn levels (***B***). ***C***, Densitometry of active and total Lgmn from ***A***, ***B***, respectively ($n = 3–5$, $t_{(6)} = 2.592$, $^*p = 0.0411$, when active Lgmn in normal mouse tongue and xenograft cancer is compared, and $t_{(6)} = 2.818$, $^*p = 0.0304$, when total Lgmn in normal mouse tongue xenograft cancer is compared, unpaired Student's *t* tests).

desensitize PAR_2-mediated Ca^{2+} signaling, HEK-FLAG-PAR_2-HA cells were preincubated with Lgmn (1 or 10 ng/µl final concentration) in MES-HBSS (pH 5.0), trypsin (10 nM final concentration) in HBSS (pH 7.4), or vehicle (buffer control) for 10 min at 37°C. Cells were washed and recovered in HBSS (pH 7.4) for 20 min at 37°C. Cells were then challenged with trypsin (10 nM). Desensitization of Ca^{2+} signals to the second challenge with trypsin was calculated as a percentage of the responses in cells preincubated with the vehicle control.

FRET assays of cAMP, protein kinase D (PKD), and ERK. Genetically encoded FRET biosensors targeted to the cytosol were used to assess cAMP, PKD and ERK activation in living cells in real time (Zhao et al., 2015). HEK-FLAG-PAR_2-HA cells were transfected with cDNA (5 µg) encoding the cAMP biosensor Cyto-EPAC (Jimenez-Vargas et al., 2018), the PKD biosensor Cyto-DKAR (Zhao et al., 2019), or the ERK biosensor Cyto-EKAR (Yarwood et al., 2017) using polyethylenimine (ratio 1:6, DNA:PEI). Cells were plated on PDL-coated 96-well plates (25,000 cells/well) and incubated overnight. Cells were washed 2× in HBSS and placed in MES-HBSS (pH 5.0) for the Lgmn assays. The cyan (470 nM) and yellow fluorescent protein (535 nM) emission ratios were measured with a CLARIOstar^{Plus} plate reader (BMG). Baseline fluorescent ratios were recorded for 5 min. Cells were challenged with Lgmn (1 or 10 ng/µl) in MES-HBSS (pH 5.0) or vehicle (buffer control), and FRET was measured for an additional 30 min. FRET ratios were normalized to the MES-HBSS vehicle control.

BRET assays of β-arrestin recruitment. HEK293 cells were transfected with cDNA encoding the PAR_2-RLuc8 (1 µg) and β-arrestin-1-YFP (4 µg) with polyethylenimine (ratio 1:6, DNA:PEI; Jensen et al., 2013). Cells were plated on PDL-coated 96-well white walled plates (30,000 cells/well) and incubated overnight. Cells were washed 2× in HBSS and placed in MES-HBSS (pH 5.0) for the Lgmn assays or HBSS (pH 7.4) for trypsin assays. Coelenterazine-h (5 µM, Nanolight, Pinetop AZ) was added to the cells and the cells were challenged with Lgmn (1 or 10 ng/µl) or trypsin (10 nM). RLuc8 luminescence (480 nm) and YFP fluorescence (530 nm) emission were measured using a CLARIOstar^{Plus} plate reader. Baseline fluorescence ratios were recorded for 2.5 min. The BRET ratio was normalized to vehicle control and baseline.

Experimental design and statistical analysis. We used GraphPad Prism 7 and 8 (GraphPad Prism, GraphPad Software) for the statistical analysis. Results are expressed as mean ± SEM. For cell-based assays, triplicate measurements were made from four to five experiments; differences were evaluated by one-way or two-way ANOVA and Dunnett's or Tukey's multiple comparisons test. One-way ANOVA and Tukey's or Sidak's multiple comparisons and Student's *t* test were used for *in vivo* behavioral experiments and comparison of rheobase. Unpaired Student's *t* test was used to compare values between two groups.

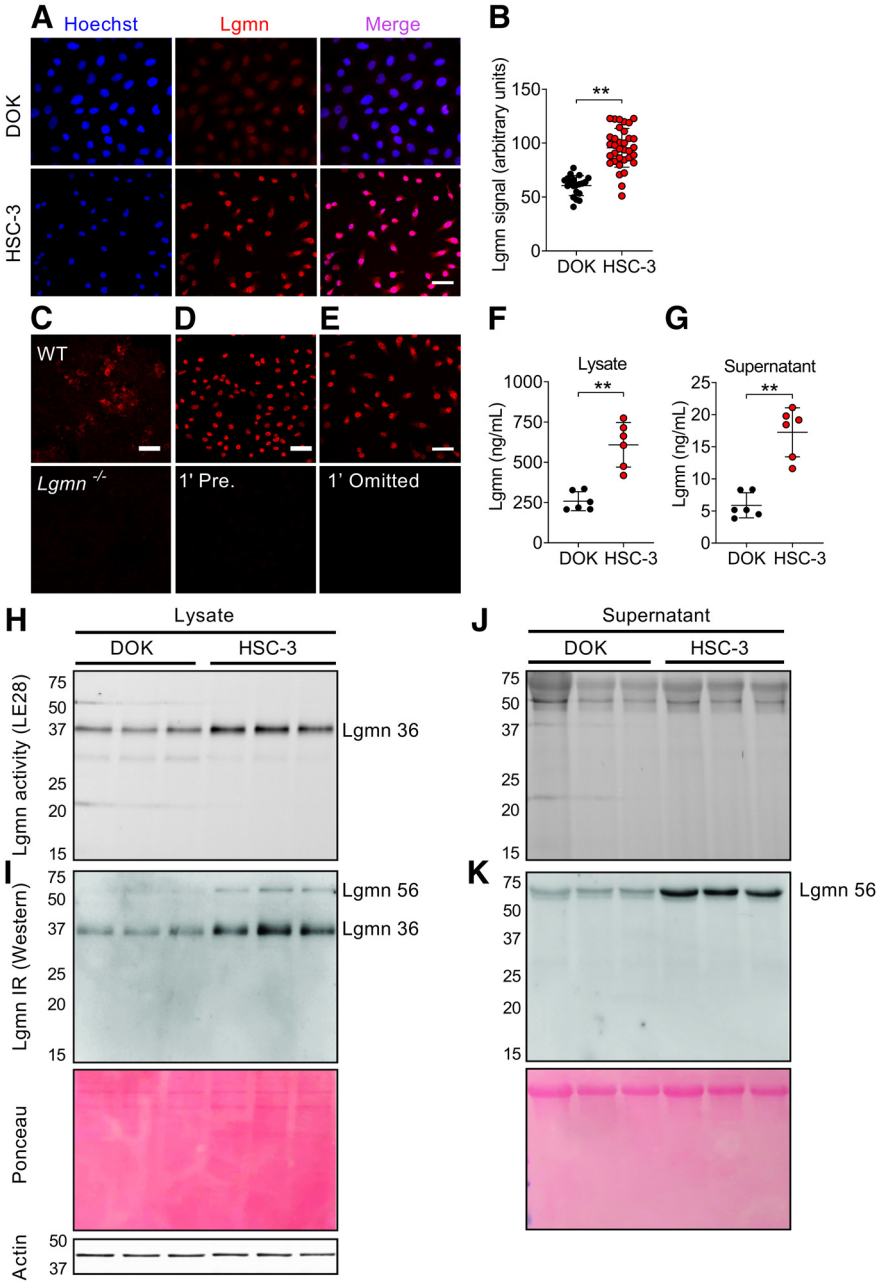


Figure 3. Expression of Lgmn in OSCC cells. ***A***, Localization of immunoreactive Lgmn (red) in DOK and HSC-3. ***B***, Lgmn signal intensity in DOK and HSC-3 was quantified in individual cells by NIH ImageJ ($t_{(52)} = 8.11$, $^{**}p = 8.53E\text{-}11$, when Lgmn signal of DOK is compared with HSC-3, $n = 20$ and 34 cells in DOK and HSC-3, respectively, unpaired Student's *t* test). ***C***, Localization of immunoreactive Lgmn in the spleen of WT and *Lgmn*$^{-/-}$ mice. ***D***, Preabsorption of Lgmn antibody with Lgmn eliminated HSC-3 staining. ***E***, Omission of the anti-Lgmn antibody resulted in lack of HSC-3 staining. ***F***, ***G***, Quantification of Lgmn protein by ELISA in DOK and HSC-3 cell lysate and supernatant. The concentration of Lgmn in HSC-3 cell lysate and supernatant was three times higher than that of DOK. $N = 6$ experiments in each group (in ***F***, $t_{(10)} = 5.70$, $^{**}p = 0.0002$, when the Lgmn concentration in supernatant from HSC-3 is compared with the Lgmn protein concentration in supernatant from DOK, unpaired Student's *t* test. In ***G***, $t_{(10)} = 6.49$, $^{**}p = 0.000069$, when the Lgmn concentration in lysate from HSC-3 is compared with the Lgmn concentration in lysate from DOK, unpaired Student's *t* test). Scale bar in ***A***, ***C***, ***D***, ***E***: 50 µm. ***H***, Labeling of active Lgmn with LE28 in DOK and HSC-3 cell lysate, as shown by in-gel fluorescence. ***I***, Lgmn immunoblot in DOK and HSC-3 cell lysate in ***H***, with ponceau stain and actin immunoblot to verify equal loading. ***J***, Labeling of Lgmn with LE28 in DOK and HSC-3 cell supernatant, as shown by in-gel fluorescence. ***K***, Immunoblot of Lgmn from DOK and HSC-3 cell supernatant.

Results

Lgmn is activated in human and murine OSCC

To determine whether Lgmn is activated in OSCCs, we collected OSCC specimens and matched normal oral mucosa from seven

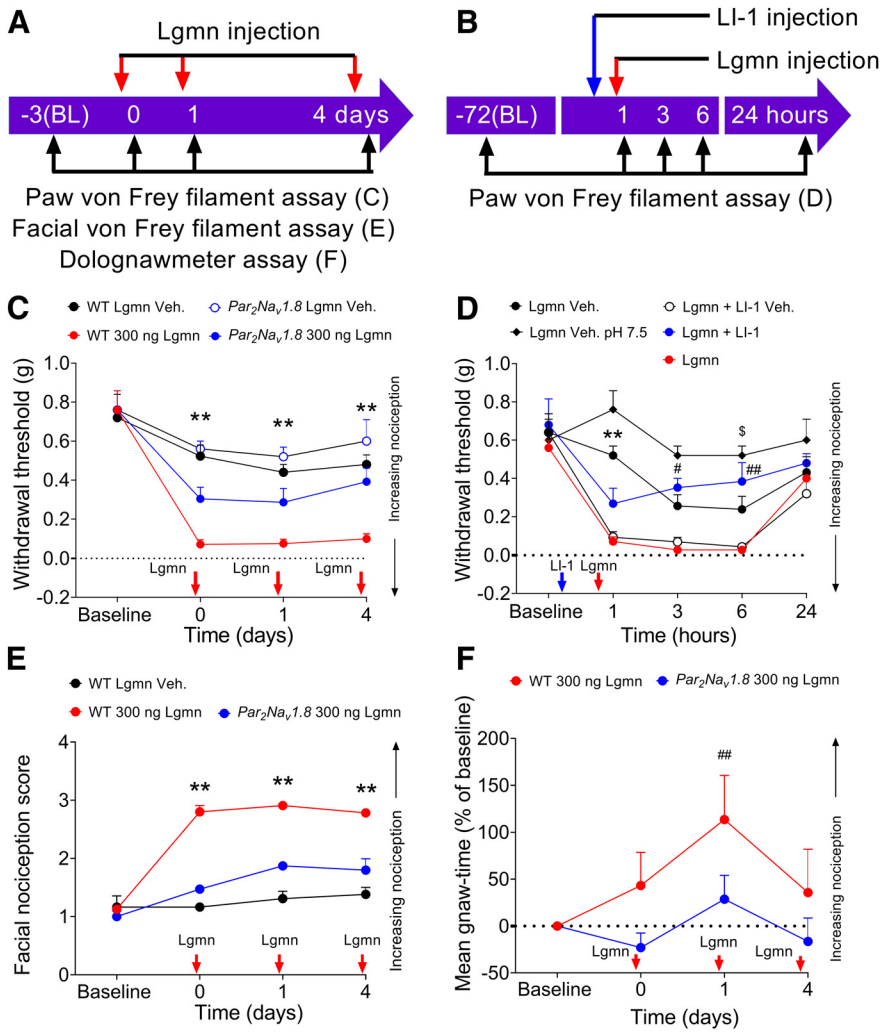


Figure 4. Lgmn-evoked nociception. ***A***, Experiment timeline to test the effect of Lgmn (red arrow) on paw, facial mechanical nociception, and oral function on WT and *$Par_2Na_v1.8$* mice. ***B***, Experiment timeline to test the effect of Lgmn (red arrow) and LI-1 (blue arrow) on paw mechanical nociception on WT mice. ***C***, Effects of Lgmn or vehicle (Veh) on paw withdrawal in WT and *$Par_2Na_v1.8$* mice. Arrows indicate time of Lgmn or vehicle injection. Relative to WT Veh. mice, withdrawal thresholds were significantly lower in WT Lgmn mice, but not *$Par_2Na_v1.8$* mice, at days 0, 1, and 4 (interaction $F_{(9,64)} = 2.47$, $p = 0.02$; $^{**}p = 0.0002$ at d0, $^{**}p = 0.0033$ at d1, $^{**}p = 0.002$ at d4, respectively, when WT mice treated with 300 ng Lgmn are compared with WT mice treated with Lgmn vehicle, $n = 5$ in each group, two-way ANOVA, Tukey's multiple comparisons). ***D***, Effects of LI-1 on Lgmn-evoked mechanical allodynia in WT mice. Blue arrow indicates time of LI-1 or vehicle administration. Red arrow indicates time of Lgmn or Lgmn vehicle injection. Withdrawal thresholds were measured at 1, 3, 6, and 24 h after Lgmn injection. The effect of Lgmn varied with time (interaction $F_{(16,100)} = 2.98$, $p = 0.005$, two-way ANOVA, $n = 5$ in each group, Tukey's multiple comparisons). One hour after injection of LI-1, mean withdrawal threshold was lower in Lgmn versus Lgmn vehicle ($^{**}p = 0.0002$). LI-1 prevented the nociceptive effect of Lgmn at 3 and 6 h after Lgmn injection ($^{\#}p = 0.04$ and $^{\#\#}p = 0.009$, respectively, when Lgmn plus LI-1 is compared with Lgmn plus LI-1 vehicle), but not 1 h after LI-1 injection ($p = 0.30$). Lgmn Veh. at pH 5 reduced the withdrawal threshold more than Lgmn Veh. at pH 7.5 at 6 h after paw injection ($F_{(4,100)} = 24.5$, $^{\$}p = 0.04$, when Lgmn Veh. at pH 5.0 is compared with Lgmn Veh. at pH 7.5, two-way ANOVA, Tukey's multiple comparisons). ***E***, Lgmn (300 ng) was injected into the cheek at days 0, 1, and 4 following baseline facial withdrawal measurements. Arrows indicate Lgmn injection into the cheek. Lgmn induced facial mechanical allodynia in WT but not *$Par_2Na_v1.8$* mice. The means of the facial nociception score were significantly increased in WT mice versus *$Par_2Na_v1.8$* mice at days 0, 1, and 4 ($F_{(3,36)} = 71.69$, $^{**}p = 2.98\text{E-}15$ at d0, d1, and d4, when WT 300 ng Lgmn is compared with *$Par_2Na_v1.8$* 300 ng Lgmn, $n = 5$ in each group, two-way ANOVA, Sidak's multiple comparisons). ***F***, Lgmn (300 ng) significantly increased gnaw-time at 1 d after injection in WT mice versus baseline, but not in *$Par_2Na_v1.8$* mice ($F_{(3,33)} = 3.26$, $^{\#\#}p = 0.0045$ at d1, when WT 300 ng Lgmn is compared with baseline, $n = 8$ and 6 in WT and *$Par_2Na_v1.8$* mice, respectively, two-way ANOVA, Tukey's multiple comparisons).

patients (Table 1). Specimens were incubated with a fluorescently quenched activity-based probe (LE28) selective for Lgmn (Edgington et al., 2013). Two LE28-labeled species of 36 kDa and 25 kDa were activated in OSCC versus normal tissue (Fig. 1*A–D*). Immunoprecipitation with a Lgmn-specific antibody confirmed the identity of mature forms of Lgmn (Fig. 1*D*). Immunoblotting revealed total levels of mature Lgmn 36 kDa increased in all OSCC versus normal tissue (Fig. 1*A*). The 56 kDa inactive Lgmn zymogen (pro-Lgmn) was detected in all specimens. Total Lgmn and Lgmn activity of 36 kDa were upregulated in a murine OSCC xenograft model (human OSCC cells (HSC-3) inoculated in nude mouse tongues) versus normal (Fig. 2*A–C*).

We examined Lgmn expression in HSC-3 and dysplastic oral keratinocytes (DOK, non-cancer cell line) by immunofluorescence and ELISA. Immunoreactive Lgmn was detected in cytosolic granules of HSC-3 and DOK cells, and expression was confirmed by ELISA of cell lysate and conditioned medium (supernatant; Fig. 3*A*,*F*,*G*). The intensity of Lgmn staining was higher in HSC-3 (Fig. 3*B*). Controls for the selectivity of the Lgmn antibody included absence of staining of spleen from *$Lgmn^{-/-}$* mice (Fig. 3*C*), abolition of Lgmn staining by Lgmn antibody preabsorption with Lgmn (Fig. 3*D*), and lack of staining when the Lgmn antibody was omitted (Fig. 3*E*). The Lgmn protein concentration in lysate and supernatant from HSC-3 was higher than the concentration from DOK (Fig. 3*F*,*G*). The levels of Lgmn in lysate (Fig. 3*H*,*I*) and supernatant (Fig. 3*J*,*K*) were higher in HSC-3 compared with DOK. Immunoblotting revealed upregulation of Lgmn 56-kDa zymogen and Lgmn 36-kDa mature form in HSC-3 versus DOK (Fig. 3*I*). HSC-3 cells also secreted more pro-Lgmn than DOKs (Fig. 3*J*,*K*). These results suggest that OSCC cells express and release more Lgmn than dysplastic keratinocytes.

PAR_2 expression on $Na_V1.8$-positive nociceptors is necessary for Lgmn-induced mechanical allodynia

To investigate whether Lgmn causes allodynia by activating PAR_2 on nociceptors, we administered Lgmn (300 ng intraplantar injection) for 3 d (0, 1, 4 d) to WT (C57BL/6J) and *$Par_2Na_v1.8$* mice, which lack PAR_2 in $Na_V1.8$-positive neurons. We measured paw withdrawal responses to stimulation of the plantar surface with von Frey filaments at baseline and 1 h after each Lgmn injection (Fig. 4*A*). Lgmn induced mechanical allodynia on all 3 d in WT mice; however, mechanical allodynia was attenuated in *$Par_2Na_v1.8$* mice by 51% on day 0

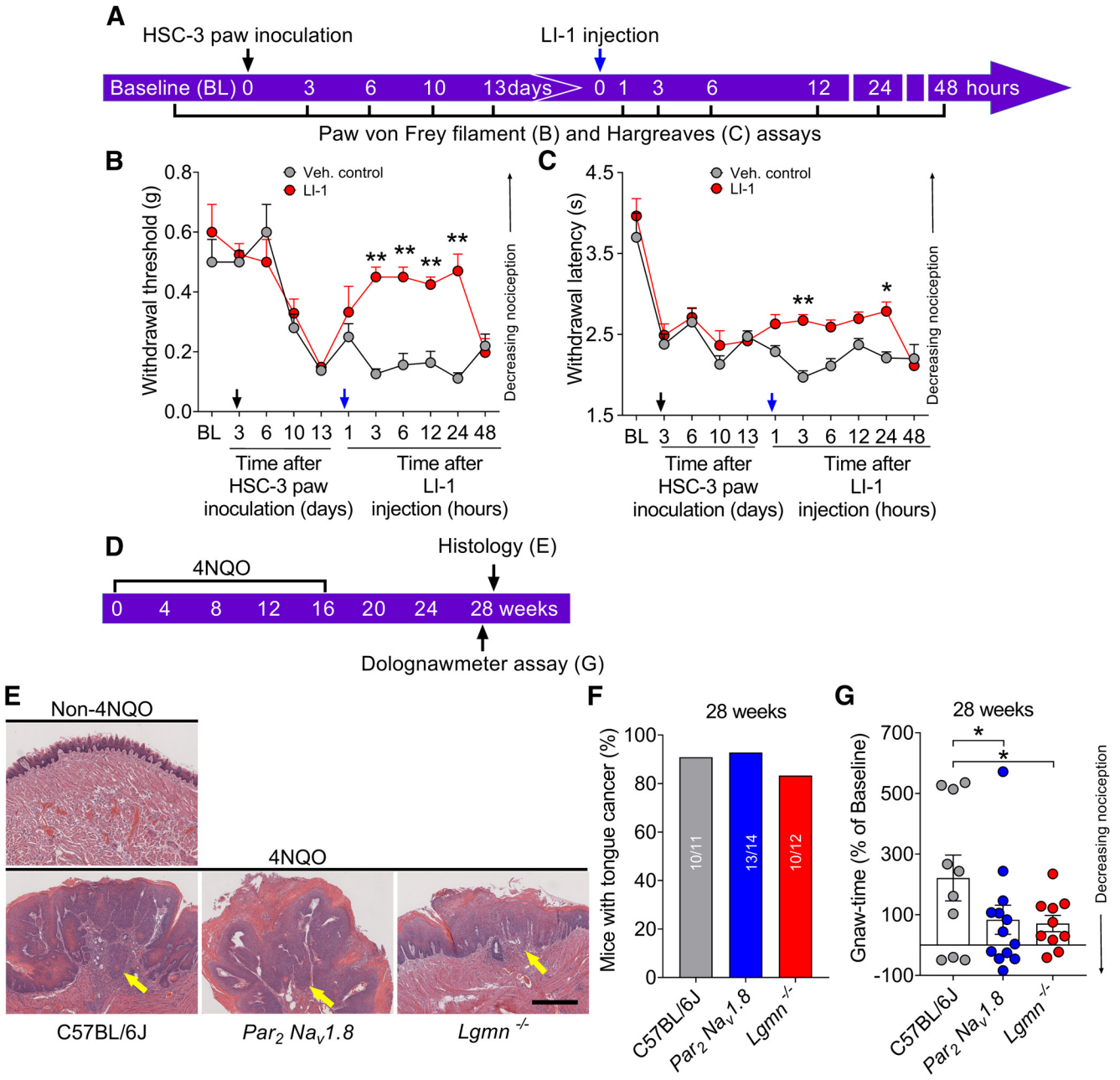


Figure 5. Contributions of Lgmn and PAR_2 to OSCC pain. ***A***, The experimental protocol included baseline measurements of withdrawal threshold to mechanical stimulation and withdrawal latency to thermal stimulation, HSC-3 inoculation, injection of LI-1, and measurements of nociception. ***B***, Mechanical allodynia. HSC-3 inoculation (black arrow) produced mechanical allodynia after 10 d. LI-1 (blue arrow) reversed cancer-induced mechanical nociception versus vehicle control after 3, 6, 12, and 24 h following injection but not after 48 h ($F_{(1,77)} = 32.42$, $^{**}p = 0.0003$ at 3 h, $^{**}p = 0.0015$ at 6 h, $^{**}p = 0.0068$ at 12 h, $^{**}p = 2.15E\text{-}07$ at 24 h, when Veh. control is compared with LI-1, $n = 8$ in each group, two-way ANOVA, Sidak's multiple comparisons). ***C***, Thermal hyperalgesia. HSC-3 inoculation (black arrow) produced thermal hyperalgesia beginning at 3 d. LI-1 (blue arrow), versus vehicle control, reduced thermal hyperalgesia after 3 and 24 h but not after 48 h ($F_{(10,140)} = 24.45$, $^{**}p = 0.0029$ at 3 h, $^{*}p = 0.0278$ at 24 h, when Veh. control is compared with LI-1, $n = 8$ in each group, two-way ANOVA, Sidak's multiple comparisons). ***D***, The experimental protocol included administration of 4NQO to the mice for 16 weeks, measurement of OSCC nociception (gnaw-time) with the dolognawmeter, and histologic analysis of the tongue to confirm cancer. ***E***, Representative histologic images of the tongue from C57BL/6J mice that did not receive 4NQO, and of the tongues from C57BL/6J, *$Par_2Na_v1.8$*, and *$Lgmn^{-/-}$* mice at 28 weeks following 4NQO administration. Arrows indicate tongue carcinoma. Scale bar: 100 µm. ***F***, The percentage of C57BL/6J, *$Par_2Na_v1.8$*, and *$Lgmn^{-/-}$* mice that developed tongue cancer at 28 weeks after 4NQO administration. ***G***, Change of gnaw-time versus baseline (percentage change of gnaw-time at baseline was set as 0%; data not shown) of C57BL/6J ($n = 10$), *$Par_2Na_v1.8$* ($n = 13$), and *$Lgmn^{-/-}$* ($n = 10$) mice with 4NQO-induced tongue cancer ($F_{(1,30)} = 16.28$, $^{*}p = 0.029$, when C57BL/6J is compared with *$Par_2Na_v1.8$*, $^{*}p = 0.024$, when C57BL/6J is compared with *$Lgmn^{-/-}$*, two-way ANOVA with Tukey's multiple comparisons).

(Fig. 4*C*). To confirm that the nociceptive action of Lgmn required enzymatic activity and to test the analgesic potential of a Lgmn inhibitor, we administered the Lgmn-selective inhibitor, LI-1 (10 mM, 100 µl, i.v.; Edgington-Mitchell, 2016) to WT mice 120 min before intraplantar injection of Lgmn and measured paw withdrawal at 1, 3, 6, and 24 h after Lgmn injection (Fig. 4*B*). LI-1 attenuated Lgmn-induced mechanical allodynia by 44% 1 h after Lgmn injection (Fig. 4*D*). Thus, Lgmn-induced mechanical allodynia in mice requires PAR_2 expression on $Na_v1.8$-expressing nociceptors and Lgmn enzymatic activity.

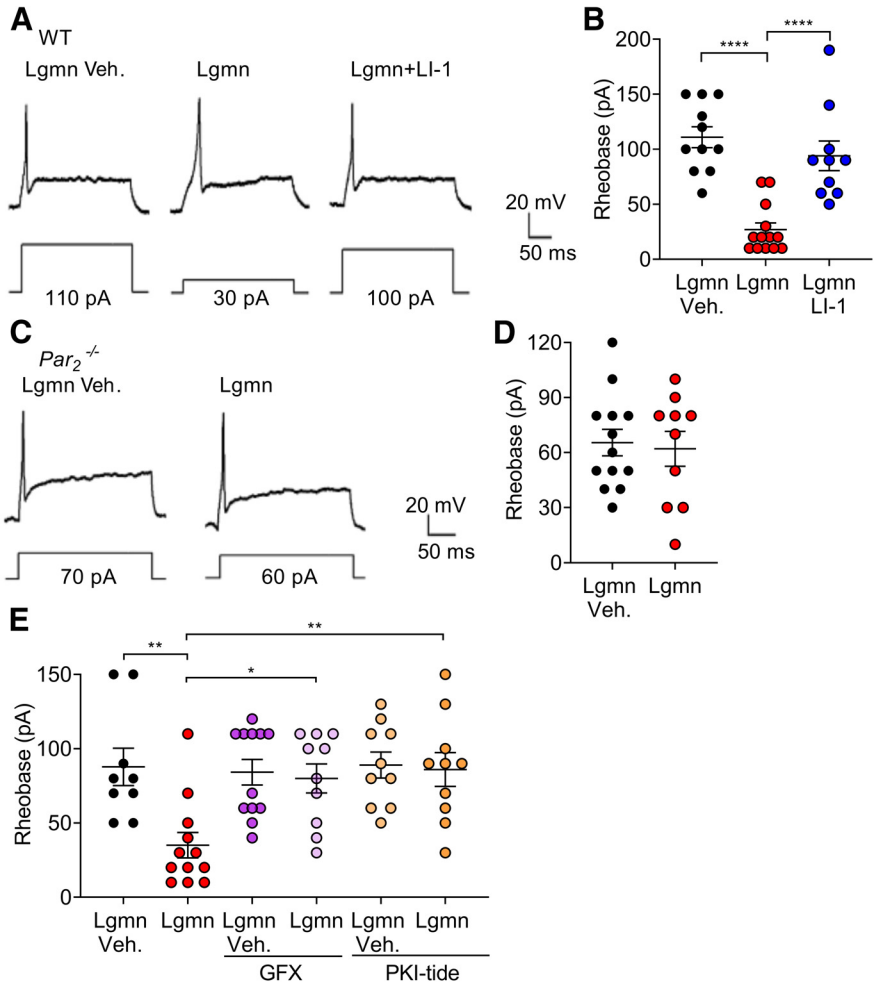


Figure 6. PAR_2 mediated Lgmn-induced hyperexcitability in TG neurons. ***A***, Representative raw traces of whole-cell patch-clamp recordings showing membrane potential response at rheobase of TG neurons from WT mice treated with Lgmn vehicle, Lgmn, and Lgmn + LI-1. ***B***, Rheobase of TG neurons in different treatment groups. Lgmn vehicle: 110.0 ± 31.4 pA, $n = 11$; Lgmn: 26.9 ± 22.1 pA, $n = 13$; Lgmn + LI-1: 94.0 ± 42.4 pA, $n = 10$ ($F_{(2,31)} = 23.14$, ****$p = 1.23E-6$, when Lgmn and Lgmn vehicle are compared, ****$p = 6.93E-5$, when Lgmn and Lgmn + LI-1 are compared, one-way ANOVA with Tukey's multiple comparisons). ***C***, Representative raw traces of whole-cell patch-clamp recordings showing membrane potential response at rheobase of TG neurons from $Par_2^{-/-}$ mice treated with Lgmn and Lgmn vehicle. ***D***, Rheobase of TG neurons from $Par_2^{-/-}$ mice. Lgmn vehicle: 65.3 ± 26.0 pA, $n = 13$; Lgmn: 62.0 ± 30.1 pA, $n = 10$. ***E***, Lgmn induced hyperexcitability and PKC-dependent or PKA-dependent pathways. Perforated patch-clamp recordings were used to measure rheobase of TG neurons. Neurons were preincubated with GFX 1 μM and PKI-tide 1 μM before Lgmn or Lgmn vehicle treatments. Rheobase was measured after neurons were challenged with Lgmn and Lgmn vehicle. Lgmn vehicle, 87.7 ± 12.5 pA, $n = 9$; Lgmn, 35.6 ± 8.5 pA, $n = 12$; GFX + Lgmn vehicle, 84.1 ± 8.5 pA, $n = 12$; GFX + Lgmn, 80.0 ± 9.7 pA, $n = 10$; PKI-tide + Lgmn vehicle, 89.0 ± 8.7 pA, $n = 10$; PKI-tide + Lgmn, 86.0 ± 11.3 pA, $n = 10$ ($F_{(5,57)} = 4.93$, **$p = 0.0052$, when Lgmn and Lgmn vehicle are compared, *$p = 0.0198$ when the Lgmn and Lgmn + GFX are compared, **$p = 0.0198$, when Lgmn and Lgmn + PKI-tide are compared, one-way ANOVA with Tukey's multiple comparisons).

PAR_2 expression on $Na_V1.8$-positive nociceptors is necessary for Lgmn-induced orofacial nociception

We used reflexive and operant assays to test whether Lgmn induces nociception in the orofacial region. We injected Lgmn into the cheek and measured facial withdrawal to stimulation with von Frey filaments. Lgmn (300 ng) was injected subcutaneously for 3 d (0, 1, 4 d) to WT and $Par_2Na_v1.8$ mice. Withdrawal was measured at baseline and 1 h after each injection (Fig. 4*A*). Lgmn induced facial mechanical allodynia on all 3 d in WT mice, but the nociceptive effect was attenuated in $Par_2Na_v1.8$ mice by 81% on day 0 (Fig. 4*E*). For operant behavioral testing, Lgmn (300 ng) was injected into the tongue. Dolognawmeters quantified a behavioral index of nociception 1 h after injection (Fig. 4*A*). Lgmn induced orofacial dysfunction in WT but not $Par_2Na_v1.8$ mice (Fig. 4*F*). Thus, expression of PAR_2 in $Na_V1.8$-expressing nociceptors is necessary for Lgmn-induced pain.

Lgmn mediates OSCC nociception

We used LI-1 to study whether Lgmn secreted from HSC-3 contributes to nociception in the xenograft paw cancer model. After measuring baseline mechanical withdrawal and thermal latency in the paws of NU/J $Foxn1^{nu}$ athymic mice, we inoculated HSC-3 cells, which highly express Lgmn (Fig. 5*A*). Post-inoculation withdrawal measurements verified cancer-generated mechanical allodynia or thermal hyperalgesia. Mice were then treated with LI-1, and mechanical and thermal nociception were assessed (Fig. 5*A*). LI-1 reversed OSCC-induced mechanical withdrawal at 3, 6, 12, and 24 h after injection (Fig. 5*B*), and reversed thermal hyperalgesia at 3 and 24 h postinjection (Fig. 5*C*). LI-1 had no effect 48 h postinjection. An OSCC mouse model was generated with 4NQO administered over 16 weeks in $Lgmn^{-/-}$, $Par_2Na_v1.8$ and WT mice. Oral mechanical allodynia was measured with dolognawmeters at week 28. Tongues were removed, sectioned, stained with H & E, and reviewed independently by two pathologists (Fig. 5*D*). OSCC was confirmed in all groups (Fig. 5*E*). OSCC incidence was >80% at 28 weeks after the administration of 4NQO in all groups (Fig. 5*F*). $Lgmn^{-/-}$ and $Par_2Na_v1.8$ showed significantly less mechanical allodynia than the WT mice (Fig. 5*G*).

Lgmn induces PAR_2-dependent hyperexcitability of trigeminal neurons

To determine whether Lgmn causes PAR_2-dependent hyperexcitability of TG neurons, we measured rheobase in WT mice using whole-cell patch-clamp. Neurons were studied in acidic buffer (external solution, pH 5.5). Lgmn (20 ng/ml, 10 min) decreased rheobase versus vehicle. There was no significant difference between the resting membrane potentials of TG neurons from WT mice pretreated with Lgmn versus Lgmn vehicle (Lgmn: −55.7 ± 2.2 mV, $n = 13$; Lgmn vehicle: −56.6 ± 3.9 mV; $n = 11$, $t_{(22)} = 0.207$, $p = 0.8378$, unpaired Student's t test). The mean input resistance was increased in TG neurons pretreated with Lgmn compared with Lgmn vehicle, but there was no statistically significant difference (Lgmn: 659.3 ± 93.9 MΩ, $n = 13$; Lgmn vehicle: 526.9 ± 79.9 MΩ; $n = 11$, $t_{(22)} = 1.052$, $p = 0.3443$, unpaired Student's t test). To investigate requirement for activity, we preincubated Lgmn with LI-1 (10 μM, 10 min) or vehicle. LI-1 prevented the effect of Lgmn on

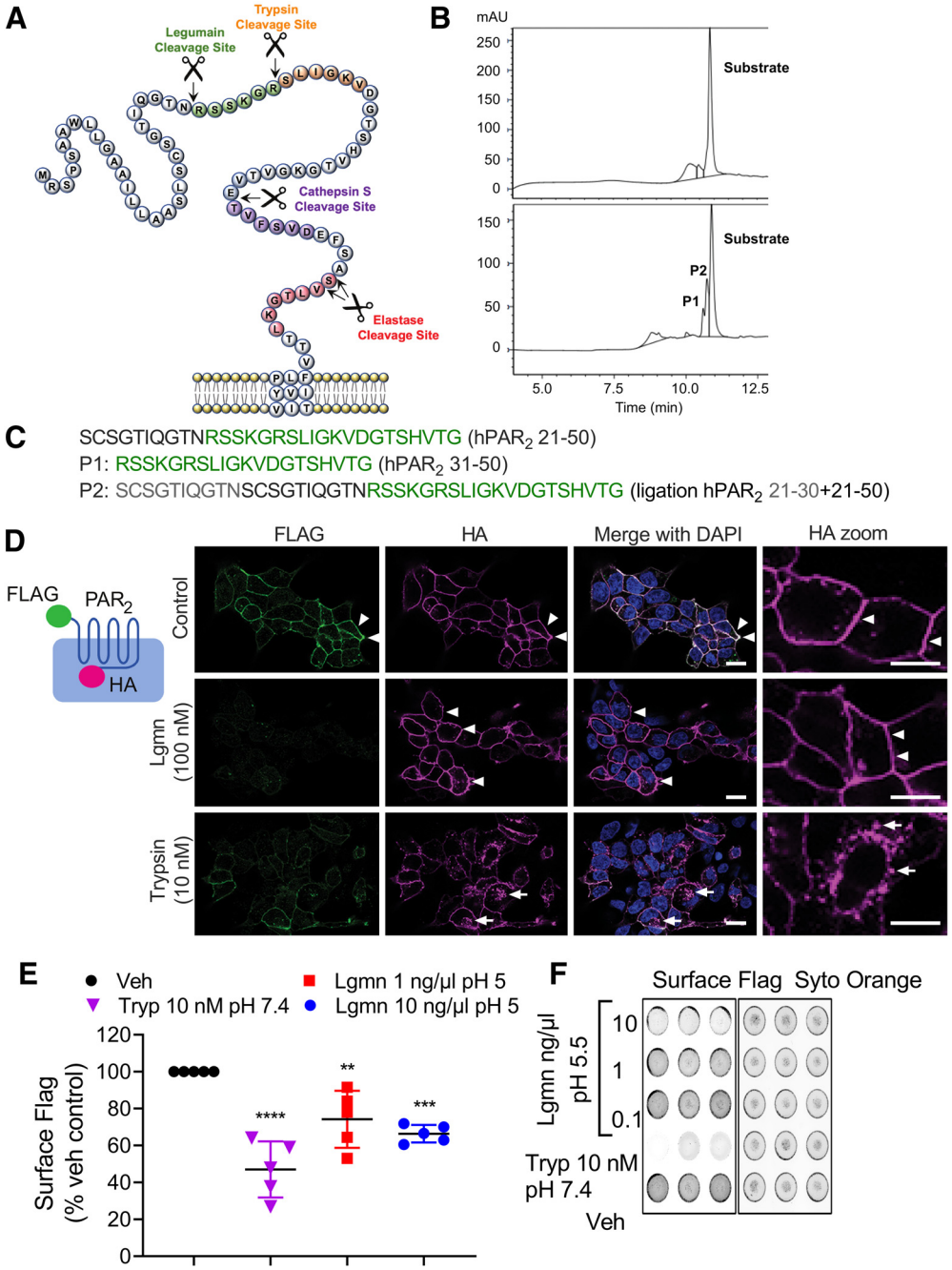


Figure 7. Lgmn cleavage of PAR_2. ***A***, Lgmn PAR_2 cleavage sites and PAR_2 N terminus indicating known cleavage sites. ***B***, ***C***, HPLC chromatograms (***B***) and product identification by mass spectrometry (***C***) of degradation of a fragment of PAR_2 ($hPAR_2^{21-50}$) by Lgmn, showing that Lgmn cleaves PAR_2 at $Asn^{30}\downarrow Arg^{31}$. ***D***, Localization of PAR_2 using antibodies to extracellular N-terminal FLAG and intracellular C-terminal HA epitopes (inset) in HEK-FLAG-PAR_2-HA cells incubated with vehicle (control), Lgmn, or trypsin. Arrows denote plasma membrane localization; arrowheads denote endosomal localization. Scale bar: 20 µm. ***E***, ***F***, On-cell Western showing that trypsin and Lgmn remove the extracellular N-terminal FLAG epitope from HEK-FLAG-PAR_2-HA cells. ***E***, Quantification of triplicate observations from $n = 5$ individual experiments ($F_{(5,22)} = 16.03$, $^{**}p = 0.0034$, Lgmn 1 ng/µl compared with vehicle, $^{***}p = 0.0002$, Lgmn 100 ng/µg compared with vehicle, $^{****}p = 2.5E\text{-}7$ trypsin compared with vehicle, one-way ANOVA with Dunnett's test, $n = 5$). ***F***, Representative images of FLAG immunoreactivity and Syto Orange stain.

rheobase (Fig. 6*A*,*B*). To investigate the contribution of PAR_2, we analyzed Lgmn-induced hyperexcitability in TG neurons from $Par_2^{-/-}$ mice. Lgmn (20 ng/ml, 10 min) did not affect rheobase of $Par_2^{-/-}$ neurons (Fig. 6*C*,*D*).

To evaluate the signaling pathway that mediates effects of Lgmn on excitability, perforated patch-clamp recordings were made from TG neurons pretreated with inhibitors of protein kinase C (PKC; GFX, 1 μM; Coultrap et al., 1999) or protein kinase A (PKA; PKI-tide, 1 μM; Ohlstein et al., 1990) for 30 min at 37°C before treatment with Lgmn (20 ng/ml) or vehicle. GFX and PKI-tide prevented Lgmn-induced hyperexcitability (Fig. 6*E*). Thus, Lgmn causes hyperexcitability of TG nociceptors through Lgmn enzymatic activity, expression of PAR_2, PKC activity, and PKA activity.

Lgmn cleaves PAR_2

To determine whether Lgmn can cleave PAR_2 and identify the cleavage site, Lgmn (200 nM in acetate buffer, pH 4.5)

Table 2. Masses of $hPAR_2$ N-terminal peptide cleavage products identified by mass spectrometry

Peptide	Expected	Found
Substrate:	M: 2991.268	
SCSGTIQGTNRSSKGRSLIGKV$_D$GTSHVTG	(M + 2)/2: 1496.64	1496.45
	(M + 3)/2: 998.10	998.10
	(M + 4)/4: 748.83	748.80
Product 1:	M: 2042.263	
RSSKGRSLIGKV$_D$GTSHVTG	(M + 2)/2: 1022.14	1022.45
	(M + 3)/3: 681.76	681.95
	(M + 4)/4: 511.57	
Product 2:	M: 3958.274	
SCSGTIQGTNSCSGTIQGTNRSSKGRSLIGKV$_D$GTSHVTG•H_2O	(M + 2)/2: 1980.15	
	(M + 3)/3: 1320.43	1320.10
	(M + 4)/4: 990.58	990.40

was incubated with a peptide corresponding to residues 21–50 (S^{21}CSGTIQGTNRSSKGRSLIGKVDGTSHVTG^{50}) of the extracellular N terminus of $hPAR_2$ (200 μM). Digest was analyzed by HPLC and mass spectrometry. Cleavage products were detected corresponding to $PAR_2^{31–50}$ and $PAR_2^{21–30}$ fused to $PAR_2^{21–50}$ (Fig. 7*A–C*; Table 2). Thus, Lgmn cleaves the N terminus of $hPAR_2$ at Asn^{30}↓Arg^{31} consistent with its preference for asparagine residues and ability to ligate peptides with C-terminal asparagine residues to free N termini (Mikula et al., 2017).

To determine whether Lgmn cleaves intact PAR_2 at the plasma membrane, $hPAR_2$ with an extracellular FLAG epitope and intracellular HA epitope was expressed in HEK293 cells (Fig. 7*D*). HEK-FLAG-PAR_2-HA cells were incubated with Lgmn (100 nM, HBSS pH 5.0), trypsin (10 nM, HBSS pH 7.4), or vehicle (buffer control). FLAG and HA were localized by immunofluorescence and confocal microscopy. In vehicle-treated cells, FLAG and HA colocalized at the plasma membrane (Fig. 7*D*). After incubation with Lgmn, FLAG was depleted from the plasma membrane whereas HA was retained at the plasma membrane, consistent with PAR_2 cleavage and removal of the extracellular FLAG epitope. After incubation with trypsin, FLAG was depleted from the plasma membrane, and HA was detected within endosomes, consistent with PAR_2 cleavage and endocytosis (Böhm et al., 1996a).

On-cell Western was used to quantify removal of the FLAG epitope. In Lgmn incubated cells (1 or 10 ng/μl, MES-HBSS pH 5.0, 30 min, 37°C), FLAG immunoreactivity was reduced 26 ± 7% (1 ng/μl) or 34 ± 2% (10 ng/μl) versus vehicle-treated cells (Fig. 7*E*,*F*). After trypsin incubation (10 nM, HBSS pH 7.4, 30 min, 37°C), FLAG immunoreactivity was reduced 53 ± 7% versus vehicle-treated cells. Nuclear stain (Syto Orange) confirmed that proteases did not remove cells from the plate (Fig. 7*F*).

Thus, Lgmn can cleave intact PAR_2 at the surface of HEK cells and remove the extracellular FLAG epitope. Lgmn cleaves PAR_2 at Asn^{30}↓Arg^{31}, proximal to the trypsin cleave site (Arg^{36}↓Ser^{37}). Lgmn does not evoke endocytosis of PAR_2.

Lgmn activity and Lgmn-induced Ca^{2+} signaling are pH dependent

Trypsin, tryptase, and kallikreins cleave PAR_2 at Arg^{36}↓Ser^{37} and induce coupling to $G_{\alpha q}$ and mobilization of intracellular Ca^{2+} (Böhm et al., 1996a; Corvera et al., 1999; Oikonomopoulou et al., 2006). To examine whether Lgmn can mobilize Ca^{2+}, HEK-FLAG-PAR_2-HA cells were challenged with Lgmn (1 or 10 ng/μl, MES-HBSS pH 5.0, 5.5, 6.0 or HBSS pH 7.4), trypsin (10 nM, HBSS pH 7.4), or vehicle (buffer control). Change in intracellular Ca^{2+} was measured using fura-2 AM. Trypsin increased Ca^{2+}, reflected by increased F340/380 nm emission, which rapidly declined toward basal (Fig. 8*A*). At pH 7.4, 10 ng/μl Lgmn induced a small increase in Ca^{2+}, whereas 1 ng/μl Lgmn did not elicit a Ca^{2+} response (Fig. 8*A*). At a lower pH of 5.0, 1 and 10 ng/μl Lgmn caused sustained and concentration-dependent increases in Ca^{2+} (Fig. 8*B*,*E*). At pH 5.0 and 5.5, 10 ng/μl Lgmn increased Ca^{2+}, compared with pH 6.0 and 7.4 (Fig. 8*C*,*D*); however, at pH 5, 1 ng/μl Lgmn increased Ca^{2+} compared with pH 5.5 and 6.0 (Fig. 8*E*,*F*). Lgmn activity assays confirmed the acidic pH optimum of Lgmn, which was active at pH 5.0 and 5.5 but not pH >6.0 (Fig. 8*G*). Lgmn increased Ca^{2+}, in the absence of extracellular Ca^{2+}, indicating intracellular mobilization (Fig. 8*H*). The Lgmn inhibitors, QDD100531 (1 μM) and QD123427 (100 nM), prevented Lgmn-evoked (1 ng/μl) Ca^{2+} signals (Fig. 8*I*,*J*), and caused concentration-dependent inhibition of activity (Fig. 8*K*; Ness et al., 2015).

Lgmn induces Ca^{2+} signaling through PAR_2

To determine whether Lgmn induces Ca^{2+} signaling through PAR_2, we used specific antagonists for PAR_2 and cells genetically deleted for PAR_2. PAR_2 antagonists, I-343 and GB88 (10 μM; Farmer, 2013; Lieu et al., 2016; Jimenez-Vargas et al., 2018) abolished Lgmn-stimulated (1 and 10 ng/μl) Ca^{2+} responses (Fig. 9*A–C*). I-343 and GB88 did not inhibit the enzymatic activity of Lgmn (1 ng/μl), which was slightly increased in the presence of these antagonists (Fig. 9*D*). To determine whether Lgmn induced a Ca^{2+} increase through PAR_1, we used the specific PAR_1 antagonist SCH79797 (Ahn et al., 2000). SCH79797 (200 nM) did not alter Lgmn-induced Ca^{2+} responses (Fig. 9*E*,*F*). To confirm the pharmacologic evidence that PAR_2, and not PAR_1, mediated Lgmn-evoked Ca^{2+} signals, PAR_2 or PAR_1 was deleted from HEK293 cells using CRISPR/Cas9 (Ungefroren et al., 2017). In PAR_2-KO cells, the PAR_2 selective agonist 2-Furoyl-LIGRLO-NH_2 did not increase Ca^{2+} (Fig. 9*G*); however, the PAR_1 selective agonist TFLLR-NH_2 increased Ca^{2+} in PAR_2-KO cells (Fig. 9*H*). In PAR_1-KO cells, TFLLR-NH_2 did not increase Ca^{2+} except at a high concentration (10 μM; Fig. 9*I*), whereas 2-Furoyl-LIGRLO-NH_2 increased Ca^{2+} in PAR_1-KO cells (Fig. 9*J*). Lgmn (10 ng/μl) mobilized Ca^{2+} in PAR_1-KO but not PAR_2-KO cells (Fig. 9*K*).

To confirm that Lgmn activates PAR_2 by cleavage at the Asn^{30}↓Arg^{31} site, we generated a mutant receptor in which the Asn^{30} residue was mutated to Ala, which would not be recognized by Lgmn. PAR_2-ΔN30A was transfected into PAR_2-KO HEK cells. 2-Furoyl-LIGRLO-NH_2 (10 μM) robustly increased Ca^{2+} in HEK-PAR_2ΔN30A cells, whereas Lgmn (10 ng/μl) had no effect (Fig. 9*L*). To determine whether Lgmn activates PAR_2 by exposure of a tethered ligand, we synthesized a hexapeptide, R^{31}SSKGR^{36}, corresponding to a potential tethered ligand revealed by Lgmn cleavage of PAR_2 at the Asn^{30}↓Arg^{31} site. However, R^{31}SSKGR^{36} (10 μM to 0.01 nM) did not alter Ca^{2+} in HEK-PAR_2 cells (Fig. 9*M*). These data confirm that the Lgmn-driven Ca^{2+} response is PAR_2 dependent but does not involve exposure of a tethered ligand domain.

Lgmn desensitizes PAR_2, but does not induce an association between PAR_2 and β-arrestin-1

Processes that terminate PAR_2 signaling at the plasma membrane include β-arrestin-mediated desensitization of PAR_2,

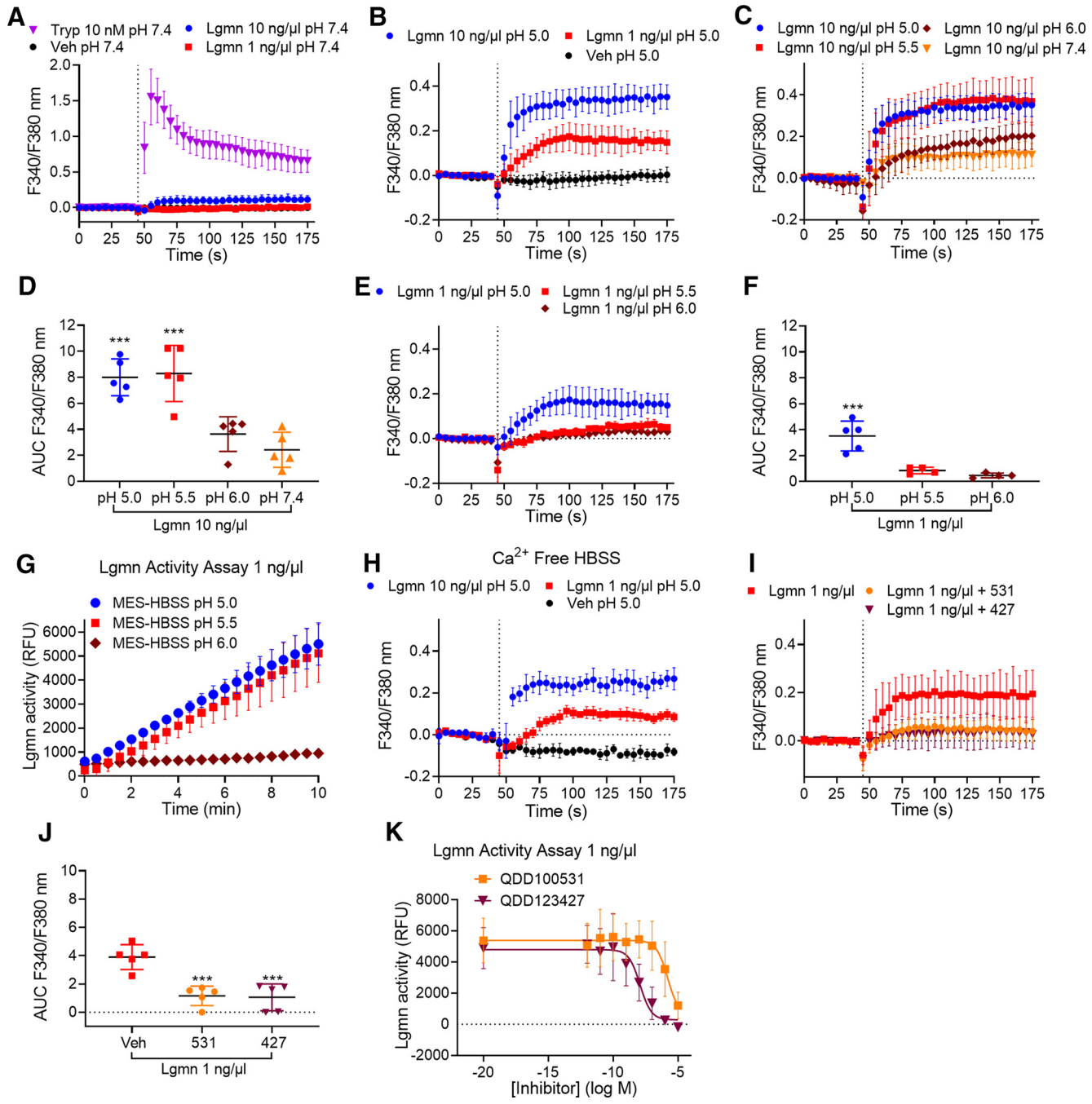


Figure 8. pH dependence of Lgmn activity and stimulation of Ca^{2+} signaling. Time course (***A–C***) and area under curve (AUC; ***D***) of trypsin-evoked and Lgmn-evoked Ca^{2+} signaling in HEK-FLAG-PAR_2-HA cells at pH 7.4, 6.0, 5.5, and 5.0 ($F_{(3,16)} = 17.5$ ***$p = 0.003$, pH 5.0 compared with pH 7.4, ***$p = 0.0001$, pH 5.5 compared with pH 7.4, one-way ANOVA with Tukey's test, $n = 5$). ***E***, ***F***, Time course (***E***) and AUC (***F***) of Lgmn (1 ng/µl)-evoked Ca^{2+} signaling in HEK-FLAG-PAR_2-HA cells at pH 6.0, 5.5, and 5.0 ($F_{(2,10)} = 22.68$, ***$p = 0.0009$ for pH 5.0 compared with pH 5.5 and ***$p = 0.0003$ for pH 5.0 compared with pH 6.0, one-way ANOVA with Tukey's test, $n = 5$). ***G***, Lgmn activity assays at pH 5.0, 5.5, and 6.0. ***H***, Effects of depletion of extracellular Ca^{2+} on Lgmn responses. ***I***, ***J***, Time course (***I***) and AUC (***J***) of the effects of the Lgmn inhibitors QDD100531 (531) and QD123427 (427) on Lgmn Ca^{2+} signals ($F_{(2,12)} = 22.32$, ***$p = 0.0002$ for 531 and ***$p = 0.0002$ for 427 compared with vehicle, one-way ANOVA with Tukey's test, $n = 5$). ***K***, Lgmn activity assay in the presence of graded concentrations of Lgmn inhibitors QDD100531 and QDD123427 (pH 5.0).

PAR_2 cleavage and removal of activation sites and tethered ligand domains, and PAR_2 endocytosis (Böhm et al., 1996a; Déry et al., 1999; DeWire et al., 2007). Since Lgmn cleaves PAR_2 proximal to the trypsin site, subsequent inhibition of trypsin signaling would likely reflect PAR_2 desensitization. To examine desensitization, HEK-FLAG-PAR_2-HA cells were incubated with Lgmn (1 or 10 ng/µl, MES-HBSS pH 5.0), trypsin (10 nM, HBSS pH 7.4), or vehicle (buffer control; Fig. 10*A*). Cells were washed and recovered in HBSS pH 7.4 for 20 min and then challenged with trypsin (10 nM). In cells preincubated with vehicle, trypsin challenge at 30 min robustly increased Ca^{2+} (Fig. 10*B*,*C*). Initial challenge with trypsin also increased Ca^{2+}, but response to a second challenge at 30 min was reduced by 53.7 ± 6.3% versus the response in vehicle-treated cells, consistent with desensitization and endocytosis of PAR_2. Initial challenge with Lgmn (10 ng/µl) slightly increased Ca^{2+}, but the response to a second challenge at

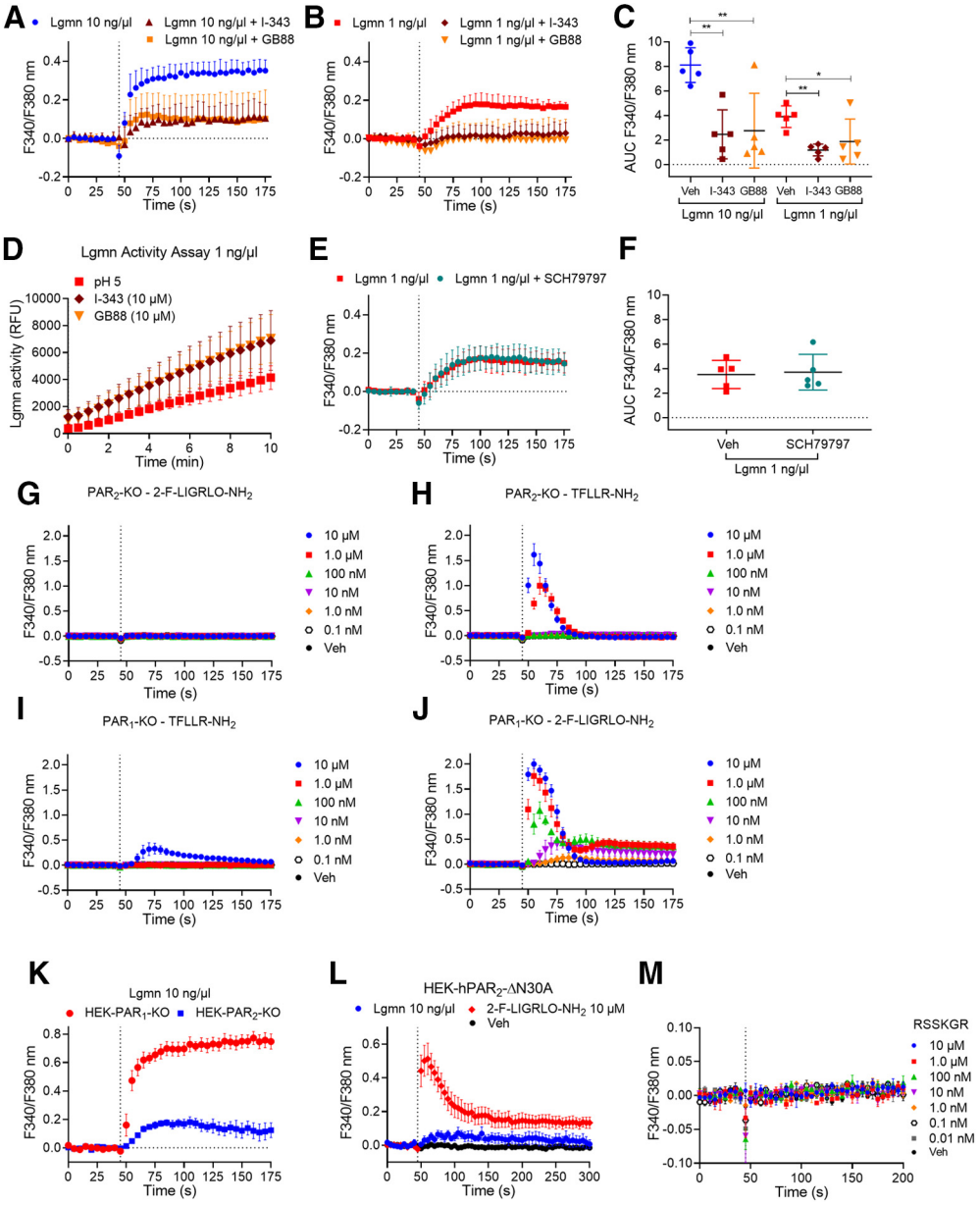


Figure 9. Lgmn signals through PAR_2. ***A–C***, Time course (***A***, ***B***) and area under curve (***C***) of the effects of the PAR_2 antagonists I-343 and GB88 on Lgmn Ca^{2+} signals ($F_{(2,12)} = 9.89$ for Lgmn 10 ng/µl with $^{**}p = 0.0036$ for I-343 and $^{**}p = 0.0052$ for GB88 compared with vehicle, $F_{(2,12)} = 6.84$ for Lgmn 1 ng/µl with $^{**}p = 0.0073$ for I-343 and $^{*}p = 0.0384$ for GB88 compared with vehicle, one-way ANOVA with Tukey's test, $n = 5$). ***D***, Lgmn activity assays in the presence of the PAR_2 antagonists I-343 and GB88 (pH 5.0). Triplicate observations from $n = 5$ individual experiments. ***E***, ***F***, Time course (***E***) and area under curve (***F***) of the effects of the PAR_1 antagonist SCH79797 on Lgmn Ca^{2+} signals. ***G–J***, Effects of the PAR_2 agonist 2-Furoyl-LIGRLO-NH_2 and the PAR_1 agonist TFLLR-NH_2 on Ca^{2+} signals in PAR_2-KO (***G***, ***H***) and PAR_1-KO HEK293 (***I***, ***J***) cells. ***K***, Time course of Lgmn Ca^{2+} signals in HEK-PAR_1-KO and HEK-PAR_2-KO cells. ***L***, Time course of Lgmn Ca^{2+} signals in HEK-PAR_2ΔR30A cells. ***M***, Effects of potential PAR_2 activating peptide $R^{31}SSKGR^{36}$ Ca^{2+} signaling in HEK-FLAG-PAR_2-HA cells.

30 min was reduced by 49.9 ± 6.9% versus response in vehicle-treated cells, consistent with desensitization of PAR_2.

Given that Lgmn desensitizes PAR_2, we sought to determine whether Lgmn recruits β-arrestin-1 to PAR_2. After trypsin cleavage, PAR_2 becomes phosphorylated by GPCR kinases and interacts with β-arrestins, which mediate desensitization and endocytosis (Corvera et al., 1999). However, after cathepsin S or elastase cleavage, PAR_2 neither recruits β-arrestins nor induces endocytosis (Zhao et al., 2014, 2015). We showed that Lgmn does not induce PAR_2 endocytosis (Fig. 7*D*). It is unknown whether PAR_2 associates with β-arrestin-1 following Lgmn cleavage. Thus, we examined BRET between PAR_2-Rluc8 and β-arrestin-1-YFP following treatment with Lgmn. Trypsin (10 nM), but not Lgmn (1 or 10 ng/µl), stimulated PAR_2-Rluc8/β-arrestin-1-YFP BRET (Fig. 10*D*,*E*). These results accord with the inability of Lgmn to evoke PAR_2 endocytosis.

Lgmn activates PAR_2-mediated cAMP formation and activation of PKD and ERK in HEK293 cells

After activation by trypsin, PAR_2 couples to $G_{\alpha q}$, leading to mobilization of intracellular Ca^{2+}, generation of cAMP, and activation of ERK and PKD (DeFea et al., 2000; Amadesi et al., 2009). ERK contributes to sensitization of nociceptors (Ji et al., 1999), and PKD promotes mobilization of PAR_2 from Golgi and recovery of responses to extracellular proteases (Amadesi et al., 2009; Zhao et al., 2019). To examine whether Lgmn-activated PAR_2

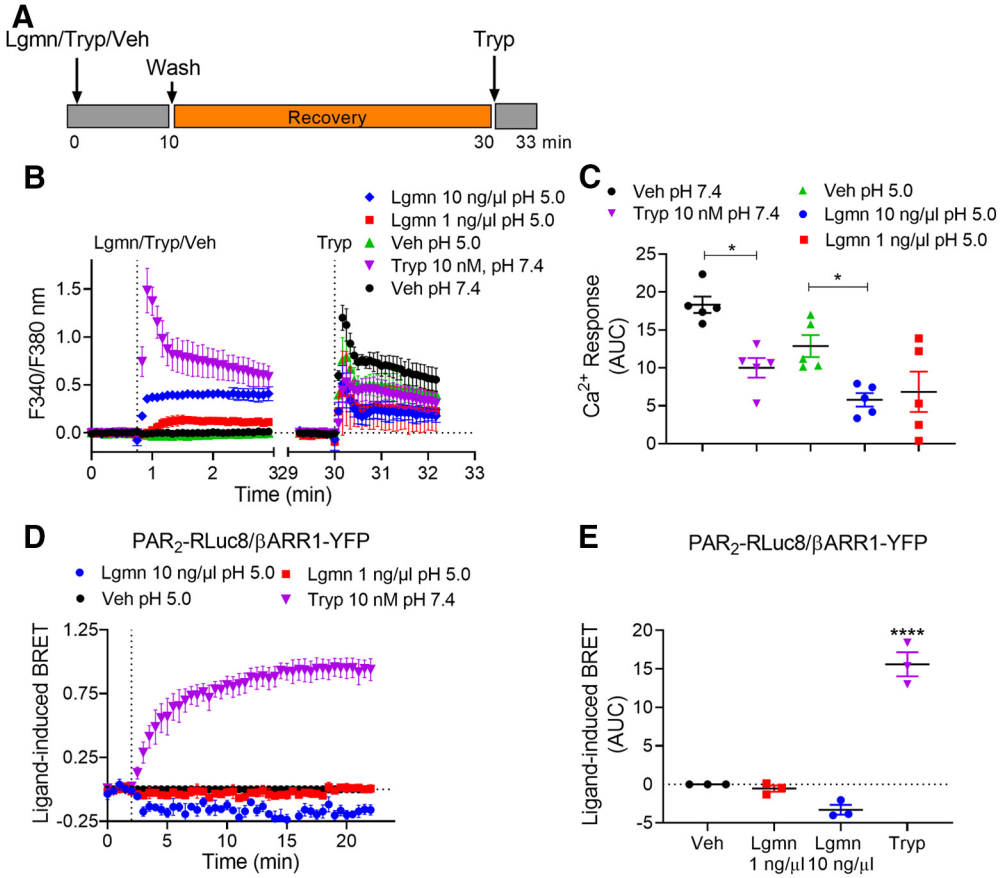


Figure 10. Lgmn desensitization of PAR_2 Ca^{2+} signaling and recruitment of β-arrestin-1. ***A***, HEK-FLAG-PAR_2-HA cells were exposed to trypsin or Lgmn for 10 min, washed, and then challenged with trypsin 20 min after washing. ***B***, Time course of Ca^{2+} signaling. ***C***, Recovery of trypsin responses [area under curve (AUC) from ***B***] in cells pretreated with vehicle, trypsin, or Lgmn ($F_{(4,20)} = 1.61$, $^*p = 0.0116$ for trypsin, and $^*p = 0.0372$ for Lgmn 10 ng/µl compared with vehicle, one-way ANOVA with Tukey's test $n = 5$). ***D***, ***E***, BRET assays of recruitment of β-arrestin-1 to PAR_2. ***D***, Time courses. ***E***, AUC ($F_{(3,8)} = 96.95$, **** $p = 1.25E\text{-}6$ for trypsin versus vehicle, one-way ANOVA with Tukey's test, $n = 5$). All assays were done in triplicate.

couples to a similar range of downstream effectors, we expressed FRET biosensors of cytosolic cAMP (Cyto-Epac), cytosolic PKD (Cyto-DKAR), and cytosolic ERK (Cyto-EKAR) in HEK-FLAG-PAR_2-HA cells. Lgmn caused concentration-dependent activation of cAMP (Fig. 11*A*,*B*), PKD (Fig. 11*C*,*D*), and ERK (Fig. 11*E*,*F*) within the cytosol. cAMP and PKD responses were robust; however, the ERK response was small and detected only after treatment with a higher Lgmn concentration.

Discussion

We report that Lgmn is secreted from OSCC cells and is robustly and reproducibly activated in human and mouse OSCCs compared with normal mucosa. Under acidic conditions, Lgmn cleaves and activates PAR_2 by biased mechanisms to evoke sustained hyperexcitability of nociceptors. We confirmed that PAR_2 and Lgmn contribute to OSCC pain in OSCC mouse models that recapitulate the progression of OSCC observed in humans; genes for Lgmn and PAR_2 on nociceptors were deleted in these mice. Lgmn contributes to cancer hallmarks including proliferation, invasion, and metastasis (Murthy et al., 2005; Vasiljeva et al., 2006; Li et al., 2013; Ohno et al., 2013; Edgington-Mitchell et al., 2015). While Lgmn has been reported to produce bone cancer pain through neurotrophin receptors (Yao et al., 2017), the role of the Lgmn/PAR_2 axis has not been described and could be therapeutically exploited.

The mechanism responsible for Lgmn activation in oral cancer is unresolved. Lgmn is synthesized as pro-Lgmn and traffics through the endoplasmic reticulum and Golgi (Dall and Brandstetter, 2016). Lgmn is packaged and activated in the acidic environment of lysosomes (Dall and Brandstetter, 2016). At pH >6.0, acidic residues unfold and lose proteolytic activity. pH in cancers varies (5.4–6.7; Meyer et al., 1948; Vaupel et al., 1981; Newell et al., 1993; Gillies et al., 1994); the Lgmn activation mechanism remains obscure (Dall and Brandstetter, 2012). Exosomes released from OSCC might exhibit a pH low enough to activate Lgmn. A single report reveals acidic exosomes in cancer patients (Logozzi et al., 2019). Cells from human OSCCs, including the cell line used in this study (HSC-3), secrete exosomes (Dayan et al., 2012; Li et al., 2019). Stabilization between a RGD motif in the catalytic domain and the integrin $\alpha_v\beta_3$ might also activate Lgmn at a higher pH (Liu et al., 2012).

We demonstrated that Lgmn causes cancer-associated nociception through PAR_2 activation on $Na_v1.8$-expressing neurons. While all nociceptors express *$Na_v1.8$*, some non-nociceptors, including low-threshold mechanoreceptors that mediate touch sensation, also express *$Na_v1.8$* (Shields et al., 2012). Since Lgmn activates cathepsins (Edgington-Mitchell et al., 2016), which can also activate PAR_2 (Zhao et al., 2014), it is possible that Lgmn activates PAR_2 directly or indirectly (Edgington-Mitchell et al., 2016). However, we found that Lgmn directly cleaves a fragment of $hPAR_2$ at a unique $Asn^{30}\downarrow Arg^{31}$ site, consistent with known Lgmn selectivity. Site mutation prevented Lgmn-evoked signaling, confirming this mechanism of proteolytic activation. Lgmn evoked hypersensitivity of TG neurons from WT mice

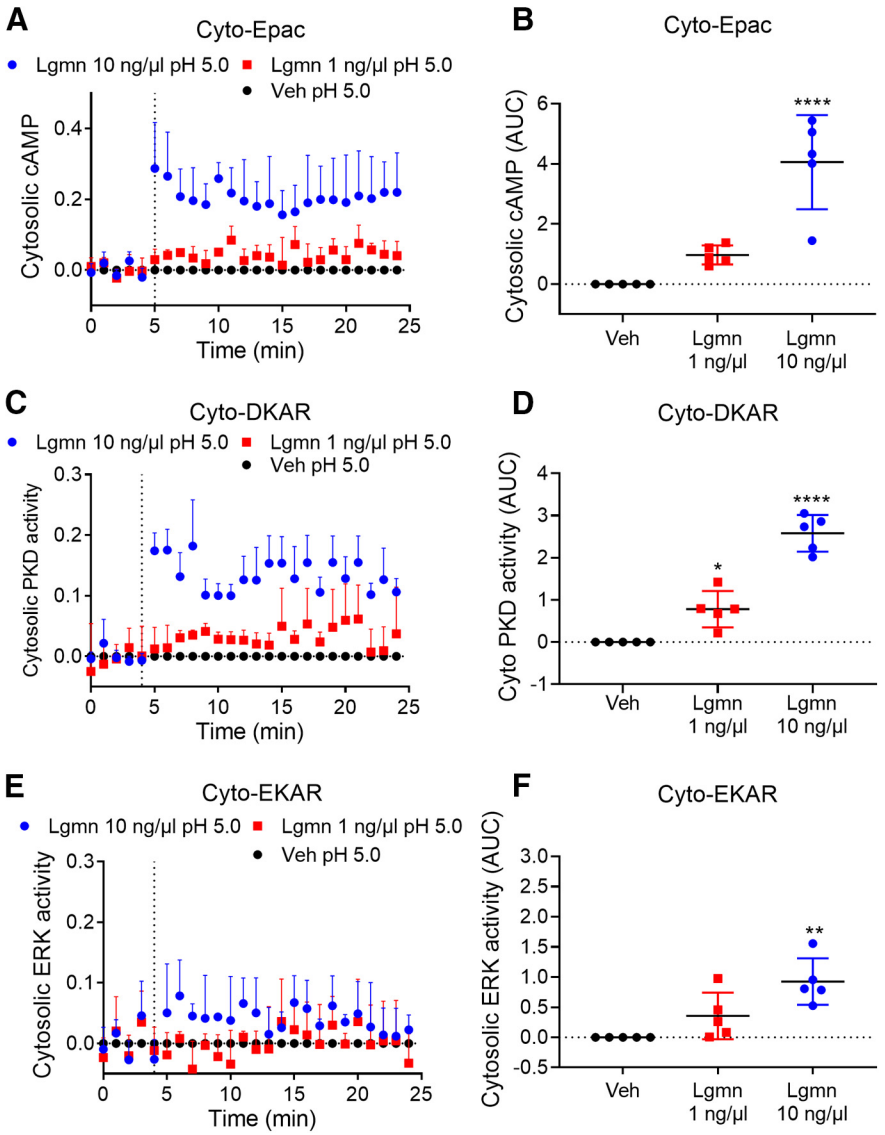


Figure 11. Lgmn activation of cAMP, PKD and ERK signaling and recruitment of β-arrestin-1. ***A–F***, FRET assays of cytosolic cAMP (***A***, ***B***), cytosolic PKD (***C***, ***D***), and cytosolic ERK (***E***, ***F***) in HEK-FLAG-PAR_2-HA cells. ***A***, ***C***, ***E***, Time courses. ***B***, Area under curve (AUC) for cytosolic cAMP ($F_{(2,12)} = 26.43$, ****$p = 0.00{,}004$ for Lgmn 10 ng/µl compared with vehicle, one-way ANOVA with Tukey's test, $n = 5$). ***D***, AUC for cytosolic DKAR ($F_{(2,12)} = 69.77$, ****$p = 2.5E\text{-}7$ for Lgmn 10 ng/µl and *$p = 0.0117$ for Lgmn 1 ng/µl compared with vehicle, one-way ANOVA with Tukey's test, $n = 5$). ***F***, AUC for cytosolic ERK ($F_{(2,12)} = 10.99$, **$p = 0.0015$ for Lgmn 10 ng/µl compared with vehicle, one-way ANOVA with Tukey's test, $n = 5$).

(determined by patch clamp). These effects of Lgmn were prevented by a Lgmn inhibitor and absent in neurons from mice lacking PAR_2, confirming necessity of PAR_2 activation. The nociceptive behavior we measured accords with Lgmn-induced neuronal hypersensitivity. Lgmn induced nociceptive responses in anatomic regions innervated by DRG (paw) and TG (craniofacial) neurons; a Lgmn inhibitor and selective deletion of PAR_2 in $Na_v1.8$ neurons attenuated nociceptive responses. A Lgmn inhibitor eliminated chronic mechanical and thermal nociception in mice inoculated with OSCC cells.

OSCC patients complain of mechanical-induced and function-induced pain and not spontaneous pain (Connelly and Schmidt, 2004; Kolokythas et al., 2007). Our operant orofacial pain assay and automated device to perform the assay (dolognawmeter) quantifies a behavioral index of mechanical allodynia during gnawing (comparable to chewing in humans). Lgmn-induced mechanical allodynia and heat hyperalgesia in OSCC patients might involve PAR_2 sensitization of TRPV4 and TRPV1 ion channels, respectively (Grant et al., 2007; Sipe et al., 2008). TRPV4 mediates mechanosensation, while TRPV1 responds to heat and acids (Caterina et al., 1999; Liedtke and Friedman, 2003; Liedtke et al., 2003; Suzuki et al., 2003a,b). TRPV4 and TRPV1 are sensitized by adenylyl cyclase-dependent, PKA-dependent, and PKCε-dependent mechanisms, which yield ion channel phosphorylation (Numazaki et al., 2002; Amadesi et al., 2006; Zhao et al., 2019). We showed that Lgmn cleavage of PAR_2 activates adenylyl cyclase and cAMP formation; cAMP unleashes catalytic subunits of PKA, which subsequently phosphorylate TRPV channels. We also showed that Lgmn alters rheobase through PKC. Lgmn robustly activates PKD, which likely contributes to PAR_2 trafficking from Golgi to plasma membrane (Zhao et al., 2019).

HEK293 cell experiments revealed that Lgmn mobilizes intracellular calcium, stimulates formation of cAMP, and activates PKD and ERK. Selective inhibitors of Lgmn abolished the

calcium responses; we therefore infer that protease activity is necessary. Lgmn-evoked signals were detected only under mildly acidic conditions, consistent with the acidic pH optimum of Lgmn. We infer that Lgmn-evoked calcium signaling required cleavage/activation of PAR_2 because PAR_2 antagonism or deletion and mutation of the cleavage site abolished signals. PAR_1 antagonism or deletion had no effect. Further studies are needed to reveal mechanisms by which Lgmn activated PAR_2 signals to regulate channel activity and nociception. Trypsin activation of PAR_2 involves exposure of a tethered ligand domain; peptides mimicking the tethered ligand activate the receptor (Hollenberg et al., 1996). Lgmn activation does not involve a tethered ligand; a synthetic peptide corresponding to the revealed N terminus was inactive. Trypsin-activated PAR_2 recruits β-arrestins and then internalizes; Lgmn did not promote β-arrestin recruitment or receptor endocytosis. Thus, like cathepsin S and elastase (Zhao et al., 2014, 2015), Lgmn activates PAR_2 by biased mechanisms to evoke pain.

Our findings are relevant for OSCC patients with pain. While the role of PAR_2 in OSCC pain is clear, antagonism of PAR_2 as a pain therapy approach is challenging. Access to the PAR_2 binding pocket frustrates development of a clinically viable PAR_2 antagonist (Goh et al., 2009; Suen et al., 2014; Boitano et al., 2015). Moreover, PAR_2 continues to signal following cleavage and endocytosis (Jimenez-Vargas et al., 2018); however, we showed that Lgmn-cleaved PAR_2 was not endocytosed. Furthermore, blockade of the Lgmn/PAR_2 axis with a Lgmn inhibitor abrogates OSCC pain in mice. Accordingly, a pain therapy strategy that utilizes blockade of Lgmn is physiologically expedient and holds great clinical potential.

References

Ahn HS, Foster C, Boykow G, Stamford A, Manna M, Graziano M (2000) Inhibition of cellular action of thrombin by N3-cyclopropyl-7-[[4-(1-methylethyl)phenyl]methyl]-7H-pyrrolo[3, 2-f]quinazoline-1,3-diamine (SCH 79797), a nonpeptide thrombin receptor antagonist. Biochem Pharmacol 60:1425–1434.

Amadesi S, Cottrell GS, Divino L, Chapman K, Grady EF, Bautista F, Karanjia R, Barajas-Lopez C, Vanner S, Vergnolle N, Bunnett NW (2006) Protease-activated receptor 2 sensitizes TRPV1 by protein kinase Cepsilon- and A-dependent mechanisms in rats and mice. J Physiol 575:555–571.

Amadesi S, Grant AD, Cottrell GS, Vaksman N, Poole DP, Rozengurt E, Bunnett NW (2009) Protein kinase D isoforms are expressed in rat and mouse primary sensory neurons and are activated by agonists of protease-activated receptor 2. J Comp Neurol 516:141–156.

Angelo PF, Lima AR, Alves FM, Blaber SI, Scarisbrick IA, Blaber M, Juliano L, Juliano MA (2006) Substrate specificity of human kallikrein 6: salt and glycosaminoglycan activation effects. J Biol Chem 281:3116–3126.

Böhm SK, Khitin LM, Grady EF, Aponte G, Payan DG, Bunnett NW (1996a) Mechanisms of desensitization and resensitization of proteinase-activated receptor-2. J Biol Chem 271:22003–22016.

Böhm SK, Kong W, Bromme D, Smeekens SP, Anderson DC, Connolly A, Kahn M, Nelken NA, Coughlin SR, Payan DG, Bunnett NW (1996b) Molecular cloning, expression and potential functions of the human proteinase-activated receptor-2. Biochem J 314:1009–1016.

Boitano S, Hoffman J, Flynn AN, Asiedu MN, Tillu DV, Zhang Z, Sherwood CL, Rivas CM, DeFea KA, Vagner J, Price TJ (2015) The novel PAR2 ligand C391 blocks multiple PAR2 signalling pathways in vitro and in vivo. Br J Pharmacol 172:4535–4545.

Caterina MJ, Rosen TA, Tominaga M, Brake AJ, Julius D (1999) A capsaicin-receptor homologue with a high threshold for noxious heat. Nature 398:436–441.

Connelly ST, Schmidt BL (2004) Evaluation of pain in patients with oral squamous cell carcinoma. J Pain 5:505–510.

Corvera CU, Déry O, McConalogue K, Böhm SK, Khitin LM, Caughey GH, Payan DG, Bunnett NW (1997) Mast cell tryptase regulates rat colonic myocytes through proteinase-activated receptor 2. J Clin Invest 100:1383–1393.

Corvera CU, Déry O, McConalogue K, Gamp P, Thoma M, Al-Ani B, Caughey GH, Hollenberg MD, Bunnett NW (1999) Thrombin and mast cell tryptase regulate guinea-pig myenteric neurons through proteinase-activated receptors-1 and -2. J Physiol 517:741–756.

Coultrap SJ, Sun H, Tenner TE Jr, Machu TK (1999) Competitive antagonism of the mouse 5-hydroxytryptamine3 receptor by bisindolylmaleimide I, a "selective" protein kinase C inhibitor. J Pharmacol Exp Ther 290:76–82.

Dai Y, Wang S, Tominaga M, Yamamoto S, Fukuoka T, Higashi T, Kobayashi K, Obata K, Yamanaka H, Noguchi K (2007) Sensitization of TRPA1 by PAR2 contributes to the sensation of inflammatory pain. J Clin Invest 117:1979–1987.

Dall E, Brandstetter H (2012) Activation of legumain involves proteolytic and conformational events, resulting in a context- and substrate-dependent activity profile. Acta Crystallogr Sect F Struct Biol Cryst Commun 68:24–31.

Dall E, Brandstetter H (2016) Structure and function of legumain in health and disease. Biochimie 122:126–150.

Dayan D, Salo T, Salo S, Nyberg P, Nurmenniemi S, Costea DE, Vered M (2012) Molecular crosstalk between cancer cells and tumor microenvironment components suggests potential targets for new therapeutic approaches in mobile tongue cancer. Cancer Med 1:128–140.

DeFea KA, Zalevsky J, Thoma MS, Déry O, Mullins RD, Bunnett NW (2000) Beta-arrestin-dependent endocytosis of proteinase-activated receptor 2 is required for intracellular targeting of activated ERK1/2. J Cell Biol 148:1267–1281.

Déry O, Thoma MS, Wong H, Grady EF, Bunnett NW (1999) Trafficking of proteinase-activated receptor-2 and beta-arrestin-1 tagged with green fluorescent protein. beta-Arrestin-dependent endocytosis of a proteinase receptor. J Biol Chem 274:18524–18535.

Deseure K, Koek W, Adriaensen H, Colpaert FC (2003) Continuous administration of the 5-hydroxytryptamine1A agonist (3-chloro-4-fluoro-phenyl)-[4-fluoro-4-[[(5-methyl-pyridin-2-ylmethyl)-amino]-methyl] piperidin-1-yl]-methadone (F 13640) attenuates allodynia-like behavior in a rat model of trigeminal neuropathic pain. J Pharmacol Exp Ther 306:505–514.

DeWire SM, Ahn S, Lefkowitz RJ, Shenoy SK (2007) Beta-arrestins and cell signaling. Annu Rev Physiol 69:483–510.

Dolan JC, Lam DK, Achdjian SH, Schmidt BL (2010) The dolognawmeter: a novel instrument and assay to quantify nociception in rodent models of orofacial pain. J Neurosci Methods 187:207–215.

Edgington LE, Verdoes M, Ortega A, Withana NP, Lee J, Syed S, Bachmann MH, Blum G, Bogyo M (2013) Functional imaging of legumain in cancer using a new quenched activity-based probe. J Am Chem Soc 135:174–182.

Edgington-Mitchell LE (2016) Pathophysiological roles of proteases in gastrointestinal disease. Am J Physiol Gastrointest Liver Physiol 310:G234–G239.

Edgington-Mitchell LE, Rautela J, Duivenvoorden HM, Jayatilleke KM, van der Linden WA, Verdoes M, Bogyo M, Parker BS (2015) Cysteine cathepsin activity suppresses osteoclastogenesis of myeloid-derived suppressor cells in breast cancer. Oncotarget 6:27008–27022.

Edgington-Mitchell LE, Wartmann T, Fleming AK, Gocheva V, van der Linden WA, Withana NP, Verdoes M, Aurelio L, Edgington-Mitchell D, Lieu T, Parker BS, Graham B, Reinheckel T, Furness JB, Joyce JA, Storz P, Halangk W, Bogyo M, Bunnett NW (2016) Legumain is activated in macrophages during pancreatitis. Am J Physiol Gastrointest Liver Physiol 311:G548–G560.

Farmer LJ (2013) Imidazopyridazines useful as inhibitors of the PAR-2 signaling pathway. U.S. Patent Application WO 2015/048245.

Gillies RJ, Liu Z, Bhujwalla Z (1994) 31P-MRS measurements of extracellular pH of tumors using 3-aminopropylphosphonate. Am J Physiol 267: C195–C203.

Goh FG, Ng PY, Nilsson M, Kanke T, Plevin R (2009) Dual effect of the novel peptide antagonist K-14585 on proteinase-activated receptor-2-mediated signalling. Br J Pharmacol 158:1695–1704.

Grant AD, Cottrell GS, Amadesi S, Trevisani M, Nicoletti P, Materazzi S, Altier C, Cenac N, Zamponi GW, Bautista-Cruz F, Lopez CB, Joseph EK, Levine JD, Liedtke W, Vanner S, Vergnolle N, Geppetti P, Bunnett NW (2007) Protease-activated receptor 2 sensitizes the transient receptor

potential vanilloid 4 ion channel to cause mechanical hyperalgesia in mice. J Physiol 578:715–733.

Hachem JP, Crumrine D, Fluhr J, Brown BE, Feingold KR, Elias PM (2003) pH directly regulates epidermal permeability barrier homeostasis, and stratum corneum integrity/cohesion. J Invest Dermatol 121:345–353.

Hachem JP, Behne M, Aronchik I, Demerjian M, Feingold KR, Elias PM, Mauro TM (2005) Extracellular pH Controls NHE1 expression in epidermis and keratinocytes: implications for barrier repair. J Invest Dermatol 125:790–797.

Hollenberg MD, Saifeddine M, al-Ani B (1996) Proteinase-activated receptor-2 in rat aorta: structural requirements for agonist activity of receptor-activating peptides. Mol Pharmacol 49:229–233.

Jensen DD, Godfrey CB, Niklas C, Canals M, Kocan M, Poole DP, Murphy JE, Alemi F, Cottrell GS, Korbmacher C, Lambert NA, Bunnett NW, Corvera CU (2013) The bile acid receptor TGR5 does not interact with β-arrestins or traffic to endosomes but transmits sustained signals from plasma membrane rafts. J Biol Chem 288:22942–22960.

Ji RR, Baba H, Brenner GJ, Woolf CJ (1999) Nociceptive-specific activation of ERK in spinal neurons contributes to pain hypersensitivity. Nat Neurosci 2:1114–1119.

Jiang Y, Yau MK, Lim J, Wu KC, Xu W, Suen JY, Fairlie DP (2018) A potent antagonist of protease-activated receptor 2 that inhibits multiple signaling functions in human cancer cells. J Pharmacol Exp Ther 364:246–257.

Jimenez-Vargas NN, Pattison LA, Zhao P, Lieu T, Latorre R, Jensen DD, Castro J, Aurelio L, Le GT, Flynn B, Herenbrink CK, Yeatman HR, Edgington-Mitchell L, Porter CJH, Halls ML, Canals M, Veldhuis NA, Poole DP, McLean P, Hicks GA, et al. (2018) Protease-activated receptor-2 in endosomes signals persistent pain of irritable bowel syndrome. Proc Natl Acad Sci USA 115:E7438–E7447.

Kembhavi AA, Buttle DJ, Knight CG, Barrett AJ (1993) The two cysteine endopeptidases of legume seeds: purification and characterization by use of specific fluorometric assays. Arch Biochem Biophys 303:208–213.

Kolokythas A, Connelly ST, Schmidt BL (2007) Validation of the University of California San Francisco oral cancer pain questionnaire. J Pain 8:950–953.

Lam DK, Schmidt BL (2010) Serine proteases and protease-activated receptor 2-dependent allodynia: a novel cancer pain pathway. Pain 149:263–272.

Lam DK, Dang D, Zhang J, Dolan JC, Schmidt BL (2012) Novel animal models of acute and chronic cancer pain: a pivotal role for PAR2. J Neurosci 32:14178–14183.

Lee J, Bogyo M (2010) Development of near-infrared fluorophore (NIRF)-labeled activity-based probes for in vivo imaging of legumain. ACS Chem Biol 5:233–243.

Li C, Zhou Y, Liu J, Su X, Qin H, Huang S, Huang X, Zhou N (2019) Potential markers from serum-purified exosomes for detecting oral squamous cell carcinoma metastasis. Cancer Epidemiol Biomarkers Prev 28:1668–1681.

Li N, Liu Q, Su Q, Wei C, Lan B, Wang J, Bao G, Yan F, Yu Y, Peng B, Qiu J, Yan X, Zhang S, Guo F (2013) Effects of legumain as a potential prognostic factor on gastric cancers. Med Oncol 30:621.

Liedtke W, Friedman JM (2003) Abnormal osmotic regulation in trpv4-/- mice. Proc Natl Acad Sci USA 100:13698–13703.

Liedtke W, Tobin DM, Bargmann CI, Friedman JM (2003) Mammalian TRPV4 (VR-OAC) directs behavioral responses to osmotic and mechanical stimuli in *Caenorhabditis elegans*. Proc Natl Acad Sci USA 100 [Suppl 2]:14531–14536.

Lieu T, Savage E, Zhao P, Edgington-Mitchell L, Barlow N, Bron R, Poole DP, McLean P, Lohman RJ, Fairlie DP, Bunnett NW (2016) Antagonism of the proinflammatory and pronociceptive actions of canonical and biased agonists of protease-activated receptor-2. Br J Pharmacol 173:2752–2765.

Liu Y, Bajjuri KM, Liu C, Sinha SC (2012) Targeting cell surface alpha(v)beta (3) integrin increases therapeutic efficacies of a legumain protease-activated auristatin prodrug. Mol Pharm 9:168–175.

Logozzi M, Capasso C, Di Raimo R, Del Prete S, Mizzoni D, Falchi M, Supuran CT, Fais S (2019) Prostate cancer cells and exosomes in acidic condition show increased carbonic anhydrase IX expression and activity. J Enzyme Inhib Med Chem 34:272–278.

Matthews SP, Werber I, Deussing J, Peters C, Reinheckel T, Watts C (2010) Distinct protease requirements for antigen presentation in vitro and in vivo. J Immunol 184:2423–2431.

Meyer KA, Kammerling EM, Amtman L, Koller M, Hoffman SJ (1948) pH studies of malignant tissues in human beings. Cancer Res 8:513–518.

Mikula KM, Tascón I, Tommila JJ, Iwaï H (2017) Segmental isotopic labeling of a single-domain globular protein without any refolding step by an asparaginyl endopeptidase. FEBS Lett 591:1285–1294.

Murthy R, Xiong H, Nunez R, Cohen AC, Barron B, Szklaruk J, Madoff DC, Gupta S, Wallace MJ, Ahrar K, Hicks ME (2005) Yttrium 90 resin microspheres for the treatment of unresectable colorectal hepatic metastases after failure of multiple chemotherapy regimens: preliminary results. J Vasc Interv Radiol 16:937–945.

Ness KA, Eddie SL, Higgins CA, Templeman A, D'Costa Z, Gaddale KK, Bouzzaoui S, Jordan L, Janssen D, Harrison T, Burkamp F, Young A, Burden R, Scott CJ, Mullan PB, Williams R (2015) Development of a potent and selective cell penetrant Legumain inhibitor. Bioorg Med Chem Lett 25:5642–5645.

Newell K, Franchi A, Pouyssegur J, Tannock I (1993) Studies with glycolysis-deficient cells suggest that production of lactic acid is not the only cause of tumor acidity. Proc Natl Acad Sci USA 90:1127–1131.

Numazaki M, Tominaga T, Toyooka H, Tominaga M (2002) Direct phosphorylation of capsaicin receptor VR1 by protein kinase Cepsilon and identification of two target serine residues. J Biol Chem 277:13375–13378.

Nystedt S, Emilsson K, Larsson AK, Strömbeck B, Sundelin J (1995) Molecular cloning and functional expression of the gene encoding the human proteinase-activated receptor 2. Eur J Biochem 232:84–89.

Ohlstein EH, Vickery L, Sauermelch C, Willette RN (1990) Vasodilation induced by endothelin: role of EDRF and prostanoids in rat hindquarters. Am J Physiol 259:H1835–H1841.

Ohno Y, Nakashima J, Izumi M, Ohori M, Hashimoto T, Tachibana M (2013) Association of legumain expression pattern with prostate cancer invasiveness and aggressiveness. World J Urol 31:359–364.

Oikonomopoulou K, Hansen KK, Saifeddine M, Tea I, Blaber M, Blaber SI, Scarisbrick I, Andrade-Gordon P, Cottrell GS, Bunnett NW, Diamandis EP, Hollenberg MD (2006) Proteinase-activated receptors, targets for kallikrein signaling. J Biol Chem 281:32095–32112.

Ono K, Ye Y, Viet CT, Dang D, Schmidt BL (2015) TRPV1 expression level in isolectin B4-positive neurons contributes to mouse strain difference in cutaneous thermal nociceptive sensitivity. J Neurophysiol 113:3345–3355.

Pickering V, Gupta JR, Quang P, Jordan RC, Schmidt BL (2008) Effect of peripheral endothelin-1 concentration on carcinoma-induced pain in mice. Eur J Pain 12:293–300.

Ramachandran R, Mihara K, Mathur M, Rochdi MD, Bouvier M, Defea K, Hollenberg MD (2009) Agonist-biased signaling via proteinase activated receptor-2: differential activation of calcium and mitogen-activated protein kinase pathways. Mol Pharmacol 76:791–801.

Scheff NN, Bhattacharya A, Dowse E, Dang RX, Dolan JC, Wang S, Kim H, Albertson DG, Schmidt BL (2018) Neutrophil-mediated endogenous analgesia contributes to sex differences in oral cancer pain. Front Integr Neurosci 12:52.

Schmidt BL, Pickering V, Liu S, Quang P, Dolan J, Connelly ST, Jordan RC (2007) Peripheral endothelin A receptor antagonism attenuates carcinoma-induced pain. Eur J Pain 11:406–414.

Shields SD, Ahn HS, Yang Y, Han C, Seal RP, Wood JN, Waxman SG, Dib-Hajj SD (2012) Nav1.8 expression is not restricted to nociceptors in mouse peripheral nervous system. Pain 153:2017–2030.

Sipe WE, Brierley SM, Martin CM, Phillis BD, Cruz FB, Grady EF, Liedtke W, Cohen DM, Vanner S, Blackshaw LA, Bunnett NW (2008) Transient receptor potential vanilloid 4 mediates protease activated receptor 2-induced sensitization of colonic afferent nerves and visceral hyperalgesia. Am J Physiol Gastrointest Liver Physiol 294:G1288–G1298.

Steinhoff M, Vergnolle N, Young SH, Tognetto M, Amadesi S, Ennes HS, Trevisani M, Hollenberg MD, Wallace JL, Caughey GH, Mitchell SE, Williams LM, Geppetti P, Mayer EA, Bunnett NW (2000) Agonists of proteinase-activated receptor 2 induce inflammation by a neurogenic mechanism. Nat Med 6:151–158.

Suen JY, Barry GD, Lohman RJ, Halili MA, Cotterell AJ, Le GT, Fairlie DP (2012) Modulating human proteinase activated receptor 2 with a novel antagonist (GB88) and agonist (GB110). Br J Pharmacol 165:1413–1423.

Suen JY, Cotterell A, Lohman RJ, Lim J, Han A, Yau MK, Liu L, Cooper MA, Vesey DA, Fairlie DP (2014) Pathway-selective antagonism of proteinase activated receptor 2. Br J Pharmacol 171:4112–4124.

Suzuki M, Mizuno A, Kodaira K, Imai M (2003a) Impaired pressure sensation in mice lacking TRPV4. J Biol Chem 278:22664–22668.

Suzuki M, Watanabe Y, Oyama Y, Mizuno A, Kusano E, Hirao A, Ookawara S (2003b) Localization of mechanosensitive channel TRPV4 in mouse skin. Neurosci Lett 353:189–192.

Ungefroren H, Witte D, Mihara K, Rauch BH, Henklein P, Jöhren O, Bonni S, Settmacher U, Lehnert H, Hollenberg MD, Kaufmann R, Gieseler F (2017) Transforming growth factor-β1/activin receptor-like kinase 5-mediated cell migration is dependent on the protein proteinase-activated receptor 2 but not on proteinase-activated receptor 2-stimulated Gq-calcium signaling. Mol Pharmacol 92:519–532.

van den Beuken-van Everdingen MH, de Rijke JM, Kessels AG, Schouten HC, van Kleef M, Patijn J (2007) Prevalence of pain in patients with cancer: a systematic review of the past 40 years. Ann Oncol 18:1437–1449.

Vasiljeva O, Papazoglou A, Krüger A, Brodoefel H, Korovin M, Deussing J, Augustin N, Nielsen BS, Almholt K, Bogyo M, Peters C, Reinheckel T (2006) Tumor cell-derived and macrophage-derived cathepsin B promotes progression and lung metastasis of mammary cancer. Cancer Res 66:5242–5250.

Vaupel PW, Frinak S, Bicher HI (1981) Heterogeneous oxygen partial pressure and pH distribution in C3H mouse mammary adenocarcinoma. Cancer Res 41:2008–2013.

Vergnolle N, Bunnett NW, Sharkey KA, Brussee V, Compton SJ, Grady EF, Cirino G, Gerard N, Basbaum AI, Andrade-Gordon P, Hollenberg MD, Wallace JL (2001) Proteinase-activated receptor-2 and hyperalgesia: a novel pain pathway. Nat Med 7:821–826.

Yamano S, Viet CT, Dang D, Dai J, Hanatani S, Takayama T, Kasai H, Imamura K, Campbell R, Ye Y, Dolan JC, Kwon WM, Schneider SD, Schmidt BL (2017) Ex vivo nonviral gene delivery of μ-opioid receptor to attenuate cancer-induced pain. Pain 158:240–251.

Yao P, Ding Y, Han Z, Mu Y, Hong T, Zhu Y, Li H (2017) Suppression of asparaginyl endopeptidase attenuates breast cancer-induced bone pain through inhibition of neurotrophin receptors. Mol Pain 13:1744806917708127.

Yarwood RE, Imlach WL, Lieu T, Veldhuis NA, Jensen DD, Klein Herenbrink C, Aurelio L, Cai Z, Christie MJ, Poole DP, Porter CJH, McLean P, Hicks GA, Geppetti P, Halls ML, Canals M, Bunnett NW (2017) Endosomal signaling of the receptor for calcitonin gene-related peptide mediates pain transmission. Proc Natl Acad Sci USA 114:12309–12314.

Ye Y, Dang D, Zhang J, Viet CT, Lam DK, Dolan JC, Gibbs JL, Schmidt BL (2011) Nerve growth factor links oral cancer progression, pain, and cachexia. Mol Cancer Ther 10:1667–1676.

Ye Y, Bae SS, Viet CT, Troob S, Bernabé D, Schmidt BL (2014a) IB4(+) and TRPV1(+) sensory neurons mediate pain but not proliferation in a mouse model of squamous cell carcinoma. Behav Brain Funct 10:5.

Ye Y, Ono K, Bernabé DG, Viet CT, Pickering V, Dolan JC, Hardt M, Ford AP, Schmidt BL (2014b) Adenosine triphosphate drives head and neck cancer pain through P2X2/3 heterotrimers. Acta Neuropathol Commun 2:62.

Zhao P, Lieu T, Barlow N, Metcalf M, Veldhuis NA, Jensen DD, Kocan M, Sostegni S, Haerteis S, Baraznenok V, Henderson I, Lindström E, Guerrero-Alba R, Valdez-Morales EE, Liedtke W, McIntyre P, Vanner SJ, Korbmacher C, Bunnett NW (2014) Cathepsin S causes inflammatory pain via biased agonism of PAR2 and TRPV4. J Biol Chem 289:27215–27234.

Zhao P, Lieu T, Barlow N, Sostegni S, Haerteis S, Korbmacher C, Liedtke W, Jimenez-Vargas NN, Vanner SJ, Bunnett NW (2015) Neutrophil elastase activates protease-activated receptor-2 (PAR2) and transient receptor potential vanilloid 4 (TRPV4) to cause inflammation and pain. J Biol Chem 290:13875–13887.

Zhao P, Pattison LA, Jensen DD, Jimenez-Vargas NN, Latorre R, Lieu T, Jaramillo JO, Lopez-Lopez C, Poole DP, Vanner SJ, Schmidt BL, Bunnett NW (2019) Protein kinase D and G$\beta\gamma$ mediate sustained nociceptive signaling by biased agonists of protease-activated receptor-2. J Biol Chem 294:10649–10662.

Nano Today 39 (2021) 101223

Contents lists available at ScienceDirect

Nano Today

journal homepage: www.elsevier.com/locate/nanotoday

Review

Nanotechnology for pain management: Current and future therapeutic interventions

Divya Bhansali[a], Shavonne L. Teng[b,c,d], Caleb S. Lee[a], Brian L. Schmidt[e], Nigel W. Bunnett[c,d], Kam W. Leong[a,f,*]

[a] Department of Biomedical Engineering, Columbia University, New York, NY 10027, United States
[b] Department of Physiology and Cellular Biophysics, Columbia University, New York, NY 10032, United States
[c] Department of Molecular Pathobiology, New York University College of Dentistry, New York, NY 10010, United States
[d] Department of Neuroscience and Physiology, Neuroscience Institute, New York University Langone School of Medicine, New York, NY 10010, United States
[e] Bluestone Center for Clinical Research, New York University College of Dentistry, New York, NY 10010, United States
[f] Department of Systems Biology, Columbia University, New York, NY 10027, United States

ARTICLE INFO

Article history:
Received 7 April 2021
Received in revised form 29 May 2021
Accepted 10 June 2021
Available online 19 June 2021

Keywords:
Pain
Nanomedicine
Drug delivery
Gene therapy
CRISPR
ROS scavenging

ABSTRACT

Pain is one of the most common medical conditions and affects more Americans than diabetes, heart disease, and cancer combined. Current pain treatments mainly rely on opioid analgesics and remain unsatisfactory. The life-threatening side effects and addictive properties of opioids demand new therapeutic approaches. Nanomedicine may be able to address these challenges as it allows for sensitive and targeted treatments without some of the burdens associated with current clinical pain therapies. This review discusses the physiology of pain, the current landscape of pain treatment, novel targets for pain treatment, and recent and ongoing efforts to effectively treat pain using nanotechnology-based approaches. We highlight advances in nanoparticle-based drug delivery to reduce side effects, gene therapy to tackle the source of pain, and nanomaterials-based scavenging to proactively mediate pain signaling.

© 2021 Elsevier Ltd. All rights reserved.

Contents

Introduction . . . 2
The physiology of pain . . . 2
Acute and chronic pain . . . 3
Pain pathways . . . 3
Central and peripheral sensitization . . . 4
Pain and inflammation . . . 4
Nociceptive, neuropathic, and nociplastic pain . . . 4
Current pain treatments and new targets . . . 4
Current pain treatments . . . 4
Non-opioid pain medications . . . 4
Opioids . . . 5
Other pain treatments . . . 5
New targets . . . 6
Voltage-gated sodium channels . . . 6
Nerve growth factor and TrkA . . . 6
Endosomal targets . . . 6
Other targets . . . 6
Nanoparticles for pain management . . . 6

* Correspondence to: Columbia University Medical Center, 3960 Broadway, Lasker Room 450C, New York, NY 10032, United States.
E-mail address: kwl2121@columbia.edu (K.W. Leong).

https://doi.org/10.1016/j.nantod.2021.101223
1748-0132/© 2021 Elsevier Ltd. All rights reserved.

Analgesic nanoparticulate drug delivery systems . . . 7
Systemic pain: opioids and new approaches . . . 7
Neuropathic pain: local anesthetics . . . 8
Neuropathic pain: neurotoxins . . . 8
Chronic pain . . . 9
Localized pain . . . 9
Enhancing drug targeting . . . 9
Light-responsive NDDSs . . . 9
Ultrasound-responsive NDDSs . . . 10
Magnetic field-responsive NDDSs . . . 11
Nanoparticles to detect molecular sources of pain . . . 12
Multiplexed detection of pain markers . . . 12
Localization of neuropathic pain . . . 12
Future use of nanoparticles in pain management . . . 12
Gene therapy for pain . . . 12
Vectors for delivery of gene therapy for pain . . . 12
Herpes simplex virus type 1 . . . 12
Adenoviruses . . . 13
Adeno-associated viruses . . . 13
Lentiviruses . . . 13
Non-viral vectors . . . 14
Future use of gene therapy for treating chronic pain . . . 15
Clinical trials . . . 15
CRISPR-Cas for pain . . . 15
Repressing $Na_v1.7$ via SCN9A . . . 15
Blocking proinflammatory signaling . . . 16
Alleviating osteoarthritic pain . . . 16
Future use of CRISPR-Cas9 for treating chronic pain . . . 16
Scavengers . . . 16
Nucleic acid-binding scavengers . . . 16
ROS-scavenging molecules . . . 17
Conclusions . . . 18
CRediT authorship contribution statement . . . 18
Declaration of Competing Interest . . . 18
Acknowledgments . . . 18
References . . . 18

Introduction

Pain is among the most common reasons for medical care visits [1]. Globally, an estimated 20% of all patients experience pain, and 10% are diagnosed with chronic pain [2]. Over 40% of patients treated for primary pain report inadequate pain relief [3], and many pain relievers have debilitating side effects such as hepatotoxicity, depression, respiratory depression and addiction. The recent opioid epidemic—the leading cause of medication-induced overdose—highlights the urgent need for better treatment options for chronic pain. Chronic pain affects over 20% of the adult population in the United States [4,5], and is associated with diseases such as cancer, diabetes, cystic fibrosis, inflammatory diseases, and with trauma due to injury or surgery. Sufferers of chronic pain have the additional risk of anxiety and depressive disorders, sleep disorders, addiction, and disability [6]. The burden of pain for an individual includes not only physical and mental impairment but also medical costs, strained social relationships, and reduced work productivity. Chronic pain is also a financial burden for countries, costing the United States an estimated $635 billion annually [7,8], due to the socioeconomic costs of healthcare expenses and lost productivity. Chronic pain is more prevalent as the aging population grows. Ultimately, pain negatively impacts the quality of life and is one of the leading causes of long-term disability. Despite this clear need, chronic pain remains difficult to treat effectively and without undesirable side effects.

Nanomedicine is a rapidly growing field, but its application to pain management has been limited by the complexity of pain physiology and the intractable nature of chronic pain. Nevertheless, nanotechnology is playing a major role in the next generation of pain treatments. New nanomaterials serve as drug carriers that target specific tissues, cell types and organelles with stimuli-sensitive release, and as nanodevices that detect the molecular source of pain. Nanoparticle drug carriers exhibit improved efficacy with smaller analgesic doses and longer-term relief of pain symptoms. Gene therapy delivery using nanoparticles is improving the long-term treatment of chronic pain, and both viral and non-viral vectors for gene therapy have proven effective in clinical trials. CRISPR is being used to modulate gene expression to reduce pain without eliminating sensitization. Scavengers of proinflammatory reactive oxygen species and free nucleic acids represent a proactive approach to pain management: instead of treating the symptoms of pain, scavengers remove molecules that trigger nociceptors and that cause sensitization. The application of nanotechnology to pain management represents a frontier for nanomedicine and is the subject of this review.

The physiology of pain

A better understanding of the physiology of pain is needed to develop new therapies that act on specific targets to reduce dosage and toxicity. Pain is an unpleasant, multifaceted sensory and emotional experience associated with actual or potential tissue damage [9], and involves physical, emotional, and psychosocial elements. Pain is difficult to treat and study in part because it is subjective; the perception of pain and its severity varies between individuals. Multimodal pain care regimens are often used to address the complex nature of pain. Pharmaceutical treatments are mechanism-based and consider both pain physiology and psychological factors. To better assess pain, provide personalized pain treatment, and to develop

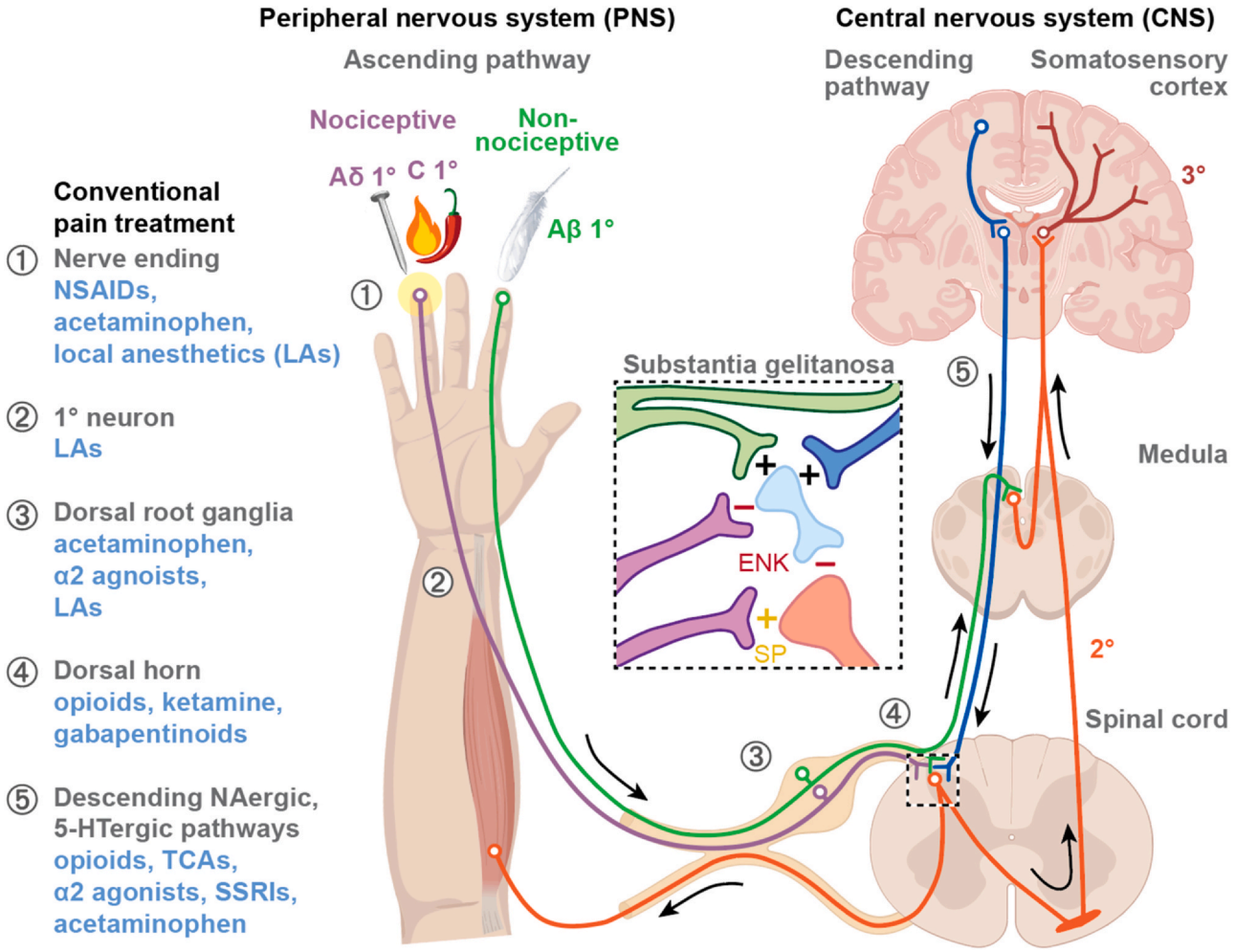


Fig. 1. Pain pathways and current pain treatments. The ascending pathway transmits pain and sensory information from the periphery to the brain. Painful stimuli activate primary afferent nociceptors of mechanosensitive Aδ and mechanothermal C fibers, which send signals to second-order neurons in the spinal cord. This information is transmitted up the spinothalamic tract to tertiary neurons in the thalamus, and pain is perceived in the somatosensory cortex. The descending pathway inhibits pain via noradrenergic/serotonergic neurons and Aβ fibers. Upon activation, interneurons in the substantia gelatinosa (central box) release enkephalin (ENK) or endogenous opioids that inhibit ascending impulses. Conventional pain treatments (blue text on the left) and their locations of action (circled numbers) are shown. Abbrev: NSAIDs, nonsteroidal anti-inflammatory drugs; α2 agonists, α2 adrenergic receptor agonists; TCA, tricyclic antidepressants; SSRI, selective serotonin reuptake inhibitor; SP, substance P; +, stimulation; −, inhibition.

more effective nanotherapeutics, the physiological mechanisms underlying different types of pain must be better understood.

Acute and chronic pain

Pain is categorized as acute or chronic. *Acute pain* is temporary and resolves once the primary cause is removed (e.g., by wound healing), and functions as a signal to prevent further harm. Treatments for acute pain typically address the underlying cause, which is often injury or disease. *Chronic pain* is long-lasting, often arises without injury or disease, and does not always resolve once the primary cause is removed. The biological purpose of chronic pain is unclear, and often there is no recognizable endpoint. The mechanisms underlying chronic pain and the transition from acute pain to chronic pain remain poorly understood.

Pain pathways

Pain pathways involve both the peripheral and central nervous systems (Fig. 1). Pain sensation occurs when mechanical, chemical, or thermal stimuli activate receptors called nociceptors, which are located on sensory neurons called A- or C-type primary afferent fibers. Aδ-type fibers are large, myelinated fibers that rapidly conduct sharp, well-localized pain; in contrast, C-type fibers are small, unmyelinated fibers that transmit slow, dull, poorly-localized pain. Noxious stimuli (stimuli that have the potential to damage tissue) cause epithelial cells, immune cells, and cells in the circulatory system to release molecules that stimulate G-protein coupled receptors (GPCRs), ionotropic receptors, and tyrosine kinase receptors on the peripheral terminals of primary spinal afferent neurons; these released stimulatory molecules includes lipids (e.g., prostaglandins), proteases, neurotrophins (e.g., nerve growth factor), and peptides. Neurogenic inflammation occurs when the terminals release neuropeptides such as substance P and calcitonin gene-related proteins (CGRP) that activate receptors within the vasculature, on epithelial cells and immune cells [10]. Activation of receptors and channels of primary sensory neurons evokes central transmission of action potentials and subsequent release of glutamate, substance P, and CGRP within the dorsal horn of the spinal cord. These transmitters activate receptors on second-order neurons in the dorsal horn of the spinal cord. Pain perception occurs when these signals are transmitted through the spinothalamic tract to the cortex.

Central and peripheral sensitization

Structural and functional changes in pain pathways such as increases in long-term potentiation at synapses and neuronal hypersensitivity prevent further harm following injury or damage. Elevated sensitivity to noxious stimuli causes hyperalgesia (enhanced sensitivity to pain), and can occur following surgery or opioid use; non-noxious stimuli such as light touch or warmth can also elicit pain (allodynia or pain from stimuli that are not normally painful), which can occur due to other medical disorders or following injury. Hypersensitivity via increased intracellular Ca^{2+} can occur by activation of N-methyl-D-aspartate (NMDA) receptors following injury. Influx of calcium ions causes upregulation of a-amino-3-hydroxy-5-methyl-4-isoxazolepropionic acid (AMPA) receptors. Increase of AMPA receptors enhances postsynaptic excitation and activates protein kinases such as calmodulin dependent protein kinase II (a kinase that plays a role in synaptic plasticity, learning, and memory). Calcium influx also upregulates calcium-dependent kinases including cyclooxygenases (COXs) and nitric oxide synthases. This results in production of prostaglandin E2 and nitric oxide that causes neurotransmitter release and activation of downstream second messenger signaling via the cyclic adenosine monophosphate (cAMP)/protein kinase A (PKA) pathways.

Peripheral and central sensitization (heightened sensitivity to stimuli) play critical roles in chronic pain. *Central sensitization* occurs when nociceptive neurons in the central nervous system fire at subthresholds, resulting in neuronal hyperexcitability. Activated neurons in the dorsal horn of the spinal cord release glutamate and neuropeptides that bind receptors and generate action potential firing. Microglia and astrocytes in the spinal cord release cytokines and chemokines that stimulate neuronal firing [11]. *Peripheral sensitization* is hyperexcitability at primary afferent neurons. Activation of peripheral receptors is regulated by ion channels that include transient receptor potential ion channels (TRPs) such as transient receptor potential ankyrin 1 (TRPA1) and transient receptor potential vanilloid type 1 (TRPV1), and sodium channels such as $Na_v1.7$, $Na_v1.8$, and $Na_v1.9$ [12,13].

Pain and inflammation

Pain and inflammation are tightly connected. Damage to vascularized tissue triggers inflammatory responses, causing T cells, neutrophils, mast cells, and macrophages to release inflammatory mediators such as hydrogen ions, adenosine triphosphate (ATP), serotonin, and substance P, which in turn induce vasodilation, increased vascular permeability, and plasma extravasation. These inflammatory molecules also activate pain receptors, increasing an inflow of calcium and sodium ions into neurons and inducing action potential firing. Proinflammatory mediators promote the release of injury byproducts such as prostaglandins, bradykinin, and histamines that stimulate pain neurons to release additional inflammatory neuropeptides and cytokines that exacerbate inflammation. Proinflammatory chemokines (CCL2, CXCL5) and cytokines such as tumor necrosis factor-α (TNF-α) and interleukin 1β (IL-1β) bind receptors and ion channels to sustain the inflammatory response [14]. Damaged cells release phospholipids that are converted to prostaglandin H2 (PGH2) via COXs. Prostaglandin synthases convert PGH2 to PGE2, prostacyclin (PGI2), and PGF2, which mediate fever, enhanced pain, and inflammation, or to thromboxane A2 (TXA2) which mediates platelet aggregation. Inflammation usually subsides when damaged tissues have recovered, but can become chronic inflammation, which continues past the healing period and persists for months or years.

Following inflammatory response, phospholipase A2 is released, which is then converted into arachidonic acid. The COX enzymatic pathway, which includes COX-1 and COX-2, is responsible for converting arachidonic acid into prostaglandins (PGs). Normally, COX-1 produces thromboxane and PGs in platelets, gastrointestinal mucosal cells, and renal tubule cells. COX-2 is upregulated at sites of inflammation and produces PGs that cause inflammation and pain. Inhibition of COX-2 reduces production of PGs to result in anti-inflammatory and analgesic effects.

Nociceptive, neuropathic, and nociplastic pain

Identifying the pathophysiological origin of pain is important for determining an appropriate treatment. Pain is classified into neuropathic, nociceptive, and nociplastic pain. *Nociceptive pain* arises through nociceptor activation from noxious stimuli (mechanical, chemical, or thermal stimuli that have the potential to damage tissue). Nerve cells are responsible for propagation of pain signals from peripheral nerve fibers to the spinal cord and the brain. Nociceptive pain typically results from physical injury and presents as somatic pain, a well-defined, precisely-located pain from injury to skin, joints, and muscles, or visceral pain, a type of pain due to injury to internal organs or viscera that is often diffuse and difficult to localize [15].

Neuropathic pain originates from injury or dysfunction of the somatosensory system and is categorized into central and peripheral neuropathic pain. Central neuropathic pain stems from injury lesions to the spinal cord or brain and can be caused by diseases such as Parkinson's disease. Peripheral neuropathic pain results from nerve damage, which often occurs in the hands and feet and manifests as a chronic stabbing or burning sensation. Roughly 20% of patients who experience chronic pain suffer from neuropathic pain [16].

Nociplastic pain is a new mechanistic descriptor that encompasses pain with an unknown origin or altered nociception. The mechanisms underlying nociplastic pain include changes in nociceptive signaling that result in peripheral and central sensitization. While traditionally pain has been considered a symptom of injury or damage to the nervous system, nociplastic pain considers forms of chronic pain without a clear origin to be disease states themselves. Common examples of nociplastic pain include chronic musculoskeletal and visceral pain including fibromyalgia and lower back pain [17].

Current pain treatments and new targets

Current pain treatments

Non-opioid pain medications

Treatment for chronic pain typically begins with a low-risk, non-opioid analgesic, such as acetaminophen (Tylenol), non-steroidal anti-inflammatory drugs (NSAIDs), and adjuvant medications (e.g., antidepressants, anticonvulsants, and corticosteroids). Acetaminophen is a first line treatment for mild musculoskeletal pain (e.g., osteoarthritis, lower back pain). Acetaminophen blocks proinflammatory prostaglandin synthesis by oxidized cyclooxygenases (COX), with analgesic and antipyretic (fever-reducing) effects [18,19]. Acetaminophen is effective in low doses for short durations, but long-term use or high doses can cause hepatotoxicity [20].

NSAIDs such as aspirin, ibuprofen (Advil, Motrin), and naproxen (Aleve) are the most common first line treatments for inflammation-associated pain. Unlike acetaminophen, NSAIDs relieve both pain and inflammation. Many NSAIDs are COX inhibitors that reduce prostaglandin production to relieve inflammation; these include COX-1 inhibitors (low-dose aspirin), COX-2 inhibitors (celecoxib), and non-selective COX inhibitors (ibuprofen, naproxen). However,

since cyclooxygenases mediate multiple physiological functions, prolonged use of NSAIDs at high dosage can have negative effects such as gastric bleeding, peptic ulcers, kidney damage, myocardial infarction, or stroke.

Adjuvant analgesics such as antidepressants and anticonvulsants are increasingly being used to treat neuropathic and nociplastic pain. Antidepressants do not act as acute analgesics but can be used to treat chronic pain. The requirement of a longer treatment duration when using antidepressants suggests that long-term neuronal plasticity is involved in chronic pain. Antidepressants used to treat neuropathic pain include tricyclic antidepressants (TCAs) such as amitriptyline, serotonin-norepinephrine inhibitors (SNRIs) such as duloxetine, and selective serotonin reuptake inhibitors (SSRIs) such as paroxetine. TCAs inhibit the presynaptic reuptake of norepinephrine and serotonin, and block α2 adrenergic, H1-histaminergic, and muscarinic cholinergic receptors, and are effective in 33–50% of patients with chronic pain [21]. SNRIs are balanced noradrenaline and serotonergic inhibitors that rely on drug dosage and concentration and are effective in 20–25% of patients. Duloxetine has a high affinity for norepinephrine and serotonin reuptake transporters and is effective for treatment of diabetic peripheral neuropathic pain [22]. Only ~ 14% of patients are relieved of pain with SSRIs, which block serotonin reuptake [23]. The differing efficacy of antidepressants with different mechanisms of action suggests that noradrenaline plays a more important role in relieving pain than serotonin. The anticonvulsants gabapentin and pregabalin are currently used to treat neuropathic pain, especially postherpetic neuralgia and peripheral diabetic neuropathy. Gabapentin is a gamma-amino-butyric acid (GABA) analog that binds the α2δ subunit of the voltage-gated calcium channel complex to block the presynaptic neurotransmitter release. Like gabapentin, pregabalin binds the calcium channel α2δ subunit, but with six times the potency. These anticonvulsants address the increased sensitivity associated with chronic pain and work by reducing action potential firing at nerve terminals.

Other non-opioid pain treatments include local anesthetics and steroids. Local anesthetics such as lidocaine are commonly used for short-acting pain relief. Lidocaine reduces sharp burning pain such as postherpetic neuralgia in shingles by blocking voltage-dependent sodium channels to mediate pain transmission. Lidocaine can be applied topically as a local anesthetic to relieve pain or carefully injected as a nerve block to lessen pain and discomfort from medical procedures. Capsaicin is a topical cream that targets nociceptors and is a highly selective agonist of noxious heat-sensing TRPV1 in nociceptors. Persistent activation of TRPV1 by capsaicin reduces receptor function and pain sensitivity for an extended period of time [24]. Steroids are also used for chronic pain management. Glucocorticoids relieve pain by targeting proinflammatory responses associated with pain, for example by blocking prostaglandin synthesis and reducing vascular permeability to treat inflammation and tissue edema [25]. Dexamethasone, a synthetic corticosteroid, is the most frequently used steroid for pain relief due to its high potency, long half-life, and low mineralocorticoid activity which results in less fluid retention. However, the side effects of dexamethasone include gastric bleeding and muscle myopathy. Prednisolone, another steroid used for pain relief, has fewer side effects than dexamethasone and acts by stimulating glucocorticoid receptors to address the inflammatory component of pain. Recently, α2-adrenergic agonists have been used for anesthetic management alone or in combination with local anesthetics. Clonidine, an α2-adrenergic agonist in combination with local anesthetics extends the length of peripheral nerve blocks. Dexmedetomidine, a more selective α2-adrenergic agonists, has also been used in combination with local anesthetics to prolong the anesthetic effects with both central and peripheral nerve blockers [26–29].

Opioids

Opioids are used when nociceptive symptoms become more severe and when non-opioid analgesic regimens are inadequate. Opioids are potent analgesics and have been considered the most effective pain medications for non-neuropathic pain. Opioid medications act like endogenous opioids, which bind opioid receptors throughout the peripheral and central nervous systems. Opioid receptors are GPCRs that, when activated on the presynaptic terminal, cause the beta-gamma subunit to inhibit voltage-gated calcium channels, preventing release of the neurotransmitter glutamate and the neuropeptides substance P and CGRP [30]. When opioid receptors are activated on postsynaptic terminals, G protein-coupled inwardly rectifying potassium channels (GIRK) are opened to allow outflow of potassium, preventing depolarization of the neuron. The Gα subunit also binds phospholipase C and adenylyl cyclase to cause downstream signaling such as cAMP production to modulate neurotransmitter release [31]. Overall, activation of opioid receptors is antinociceptive by reducing action potential firing and neuronal sensitivity. Activation of opioid receptors at the brainstem and spinal cord removes inhibition of GABAergic neurons, causing GABA release and hyperpolarization to prevent pain transmission.

Many opioid drugs activate the μ and κ opioid receptors for pain relief. Morphine is a natural opiate used to treat moderate to severe pain. Synthetic opioids, including fentanyl, hydrocodone, methadone, and oxycodone, mimic endogenous opioid peptides but with higher potency [32]. Methadone is used to relieve both nociceptive and neuropathic pain since it antagonizes NMDA receptors and acts as a serotonin-norepinephrine inhibitor.

Although opioids effectively relieve acute pain, prolonged use causes serious side effects. Constipation is a common on-target effect due to the presence of opioid receptors in the small intestine that control gut motility. Nausea occurs with opioid use due to chemoreceptor binding in the medulla [33]. Dose-dependent respiratory depression is a dangerous side effect of opioid drug use. A high dosage of opioids can lead to activation of opioid receptors of interneurons in the pons and the Pre-botzinger complex of the medulla, leading to suppression of respiratory activity. Other dangerous side effects of opioids are related to addiction, dependence, and tolerance. Opioid drugs activate opioid receptors in the brainstem and in the ventral tegmental area of the brain, which inhibits GABA release at presynaptic terminals, promoting dopaminergic activity in the reward system [34]. Chronic opioid usage causes receptor desensitization and tolerance. When opioid use is reduced or stopped, withdrawal symptoms include diarrhea, anxiety, and dysphoria. The recent opioid epidemic was driven by increased opioid prescriptions and overuse, which led to addiction, overdoses and deaths [35]. Opioid abuse is now thought to be responsible for more deaths than motor vehicle accidents and suicide combined. The devastation of the recent opioid epidemic highlights the urgent need for better treatment options to address chronic pain.

Other pain treatments

Other methods of pain treatment include nerve blockers and electrical stimulation. Nerve blockers are used to treat chronic pain when other drugs do not provide relief or to avoid side effects, and include epidural steroid injections and peripheral nerve blockers [36]. Local anesthetics and neurotoxins are two common forms of nerve block agents. Epidural steroid injections are commonly administered for spine-related pain. Continuous peripheral nerve blockers, which have been traditionally used for perioperative or postoperative periods, are now also used for chronic pain. Continuous administration of peripheral nerve blockers uses a lower initial bolus, resulting in reduced systemic toxicity and reduced supplemental opioid usage and side effects [37].

Transcutaneous electrical nerve stimulation (TENS) is a non-pharmacological method of pain relief. TENS uses a small

battery-powered device to apply a mild electrical current to activate endogenous inhibitory mechanisms in the central nervous system. TENS activates opioid receptors in the descending inhibitory pathway of the rostral ventromedial medulla, spinal cord, and periaqueductal gray [38]. TENS also activates muscarinic receptors and GABA-A receptors in the spinal cord to reduce hyperalgesia. A spinal cord stimulator (SCS) is an implanted device that is inserted into the dorsal epidural space that sends low currents of electricity into the spinal cord for chronic neuropathic pain relief. The specific mechanism of action of SCS is unclear, but has been shown to increase the release of GABA to suppress dorsal horn neuronal hyperexcitability [39].

New targets

Current pain medications are inadequate due to lack of specificity and serious side effects. Recent studies have investigated novel pain targets and novel methods for pain treatment. Advances in pain therapy include specific targeting of ion channels, pain receptors, and mediators of inflammation, described below.

Voltage-gated sodium channels

Voltage-gated sodium channels are an attractive target for pain treatment. An influx of sodium through the channel shifts a neuron's membrane potential towards action potential depolarization and neuronal firing. Sodium channel $Na_v1.7$, which is expressed in peripheral sensory neurons, dorsal horn neurons, and sympathetic ganglion neurons, is associated with pain transmission [40]. Loss-of-function mutations in the gene encoding $Na_v1.7$, *SCN9A*, leads to congenital insensitivity to pain, and gain-of-function mutations are associated with familial pain disorders such as paroxysmal extreme pain disorder and inherited primary erythromelalgia [41]. Recent studies have targeted the $Na_v1.7$ channel with a monoclonal antibody specific to voltage-sensor regions that allosterically control channel gating [16].

Nerve growth factor and TrkA

Another target for pain treatment is nerve growth factor (NGF) and its receptor, tropomyosin-related kinase A (TrkA). NGF is a neurotrophin that is released from all innervated peripheral tissues, immune cells, CNS, and PNS, and promotes the growth and survival of sensory and sympathetic neurons and ganglia. NGF levels increase in response to noxious stimuli from injury, neuroinflammation, and chronic pain. The binding of NGF to TrkA receptors in Aδ- and C-type fibers and mast cells releases proinflammatory mediators such as histamine and protons, and exacerbates inflammation. Tanezumab is a humanized monoclonal IgG2 antibody that blocks NGF-TrkA binding, and was fast-tracked by the FDA for patients with osteoarthritis and chronic lower back pain [42]. The cost of Tanezumab is high, but it can be administered only once every eight weeks and does not have the adverse side effects seen with opioids and some NSAIDs. Tanezumab can also be administered at home with a single subcutaneous injection, avoiding medical visit costs [43]. Another promising antibody for treating osteoarthritis is fasinumab, by Regeneron, a recombinant fully-human anti-NGF antibody that is currently in clinical trials.

Endosomal targets

Endosomes are commonly described as conduits for biomolecule degradation or recycling, but are also the site of persistent signals from GPCRs that control pain transmission and thus are a promising target for treating chronic pain. GPCRs in pain pathways were once thought to signal solely at the plasma membrane, and drug discovery was focused on targeting receptors at the cell surface. However, many of these drugs were found to be unsuccessful in clinical trials. Although such drugs might fail for multiple reasons, one possibility could be related to their inability to antagonize GPCRs within the acidic microenvironment of endosomes. Thus, the targeted delivery of GPCR agonists and antagonists to endosomes may result in more effective mediation of GPCR pain signaling.

Endosomal signaling from GPCRs such as the neurokinin 1 receptor (NK_1R), calcitonin-like receptor (CLR), and protease-activated receptor 2 (PAR_2) might regulate the expression of genes in the nucleus and the activity of ion channels at the plasma membrane that control neuronal excitation and chronic pain [44–46]. For example, substance P, a ligand of the neurokinin 1 receptor, causes increased activation of extracellular signal-regulated kinase (ERK) in the nucleus and protein kinase C (PKC) and cAMP in the cytosol [44]. These signals mediate sustained excitation of spinal neurons and pain transmission in the spinal cord. Inhibitors of clathrin and dynamin suppress substance P-induced signaling by ERK, PKC, and cAMP as well as abolishing persistent neuronal firing, suggesting that endosomal signaling mediates neuronal excitability. Studies are now examining GPCRs in endosomes as a therapeutic target for chronic pain treatment. Conjugation of transmembrane lipid cholestenol with an NK1R antagonist promotes drug delivery to endosomes, allowing antagonism of endosomal NK_1R signaling. Nanoparticle technology (described in Section 4) is being used to deliver antagonists of pro-nociceptive receptors to endosomes—which have an acidic and reducing environment that can be exploited for targeted delivery of these GPCR inhibitors.

Other targets

Other targets for pain treatment include purinergic P2X receptor channels and the angiotensin II receptor. P2X receptors are ligand-gated cation channels found on peripheral afferents (the axons of sensory neurons). Damaged and inflamed tissues release ATP which binds and activates P2X receptors, leading to influx of Ca^{2+} and Na^{+} into the cytoplasm for membrane potential depolarization. Animals with a P2X3 knockdown or siRNA-silenced P2X3 expression exhibit decreased pain behavior [47]. P2X3 antagonists are a potential therapy for neuropathic pain [48]. Abbott Laboratories developed the P2X3 antagonist A-317491, which reduced pain in chronic and inflammatory pain models. Afferent Pharmaceuticals' potent P2X3 antagonist, AF-219, is currently in Phase 2 trials for cystitis/bladder pain syndrome. Additional, second-generation P2X3 antagonists that have a reduced risk of hyperbilirubinemia are being developed [49].

The angiotensin II-receptor (AT2R) is another target for treating chronic pain. Angiotensin II is a mediator of the renin-angiotensin system and has been implicated in pain modulation. $G_{\alpha s}$-coupled AT2R signaling modulates sensory neuron firing, and $G_{\alpha i}$-coupled AT2R signaling leads to analgesia in mice [50]. Activation of AT2R on macrophages causes mechanical and cold pain hypersensitivity in mouse models of neuropathic pain and chronic inflammatory pain [51]. Other targets of chronic pain drugs currently in development include CGRP pathways, TNF-α, epidermal growth factor receptor, and TRP channels.

Nanoparticles for pain management

Nanomedicine aims to apply nanotechnology to enhancing the efficacy and safety of drugs, for example by encapsulating naked drugs in biocompatible nanocarriers such as nanoparticles, liposomes, micelles, and dendrimers. Nanoparticulate drug delivery systems (NDDSs, Fig. 2) have design parameters such as size, shape, surface charge, and cargo dose that can be optimized to prolong drug circulation and to target specific tissues or subcellular organelles [52,53]. NDDS surfaces can be functionalized with cell-penetrating peptides or ligands to deliver therapeutics across the blood-brain barrier and to the central nervous system. NDDSs can achieve enhanced therapeutic efficacy by regulating spatial localization and reducing dosage and side effects. Therapeutic potency can be

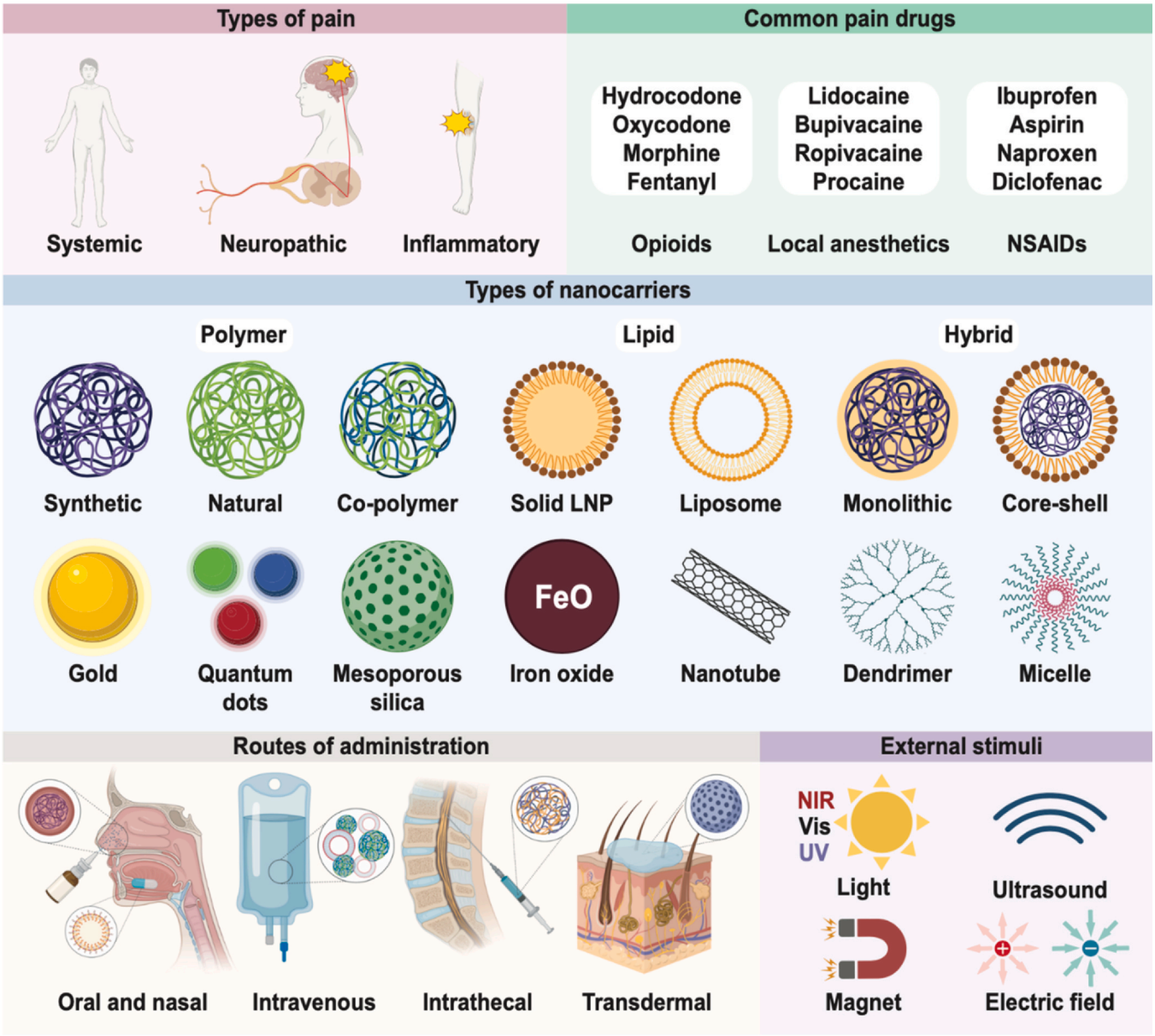


Fig. 2. Nanoparticles for pain relief. Design considerations for analgesic nanoparticulate drug delivery systems include the type and location of pain (top left), what drugs are clinically available (top right), nanocarrier composition (middle), route of administration (lower left), and accessible external stimuli (lower right).

enhanced by using a nanocarrier containing multiple analgesics or by using small molecules that target pain signaling receptors. Such approaches might overcome the redundancy that is inherent in essential processes, such as pain transmission. NDDSs are being developed to treat systemic, neuropathic, localized, and disease-associated pain with reduced risk of addiction. Theragnostic nanoparticles are also being developed to detect the source of pain.

Analgesic nanoparticulate drug delivery systems

Analgesic nanoparticulate drug delivery systems (Fig. 2) can be used for relief of systemic, neuropathic, and inflammation-related pain by serving as nanocarriers of drug cargo and targeting molecules. For example, targeting opioid receptors to create safer drugs is an active area of research, and pain medicine is moving towards more effective delivery of non-opioid analgesics and less addictive opioids. Intraoral, intranasal, and transdermal administration are preferred routes of administration for patient compliance, while local and systemic administration via injection in clinics is useful for treatments that require longer time periods between doses. Localized administration of local anesthetic-loaded NDDSs can block pathways related to perioperative pain. Neurotoxins traditionally considered too dangerous can benefit from NDDSs to become new local anesthetic candidates.

Systemic pain: opioids and new approaches

Conventional pain treatments with naked drugs provide uncontrolled drug release; often, several doses are taken daily to achieve and maintain sufficient plasma concentrations. However, such intermittent administration causes fluctuations in plasma drug levels, which can fall below the effective concentration or exceed the toxic concentration threshold [54]. Liposomes and polymeric nanoparticles have been used since the 1990s to encapsulate opioids for extended-release (ER) and reduced systemic toxicity [55–58]. These efforts led to FDA approval and commercialization of two ER morphine NDDSs, Depodur and Avinza. Depodur uses proprietary DepoFoam, a multivesicular liposomal delivery system that encompasses numerous non-concentric aqueous chambers

containing a drug [59]. Single epidural injection of Depodur achieves 48 h of analgesia [60]. Orally delivered Avinza contains ER morphine capsules in proprietary beads consisting of ammonium-methacrylate copolymers that are solubilized by gastrointestinal fluids [61]. The drug solution then diffuses out of the capsule, providing therapeutic plasma levels for up to 24 h [59].

Other formulations of opioids with ER profiles have been studied extensively and are commercially available [59]. Liposomes and polymeric nanoparticles used in these ER formulations are generally considered as safe carriers at therapeutic concentrations. Modifications such as liposome PEGylation and cationic coating can potentially improve safety only when the inherent toxicity of the functionalization is accounted for. ER opioids offer advantages such as stabilized plasma drug levels, but suffer from misuse and abuse, and drug tolerance further complicates their safety and analgesic efficacy. A growing number of investigations are focused on therapeutics with lower abuse potential [62,63].

Enkephalin (ENK) is an attractive neuropeptide analgesic; this endogenous neuropeptide preferentially binds δ-opioid receptors, which are less correlated with abuse and tolerance than μ-opioid receptors [64]. Leu-enkephalin (LENK) has been conjugated with lipid squalene to target proinflammatory mediators [65]. LENK-squalene bioconjugate nanoformulated in dextrose allowed a higher drug payload than ENK-loaded liposomes or poly(lactic-co-glycolic acid) (PLGA) nanoparticles. Animal studies showed that an intravenous injection of LENK-squalene nanoparticles achieves a greater anti-hyperalgesic effect than morphine, without causing tolerance. Further, using a microparticulate formulation of clustered nanoparticles, intranasal administration can be used to deliver LENK-squalene specifically to the brain [66].

As an alternative to opioids, new pain medications in development target GPCRs including adrenergic, cannabinoid, and serotonin receptors [67]. PLGA-PEG nanoparticles containing the synthetic cannabinoid CB13 have achieved an analgesic effect for up to 11 days after one oral dose in a murine neuropathic pain model [68]. Mesoporous silica nanoparticles (MSNs) are well-suited for systemic and local delivery due to their dual surfaces (internal cylindrical pores and exterior particle surface), which enable a multistage delivery. MSNs loaded with the cannabinoid Δ9-THC and the erythropoietin-derived polypeptide ARA290 provide sustained systemic and neuropathic pain relief. THC-MSN-ARA290 nanocomplexes represent a combinatorial delivery system in which THC diffuses into the circulation while ARA290 is released upon the cleavage of a disulfide bond triggered by glutathione. With two intraperitoneal (IP) injections, an analgesic effect was seen for four weeks in mouse models of thermal hyperalgesia and mechanical allodynia [69].

pH-responsive MSNs functionalized with a PEGylated liposome coating (lipoMSN) and loaded with a δ-opioid receptor agonist DADLE ([D-Ala^2, D-Leu^5]-Enkephalin) can target endosomal δ-opioid receptors and provide sustained inflammatory pain relief. The pH-responsiveness of the lipoMSN allows for preferential delivery to the acidified endosome while the DADLE-functionalized liposomal coating helps to cloak the MSN core and selectively target δ-opioid receptor-expressing neurons. One intrathecal injection of the lipoMSN can provide an analgesic effect lasting for 6 h in a mouse model of inflammatory nociception [70]. This study suggests that endosomal signaling of DOPr may provide relief from inflammatory pain, which presents a unique opportunity for NDDSs because of the natural and efficient trafficking of nanoparticles to endosomes.

Neuropathic pain: local anesthetics

NDDSs can enhance the therapeutic potential of local anesthetics to for perioperative pain management. Local anesthetics such as lidocaine and prilocaine are widely used for perioperative pain management, and act by blocking specific nerve pathways [71]. ER local anesthetics have been developed to prolong their analgesic effect while preventing adverse events.

Traditional local anesthetic formulations for postsurgical analgesia have a short duration of effect, lasting no longer than 24 h with a single injection [72,73]. Several approaches have been used to encapsulate local anesthetics in polymeric nanoparticles (e.g., PLA, PLGA, PCL, alginate, chitosan, and copolymers), resulting in long-term stability, sustained release, and enhanced anesthetic efficacy in vivo [74–77]. The only FDA-approved liposomal bupivacaine, Exaparel, which also uses the DepoFoam platform, can reduce postoperative pain for up to 3 days after a single infiltration [78].

The $Na_v1.4$ inhibitor lamotrigine has demonstrated efficacy for neuropathic pain treatment in multiple randomized controlled trials [79,80]. However, its clinical applications in neuropathic pain are limited by the risk of severe rash, and it has a poor pharmacokinetic profile due to nonselective distribution to organs other than the brain. Lamotrigine-carrying PLGA nanoparticles were functionalized with transferrin or lactoferrin to enhance blood-brain barrier permeability [79]. Preferential distribution of these nanoparticles to the brain and reduced accumulation in non-target organs were observed in a partial sciatic nerve injury mouse model, with lactoferrin being superior to transferrin as the targeting ligand.

In labor pain, epidural local anesthetics are injected into the lower spinal nerves. Epidurals have a short-lasting effect and can have side effects such as infection and nerve damage. Solid lipid nanoparticles (SLNs) can be used as drug carriers for epidurals, and can double their longevity via controlled release and reduce side effects [81]. Lidocaine-loaded SLNs allow longer-lasting effects than free lidocaine with more effective sensory and motor blocks [82]. However, the toxicity of SLNs is not well characterized; ongoing research on nanoparticles for delivering epidurals aims to reduce motor weakness and systemic absorption, optimize controlled release, and reduce the dosage required for an analgesic effect.

Neuropathic pain: neurotoxins

NDDSs can enable the safe use of otherwise toxic analgesic molecules. For example, conventional local anesthetics are nonspecific Na_v channel blockers, and their use can result in rare but life-threatening systemic toxicity upon leakage into the cardiovascular system or central nervous system [83–85]. Neurotoxins are also potent and specific Na_v blockers with slightly less serious complications (e.g., muscle paralysis) [86]. Guanidinium toxins, tetrodotoxin (TTX) and saxitoxin (STX), are Na_v blockers that synergistically prolong anesthesia when combined with other local anesthetics [87,88]. Clinical use of these neurotoxins has been limited due to their systemic toxicity. One way to circumvent this toxicity is to slowly release a therapeutic amount. Conjugating TTX with poly(triol dicarboxylic acid)-co-PEG (TDP) has achieved nerve blocks in rat sciatic nerves from several hours to 3 days, depending on the dose. Minimal systemic or local toxicity was induced, and TTX release could be adjusted by tuning the hydrophilicity of the TDP polymer [89]. Local administration is another method to circumvent toxicity while simultaneously increase efficacy. Local injection of hollow silica nanoparticles loaded with TTX to the sciatic nerve increased the duration of nerve block while decreasing toxicity. The nanoparticles could penetrate the sciatic nerve in a size dependent manner, enhancing efficacy while improving safety [90]. STX and dexamethasone have also been encapsulated in liposomes for treatment of neuropathic pain [91]; a single percutaneous injection of STX-dexamethasone nanoparticles provided a nerve block that lasts for about a week in a rat spared nerve injury model [92]. Crotoxin, a rattlesnake venom-derived neurotoxin with prolonged anti-inflammatory and antinociceptive activity, was encapsulated in inert SBA-15 MSNs to treat neuropathic pain, resulting in reduced toxicity of crotoxin and enhanced analgesic effect after subcutaneous and oral delivery in a mouse neuropathic pain model [93].

Chronic pain

NSAIDs and acetaminophen are generally safe in low doses, but prolonged use can cause side effects in the stomach and liver, respectively. NDDSs are effective chronic pain treatment options due to their controlled release kinetics and versatility of nanoformulation.

Drug-induced acute liver failure has a high morbidity and mortality rate, with the leading cause being acetaminophen overdose [94]. Milk thistle-extracted silymarin has shown hepatoprotective properties due to its antioxidant, anti-inflammatory, and antifibrotic effects [95]. Silymarin nanoparticles entrap acetaminophen via nanoprecipitation, and upon intraperitoneal injection, glutathione is generated to counter hepatic damage [96]. In an animal model of acetaminophen-induced hepatotoxicity, no death occurred even when the drug was administered after established hepatic necrosis. Similar NDDS-based approaches can reduce the side effects of long-term NSAID use for chronic pain.

Osteoarthritis is a disease of the cartilage and bone and is marked by chronic pain. Most osteoarthritis drugs are aimed at mediating this pain. Osteoarthritis is typically treated with NSAIDs, cyclooxygenase-2 inhibitors, or experimental therapeutics such as MAPK-inhibiting drugs. Targeting these drugs to the cartilage matrix and subchondral bone can be achieved by using nanocarriers (< 40 nm diameter) with positive surface charges, such as micelles and dendrimers. Targeting the cartilage surface, synovial membrane, intra-articular space, or infrapatellar fat pad requires larger nanoparticles (> 60 nm) to avoid penetration into cartilage, making liposomes, high-generation dendrimer micelles, and other larger nanoparticles more suitable nanocarriers for these applications. The combination of osteoarthritis drugs with appropriate nanocarriers for targeting will lead to more effective treatments of osteoarthritis-associated pain with fewer side effects [97].

Other sources of chronic pain include receptor signaling from subcellular compartments, such as the GPCR cascade. Endocytosed neurokinin 1 receptor (NK_1R), a GPCR in the central and peripheral nervous systems, mediates pain and offers a new target for treating chronic pain [44]. pH-responsive nanoparticles loaded with the NK_1R antagonist aprepitant deliver the drug to acidic endosomes environment to block NK_1R signaling [98]. These nanoparticles exhibit greater and more sustained pain relief than standard therapy with free drugs in animal models of nociceptive, neuropathic, and inflammatory pain (Fig. 3).

Localized pain

Localized pain in joints, burns, surgical sites, and in many diseases is commonly treated with NSAIDs and pain receptor inhibitors, but opioids are often used when the pain becomes severe. NDDSs can target specific pain receptors and treat the underlying source of localized pain.

Functionalization of liposomes with monoclonal antibodies or antibody fragments (immunoliposomes) is a popular targeted drug delivery strategy that reduces doses and thus side effects [99]. For example, the antidiarrheal loperamide was converted to the first peripherally-selective analgesic by intravenous use of anti-intracellular adhesion molecule 1 (ICAM-1) immunoliposomes [100]. This NDDS showed antinociceptive and anti-inflammatory effects exclusively in peripheral inflamed tissue in a rat local inflammation model. In a follow-up study, conjugation of the NDDS with anti-oxytocin receptor increased immunoliposome localization at the uterus of pregnant mice by 7-fold; localization was not detected in the maternal brain or fetus, preventing inflammation-induced preterm labor [101].

For migraine treatment, Girotra et al. encapsulated the GPCR agonists sumatriptan and zolmitriptan in various nanoparticles (chitosan solid lipid, ApoE-bovine serum albumin, and PLGA-poloxamer) to enhance brain targeting [102–104]. This group applied *in silico* models to virtually screen ligands from Drugbank, and identified nystatin as the lead ligand against four receptors that are responsible for migraine pathogenesis, including CGRP (PDB ID: 3N7R). Mice studies using nystatin-chitosan nanoparticles revealed an analgesic effect via IP injection and greater accumulation of nanoparticles in the brain than in other organs such as the liver and spleen [104].

Metastatic cancer can be excruciatingly painful, and the success rate of treatment is low. Between 30% and 50% of patients with tumors receiving active treatment and 70–90% with advanced-stage disease experience chronic pain [105]. Prostate cancer tends to metastasize to the bone, where it often becomes untreatable and causes intractable pain. Gdowski et al. developed alendronate-conjugated PLGA-cabazitaxel nanoparticles to target bone metastases to treat bone pain. In mice orthoptic bone tumor models, the targeted nanoparticle-treated group showed lower pain as well as reduced tumor burden and improved maintenance of bone structure than the free drug-treated group, alleviating long-term pain and other complications [106].

Enhancing drug targeting

Conventional pain treatment relies on drugs with continuous release profiles to sustain the pharmacological effect until the payload is exhausted. Most NDDSs aim to prolong the therapeutic effect; however, an alternative approach is to use external stimuli-responsive NDDSs that allow drug release on demand.

Current treatment of perioperative and other acute pain relies on opioids and local anesthetics. By using stimuli such as light, heat, ultrasound, magnetic field, and electric field, the location and timing of drug release can be controlled to maximize efficacy and reduce opioid use to minimize side effects. For example, emerging evidence suggests that chronotherapy of NSAIDs can be effective, and on-demand drug release may improve pain relief by limiting treatment to the active phase of the circadian rhythm [107]. In addition, theragnostic nanoparticles can be designed to accumulate in targets of interest to both detect pain and deliver a drug on demand, for precision pain management [108].

Light-responsive NDDSs

Light used as a non-invasive exogenous trigger can enable multiple drug administrations with precise spatiotemporal control. Light-activated NDDSs include photosensitive molecules with labile bonds that are photochemically cleaved upon ultraviolet (UV), visible, or near-infrared (NIR) light irradiation [109]. Short-wavelength light (UV) is potent enough to disrupt chemical structures but can damage DNA and proteins [109,110]. NIR-triggered NDDSs have been developed since NIR can achieve deeper tissue penetration than UV or visible light [110]. The mechanisms of NIR-triggered NDDS include photodynamic reactions via photosensitizer-loaded liposomes and the photothermal effect via plasmonic nanoparticles [111].

Rwei et al. developed NIR-light-triggered liposomes loaded with TTX and photosensitizer, allowing peroxidation of liposomal lipids and drug release upon irradiation at 730 nm. This NDDS exhibited adjustable on-demand local anesthesia lasting 14 h following injection in a rat sciatic nerve [112]. The photosensitivity and repeatability of this system was enhanced by an additional tethering of gold nanorods excitable at the same NIR wavelength as the photosensitizer [113].

By combining the photothermal effect of copper sulfide (CuS) nanoparticles upon NIR excitation and the thermoresponsive behavior of amine-terminated copolymer P(MEO_2MA-*co*-OEGMA), de Solorzano et al. achieved repeated on-demand release of bupivacaine after NIR excitation [114]. This copolymer can be functionalized with disulfides for gold nanoparticle binding [115]. These

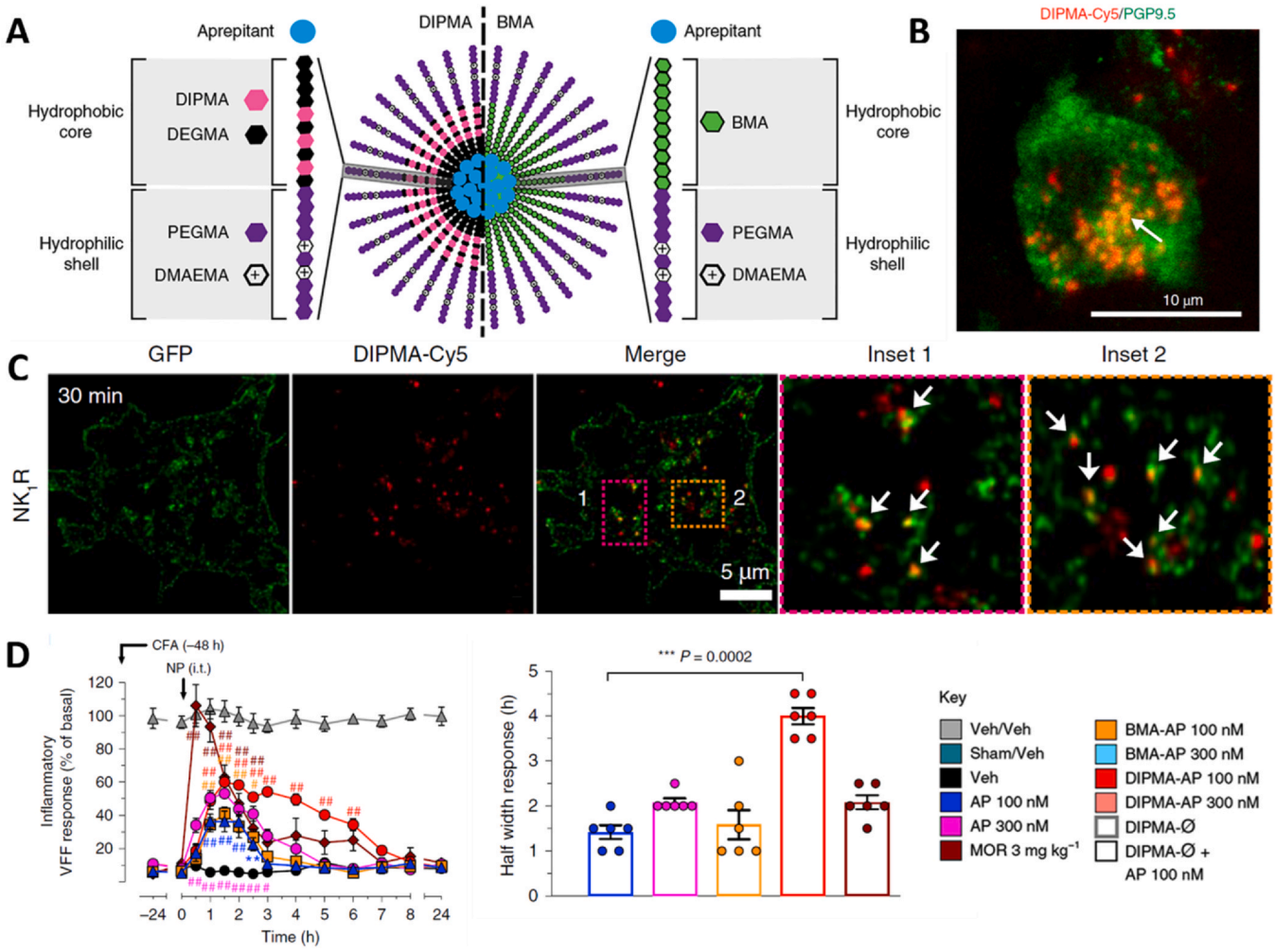


Fig. 3. pH-responsive nanoparticles target NK_1R in the endosome to target chronic pain. A) Structure of pH-responsive DIPMA and pH-non-responsive BMA nanoparticles. The nanoparticles share the same hydrophilic shell, P(PEGMA-co-DMAEMA), but have different hydrophobic cores. B) Accumulation of nanoparticles in spinal neurons, the target of the encapsulated Aprepitant. C) pH-responsive nanoparticles target NK_1R in endosomes. D) DIPMA-Aprepitant (AP) nanoparticles are more effective than morphine in mouse models of inflammatory pain [98].

studies showed a successful drug release of ~50%, demonstrating the potential for POEGMA-based light-activated systems for pain management.

NIR-triggered NDDSs have also been applied to patient-controlled transdermal analgesia systems. Microneedles composed of PCL, plasmonic lanthanum hexaboride nanoparticles, and lidocaine can release drugs in a pulsatile and programmed manner by varying the duration of irradiation and turning a laser on and off. Lidocaine delivered via implanted microneedle is rapidly absorbed into the blood circulation within 10 min and has a bioavailability of at least 95% relative to subcutaneous injection (Fig. 4A and B) [116].

One limitation of NIR light as a trigger is that its tissue penetration is only 1–5 mm; cytotoxicity and burning are risks of deeper penetration [117–119]. Moreover light-responsive NDDSs are designed to be controlled by the intensity and localization of the light. However, there can be variability in the depth of light penetration from patient to patient due to factors including tissue thickness, tissue type, ratio of muscle vs fat, and amount of body hair in the effected region, all of which affect the translatability of such a platform.

Ultrasound-responsive NDDSs

Ultrasound, with its proven clinical utility and tissue penetration, which is an order of magnitude deeper than NIR, is well-suited as a non-invasive external trigger for on-demand local anesthesia. Ultrasound alone or combined with contrast agent microbubbles is widely used clinically to deliver drugs and to diagnose cancers, stroke, osteoarthritis, and chronic pain [120–122]. Sonoporation, cavitation, and hyperthermia are well-known biophysical effects of ultrasound that can be applied to enhance the efficacy of pain relievers [123]. Local anesthetics and hydrophilic molecules such as TTX are impeded by tissue barriers that restrict access to nerve cells. Using ultrasound alone, the peripheral nerve blockade capacity of TTX is enhanced, but the same effect is not seen with the more hydrophobic bupivacaine [124]. While ultrasound is a highly translatable method to control drug targeting due to its safety and deep tissue penetration, it does suffer from poor spatial resolution compared to other methods.

Rwei et al. have shown that the timing, intensity, and duration of nerve blocks can be controlled when using ultrasound-triggered delivery of anesthetic via liposomes by varying ultrasound parameters (Fig. 4C and D). Upon insonation, the encapsulated sonosensitizer protoporphyrin IX (PPIX) produces ROS that react with the liposomal membrane, leading to TTX release. The liposome-PPIX-TTX induces an initial nerve block that lasts for over 8 h in rats; subsequent insonation can reproduce nerve blocks twice more for 0.7 and 0.2 h. Co-administration of liposome-DMED and liposome-PPIX-TTX significantly extends the initial nerve block to 35 h. As the

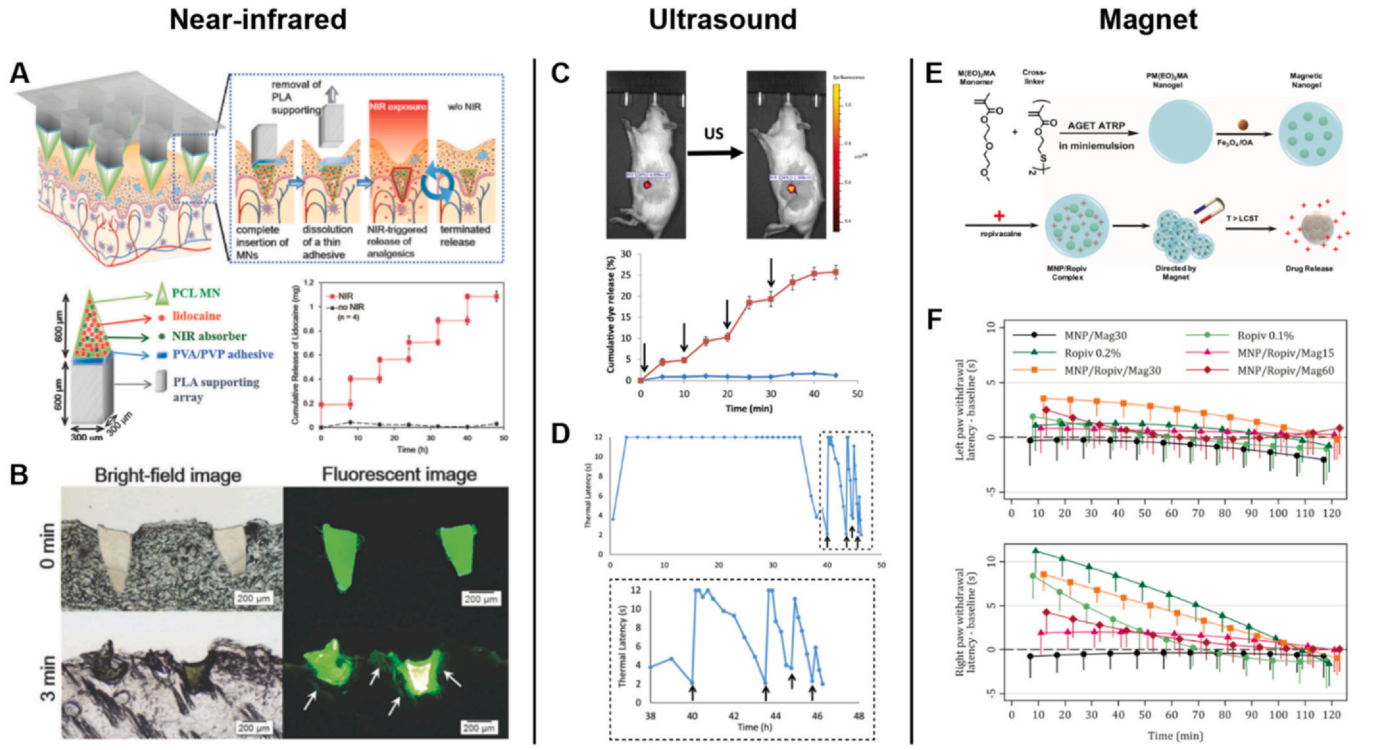


Fig. 4. Local on-demand delivery of analgesia using external stimuli. A) Schematic of NIR-triggered NDDS and implanted polymeric microneedles for on-demand transdermal delivery of lidocaine. The plot shows an in vitro drug release profile after intermittent laser irradiation. B) Histological sections of rat skin with microneedles after NIR exposure for 0 and 3 min [116]. C) Ultrasound (US)-triggered release of liposome-PPIX-red dye. Insonation is indicated by arrows. D) Combined use of liposome-PPIX-TTX and liposome-DMED shows initial nerve block of 35 h, followed by repeated US-triggered analgesia [119]. E) Schematic of magnetic microgels containing iron oxide (magnetite) nanoparticles and ropivacaine. Magnetic nanoparticles in circulation are attracted to the ankle upon magnet application. F) Withdrawal latency trends of untreated left paw and treated right paw [130].

duration of anesthesia depends on the extent and intensity of insonation, further development of similar NDDSs could achieve ultrasound-triggered local anesthesia with shorter or longer initial nerve blocks or a greater number of triggerable events. Such control will provide on-demand, personalized pain treatment [119].

Kim et al. have developed theragnostic PVAX nanoparticles that serve as ultrasonographic contrast agents and therapeutic agents by leveraging poly(vanillyl alcohol-*co*-oxalate) (PVAX) nanoparticles that generate CO_2 bubbles through H_2O_2-triggered hydrolysis. The PVAX nanoparticles rapidly scavenge H_2O_2 and exert antioxidant and anti-inflammatory effects for musculoskeletal injuries associated with overproduction of H_2O_2 [125]. This group also loaded curcumin in PVAX (CUR-PVAX) nanoparticles to increase therapeutic capacity. Along with suppression of the proinflammatory cytokines TNFα and IL-1β, significantly enhanced VEGF and PECAM-1 levels led to blood perfusion into ischemic mice tissues [126].

Magnetic field-responsive NDDSs

Targeted delivery of chemotherapeutics with magnetic nanoparticles (MNPs) has been achieved in animals and humans. MNPs improve spatiotemporal localization of therapeutics by controlling hyperthermia (magnetite, maghemite, and ferrite MNPs), mechanical deformation, and magnetic guiding [84,111]. In hybrid NDDS approaches, alginate-based ferrogels and chitosan-based nanoparticles have been used to induce pore formation and drug release upon magnetic stimulation [84].

Preemptive nerve blocking at the ankle is a common technique to provide analgesia before foot surgeries for reduced central sensitization, postoperative pain, and analgesic consumption [127]. The use of ultrasound-guided techniques has become the gold standard for regional anesthesia or peripheral nerve blocks, providing minimal complications [128]. However, rare but devastating complications such as nerve injury, catheter infection, bleeding, and LAST may arise, calling for finer spatiotemporal control of therapy [129].

In proof-of-concept studies, intravenous injections of MNP complexes with ropivacaine and bupivacaine followed by magnet application at the ankle significantly improved anesthesia [130,131]. Using magnetic nanogels of $PM(EO)_2MA$, magnetite, and ropivacaine, Mantha et al. showed increased thermal antinociceptive response and ankle ropivacaine concentration when an external magnet was applied for 30 min (Fig. 4E and F) [130]. Similar results were obtained from nanogels containing NIPAAM-MAA and bupivacaine [131]. The plasma concentration of complexed ropivacaine was several-fold higher than for direct drug injection [130].

The lack of formal toxicity assessments in these studies means that further research is required before clinical translation. Several reports indicate that MNPs can have significant dose-dependent cytotoxicity as seen in both morphological changes and apoptosis in chicken embryos and human umbilical vein endothelial cells [108,132–135]. In contrast, dose-dependent pain relief by ultrasmall (6–10 nm) magnetite (Fe_3O_4) nanoparticles even without drug cargo has been shown to reduce inflammatory cells, proinflammatory markers, and ROS production in rat paw lesions [136]. The ability of MNPs to scavenge free radicals provides a safer and more effective alternative to traditional pain management, and is discussed further in Section 6.

Several iron oxide nanoparticles (IONPs) including Feridex, Gastromark, and Feraheme are FDA-approved for contrast enhancement in magnetic resonance imaging (MRI) [137]. With greater bioavailability and visibility with MRI, IONPs offer optimal pain treatment. Superparamagnetic iron oxide nanoparticles (SPIONs) also increase the blood circulation time of quercetin, a well-established anti-inflammatory, antioxidant, and analgesic agent [138,139].

Nanoparticles to detect molecular sources of pain

Successful pain treatment relies on locating the source of pain, yet this process is currently imprecise and laborious. A point-of-care system that accurately and efficiently determines the origins of pain by using specific pain biomarkers has the potential to streamline the process, eliminating weeks-long testing and allowing rapid treatment of patients. Researchers are elucidating biomarkers for pain in disease states such as matrix metalloproteinases (MMPs) in neuropathic pain, IL-6 in osteoarthritis, various serum markers in lower back pain, and cytokine IL-6 and P neuropeptide in cerebrospinal fluid in fibromyalgia.

Multiplexed detection of pain markers

Multiplexed point-of-care detection of pain biomarkers can be achieved using nanotechnology, as demonstrated with cancer biomarkers [136,140]. Quantum dot nanoparticles (Qdots) are particularly applicable, owing to their tunable optical properties [82,141]. Bioconjugated Qdots with varying diameters, emission spectra, and antibody motifs can determine pain sources from patient samples [82]. This system allows pain-specific biomarkers to be quantified in a point-of-care modality based on the unique fluoroscopic signature of the Qdot, obviating the need for a physician to run multiple tests to check for individual biomarkers, for determination of the specific source of pain. This system is unique in that it tests for a variety of biomarkers and pain sources at once in a rapid manner, rather than by using multiple biomarker tests. Efficient determination of the pain source will facilitate localized treatment and reduce unnecessary systemic treatments that are commonplace today.

Localization of neuropathic pain

Neuropathic pain is a consequence of neural pathology such as nerve lesions that interrupt axonal continuity and cause peripheral sensitization, or diseases such as diabetes mellitus that are associated with nerve damage. Neuropathy is a common form of chronic pain and remains difficult to treat. Diagnosis and treatment of neuropathic pain require locating the lesion or pain source; however, current clinical determination of neuropathic pain relies on questionnaires and electrodiagnostic tests that are unable to locate the exact source of pain [142]. Nanoparticles are uniquely suited to determine sources of lesions as they can be modified to target regions with high levels of biomarkers and can be imaged. The largest obstacle to using nanoparticles for locating lesions is the lack of well-defined biomarkers.

Recently, Husain et al. illustrated the feasibility and efficacy of using nanoparticles to locate lesions responsible for neuropathic pain by targeting MMPs. MMPs are upregulated after nerve injury and have elevated levels for ~ 20 days as they maintain neuroinflammation. To test the hypothesis that MMP upregulation is a biomarker for peripheral and spinal lesions, the group used magnetic IONPs to target MMP-12 in spinal nerve ligations. MRI scans and histological studies showed significant uptake of the MMP-12-targeted probe at the lesion. Stable and non-toxic in vitro, the IONP probe appears promising as a tool for harvesting biomarkers for clinical determination of neuropathic pain sources. Other proteins which are over-expressed in injured nerves, such as aquaporin-4, interleukin 1 receptor-like 1, and periaxin, can be targeted using a similar approach [142].

Future use of nanoparticles in pain management

Successful pain treatment requires determining biomarkers to identify the location of pain and to target the source of pain. Using biomarkers to locate the source of pain will be a major breakthrough in the field as it will allow pain to be managed locally instead of through systemic treatments; this will lower dosages, side effects, and cytotoxicity while providing better pain therapies to patients. Another new and attractive area is treating pain by targeting intracellular signaling molecules to mitigate nociception and neuropathy at the source. Nanoparticles play a crucial role in this effort as they can target receptors and allow controlled release of drugs at the receptor location [82]. Nanoparticles are also being used to replace opioids via receptor targeting. Compounds such as MAPK inhibitors are being developed to treat a wide variety of chronic pain, but their delivery cannot be systemic. Nanoparticles represent a major step towards treating pain in a site-specific manner with minimal systemic uptake, which is vital to long-term chronic pain management without negative systemic side effects and addiction [97].

Gene therapy for pain

Gene therapy allows for specific targeting of the pain source by tailoring three parameters, vector, transgene, and promoter, to a known pathophysiology. This level of control makes gene therapy powerful by enabling both specific targeting of a disease or gene causing the pain, and localized delivery to the source of the pain. Co-treatment with other approved drugs can enhance the palliative effect of gene therapy. For treatment of chronic pain, transgenes can reduce nociception by inducing overexpression of analgesic genes and anti-inflammatory cytokines or by inhibiting a pain-producing gene (Fig. 5).

Recently, extensive research efforts have developed safe viral vectors that transfer therapeutic genetic materials. Herpes simplex virus type 1 (HSV-1), adeno-associated viruses (AAVs), adenoviruses (AVs), and lentiviruses (LVs) have become the four main viral vectors for pain gene therapy as they can target non-dividing cells such as neurons (Fig. 6). Retroviruses cannot transfect non-dividing cells and thus have not been useful in targeting chronic pain. HSV-1 is an ideal viral carrier for pain treatment given its high packaging capacity and innate neurotropism, allowing delivery to be as simple as a dermal application or subdermal injection. AAVs are commonly used as carriers to produce opioids. AAVs are used to deliver genes via intrathecal injection, targeting, and triggering neuronal cells to secrete opiate-like proteins in low and sustained amounts. This novel treatment can potentially reduce pain without exposing patients to the risk of opiate abuse [143].

Vectors for delivery of gene therapy for pain

Herpes simplex virus type 1

HSV-1 is one of the most commonly used viral vectors for pain management in large part due to its high packaging capacity and neurotropism. HSV-1 has become the vector of choice in a number of disease models for pain management after its proven efficacy in the NP2 clinical trial described in section *Clinical trials*. A common use of HSV is to express ENK and PENK, naturally occurring endogenous opioids that, upon transfection, can improve the body's ability to release endogenous opioids.

The anti-nociceptive, anti-neuropathic, and anti-inflammatory effects of HSV vectors expressing ENK and PENK have been demonstrated in a number of in vivo models, including pancreatic inflammation [144], rheumatoid arthritis using the adjuvant-induced polyarthritis model, [145], facial pain from the infraorbital nerve constriction [146], arthritis induced by injection of complete Freund's adjuvant [147], nerve injury [147], and bone cancer pain [148]. Induction of glycine receptor (GlyR) expression using HSV can function as an endogenous opioid that is not ordinarily present in sensory neurons, maximizing therapeutic selectivity and minimizing immunogenicity [149].

HSV vectors have also been used to express IL-10 in a model of type I diabetes to alleviate pain by reducing the Toll-like receptor 4 (TLR4) expression, which reduces macrophage activation and

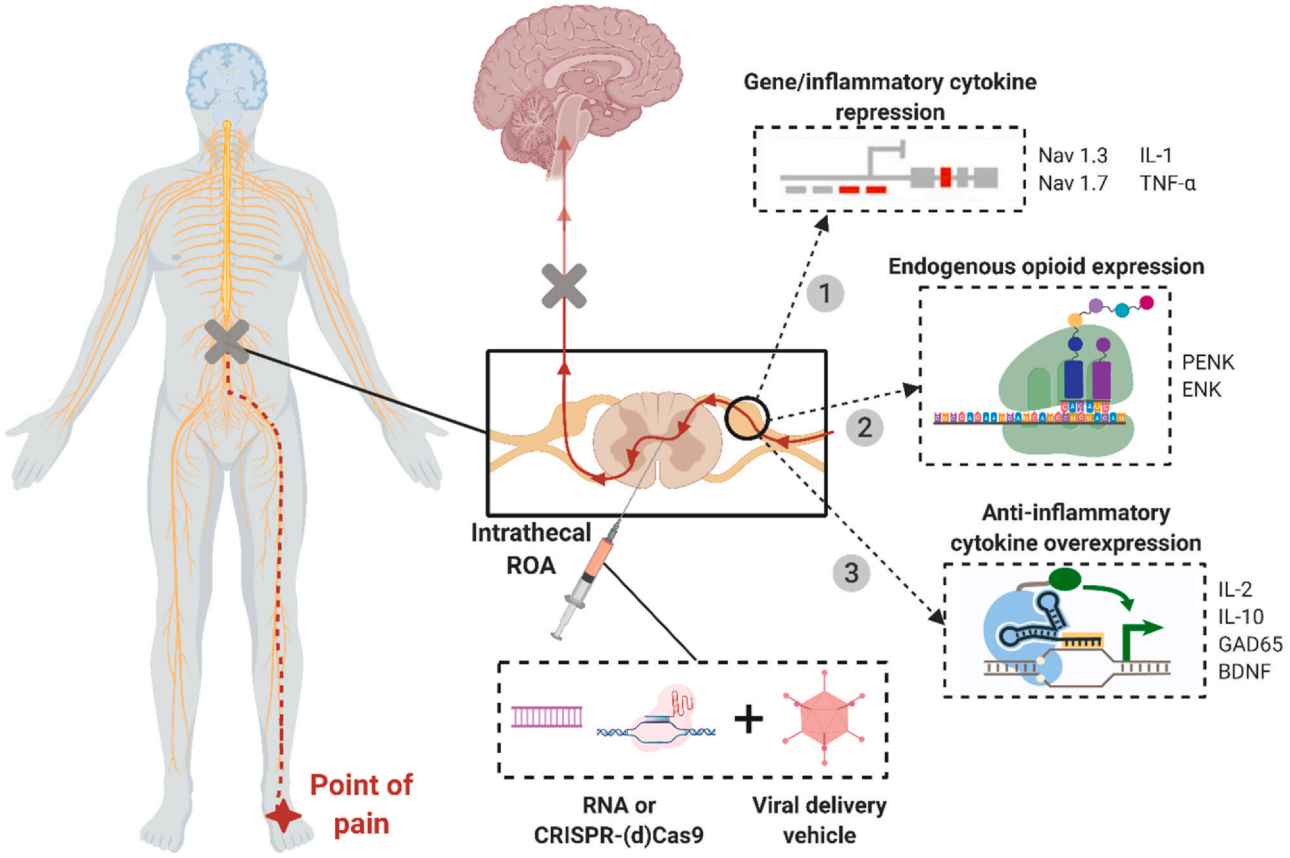


Fig. 5. Methods of viral gene therapy for pain treatment. Schematic showing various methods of gene therapy for pain treatment. 1) Repression of genes ($Na_v1.3$, $Na_v1.7$) or inflammatory cytokines (IL-1, TNF-α) to reduce pain signaling and inflammation in affected areas. 2) Expression of preproenkephalin (PENK) and enkephalin (ENK), which act as endogenous opioids by binding to opioid receptors and mediating pain. 3) Overexpression of anti-inflammatory cytokines (IL-2, IL-10, GAD65, BDNF) to reduce inflammation, immune response, and inflammatory pain.

inhibits painful neuropathy [150]. Another application of HSV vectors is suppressing neuropathic pain induced by HIV by transfecting the *gad1* gene that expresses GAD67, which synthesizes GABA for neuronal activity [151,152]. The expression of TRPV1 using HSV vectors has been found effective in treating interstitial cystitis/bladder pain syndrome [153].

Adenoviruses

Adenoviruses can be used for gene transfer to both dividing and non-dividing cells and are commonly used in gene therapy due to their low host specificity and high immunogenicity, as most people have been exposed to AV serotypes 2 and 5. AVs have moderate packaging ability and short-term transgene expression, making them ideal for acute pain treatment. AVs have been used as a vector for GAD65 and IL-10. AVs expressing GAD65 and targeting glial cells were shown to be effective in a facial pain model, where GAD expression reduced pain by acting on GABA receptors on neurons [154]. AVs encoding IL-10 blocked both nerve pain and allodynia in three models of neuropathic pain nerve injury [155]. Researchers have used AVs to express IL-2 to mediate nociceptive pain. IL-2 has analgesic effects in both the PNS and CNS, mediated by opioid receptor binding. AVs expressing IL-2 delivered to nerve injury (CCI) models via intrathecal injection have a nearly week-long effect [156]. GLT-1, a glial glutamate transporter, has been expressed by AVs and delivered to the spinal cord to treat inflammatory and neuropathic pain. GLT-1 attenuates the induction of inflammatory and neuropathic pain but has little effect on mediating pre-existing pain, making it an excellent candidate to administer in clinical procedures that induce pain, such as chemotherapy [157].

Adeno-associated viruses

Adeno-associated viruses are similar to AVs but have deficiencies in their replication and pathogenicity, making them safer than AVs. AAVs have been used as a vector for pain management to knockdown $Na_v1.3$ in a diabetic model to alleviate tactile allodynia, and in a nerve injury neuropathic pain model. $Na_v1.3$ is a voltage-gated sodium channel that is upregulated in both the PNS and CNS after nerve injury and in dorsal root ganglion neurons in diabetes. The increase in $Na_v1.3$ contributes to chronic pain. Knocking down $Na_v1.3$ via siRNA to reduce $Na_v1.3$ levels via AAV is effective in alleviating diabetic allodynia (neuropathic pain) and nerve injury-induced neuropathic pain [158,159].

Overexpression of GAD65 after peripheral nerve injury is effective in alleviating neuropathic pain by increasing GABA levels. However, the increased levels of GAD65 remain for less than a week from the time of injury. Recombinant AAVs expressing GAD65 have attenuated neuropathic pain for longer periods via administration to the sciatic nerve and dorsal root ganglion [160,161].

The use of AAVs to express the analgesic prepro-β-endorphin and IL-10 through lumbar puncture reduced neuropathic pain in a L5 spinal ligation (SNL) chronic neuropathic pain model [143], as did overexpression of brain-derived neurotrophic factor (BDNF) via injection into the dorsal root ganglion after chronic constriction injury of the sciatic nerve (CCI model of neuropathic pain) [162].

Lentiviruses

Lentiviruses naturally integrate with non-diving cells and provide stable long-term expression of transgenes with low immunogenicity, making them uniquely suited for pain therapy. Knocking down the transcription factor NF-κB using siRNA has been

Comparison of common viral vectors used in chronic pain therapy

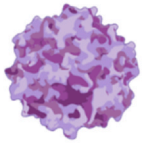
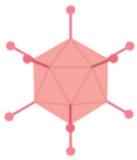
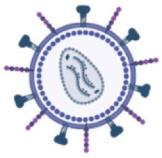
	HSV-1	AAV	AV	LV
Vector				
Genome	dsDNA	ssDNA	dsDNA	ssRNA
Packaging capacity	High (40kB)	Low (<5kB)	Moderate (7kB)	Moderate (8kB)
Immunogenicity	Low	Low-Moderate	High	Low
Common Pain models	NeuP, NocP, IP	NeuP, IP	NeuP, NocP, IP	NeuP
Integrates into the host genome	No	Yes	No	Yes
Transgene expression	>1 year	>1 year	Days to Weeks	Lifelong
Advantages	Neurotropic Can be delivered dermally subdermally	Some target cell specificity High transduction efficiency	Some target cell specificity High transduction efficiency Vector can have high cloning capacity (30-40kB)	High target cell specificity Does not require cells to be dividing for transfection (unlike other retroviruses)
Disadvantages	Transient transgene expression in non-neuronal cells			

Fig. 6. Comparison of common viral vector carriers used in gene therapy for pain: herpes simplex virus 1 (HSV-1), adeno-associated virus (AAV), adenovirus (AV), and lentivirus (LV). Abbrev: NeuP, neuropathic pain; NocP, nociceptive pain; IP, inflammatory pain.

a major focus of research, as NF-κB controls multiple genes that encode inflammatory and pain responses. Selectively knocking down NF-κB super-repressor IκBα results in inhibition of the NF-κB pathway in nerve injury models and attenuation of neuropathic pain [163]. Using lentiviral vectors to deliver short hairpin DNA targeting NF-κB65 to silence NF-κB inhibits proinflammatory TNF-α, IL-1β, and IL-6 and moderates neuropathic pain and allodynia for over four weeks [164].

Lentiviral vectors have also been used to knockdown PKC to treat nerve injury-based neuropathic pain and reverse morphine tolerance in patients with chronic pain. PKCγ is an important second messenger as its activation is involved in chronic neuropathic pain. Lentiviral delivery of RNAi can silence the PKCγ gene and reduce pain and allodynia in rat nerve-injury models for over six weeks [165]. PKCγ is also thought to play a role in morphine tolerance. To combat increased tolerance, lentiviral vectors of PKCγ short hairpin RNA are delivered to morphine-tolerant rats via intrathecal injection. After injection, downregulation of expression of PKCγ was observed along with a reversal in morphine tolerance, which is useful for patients already taking opioids [166].

Non-viral vectors

While most gene therapy for pain is accomplished using viral vectors, many non-viral vectors are also to treat pain. Non-viral vectors are less immunogenic, more stable, and safer than their viral counterparts, but are much less efficient [167]. Non-viral vectors include cationic lipids and polymers, plasmids, naked DNA, and lipid-polymers. Non-viral vectors have been extensively used in gene therapy-based treatment of peripheral and coronary artery disease using VEGF165 and VEGF-2; however, clinical trials using plasmid DNA (phVEGF165 and phVEGF-2) have shown varying degrees of success [168–174].

IL-2 and IL-10 have become popular targets for non-viral gene therapy of neuropathic pain. IL-2 is unsuitable as an analgesic as it is short-lived in vivo and requires constant administration. However, IL-2 gene therapy may be suitable for short-term neuropathic pain therapy. Humanized IL-2-expressing plasmids administered via a spinal catheter in CCI rat models have shown dose-dependent pain reduction [175]. Long-term control of neuropathic pain has also been established using IL-10 to control glial inflammation, mediating neuropathic pain [176–179].

One form of non-viral treatment requires an intrathecal 'priming' injection of DNA to induce accumulation of immune cells and short-term pain reversal before a second intrathecal injection; one DNA used was a naked plasmid-encoded IL-10^{F129S} transgene for long-term pain reduction. The injections achieved pain relief for over three months in peripheral nerve injuries. The priming shot, given from 5 h to 3 d before the second injection, potentiated long-term pain relief in a time- and dose-dependent manner [180].

Intrathecal IL-10 transgene expression induces an anti-inflammatory environment in the dorsal root ganglion and in the lumbar spinal cord. Co-injection of naked IL-10-encoded plasmids with D-mannose, an immune cell adjuvant, allows stable long-term neuropathic pain relief following a single intrathecal injection in CCI and IL-10 deficient rat models [167]. D-mannose is a mannose receptor-specific ligand that increases mannose receptor expression, which is associated with anti-inflammatory macrophage polarization, anti-inflammatory signaling, and transient pain relief. Treatment with D-mannose optimizes IL-10 transgene expression, and co-injection of mannose with a 25-fold lower

transgene dose produces prolonged pain suppression in CCI rat models [178].

The μ-opioid receptor OPRM1 has been a target of non-viral gene delivery to attenuate cancer-associated pain. A non-viral hybrid vector, modified HIV-1 Tat, was used to transfect HSC-3 (human tongue squamous cell carcinoma) cells with OPRM1. These cells were then inoculated into athymic SCC (oral cancer) mouse models and were found to have an analgesic effect. This non-viral approach is superior to viral approaches as the vector has a much smaller size, allowing greater transfection efficiency and lower sufficient dosages [181].

Non-viral gene transfer has also been used to prevent drug-induced neuropathy. Cisplatin is a powerful chemotherapeutic but causes dose-dependent neuropathy with slow and often partial recovery. Neurotrophin-3 (NT-3) is a promising agent for preventing and treating cisplatin-induced neuropathy as it readily reaches the dorsal root ganglion, the main target of cisplatin toxicity. However, the administration of NT-3 is complicated as its plasma half-life is ~ 1 min. Non-viral gene transfer of NT-3 using a recombinant plasmid followed by electroporation can protect against cisplatin-induced neuropathy. NT-3-encoded plasmids were intramuscularly injected followed by four square-wave pulses of 100 V and 20 ms duration delivered at a frequency of 1 Hz in a cisplatin-treated mouse model. This treatment caused only slight muscle toxicity and no general side effects while reducing neuropathic pain, making it a robust platform to treat chemo-induced neuropathy and peripheral neuropathies [182].

Future use of gene therapy for treating chronic pain

Future opportunities for applications of gene editing to pain are expansive. Current gene therapy can be enhanced, for example, by designing a specific transgene to allow better targeting of cells of interest and longer-lasting expression of the genetic modification. With improved knowledge of patient profiles and how they correspond to transgene selection, treatments can be made more effective. AAV-mediated transfer of Kv1.2 sense RNA for reduction of dorsal root ganglion neuronal excitability [183], and viral vector-mediated overexpression of anti-inflammatory cytokines to counter over-inflammation are promising methods to treat pain using gene therapy. Other long-term goals for gene therapy include specific delivery to the brain to target pain control centers, which is currently difficult due to the complexity of the neural circuits of the brain in comparison to the spinal cord.

Clinical trials

Gene therapy was proven effective for treating pain in humans in 2011, in the first clinical trial of gene transfer as a treatment for pain. In the phase 1 trial, cancer patients were treated with NP2, a replication-defective HSV-based vector expressing human preproenkephalin (PENK). PENK induces the release of enkephalin peptides which activate opioid receptors, inhibiting the transmission of pain signals to neurons. NP2 was transdermally injected into the pain location as perceived by the patients. NP2 was well tolerated and caused no adverse effects, and patients given moderate to high doses of NP2 saw pain relief over the course of treatment [184,185]. A phase 2 clinical trial of NP2 was conducted with 33 participants with intractable pain due to malignant cancer in 2013 [185].

A phase 1 trial to treat osteopathic pain using XT-150 was conducted by Xalud Pharmaceuticals. Instead of blocking pain signaling, XT-150 treats the inflammation responsible for chronic pain through the expression of a variant of IL-10, a naturally occurring anti-inflammatory protein that suppresses TNF-α, IL-1β, and IL-6, downregulates cytokine receptors, and upregulates cytokine antagonists. Prior to clinical trials, upregulation of IL-10 to mediate pain was conducted in CCI rat models of neuropathic pain with positive results [176]. XT-150 is similar to XT-101, a predecessor that was shown to successfully treat pain in models of multiple sclerosis (MS) and enhanced pain states in rats [177,179,180]. In this trial, XT-150 was administered via injection into the knee synovial capsule. The study followed patients for six months, monitoring their pain levels and blood levels of the IL-10 variant. While phase 1 results are yet to be published, phase 2 trials of XT-150 for elderly patients with musculoskeletal pain are currently underway [186,187].

An ongoing FDA fast-tracked Phase 1/2 trial to treat refractory angina using XC001 is being conducted by XyloCor Therapeutics. Refractory angina is chronic chest pain in coronary artery disease that cannot be treated otherwise. Angina in these patients is severe and debilitating, affecting daily activities and quality of life. XC001, also known as AdVEGF-All6A+, is a novel gene therapy consisting of a replication-deficient adenovirus vector that expresses a hybrid variant of VEGF. XC001 is being used to treat angina by promoting angiogenesis (revascularization), which would increase myocardial blood flow. Angiogenesis can relieve myocardial ischemia and improve ventricular performance [188,189].

There is also an ongoing phase 1 trial to treat refractory angina using Ad5FGF-4 (AFFIRM). Ad5FGF-4 is a replication-deficient serotype 5 adenovirus expressing the gene for human fibroblast growth factor-4 (FGF-4) driven by a cytomegalovirus promoter [190]. Ad5FGF-4 was previously tested in clinical trials AGENT-3 and AGENT-4 in 2008 to treat chronic angina. After preclinical successes, the trials were cut short after it became clear that 12 weeks would not be long enough to reach significance. The AGENT trials enrolled over 500 participants and found that while not effective in men, Ad5FGF-4 was effective in women. This was the first clinical report to show a gender difference in the treatment of angina [191,192]. The purpose of this ongoing study is to determine whether Ad5FGF-4 is effective in reducing debilitation from angina, including increasing the duration of exercise, reducing the frequency of angina attacks, and improving overall quality of life [193].

CRISPR-Cas for pain

CRISPR-Cas offers a new mechanism to combat chronic pain. CRISPR-Cas is a gene-editing system that allows genes to be added, deleted, or altered at particular locations in the genome. CRISPR-Cas9 is one form of CRISPR-Cas, and is adapted from a naturally occurring genome editing system in bacteria. CRISPR-Cas9 is faster, cheaper, more accurate, and more efficient than other gene-editing tools. One obstacle when using CRISPR is that the target must be specific to the cells being modified—this is particularly important in the context of pain. The goal of CRISPR in the context of pain therapy is to edit cells to make them more resistant to pain. Off-target editing or over-editing could lead to cells that are completely resistant to pain, which would have serious negative repercussions. Since CRISPR permanently edits cells, CRISPR-based therapies must be extensively tested to ensure that they are not too potent and that they can be delivered in a strictly targeted manner. Pain is biologically important to alert and protect the body from harm; permanently removing pain sensation via CRISPR would be detrimental, while limiting the amount of pain in specific cells could bring relief to those suffering from debilitating chronic pain.

Repressing $Na_v1.7$ via SCN9A

One way to make CRISPR safe and controlled for pain management is to use inactivated or 'dead' Cas9 (dCas9). dCas9 does not cleave DNA but maintains other functions—binding to guide RNA and the DNA strand being targeted—and can modify and employ transcriptional activators to modulate gene expression. This dCas9 mechanism is being studied in the context of the rare SCN9A gene mutation. SCN9A is responsible for production of $Na_v1.7$, which plays a role in transmitting pain from nerves to the brain. Loss-of-function

mutations in $Na_v1.7$ cause congenital insensitivity to pain (CIP), a phenomenon that can lead to lack of pain perception to noxious stimuli [194].

Some mutations of the *SCN9A* gene cause people to feel more or less pain, or, in the extreme case of CIP where *SCN9A* has been disabled completely, no pain at all. While this discovery has led to advances in pain treatment research, it also shows why researchers need to be cognizant of the level of pain attenuation. Pain is essential for survival, as can be seen from those who suffer from CIP: individuals with CIP are often mistakenly injured as evidenced by limping or missing pieces of their tongue that they unknowingly bit off because their bodies lack a mechanism to indicate damage. The goal of using CRISPR should not be to eliminate pain but to attenuate it, such that people do not suffer from debilitating chronic pain, while retaining the ability to feel pain [16,40,41]. The Mali group has been studying this mutation and how to pair it with CRISPR to mediate pain in people with chronic pain conditions. CRISPR is advantageous for blocking NaV1.7 as small molecules and antibodies targeting $Na_v1.7$ have overwhelming off-target effects in the Na_v family. CRISPR was used to block $Na_v1.7$ in mice, in the first use of CRISPR for pain management. AAV was the vector for CRISPR-dCas9 (inactivated Cas9) and zinc finger protein (ZFP), which was injected into the spine to infiltrate neuron cells in inflammatory, neuropathic, and BzATP-induced pain models. CRISPR and ZFP reduced neuropathic (lesion and chemotherapy-induced) and nociceptive pain. Knockdown of $Na_v1.7$ did not affect inflammation. These CRISPR-based systems are a successful proof of concept, but must be further tested to see how long $Na_v1.7$ stays knocked out; researchers expect the $Na_v1.7$ knockout period to be six months to one year [195]. dCAS9 can activate or repress a gene of interest without creating permanent changes. This behavior is ideal because gene expression can be modulated to suit the patient's needs and can be reversed. This study serves as a platform for gene therapy that would last for months at a time, ideal for shorter-lived chronic pain such as that of chemotherapy patients.

Blocking proinflammatory signaling

The use of CRISPR to treat pain has been studied by blocking proinflammatory signaling in vitro. CRISPR can prevent tissue damage and chronic pain by modulating gene expression to reduce proinflammatory signaling. Inhibition of TNF-α and IL-1, which upregulate NF-κB, can reduce inflammation. Researchers built lentiviral vectors encoding TNF-α and IL-1 receptors, TNFR1 and IL1R1, and targeted CRISPR-based transcriptional repressors (Fig. 5). These vectors inhibit NF-κB activation while promoting cell survival, demonstrating that CRISPR-based epigenome editing can be used to modulate inflammation [196].

Alleviating osteoarthritic pain

Osteoarthritis is marked by chronic pain and inflammation in joints, affects over 10% of adults, and has no cure. CRISPR-Cas9 provides a new platform for osteoarthritis therapy. Osteoarthritis is marked by upregulation of NGF, IL-1β, and MMP13. AAVs expressing CRISPR-Cas9 have been used to target NGF, IL-1β, and/or MMP13 via injection into arthritic sites in a surgical mouse model. Shutting off NGF resulted in reduction of pain, but joint damage increased. Shutting off NGF, IL-1β, and MMP13 together reduced pain and inhibited disease progression [197], suggesting that CRISPR-based gene editing can be useful in treating osteoarthritis.

Future use of CRISPR-Cas9 for treating chronic pain

From these studies, the potential for CRISPR-based gene editing and replacement in pain therapy is clear. CRISPR can treat chronic pain by editing the genes that are responsible for pain in a specific manner, reducing the use of pain medication, and can be done in a way that relieves pain but preserves some healthy sensation of pain. CRISPR can also be used to modulate gene expression, for example to upregulate expression of anti-inflammatory cytokines, an exciting new direction for chronic pain management.

A new CRISPR approach uses nanoparticles rather than viral vectors to deliver CRISPR-Cas machinery. These nanoparticle delivery systems, such as CRISPR-Gold, have been administered successfully and with high specificity [198]. Nanoparticle-mediated delivery minimizes the immunogenicity, risk of genomic damage [198], barriers to large-scale production, and limited insertion size [199] associated with viral delivery. Nanoparticle systems can be developed to tag specific cell types and overcome physiological barriers to aid in localized delivery. Examples of specialized nanoparticle carriers are CRISPR-Gold, which can target neurons and muscle cells [198]; selective organ targeting lipid nanoparticles, which selectively target the lung, spleen, and liver [200]; biomimetic mineralized ribonucleoprotein nanoparticles [201]; and magnetic nanoparticles; some of these systems have unique properties such as the ability to pass through cellular barriers or magnetic field-responsiveness for magnetic field-triggered genome editing [202].

These advances in using CRISPR will allow the development of platforms for monitoring patients' chronic pain and inflammation and modulating their gene expression to healthy levels as needed.

Scavengers

Acute pain can cause and reinforce the accumulation of molecules that cause unwanted immune activation and central sensitization, which in turn can increase pain and cause chronic pain. Scavengers of such molecules can improve therapeutic outcomes without off-target effects and loss of biological activity of immune agents. Scavengers are therapeutic immunomodulatory nanomaterials that are uniquely designed to proactively remove overproduced molecules to reduce chronic pain. Scavengers are a promising agent for treating chronic pain and inflammatory pain due to their structure and mechanism of action. Two of the most promising types of scavengers are nucleic acid-binding scavengers (NABS) and ROS scavengers.

NABS are highly charged polymers and nanoparticles that recognize danger- and pathogen-associated molecular patterns (DAMPs and PAMPs) that stimulate TLRs and activate an innate immune response. DAMPs and PAMPs effectively regulate immune response in healthy cells, but in chronic disease, they overstimulate TLRs leading to chronic pain and inflammation. NABS can reduce TLR overactivation, relieving inflammation and pain.

ROS scavengers remove excess ROS that are yet to be metabolized by cellular enzymes. Increased levels of ROS cause central sensitization and promote chronic pain. Scavenging excess ROS reverses central sensitization and reduces pain by increasing the threshold for pain.

Nucleic acid-binding scavengers

In chronic pain, TLRs are over-activated and cause undesirable chronic immune responses. Nucleic acid-binding scavengers (NABS) that remove the DAMPs and PAMPs that cause chronic inflammation and pain reduce both inflammation and pain. These scavengers function proactively (Fig. 7A) [203]. Instead of treating the symptoms of pain, scavengers eliminate the cause of pain by removing the agonists that cause TLR overexpression. Scavengers are unique in that the immune response is reduced in a dose-dependent manner, which can eliminate overactivation without eliminating baseline healthy activation.

DAMPs and PAMPs are molecular signaling molecules that activate an immune response. DAMPs are released by damaged cells and injured tissue into the blood and tissue fluid; PAMPs result from infection, bacteria, and viruses. Both are recognized by pattern

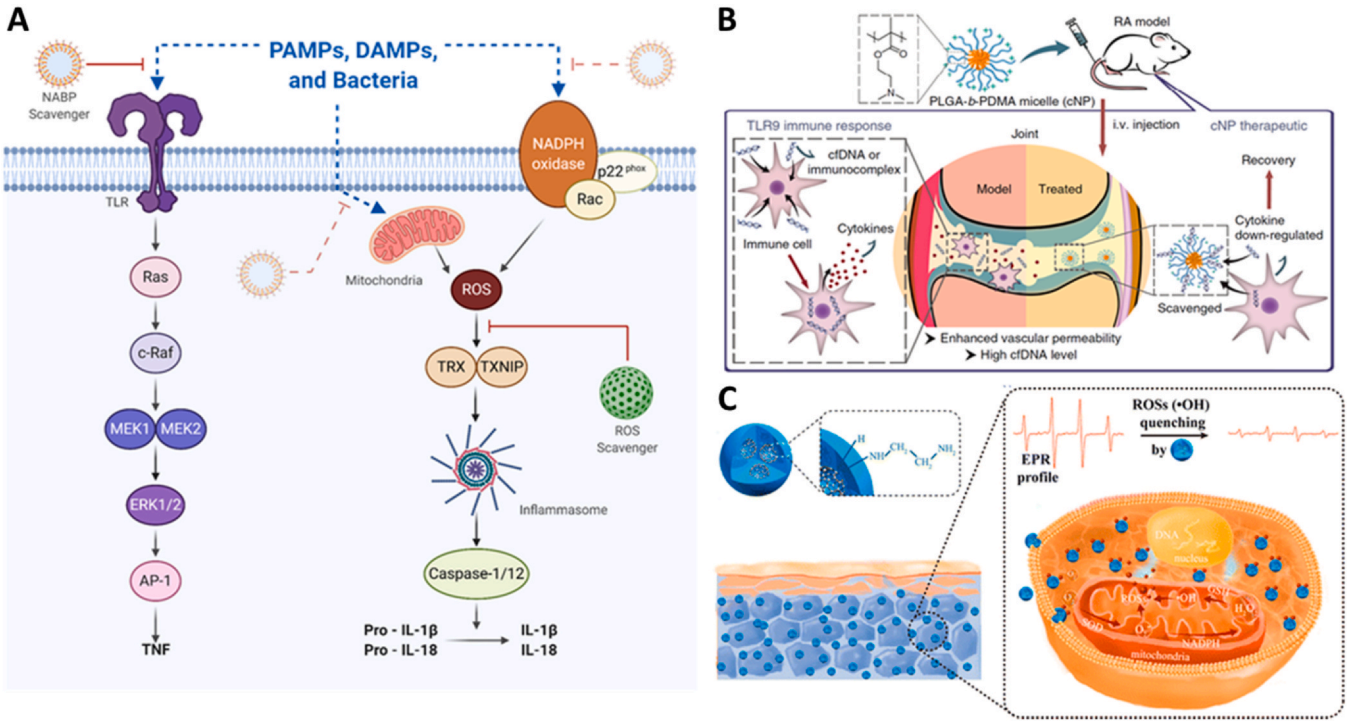


Fig. 7. Role of scavengers in pain mediation. A) The role of scavengers in mediating PAMP-, DAMP-, bacteria-, and ROS-associated pain pathways. B) Nucleic acid binding PLGA-b-PDMA nanoparticles in a rheumatoid arthritis model [203]. C) Water soluble Gd@C_{82}-(ethylenediamine)$_8$ nanoparticles act as efficient and biocompatible ROS scavengers as can be seen through decreased electron paramagnetic resonance (EPR) signal. These nanoparticles also exhibit a cytoprotective effect [219].

recognition receptors (PRRs) and trigger intracellular signaling cascades, leading to upregulation of inflammatory cytokines and type 1 interferons (Fig. 7A). TLRs are a type of PRR that recognize specific molecular patterns associated with pathogens and damaged tissue, which allow them to act as a 'guard' of the innate immune system. When TLRs recognize a PAMP or DAMP, they immediately activate an innate immune response, which leads to expression of inflammatory cytokines, immune-stimulatory cytokines, and chemokines that destroy invading pathogens and promote tissue regeneration [204]. However, inappropriate activation of TLRs contributes to the development of diseases such as autoimmune disease [205], inflammatory disease [203,206,207], sepsis [208], arthritis [203], and cancer [209] (Fig. 7B), making TLRs an attractive therapeutic target for disease-associated pain, tissue damage-associated neuropathic pain [210], and inflammatory pain [211].

NABSs are highly cationic polymers and nanoparticles that act as molecular scavengers and counteract the activity of nucleic acid aptamers, as well as inhibiting RNA- and DNA-mediated activation of TLRs and inflammation. Their positive charge allows them to bind nucleic acids and other free negatively-charged molecules, including DAMPs and PAMPs. When NABSs capture nucleic acids, the ability of those DAMPs and PAMPs to activate TLRs is neutralized. NABSs block TLR activation by nucleic acids in a controlled and localized manner without interfering with the normal course of an immune response or compromising TLR responses to non-nucleic acid, pathogenic stimulators. NABSs cannot neutralize the ability of non-nucleic acid DAMPS to induce cell death.

ROS-scavenging molecules

Reactive oxygen species are byproducts of cellular functions such as oxidative phosphorylation, an act as secondary messengers in cell-to-cell signaling and pathogen defense. In healthy cells, ROS levels are maintained by specialized enzymes, but in pathological conditions, excess ROS causes inflammation, cell and tissue damage, and pain [212,213]. Excess ROS has long been known to have a role in persistent inflammatory and neuropathic pain [214]. Elevated ROS phosphorylate NMDA receptors in the spinal cord which leads to central sensitization, a persistent state of high reactivity where the threshold of pain is reduced, creating a state of chronic pain. Reducing ROS in neuropathic pain models has dramatic analgesic effects by rapidly and effectively reversing central sensitization [214]. One way to reduce ROS levels to treat chronic pain is to use ROS-scavenging molecules.

ROS scavengers include alpha-phenyl N-tertiary-butyl nitrone (PBN), 5,5-dimethyl-pyrroline N-oxide (DMPO), 2,2,6,6-tetramethylpiperidine-N-oxyl (TEMPO), 4-hydroxy-2,2,6,6-tetramethylpiperidine-1-oxyl (TEMPOL), and vitamin E [213–216]. 'Spin trap' reagents (e.g. PBN and DMPO) are the most potent ROS scavengers as they covalently react with radicals to create stable adducts. However, these ROS scavengers are nonspecific, lack self-propulsion, and can be cytotoxic, limiting clinical translation [217]. The next generation of ROS scavengers is addressing these issues for greater efficiency and biocompatibility.

Nanoparticles can also be used to scavenge ROS. Like other nanoscavengers, mesoporous silica nanoparticles (MSN) have low motility and difficulty reaching some intracellular locations. Hollow MSN loaded with hemin has harnessed the chemical free energy of catalytic reactions and achieved 3.5-fold higher average speed than solid nanoparticles [217]. The motility can be controlled by modulating the thickness of the nanoparticle shell and presents as a new model to scavenge ROS in a more controlled manner [217].

MSN have also been decorated with ultrasmall ceria nanocrystals to create a ROS-scavenging nanocomposite that scavenges ROS in a localized manner and facilitates wound repair [136]. MSN-ceria nanocomposites can be useful in inflammatory pain especially in cases of chronic inflammation that causes tissue damage. The MSN-ceria scavenge ROS while facilitating tissue repair, reducing the likelihood of future neuropathic pain.

Another way to improve ROS scavenging is to render the nanoparticulate surface more biocompatible. Endohedral metallofullerenol nanoparticles are ROS-scavengers that inhibit lipid peroxidation, protect cells from further oxidative stress, and can potentially reverse central sensitization long-term [218]. These nanoparticles could be useful as their ability to protect cells from further stress would be beneficial when reversing central sensitization, as they could reduce oxidative stress for extended periods. Metallofullerene Gd@C_{82} nanoparticles have been modified with ethylenediamine (EDA) to create a positive zeta potential and a water-soluble surface (Fig. 7C) [218]. Even at low concentrations, Gd@C_{82}-$(EDA)_8$ nanoparticles exhibit excellent hydroxyl radical scavenging and cytoprotective effects suitable for antioxidants. Moreover, the naked amino groups on the surface can be sites of further surface functionalization, making Gd@C_{82}-$(EDA)_8$ attractive for a host of applications, including biomaterials and dietary supplements [219].

pH-responsive scavengers have been developed for targeted ROS scavenging. pH-responsive nitroxide radical-containing nanoparticles were developed to disintegrate in acidic lesions and release nitroxide radicals locally, neutralizing ROS [215]. This scavenging approach is attractive for localized injury as it can remove excess ROS in a lesion, relieving neuropathic pain without affecting the rest of the body.

NABSs may also be useful in mediating ROS-induced pain as NABSs can remove DAMPs and PAMPs before ROS generation, thereby proactively preventing ROS-related pain sensitization (Fig. 7A).

Conclusions

Nanomedicine has become an important field in therapeutic research, but nanotherapeutics have only begun to be explored in the context of pain management, in part due to the complex nature of pain. Chronic pain is associated with many diseases and with post-operative care, is difficult to treat, and costs the U.S. healthcare system over $635 billion annually. Current therapeutics for chronic pain do not provide adequate relief and many debilitating side effects. Advances in nanomaterials and nanoparticles are improving the targeting and detection of the molecular sources of pain to reduce dosage and improve long-term efficacy and safety. Gene therapy is also enabling more effective and longer-term treatment of chronic pain, with both viral and non-viral vectors for gene therapy showing effectiveness in clinical trials. CRISPR allows modulating the gene expression of newly identified targets to mediate pain without eliminating sensitization. Scavengers represent a proactive approach to treating pain by removing molecules that cause pain and pain sensitization (such as free nucleic acids and reactive oxygen species) rather than merely treating the symptoms of pain. Applying nanotechnology to new molecular pain targets and to detecting the molecular sources of pain is a frontier in nanomedicine and pain management.

CRediT authorship contribution statement

Divya Bhansali: Conceptualization, Writing - original draft, Writing - review & editing, Visualization. **Shavonne L. Teng:** Writing - original draft, Writing - review & editing. **Caleb S. Lee:** Writing - original draft, Writing - review & editing, Visualization. **Brian L. Schmidt:** Writing - review & editing. **Nigel W. Bunnett:** Writing - review & editing. **Kam W. Leong:** Conceptualization, Writing - review & editing.

Declaration of Competing Interest

The authors declare the following financial interests/personal relationships which may be considered as potential competing interests: Nigel W. Bunnett is a founding scientist of Endosome Therapeutics Inc.

Acknowledgments

Support by National Institutes of Health (NS102722, DE026806, DK118971, DE029951, NWB, BLS) and Department of Defense (W81XWH1810431, NWB, BLS) is acknowledged. Images were created with the assistance of Biorender.com.

References

[1] S.M. Schappert, C.W. Burt, Ambulatory Care Visits to Physician Offices, Hospital Outpatient Departments, and Emergency Departments: United States, 2001–02, Vital and Health Statistics, Series 13, Data from the National Health Survey 13, 2006, pp. 1–66.
[2] A. Enright, R. Goucke, The global burden of pain: the tip of the iceberg? Anesth. Analg. 123 (2016) 529–530.
[3] C.E. Whitten, M. Donovan, K. Cristobal, Treating chronic pain: new knowledge, more choices, Perm. J. 9 (2005) 9–18.
[4] A. Tsang, M. Von Korff, S. Lee, J. Alonso, E. Karam, M.C. Angermeyer, G.L. Borges, E.J. Bromet, K. Demytteneare, G. de Girolamo, R. de Graaf, O. Gureje, J.P. Lepine, J.M. Haro, D. Levinson, M.A. Oakley Browne, J. Posada-Villa, S. Seedat, M. Watanabe, Common chronic pain conditions in developed and developing countries: gender and age differences and comorbidity with depression-anxiety disorders, J. Pain 9 (2008) 883–891.
[5] J. Dahlhamer, J. Lucas, C. Zelaya, R. Nahin, S. Mackey, L. DeBar, R. Kerns, M. Von Korff, L. Porter, C. Helmick, Prevalence of chronic pain and high-impact chronic pain among adults – United States, 2016, MMWR Morb. Mortal. Wkly. Rep. 67 (2018) 1001–1006.
[6] J.A. Davis, R.L. Robinson, T.K. Le, J. Xie, Incidence and impact of pain conditions and comorbid illnesses, J. Pain Res. 4 (2011) 331–345.
[7] D.J. Gaskin, P. Richard, The economic costs of pain in the United States, J. Pain 13 (2012) 715–724.
[8] T.J. Smith, B.E. Hillner, Some orthodontists' experiences of volunteering for a community orthodontic initiative, Am. J. Orthod. Dentofac. Orthop. Off. Publ. Am. Assoc. Orthod. Const. Soc. Am. Board Orthod. 155 (2019) 552–559 e191532-e191532.
[9] Classification of Chronic Pain, Descriptions of Chronic Pain Syndromes and Definitions of Pain Terms, Prepared by the International Association for the Study of Pain, Subcommittee on Taxonomy, Pain, Suppl. 3, 1986, pp. 1–226.
[10] P. Geppetti, N.A. Veldhuis, T. Lieu, N.W. Bunnett, G Protein-coupled receptors: dynamic machines for signaling pain and itch, Neuron 88 (2015) 635–649.
[11] R.D. Gosselin, M.R. Suter, R.R. Ji, I. Decosterd, Glial cells and chronic pain, Neuroscientist 16 (2010) 519–531.
[12] L.S. Premkumar, P. Sikand, TRPV1: a target for next generation analgesics, Curr. Neuropharmacol. 6 (2008) 151–163.
[13] A.M. Habib, J.N. Wood, J.J. Cox, Sodium channels and pain, Handbook of Experimental Pharmacology, (2015), pp. 39–56.
[14] Y.Q. Zhou, Z. Liu, Z.H. Liu, S.P. Chen, M. Li, A. Shahveranov, D.W. Ye, Y.K. Tian, Interleukin-6: an emerging regulator of pathological pain, J. Neuroinflamm. 13 (2016) 141.
[15] F. Cervero, Visceral versus somatic pain: similarities and differences, Dig. Dis. 27 Suppl. 1 (Suppl. 1) (2009) S3–S10.
[16] S.P. Cohen, J. Mao, Neuropathic pain: mechanisms and their clinical implications, BMJ Clin. Res. Ed. 348 (2014) 7656.
[17] A.P. Trouvin, S. Perrot, New concepts of pain, Best Pract. Res. Clin. Rheumatol. 33 (2019) 101415.
[18] C.I. Ghanem, M.J. Pérez, J.E. Manautou, A.D. Mottino, Acetaminophen from liver to brain: new insights into drug pharmacological action and toxicity, Pharmacol. Res. 109 (2016) 119–131.
[19] Y.S. Karandikar, P. Belsare, A. Panditrao, Effect of drugs modulating serotonergic system on the analgesic action of paracetamol in mice, Indian J. Pharmacol. 48 (2016) 281–285.
[20] E. Yoon, A. Babar, M. Choudhary, M. Kutner, N. Pyrsopoulos, Acetaminophen-induced hepatotoxicity: a comprehensive update, J. Clin. Transl. Hepatol. 4 (2016) 131–142.
[21] S.H. Sindrup, M. Otto, N.B. Finnerup, T.S. Jensen, Antidepressants in the treatment of neuropathic pain, Basic Clin. Pharmacol. Toxicol. 96 (2005) 399–409.
[22] M.P. Lunn, R.A. Hughes, P.J. Wiffen, Duloxetine for treating painful neuropathy, chronic pain or fibromyalgia, Cochrane Database Syst. Rev. (2014) 007115.
[23] H. Obata, Analgesic mechanisms of antidepressants for neuropathic pain, Int. J. Mol. Sci. 18 (2017).
[24] J. Neill, C. Brock, A.E. Olesen, T. Andresen, M. Nilsson, A.H. Dickenson, Unravelling the mystery of capsaicin: a tool to understand and treat pain, Pharmacol. Rev. 64 (2012) 939–971.

[25] M. Vyvey, Steroids as pain relief adjuvants, Can. Fam. Physician 56 (2010) 1295–1297.
[26] D. Memiş, A. Turan, B. Karamanlioğlu, Z. Pamukçu, I. Kurt, Adding dexmedetomidine to lidocaine for intravenous regional anesthesia, Anesth. Analg. 98 (2004) 835–840.
[27] J.A. Calasans-Maia, G. Zapata-Sudo, R.T. Sudo, Dexmedetomidine prolongs spinal anaesthesia induced by levobupivacaine 0.5% in guinea-pigs, J. Pharm. Pharmacol. 57 (2005) 1415–1420.
[28] G.E. Kanazi, M.T. Aouad, S.I. Jabbour-Khoury, M.D. Al Jazzar, M.M. Alameddine, R. Al-Yaman, M. Bulbul, A.S. Baraka, Effect of low-dose dexmedetomidine or clonidine on the characteristics of bupivacaine spinal block, Acta Anaesthesiol. Scand. 50 (2006) 222–227.
[29] T. Yoshitomi, A. Kohjitani, S. Maeda, H. Higuchi, M. Shimada, T. Miyawaki, Dexmedetomidine enhances the local anesthetic action of lidocaine via an alpha-2A adrenoceptor, Anesth. Analg. 107 (2008) 96–101.
[30] K.R. Ashish, S.J. Amteshwar, S. Nirmal, Opioid withdrawal syndrome: emerging concepts and novel therapeutic targets, CNS Neurol. Disord. Drug Targets 12 (2013) 112–125.
[31] G. Corder, D.C. Castro, M.R. Bruchas, G. Scherrer, Endogenous and exogenous opioids in pain, Annu. Rev. Neurosci. 41 (2018) 453–473.
[32] E.A. Kiyatkin, Respiratory depression and brain hypoxia induced by opioid drugs: morphine, oxycodone, heroin, and fentanyl, Neuropharmacology 151 (2019) 219–226.
[33] H. Khademi, F. Kamangar, P. Brennan, R. Malekzadeh, Opioid therapy and its side effects: a review, Arch. Iran. Med. 19 (2016) 870–876.
[34] G. Del Vecchio, V. Spahn, C. Stein, Novel opioid analgesics and side effects, ACS Chem. Neurosci. 8 (2017) 1638–1640.
[35] P. Skolnick, The opioid epidemic: crisis and solutions, Annu. Rev. Pharmacol. Toxicol. 58 (2018) 143–159.
[36] S.M. Hayek, A. Shah, Nerve blocks for chronic pain, Neurosurg. Clin. N. Am. 25 (2014) 809–817.
[37] J. Aguirre, A. Del Moral, I. Cobo, A. Borgeat, S. Blumenthal, The role of continuous peripheral nerve blocks, Anesthesiol. Res. Pract. 2012 (2012) 560879.
[38] G. Leonard, P. Goffaux, S. Marchand, Deciphering the role of endogenous opioids in high-frequency TENS using low and high doses of naloxone, Pain 151 (2010) 215–219.
[39] T. Wolter, Spinal cord stimulation for neuropathic pain: current perspectives, J. Pain Res. 7 (2014) 651–663.
[40] S.D. Dib-Hajj, Y. Yang, J.A. Black, S.G. Waxman, The Na(V)1.7 sodium channel: from molecule to man, Nat. Rev. Neurosci. 14 (2013) 49–62.
[41] C.G. Faber, J.G. Hoeijmakers, H.S. Ahn, X. Cheng, C. Han, J.S. Choi, M. Estacion, G. Lauria, E.K. Vanhoutte, M.M. Gerrits, S. Dib-Hajj, J.P. Drenth, S.G. Waxman, I.S. Merkies, Gain of function Naν1.7 mutations in idiopathic small fiber neuropathy, Ann. Neurol. 71 (2012) 26–39.
[42] B. Bannwarth, M. Kostine, Nerve growth factor antagonists: is the future of monoclonal antibodies becoming clearer? Drugs 77 (2017) 1377–1387.
[43] A.S. Nair, Tanezumab: finally a monoclonal antibody for pain relief, Indian J. Palliat. Care 24 (2018) 384–385.
[44] D.D. Jensen, T. Lieu, M.L. Halls, N.A. Veldhuis, W.L. Imlach, Q.N. Mai, D.P. Poole, T. Quach, L. Aurelio, J. Conner, C.K. Herenbrink, N. Barlow, J.S. Simpson, M.J. Scanlon, B. Graham, A. McCluskey, P.J. Robinson, V. Escriou, R. Nassini, S. Materazzi, P. Geppetti, G.A. Hicks, M.J. Christie, C.J.H. Porter, M. Canals, N.W. Bunnett, Neurokinin 1 receptor signaling in endosomes mediates sustained nociception and is a viable therapeutic target for prolonged pain relief, Sci. Transl. Med. 9 (2017).
[45] R.E. Yarwood, W.L. Imlach, T. Lieu, N.A. Veldhuis, D.D. Jensen, C. Klein Herenbrink, L. Aurelio, Z. Cai, M.J. Christie, D.P. Poole, C.J.H. Porter, P. McLean, G.A. Hicks, P. Geppetti, M.L. Halls, M. Canals, N.W. Bunnett, Endosomal signaling of the receptor for calcitonin gene-related peptide mediates pain transmission, Proc. Natl. Acad. Sci. USA 114 (2017) 12309–12314.
[46] N.N. Jimenez-Vargas, L.A. Pattison, P. Zhao, T. Lieu, R. Latorre, D.D. Jensen, J. Castro, L. Aurelio, G.T. Le, B. Flynn, C.K. Herenbrink, H.R. Yeatman, L. Edgington-Mitchell, C.J.H. Porter, M.L. Halls, M. Canals, N.A. Veldhuis, D.P. Poole, P. McLean, G.A. Hicks, N. Scheff, E. Chen, A. Bhattacharya, B.L. Schmidt, S.M. Brierley, S.J. Vanner, N.W. Bunnett, Protease-activated receptor-2 in endosomes signals persistent pain of irritable bowel syndrome, Proc. Natl. Acad. Sci. USA 115 (2018) 7438.
[47] C.E. Müller, Emerging structures and ligands for P2X(3) and P2X(4) receptors-towards novel treatments of neuropathic pain, Purinergic Signal. 6 (2010) 145–148.
[48] Y.H. Jung, Y.O. Kim, H. Lin, J.H. Cho, J.H. Park, S.D. Lee, J. Bae, K.M. Kang, Y.G. Kim, A.N. Pae, H. Ko, C.S. Park, M.H. Yoon, Y.C. Kim, Discovery of potent antiallodynic agents for neuropathic pain targeting P2X3 receptors, ACS Chem. Neurosci. 8 (2017) 1465–1478.
[49] A.T. Ginnetti, D.V. Paone, S.R. Stauffer, C.M. Potteiger, A.W. Shaw, J. Deng, J.J. Mulhearn, D.N. Nguyen, C. Segerdell, J. Anquandah, A. Calamari, G. Cheng, M.D. Leitl, A. Liang, E. Moore, J. Panigel, M. Urban, J. Wang, K. Fillgrove, C. Tang, S. Cook, S. Kane, C.A. Salvatore, S.L. Graham, C.S. Burgey, Identification of second-generation P2X3 antagonists for treatment of pain, Bioorg. Med. Chem. Lett. 28 (2018) 1392–1396.
[50] E. Marion, O.R. Song, T. Christophe, J. Babonneau, D. Fenistein, J. Eyer, F. Letournel, D. Henrion, N. Clere, V. Paille, N.C. Guerineau, J.P. Saint Andre, P. Gersbach, K.H. Altmann, T.P. Stinear, Y. Comoglio, G. Sandoz, L. Preisser, Y. Delneste, E. Yeramian, L. Marsollier, P. Brodin, Mycobacterial toxin induces analgesia in buruli ulcer by targeting the angiotensin pathways, Cell 157 (2014) 1565–1576.
[51] A.J. Shepherd, A.D. Mickle, J.P. Golden, M.R. Mack, C.M. Halabi, A.D. de Kloet, V.K. Samineni, B.S. Kim, E.G. Krause, R.Wt Gereau, D.P. Mohapatra, Macrophage angiotensin II type 2 receptor triggers neuropathic pain, Proc. Natl. Acad. Sci. USA 115 (2018) 8057.
[52] J.P. Almeida, A.L. Chen, A. Foster, R. Drezek, In vivo biodistribution of nanoparticles, Nanomedicine 6 (2011) 815–835 (Lond).
[53] E. Blanco, H. Shen, M. Ferrari, Principles of nanoparticle design for overcoming biological barriers to drug delivery, Nat. Biotechnol. 33 (2015) 941–951.
[54] M.I. Noordin, Advance Delivery System Dosage Form for Analgesic, their Rationale, and Specialty, 2017.
[55] C.M. Bernards, T.J. Luger, A.B. Malmberg, H.F. Hill, T.L. Yaksh, Liposome encapsulation prolongs alfentanil spinal analgesia and alters systemic redistribution in the rat, Anesthesiology 77 (1992) 529–535.
[56] G.J. Grant, K. Vermeulen, M.I. Zakowski, M. Stenner, H. Turndorf, L. Langerman, Prolonged analgesia and decreased toxicity with liposomal morphine in a mouse model, Anesth. Analg. 79 (1994) 706–709.
[57] T.L. Yaksh, J.C. Provencher, M.L. Rathbun, F.R. Kohn, Pharmacokinetics and efficacy of epidurally delivered sustained-release encapsulated morphine in dogs, Anesthesiology 90 (1999) 1402–1412.
[58] R.N. Alyautdin, V.E. Petrov, K. Langer, A. Berthold, D.A. Kharkevich, J. Kreuter, Delivery of loperamide across the blood-brain barrier with polysorbate 80-coated polybutylcyanoacrylate nanoparticles, Pharm. Res. 14 (1997) 325–328.
[59] A. Sao Pedro, R. Fernandes, C.F. Villarreal, R. Fialho, E.C. Albuquerque, Opioid-based micro and nanoparticulate formulations: alternative approach on pain management, J. Microencapsul. 33 (2016) 18–29.
[60] M. Alam, C.T. Hartrick, Extended-release epidural morphine (DepoDur): an old drug with a new profile, Pain Pract. 5 (2005) 349–353.
[61] R.J. Balch, A. Trescot, Extended-release morphine sulfate in treatment of severe acute and chronic pain, J. Pain Res. 3 (2010) 191–200.
[62] K. Park, A. Otte, Prevention of opioid abuse and treatment of opioid addiction: current status and future possibilities, Annu. Rev. Biomed. Eng. 21 (2019) 61–84.
[63] K. Simon, Abuse-deterrent formulations: transitioning the pharmaceutical market to improve public health and safety-reply, Ther. Adv. Drug Saf. 6 (2015) 198–199.
[64] C. Contet, B.L. Kieffer, K. Befort, Mu opioid receptor: a gateway to drug addiction, Curr. Opin. Neurobiol. 14 (2004) 370–378.
[65] A. Cárdeno, M. Aparicio-Soto, S. Montserrat-de la Paz, B. Bermudez, F.J.G. Muriana, C. Alarcón-de-la-Lastra, Squalene targets pro- and anti-inflammatory mediators and pathways to modulate over-activation of neutrophils, monocytes and macrophages, J. Funct. Foods 14 (2015) 779–790.
[66] J. Feng, S. Lepetre-Mouelhi, A. Gautier, S. Mura, C. Cailleau, F. Coudore, M. Hamon, P. Couvreur, A new painkiller nanomedicine to bypass the blood-brain barrier and the use of morphine, Sci. Adv. 5 (2019) 5148.
[67] F.A. Oladosu, W. Maixner, A.G. Nackley, Alternative splicing of G protein-coupled receptors: relevance to pain management, Mayo Clin. Proc. 90 (2015) 1135–1151.
[68] E. Berrocoso, R. Rey-Brea, M. Fernandez-Arevalo, J.A. Mico, L. Martin-Banderas, Single oral dose of cannabinoid derivate loaded PLGA nanocarriers relieves neuropathic pain for eleven days, Nanomedicine 13 (2017) 2623–2632.
[69] J. Xie, D. Xiao, J. Zhao, N. Hu, Q. Bao, L. Jiang, L. Yu, Mesoporous silica particles as a multifunctional delivery system for pain relief in experimental neuropathy, Adv. Healthc. Mater. 5 (2016) 1213–1221.
[70] N.N. Jimenez-Vargas, J. Gong, M.J. Wisdom, D.D. Jensen, R. Latorre, A. Hegron, S. Teng, J.J. DiCello, P. Rajasekhar, N.A. Veldhuis, S.E. Carbone, Y. Yu, C. Lopez-Lopez, J. Jaramillo-Polanco, M. Canals, D.E. Reed, A.E. Lomax, B.L. Schmidt, K.W. Leong, S.J. Vanner, M.L. Halls, N.W. Bunnett, D.P. Poole, Endosomal signaling of delta opioid receptors is an endogenous mechanism and therapeutic target for relief from inflammatory pain, Proc. Natl. Acad. Sci. USA 117 (2020) 15281–15292.
[71] B.V. Muniz, D. Baratelli, S. Di Carla, L. Serpe, C.B. da Silva, V.A. Guilherme, L.N.M. Ribeiro, C.M.S. Cereda, E. de Paula, M.C. Volpato, F.C. Groppo, L.F. Fraceto, M. Franz-Montan, Hybrid hydrogel composed of polymeric nanocapsules co-loading lidocaine and prilocaine for topical intraoral anesthesia, Sci. Rep. 8 (2018) 17972.
[72] J. Gadsden, W.J. Long, Time to analgesia onset and pharmacokinetics after separate and combined administration of liposome bupivacaine and bupivacaine HCl: considerations for clinicians, Open Orthop. J. 10 (2016) 94–104.
[73] B.M. Ilfeld, Continuous peripheral nerve blocks: a review of the published evidence, Anesth. Analg. 113 (2011) 904–925.
[74] N.F. De Melo, D.R. De Araújo, R. Grillo, C.M. Moraes, A.P. De Matos, E. de Paula, A.H. Rosa, L.F. Fraceto, Benzocaine-loaded polymeric nanocapsules: study of the anesthetic activities, J. Pharm. Sci. 101 (2012) 1157–1165.
[75] N.F. Silva de Melo, E.V. Campos, C.M. Goncalves, E. de Paula, T. Pasquoto, R. de Lima, A.H. Rosa, L.F. Fraceto, Development of hydrophilic nanocarriers for the charged form of the local anesthetic articaine, Colloids Surf. B Biointerfaces 121 (2014) 66–73.
[76] N.F.S. Melo, E.V.R. Campos, M. Franz-Montan, E. Paula, C. Silva, C.R. Maruyama, T.P. Stigliani, R. Lima, D.R. Araujo, L.F. Fraceto, Characterization of articaine-loaded poly(ε-caprolactone) nanocapsules and solid lipid nanoparticles in hydrogels for topical formulations, J. Nanosci. Nanotechnol. 18 (2018) 4428–4438.
[77] E.V. Ramos Campos, N.F. Silva de Melo, V.A. Guilherme, E. de Paula, A.H. Rosa, D.R. de Araújo, L.F. Fraceto, Preparation and characterization of poly(ε-caprolactone) nanospheres containing the local anesthetic lidocaine, J. Pharm. Sci. 102 (2013) 215–226.

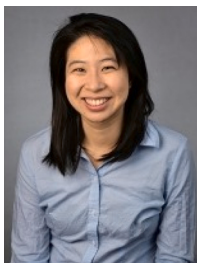
[78] O. Malik, A.D. Kaye, A. Kaye, K. Belani, R.D. Urman, Emerging roles of liposomal bupivacaine in anesthesia practice, J. Anaesthesiol. Clin. Pharmacol. 33 (2017) 151–156.
[79] J. Lalani, S. Patil, A. Kolate, R. Lalani, A. Misra, Protein-functionalized PLGA nanoparticles of lamotrigine for neuropathic pain management, AAPS PharmSciTech 16 (2015) 413–427.
[80] Y. Nakatani, H. Masuko, T. Amano, Effect of lamotrigine on Na(v)1.4 voltage-gated sodium channels, J. Pharmacol. Sci. 123 (2013) 203–206.
[81] F. Leng, J. Wan, W. Liu, B. Tao, X. Chen, Prolongation of epidural analgesia using solid lipid nanoparticles as drug carrier for lidocaine, Reg. Anesth. Pain Med. 37 (2012) 159–165.
[82] K.V. Chakravarthy, F.J. Boehm, P.J. Christo, Nanotechnology: a promising new paradigm for the control of pain, Pain Med. 19 (2018) 232–243.
[83] K. El-Boghdadly, A. Pawa, K.J. Chin, Local anesthetic systemic toxicity: current perspectives, Local Reg. Anesth. 11 (2018) 35–44.
[84] Y. He, L. Qin, Y. Huang, C. Ma, Advances of nano-structured extended-release local anesthetics, Nanoscale Res. Lett. 15 (2020) 13.
[85] K. Sekimoto, M. Tobe, S. Saito, Local anesthetic toxicity: acute and chronic management, Acute Med. Surg. 4 (2017) 152–160.
[86] P. Vadhanan, D.K. Tripaty, S. Adinarayanan, Physiological and pharmacologic aspects of peripheral nerve blocks, J. Anaesthesiol. Clin. Pharmacol. 31 (2015) 384–393.
[87] D.S. Kohane, J. Yieh, N.T. Lu, R. Langer, G.R. Strichartz, C.B. Berde, A re-examination of tetrodotoxin for prolonged duration local anesthesia, Anesthesiology 89 (1998) 119–131.
[88] C.S. Barnet, J.Y. Tse, D.S. Kohane, Site 1 sodium channel blockers prolong the duration of sciatic nerve blockade from tricyclic antidepressants, Pain 110 (2004) 432–438.
[89] C. Zhao, A. Liu, C.M. Santamaria, A. Shomorony, T. Ji, T. Wei, A. Gordon, H. Elofsson, M. Mehta, R. Yang, D.S. Kohane, Polymer-tetrodotoxin conjugates to induce prolonged duration local anesthesia with minimal toxicity, Nat. Commun. 10 (2019) 2566.
[90] Q. Liu, C.M. Santamaria, T. Wei, C. Zhao, T. Ji, T. Yang, A. Shomorony, B.Y. Wang, D.S. Kohane, Hollow silica nanoparticles penetrate the peripheral nerve and enhance the nerve blockade from tetrodotoxin, Nano Lett. 18 (2018) 32–37.
[91] J. Curley, J. Castillo, J. Hotz, M. Uezono, S. Hernandez, J.O. Lim, J. Tigner, M. Chasin, R. Langer, C. Berde, Prolonged regional nerve blockade. Injectable biodegradable bupivacaine/polyester microspheres, Anesthesiology 84 (1996) 1401–1410.
[92] S.A. Shankarappa, J.H. Tsui, K.N. Kim, G. Reznor, J.C. Dohlman, R. Langer, D.S. Kohane, Prolonged nerve blockade delays the onset of neuropathic pain, Proc. Natl. Acad. Sci. USA 109 (2012) 17555–17560.
[93] M.B. Sant'Anna, F.S.R. Lopes, L.F. Kimura, A.C. Giardini, O.A. Sant'Anna, G. Picolo, Crotoxin conjugated to SBA-15 nanostructured mesoporous silica induces long-last analgesic effect in the neuropathic pain model in mice, Toxins 11 (2019) (Basel).
[94] B.L. Woolbright, H. Jaeschke, Role of the inflammasome in acetaminophen-induced liver injury and acute liver failure, J. Hepatol. 66 (2017) 836–848.
[95] A. Federico, M. Dallio, C. Loguercio, Silymarin/silybin and chronic liver disease: a marriage of many years, Molecules 22 (2017).
[96] S. Das, P. Roy, R.G. Auddy, A. Mukherjee, Silymarin nanoparticle prevents paracetamol-induced hepatotoxicity, Int. J. Nanomed. 6 (2011) 1291–1301.
[97] P. Chinnagounder Periyasamy, J.C.H. Leijten, P.J. Dijkstra, M. Karperien, J.N. Post, Nanomaterials for the local and targeted delivery of osteoarthritis drugs, J. Nanomater. 2012 (2012) 1–13.
[98] P.D. Ramirez-Garcia, J.S. Retamal, P. Shenoy, W. Imlach, M. Sykes, N. Truong, L. Constandil, T. Pelissier, C.J. Nowell, S.Y. Khor, L.M. Layani, C. Lumb, D.P. Poole, T. Lieu, G.D. Stewart, Q.N. Mai, D.D. Jensen, R. Latorre, N.N. Scheff, B.L. Schmidt, J.F. Quinn, M.R. Whittaker, N.A. Veldhuis, T.P. Davis, N.W. Bunnett, A pH-responsive nanoparticle targets the neurokinin 1 receptor in endosomes to prevent chronic pain, Nat. Nanotechnol. 14 (2019) 1150–1159.
[99] J.O. Eloy, R. Petrilli, L.N.F. Trevizan, M. Chorilli, Immunoliposomes: a review on functionalization strategies and targets for drug delivery, Colloids Surf. B Biointerfaces 159 (2017) 454–467.
[100] S. Hua, P.J. Cabot, Targeted nanoparticles that mimic immune cells in pain control inducing analgesic and anti-inflammatory actions: a potential novel treatment of acute and chronic pain condition, Pain Physician 16 (2013) 199–216.
[101] J.W. Paul, S. Hua, M. Ilicic, J.M. Tolosa, T. Butler, S. Robertson, R. Smith, Drug delivery to the human and mouse uterus using immunoliposomes targeted to the oxytocin receptor, Am. J. Obstet. Gynecol. 216 (2017) 283.
[102] P. Girotra, S.K. Singh, A comparative study of orally delivered PBCA and ApoE coupled BSA nanoparticles for brain targeting of sumatriptan succinate in therapeutic management of migraine, Pharm. Res. 33 (2016) 1682–1695.
[103] P. Girotra, S.K. Singh, G. Kumar, Development of zolmitriptan loaded PLGA/poloxamer nanoparticles for migraine using quality by design approach, Int. J. Biol. Macromol. 85 (2016) 92–101.
[104] P. Girotra, A. Thakur, A. Kumar, S.K. Singh, Identification of multi-targeted anti-migraine potential of nystatin and development of its brain targeted chitosan nanoformulation, Int. J. Biol. Macromol. 96 (2017) 687–696.
[105] R.K. Portenoy, P. Lesage, Management of cancer pain, Lancet 353 (1999) 1695–1700.
[106] A.S. Gdowski, A. Ranjan, M.R. Sarker, J.K. Vishwanatha, Bone-targeted cabazitaxel nanoparticles for metastatic prostate cancer skeletal lesions and pain, Nanomedicine 12 (2017) 2083–2095 (Lond).
[107] H. Al-Waeli, B. Nicolau, L. Stone, L. Abu Nada, Q. Gao, M.N. Abdallah, E. Abdulkader, M. Suzuki, A. Mansour, A. Al Subaie, F. Tamimi, Chronotherapy of non-steroidal anti-inflammatory drugs may enhance postoperative recovery, Sci. Rep. 10 (2020) 468.
[108] G. Liu, J. Gao, H. Ai, X. Chen, Applications and potential toxicity of magnetic iron oxide nanoparticles, Small 9 (2013) 1533–1545.
[109] G. Mendoza, M. Arruebo, Light-triggered nanoparticles for pain management, Expert Opin. Drug Deliv. 17 (2020) 627–633.
[110] C.S. Linsley, B.M. Wu, Recent advances in light-responsive on-demand drug-delivery systems, Ther. Deliv. 8 (2017) 89–107.
[111] Y. Wang, D.S. Kohane, External triggering and triggered targeting strategies for drug delivery, Nat. Rev. Mater. 2 (2017) 17020.
[112] A.Y. Rwei, J.J. Lee, C. Zhan, Q. Liu, M.T. Ok, S.A. Shankarappa, R. Langer, D.S. Kohane, Repeatable and adjustable on-demand sciatic nerve block with phototriggerable liposomes, Proc. Natl. Acad. Sci. USA 112 (2015) 15719–15724.
[113] A.Y. Rwei, B.Y. Wang, T. Ji, C. Zhan, D.S. Kohane, Enhanced triggering of local anesthetic particles by photosensitization and photothermal effect using a common wavelength, Nano Lett. 17 (2017) 7138–7145.
[114] I. Ortiz de Solorzano, T. Alejo, M. Abad, C. Bueno-Alejo, G. Mendoza, V. Andreu, S. Irusta, V. Sebastian, M. Arruebo, Cleavable and thermo-responsive hybrid nanoparticles for on-demand drug delivery, J. Colloid Interface Sci. 533 (2019) 171–181.
[115] T. Alejo, V. Andreu, G. Mendoza, V. Sebastian, M. Arruebo, Controlled release of bupivacaine using hybrid thermoresponsive nanoparticles activated via photothermal heating, J. Colloid Interface Sci. 523 (2018) 234–244.
[116] M.C. Chen, H.A. Chan, M.H. Ling, L.C. Su, Implantable polymeric microneedles with phototriggerable properties as a patient-controlled transdermal analgesia system, J. Mater. Chem. B 5 (2017) 496–503.
[117] M.V. Padalkar, N. Pleshko, Wavelength-dependent penetration depth of near infrared radiation into cartilage, Analyst 140 (2015) 2093–2100.
[118] M.V. Vedunova, T.A. Mishchenko, E.V. Mitroshina, N.V. Ponomareva, A.V. Yudintsev, A.N. Generalova, S.M. Deyev, I.V. Mukhina, A.V. Semyanov, A.V. Zvyagin, Cytotoxic effects of upconversion nanoparticles in primary hippocampal cultures, RSC Adv. 6 (2016) 33656–33665.
[119] A.Y. Rwei, J.L. Paris, B. Wang, W. Wang, C.D. Axon, M. Vallet-Regi, R. Langer, D.S. Kohane, Ultrasound-triggered local anaesthesia, Nat. Biomed. Eng. 1 (2017) 644–653.
[120] Q. Yang, G.K. Nanayakkara, C. Drummer, Y. Sun, C. Johnson, R. Cueto, H. Fu, Y. Shao, L. Wang, W.Y. Yang, P. Tang, L.W. Liu, S. Ge, X.D. Zhou, M. Khan, H. Wang, X. Yang, Low-intensity ultrasound-induced anti-inflammatory effects are mediated by several new mechanisms including gene induction, immunosuppressor cell promotion, and enhancement of exosome biogenesis and docking, Front. Physiol. 8 (2017) 818.
[121] D.L. Miller, N.B. Smith, M.R. Bailey, G.J. Czarnota, K. Hynynen, I.R. Makin, Bioeffects committee of the American Institute of Ultrasound, J. Ultrasound Med. 31 (2012) 623–634.
[122] R. Aiyer, S.A. Noori, K.V. Chang, B. Jung, A. Rasheed, N. Bansal, E. Ottestad, A. Gulati, Pain Med. (2019).
[123] P. Tharkar, R. Varanasi, W.S.F. Wong, C.T. Jin, W. Chrzanowski, Nano-enhanced drug delivery and therapeutic ultrasound for cancer treatment and beyond, Front. Bioeng. Biotechnol. 7 (2019) 324.
[124] K. Cullion, L.C. Petishnok, T. Sun, C.M. Santamaria, G.L. Pemberton, N.J. McDannold, D.S. Kohane, Local anesthesia enhanced with increasing high-frequency ultrasound intensity, Drug Deliv. Transl. Res. 10 (2020) 1507–1516.
[125] G.W. Kim, C. Kang, Y.B. Oh, M.H. Ko, J.H. Seo, D. Lee, Ultrasonographic imaging and anti-inflammatory therapy of muscle and tendon injuries using polymer nanoparticles, Theranostics 7 (2017) 2463–2476.
[126] E. Jung, J. Noh, C. Kang, D. Yoo, C. Song, D. Lee, Ultrasound imaging and on-demand therapy of peripheral arterial diseases using H2O2-activated bubble generating anti-inflammatory polymer particles, Biomaterials 179 (2018) 175–185.
[127] A. van Walsem, S. Pandhi, R.M. Nixon, P. Guyot, A. Karabis, R.A. Moore, Relative benefit-risk comparing diclofenac to other traditional non-steroidal anti-inflammatory drugs and cyclooxygenase-2 inhibitors in patients with osteoarthritis or rheumatoid arthritis: a network meta-analysis, Arthritis Res. Ther. 17 (2015) 66.
[128] C.R. Falyar, Ultrasound-guided ankle blocks: a review of current practices, AANA J. 83 (2015) 357–364.
[129] C.L. Jeng, T.M. Torrillo, M.A. Rosenblatt, Complications of peripheral nerve blocks, Br. J. Anaesth. 105 Suppl. 1 (Suppl. 1) (2010) S97–S107.
[130] V.R. Mantha, H.K. Nair, R. Venkataramanan, Y.Y. Gao, K. Matyjaszewski, H. Dong, W. Li, D. Landsittel, E. Cohen, W.R. Lariviere, Nanoanesthesia: a novel, intravenous approach to ankle block in the rat by magnet-directed concentration of ropivacaine-associated nanoparticles, Anesth. Analg. 118 (2014) 1355–1362.
[131] S. Nadri, H. Mahmoudvand, A. Eatemadi, Magnetic nanogel polymer of bupivacaine for ankle block in rats, J. Microencapsul. 33 (2016) 656–662.
[132] S. Patel, S. Jana, R. Chetty, S. Thakore, M. Singh, R. Devkar, Toxicity evaluation of magnetic iron oxide nanoparticles reveals neuronal loss in chicken embryo, Drug Chem. Toxicol. 42 (2019) 1–8.

[133] M.A. Agotegaray, A.E. Campelo, R.D. Zysler, F. Gumilar, C. Bras, A. Gandini, A. Minetti, V.L. Massheimer, V.L. Lassalle, Magnetic nanoparticles for drug targeting: from design to insights into systemic toxicity. Preclinical evaluation of hematological, vascular and neurobehavioral toxicology, Biomater. Sci. 5 (2017) 772–783.
[134] Y.G. Toropova, A.S. Golovkin, A.B. Malashicheva, D.V. Korolev, A.N. Gorshkov, K.G. Gareev, M.V. Afonin, M.M. Galagudza, In vitro toxicity of FemOn, FemOn-SiO2 composite, and SiO2-FemOn core-shell magnetic nanoparticles, Int. J. Nanomed. 12 (2017) 593–603.
[135] M. Agotegaray, S. Palma, V. Lassalle, Novel chitosan coated magnetic nanocarriers for the targeted diclofenac delivery, J. Nanosci. Nanotechnol. 14 (2014) 3343–3347.
[136] H. Wu, F. Li, S. Wang, J. Lu, J. Li, Y. Du, X. Sun, X. Chen, J. Gao, D. Ling, Ceria nanocrystals decorated mesoporous silica nanoparticle based ROS-scavenging tissue adhesive for highly efficient regenerative wound healing, Biomaterials 151 (2018) 66–77.
[137] L. Zhu, Z. Zhou, H. Mao, L. Yang, Magnetic nanoparticles for precision oncology: theranostic magnetic iron oxide nanoparticles for image-guided and targeted cancer therapy, Nanomedicine 12 (2017) 73–87 (Lond).
[138] E. Amanzadeh, A. Esmaeili, R.E.N. Abadi, N. Kazemipour, Z. Pahlevanneshan, S. Beheshti, Quercetin conjugated with superparamagnetic iron oxide nanoparticles improves learning and memory better than free quercetin via interacting with proteins involved in LTP, Sci. Rep. 9 (2019) 6876.
[139] R. Enteshari Najafabadi, N. Kazemipour, A. Esmaeili, S. Beheshti, S. Nazifi, Using superparamagnetic iron oxide nanoparticles to enhance bioavailability of quercetin in the intact rat brain, BMC Pharmacol. Toxicol. 19 (2018) 59.
[140] R. Bilan, I. Nabiev, A. Sukhanova, Quantum dot-based nanotools for bioimaging, diagnostics, and drug delivery, ChemBioChem 17 (2016) 2103–2114.
[141] T.R. Pisanic 2nd, Y. Zhang, T.H. Wang, Quantum dots in diagnostics and detection: principles and paradigms, Analyst 139 (2014) 2968–2981.
[142] S.F. Husain, R.W.M. Lam, T. Hu, M.W.F. Ng, Z.Q.G. Liau, K. Nagata, S. Khanna, Y. Lam, K. Bhakoo, R.C.M. Ho, H.K. Wong, Locating the site of neuropathic pain in vivo using MMP-12-targeted magnetic nanoparticles, Pain Res. Manag. 2019 (2019) 9394715.
[143] B. Storek, M. Reinhardt, C. Wang, W.G.M. Janssen, N.M. Harder, M.S. Banck, J.H. Morrison, A.S. Beutler, Sensory neuron targeting by self-complementary AAV8 via lumbar puncture for chronic pain, Proc. Natl. Acad. Sci. USA 105 (2008) 1055–1060.
[144] Y. Lu, T.A. McNearney, W. Lin, S.P. Wilson, D.C. Yeomans, K.N. Westlund, Treatment of inflamed pancreas with enkephalin encoding HSV-1 recombinant vector reduces inflammatory damage and behavioral sequelae, Mol. Ther. J. Am. Soc. Gene Ther. 15 (2007) 1812–1819.
[145] J. Braz, C. Beaufour, A. Coutaux, A.L. Epstein, F. Cesselin, M. Hamon, M. Pohl, Therapeutic efficacy in experimental polyarthritis of viral-driven enkephalin overproduction in sensory neurons, J. Neurosci. 21 (2001) 7881–7888.
[146] A. Meunier, A. Latrémolière, A. Mauborgne, S. Bourgoin, V. Kayser, F. Cesselin, M. Hamon, M. Pohl, Attenuation of pain-related behavior in a rat model of trigeminal neuropathic pain by viral-driven enkephalin overproduction in trigeminal ganglion neurons, Mol. Ther. 11 (2005) 608–616.
[147] C. Hu, Z. Cai, Y. Lu, X. Cheng, Q. Guo, Z. Wu, Q. Zhang, Nonviral vector plasmid DNA encoding human proenkephalin gene attenuates inflammatory and neuropathic pain-related behaviors in mice, Neurosci. Lett. 634 (2016) 87–93.
[148] J.R. Goss, C.F. Harley, M. Mata, M.E. O'Malley, W.F. Goins, X. Hu, J.C. Glorioso, D.J. Fink, Herpes vector-mediated expression of proenkephalin reduces bone cancer pain, Ann. Neurol. 52 (2002) 662–665.
[149] J.R. Goss, M. Cascio, W.F. Goins, S. Huang, D.M. Krisky, R.J. Clarke, J.W. Johnson, H. Yokoyama, N. Yoshimura, M.S. Gold, J.C. Glorioso, HSV delivery of a ligand-regulated endogenous ion channel gene to sensory neurons results in pain control following channel activation, Mol. Ther. J. Am. Soc. Gene Ther. 19 (2011) 500–506.
[150] V. Thakur, M. Gonzalez, K. Pennington, M. Chattopadhyay, Viral vector mediated continuous expression of interleukin-10 in DRG alleviates pain in type 1 diabetic animals, Mol. Cell. Neurosci. 72 (2016) 46–53.
[151] H. Kanda, M. Kanao, S. Liu, H. Yi, T. Iida, R.C. Levitt, K.A. Candiotti, D.A. Lubarsky, S. Hao, HSV vector-mediated GAD67 suppresses neuropathic pain induced by perineural HIV gp120 in rats through inhibition of ROS and Wnt5a, Gene Ther. 23 (2016) 340–348.
[152] M. Kanao, H. Kanda, W. Huang, S. Liu, H. Yi, K.A. Candiotti, D.A. Lubarsky, R.C. Levitt, S. Hao, Gene transfer of glutamic acid decarboxylase 67 by herpes simplex virus vectors suppresses neuropathic pain induced by human immunodeficiency virus gp120 combined with ddC in rats, Anesth. Analg. 120 (2015) 1394–1404.
[153] T. Majima, Y. Funahashi, S. Takai, W.F. Goins, M. Gotoh, P. Tyagi, J.C. Glorioso, N. Yoshimura, Herpes simplex virus vector-mediated gene delivery of poreless TRPV1 channels reduces bladder overactivity and nociception in rats, Hum. Gene Ther. 26 (2015) 734–742.
[154] J.-P. Vit, P.T. Ohara, C. Sundberg, B. Rubi, P. Maechler, C. Liu, M. Puntel, P. Lowenstein, M. Castro, L. Jasmin, Adenovector GAD65 gene delivery into the rat trigeminal ganglion produces orofacial analgesia, Mol. Pain 5 (2009) 42.
[155] E.D. Milligan, R.G. Soderquist, S.M. Malone, J.H. Mahoney, T.S. Hughes, S.J. Langer, E.M. Sloane, S.F. Maier, L.A. Leinwand, L.R. Watkins, M.J. Mahoney, Intrathecal polymer-based interleukin-10 gene delivery for neuropathic pain, Neuron Glia Biol. 2 (2006) 293–308.
[156] M.Z. Yao, J.F. Gu, J.H. Wang, L.Y. Sun, H. Liu, X.Y. Liu, Adenovirus-mediated interleukin-2 gene therapy of nociception, Gene Ther. 10 (2003) 1392–1399.
[157] S. Maeda, A. Kawamoto, Y. Yatani, H. Shirakawa, T. Nakagawa, S. Kaneko, Gene transfer of GLT-1, a glial glutamate transporter, into the spinal cord by recombinant adenovirus attenuates inflammatory and neuropathic pain in rats, Mol. Pain 4 (2008) 65.
[158] A.M. Tan, O.A. Samad, S.D. Dib-Hajj, S.G. Waxman, Virus-mediated knockdown of Nav1.3 in dorsal root ganglia of STZ-induced diabetic rats alleviates tactile allodynia, Mol. Med. 21 (2015) 544–552 (Cambridge, Mass.).
[159] O.A. Samad, A.M. Tan, X. Cheng, E. Foster, S.D. Dib-Hajj, S.G. Waxman, Virus-mediated shRNA knockdown of Na(v)1.3 in rat dorsal root ganglion attenuates nerve injury-induced neuropathic pain, Mol. Ther. J. Am. Soc. Gene Ther. 21 (2013) 49–56.
[160] J. Kim, S.J. Kim, H. Lee, J.W. Chang, Effective neuropathic pain relief through sciatic nerve administration of GAD65-expressing rAAV2, Biochem. Biophys. Res. Commun. 388 (2009) 73–78.
[161] B. Lee, J. Kim, S.J. Kim, H. Lee, J.W. Chang, Constitutive GABA expression via a recombinant adeno-associated virus consistently attenuates neuropathic pain, Biochem. Biophys. Res. Commun. 357 (2007) 971–976.
[162] M.J. Eaton, B. Blits, M.J. Ruitenberg, J. Verhaagen, M. Oudega, Amelioration of chronic neuropathic pain after partial nerve injury by adeno-associated viral (AAV) vector-mediated over-expression of BDNF in the rat spinal cord, Gene Ther. 9 (2002) 1387–1395.
[163] A. Meunier, A. Latrémolière, E. Dominguez, A. Mauborgne, S. Philippe, M. Hamon, J. Mallet, J.-J. Benoliel, M. Pohl, Lentiviral-mediated targeted NF-κB blockade in dorsal spinal cord glia attenuates sciatic nerve injury–induced neuropathic pain in the rat, Mol. Ther. 15 (2007) 687–697.
[164] T. Sun, J. Luo, M. Jia, H. Li, K. Li, Z. Fu, Small interfering RNA-mediated knockdown of NF-κBp65 attenuates neuropathic pain following peripheral nerve injury in rats, Eur. J. Pharmacol. 682 (2012) 79–85.
[165] Z. Song, W. Zou, C. Liu, Q. Guo, Gene knockdown with lentiviral vector-mediated intrathecal RNA interference of protein kinase C gamma reverses chronic morphine tolerance in rats, J. Gene Med. 12 (2010) 873–880.
[166] W. Zou, Z. Song, Q. Guo, C. Liu, Z. Zhang, Y. Zhang, Intrathecal lentiviral-mediated RNA interference targeting PKCγ attenuates chronic constriction injury-induced neuropathic pain in rats, Hum. Gene Ther. 22 (2011) 465–475.
[167] A.G. Vanderwall, S. Noor, M.S. Sun, J.E. Sanchez, X.O. Yang, L.L. Jantzie, N. Mellios, E.D. Milligan, Effects of spinal non-viral interleukin-10 gene therapy formulated with d-mannose in neuropathic interleukin-10 deficient mice: behavioral characterization, mRNA and protein analysis in pain relevant tissues, Brain Behav. Immun. 69 (2018) 91–112.
[168] J.M. Isner, K. Walsh, J. Symes, A. Pieczek, S. Takeshita, J. Lowry, S. Rossow, K. Rosenfield, L. Weir, E. Brogi, R. Schainfeld, Arterial gene therapy for therapeutic angiogenesis in patients with peripheral artery disease, Circulation 91 (1995) 2687–2692.
[169] I. Baumgartner, A. Pieczek, O. Manor, R. Blair, M. Kearney, K. Walsh, J.M. Isner, Constitutive expression of phVEGF165 after intramuscular gene transfer promotes collateral vessel development in patients with critical limb ischemia, Circulation 97 (1998) 1114–1123.
[170] J.M. Isner, I. Baumgartner, G. Rauh, R. Schainfeld, R. Blair, O. Manor, S. Razvi, J.F. Symes, Treatment of thromboangiitis obliterans (Buerger's disease) by intramuscular gene transfer of vascular endothelial growth factor: preliminary clinical results, J. Vasc. Surg. 28 (1998) 964–973.
[171] D.W. Losordo, P.R. Vale, J.F. Symes, C.H. Dunnington, D.D. Esakof, M. Maysky, A.B. Ashare, K. Lathi, J.M. Isner, Gene therapy for myocardial angiogenesis: initial clinical results with direct myocardial injection of phVEGF165 as sole therapy for myocardial ischemia, Circulation 98 (1998) 2800–2804.
[172] P.R. Vale, D.W. Losordo, C.E. Milliken, M.C. McDonald, L.M. Gravelin, C.M. Curry, D.D. Esakof, M. Maysky, J.F. Symes, J.M. Isner, Randomized, single-blind, placebo-controlled pilot study of catheter-based myocardial gene transfer for therapeutic angiogenesis using left ventricular electromechanical mapping in patients with chronic myocardial ischemia, Circulation 103 (2001) 2138–2143.
[173] D.W. Losordo, P.R. Vale, R.C. Hendel, C.E. Milliken, F.D. Fortuin, N. Cummings, R.A. Schatz, T. Asahara, J.M. Isner, R.E. Kuntz, Phase 1/2 placebo-controlled, double-blind, dose-escalating trial of myocardial vascular endothelial growth factor 2 gene transfer by catheter delivery in patients with chronic myocardial ischemia, Circulation 105 (2002) 2012–2018.
[174] J. Kastrup, E. Jørgensen, A. Rück, K. Tägil, D. Glogar, W. Ruzyllo, H.E. Bøtker, D. Dudek, V. Drvota, B. Hesse, L. Thuesen, P. Blomberg, M. Gyöngyösi, C. Sylvén, Direct intramyocardial plasmid vascular endothelial growth factor-A165 gene therapy in patients with stable severe angina pectoris A randomized double-blind placebo-controlled study: the Euroinject one trial, J. Am. Coll. Cardiol. 45 (2005) 982–988.
[175] M.Z. Yao, J.F. Gu, J.H. Wang, L.Y. Sun, M.F. Lang, J. Liu, Z.Q. Zhao, X.Y. Liu, Interleukin-2 gene therapy of chronic neuropathic pain, Neuroscience 112 (2002) 409–416.
[176] E.D. Milligan, S.J. Langer, E.M. Sloane, L. He, J. Wieseler-Frank, K. O'Connor, D. Martin, J.R. Forsayeth, S.F. Maier, K. Johnson, R.A. Chavez, L.A. Leinwand, L.R. Watkins, Controlling pathological pain by adenovirally driven spinal production of the anti-inflammatory cytokine, interleukin-10, Eur. J. Neurosci. 21 (2005) 2136–2148.

[177] R.G. Soderquist, E.D. Milligan, J.A. Harrison, R.A. Chavez, K.W. Johnson, L.R. Watkins, M.J. Mahoney, PEGylation of interleukin-10 for the mitigation of enhanced pain states, J. Biomed. Mater. Res. A 93 (2010) 1169–1179.
[178] E.C. Dengler, L.A. Alberti, B.N. Bowman, A.A. Kerwin, J.L. Wilkerson, D.R. Moezzi, E. Limanovich, J.A. Wallace, E.D. Milligan, Improvement of spinal non-viral IL-10 gene delivery by D-mannose as a transgene adjuvant to control chronic neuropathic pain, J. Neuroinflamm. 11 (2014) 92.
[179] P.M. Grace, L.C. Loram, J.P. Christianson, K.A. Strand, J.G. Flyer-Adams, K.R. Penzkover, J.R. Forsayeth, A.-M. van Dam, M.J. Mahoney, S.F. Maier, R.A. Chavez, L.R. Watkins, Behavioral assessment of neuropathic pain, fatigue, and anxiety in experimental autoimmune encephalomyelitis (EAE) and attenuation by interleukin-10 gene therapy, Brain Behav. Immun. 59 (2017) 49–54.
[180] E. Sloane, S. Langer, B. Jekich, J. Mahoney, T. Hughes, M. Frank, W. Seibert, G. Huberty, B. Coats, J. Harrison, D. Klinman, S. Poole, S. Maier, K. Johnson, R. Chavez, L.R. Watkins, L. Leinwand, E. Milligan, Immunological priming potentiates non-viral anti-inflammatory gene therapy treatment of neuropathic pain, Gene Ther. 16 (2009) 1210–1222.
[181] S. Yamano, C.T. Viet, D. Dang, J. Dai, S. Hanatani, T. Takayama, H. Kasai, K. Imamura, R. Campbell, Y. Ye, J.C. Dolan, W.M. Kwon, S.D. Schneider, B.L. Schmidt, Ex vivo nonviral gene delivery of μ-opioid receptor to attenuate cancer-induced pain, Pain 158 (2017) 240–251.
[182] P.F. Pradat, F. Finiels, P. Kennel, S. Naimi, C. Orsini, P. Delaere, F. Revah, J. Mallet, Partial prevention of cisplatin-induced neuropathy by electroporation-mediated nonviral gene transfer, Hum. Gene Ther. 12 (2001) 367–375.
[183] J.-M.G. Guedon, S. Wu, X. Zheng, C.C. Churchill, J.C. Glorioso, C.-H. Liu, S. Liu, L. Vulchanova, A. Bekker, Y.-X. Tao, P.R. Kinchington, W.F. Goins, C.A. Fairbanks, S. Hao, Current gene therapy using viral vectors for chronic pain, Mol. Pain 11 (2015) 27.
[184] D.J. Fink, J. Wechuck, M. Mata, J.C. Glorioso, J. Goss, D. Krisky, D. Wolfe, Gene therapy for pain: results of a phase I clinical trial, Ann. Neurol. 70 (2011) 207–212.
[185] ⟨https://ClinicalTrials.gov/show/NCT01291901⟩.
[186] ⟨https://ClinicalTrials.gov/show/NCT03477487⟩.
[187] ⟨https://ClinicalTrials.gov/show/NCT04124042⟩.
[188] X. Therapeutics, 2021. ⟨http://xylocor.com/angina_trial.html⟩.
[189] ⟨https://ClinicalTrials.gov/show/NCT04125732⟩.
[190] C. Grines, G.M. Rubanyi, N.S. Kleiman, P. Marrott, M.W. Watkins, Angiogenic gene therapy with adenovirus 5 fibroblast growth factor-4 (Ad5FGF-4): a new option for the treatment of coronary artery disease, Am. J. Cardiol. 92 (2003) 24–31.
[191] T.D. Henry, C.L. Grines, M.W. Watkins, N. Dib, G. Barbeau, R. Moreadith, T. Andrasfay, R.L. Engler, Effects of Ad5FGF-4 in patients with angina: an analysis of pooled data from the AGENT-3 and AGENT-4 trials, J. Am. Coll. Cardiol. 50 (2007) 1038–1046.
[192] ⟨https://ClinicalTrials.gov/show/NCT00346437⟩.
[193] ⟨https://ClinicalTrials.gov/show/NCT02928094⟩.
[194] L.A. McDermott, G.A. Weir, A.C. Themistocleous, A.R. Segerdahl, I. Blesneac, G. Baskozos, A.J. Clark, V. Millar, L.J. Peck, D. Ebner, I. Tracey, J. Serra, D.L. Bennett, Defining the functional role of NaV1.7 in human nociception, Neuron 101 (2019) 905–919.
[195] A.M. Moreno, F. Alemán, G.F. Catroli, M. Hunt, M. Hu, A. Dailamy, A. Pla, S.A. Woller, N. Palmer, U. Parekh, D. McDonald, A.J. Roberts, V. Goodwill, I. Dryden, R.F. Hevner, L. Delay, G. Gonçalves dos Santos, T.L. Yaksh, P. Mali, Long-lasting analgesia via targeted in situ repression of NaV1.7 in mice, Sci. Transl. Med. 13 (2021) eaay9056.
[196] N. Farhang, J.M. Brunger, J.D. Stover, P.I. Thakore, B. Lawrence, F. Guilak, C.A. Gersbach, L.A. Setton, R.D. Bowles, CRISPR-based epigenome editing of cytokine receptors for the promotion of cell survival and tissue deposition in inflammatory environments, Tissue Eng. Part A 23 (2017) 738–749.
[197] L. Zhao, J. Huang, Y. Fan, J. Li, T. You, S. He, G. Xiao, D. Chen, Exploration of CRISPR/Cas9-based gene editing as therapy for osteoarthritis, Ann. Rheum. Dis. 78 (2019) 676–682.
[198] B. Lee, K. Lee, S. Panda, R. Gonzales-Rojas, A. Chong, V. Bugay, H.M. Park, R. Brenner, N. Murthy, H.Y. Lee, Nanoparticle delivery of CRISPR into the brain rescues a mouse model of fragile X syndrome from exaggerated repetitive behaviours, Nat. Biomed. Eng. 2 (2018) 497–507.
[199] M. Hryhorowicz, B. Grześkowiak, N. Mazurkiewicz, P. Śledziński, D. Lipiński, R. Słomski, Improved delivery of CRISPR/Cas9 system using magnetic nanoparticles into porcine fibroblast, Mol. Biotechnol. 61 (2019) 173–180.
[200] Q. Cheng, T. Wei, L. Farbiak, L.T. Johnson, S.A. Dilliard, D.J. Siegwart, Selective organ targeting (SORT) nanoparticles for tissue-specific mRNA delivery and CRISPR-Cas gene editing, Nat. Nanotechnol. 15 (2020) 313–320.
[201] S. Li, Z. Song, C. Liu, X.-L. Chen, H. Han, Biomimetic mineralization-based CRISPR/Cas9 ribonucleoprotein nanoparticles for gene editing, ACS Appl. Mater. Interfaces 11 (2019) 47762–47770.
[202] S.S. Rohiwal, N. Dvorakova, J. Klima, M. Vaskovicova, F. Senigl, M. Slouf, E. Pavlova, P. Stepanek, D. Babuka, H. Benes, Z. Ellederova, K. Stieger, Polyethylenimine based magnetic nanoparticles mediated non-viral CRISPR/Cas9 system for genome editing, Sci. Rep. 10 (2020) 4619.
[203] H. Liang, B. Peng, C. Dong, L. Liu, J. Mao, S. Wei, X. Wang, H. Xu, J. Shen, H.-Q. Mao, X. Gao, K.W. Leong, Y. Chen, Cationic nanoparticle as an inhibitor of cell-free DNA-induced inflammation, Nat. Commun. 9 (2018) 4291.
[204] E.K. Holl, K.L. Shumansky, G. Pitoc, E. Ramsburg, B.A. Sullenger, Nucleic acid scavenging polymers inhibit extracellular DNA-mediated innate immune activation without inhibiting anti-viral responses, PLoS One 8 (2013) 69413.
[205] E.K. Holl, K.L. Shumansky, L.B. Borst, A.D. Burnette, C.J. Sample, E.A. Ramsburg, B.A. Sullenger, Scavenging nucleic acid debris to combat autoimmunity and infectious disease, Proc. Natl. Acad. Sci. USA 113 (2016) 9728–9733.
[206] J. Lee, J.G. Jackman, J. Kwun, M. Manook, A. Moreno, E.A. Elster, A.D. Kirk, K.W. Leong, B.A. Sullenger, Nucleic acid scavenging microfiber mesh inhibits trauma-induced inflammation and thrombosis, Biomaterials 120 (2017) 94–102.
[207] J. Lee, J.W. Sohn, Y. Zhang, K.W. Leong, D. Pisetsky, B.A. Sullenger, Nucleic acid-binding polymers as anti-inflammatory agents, Proc. Natl. Acad. Sci. USA 108 (2011) 14055–14060.
[208] F. Liu, S. Sheng, D. Shao, Y. Xiao, Y. Zhong, J. Zhou, C.H. Quek, Y. Wang, Z. Hu, H. Liu, Y. Li, H. Tian, K.W. Leong, X. Chen, Propagation of spin waves in a 2D vortex network, Nano Lett. 21 (2021) 4708–4714.
[209] I. Naqvi, R. Gunaratne, J.E. McDade, A. Moreno, R.E. Rempel, D.C. Rouse, S.G. Herrera, D.S. Pisetsky, J. Lee, R.R. White, B.A. Sullenger, Polymer-mediated inhibition of pro-invasive nucleic acid DAMPs and microvesicles limits pancreatic cancer metastasis, Mol. Ther. 26 (2018) 1020–1031.
[210] E.K. Holl, J.E. Bond, M.A. Selim, T. Ehanire, B. Sullenger, H. Levinson, The nucleic acid scavenger polyamidoamine third-generation dendrimer inhibits fibroblast activation and granulation tissue contraction, Plast. Reconstr. Surg. 134 (2014) 420.
[211] D.S. Pisetsky, J. Lee, K.W. Leong, B.A. Sullenger, Nucleic acid-binding polymers as anti-inflammatory agents: reducing the danger of nuclear attack, Expert Rev. Clin. Immunol. 8 (2012) 1–3.
[212] M. Mittal, M.R. Siddiqui, K. Tran, S.P. Reddy, A.B. Malik, Reactive oxygen species in inflammation and tissue injury, Antioxid. Redox Signal. 20 (2014) 1126–1167.
[213] H.K. Kim, S.K. Park, J.L. Zhou, G. Taglialatela, K. Chung, R.E. Coggeshall, J.M. Chung, Reactive oxygen species (ROS) play an important role in a rat model of neuropathic pain, Pain 111 (2004) 116–124.
[214] X. Gao, H.K. Kim, J.M. Chung, K. Chung, Reactive oxygen species (ROS) are involved in enhancement of NMDA-receptor phosphorylation in animal models of pain, Pain 131 (2007) 262–271.
[215] T. Yoshitomi, A. Hirayama, Y. Nagasaki, The ROS scavenging and renal protective effects of pH-responsive nitroxide radical-containing nanoparticles, Biomaterials 32 (2011) 8021–8028.
[216] M. Fidanboylu, L.A. Griffiths, S.J. Flatters, Global inhibition of reactive oxygen species (ROS) inhibits paclitaxel-induced painful peripheral neuropathy, PLoS One 6 (2011) 25212.
[217] M. Lian, Z. Xue, X. Qiao, C. Liu, S. Zhang, X. Li, C. Huang, Q. Song, W. Yang, X. Chen, T. Wang, Movable hollow nanoparticles as reactive oxygen scavengers, Chem 5 (2019) 2378–2387.
[218] J.J. Yin, F. Lao, J. Meng, P.P. Fu, Y. Zhao, G. Xing, X. Gao, B. Sun, P.C. Wang, C. Chen, X.J. Liang, Inhibition of tumor growth by endohedral metallofullerenol nanoparticles optimized as reactive oxygen species scavenger, Mol. Pharmacol. 74 (2008) 1132–1140.
[219] J. Li, M. Guan, T. Wang, M. Zhen, F. Zhao, C. Shu, C. Wang, Gd@C82-(ethylenediamine)8 nanoparticle: a new high-efficiency water-soluble ROS scavenger, ACS Appl. Mater. Interfaces 8 (2016) 25770–25776.



Divya Bhansali obtained her Bachelors of Science in Biomedical Engineering from the University of Miami. She is currently a Ph.D. student in the Department of Biomedical Engineering at Columbia University. Her research interests include investigating nanoparticles and their application in therapeutic platforms for cancer treatment, pain management, and inflammation modulation. She is a recipient the NSF Graduate Research Fellowship and Columbia University's Blavatnik Presidential Fellowship.



Shavonne L. Teng obtained her Bachelor of Science in Neuroscience and Behavioral Biology from Emory University. She is currently a Ph.D. graduate student in the Department of Physiology and Cellular Biophysics at Columbia University Medical Center. She is mentored by Dr. Kam Leong at Columbia and Dr. Nigel Bunnett at NYU. Her research interests include utilizing nanoparticles to probe the mechanisms of endosomal signaling of GPCRs and to understand the role of GPCR signaling in chronic pain.



Caleb S. Lee received his B.S. in biological engineering and materials science and engineering at University of California, Berkeley. He is a Biomedical Engineering Ph.D. student at Columbia University jointly advised by Dr. Kam Leong and Dr. Raju Tomer to investigate brain disorders and nanomedicine.



Dr. Brian L. Schmidt is a surgeon and scientist. He earned his advanced degrees at the University of California, San Francisco. He is a Professor in the Departments of Oral and Maxillofacial Surgery and Neuroscience and Physiology. He directs Bluestone Center for Clinical Research at New York University as well as the NYU Oral Cancer Center. Dr. Schmidt's clinical efforts are dedicated to comprehensive surgical management of oral cancer; his scientific work explores the neurobiology of oral cancer pain. His clinical and basic science research have been funded by the NIH since 2005.



Nigel W. Bunnett obtained a Ph.D. from the University of Cambridge. Nigel serves as Professor and Chair of the Department of Molecular Pathobiology, Professor of Neuroscience and Physiology, and Member of Neuroscience Institute at New York University College. Nigel's laboratory investigates the mechanisms by which G protein-coupled receptors signal chronic pain and neurogenic inflammation. His laboratory has developed novel therapies that target receptors in endosomes and provide more effective and selective relief from chronic pain and inflammation. Nigel has ~ 350 peer-reviewed publications, which have received > 36,000 citations. Nigel is Editor-in-Chief of the American Journal of Physiology, Gastrointestinal and Liver Physiology.



Kam W. Leong is the Samuel Y. Sheng Professor of Biomedical Engineering at Columbia University. He received his Ph.D. in Chemical Engineering from the University of Pennsylvania. He has published ~ 450 peer-reviewed and holds more than 60 issued patents. The lab focuses on three major research directions: 1) Design of biomaterials for inflammation modulation; 2) Construction of patient-specific iPSC-derived brain organoids for disease modeling and drug discovery; 3) Development of nonviral gene editing systems in vivo. He is the Editor-in-Chief of Biomaterials, a member of the USA National Academy of Inventors, National Academy of Engineering, and National Academy of Medicine.

Laboratory Investigation
https://doi.org/10.1038/s41374-021-00593-7

ARTICLE

Serotonin-induced vascular permeability is mediated by transient receptor potential vanilloid 4 in the airways and upper gastrointestinal tract of mice

Jeffri S. Retamal[1,2] · Megan S. Grace[3,4,5,6] · Larissa K. Dill[3,7] · Paulina Ramirez-Garcia[1,2] · Scott Peng[1,2] · Arisbel B. Gondin[1,2] · Felix Bennetts[1] · Sadia Alvi[1] · Pradeep Rajasekhar[1,2] · Juhura G. Almazi[3] · Simona E. Carbone[1,2] · Nigel W. Bunnett[1,2,8] · Thomas P. Davis[2] · Nicholas A. Veldhuis[1,2] · Daniel P. Poole[1,2] · Peter McIntyre[3,9]

Received: 14 September 2020 / Revised: 12 March 2021 / Accepted: 14 March 2021
© The Author(s), under exclusive licence to United States and Canadian Academy of Pathology 2021

Abstract

Endothelial and epithelial cells form physical barriers that modulate the exchange of fluid and molecules. The integrity of these barriers can be influenced by signaling through G protein-coupled receptors (GPCRs) and ion channels. Serotonin (5-HT) is an important vasoactive mediator of tissue edema and inflammation. However, the mechanisms that drive 5-HT-induced plasma extravasation are poorly defined. The Transient Receptor Potential Vanilloid 4 (TRPV4) ion channel is an established enhancer of signaling by GPCRs that promote inflammation and endothelial barrier disruption. Here, we investigated the role of TRPV4 in 5-HT-induced plasma extravasation using pharmacological and genetic approaches. Activation of either TRPV4 or 5-HT receptors promoted significant plasma extravasation in the airway and upper gastrointestinal tract of mice. 5-HT-mediated extravasation was significantly reduced by pharmacological inhibition of the 5-HT_{2A} receptor subtype, or with antagonism or deletion of TRPV4, consistent with functional interaction between 5-HT receptors and TRPV4. Inhibition of receptors for the neuropeptides substance P (SP) or calcitonin gene-related peptide (CGRP) diminished 5-HT-induced plasma extravasation. Supporting studies assessing treatment of HUVEC with 5-HT, CGRP, or SP was associated with ERK phosphorylation. Exposure to the TRPV4 activator GSK1016790A, but not 5-HT, increased intracellular Ca^{2+} in these cells. However, 5-HT pre-treatment enhanced GSK1016790A-mediated Ca^{2+} signaling, consistent with sensitization of TRPV4. The functional interaction was further characterized in HEK293 cells expressing 5-HT_{2A} to reveal that TRPV4 enhances the duration of 5-HT-evoked Ca^{2+} signaling through a PLA_2 and PKC-dependent mechanism. In summary, this study demonstrates that TRPV4 contributes to 5-HT_{2A}-induced plasma extravasation in the airways and upper GI tract, with evidence supporting a mechanism of action involving SP and CGRP release.

These authors contributed equally: Jeffri S. Retamal, Megan S. Grace

✉ Nicholas A. Veldhuis
Nicholas.Veldhuis@monash.edu

✉ Daniel P. Poole
Daniel.Poole@monash.edu

[1] Drug Discovery Biology Theme, Monash Institute of Pharmaceutical Sciences, Monash University, Parkville, VIC, Australia

[2] ARC Centre of Excellence in Convergent Bio-Nano Science & Technology, Monash University, Parkville, VIC, Australia

[3] School of Medical Sciences and Health Innovations Research Institute, RMIT University, Bundoora, VIC, Australia

[4] Department of Physiology, School of Medicine Nursing and Health Sciences, Monash University, Clayton, VIC, Australia

[5] Baker IDI Heart and Diabetes Institute, Melbourne, VIC, Australia

[6] School of Clinical Medicine, Faculty of Medicine, University of Queensland, Brisbane, QLD, Australia

[7] Department of Neuroscience, Central Clinical School, Monash University, Melbourne, VIC, Australia

[8] Department of Molecular Pathobiology, New York University College of Dentistry, New York, NY, USA

[9] The Florey Institute of Neuroscience and Mental Health, Parkville, VIC, Australia

Published online: 15 April 2021

Introduction

The vasculature performs several important functions that are essential for maintaining fluid homeostasis. Endothelial cells make up the physical barrier in blood vessels that enables the control of fluid and molecule exchange from the circulation to the surrounding tissues. Physiological regulation of these barriers controls the extravasation of plasma proteins through inter-endothelial gaps, where cytoskeletal reorganization and disassembly of VE-cadherin junctions are essential regulators of endothelial permeability [1]. Disruption of these processes, as occurs in disease, is associated with unregulated movement and accumulation of fluids, leading to tissue edema.

Several inflammatory mediators, including proteases (e.g., thrombin), histamine, substance P (SP), and serotonin (5-HT) can activate specific receptors on vascular endothelial cells to promote changes in endothelial permeability. These changes can be mediated by an increase in intracellular calcium ($[Ca^{2+}]_i$) and activation of signaling pathways that regulate the contractile apparatus of cells, leading to cytoskeletal remodeling and disassembly of VE-Cadherin junctions [2]. This, in turn, causes endothelial cell contraction and cell junction disruption, resulting in increased endothelial permeability and tissue edema [2–6]. For example, increased endothelial $[Ca^{2+}]_i$ in pulmonary blood vessels leads to their constriction and to subsequent edema formation [3, 7, 8].

It has been demonstrated that systemic administration of 5-HT produces detrimental effects on the integrity of the endothelial barrier, leading to plasma extravasation into the surrounding tissue [9]. The biological actions of 5-HT are mediated through specific serotonin receptors ($5\text{-}HT_{1-7}$) [10], all of which are G protein-coupled receptors (GPCRs), with the notable exception of the $5\text{-}HT_3$ ligand-gated ion channel [11]. In addition to their well-defined roles in neurotransmission and clinical association with the pathogenesis of neurological diseases and neuropsychiatric disorders, 5-HT receptors are also key regulators of the homeostatic control of vasoconstriction and vascular permeability [12–14].

As previously described, elevated $[Ca^{2+}]_i$ in endothelial cells is required to cause barrier dysfunction. This elevation in $[Ca^{2+}]_i$ is triggered by mechanical stimuli or by activation of GPCRs and occurs in two phases, initiated by the release of Ca^{2+} from ER-stores and followed by entry of extracellular Ca^{2+} through cation channels [15]. Additionally, GPCR activation can also promote Ca^{2+} entry by activating cation channels, including transient receptor potential channels (TRP), which are the main non-selective cation channels in endothelial cells [1, 16]. The principal TRP channels that mediate endothelial cell permeability are TRPM2, TRPC1, 4 and 6 and vanilloid family members TRPV1 and 4 [17].

Transient Receptor Potential Vanilloid 4 (TRPV4) is an established enhancer of vascular permeability and edema that is expressed by a variety of cells including endothelia, peripheral sensory neurons, and immune cells [18–21]. TRPV4 is also a recognized promoter of neurogenic inflammation through enhanced release of neuropeptides, including SP and calcitonin gene-related peptide (CGRP), from peptidergic peripheral nerve endings [22, 23]. The sensitivity to ligand or mechanical activation, as well as the magnitude and duration of TRPV4 activity can be augmented by functional interactions (termed 'coupling') with GPCRs. These interactions are also known to be reciprocal, where functional coupling of a GPCR to an ion channel such as TRPV4 can lead to augmentation of GPCR signaling outputs. Furthermore, coupling between GPCRs and TRPV4 is proposed to contribute to disease-associated processes, including neurogenic inflammation and pain [24].

A well-characterized example of reciprocal coupling is illustrated through functional interactions between protease-activated receptors 1 and 2 (PAR1 and PAR2) and TRPV4 [20, 25, 26]. PAR activation can "sensitize" or reduce the activation threshold through channel phosphorylation and enhance TRPV4 signaling through the production of endogenous TRPV4 activators (e.g., arachidonic acid and 5′,6′-EET) [25–27]. Conversely, TRPV4 activity augments PAR1- and PAR2-dependent signaling, and this bidirectional PAR-TRPV4 relationship drives a significant component of PAR-evoked edema [20, 26, 27].

A variety of cell types co-express 5-HT receptors and TRPV4, highlighting their broader potential to functionally interact. Indeed, studies have demonstrated an important role for TRPV4 as an enhancer of 5-HT signaling associated with arterial smooth muscle proliferation [28, 29], pulmonary artery smooth muscle contraction [8, 19], itch [30], and visceral pain [31]. Immunohistochemistry and in situ hybridization studies have demonstrated that nociceptive dorsal root ganglion neurons mainly express 5-HT receptor subtypes 2A and 3 [32, 33]. Activation of $5\text{-}HT_{2A}$ expressed by these neurons promotes 5-HT-induced nociception and the release of SP and CGRP from peripheral nerve terminals, leading to a sustained increase in vascular permeability [34–38]. Neurogenic inflammation is initiated by the release of these neuropeptides [36, 39] and further studies have supported the involvement of neurogenic inflammation in 5-HT-evoked plasma extravasation by demonstrating significant inhibition of plasma protein extravasation with antimigraine drugs [40, 41].

Although there is strong evidence to support the importance of TRPV4 as an amplifier of 5-HT receptor signaling, the relative contribution of TRPV4 to 5-HT-induced edema

has not been defined in detail. We hypothesized that 5-HT-induced plasma extravasation is augmented by TRPV4 activity and is mediated, in part, through release of SP and CGRP from nerve fibers associated with microvasculature. In the present study, we found that the systemic administration of 5-HT-induced plasma extravasation in the airway and upper GI tract, particularly by the activation of $5HT_{2A}$, where the pharmacological inhibition or genetic deletion of TRPV4 attenuates 5-HT-induced plasma extravasation in the airways and upper GI tract, indicating a reciprocal coupling between 5-HT_{2A} and TRPV4 in vivo. In addition, in vitro studies indicated that 5-HT_{2A} interact with TRPV4 through the activation of PLA_2 and PKC. Moreover, we establish that inhibitors of NK_1R (SR140333) or the CGRP receptor (Olcegepant; BIBN4096) block 5-HT- and TRPV4-induced plasma extravasation in mice. These observations provide further mechanistic understanding of the important contribution that GPCR-TRP channel interactions have in fundamental biological processes, including the control of vascular permeability.

Materials and methods

Drugs and reagents

Evans Blue dye and GSK1016790A were purchased from Sigma-Aldrich (St. Louis, MO); 5-HT, HC067047, SR140333, GF 109203X (GFX), and BIBN 4096 (Olcegepant) were purchased from Tocris Bioscience (Bristol, UK); YM 26734 was from Cayman Chemical; WAY-100635 Maleate, GR 55562 dihydrochloride, GR113808 and SB 269970 hydrochloride were purchased from Abcam Australia (Melbourne, VIC Australia). Ketanserin and RS-127445 were purchased from Selleck Chemicals (Houston, TX. USA); Evans Blue was dissolved in sterile 0.9% saline. All drugs administered to mice were prepared on the day of experimentation in sterile 1% dimethyl sulfoxide (DMSO) in 0.9% saline.

Animals

All animal experiments adhered to the ARRIVE guidelines [42] and were carried out in accordance with the Guide for the Care and Use of Laboratory Animals. This study was approved by the Animal Ethics Committees of RMIT and Monash Institute of Pharmaceutical Sciences. Wild-type C57Bl/6J and $TRPV4^{-/-}$ (kindly provided by Dr. W Liedtke, Duke University) (6–12 weeks, male) were obtained from the Animal Resources Center (Canning Vale, WA), or from Monash Animal Research Platform, Monash University. All animals were maintained in a temperature-controlled (24 °C) environment with a 12 h light/dark cycle and with access to food and water ad libitum.

Measurement of plasma extravasation

Mice were anaesthetized with a combination of Ketamine (100 mg/kg i.p.) and Xylazine (10 mg/kg i.p.) and kept on a warming pad. The skin at the throat was removed to expose the jugular veins. Substances were i.v. administered by passing a needle through the *pectoralis major* muscle to prevent bleeding on withdrawal. Evans Blue dye (20 mg/kg) or 0.9% saline were administered into the jugular vein, 1 min before injection of agonist (5-HT or GSK1016790A, dosing as indicated in relevant sections) or vehicle (1% DMSO in 0.9% saline). Mice were killed (5 min post-agonist administration) by exsanguination and perfused with saline solution. Tissue samples were collected, weighed, and placed in formamide (≥18 h at 37 °C) to facilitate dye extraction. Absorbance of the extracts was determined against standard concentrations of Evans Blue at 620 nm using a FlexStation III plate reader (Molecular Devices, Sunnyvale, CA). Antagonists of 5-HT_{1A} (WAY-100635, 80 µg/kg) [43], 5-HT_{1B} (GR 55562, 300 µg/kg) [44], 5-HT_{2A} (ketanserin, 2 mg/kg) [45], 5-HT_{2B} (RS-127445, 300 µg/kg) [46], 5-HT_4 (GR 113808, 1 mg/kg) [47], 5-HT_7 (SB269973, 300 µg/kg) [46], TRPV4 (HC0670471, 10 mg/kg), NK_1R (SR140333, 1 mg/kg), or CGRP receptor (Olcegepant, 1 mg/kg) were i.p. injected 60 min prior to anesthetics. Results were expressed as the amount of Evans Blue dye per wet weight tissue (ng of EB/mg of tissue).

Human umbilical vein endothelial cell (HUVEC) culture

HUVEC were grown in endothelial growth medium (EGM, Lonza, Mount Waverley, VIC, Australia) containing 2% fetal bovine serum and a SingleQuots Supplement Pack (Lonza) as described [20].

Transient transfection

Constructs of pcDNA3.1$^+$ human 5-HT receptors subtype 1A, 1B, 2A, 2B, 4, and 7 (hHT_{1A-7}) plasmids were purchased from the cDNA Resource Center (Bloomsburg, PA, USA). Human Embryonic Kidney 293 cell line with tetracycline-inducible (T-Rex™ 293) TRPV4 overexpression (HEK-TRPV4) was grown at 37 °C in 5% CO_2 in DMEM containing 10% FBS (5 µg/mL blasticidin S). Cells were transiently transfected with hHT_{1A-7} plasmids (75 ng DNA/well, HEK-5-HT_{1A-7}) using the standard protocol for the FuGENE reagent system (Promega

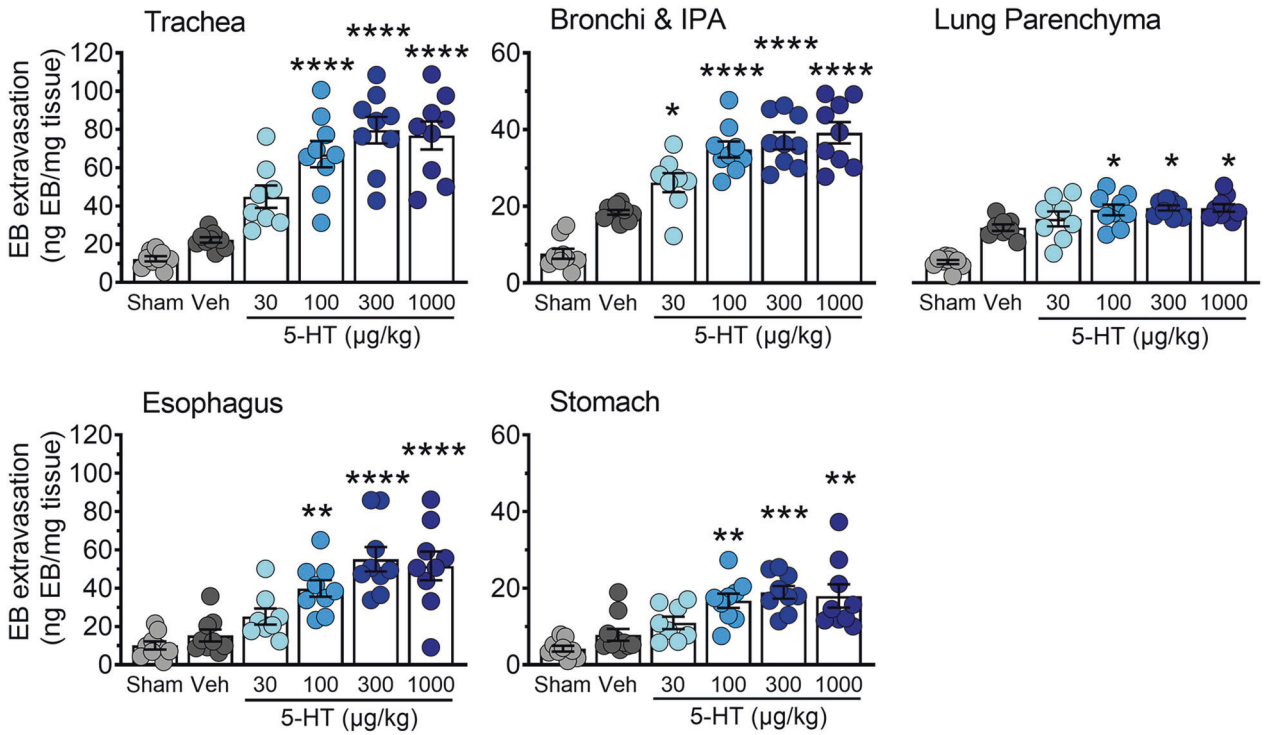


Fig. 1 5-HT causes vascular hyperpermeability in the airways and upper GI tract. Vascular hyperpermeability was assessed by the presence of Evans Blue in tissues of the airways, esophagus, and stomach following the intravenous injection of increasing concentrations of 5-HT (30–1000 µg/kg). Data are expressed as mean ± S.E.M., $n = 6$–9 mice per group. *$p < 0.05$; **$p < 0.01$; ***$p < 0.001$; ****$p < 0.0001$; significantly different compared to vehicle treatment (1% DMSO in 0.9% saline); one-way ANOVA and Dunnett's multiple comparisons test.

Corporation Madison, WI USA). Expression of TRPV4 was induced overnight with 0.1 µg/mL tetracycline.

Ca^{2+} signaling assays

HUVEC or HEK cells were seeded onto poly-D-lysine coated 96-well plates (15,000 cells/well) and cultured for 48 h. Cells were loaded with Fura2-AM ester (1 µM) in Hank's Balanced Salt Solution (HBSS) supplemented with probenecid (2 mM) and pluronic acid (0.5 µM) for 45 min at 37 °C. Fluorescence was measured at 340/380 nm excitation and 530 nm emission wavelengths using a FlexStation III plate reader. Baseline measurements were recorded for 20 s prior to agonist addition. Responses to agonists were recorded for 200 s post-addition. For the PKC and PLA_2 inhibition assay, cells were incubated 30 min prior to 5-HT addition, as previously described with GF 109203X (GFX, 100 nM) [26] or YM26734 (30 µM) [48].

ERK phosphorylation assays

HUVEC were seeded onto non-coated 96-well plates (15,000 cells/well) and cultured for 48 h. Cells were serum starved for 6 h and treated as described in the results section. Phospho-ERK 1/2 (pERK1/2) was measured using the AlphaScreen SureFire p-ERK 1/2 (Thr202/Tyr204) Assay Kit (PerkinElmer, USA), according to the manufacturer's specifications. Fluorescence was measured using the EnVision multilabel plate reader (PerkinElmer). Data were normalized to the positive control (PDBu, 1 µM).

Statistical analysis

Data were analyzed using GraphPad Prism 8 software (GraphPad Software, San Diego, CA, USA). All treatments were analyzed using one-way ANOVA with Dunnett's post-test. All data are presented as mean ± S.E.M., with a p value < 0.05 considered to be significantly different to the null hypothesis at the 95% confidence level.

Results

5-HT induces plasma extravasation in the airways and upper gastrointestinal tract

Evans Blue dye is commonly used as an indicator of altered vascular permeability to macromolecules due to its high

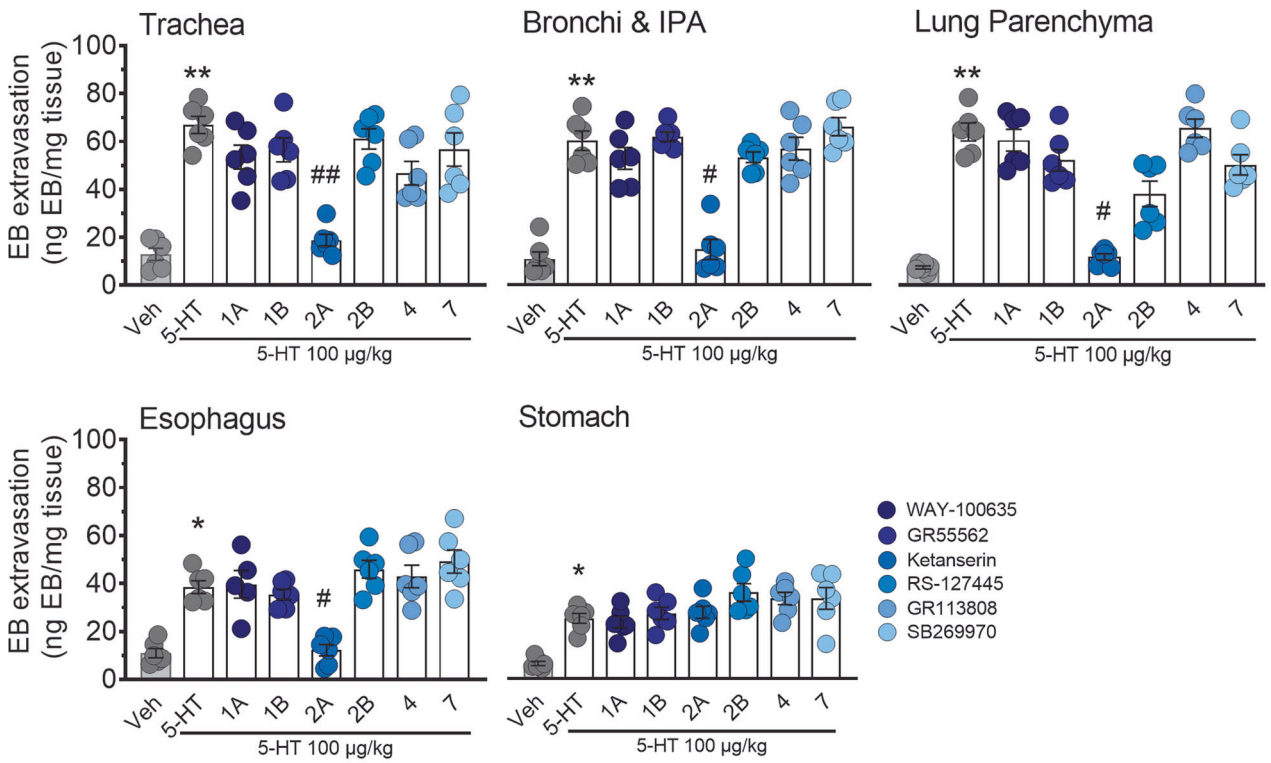


Fig. 2 5-HT-induced vascular hyperpermeability is inhibited in the airways and upper GI tract by the 5-HT$_{2A}$ selective antagonist ketanserin. Effect of WAY-100635 (5-HT$_{1A}$ antagonist, 80 µg/kg), GR 55562 (5-HT$_{1B}$ antagonist, 300 µg/kg), RS-127445 (5-HT$_{2B}$ antagonist, 300 µg/kg), GR 113808 (5-HT$_4$ antagonist, 1 mg/kg), or SB269973 (5-HT$_7$ antagonist, 300 µg/kg) in the airways and upper GI tract. Data are expressed as mean ± SEM for $n = 5$–6 experiments. *$p < 0.05$; **$p < 0.01$; One-way ANOVA and Dunnett's multiple comparisons test. * Indicates statistical significance compared to vehicle treatment, # indicates statistical significance compared to 5-HT 100 µg/kg treatment.

affinity for albumin. Under normal conditions, the vascular endothelium is impermeable to albumin, restricting albumin-bound Evans Blue to blood vessels. When inflammation occurs, albumin-bound Evans Blue is able to diffuse into surrounding tissues under conditions due to regulated, increased permeability of the vascular endothelium. Known as plasma extravasation, this process is important for promoting leukocyte infiltration, to initiate wound healing processes and subsequent swelling can also physically protect affected tissue [49].

To determine the effect of 5-HT on plasma extravasation, we examined the tissue distribution of Evans Blue following the administration of either vehicle (1% DMSO in 0.9% saline) or 5-HT (30–1000 µg/kg). For assessment of the natural absorbance of each tissue, an additional control group received an injection of saline solution without Evans Blue, followed by vehicle treatment. The vehicle treatment group did not exhibit significant basal leakiness of Evans Blue in the airways (trachea, bronchi and lung parenchyma) and upper gastrointestinal (GI) tract (esophagus and stomach) (Fig. 1). In contrast, the systemic administration of 5-HT elicited a dose-dependent increase in the amount of Evans Blue in tissues of the airways and upper GI tract, indicative of plasma extravasation (Fig. 1). A submaximal dose of 5-HT (100 µg/kg) was used in all subsequent experiments.

The pharmacological inhibition of 5-HT$_{2A}$ attenuates plasma extravasation in the airways and esophagus

To study the specific subtype of 5-HT receptor that is involved in 5-HT-induced plasma extravasation, mice were pre-treated with selective antagonists for 5-HT subtypes 1A (WAY-100635), 1B (GR 55562), 2A (ketanserin), 2B (RS-127445), 4 (GR 113808), or 7 (SB269973). The inhibition of 5-HT$_{2A}$ by ketanserin significantly attenuated plasma extravasation compared with vehicle pre-treated mice in the airways and esophagus (Fig. 2). However, ketanserin did not attenuate 5-HT-induced plasma extravasation in the stomach (Fig. 2). The inhibition of the 5-HT receptor subtypes 1A, 1B, 2B, 4, and 7 had no significant effect on 5-HT-induced plasma extravasation in the airways and upper GI tract compared with vehicle pre-treated mice, indicating that only 5-HT$_{2A}$ plays an important role on plasma extravasation.

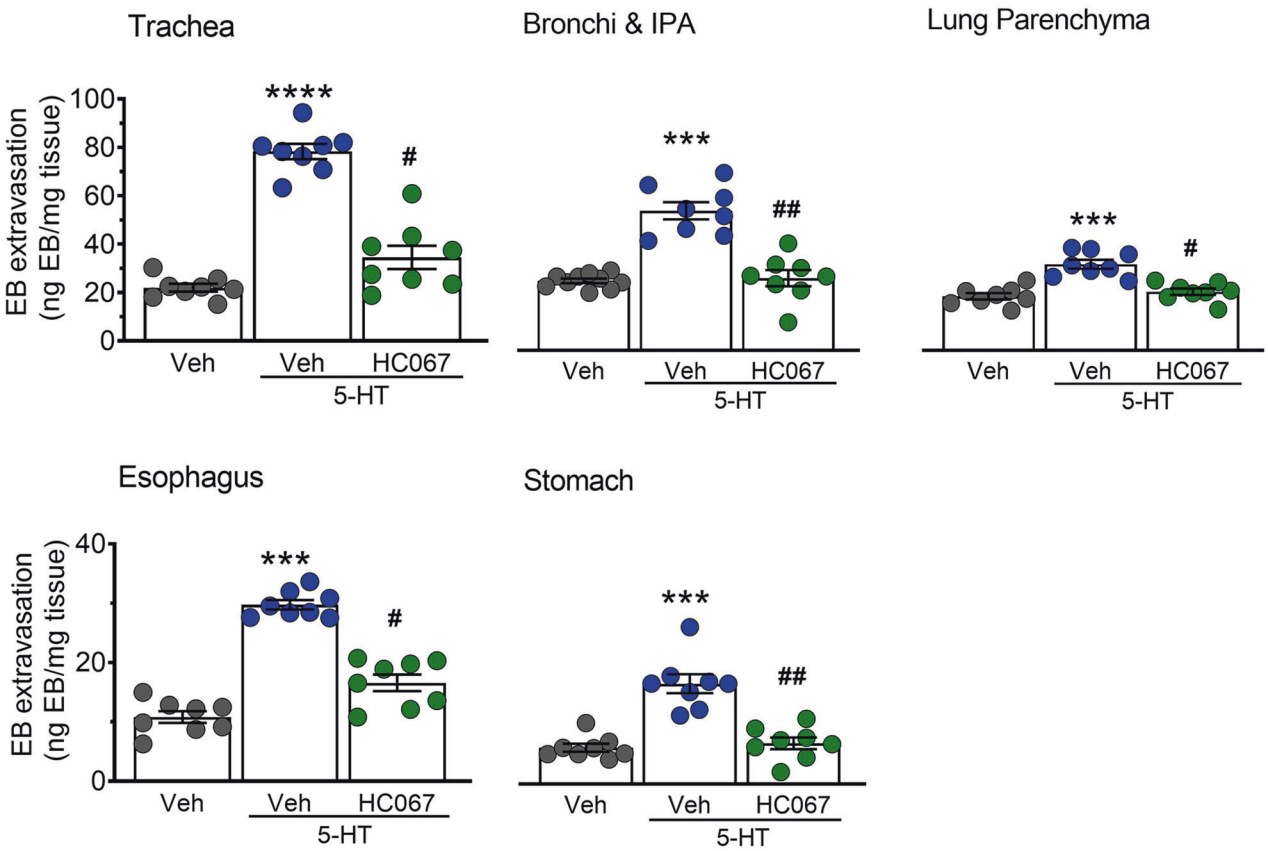


Fig. 3 Selective inhibition of TRPV4 suppresses 5-HT-induced edema. Effects of pre-treatment with the TRPV4 inhibitor HC067047 (10 mg/kg, HC067) on 5HT-induced plasma extravasation. HC067 significantly reduced Evans Blue leakage induced by 5-HT (100 µg/kg, i.v.). Data are expressed as mean ± S.E.M., $n = 8$ mice per group. $^{***}p < 0.001$; $^{****}p < 0.0001$; significantly different compared to vehicle treatment. $^{\#}p < 0.05$; $^{\#\#}p < 0.01$; significantly different compared to 5-HT treatment; one-way ANOVA and Dunnett's multiple comparisons test.

TRPV4 mediates 5-HT-induced plasma extravasation in the airways and upper GI tract

We have previously demonstrated that TRPV4 contributes to PAR1- and PAR2-dependent intracellular signaling and to PAR2-induced plasma extravasation [20, 26]. To determine whether TRPV4 plays an equivalent role in 5-HT-induced plasma extravasation, we administered the selective TRPV4 blocker HC067047 (HC067; 10 mg/kg, i.p.) prior to delivery of 5-HT. Inhibition of TRPV4 significantly decreased 5-HT-induced Evans Blue extravasation in the airways and upper GI tract, consistent with a TRPV4-dependent mechanism of action (Fig. 3).

5-HT-induced plasma extravasation requires TRPV4 expression

To confirm that 5-HT-induced plasma extravasation requires TRPV4 expression, we performed equivalent studies in TRPV4$^{-/-}$ mice or matched TRPV4$^{+/+}$ littermates. Previously, we reported that the selective TRPV4 activator GSK1016790A (GSK101) induced a dose-dependent increase in plasma extravasation in wild-type mice [20]. Consistent with our prior report, the administration of GSK101 (100 µg/kg) to wild-type mice induced a significant increase in plasma extravasation in the airways and upper GI tract (Fig. 4). Both GSK101- and 5-HT-induced plasma extravasation were abolished in TRPV4$^{-/-}$ mice (Fig. 4) when compared to TRPV4$^{+/+}$ mice. These data demonstrate the TRPV4-dependence of the 5-HT-evoked extravasation described.

TRPV4 enhanced 5-HT$_{2A}$ calcium signaling in HEK cells

The direct effect of 5-HT receptor signaling on TRPV4 activity was examined in an isolated cell system using HEK cells expressing the serotonin receptors (1A, 1B, 2A, 2B, or 4) alone or with co-expression of TRPV4. Assessment of 5-HT-mediated Ca^{2+} signaling over time (100 µM) demonstrated that HEK cells expressing 5-HT$_{1A,\ 1B,\ 2B}$ did not exhibit increased $[Ca^{2+}]_i$ in response to 5-HT (Fig. 5A).

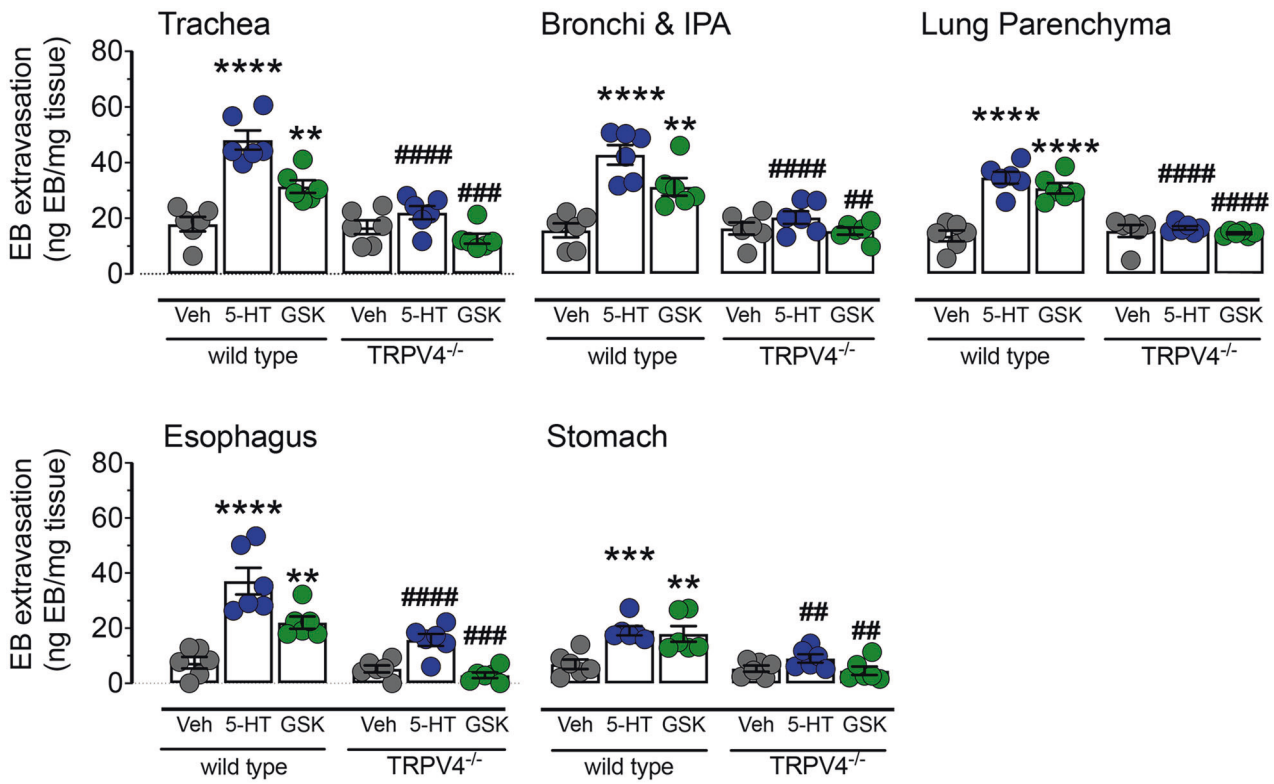


Fig. 4 5-HT and TRPV4-induced edema is absent in TRPV4$^{-/-}$ mice. The TRPV4 agonist GSK1016790A (100 µg/kg, i.v.; GSK) or 5-HT (100 µg/kg, i.v.) caused significant leakage of Evans Blue in the airway and upper GI tract of wild-type mice. Both 5-HT- and TRPV4-induced edema was significantly reduced in TRPV4$^{-/-}$ mice compared to wild-type littermate controls. Data are presented as mean ± S.E.M., $n = 6$ mice per group. * Significantly different compared to vehicle treated wild-type; $^{*}p < 0.05$; $^{**}p < 0.01$; $^{***}p < 0.001$; $^{****}p < 0.0001$. # Significantly different compared to 5-HT- or GSK1016790A-treated wild-type; $^{\#}p < 0.05$; $^{\#\#}p < 0.01$; $^{\#\#\#}p < 0.001$; $^{\#\#\#\#}p < 0.0001$; one-way ANOVA and Dunnett's multiple comparisons test.

Expression of TRPV4 did not influence this response. In contrast, stimulation of HEK-5-HT$_{2A}$ cells resulted in a rapid, transient elevation in $[Ca^{2+}]_i$ that returned to baseline within 40 s, consistent with Gq-coupled signaling. Furthermore, the duration of the Ca^{2+} response was markedly sustained in cells functionally expressing TRPV4 (Fig. 5B). Stimulation of HEK-5HT$_4$ also revealed a Ca^{2+} transient that was only moderately enhanced in cells co-expressing TRPV4 (Fig. 5C).

Based on the robust nature of 5HT$_{2A}$-TRPV4 coupling, we focused on 5-HT$_{2A}$ and used known mediators of GPCR-TRPV4 coupling [24] to define the signaling mechanisms involved. The 5-HT$_{2A}$ dependence of the Ca^{2+} response was initially confirmed using ketanserin (Fig. 5B). Changes in $[Ca^{2+}]_i$ were then quantified over time by assessing the amplitude of the acute phase after 5-HT stimulation (0–20 s) and the magnitude of the sustained plateau phase (20–80 s post-stimulation). 5-HT$_{2A}$ transactivates phospholipase A2 (PLA_2) to generate arachidonic acid (AA), an endogenous activator of TRPV4 [50–53]. G_q-coupled activation of Protein Kinase C (PKC) can lead to rapid phosphorylation of intracellular regulatory domains of non-selective cation channels to modulate their ionic permeability [24]. To determine if PLA_2 and PKC serve as intermediates of 5-HT$_{2A}$-TRPV4 coupling, cells were treated with the PLA_2 inhibitor YM 26734 (30 µM) or the PKC inhibitor GF 109203X (GFX; 100 nM). Neither inhibitor affected the initial peak of the 5-HT response (Fig. 5D, E). Both inhibitors significantly suppressed the sustained phase (Fig. 5D, F). In addition, removal of extracellular Ca^{2+} abolished the transient and sustained phase of the 5-HT-evoked $[Ca^{2+}]_i$ response (Fig. 5D). These results suggest that coupling to TRPV4 enhances 5-HT$_{2A}$ receptor signaling predominantly through influx of extracellular Ca^{2+}.

Neuropeptide receptors contribute to TRPV4- and 5-HT-induced edema

Neuropeptides including CGRP and SP are released from sensory terminals that innervate blood vessels. These neuropeptides can influence endothelial barrier function and promote tissue edema through direct actions on microvascular endothelial cells [22, 54]. We assessed the contribution of CGRP and SP receptors to 5-HT- and TRPV4-induced plasma extravasation using selective antagonists of either the CGRP receptor (Olcegepant) or NK_1R

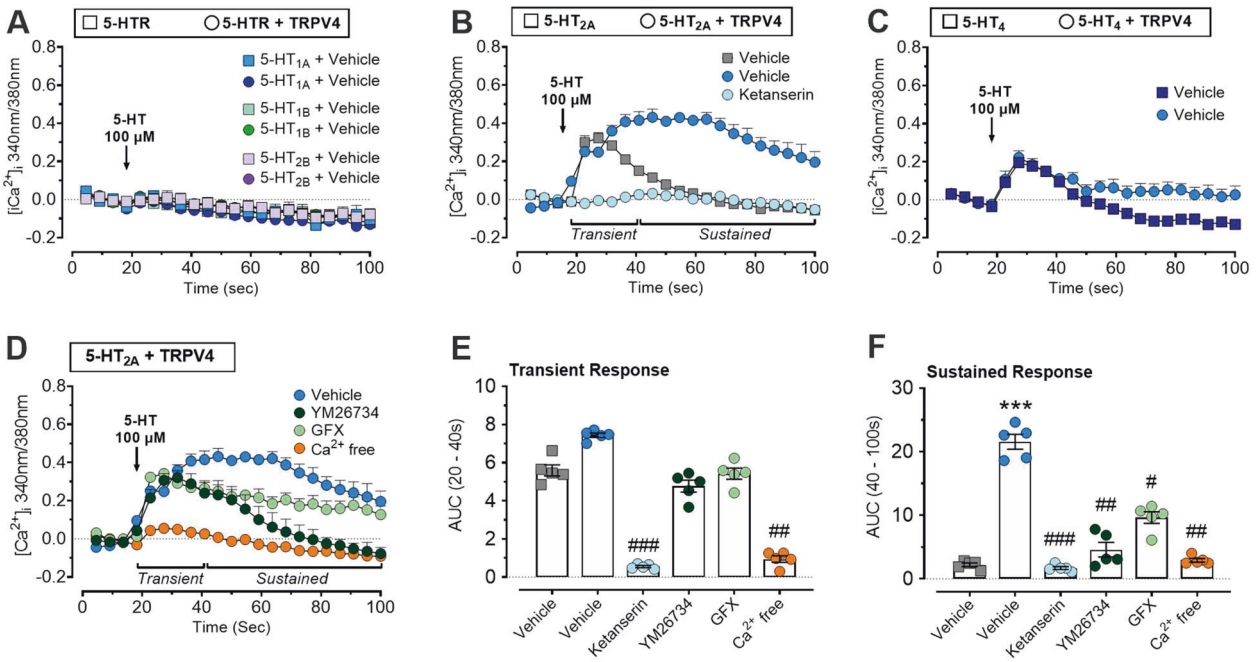


Fig. 5 5-HT induced a sustained increase in $[Ca^{2+}]_i$ in HEK cells co-expressing 5-HT_{2A} receptor and TRPV4. A Time traces showing responses to 5-HT (100 µM) by HEK cells expressing 5-HT_{1A}, 5-HT_{1B} or 5-HT_{2A} alone (circles) or with coexpression of TRPV4 (squares). **B** Time traces showing responses to 5-HT (100 µM) by HEK cells expressing 5-HT_{2A} or coexpressing 5-HT_{2A}/TRPV4. 5-HT-induced $[Ca^{2+}]_i$ was abolished by ketanserin (10 µM). **C** Time traces showing responses to 5-HT (100 µM) by HEK cells expressing 5-HT_4 alone or with coexpression of TRPV4. **D** Effect of the depletion of extracellular Ca^{2+}, PLA_2 inhibitor YM 26734 (30 µM), or PKC inhibitor GF 109203X (GFX; 100 nM) in HEK cells co-expressing 5-HT_{2A}/TRPV4. **E**, **F** Area under the curve analysis from 60 to 100 s post 5-HT (100 µM) addition. Data are expressed as mean ± SEM for n = 5–6 independent replicates. *p < 0.05; **p < 0.01; One-way ANOVA and Dunnett's multiple comparisons test. * Indicates statistical significance compared to HEK cells expressing 5-HTR subtype, # indicates statistical significance compared to HEK co-expressing 5-HTR and TRPV4.

(SR140333). Both antagonists significantly decreased tissue edema in the airways, esophagus and stomach in animals treated with GSK101 (Fig. 6) and 5-HT (Fig. 7), consistent with a neurogenic mechanism of action.

5-HT signaling in vascular endothelial cells is independent of TRPV4

The direct effects of 5-HT-TRPV4 coupling on vascular endothelial cells were examined using HUVEC, which are known to functionally express both targets [20, 55]. Focusing initially on Ca^{2+} mobilization, exposure to 100 nM or 1 µM 5-HT did not increase in $[Ca^{2+}]_i$. This is consistent with signaling through a G_q-independent mechanism (Fig. 8A). In contrast, GSK101 evoked a concentration-dependent elevation of $[Ca^{2+}]_i$ and this was attenuated with prior treatment with HC067 (Fig. 8A), thus confirming functional expression of TRPV4. Pre-treatment with 5-HT (100 nM; 30 min) enhanced GSK101-mediated $[Ca^{2+}]_i$ signaling in HUVECs (Fig. 8A, B). Specifically, 5-HT pre-treatment promoted a modest shift in pEC_{50} from −8.69 M to −9 M and increased E_{max} from 49.52 to 64.58 (Fig. 8A). This demonstrates a significant 5-HT-evoked amplification of TRPV4 signaling. Functional expression of 5-HT receptors was further confirmed by measuring levels of phosphorylated ERK (pERK), which allows for assessment of signaling through convergent pathways downstream of GPCRs. ERK activation was maximal at 2 min post-5-HT addition (100 nM or 1 µM) and decreased gradually over the 30 min assessment period. In contrast, GSK101 did not stimulate pERK in these cells (Fig. 8C). We confirmed that exposure to either SP (100 nM or 1 µM) or CGRP (100 nM or 1 µM) promotes a rapid and robust increase in pERK levels in HUVEC (Fig. 8D). Together, these data indicate that 5-HT receptors can sensitize and augment TRPV4 activity. These observations suggest that enhanced vascular permeability in response to 5-HT is potentially mediated through an indirect mechanism involving the TRPV4-dependent release of the neuropeptides SP and CGRP, possibly from external cellular sources such as primary afferent terminals.

Discussion

TRPV4 activation is important for the pathogenesis of pulmonary edema associated with heart failure or

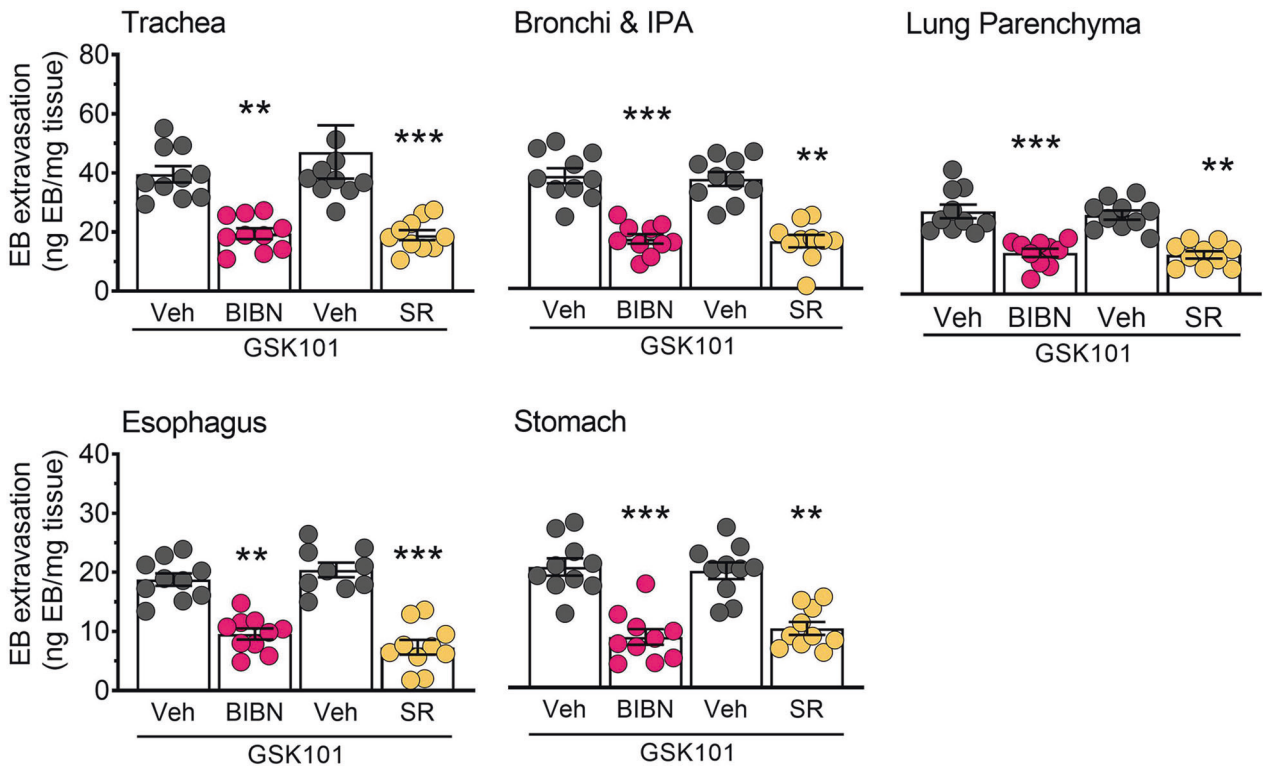


Fig. 6 TRPV4-induced edema is decreased by inhibition of CGRP or NK_1 receptors. Pre-treatment with the CGRP receptor antagonist BIBN4906 (BIBN; 1 mg/kg) or NK_1R antagonist SR140333 (SR; 1 mg/kg) significantly decreased tissue edema induced by GSK1016790A (100 µg/kg) compared to vehicle treatment in the airways and upper GI tract. Data are presented as mean ± S.E.M., $n = 9$–10 mice per group. $^{**}p < 0.01$; $^{***}p < 0.001$; One-way ANOVA and Dunnett's multiple comparisons test, significantly different compared to vehicle treated control (Veh).

chemically-induced acute lung injury [18, 21]. TRPV4 is also a mediator of sepsis-induced endothelial dysfunction and increased vascular permeability [56]. Consistent with this, 5-HT is also a potent vasoactive and signaling mediator and can promote disruption of cell–cell junctions at concentrations not much higher than those normally present under resting conditions [56, 57]. Here, we showed that 5-HT promotes pulmonary and esophageal plasma extravasation through a TRPV4-dependent mechanism. This also involves activation of NK_1R and the CGRP receptor, consistent with a putative neurogenic mechanism involving release of SP and CGRP from nerve fibers innervating the vasculature.

5-HT is mainly produced by enterochromaffin cells of the intestine, and is largely taken up and stored by platelets, or metabolized by the liver [57]. However, the lungs also play an important role in both 5-HT production and removal, and release of 5-HT by platelets may be important in the pathology of certain pulmonary diseases [57–60]. Additionally, 5-HT can be locally synthesized and released from peripheral arteries [61–63]. The 5-HT-TRPV4 signaling pathway may mediate a number of pathologies, including pulmonary hypertension, arterial smooth muscle proliferation, visceral hypersensitivity, and itch [8, 28, 30, 31]. Results of the present study suggest that the 5-HT receptor-TRPV4 axis could be an important pathway in pathologies, such as sepsis, where plasma 5-HT levels are known to be significantly elevated [64].

We have recently demonstrated that the potent and selective TRPV4 agonist, GSK101, caused dose-dependent extravasation in the airways and upper GI tract of mice, which was inhibited by the selective TRPV4 antagonist HC067 [20]. In contrast, GSK101 did not cause plasma extravasation in the bladder, heart, liver or kidney, suggesting that edema is not a general systemic effect of TRPV4 activation [20]. In the present study, we report that 5-HT induces plasma extravasation in the airways, esophagus and the stomach. Plasma extravasation induced by 5-HT was decreased by HC067 or TRPV4 deletion and limited to the tissues in which the TRPV4 activation caused edema, namely the airways and upper gut. These results support a role for TRPV4 in promoting 5-HT-induced plasma extravasation in the airways, esophagus and stomach. Extravasation in response to 5-HT was almost completely blocked by the TRPV4-specific

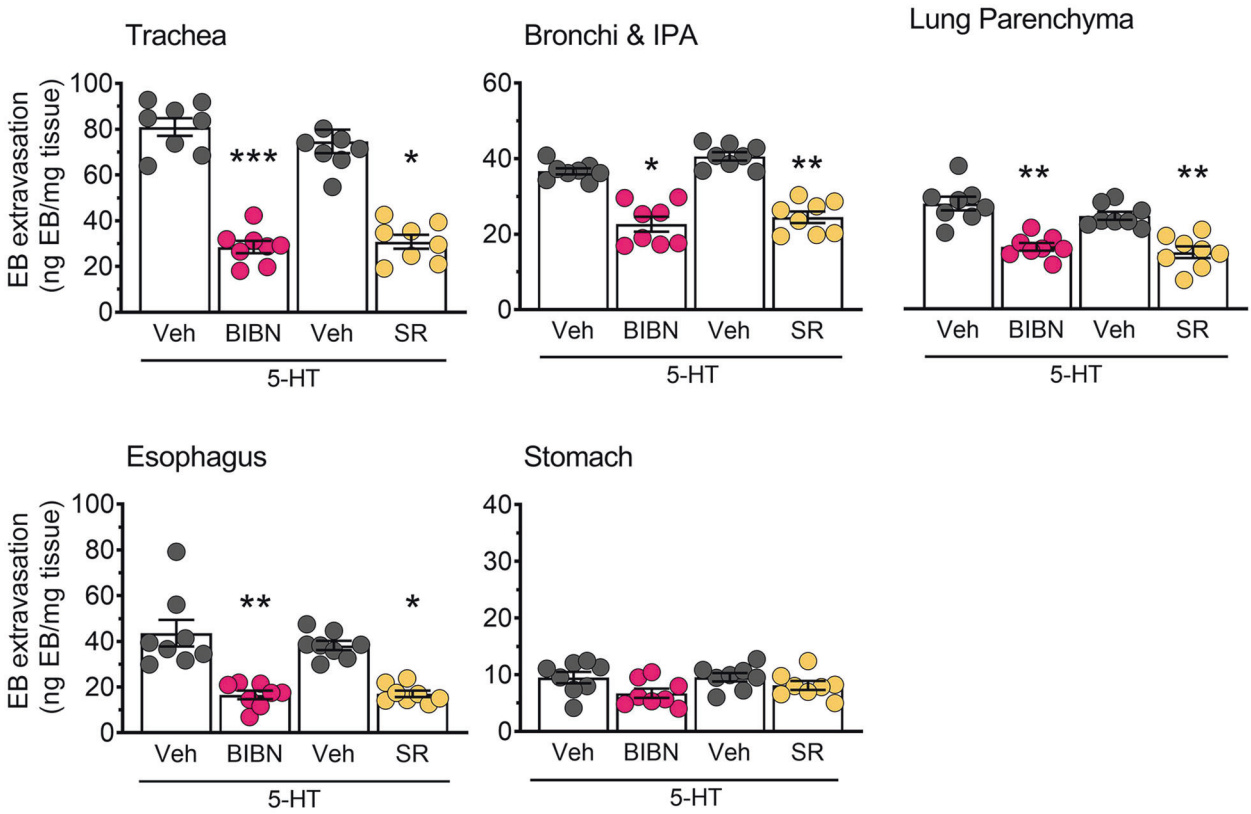


Fig. 7 Inhibition of CGRP or NK_1 receptors blocks 5-HT induced edema. Pre-treatment with the CGRP receptor antagonist BIBN4906 (BIBN; 1 mg/kg) or the NK_1R antagonist SR140333 (SR; 1 mg/kg) decreased plasma extravasation induced by 5-HT (100 µg/kg) in the airways and upper GI tract. Data are presented as mean ± S.E.M., $n = 9–10$ mice per group. $*p < 0.05$; $**p < 0.01$; $***p < 0.001$; One-way ANOVA and Dunnett's multiple comparisons test, significantly different compared to vehicle treated control (Veh).

inhibitor HC067. In contrast, the extent of GSK101-induced TRPV4-dependent vascular leak was markedly lower. Although this may be due to differences in the respective signaling pathways involved, it may also reflect the physicochemical properties of the ligands investigated and their relative bioavailability following systemic administration.

The release of neuropeptide transmitters from airway innervating nerves leads to inflammation and to vascular leak. This neurogenic response can also be initiated by exogenous irritants via airway nerves and may contribute to the development of airway pathologies [65–67]. We demonstrated that inhibitors of CGRP and SP receptors reduced TRPV4- and 5-HT-induced plasma extravasation in the airways and esophagus, supporting a mechanistic role for these neuropeptide receptors. It has been reported that CGRP does not cause microvascular leak in the airways and bladder of the guinea pig [68]. In contrast, CGRP has been reported to contribute to edema formation in mice [66] and rats [69], indicating potential species differences. Our results suggest that 5-HT-induced plasma extravasation in the airways and esophagus is mediated by activation of afferent nerves, requires TRPV4, and is likely to involve release of pro-inflammatory peptides (SP and CGRP) (Fig. 9).

Pre-clinically, TRPV4 plays important roles in pathological pulmonary edema and may therefore be a therapeutically useful target. Importantly, chronic treatment with a TRPV4 inhibitor in animal models did not affect osmoregulation or interfere with the activity of diuretics, which are often used to resolve edema in the clinic [18, 70–72]. Recently, a double-blind, placebo-controlled study using a selective TRPV4 antagonist reported that treatment with GSK2798745 resulted in a trend to improve pulmonary gas exchange in symptomatic patients with chronic heart failure [71, 73]. However, the use of inhibitors that directly target TRPV4 in pulmonary injury may be contraindicated by the role that TRPV4 plays in the complex signaling cascade that mediates hypoxic pulmonary vasoconstriction [74]. This mechanism helps to redistribute blood flow from poorly ventilated to more aerated lung areas, and inhibition of this response could be detrimental to patients with lung

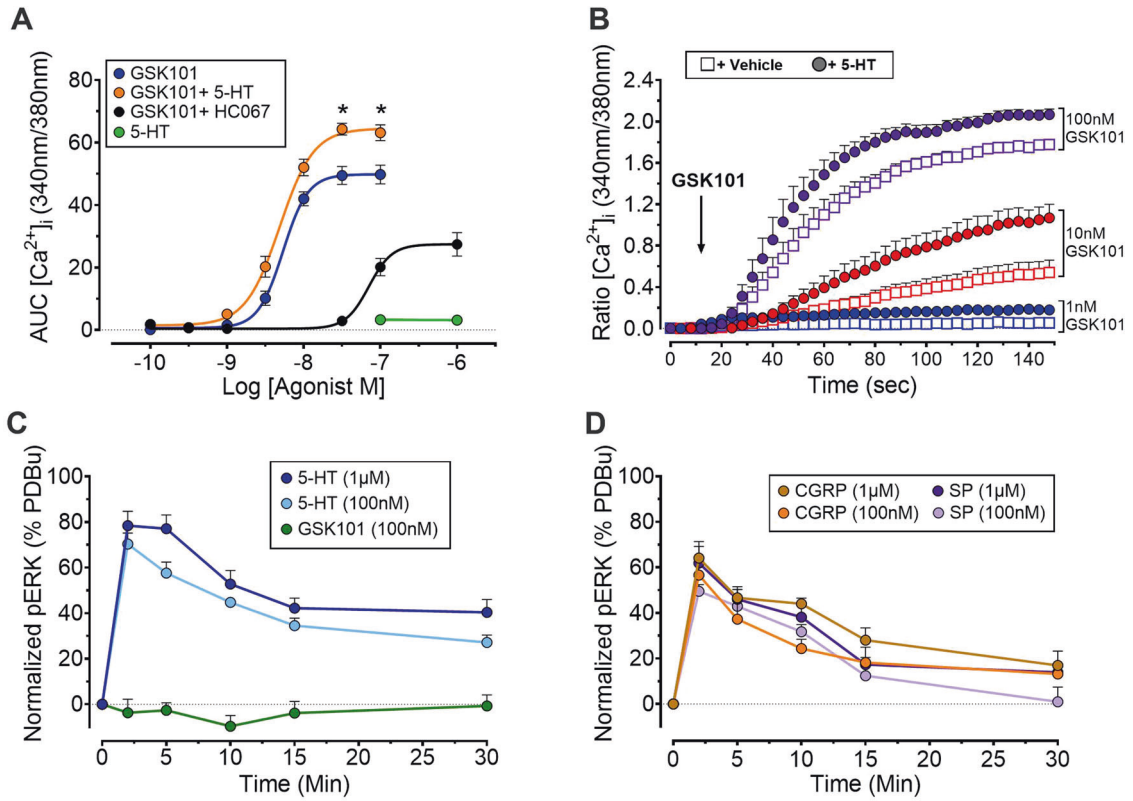


Fig. 8 Functional expression and interaction of TRPV4 and 5-HT receptors in HUVEC. A Pre-treatment with 5-HT augmented the magnitude (E_{max}) of responses to GSK101. GSK101-induced Ca^{2+} signaling was attenuated by the TRPV4 antagonist HC067. No change in $[Ca^{2+}]_i$ was detected following treatment with 5-HT. **B** Time traces demonstrating the effect of pre-treatment with 5-HT (open circle, 100 nM; 30 min) on GSK101-induced elevations in $[Ca^{2+}]_i$ (closed circles). **C**, **D** Elevated ERK phosphorylation (pERK) in response to treatment of HUVEC with 5-HT, GSK101, CGRP or SP. Data are presented as mean ± S.E.M., $n = 6$ technical replicates, pERK data are normalized to the positive control (PDBu, 1 μM).

disease [71, 73]. The benefits of TRPV4 antagonists for reducing pulmonary edema-associated lethality from severe acute respiratory syndrome coronavirus 2 (SARS-CoV-2) have also recently been proposed to outweigh the risks of contraindications such as these. Together, this highlights the need to further understand the relative cellular contribution of TRPV4 activity and also the upstream signaling mediators that lead to TRPV4 activation, to provide potential alternatives to these potent antagonists that directly inhibit TRPV4.

Our pharmacological data indicate that 5-HT_{2A} is the primary receptor subtype involved in promoting 5-HT-evoked plasma extravasation. Evidence supporting the in vivo requirement for TRPV4 activity is provided by the demonstration that 5-HT_{2A} mediated Ca^{2+} signaling is augmented by TRPV4 through a PLA_2- and PKC-dependent mechanism. Although our data support an indirect neurogenic mechanism of action involving enhanced neuropeptide release [23], the specific locations where 5-HT_{2A}-TRPV4 interactions occur (pre- or post-synaptic [75]) could not be definitively determined using available methodology. We cannot exclude a direct effect on endothelial cells as the HUVEC that we examined may not be the most suitable model for the microvasculature involved in 5-HT-dependent vascular leak as they are of a different origin and may not express the precise machinery required. Our results suggest that 5-HT and TRPV4 receptors are also expressed by endothelial cells and may cause protein leak via disruption of the vascular junctions in mice. In addition to expression by peptidergic afferent nerves [76] and vascular endothelial cells [77, 78], 5-HT receptors and TRPV4 are also expressed by immune cells, including macrophages [79–81]. Given the important immunomodulatory role of 5-HT, it is possible that the TRPV4-dependent effects of 5-HT on vascular permeability that we describe are mediated in part through immune cell activation. Future analysis to better define the relative contributions of 5-HT receptors and TRPV4 in endothelial and immune cells and on nerve endings of the different vascular beds would help to clarify the primary location of TRPV4-driven edema and the precise mechanisms involved.

In summary, we have established that TRPV4 mediates 5-HT-induced plasma extravasation in the airways and

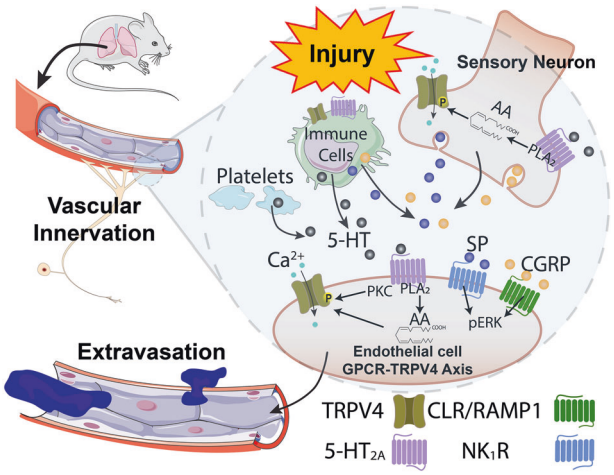


Fig. 9 Postulated neurogenic and direct mechanisms through which 5-HT receptors and TRPV4 may induce tissue edema. 5-HT activates 5-HT_{2A} receptor subtypes on afferent nerve terminals, immune cells, and vascular endothelial cells. Activation of peripheral sensory neurons or local immune cells promotes release of neuropeptides including SP and CGRP, activating NK_1R and CGRP receptors expressed by endothelial cells. Signaling downstream of these receptors leads to retraction of cell-cell junction proteins, leading to increased vascular leak and to tissue edema. Activation of 5-HT_{2A} sensitizes or activates TRPV4 through a PLA_2- and PKC-dependent mechanism, leading to enhanced neuropeptide release.

upper GI tract of mice through interaction with the 5-HT_{2A} receptor subtype. We have provided evidence to support an indirect, potentially neurogenic mechanism of action involving the neuropeptides SP and CGRP.

Data availability

Data presented in this study are available upon request from the corresponding authors.

Acknowledgements The authors thank Dr Wolfgang Liedtke (Duke University) for providing $TRPV4^{-/-}$ mice.

Author contributions *Participated in research design*: JSR, MSG, NWB, NAV, DPP, and PM. *Conducted experiments*: MSG, LKD, SP, FB, JSR, JGA, and SA. *Performed data analysis*: JSR, NAV, DPP, MSG, and PM. *Contributed to writing or critical assessment of the paper*: JSR, MSG, ABG, PR, PRG, SEC, NAV, DPP, and PM.

Funding Australian Research Council Center of Excellence in Convergent Bio-Nano Science and Technology (TPD, NWB, and NAV), NHMRC Australia 1046860 (PM, NWB), 1083480 (DPP).

Compliance with ethical standards

Conflict of interest The authors declare no competing interests.

Ethical approval Studies using mice were approved by the Animal Ethics Committees of RMIT and Monash Institute of Pharmaceutical Sciences.

Publisher's note Springer Nature remains neutral with regard to jurisdictional claims in published maps and institutional affiliations.

References

1. Tiruppathi C, Ahmmed GU, Vogel SM, Malik AB. Ca^{2+} signaling, TRP channels, and endothelial permeability. Microcirculation. 2006;13:693–708.
2. Tiruppathi C, Minshall RD, Paria BC, Vogel SM, Malik AB. Role of Ca^{2+} signaling in the regulation of endothelial permeability. Vascul Pharmacol. 2002;39:173–85.
3. Bhattacharya J, Nanjo S, Staub NC. Micropuncture measurement of lung microvascular pressure during 5-HT infusion. J Appl Physiol Respir Environ Exerc Physiol. 1982;52:634–7.
4. Friedrich EE, Hong Z, Xiong S, Zhong M, Di A, Rehman J, et al. Endothelial cell Piezo1 mediates pressure-induced lung vascular hyperpermeability via disruption of adherens junctions. Proc Natl Acad Sci USA. 2019;116:12980–5.
5. Lee HZ, Wu CH. Serotonin-stimulated increase in cytosolic Ca(2+) in cultured rat heart endothelial cells. Eur J Pharmacol. 1999;384:53–60.
6. Stolwijk JA, Zhang X, Gueguinou M, Zhang W, Matrougui K, Renken C, et al. Calcium signaling is dispensable for receptor regulation of endothelial barrier function. J Biol Chem. 2016;291:22894–912.
7. Kamiya I, Sumita T, Ishikawa N. S1-receptor participation in serotonin-induced pulmonary edema in the dog. Jpn J Pharmacol. 1987;45:121–4.
8. Xia Y, Fu Z, Hu J, Huang C, Paudel O, Cai S, et al. TRPV4 channel contributes to serotonin-induced pulmonary vasoconstriction and the enhanced vascular reactivity in chronic hypoxic pulmonary hypertension. Am J Physiol Cell Physiol. 2013;305:C704–15.
9. Majno G, Palade GE. Studies on inflammation. 1. The effect of histamine and serotonin on vascular permeability: an electron microscopic study. J Biophys Biochem Cytol. 1961;11:571–605.
10. Andrade R, Barnes NM, Baxter G, Bockaert J, Branchek T, Butler A, et al. 5-Hydroxytryptamine receptors (version 2019.4) in the IUPHAR/BPS Guide to Pharmacology Database. IUPHAR/BPS Guide to Pharmacology CITE Volume 2019, No. 4. 2019.
11. Barnes NM, Sharp T. A review of central 5-HT receptors and their function. Neuropharmacology. 1999;38:1083–152.
12. Koo JW, Balaban CD. Serotonin-induced plasma extravasation in the murine inner ear: possible mechanism of migraine-associated inner ear dysfunction. Cephalalgia. 2006;26:1310–9.
13. Ayme-Dietrich E, Aubertin-Kirch G, Maroteaux L, Monassier L. Cardiovascular remodeling and the peripheral serotonergic system. Arch Cardiovasc Dis. 2017;110:51–9.
14. Yildiz O, Smith JR, Purdy RE. Serotonin and vasoconstrictor synergism. Life Sci. 1998;62:1723–32.
15. Tran QK, Ohashi K, Watanabe H. Calcium signalling in endothelial cells. Cardiovasc Res. 2000;48:13–22.
16. Dalal PJ, Muller WA, Sullivan DP. Endothelial cell calcium signaling during barrier function and inflammation. Am J Pathol. 2020;190:535–42.
17. Thakore P, Earley S. Transient receptor potential channels and endothelial cell calcium signaling. Compr Physiol. 2019;9:1249–77.
18. Huh D, Leslie DC, Matthews BD, Fraser JP, Jurek S, Hamilton GA, et al. A human disease model of drug toxicity-induced pulmonary edema in a lung-on-a-chip microdevice. Sci Transl Med. 2012;4:159ra147.
19. Morgan JT, Stewart WG, McKee RA, Gleghorn JP. The mechanosensitive ion channel TRPV4 is a regulator of lung

development and pulmonary vasculature stabilization. Cell Mol Bioeng. 2018;11:309–20.
20. Peng S, Grace MS, Gondin AB, Retamal JS, Dill L, Darby W, et al. The transient receptor potential vanilloid 4 (TRPV4) ion channel mediates protease activated receptor 1 (PAR1)-induced vascular hyperpermeability. Lab Investig. 2020;100:1057–67.
21. Balakrishna S, Song W, Achanta S, Doran SF, Liu B, Kaelberer MM, et al. TRPV4 inhibition counteracts edema and inflammation and improves pulmonary function and oxygen saturation in chemically induced acute lung injury. Am J Physiol Lung Cell Mol Physiol. 2014;307:L158–72.
22. Queiroz BFG, Almeida MPA, Bakhle YS, Francischi JN. Calcitonin-gene related peptide is a potent inducer of oedema in rat orofacial tissue. Neuropeptides. 2018;68:43–8.
23. Vergnolle N, Cenac N, Altier C, Cellars L, Chapman K, Zamponi GW, et al. A role for transient receptor potential vanilloid 4 in tonicity-induced neurogenic inflammation. Br J Pharmacol. 2010;159:1161–73.
24. Veldhuis NA, Poole DP, Grace M, McIntyre P, Bunnett NW. The G protein-coupled receptor-transient receptor potential channel axis: molecular insights for targeting disorders of sensation and inflammation. Pharmacol Rev. 2015;67:36–73.
25. Grant AD, Cottrell GS, Amadesi S, Trevisani M, Nicoletti P, Materazzi S, et al. Protease-activated receptor 2 sensitizes the transient receptor potential vanilloid 4 ion channel to cause mechanical hyperalgesia in mice. J Physiol. 2007;578:715–33.
26. Poole DP, Amadesi S, Veldhuis NA, Abogadie FC, Lieu T, Darby W, et al. Protease-activated receptor 2 (PAR2) protein and transient receptor potential vanilloid 4 (TRPV4) protein coupling is required for sustained inflammatory signaling. J Biol Chem. 2013;288:5790–802.
27. Grace MS, Lieu T, Darby B, Abogadie FC, Veldhuis N, Bunnett NW, et al. The tyrosine kinase inhibitor bafetinib inhibits PAR2-induced activation of TRPV4 channels in vitro and pain in vivo. Br J Pharmacol. 2014;171:3881–94.
28. Ducret T, Guibert C, Marthan R, Savineau JP. Serotonin-induced activation of TRPV4-like current in rat intrapulmonary arterial smooth muscle cells. Cell Calcium. 2008;43:315–23.
29. Ahn MS, Eom YW, Oh JE, Cha SK, Park KS, Son JW, et al. Transient receptor potential channel TRPV4 mediates TGF-beta1-induced differentiation of human ventricular fibroblasts. Cardiol J. 2020;27:162–70.
30. Akiyama T, Ivanov M, Nagamine M, Davoodi A, Carstens MI, Ikoma A, et al. Involvement of TRPV4 in serotonin-evoked scratching. J Investig Dermatol. 2016;136:154–60.
31. Cenac N, Altier C, Motta JP, d'Aldebert E, Galeano S, Zamponi GW, et al. Potentiation of TRPV4 signalling by histamine and serotonin: an important mechanism for visceral hypersensitivity. Gut. 2010;59:481–8.
32. Maeshima T, Ito R, Hamada S, Senzaki K, Hamaguchi-Hamada K, Shutoh F, et al. The cellular localization of 5-HT2A receptors in the spinal cord and spinal ganglia of the adult rat. Brain Res. 1998;797:118–24.
33. Okamoto K, Imbe H, Morikawa Y, Itoh M, Sekimoto M, Nemoto K, et al. 5-HT2A receptor subtype in the peripheral branch of sensory fibers is involved in the potentiation of inflammatory pain in rats. Pain. 2002;99:133–43.
34. Chiu IM, von Hehn CA, Woolf CJ. Neurogenic inflammation and the peripheral nervous system in host defense and immunopathology. Nat Neurosci. 2012;15:1063–7.
35. Nascimento EB Jr., Seniuk JG, Godin AM, Ferreira WC, Dutra MB, Oliveira AC, et al. Peripheral 5-HT1B and 5-HT2A receptors mediate the nociceptive response induced by 5-hydroxytryptamine in mice. Pharmacol Biochem Behav. 2011;99:598–603.
36. Saria A, Lundberg JM, Skofitsch G, Lembeck F. Vascular protein linkage in various tissue induced by substance P, capsaicin, bradykinin, serotonin, histamine and by antigen challenge. Naunyn Schmiedebergs Arch Pharmacol. 1983;324:212–8.
37. Sasaki M, Obata H, Kawahara K, Saito S, Goto F. Peripheral 5-HT2A receptor antagonism attenuates primary thermal hyperalgesia and secondary mechanical allodynia after thermal injury in rats. Pain. 2006;122:130–6.
38. Sukriti S, Tauseef M, Yazbeck P, Mehta D. Mechanisms regulating endothelial permeability. Pulm Circ. 2014;4:535–51.
39. Markowitz S, Saito K, Moskowitz MA. Neurogenically mediated leakage of plasma protein occurs from blood vessels in dura mater but not brain. J Neurosci. 1987;7:4129–36.
40. Ramachandran R. Neurogenic inflammation and its role in migraine. Semin Immunopathol. 2018;40:301–14.
41. Tajti J, Szok D, Majlath Z, Tuka B, Csati A, Vecsei L. Migraine and neuropeptides. Neuropeptides. 2015;52:19–30.
42. Kilkenny C, Browne WJ, Cuthill IC, Emerson M, Altman DG. Improving bioscience research reporting: the ARRIVE guidelines for reporting animal research. PLoS Biol. 2010;8:e1000412.
43. Misane I, Ogren SO. Selective 5-HT1A antagonists WAY 100635 and NAD-299 attenuate the impairment of passive avoidance caused by scopolamine in the rat. Neuropsychopharmacology. 2003;28:253–64.
44. Hansen-Schwartz J, Lovland Hoel N, Nilsson E, Tfelt-Hansen P, Edvinsson L. Endothelium-dependent relaxant responses to selective 5-HT(1B/1D) receptor agonists in the isolated middle cerebral artery of the rat. J Vasc Res. 2003;40:561–6.
45. Ninan I, Kulkarni SK. Ketanserin reverses dizocilpine-suppression of morphine dependence but not tolerance in mice. Brain Res. 2000;876:215–9.
46. Mbaki Y, Ramage AG. Investigation of the role of 5-HT2 receptor subtypes in the control of the bladder and the urethra in the anaesthetized female rat. Br J Pharmacol. 2008;155:343–56.
47. Spohn SN, Bianco F, Scott RB, Keenan CM, Linton AA, O'Neill CH, et al. Protective actions of epithelial 5-hydroxytryptamine 4 receptors in normal and inflamed colon. Gastroenterology. 2016;151:933–44.e3.
48. Swain SM, Romac JM, Shahid RA, Pandol SJ, Liedtke W, Vigna SR, et al. TRPV4 channel opening mediates pressure-induced pancreatitis initiated by Piezo1 activation. J Clin Investig. 2020;130:2527–41.
49. Wick MJ, Harral JW, Loomis ZL, Dempsey EC. An optimized evans blue protocol to assess vascular leak in the mouse. J Vis Exp. 2018;57037.
50. Kurrasch-Orbaugh DM, Parrish JC, Watts VJ, Nichols DE. A complex signaling cascade links the serotonin2A receptor to phospholipase A2 activation: the involvement of MAP kinases. J Neurochem. 2003a;86:980–91.
51. Kurrasch-Orbaugh DM, Watts VJ, Barker EL, Nichols DE. Serotonin 5-hydroxytryptamine 2A receptor-coupled phospholipase C and phospholipase A2 signaling pathways have different receptor reserves. J Pharmacol Exp Ther. 2003b;304:229–37.
52. Qu Y, Villacreses N, Murphy DL, Rapoport SI. 5-HT2A/2C receptor signaling via phospholipase A2 and arachidonic acid is attenuated in mice lacking the serotonin reuptake transporter. Psychopharmacology. 2005;180:12–20.
53. Watanabe H, Vriens J, Prenen J, Droogmans G, Voets T, Nilius B. Anandamide and arachidonic acid use epoxyeicosatrienoic acids to activate TRPV4 channels. Nature. 2003;424:434–8.
54. Baluk P, Thurston G, Murphy TJ, Bunnett NW, McDonald DM. Neurogenic plasma leakage in mouse airways. Br J Pharmacol. 1999;126:522–8.
55. Machida T, Iizuka K, Hirafuji M. 5-hydroxytryptamine and its receptors in systemic vascular walls. Biol Pharm Bull. 2013;36:1416–9.
56. Dalsgaard T, Sonkusare SK, Teuscher C, Poynter ME, Nelson MT. Pharmacological inhibitors of TRPV4 channels reduce

cytokine production, restore endothelial function and increase survival in septic mice. Sci Rep. 2016;6:33841.
57. Egermayer P, Town GI, Peacock AJ. Role of serotonin in the pathogenesis of acute and chronic pulmonary hypertension. Thorax. 1999;54:161–8.
58. Cloutier N, Allaeys I, Marcoux G, Machlus KR, Mailhot B, Zufferey A, et al. Platelets release pathogenic serotonin and return to circulation after immune complex-mediated sequestration. Proc Natl Acad Sci USA. 2018;115:E1550–9.
59. Duerschmied D, Suidan GL, Demers M, Herr N, Carbo C, Brill A, et al. Platelet serotonin promotes the recruitment of neutrophils to sites of acute inflammation in mice. Blood. 2013;121:1008–15.
60. Ulrich S, Huber LC, Fischler M, Treder U, Maggiorini M, Eberli FR, et al. Platelet serotonin content and transpulmonary platelet serotonin gradient in patients with pulmonary hypertension. Respiration. 2011;81:211–6.
61. Neumann J, Hofmann B, Gergs U. Production and function of serotonin in cardiac cells. In Shad KF, editor. Serotonin—a chemical messenger between all types of living cells. London: IntechOpen; 2017.
62. Ni W, Geddes TJ, Priestley JR, Szasz T, Kuhn DM, Watts SW. The existence of a local 5-hydroxytryptaminergic system in peripheral arteries. Br J Pharmacol. 2008;154:663–74.
63. Rouzaud-Laborde C, Hanoun N, Baysal I, Rech JS, Mias C, Calise D, et al. Role of endothelial AADC in cardiac synthesis of serotonin and nitrates accumulation. PLoS ONE. 2012;7:e34893.
64. Li Y, Hadden C, Cooper A, Ahmed A, Wu H, Lupashin VV, et al. Sepsis-induced elevation in plasma serotonin facilitates endothelial hyperpermeability. Sci Rep. 2016;6:22747.
65. Groneberg DA, Quarcoo D, Frossard N, Fischer A. Neurogenic mechanisms in bronchial inflammatory diseases. Allergy. 2004;59:1139–52.
66. Aoki-Nagase T, Nagase T, Oh-Hashi Y, Kurihara Y, Yamaguchi Y, Yamamoto H, et al. Calcitonin gene-related peptide mediates acid-induced lung injury in mice. Respirology. 2007;12:807–13.
67. Sio SW, Puthia MK, Lu J, Moochhala S, Bhatia M. The neuropeptide substance P is a critical mediator of burn-induced acute lung injury. J Immunol. 2008;180:8333–41.
68. Rogers DF, Belvisi MG, Aursudkij B, Evans TW, Barnes PJ. Effects and interactions of sensory neuropeptides on airway microvascular leakage in guinea-pigs. Br J Pharmacol. 1988;95:1109–16.
69. Bileviciute I, Stenfors C, Theodorsson E, Lundeberg T. Unilateral injection of calcitonin gene-related peptide (CGRP) induces bilateral oedema formation and release of CGRP-like immunoreactivity in the rat hindpaw. Br J Pharmacol. 1998;125:1304–12.
70. Dietrich A. Modulators of transient receptor potential (TRP) channels as therapeutic options in lung disease. Pharmaceuticals (Basel). 2019;12:23.
71. Goyal N, Skrdla P, Schroyer R, Kumar S, Fernando D, Oughton A, et al. Clinical pharmacokinetics, safety, and tolerability of a novel, first-in-class TRPV4 ion channel inhibitor, GSK2798745, in healthy and heart failure subjects. Am J Cardiovasc Drugs. 2019;19:335–42.
72. Kuebler WM, Jordt SE, Liedtke WB. Urgent reconsideration of lung edema as a preventable outcome in COVID-19: inhibition of TRPV4 represents a promising and feasible approach. Am J Physiol Lung Cell Mol Physiol. 2020;318:L1239–43.
73. Stewart GM, Johnson BD, Sprecher DL, Reddy YNV, Obokata M, Goldsmith S, et al. Targeting pulmonary capillary permeability to reduce lung congestion in heart failure: a randomized, controlled pilot trial. Eur J Heart Fail. 2020;22:1641–5.
74. Yang XR, Lin AH, Hughes JM, Flavahan NA, Cao YN, Liedtke W, et al. Upregulation of osmo-mechanosensitive TRPV4 channel facilitates chronic hypoxia-induced myogenic tone and pulmonary hypertension. Am J Physiol Lung Cell Mol Physiol. 2012;302:L555–68.
75. Zhao H, Sprunger LK, Simasko SM. Expression of transient receptor potential channels and two-pore potassium channels in subtypes of vagal afferent neurons in rat. Am J Physiol Gastrointest Liver Physiol. 2010;298:G212–21.
76. Brierley SM, Page AJ, Hughes PA, Adam B, Liebregts T, Cooper NJ, et al. Selective role for TRPV4 ion channels in visceral sensory pathways. Gastroenterology. 2008;134:2059–69.
77. Kohler R, Heyken WT, Heinau P, Schubert R, Si H, Kacik M, et al. Evidence for a functional role of endothelial transient receptor potential V4 in shear stress-induced vasodilatation. Arterioscler Thromb Vasc Biol. 2006;26:1495–502.
78. Sonkusare SK, Bonev AD, Ledoux J, Liedtke W, Kotlikoff MI, Heppner TJ, et al. Elementary Ca^{2+} signals through endothelial TRPV4 channels regulate vascular function. Science. 2012;336:597–601.
79. Ahern GP. 5-HT and the immune system. Curr Opin Pharmacol. 2011;11:29–33.
80. Hamanaka K, Jian MY, Townsley MI, King JA, Liedtke W, Weber DS, et al. TRPV4 channels augment macrophage activation and ventilator-induced lung injury. Am J Physiol Lung Cell Mol Physiol. 2010;299:L353–62.
81. Scheraga RG, Abraham S, Niese KA, Southern BD, Grove LM, Hite RD, et al. TRPV4 mechanosensitive ion channel regulates lipopolysaccharide-stimulated macrophage phagocytosis. J Immunol. 2016;196:428–36.

JBC RESEARCH ARTICLE

A lipid-anchored neurokinin 1 receptor antagonist prolongs pain relief by a three-pronged mechanism of action targeting the receptor at the plasma membrane and in endosomes

Received for publication, July 7, 2020, and in revised form, January 20, 2021 Published, Papers in Press, January 28, 2021, https://doi.org/10.1016/j.jbc.2021.100345

Quynh N. Mai[1,2,3,4], Priyank Shenoy[1,3], Tim Quach[2], Jeffri S. Retamal[2,3], Arisbel B. Gondin[1,3], Holly R. Yeatman[1], Luigi Aurelio[1,4], Joshua W. Conner[3,4], Daniel P. Poole[1,3], Meritxell Canals[5,6], Cameron J. Nowell[1], Bim Graham[4], Thomas P. Davis[2,3,7], Stephen J. Briddon[5,6], Stephen J. Hill[5,6], Christopher J.H. Porter[2,3], Nigel W. Bunnett[1,3,8,9,*], Michelle L. Halls[1,*], and Nicholas A. Veldhuis[1,2,3,*]

From the [1]Drug Discovery Biology Theme, [2]Drug Delivery, Disposition and Dynamics Theme, [3]Australian Research Council Centre of Excellence in Convergent Bio-Nano Science and Technology, and [4]Medicinal Chemistry Theme, Monash Institute of Pharmaceutical Sciences, Monash University, Parkville, Victoria, Australia; [5]Division of Physiology, Pharmacology and Neuroscience, School of Life Sciences, The University of Nottingham Medical School, Nottingham, UK; [6]Centre of Membrane Proteins and Receptors, Universities of Birmingham and Nottingham, the Midlands, UK; [7]Australian Institute for Bioengineering and Nanotechnology, University of Queensland, Brisbane, Queensland, Australia; [8]Department of Pharmacology and Therapeutics, The University of Melbourne, Parkville, Victoria, Australia; and [9]Department of Molecular Pathobiology, New York University College of Dentistry, New York, New York, USA

Edited by Henrik Dohlman

G-protein-coupled receptors (GPCRs) are traditionally known for signaling at the plasma membrane, but they can also signal from endosomes after internalization to control important pathophysiological processes. In spinal neurons, sustained endosomal signaling of the neurokinin 1 receptor (NK_1R) mediates nociception, as demonstrated in models of acute and neuropathic pain. An NK_1R antagonist, Spantide I (Span), conjugated to cholestanol (Span-Chol), accumulates in endosomes, inhibits endosomal NK_1R signaling, and causes prolonged antinociception. However, the extent to which the Chol-anchor influences long-term location and activity is poorly understood. Herein, we used fluorescent correlation spectroscopy and targeted biosensors to characterize Span-Chol over time. The Chol-anchor increased local concentration of probe at the plasma membrane. Over time we observed an increase in NK_1R-binding affinity and more potent inhibition of NK_1R-mediated calcium signaling. Span-Chol, but not Span, caused a persistent decrease in NK_1R recruitment of β-arrestin and receptor internalization to early endosomes. Using targeted biosensors, we mapped the relative inhibition of NK_1R signaling as the receptor moved into the cell. Span selectively inhibited cell surface signaling, whereas Span-Chol partitioned into endosomal membranes and blocked endosomal signaling. In a preclinical model of pain, Span-Chol caused prolonged antinociception (>9 h), which is attributable to a three-pronged mechanism of action: increased local concentration at membranes, a prolonged decrease in NK_1R endocytosis, and persistent inhibition of signaling from endosomes. Identifying the mechanisms that contribute to the increased preclinical efficacy of lipid-anchored NK_1R antagonists is an important step toward understanding how we can effectively target intracellular GPCRs in disease

G-protein-coupled receptors (GPCRs) are tractable therapeutic targets because they have druggable sites on the cell surface and control most pathophysiological processes (1). However, many GPCRs can also signal from intracellular compartments, including endosomes, the Golgi, mitochondria, and the nucleus (2–5). These intracellular signals dictate physiological responses that are distinct from those that emanate from signaling at the plasma membrane (5–10). Drug discovery efforts typically target GPCRs at the cell surface, and as a consequence, many drugs targeting GPCRs are not designed to cross the plasma membrane. This inability to effectively engage intracellular GPCRs might explain why some drugs with high efficacy in cell-based assays of plasma membrane signaling fail in clinical trials.

For the GPCR for substance P (SP), the neurokinin 1 receptor (NK_1R), multiple NK_1R antagonists have failed in clinical trials of chronic neurological diseases, including pain (11–13). Activation of the NK_1R causes two spatially and temporally distinct rounds of signaling (Fig. S1). At the cell surface, SP-bound NK_1R rapidly activates $G\alpha_q$ G proteins to increase Ca^{2+} mobilization, protein kinase C (PKC) activity, and cyclic adenosine monophosphate (cAMP) formation in the vicinity of the plasma membrane (5, 14). Stimulation of the NK_1R also leads to transactivation of the epidermal growth factor receptor (EGFR) to increase extracellular signal-regulated kinase (ERK) activity in the cytoplasm. These signals are all relatively short-lived (<15 min) (14). During this

This article contains supporting information.

* For correspondence: Nigel W. Bunnett, nwb2@nyu.edu; Michelle L. Halls, michelle.halls@monash.edu; Nicholas A. Veldhuis, nicholas.veldhuis@monash.edu.

Present address for Quynh N. Mai: Cardiovascular Research Institute, Department of Biochemistry and Biophysics, University of California, San Francisco, CA 94158.

© 2021 THE AUTHORS. Published by Elsevier Inc on behalf of American Society for Biochemistry and Molecular Biology. This is an open access article under the CC BY license (http://creativecommons.org/licenses/by/4.0/).

time, GPCR kinases rapidly phosphorylate the NK_1R leading to association with β-arrestins and receptor endocytosis to early endosomes (<2 min) (5). Within endosomes, the SP-NK_1R complex continues to signal causing increased PKC activity and cAMP in the cytosol and increased ERK activity within the nucleus (5, 14). These signals from the endosomally localized receptor are longer-lived (>20 min). It is these sustained signals from the intracellular NK_1R that mediate persistent excitation of spinal neurons and sustained central pain transmission (7, 14, 15).

Ligands can have spatially specific or "location biased" pharmacological actions in cells (16). We have previously assessed the potential for drug delivery strategies to locally deliver NK_1R antagonists to endosomes. This includes pH-responsive nanoparticles that deliver and release the NK_1R antagonist aprepitant directly into the endosomes (17) and lipid-anchored NK_1R antagonists that accumulate in endosomal membranes (5). Both of these approaches improved drug efficacy in preclinical models of pain (2–5-fold more effective antinociception, 2–4-fold longer duration of action compared with free drug) (5, 17). The localized delivery of an NK_1R antagonist to endosomes using nanoparticles is a selective approach that bypasses any effects on receptors at the cell surface. In contrast, lipid-anchored NK_1R antagonists first partition into the plasma membrane, before they are trafficked to endosomes (5). It is therefore possible that lipid-anchored antagonists also affect the signaling and trafficking of plasma membrane-localized NK_1R, in addition to their later antagonism of endosomal receptors. This dual antagonism—initial blockade of plasma membrane receptors during partitioning into the plasma membrane and then prolonged blockade of the pathophysiologically relevant signal from endosomes—could enhance therapeutic efficacy.

In the current investigation, we used live cell imaging and biophysical approaches to assess NK_1R signaling and trafficking in subcellular compartments, in conjunction with behavioral assays of nociception to investigate the mechanisms by which a cholestanol-anchored antagonist, Spantide I (Span-Chol), inhibits endosomal signaling. We used a cholestanol-anchored fluorescent probe (Cy5-Chol) to model the lipid-dependent translocation of the antagonist. We observed that the lipid anchor allows an initial enrichment of probe concentration at the plasma membrane, which correlates with an increased antagonist potency at proximal signaling pathways (*i.e.*, Ca^{2+} mobilization). The lipid-anchored antagonist also inhibits cell surface NK_1R-β-arrestin recruitment and NK_1R endocytosis. Over time, Cy5-Chol travels from the plasma membrane to early and late endosomes. This movement deeper into the endosomal network correlates with inhibition of endosomal-selective NK_1R signaling pathways (5) by Span-Chol, including sustained cytosolic cAMP and cytosolic PKC activity. Consistent with these findings, the lipid-anchored antagonist has long-lasting antinociceptive actions in preclinical models of pain (>9 h).

We find that lipid anchors increase the local membrane concentration of GPCR antagonists, cause inhibition of receptor trafficking from the plasma membrane, and prolong the inhibition of signaling from endosomes. This three-pronged mechanism allows lipid-anchored antagonists to very effectively target endosomally derived GPCR signaling pathways of pathophysiological importance.

Results

Lipid anchors increase the available concentration of drug at the cell surface

Inspired by prior studies using lipid–drug conjugates (18, 19), we previously synthesized a series of lipid-anchored probes comprising the sterol cholestanol as a lipid conjugate for anchoring a cargo to membranes *via* a flexible polyethylene glycol linker (PEG4-PEG3-PEG4) (5). For the cargo we used Cyanine 5 (Cy5), to generate a fluorescent reporter of lipid-anchor location (Cy5-Chol), or the NK_1R antagonist, Spantide I, to generate a lipid-anchored antagonist (Span-Chol) (Fig. S2). We also generated control probes including a non-lipidated fluorescent probe (ethyl-ester group, PEG linker, Cy5; Cy5-OEt) and a lipid anchor control probe (cholestanol group, PEG linker, biotin; Chol).

Fluorescence correlation spectroscopy (FCS) enables measurement of the concentrations of fluorescent molecules within a small defined volume (<0.2 fl) (20, 21). We used this approach to determine the concentration of Cy5 probes (Cy5-Chol or the control, Cy5-OEt) in the extracellular fluid immediately above the plasma membrane and at increasing distances above the cell (30–200 μm). We chose the Cy5 probes as the simplest example of how a lipid anchor could affect the plasma membrane concentration of a cargo, independent of any receptor-dependent effects on ligand distribution (22). Consistent with our previous studies (5), brightfield and fluorescence confocal imaging confirmed that Cy5-Chol rapidly incorporated into the plasma membrane of HEK293 cells (Fig. 1*A*), but Cy5-OEt remained in extracellular fluid (Fig. 1*B*). We then used FCS to quantify the concentration of Cy5 fluorescence at the plasma membrane of cells incubated with a nominal concentration of probe (10 nM). The concentration of Cy5-Chol in the extracellular fluid at 5 μm above the plasma membrane was 23.8 ± 7.1 nM, which decreased more than fourfold to 5.6 ± 1.4 nM at 30 μm (mean ± SEM from n = 4) (Fig. 1, *C* and *E*). In contrast, the measured concentration of Cy5-OEt was 6.5 ± 1.1 nM at 5 μm above the plasma membrane, which increased more than threefold to 21.8 ± 3.8 nM at 200 μm (mean ± SEM from n = 4) (Fig. 1, *D* and *E*). A comparison of probe concentrations at increasing distances (5 μm intervals) above the plasma membrane suggested that there was an enrichment of Cy5-Chol proximal to the plasma membrane, while the Cy5-OEt reporter molecule could freely diffuse through the extracellular fluid (Fig. 1*E*). Therefore, the addition of a lipid anchor results in an enhanced association of a probe with cell membranes. This creates a high local concentration of probe at the cell surface.

Lipid anchoring increases the affinity and potency of an NK_1R antagonist

To determine whether the addition of a lipid anchor influences the affinity and potency of an NK_1R antagonist, we

ASBMB

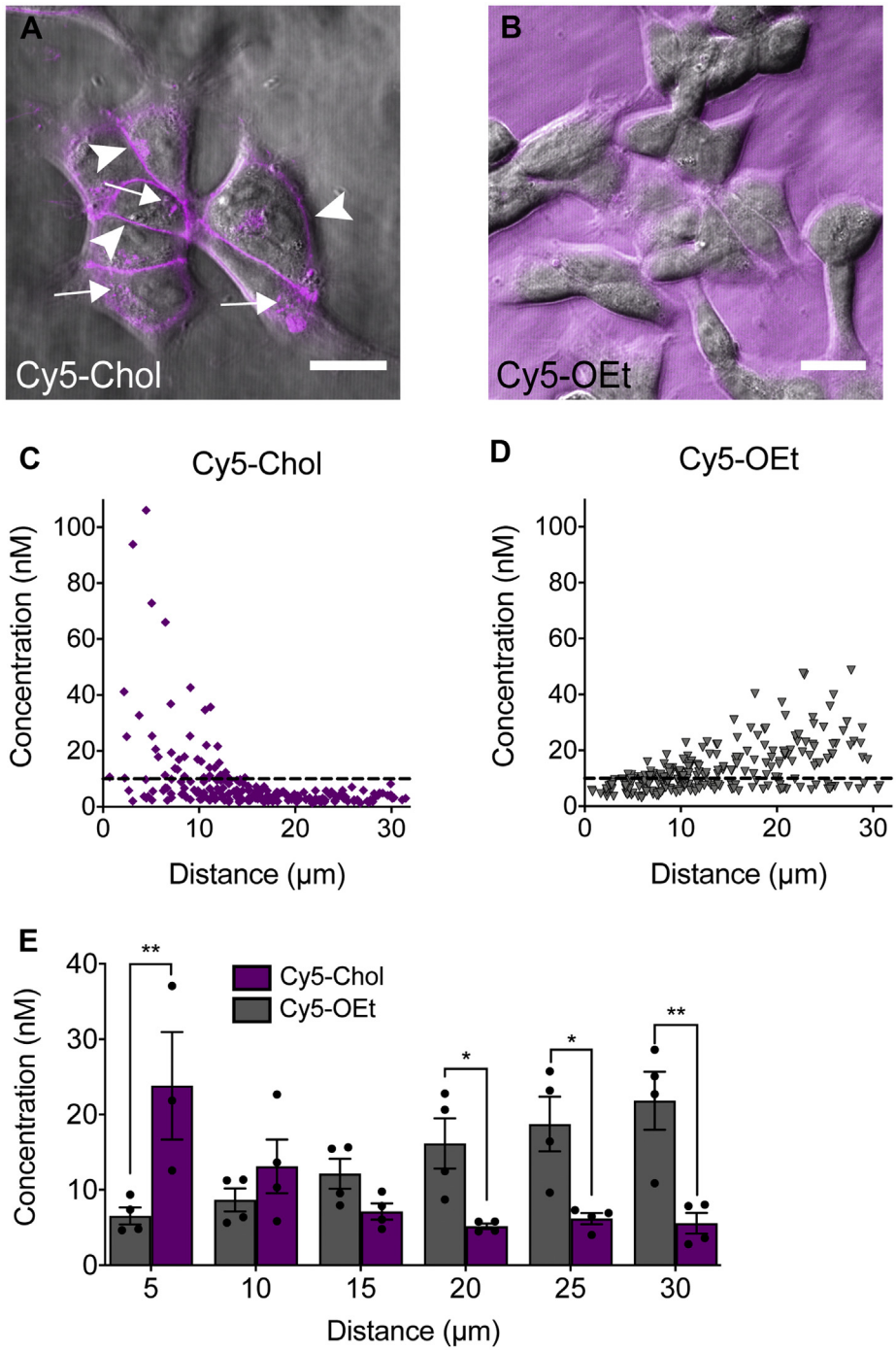


Figure 1. A cholestanol lipid anchor increases the concentration of Cy5 immediately above the plasma membrane. *A* and *B*, Confocal images of HEK293 cells after incubation with 1 μM Cy5-Chol (*A*) or Cy5-OEt (*B*). *Arrows* indicate intracellular Cy5 fluorescence, and *arrow heads* indicate Cy5 fluorescence at the plasma membrane. Scale bar, 20 μm. *C* and *D*, the concentration of 10 nM solution of Cy5-Chol (*C*) or Cy5-OEt (*D*) at increasing distances above the plasma membrane of HEK293 cells was calculated using FCS. Data points show the concentrations measured at six distance intervals averaged from 3 to 4 independent experiments. The nominal concentration of the added solution (10 nM) is shown by a *dashed line*. *E*, the concentration of Cy5-Chol and Cy5-OEt binned at increasing 5 μm intervals above the plasma membrane. Bars show the mean, error bars show the standard error of the mean (S.E.M.), and data points show the average concentrations obtained from each individual experiment (n = 4). $*p < 0.05$, $**p < 0.01$ Cy5-OEt vs Cy5-Chol; two-way ANOVA with Sidak's multiple comparison test.

compared unconjugated ("free") Spantide I (Span) and Span-Chol. A high-content imaging competition binding assay was used to evaluate the capacity of these antagonists to disrupt the binding of SP labeled with fluorescent tetramethylrhodamine (SP-TAMRA) to the NK_1R stably transfected in HEK293 cells. Cells were analyzed using an established granularity algorithm to provide a measure of total cell binding (includes both cell surface and intracellular) (21, 23). We assessed antagonist affinity at two time points following antagonist addition: 30 min, when FCS data show

Cy5-Chol enrichment at the plasma membrane (Fig. 1); and 4 h, when Span-Chol accumulates, and is pharmacologically active, within endosomal compartments (5).

To assess competition binding after 30 min, HEK-NK_1R cells were coincubated with an EC_{50} concentration of SP-TAMRA (0.5 nM) and increasing concentrations of Span or Span-Chol and equilibrated for 30 min. The affinity of Span-Chol and Span for NK_1R was similar with pIC_{50} values of 6.28 ± 0.09 and 5.99 ± 0.13, respectively (Fig. 2*A*). Therefore, peptide modification by attachment of a PEG_{12} linker and cholestanol anchor does not diminish the affinity of Spantide for the NK_1R.

To assess ligand binding after 4 h, HEK-NK_1R cells were preincubated with antagonist for 3.5 h, then with SP-TAMRA for a further 30 min (4 h total). The affinity of Span for the NK_1R was significantly reduced compared with that of Span-Chol (pIC_{50} 5.55 ± 0.17 vs 6.50 ± 0.12, p = 0.0018, unpaired *t*-test) (Fig. 2*B*). However, there was no significant change in the relative affinities of Span or Span-Chol for the NK_1R over time (p = 0.1121 and p = 0.6378, respectively; one-way ANOVA with Tukey's multiple comparisons test). This suggests that the addition of a lipid anchor improves the kinetic properties of Span by sustaining its ability to compete with SP-TAMRA at the NK_1R over a 4 h period. Our previous studies indicated no difference in stability of these ligands in spinal cord membranes (5). We therefore propose that this apparent improvement in affinity of Span-Chol for the NK_1R is due to the accumulation of Span-Chol in endosomes, allowing Span-Chol to access both plasma membrane and endosomal pools of NK_1R.

To determine if lipid conjugation influenced the potency of Span, we compared the ability of Span and Span-Chol to inhibit SP-stimulated Ca^{2+} signaling in HEK-NK_1R cells at different time points after addition. In initial experiments, HEK-NK_1R cells were preincubated with increasing concentrations of Span or Span-Chol for 30 min, prior to challenge with an EC_{80} concentration of SP (1 nM). Ca^{2+} transients were measured for 90 s poststimulation. Preincubation of cells with Span or Span-Chol caused a concentration-dependent inhibition of Ca^{2+} flux (Fig. 2*C*). A comparison of the pIC_{50} values of Span and Span-Chol (4.87 ± 0.33 and 6.25 ± 0.19, respectively) revealed a significant increase in the potency of the lipidated antagonist (p = 0.0112). This is consistent with FCS experiments (Fig. 1) and may be due to the lipid anchoring of the antagonist to the plasma membrane, thereby effectively increasing the local concentration of the antagonist near the receptor even at acute time periods (24, 25).

While lipid-anchored fluorescent probes initially partition into the plasma membrane, they are then quickly trafficked into endosomal compartments (5). As such, the continuous removal of lipidated antagonists from the plasma membrane by constitutive endocytosis could affect the relative potency of Span-Chol compared with soluble Span over time. To assess this possibility, we compared continuous exposure to the antagonists for 4 h to a "pulsed" administration whereby the cells were preincubated with antagonist for 30 min, washed to remove any excess ligand, and then left at 37°C for 3.5 h (4 h total). In both protocols, cells were challenged with 1 nM SP 4 h after the initial antagonist addition. There was no change

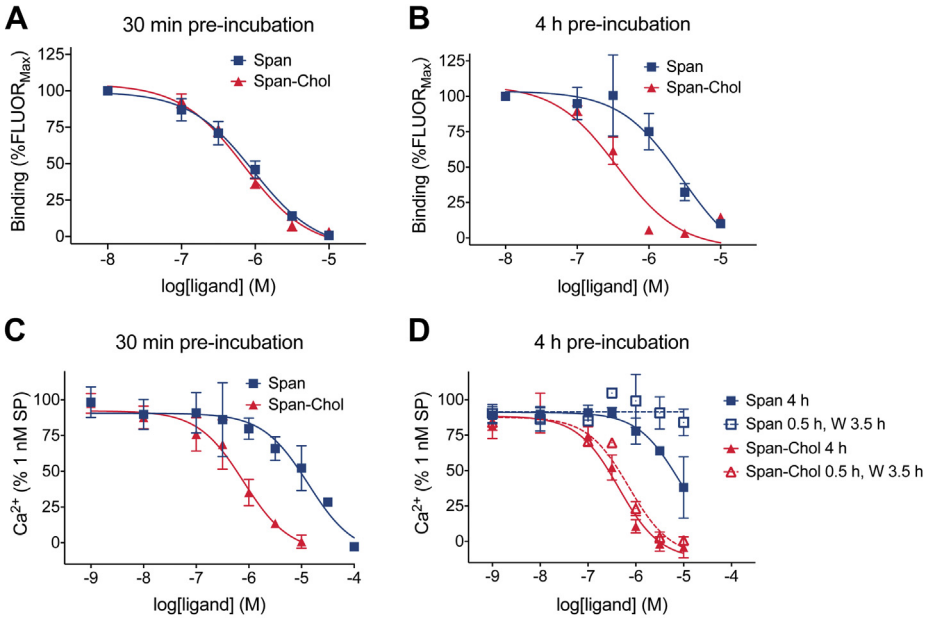


Figure 2. A cholestanol lipid anchor increases the relative affinity and potency of an NK_1R antagonist. *A* and *B*, the affinity of Span compared to Span-Chol was assessed by competition with fluorescent SP-TAMRA in HEK-NK_1R cells by high-content imaging (n = 5). HEK-NK_1R cells were preincubated with vehicle (0.1% v/v DMSO; total binding) or increasing concentrations of Span or Span-Chol for a total of 30 min (*A*) or 4 h (*B*) at 37°C prior to addition of 0.5 nM SP-TAMRA. Data are expressed as a percentage of the fluorescent intensity measured in the presence of 10 nM Span or Span-Chol (%$FLUOR_{Max}$). Symbols show means, and error bars S.E.M. of five independent experiments performed in triplicate. *C* and *D*, Calcium transients were measured in HEK-NK_1R cells in response to 1 nM SP following short (30 min; *C*) or long (4 h; *D*) preincubation with increasing concentrations of Span or Span-Chol (n = 3). Four-h preincubation experiments compared continuous exposure to antagonist (4 h) versus a "pulsed" exposure (0.5 h exposure, wash [W], 3.5 h rest). Symbols show means, and error bars S.E.M. of three independent experiments performed in triplicate.

in the pIC_{50} of the antagonists when the cells were continuously incubated with Span or Span-Chol for 4 h (5.11 ± 0.76 and 6.36 ± 0.17, respectively) compared with the 30 min preincubation (Fig. 2*D*).

After pulsed administration, only Span-Chol retained its ability to antagonize SP-stimulated Ca^{2+} signaling at 4 h (pIC_{50} 6.15 ± 0.11) (Fig. 2*D*). This is likely due to the wash step (after the initial 30 min incubation with antagonist) decreasing the available concentration of free Span in the extracellular fluid. In contrast, the potency of Span-Chol was not lost following the wash, confirming that lipidation causes an increased association of the antagonist with the cell membrane. Notably, the potency of Span-Chol was sustained over 4 h despite the increasing internalization of lipid-anchored probes over time (5). This could indicate a prolonged retention of the lipid-anchored antagonist at the plasma membrane (in addition to internalization into the endosomal network).

Together, these data demonstrate that cholestanol conjugation can enhance the potency and affinity of antagonists by increasing their retention in the plasma membrane and therefore their effective local concentration.

A lipid-anchored antagonist decreases endocytosis of the activated NK_1R

Span-Chol has a high local concentration at the cell surface (Fig. 1) and maintains antagonistic activity at cell surface receptors even after 4 h (Fig. 2). It is therefore possible that lipidated antagonists continually act at the plasma membrane to inhibit SP-induced endocytosis of the NK_1R, which could contribute to their long-lasting therapeutic efficacy. To assess this possibility, we measured the proximity between NK_1R-RLuc8 and β-arrestin2-YFP, KRas-Venus (marker of the plasma membrane), or Rab5a-Venus (marker of early endosomes) in HEK293 cells using BRET. We compared the

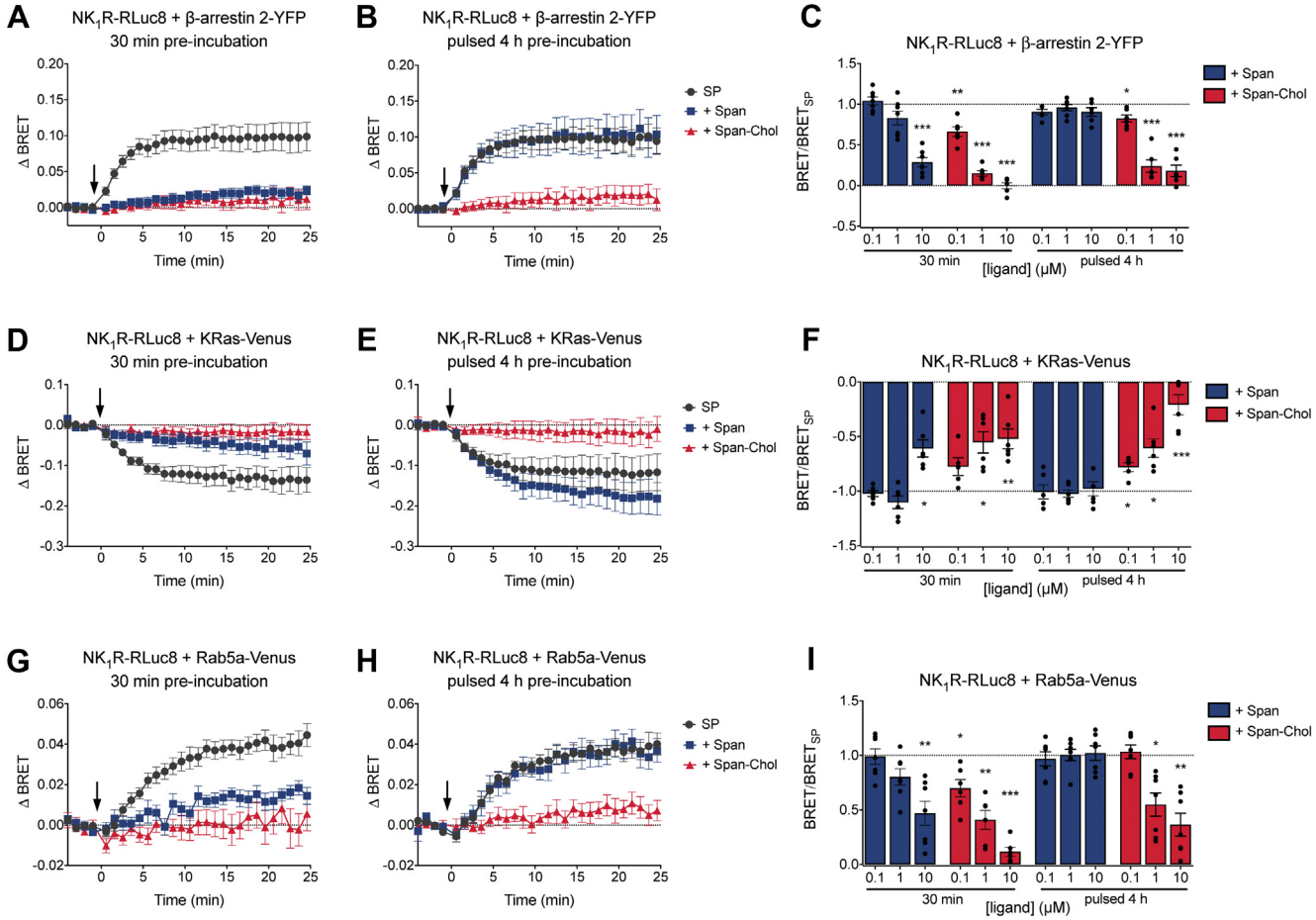


Figure 3. Span-Chol causes sustained inhibition of NK_1R-induced recruitment of β-arrestin and receptor internalization to early endosomes. The effect of short (30 min) versus long (pulsed 4 h: 30 min treatment, wash, 3.5 h recovery) preincubation with Span or Span-Chol on the NK_1R-induced recruitment of β-arrestin and receptor internalization to early endosomes was determined using BRET in HEK cells (n = 6). *A–C*, 1 nM SP-induced change in BRET between NK_1R-Rluc8 and β-arrestin 2-YFP after preincubation with 10 μM Span or Span-Chol for 30 min (*A*) or pulsed 4 h (*B*). *C*, the plateau response calculated from curve fit of the BRET time courses (as per *A* and *B*) after preincubation with 0.1 μM, 1 μM, or 10 μM antagonist, expressed relative to SP alone. *D–F*, 1 nM SP-induced change in BRET between NK_1R-Rluc8 and KRas-Venus after preincubation with 10 μM Span or Span-Chol for 30 min (*D*) or pulsed 4 h (*E*). *F*, the plateau response calculated from curve fit of the BRET time courses (as per *D* and *E*) after preincubation with 0.1 μM, 1 μM, or 10 μM antagonist, expressed relative to SP alone. *G–I*, 1 nM SP-induced change in BRET between NK_1R-Rluc8 and Rab5a-Venus after preincubation with 10 μM Span or Span-Chol for 30 min (*G*) or pulsed 4 h (*H*). *I*, the plateau response calculated from curve fit of the BRET time courses (as per *G* and *H*) after preincubation with 0.1 μM, 1 μM, or 10 μM antagonist, expressed relative to SP alone. For time courses, symbols show means and error bars S.E.M; for bar graphs, columns show means, error bars show S.E.M., and symbols show the mean of each individual experiment performed in duplicate. *$p < 0.05$, **$p < 0.01$ and ***$p < 0.001$ versus SP alone, two-way ANOVA with Dunnett's multiple comparisons test.

effectiveness of Span versus Span-Chol after short (30 min) or prolonged (4 h) incubation. In order to observe any differences between the antagonists that were due to the prolonged retention of Span-Chol at the cell surface, we used the "pulsed" incubation protocol: 30 min antagonist, wash, 3.5 h recovery (4 h total).

In control cells, SP induced an increase in NK_1R-RLuc8/β-arrestin2-YFP BRET, consistent with β-arrestin2 recruitment to NK_1R (Fig. 3, *A–C*). After 30 min preincubation, Span and Span-Chol (0.1, 1, or 10 μM) caused a concentration-dependent inhibition of SP-stimulated NK_1R-RLuc8/β-arrestin2-YFP BRET. After a pulsed 4 h preincubation with antagonists, Span had no effect on SP-stimulated NK_1R-RLuc8/β-arrestin2-YFP BRET at any concentration (Fig. 3, *B* and *C*). In contrast, Span-Chol inhibited SP-stimulated NK_1R-RLuc8/β-arrestin2-YFP BRET at the two highest concentrations of antagonist (1 and 10 μM).

Similar results were obtained when we measured the effect of Span or Span-Chol on the SP-stimulated change in BRET between NK_1R-RLuc8 and KRas-Venus (Fig. 3, *D–F*) or Rab5a-Venus (Fig. 3, *G–I*). In control cells, SP caused a decrease in BRET between NK_1R-RLuc8 and KRas-Venus (Fig. 3, *D–F*), which corresponded to an increase in BRET between NK_1R-RLuc8 and Rab5a-Venus (Fig. 3, *G–I*). This is consistent with receptor internalization from the plasma membrane (KRas) to early endosomes (Rab5a). After a 30 min preincubation, both Span and Span-Chol inhibited the SP-stimulated change in BRET between NK_1R-RLuc8 and KRas-Venus (Fig. 3, *D* and *F*) or Rab5a-Venus (Fig. 3, *G* and *I*). However, after a pulsed 4 h preincubation, only Span-Chol inhibited the SP-stimulated change in BRET between NK_1R-RLuc8 and KRas-Venus (Fig. 3, *E* and *F*) or Rab5a-Venus (Fig. 3, *H* and *I*).

Since alterations in the composition of membrane lipids could artifactually affect BRET between transmembrane and associated proteins, we also studied the effects of a control cholestanol-PEG-biotin probe (Chol). There was no effect of any tested concentration of Chol (0.1, 1, 10 μM) on the SP-induced changes in BRET between NK_1R-RLuc8 and β-arrestin2-YFP, KRas-Venus, or Rab5a-Venus (Fig. S3).

Our results show that Span-Chol can antagonize the NK_1R at the plasma membrane to inhibit β-arrestin2 recruitment and receptor endocytosis. This effect is prolonged for up to 4 h, suggesting that some Span-Chol is retained at the plasma membrane despite significant movement of the lipid-anchored antagonist into endosomes (5).

Lipid-anchored probes traffic from the plasma membrane to endosomal compartments

We have previously demonstrated that the Cy5-Chol probe accumulates in early endosomes in HEK293 cells after 4 h, as indicated by colocalization with Rab5a (5). However, we still observe effects of Span-Chol at the plasma membrane at this time point, and the distribution of lipid-anchored probes into other endosomal signaling compartments (*i.e.*, late endosomes) has not been investigated. We therefore set out to map the location of Cy5-Chol over short and longer timescales. Previous studies have shown accumulation of a fluorescent analog of Span-Chol (Cy5-Span-Chol) in NK_1R-positive endosomes in cells stimulated with SP (5). Here, we aimed to further define the role of the lipid anchor in influencing the cellular distribution of cargo when not engaged with its receptor target (Fig. 4).

HEK293 cells were infected with CellLight fluorescent fusion proteins resident to endocytic compartments, including early endosomes (EE-RFP) and late endosomes (LE-GFP). The distribution of Cy5-Chol (1.5 μM) was examined in live cells by confocal microscopy due to a loss of probe fluorescence that occurs when using standard fixation approaches. Using this approach, some of the finer endosomal structures are less evident in comparison with antibody staining of Rab GTPases in fixed cells (26). Nevertheless, live cell imaging still provides valuable insights into the distribution of lipidated probes within the endosomal network over time. After a 30 min preincubation, Cy5-Chol fluorescence was readily observed at the plasma membrane, in early endosomes (EE-RFP) and late endosomes (LE-GFP) (Fig. 4*A*). A much higher proportion of Cy5-Chol was observed at the plasma membrane, compared with intracellular compartments (Fig. 4*B*). We then assessed distribution of Cy5-Chol after a pulsed incubation protocol (30 min incubation with Cy5-Chol, wash, 3.5 h recovery; 4 h total). We observed coincident detection of Cy5-Chol with markers of early endosomes (EE-RFP) and late endosomes (LE-GFP) (Fig. 4*C*). This correlated with a change in the overall distribution of Cy5-Chol in the cell, with similar fluorescence observed at the plasma membrane and within intracellular compartments (Fig. 4*D*). To determine the long-term intracellular distribution of a lipidated probe, HEK293 cells were incubated with Cy5-Chol for 24 h (Fig. 4, *E* and *F*). After 24 h we still detected Cy5-Chol codistribution with reporters for early endosomes (EE-RFP) and late endosomes (LE-GFP) (Fig. 4*E*). However, the relative distribution of Cy5-Chol over the whole cell was enriched in intracellular compartments compared with the plasma membrane (Fig. 4*F*).

Together, these data indicate that the internalized cholestanol-conjugated reporter resides within the endocytic pathway for sustained periods. Over time, the amount of Cy5-Chol at the plasma membrane decreases, which corresponds with a movement of Cy5-Chol further into the endosomal network. These findings support the use of sterol-based lipid anchors for targeting ligands to populations of endosomal GPCRs.

Only free antagonist completely blocked plasma membrane NK_1R signaling

We then investigated in detail the capacity of Span versus Span-Chol to target NK_1R signaling in different cellular regions. Our previous analysis had focused only on ERK activity, showing selective inhibition of nuclear ERK by Span-Chol (versus Span) (5). This is because only endosomal NK_1R can increase nuclear ERK in response to SP (5). Here, we used an expanded toolbox of targeted FRET biosensors to follow the

ASBMB

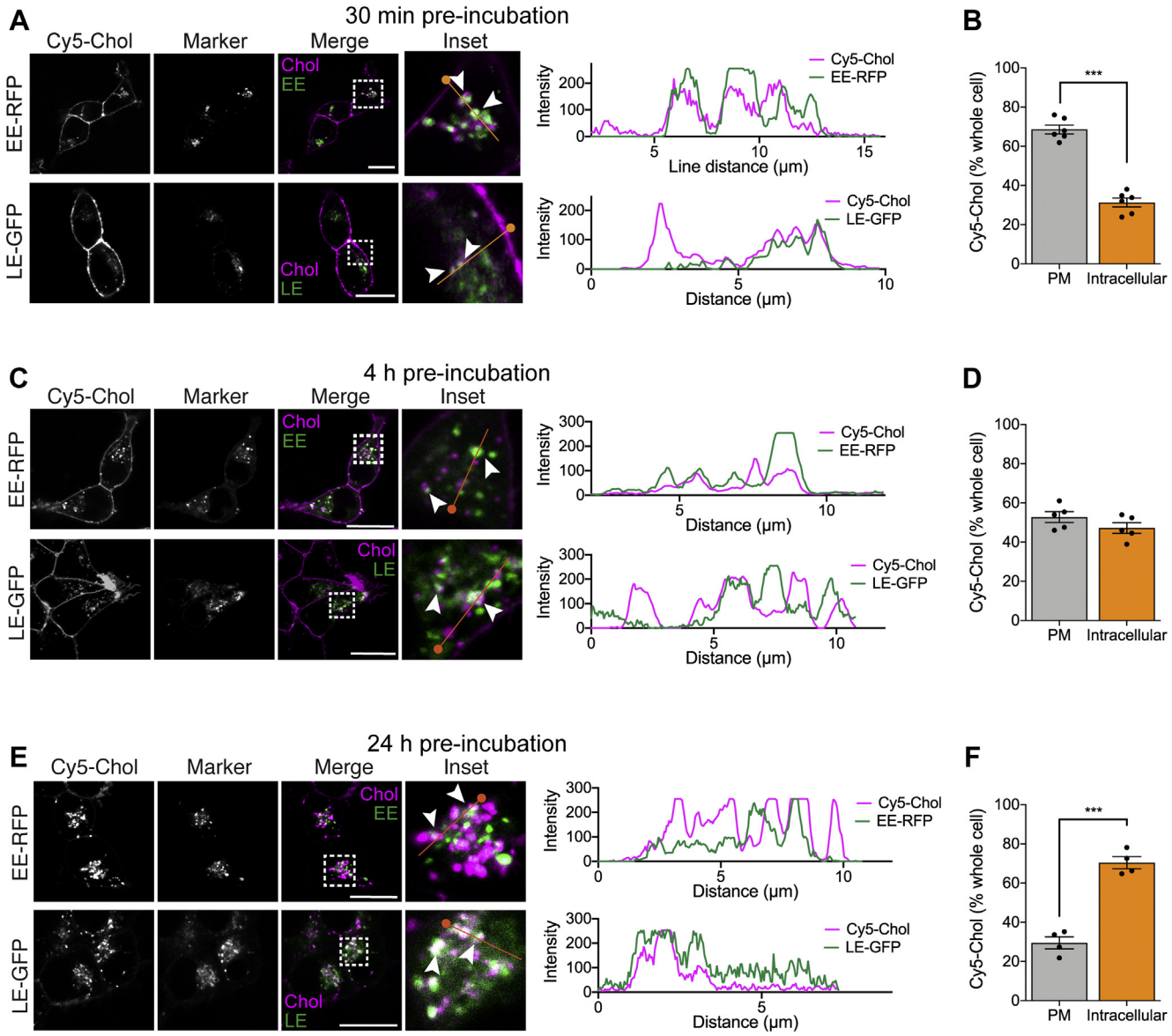


Figure 4. The cholestanol lipid anchor causes Cy5 movement from the plasma membrane deeper into endosomal pathways over 24 h. The location of the Cy5-Chol probe (1.5 μM) was determined after 30 min (*A, B*), 4 h (*C, D*) or 24 h (*E, F*) by confocal microscopy in HEK cells labeled with location markers of the endosomal network (CellLight: early endosome(EE)-RFP or late endosome(LE)-GFP) (n=4–6). *A, C, E*, representative, merged and zoomed images of HEK cells with location markers pseudocolored *green*, after 30 min incubation with Cy5-Chol (pseudocolored *magenta*). *Dotted box* indicates zoomed region for inset image. *Arrow heads* indicate coincidence of the Cy5-Chol with the location marker. *Orange line* indicates region highlighted in line scan intensity graph (right panel), with the start of the line indicated by a *circle*. Scale bar, 20 μm. *B, D, F*, the proportion of Cy5-Chol fluorescence at the plasma membrane compared with the rest of the cell (defined as intracellular Cy5). Bars show the grouped mean, and error bars represent S.E.M. of grouped cells from 4 to 6 independent experiments. ***$p < 0.001$, unpaired *t*-test.

signaling of the NK_1R in live cells as the receptor moves from the plasma membrane to early endosomes.

SP stimulation of NK_1R at the cell surface causes activation of $G\alpha_q$ signaling, which is limited to the plasma membrane (5, 14). NK_1R-$G\alpha_q$ stimulates phospholipase C (PLC)-dependent formation of inositol trisphosphate ($InsP_3$) and diacylglycerol (DAG). $InsP_3$ causes the transient release of Ca^{2+} (Fig. 2), and then both DAG and Ca^{2+} activate protein kinase C (PKC). PKC can then activate adenylyl cyclase (AC) to increase cAMP (Fig. S1).

We can measure changes in these transient signals from the NK_1R at the plasma membrane of live cells. In HEK293 cells transfected with HA-NK_1R and a PKC FRET biosensor (cytoCKAR), fast imaging shows a transient increase in PKC activity in response to SP, which declined to a steady-state level by 30 s following receptor stimulation (Fig. 5*A*). In HEK293 cells transfected with HA-NK_1R and a plasma membrane cAMP FRET biosensor (pmEpac2), this transient PKC signal was followed by a slightly delayed but also transient increase in cAMP at the plasma membrane in response to SP. With a peak at ∼5 min, the cAMP response then declined slowly toward baseline (Fig. 5*B*). This high-resolution examination of localized signaling allowed us to assemble a timescale of events at the plasma membrane following NK_1R stimulation

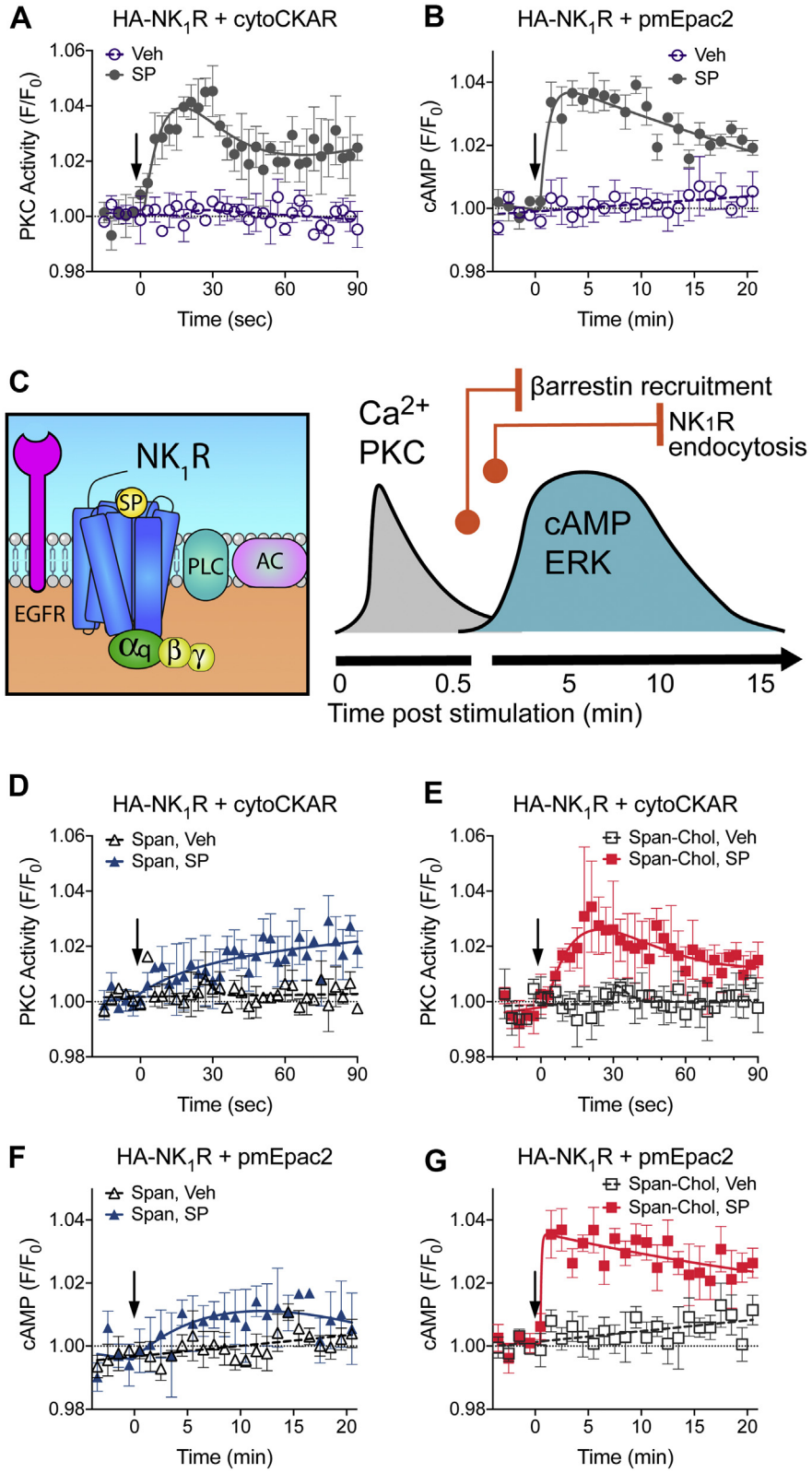


Figure 5. Only Span inhibits all NK_1R signaling from the plasma membrane. After a 4 h preincubation Span, but not Span-Chol, blocks SP-stimulated transient increases in PKC activity and cAMP (n = 3). *A* and *B*, HEK cells transfected with HA-NK_1R and cytoCKAR (*A*) or pmEpac2 (*B*) were stimulated with vehicle (0.0001% v/v MilliQ H_2O) or 1 nM SP and signaling was measured over time. *C*, Cartoon of the sequence of events following NK_1R stimulation at the plasma membrane. *Orange circles* indicate the time at which a regulatory event starts, and vertical *orange lines* indicate when it reaches a plateau. Signaling is represented by *black lines*. *D–G*, HEK cells transfected with HA-NK_1R and cytoCKAR (*D–E*) or pmEpac2 (*F–G*) were pretreated with 1 μM Span (*D*, *F*) or Span-Chol (*E*, *G*) for 4 h prior to addition of vehicle (0.0001% v/v MilliQ H_2O) or 1 nM SP. Data are expressed as the FRET relative to the baseline FRET (F/F_0). *Arrows* indicate time of vehicle/SP addition. Symbols show the mean, and error bars S.E.M. of grouped cells from three independent experiments.

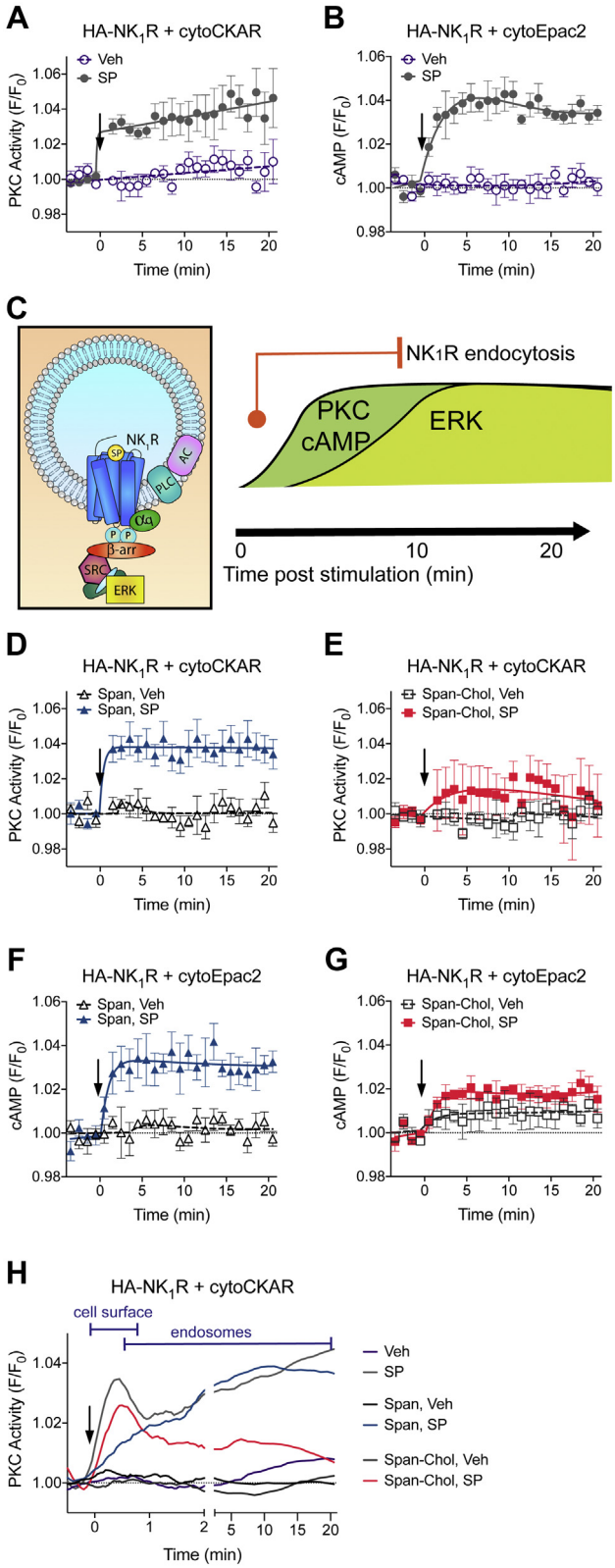


Figure 6. Only Span-Chol, and not Span, inhibits NK_1R signaling from endosomes. After a 4 h preincubation Span-Chol, but not Span, blocks SP-stimulated sustained increases in PKC and cAMP (n = 3). *A* and *B*, HEK cells transfected with HA-NK_1R and cytoCKAR (*A*) or cytoEpac2 (*B*) were stimulated with vehicle (0.0001% v/v MilliQ H2O) or 1 nM SP and signaling was measured over 20 min. *C*, cartoon of the sequence of events in endosomes following NK_1R stimulation. β-arr, β-arrestin. The *orange circle* indicates the time at which internalization starts, and the *vertical orange line* indicates when it reaches a plateau. Signaling is represented by black lines. *D–H*, HEK cells transfected with HA-NK_1R and cytoCKAR (*D–E*) or cytoEpac2 (*F–G*) were pretreated with 1 μM Span (*D, F*) or Span-Chol (*E, G*) for 4 h prior to addition of vehicle (0.0001% v/v MilliQ H2O) or 1 nM SP. Symbols show the mean, and error bars represent S.E.M. of grouped cells from three independent experiments. *H*, smoothed time course traces showing the change in effectiveness of Span versus Span-Chol at blocking SP-stimulated PKC signaling as the NK_1R transitions from the plasma membrane (data taken from Fig. 5*A*) to endosomes (data from Fig. 6*A*). Data are expressed as the FRET relative to the baseline FRET (F/F_0). *Arrows* indicate time of vehicle/SP addition.

(Fig. 5*C*). The activated receptor causes a fast peak of both Ca^{2+} and PKC activity in the first 30 s, which overlaps the start of the transient cAMP and cytosolic ERK signals. The peak of cAMP and cytosolic ERK signaling coincides with a plateau in the recruitment of β-arrestins (2–5 min post receptor stimulation) (5). The cAMP and cytosolic ERK signals then decline back toward baseline, which coincides with a plateau in the internalization of NK_1R to early endosomes (10–15 min post receptor activation) (5).

Using this timescale of events at the cell surface, we assessed the relative impact of Span versus Span-Chol on NK_1R signaling from the plasma membrane. We used a continuous incubation protocol for 4 h, so as not to wash away the free Span. This allows us to compare the spatial efficacy of both antagonists. A 4 h preincubation of the cells with Span inhibited the fast peak of PKC activity in response to SP, but there was no effect of Span-Chol on this signal (Figs. 5, *D* and *E*, S4, *A* and *B*). Similarly, a 4 h preincubation of the cells with Span inhibited the SP-induced increase in cAMP at the plasma membrane, with no effect of preincubation with Span-Chol on this signal (Figs. 5, *F* and *G*, S4, *C* and *D*).

These data suggest that while Span-Chol effectively blocks Ca^{2+} mobilization (Fig. 2), it is unable to block the PKC and cAMP signals activated by the SP-stimulated NK_1R at the plasma membrane. In contrast, free Span inhibits all signaling of the plasma-membrane-localized receptor (Ca^{2+}, PKC and cAMP).

Only a lipid-anchored antagonist can inhibit endosomal NK_1R signaling

Following NK_1R activation by SP, there is a rapid recruitment of β-arrestins and internalization of the receptor to early endosomes. Here, the NK_1R also colocalizes with $G\alpha_q$ and causes a sustained increase in PKC, cAMP, and ERK (5) (Fig. S1).

We can measure changes in these sustained signals from the NK_1R in endosomes of live cells. In HEK293 cells transfected with the HA-NK_1R and cytoCKAR, high content imaging over 20 min showed a steep increase in PKC activity by 1 min, which was sustained over the measurement period (Fig. 6*A*). Similarly, in HEK293 cells transfected with HA-NK_1R and a cytosolic cAMP FRET biosensor (cytoEpac2), we observed a prolonged increase in cAMP, which peaked by 2 min and was sustained over the 20 min period (Fig. 6*B*). This high-resolution examination of localized signaling allowed us to define a timescale of events at early endosomes following NK_1R stimulation (Fig. 6*C*). The activated NK_1R rapidly

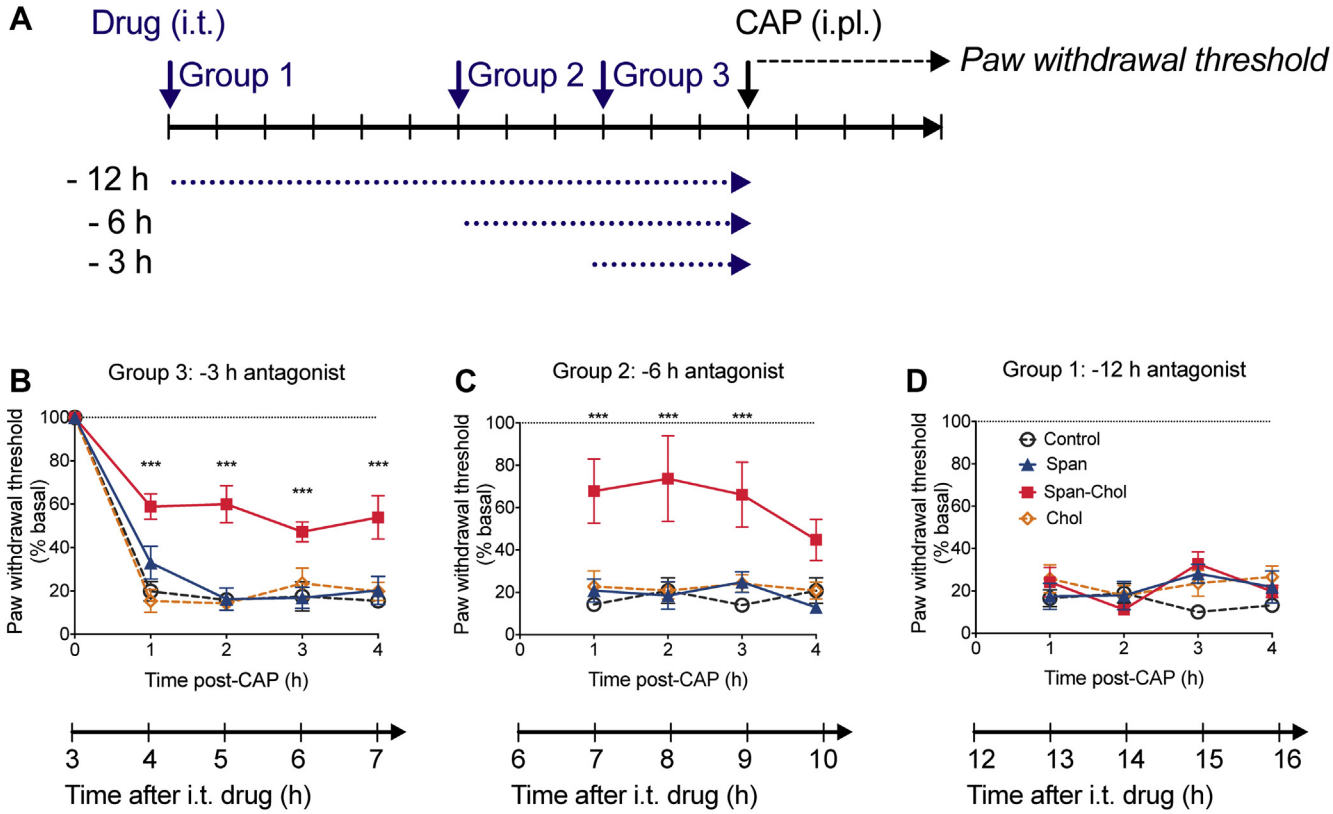


Figure 7. Span-Chol causes a prolonged antinociception in mice up to 9 h post administration. The analgesic effects of Span-Chol were assessed over 16 h in a mouse model of mechanical nociception (n = 6). *A*, illustration of the experimental protocol: Span (50 μM), Span-Chol (50 μM), Chol (50 μM), or vehicle (1% v/v DMSO/saline) was administered by intrathecal (i.t.) injection to three different groups of mice. The mice were left for 12 h (group 1), 6 h (group 2), or 3 h (group 3) before intraplantar (i.pl.) injection of capsaicin (CAP, 5 μg, 10 μl). Paw withdrawal responses to stimulation with von Frey filaments were measured hourly for 4 h. *B–D*, Paw withdrawal responses measured in the different groups of mice at 3 h (*B*), 6 h (*C*), or 12 h (*D*) after i.t. drug administration. Data are expressed relative to the baseline paw withdrawal threshold established for each mouse at the start of the experiment. Symbols show the mean, and error bars represent S.E.M. from 6 mice. ***$p < 0.001$ compared with mice that received i.t. vehicle, two-way ANOVA with Bonferroni posttest.

traffics to early endosomes that also contain $G\alpha_q$ within 1 min post receptor stimulation (5). This movement corresponds with a rapid and sustained increase in PKC activity and cAMP over very similar timescales. The sustained increase in nuclear ERK mediated by endosomal NK_1R is slightly delayed and peaks ∼10 min post receptor stimulation (5).

To compare the effect of Span versus Span-Chol on NK_1R signaling from early endosomes, we used a 4 h continuous incubation protocol. Under these conditions, Span had no effect on the SP-induced increase in PKC or cAMP (Figs. 6, *D* and *E*, S4, E–H). In contrast, preincubation for 4 h with Span-Chol inhibited SP-induced PKC and cAMP signaling (Figs. 6, *F* and *G*, S4, E–H).

Given the clear time distinction between the two PKC events stimulated by the plasma membrane versus endosomal NK_1R, we can visualize the changing spatial efficacies of the two antagonists (Figs. 6*H*, S4*I*). Under control conditions, spatiotemporal coordination of PKC activity is observed, where SP causes an initial peak in PKC activity from the plasma membrane NK_1R and then a steady increase in PKC activity from endosomal NK_1R. Signaling waves of this nature may be mediated due to spatially dependent activation of differentially localized PKC isoforms (27, 28).

A long preincubation with Span inhibits the PKC signal from cell surface NK_1R but has no effect on the PKC signals activated by endosomal NK_1R. In contrast, long preincubation with Span-Chol has no effect on the initial PKC signal from the activated cell surface NK_1R, but selectively inhibits signals from the endosomal NK_1R. These data suggest that free Span effectively inhibits plasma-membrane-delimited signaling but is unable to block signaling driven by intracellular NK_1R. In contrast, Span-Chol favors inhibition of PKC and cAMP signals activated by SP-NK_1R from endosomes.

The three-pronged mechanism of action of Span-Chol contributes to its long-lasting antinociceptive actions

We have previously demonstrated that blockade of endosomal (compared with plasma membrane) NK_1R causes much more effective antinociception (5, 17). In preclinical models of pain, the analgesic effect of Span-Chol was maintained for up to 6 h (5). However, it is unknown for how long this analgesic effect is sustained. We recently examined the analgesic effect of an NK_1R antagonist (aprepitant) over a 24 h period after directly delivering it to endosomes and found that antinociception was maintained for 6 h, before dropping back to baseline (17).

The three-pronged mechanism of Span-Chol identified in this study (higher local concentration at membranes, decreased receptor internalization, and complete inhibition of endosomal signaling) suggested that Span-Chol could provide prolonged pain relief. To evaluate this possibility, Span, Span-Chol, or controls were administered by intrathecal injection to three different groups of mice (Fig. 7*A*). Each group received an injection of capsaicin into the plantar surface of the left hindpaw at different times after intrathecal administration of the antagonists (*i.e.*, capsaicin injected 3 h, 6 h, or 12 h after antagonist administration). Mechanical nociception was evaluated by measurement of paw withdrawal responses to stimulation of the plantar surface with calibrated von Frey filaments every hour for 4 h after administration of capsaicin. As mechanical nociception to capsaicin was measured over exactly the same time period for all groups (4 h), this allowed us to build a timescale of the analgesic effect of Span-Chol over a cumulative 16 h period (Fig. 7).

In control mice receiving intrathecal vehicle, capsaicin caused a prolonged allodynia over 4 h (Fig. 7, *B–D*). Neither free Span nor the Chol control had any effect at any time tested. In contrast, Span-Chol had a marked antinociceptive action that was already present at 4 h post intrathecal injection and was fully maintained for 9 h after intrathecal injection. Thus, intrathecal delivery of Span-Chol resulted in a long duration of antinociception.

Discussion

The NK_1R is expressed throughout the nervous, immune, digestive, respiratory, and urogenital systems, where it regulates pain, inflammation, motility, and secretion (29–34). In the context of pain, noxious stimuli evoke the release of SP from peripheral and central projections of primary afferent neurons. In the dorsal horn of the spinal cord, SP then activates the NK_1R on second-order spinal neurons to mediate pain transmission (29). Despite this clear role in pain transmission, there has been limited clinical success for drug discovery programs targeting the NK_1R for chronic pain (29, 35). Previously, we reported that pain transmission is dependent on sustained signaling from the NK_1R internalized to endosomes and that we could improve analgesic effect and duration in preclinical models of pain by specifically blocking endosomal (and not cell surface) NK_1R (5, 17). Here, in addition to blockade of endosomal NK_1R, we have identified two further effects of a lipid-anchored NK_1R antagonist that contribute to its increased efficacy. First, we find that the addition of a lipid anchor causes a fourfold increase in the local concentration of a probe directly above the cell membrane. Second, although the probe quickly internalizes, 29.6% of the lipid-anchored probe remains at the plasma membrane even 24 h after administration. This residual plasma membrane localization facilitates an inhibition of NK_1R trafficking to endosomes. Together, this three-pronged mechanism—increased local concentration, inhibition of NK_1R trafficking to endosomes, and sustained blockade of endosomal signaling—contributes to the prolonged analgesic effects of lipidated antagonists in preclinical models of pain.

Cholestanol has a high affinity for sterol-rich microdomains of the outer leaflet of lipid bilayers. The binding of cholestanol to the sterol-rich microdomains then promotes internalization into endosomal compartments (36). Cholestanol has also been used to target an inhibitor of the recycling endopeptidase, β-site amyloid precursor protein cleaving enzyme 1 (BACE-1), to early endosomes (37). A lipid conjugated, but not a free antagonist, inhibited the cleavage of amyloid precursor protein at the BACE-1 ectodomain, a rate-limiting step in the production of the β-amyloid peptide. We subsequently used this approach to target an NK_1R antagonist to endosomes and observed a prolonged and seemingly selective inhibition of endosomal compared with plasma membrane NK_1R signaling (5). However, with further investigation we now find that the effects of a cholestanol-conjugated NK_1R antagonist are not limited to blockade of endosomal signaling. In addition to delivery to endosomes, we found that cholestanol conjugation causes a prolonged increase in the partitioning of the cargo into the plasma membrane. This is consistent with previous studies using Cy5-Chol or Cy5-Span-Chol that show fluorescent probe distribution in both endosomes and the plasma membrane over time (5). Increasing the lipophilic properties of soluble drugs, such as GPCR antagonists, can increase their association with membranes and may therefore enhance their local potency (24, 38). Here we found that the addition of cholestanol caused approximately fourfold increase in the concentration of Cy5 directly above the plasma membrane when we measured Cy5-Chol compared with Cy5-OEt concentrations using FCS. Although we did not directly measure the concentration of Span-Chol itself, a previous study reported a twofold local enrichment of the concentration of a GPCR ligand at the surface of cells transfected with the target GPCR, compared with nontransfected cells (22). This increase in local concentration was achieved without any change in the lipophilic properties of the ligand itself. As such, we would expect the local concentration of a lipid-anchored GPCR ligand to be *at least* fourfold higher at the surface of target cells. Consistent with this, we observed a corresponding increase in the potency and affinity of Span-Chol as compared with Span. This suggests that the blockade of endosomal signaling of the NK_1R by Span-Chol is not only due to its spatial distribution but could also be influenced by a high local concentration of Span-Chol at endosomal membranes.

Given the inherent ability of cholestanol conjugation to cause a prolonged increase in partitioning into membranes, it is important to map where the probes travel in cells. After initial incorporation into the plasma membrane, cholestanol probes translocate from the plasma membrane to endosomes. Within endosomes, cholestanol-conjugated antagonists inhibit the endosomal signaling of the NK_1R that underlies persistent excitation of spinal neurons and pain transmission (5). Consistent with our previous study, we find that Cy5-Chol is rapidly internalized into the endosomal network where it is codistributed with early and late endosomes. Despite this large movement of the Cy5-Chol into the cell, some of the probe

remains at the plasma membrane even after 24 h. This persistent partitioning of Cy5-Chol into the plasma membrane led us to look for an effect of Span-Chol on NK_1R endocytosis. BRET receptor trafficking studies revealed that up to 4 h after a pulse administration of Span-Chol, the lipid-anchored antagonist could inhibit receptor trafficking by blocking the recruitment of β-arrestins and therefore, subsequent receptor internalization to early endosomes. This inhibition of receptor movement into endosomes likely contributes to the overall decrease in endosomal signaling.

Due to the effective blockade of plasma membrane NK_1R calcium signaling (Fig. 2), β-arrestin recruitment, and receptor internalization (Fig. 3) by Span-Chol, we then examined the ability of the lipidated antagonist to affect other plasma-membrane-dependent NK_1R signaling pathways. Using an expanded toolbox of targeted FRET biosensors, we have mapped the signaling of the NK_1R as it traffics from the plasma membrane to endosomes. By comparing cAMP production detected by cytosolic and plasma-membrane-localized cAMP FRET biosensors, and delineating the temporal profiles of cytosolic PKC activity (acute versus sustained phases), we can show that Span-Chol is more effective at inhibiting endosomal-selective NK_1R signaling over sustained time periods. After 4 h of continuous administration, we find that Span effectively blocks all signaling from the plasma-membrane-localized NK_1R, but has no effect on signaling from the endosomal NK_1R. In contrast, Span-Chol was unable to block PKC or cAMP signals from the plasma membrane NK_1R but blocked all signaling from the endosomal NK_1R. It is interesting that Span-Chol appears to block NK_1R Ca^{2+} signaling and receptor internalization, but not cAMP or PKC signaling from the plasma membrane. GPCRs are highly flexible proteins that fluctuate between many different conformational states (39, 40). They may adopt different conformations at the plasma membrane versus in endosomes due to large differences in the curvature of the two membranes, the composition of the associated membrane lipids, and allosteric effects of associations with receptor signaling complexes (40–46). This could effectively facilitate slightly different binding orientations for Span-Chol in the two locations and perhaps allow location-biased antagonism. Alternatively, the enclosed and small volume of an endosome could effectively result in a much higher local concentration of the antagonist compared with the open and large volume of the extracellular space. The end result is that at the plasma membrane, Span-Chol is apparently more effective at inhibiting receptor internalization and Ca^{2+} signaling than inhibiting cAMP and PKC signaling. Signaling, in contrast to receptor internalization, is typically a highly amplified event. The recruitment of β-arrestins to a receptor, and subsequent β-arrestin-mediated internalization, is generally considered a low amplification event (47). In contrast, a single GPCR can activate multiple G proteins, which in turn switch on (or off) kinases or enzymes. For example, it is estimated that a single photon of light hitting a photosenstitive GPCR can activate between 16 and 60 G proteins, which in turn activate phosphodiesterases to hydrolyze 2000–72,000 molecules of cGMP (48). Small differences in the local concentration of Span-Chol or even its binding orientation could therefore have dramatic effects on receptor trafficking without seeming to affect downstream signaling (such as cAMP, PKC, ERK) from the receptor at the plasma membrane. Further studies involving, for example, direct measurement of NK_1R-G protein coupling at the plasma membrane compared with endosomes, may provide further insight into the mechanism of action for Span-Chol relative to Span.

We previously showed that Span-Chol could inhibit sustained pain transmission for up to 6 h following administration in preclinical models (5). Here we extended this analysis to show that the analgesic effects of Span-Chol are retained for >9 h following administration. This study demonstrates that lipidation is a viable approach, not only for enhancing membrane affinity of soluble GPCR antagonists, but also for targeting NK_1R signaling pathways of pathophysiological importance. Furthermore, this novel approach improves the pharmacological properties of an otherwise less potent NK_1R antagonist and results in potent and selective inhibition of signaling events associated with central pain transmission.

One explanation for the failure of previous drug discovery programs targeting the NK_1R for chronic pain is that they have only targeted plasma-membrane-localized NK_1R. Until very recently, GPCRs were only considered to be active at the cell surface, and therefore most drugs targeting GPCRs are not required to cross the plasma membrane. There is now clear evidence to show that activation of receptors in endosomes (compared with the cell surface) encodes for distinct physiological outcomes (5, 8, 49–52). It is therefore important to consider the subcellular location of a target GPCR, and whether they reside in, or are delivered to, a particular location. For example, the β_1-adrenoceptor is localized to two distinct pools in cells: one at the cell surface and a second at the Golgi (16). Golgi-localized signaling of the β_1-adrenoceptor requires a preexisting pool of receptors (*i.e.*, they are not delivered to the Golgi following internalization from the cell surface). In this case, as these two receptor populations are distinct, a targeting strategy involving direct delivery would be better suited than one that also facilitates inhibition of cell surface receptor endocytosis. In contrast, the two NK_1R receptor pools at the cell surface and endosomes are linked by receptor internalization. As such, blockade of the endosomal pool is further enhanced by preventing movement of the pool at the cell surface into the endosomal network. This could explain the prolonged analgesic activity of a lipidated-NK_1R antagonists versus an antagonist directly delivered to endosomes (5, 17) (Fig. 7).

Whether preventing NK_1R internalization (in addition to inhibition of endosomal NK_1R signaling) would be of benefit in situations of chronic pain is uncertain. In patients suffering from chronic visceral pain, the NK_1R is no longer available at the cell surface, but is instead found principally within intracellular compartments (35). In this case, as for the Golgi-localized β_1-adrenoceptor, there may be no added benefit of blocking receptor internalization from the cell surface. Future studies will need to directly compare different methods of

ASBMB

endosomal drug delivery and their resulting efficacy in a variety of disease models. Identifying additional mechanisms that contribute to the increased preclinical efficacy of lipid-anchored NK_1R antagonists is an important step toward understanding how we can effectively target intracellular GPCRs in disease.

Experimental procedures

Probes

The tripartite probes Span-Chol, Cy5-Chol, Cy5-OEt, and Chol were synthesized as described previously (5, 8). Tetramethylrhodamine (TAMRA)-labeled SP (SP-TAMRA) was synthesized by GL Biochem (Shanghai, China).

cDNAs

Rat NK_1R-GFP, HA-NK_1R, and NK_1R-RLuc8 have been described (14, 53). SNAP-NK_1R was from Cisbio. CytoCKAR (Addgene plasmid 14,870) was from A. Newton (54). CytoEpac2-camps was from M. Lohse (University of Wurzburg, Germany) (9), and pmEpac2-camps was from D. Cooper (University of Cambridge, UK) (55). KRas-Venus (56) and Rab5a-Venus (57) were from N. Lambert. β-arrestin 2-YFP was from M. Caron (University of North Carolina).

Cell culture and transfection

HEK293 cells (ATCC, negative for *mycoplasma* contamination) were maintained in Dulbecco's modified Eagle's medium (DMEM) supplemented with 5% (v/v) FBS. HEK293 cells were transfected using linear polyethyleneimine. HEK293-FlpIn cells stably expressing rat HA-NK_1R (HEK-NK_1R) and SNAP-NK_1R (HEK-SNAP-NK_1R) have been described (5, 15). HEK-NK_1R and HEK-SNAP-NK_1R cells were maintained in DMEM supplemented with 10% (v/v) FBS and 100 μg/ml Hygromycin B. All assay dishes and plates were coated with poly-D-lysine (5 $\mu g/cm^2$).

Fluorescence correlation spectroscopy (FCS)

FCS measurements were made using a Zeiss LSM510Meta ConfoCor 3 microscope fitted with a c-Apochromat 40x NA 1.2 water immersion objective lens (58). Cy5 was excited using a 633 nm HeNe laser, with emission collected through a 650LP filter and the pinhole diameter of 1 Airy unit. Prior to each experiment, Cy5 NHS ester (GE healthcare, Buckingham, UK) was used to calibrate the 633 nm detection volume using a literature value for diffusion coefficient (D) of 3.16×10^{-10} m^2/s, as described (22, 58).

HEK-NK_1R-SNAP was plated on Nunc Lab-Tek 8-well coverglasses (SLS, Nottingham, UK). After 24 h, Cy5-Chol and Cy5-OEt were prepared in HBSS and cells were incubated with a 10 nM solution of each ligand for 10 min at 37°C in a final volume of 400 μl. A reference confocal image of each cell was captured, before positioning the FCS detection volume in x-y using a live confocal image. A fluorescence intensity scan in the z direction was used to determine the position of the plasma membrane, and the focal point was positioned at defined distances above this point using the microscope's harmonic z-drive. FCS fluctuations were recorded at each point (ex λ: 633 nm HeNe, em λ: LP650 nm filter) for 20 s, at a laser power of ~1 kW/cm^2.

Probe dwell times and particle numbers were obtained from subsequent autocorrelation analysis of the fluctuations, performed with a 1 component, 3D Brownian model fit incorporating a triplet state pre-exponential using Zeiss 2010 Black software (22). Probe concentration and diffusion coefficients were calculated from measurements of dwell time and particle number, respectively, using the dimensions of the detection volume calculated from the Cy5 calibration data.

High-content fluorescent competition binding

HEK-NK_1R cells in black optically-clear 96 well plates were grown to 80% confluency. Cells were pretreated at 37°C with increasing concentrations of Span or Span-Chol for the indicated times, followed by an EC_{50} concentration (0.5 nM) of SP-TAMRA. Total binding was determined by preincubation with a vehicle control (0.1% v/v DMSO). Cell nuclei were stained with Hoechst 33,342 (1 μg/ml, 30 min, 37°C). Images were acquired using an ImageXpress Ultra confocal high-content plate reader (Molecular Devices, Sunnyvale, CA, USA) with Fluor 40x NA0.6 objective and the pinhole set to 4. Cells were imaged using the 405 nm and 561 nm laser excitations for Hoechst (DAPI filter) and TAMRA (Texas Red filter), respectively. The experiment was performed in triplicate with four fields of view imaged per well. Images were analyzed with MetaXpress 2.0 software (Molecular Devices), using an automated granularity module with the granule range set to 5–10 μm and intensity thresholds for granule classification set for each experiment based on the positive and negative controls (*i.e.*, total and nonspecific binding). A nuclear count from the Hoechst 33,342 image was obtained and the granularity module calculated the average intensity per cell, as previously described (23, 59). Data were fit with a competitive binding, one site, fit $logIC_{50}$ model.

Confocal imaging

To identify endosomal compartments, HEK293 cells were transduced with fluorescent fusion proteins using CellLight BacMam 2.0 virus (Life Technologies) for 16 h. CellLight fusion proteins used were as follows: early endosome-RFP, late endosome-GFP. Cells were equilibrated in Hanks' Balanced Salt Solution (HBSS) for 30 min prior to imaging.

Images were obtained using a Leica TCS SP8 Laser-scanning confocal microscope with HCX PL APO 40x (NA 1.30) and HCX PL APO 63x (NA 1.40) oil objectives in a humidified and temperature-controlled chamber at 37°C. For each cell, three baseline images were captured (4–6 optical sections) before addition of Cy5-Chol (1.5 μM). Cells were imaged at different time points following probe addition, as indicated.

Imaging was performed on at least three different days with separate drug preparations. Line scan intensity was processed using the FIJI distribution of Image J (60). The proportion of

Cy5 fluorescence at the plasma membrane compared with the rest of the cell was calculated as a percentage of the raw integrated density of the total cell area.

Measurement of intracellular Ca^{2+}

HEK-NK_1R cells in 96-well plates were washed with calcium buffer (10 mM HEPES, 0.5% w/v BSA, 10 mM D-glucose, 2.2 mM $CaCl_2$ 1.18 mM $MgCl_2$, 2.6 mM KCl, 150 mM NaCl, 4 mM probenecid, 0.05% v/v pluronic acid F127; pH 7.4) and then loaded with 1 μM Fura-2 AM ester (Life Technologies) in calcium buffer for 45 min at 37°C. For short preincubation with the antagonist, increasing concentrations of Span or Span-Chol were incubated with the cells for 30 min during Fura-2 AM loading. For longer preincubation with the antagonist, cells were incubated with increasing concentrations of Span or Span-Chol for the indicated time periods prior to Fura-2 AM loading.

Calcium was measured using a FlexStation 3 plate reader (Molecular Devices). Fluorescence (excitation: 340 nm and 380 nm; emission: 520 nm) was measured at 4 s intervals for a total of 45 s. After establishing baseline fluorescence, cells were stimulated with vehicle, 1 nM SP, or 1 μM ionomycin (to obtain a maximal response). SoftMax Pro (v5.4.4) software was used to calculate the area under the curve from the kinetic data from at least four experiments performed in duplicate.

Receptor trafficking using BRET

HEK293 cells in 10 cm dishes were cotransfected with 1 μg of NK_1R-RLuc8 and 4 μg β-arrestin 2-YFP, KRas-Venus or Rab5a-Venus. After 24 h, cells were replated in 96-well white opaque culture plates (CulturPlate-96; PerkinElmer). Forty-eight h after transfection, cells were pretreated with antagonists. For short preincubations, cells were incubated with increasing concentrations of Span, Span-Chol, or Chol in HBSS for 30 min. For "pulsed" long preincubations, cells were incubated with increasing concentrations of Span, Span-Chol, or Chol for 30 min, washed, media was replaced for 3 h, prior to equilibration for 30 min in HBSS (4 h total). Coelenterazine h (Promega) was added at a final concentration of 5 μM, and the cells were incubated for a further 5 min.

The BRET baseline was measured every 1 min for 4 min, before addition of vehicle or 1 nM SP, with BRET measurements continued every 1 min for 25 min. BRET was measured using a PHERAstar Omega microplate reader (BMG Labtech) with sequential integration of the signals detected at 475 ± 30 nm and 535 ± 30 nm with filters with the appropriate band pass. Data are shown as the BRET ratio (calculated as the ratio of the YFP/Venus signal to the RLuc8 signal) expressed as the SP-induced change in BRET (corrected for vehicle) for time course graphs. Curve fitting of time course data used exponential equations in GraphPad Prism version 8.4.3 (plateau followed by one-phase association for Rab5a and β-arrestin2 BRET or one-phase decay for KRas BRET). The plateau was derived from the curve fit for each independent experiment and is shown relative to the control SP response ($BRET/BRET_{SP}$) for bar graphs. Normal distribution of the data was confirmed using normality (QQ) plots in GraphPad Prism prior to statistical analysis.

Spatial PKC and cAMP using high-content and confocal ratiometric FRET imaging

High-content ratiometric FRET imaging was performed as described previously (61). HEK293 cells in black, optically clear 96-well plates were grown to 70% confluency before cotransfection with 55 ng/well HA-NK_1R and 40 ng/well cytoCKAR, pmEpac2, or cytoEpac2 for 48 h. Before the experiment, cells were partially serum-restricted overnight in 0.5% (v/v) FBS DMEM. On the day of the experiment, cells were preincubated with Span or Span-Chol (both 1 μM) for 4 h before the medium was replaced with HBSS and cells were equilibrated for 30 min at 37°C. High-content fluorescence imaging was performed using the INCell 2000 Analyzer with a Nikon Plan Fluor ELWD 40× (NA, 0.6) objective and FRET module (GE Healthcare) (14, 61). Cells were sequentially excited using a CFP filter (430/24) with emission measured using YFP (535/30) and CFP (470/24) filters with a polychroic optimized for this filter pair (Quad 3). The FRET baseline was measured every 1 min for 4 min, before addition of vehicle control (0.0001% v/v MilliQ H_2O) or 1 nM SP, with image capture continued for 20 min. At the end of each experiment, the same cells were stimulated with positive controls to maximally activate the biosensor: 200 nM phorbol 12,13-dibutyrate (PDBu) with phosphatase inhibitor cocktail (Merck) for CKAR, or 10 μM forskolin with 100 μM 3-isobutyl-1-methylxanthine for Epac2. After 10 min incubation, images were captured every 1 min for a final 4 min.

For fast confocal imaging experiments, HEK293 cells in 8-well Ibidi chamber slides were grown to 50% confluency before cotransfection with 110 ng/well HA-NK_1R and 80 ng/well cytoCKAR. Before the experiment, cells were partially serum-restricted overnight in 0.5% (v/v) FBS DMEM. Forty-eight h after transfection, cells were preincubated with Span or Span-Chol (both 1 μM) for 4 h before the medium was replaced with HBSS and cells were equilibrated for 30 min at 37°C. Fast capture imaging was performed using a Zeiss LSM710 confocal fluorescence microscope with a Zeiss 40x NA1.34, oil immersion objective, with pinhole set to 2 AU. Cells were excited at 458 nm (CFP), with dual emission measured at 481 nm (CFP) and 540 nm (YFP). The FRET baseline was measured every 3 s for 30 s, before addition of vehicle control (0.0001% v/v MilliQ H_2O) or 1 nM SP, with image capture continued every 3 s for 2 min. At the end of each experiment, the same cells were stimulated with a positive control, 200 nM PDBu, and imaged for a further 5 min.

For both high-content and fast imaging experiments, only cells with >3% change in F/F_0 (FRET ratio relative to baseline for each cell) after stimulation with the positive controls were selected for analysis. The average F/F_0 was calculated for each experiment and combined. Data were analyzed using in-house scripts written for the Fiji distribution of Image J (60), as described previously (61), with some modifications. The updated scripts are freely available from the Monash

ASBMB

University online repository, Bridges (https://doi.org/10.26180/13289105) (62). Data were fit using a Pharmechanics "rise and fall" time course equation ("baseline then rise-and-fall to baseline time course with drift"), which is freely available (https://www.pharmechanics.com/time-course-tool-pack).

Animal models of mechanical nociception

A total of 72 male C57Bl/6 mice (6–12 weeks old) were used in this study. Mice were maintained in a temperature and humidity-controlled room (23°C ± 2° C) under a 12 h light/dark cycle with food and water *ad libitum*. The study was conducted in accordance with the requirements of the Australian Code for the Care and Use of Animals for Scientific Purposes (eighth edition, 2013) and the ethical guidelines of the International Association for the Study of Pain (63), and was approved by the animal ethics committee of Monash Institute of Pharmaceutical Sciences, Monash University. Mice were randomly assigned to experimental groups.

Mice were acclimatized to the experimental conditions on two successive days for 1–2 h. On the day of the study, withdrawal thresholds were measured in duplicate to establish baseline readings for each mouse. Span, Span-Chol, Chol (all 50 μM), or vehicle (1% v/v DMSO in 0.9% w/v saline) was injected intrathecally (5 μl, L3-L4) into the mice (n = 6 per group) anesthetized with isoflurane inhalation (2–5% delivered in oxygen). At 3, 6, and 12 h after drug administration, capsaicin (5 μg, vehicle: 20% ethanol, 10% Tween 80, 70% saline; v/v; 10 μl/mouse) was administered by intraplantar injection under isoflurane anesthesia (2–5% delivered in oxygen) to the left hindpaw. Nociception was assessed by measuring paw withdrawal thresholds with von Frey filaments of ascending force, applied to the plantar surface of the hindpaws as previously described (5, 64). Paw withdrawal thresholds were measured for both the ipsilateral and contralateral hindpaws every hour for 4 h. The data were subsequently normalized to the baseline paw withdrawal threshold for each animal. Investigators were blinded to drug treatments and experimental groups.

Data analysis

Graphs were generated using GraphPad Prism 8 (San Diego, CA). Data are presented as mean ± S.E.M, unless otherwise stated.

Data availability

All data are contained within the article.

Author contributions—N. W. B., M. L. H., N. A. V., Q. N. M. conceived and designed the study; Q. N. M., P. S., T. Q., J. S. R., A. B. G., H. R. Y., L. A., J. W. C., and C. J. N. generated compounds, acquired data and wrote analysis scripts; Q. N. M., P. S., J. S. R., A. B. G., H. R. Y., S. J. B., S. J. H., C. J. H. P., N. W. B, M. L. H., and N. A. V. analysed and interpreted data; D. P. P., M. C., B. G., T. P. D., S. J. B., S. J. H., C. J. H. P., N. W. B., M. L. H., and N. A. V. supervised the study; Q. N. M, M. L. H., and N. A. V. wrote the manuscript. All authors critically revised and approved the manuscript.

Funding and additional information—This work was supported by grants from the National Institutes of Health (NS102722, DE026806, DE029951, DK118971 to N. W. B), Department of Defence (W81XWH1810431 to N. W. B.), National Health and Medical Research Council (63303 to N. W. B., 1049682 to N. W. B. and B. G., 1031886 to N. W. B. and D. P. P, 1083054 to N. W. B., M. L. H., M. C., C. J. P., and T. P. D.), ARC Centre of Excellence in Convergent Bio-Nano Science and Technology (CE14100036 to N. W. B., T. P. D., C. J. P., N. A. V.), and Medical Research Council (MR/N020081/1 to S. J. B., S. J. H.). M. L. H. was an NHMRC RD Wright Fellow (1061687). Q. N. M. was part of the Joint Award Doctoral Training Centre in Molecular Pharmacology and Drug Discovery at Monash University (Australia) and the University of Nottingham (UK).

Conflict of interest—N. W. B. is a founding scientist of Endosome Therapeutics Inc. Research in the laboratories of N. W. B., N. A. V., and D. P. P. is funded in part by Takeda Pharmaceuticals Inc and Endosome Therapeutics Inc (N. A. V. and D. P. P.).

Abbreviations—The abbreviations used are: AC, adenylyl cyclase; BACE-1, β-site amyloid precursor protein cleaving enzyme 1; BRET, bioluminescence resonance energy transfer; cAMP, cyclic adenosine monophosphate; Chol, biotin conjugated to cholestanol *via* a PEG linker; CFP, cyan fluorescent protein; Cy5, cyanine 5; Cy5-Chol, cyanine 5 with cholestanol linked via PEG; Cy5-OEt, cyanine 5 with an ethyl ester linked via PEG; cytoCKAR, cytosolic C kinase activity reporter FRET biosensor; cytoEpac2, cytosolic Epac2-camps FRET biosensor; DAG, diacylglycerol; DMEM, Dulbecco's modified Eagle's medium; EGFR, epidermal growth factor receptor; ERK, extracellular signal regulated kinase (mitogen activated protein kinase); FBS, fetal bovine serum; FCS, fluorescence correlation spectroscopy; GPCR, G protein-coupled receptor; $InsP_3$, inositol trisphosphate; NK_1R, neurokinin 1 receptor; OEt, ethyl ester; PKA, protein kinase A; PKC, protein kinase C; pmEpac2, plasma membrane localized Epac2-camps FRET biosensor; RLuc8, Renilla luciferase; SP, substance P; Span, Spantide I; Span-Chol, Spantide I conjugated to cholestanol via PEG linker; TAMRA, tetramethylrhodamine; YFP, yellow fluorescent protein.

References

1. Hauser, A. S., Attwood, M. M., Rask-Andersen, M., Schioth, H. B., and Gloriam, D. E. (2017) Trends in GPCR drug discovery: New agents, targets and indications. *Nat. Rev. Drug Discov.* **16**, 829–842
2. Luttrell, L. M., Ferguson, S. S., Daaka, Y., Miller, W. E., Maudsley, S., Della Rocca, G. J., Lin, F., Kawakatsu, H., Owada, K., Luttrell, D. K., Caron, M. G., and Lefkowitz, R. J. (1999) Beta-arrestin-dependent formation of beta2 adrenergic receptor-Src protein kinase complexes. *Science* **283**, 655–661
3. Slessareva, J. E., Routt, S. M., Temple, B., Bankaitis, V. A., and Dohlman, H. G. (2006) Activation of the phosphatidylinositol 3-kinase Vps34 by a G protein alpha subunit at the endosome. *Cell* **126**, 191–203
4. Sorkin, A., and von Zastrow, M. (2009) Endocytosis and signalling: Intertwining molecular networks. *Nat. Rev. Mol. Cell Biol.* **10**, 609–622
5. Jensen, D. D., Lieu, T., Halls, M. L., Veldhuis, N. A., Imlach, W. L., Mai, Q. N., Poole, D. P., Quach, T., Aurelio, L., Conner, J., Herenbrink, C. K., Barlow, N., Simpson, J. S., Scanlon, M. J., Graham, B., *et al.* (2017) Neurokinin 1 receptor signaling in endosomes mediates sustained nociception and is a viable therapeutic target for prolonged pain relief. *Sci. Transl. Med.* **9**, eaal3447
6. Irannejad, R., Tomshine, J. C., Tomshine, J. R., Chevalier, M., Mahoney, J. P., Steyaert, J., Rasmussen, S. G., Sunahara, R. K., El-Samad, H., Huang, B., and von Zastrow, M. (2013) Conformational biosensors reveal GPCR signalling from endosomes. *Nature* **495**, 534–538

7. Murphy, J. E., Padilla, B. E., Hasdemir, B., Cottrell, G. S., and Bunnett, N. W. (2009) Endosomes: A legitimate platform for the signaling train. *PNAS* **106**, 17615–17622
8. Yarwood, R. E., Imlach, W. L., Lieu, T., Veldhuis, N. A., Jensen, D. D., Herenbrink, C. K., Aurelio, L., Cai, Z., Christie, M. J., and Poole, D. P. (2017) Endosomal signaling of the receptor for calcitonin gene-related peptide mediates pain transmission. *Proc. Natl. Acad. Sci.* **114**, 12309–12314
9. Nikolaev, V. O., Bunemann, M., Hein, L., Hannawacker, A., and Lohse, M. J. (2004) Novel single chain cAMP sensors for receptor-induced signal propagation. *J. Biol. Chem.* **279**, 37215–37218
10. Calebiro, D., Nikolaev, V. O., Gagliani, M. C., de Filippis, T., Dees, C., Tacchetti, C., Persani, L., and Lohse, M. J. (2009) Persistent cAMP-signals triggered by internalized G-protein-coupled receptors. *Plos Biol.* **7**, e1000172
11. Dionne, R. A., Max, M. B., Gordon, S. M., Parada, S., Sang, C., Gracely, R. H., Sethna, N. F., and MacLean, D. B. (1998) The substance P receptor antagonist CP-99,994 reduces acute postoperative pain. *Clin. Pharmacol. Ther.* **64**, 562–568
12. Diener, H. C., and Group, R. P. R. S. (2003) RPR100893, a substance-P antagonist, is not effective in the treatment of migraine attacks. *Cephalalgia* **23**, 183–185
13. Goldstein, D. J., Wang, O., Saper, J. R., Stoltz, R., Silberstein, S. D., and Mathew, N. T. (1997) Ineffectiveness of neurokinin-1 antagonist in acute migraine: A crossover study. *Cephalalgia* **17**, 785–790
14. Jensen, D. D., Halls, M. L., Murphy, J. E., Canals, M., Cattaruzza, F., Poole, D. P., Lieu, T., Koon, H. W., Pothoulakis, C., and Bunnett, N. W. (2014) Endothelin-converting enzyme 1 and beta-arrestins exert spatio-temporal control of substance P-induced inflammatory signals. *J. Biol. Chem.* **289**, 20283–20294
15. Cottrell, G. S., Padilla, B. E., Amadesi, S., Poole, D. P., Murphy, J. E., Hardt, M., Roosterman, D., Steinhoff, M., and Bunnett, N. W. (2009) Endosomal endothelin-converting enzyme-1: A regulator of beta-arrestin-dependent ERK signaling. *J. Biol. Chem.* **284**, 22411–22425
16. Irannejad, R., Pessino, V., Mika, D., Huang, B., Wedegaertner, P. B., Conti, M., and von Zastrow, M. (2017) Functional selectivity of GPCR-directed drug action through location bias. *Nat. Chem. Biol.* **13**, 799–806
17. Ramirez-Garcia, P. D., Retamal, J. S., Shenoy, P., Imlach, W., Sykes, M., Truong, N., Constandil, L., Pelissier, T., Nowell, C. J., Khor, S. Y., Layani, L. M., Lumb, C., Poole, D. P., Lieu, T., Stewart, G. D., *et al.* (2019) A pH-responsive nanoparticle targets the neurokinin 1 receptor in endosomes to prevent chronic pain. *Nat. Nanotechnol.* **14**, 1150–1159
18. Rajendran, L., Schneider, A., Schlechtingen, G., Weidlich, S., Ries, J., Braxmeier, T., Schwille, P., Schulz, J. B., Schroeder, C., Simons, M., Jennings, G., Knolker, H. J., and Simons, K. (2008) Efficient inhibition of the Alzheimer's disease beta-secretase by membrane targeting. *Science* **320**, 520–523
19. Linning, P., Haussmann, U., Beyer, I., Weidlich, S., Schieb, H., Wiltfang, J., Klafki, H. W., and Knolker, H. J. (2012) Optimisation of BACE1 inhibition of tripartite structures by modification of membrane anchors, spacers and pharmacophores - development of potential agents for the treatment of Alzheimer's disease. *Org. Biomol. Chem.* **10**, 8216–8235
20. Briddon, S. J., and Hill, S. J. (2007) Pharmacology under the microscope: The use of fluorescence correlation spectroscopy to determine the properties of ligand-receptor complexes. *Trends Pharmacol. Sci.* **28**, 637–645
21. Stoddart, L. A., Vernall, A. J., Denman, J. L., Briddon, S. J., Kellam, B., and Hill, S. J. (2012) Fragment screening at adenosine-A(3) receptors in living cells using a fluorescence-based binding assay. *Chem. Biol.* **19**, 1105–1115
22. Gherbi, K., Briddon, S. J., and Charlton, S. J. (2018) Micro-pharmacokinetics: Quantifying local drug concentration at live cell membranes. *Sci. Rep.* **8**, 3479
23. Stoddart, L. A., Vernall, A. J., Briddon, S. J., Kellam, B., and Hill, S. J. (2015) Direct visualisation of internalization of the adenosine A3 receptor and localization with arrestin3 using a fluorescent agonist. *Neuropharmacology* **98**, 68–77
24. Vauquelin, G., and Charlton, S. J. (2010) Long-lasting target binding and rebinding as mechanisms to prolong *in vivo* drug action. *Br. J. Pharmacol.* **161**, 488–508
25. Sykes, D. A., Parry, C., Reilly, J., Wright, P., Fairhurst, R. A., and Charlton, S. J. (2014) Observed drug-receptor association rates are governed by membrane affinity: The importance of establishing "micro-pharmacokinetic/pharmacodynamic relationships" at the beta2-adrenoceptor. *Mol. Pharmacol.* **85**, 608–617
26. Pelayo, J. C., Poole, D. P., Steinhoff, M., Cottrell, G. S., and Bunnett, N. W. (2011) Endothelin-converting enzyme-1 regulates trafficking and signalling of the neurokinin 1 receptor in endosomes of myenteric neurones. *J. Physiol.* **589**, 5213–5230
27. Collazos, A., Diouf, B., Guerineau, N. C., Quittau-Prevostel, C., Peter, M., Coudane, F., Hollande, F., and Joubert, D. (2006) A spatiotemporally coordinated cascade of protein kinase C activation controls isoform-selective translocation. *Mol. Cell Biol.* **26**, 2247–2261
28. Mukherjee, A., Roy, S., Saha, B., and Mukherjee, D. (2016) Spatio-temporal regulation of PKC isoforms Imparts signaling specificity. *Front Immunol.* **7**, 45
29. Steinhoff, M. S., von Mentzer, B., Geppetti, P., Pothoulakis, C., and Bunnett, N. W. (2014) Tachykinins and their receptors: Contributions to physiological control and the mechanisms of disease. *Physiol. Rev.* **94**, 265–301
30. Caberlotto, L., Hurd, Y. L., Murdock, P., Wahlin, J. P., Melotto, S., Corsi, M., and Carletti, R. (2003) Neurokinin 1 receptor and relative abundance of the short and long isoforms in the human brain. *Eur. J. Neurosci.* **17**, 1736–1746
31. Hargreaves, R. (2002) Imaging substance P receptors (NK1) in the living human brain using positron emission tomography. *J. Clin. Psychiatry* **63**(Suppl 11), 18–24
32. Renzi, D., Pellegrini, B., Tonelli, F., Surrenti, C., and Calabro, A. (2000) Substance P (neurokinin-1) and neurokinin A (neurokinin-2) receptor gene and protein expression in the healthy and inflamed human intestine. *Am. J. Pathol.* **157**, 1511–1522
33. Pinto, F. M., Almeida, T. A., Hernandez, M., Devillier, P., Advenier, C., and Candenas, M. L. (2004) mRNA expression of tachykinins and tachykinin receptors in different human tissues. *Eur. J. Pharmacol.* **494**, 233–239
34. Greeno, E. W., Mantyh, P., Vercellotti, G. M., and Moldow, C. F. (1993) Functional neurokinin 1 receptors for substance P are expressed by human vascular endothelium. *J. Exp. Med.* **177**, 1269–1276
35. Jarcho, J. M., Feier, N. A., Bert, A., Labus, J. A., Lee, M., Stains, J., Ebrat, B., Groman, S. M., Tillisch, K., Brody, A. L., London, E. D., Mandelkern, M. A., and Mayer, E. A. (2013) Diminished neurokinin-1 receptor availability in patients with two forms of chronic visceral pain. *Pain* **154**, 987–996
36. Levental, I., Grzybek, M., and Simons, K. (2010) Greasing their way: Lipid modifications determine protein association with membrane rafts. *Biochemistry* **49**, 6305–6316
37. Rajendran, L., and Annaert, W. (2012) Membrane trafficking pathways in Alzheimer's disease. *Traffic* **13**, 759–770
38. Rose, R. H., Briddon, S. J., and Hill, S. J. (2012) A novel fluorescent histamine H(1) receptor antagonist demonstrates the advantage of using fluorescence correlation spectroscopy to study the binding of lipophilic ligands. *Br. J. Pharmacol.* **165**, 1789–1800
39. Kobilka, B. K., and Deupi, X. (2007) Conformational complexity of G-protein-coupled receptors. *Trends Pharmacol. Sci.* **28**, 397–406
40. Latorraca, N. R., Venkatakrishnan, A. J., and Dror, R. O. (2017) GPCR Dynamics: Structures in motion. *Chem. Rev.* **117**, 139–155
41. Jarsch, I. K., Daste, F., and Gallop, J. L. (2016) Membrane curvature in cell biology: An integration of molecular mechanisms. *J. Cell Biol* **214**, 375–387
42. McMahon, H. T., and Boucrot, E. (2015) Membrane curvature at a glance. *J. Cell Sci.* **128**, 1065–1070
43. Civciristov, S., Ellisdon, A. M., Suderman, R., Pon, C. K., Evans, B. A., Kleifeld, O., Charlton, S. J., Hlavacek, W. S., Canals, M., and Halls, M. L. (2018) Preassembled GPCR signaling complexes mediate distinct cellular responses to ultralow ligand concentrations. *Sci. Signal* **11**, eaan118
44. Huang, W., Masureel, M., Qu, Q., Janetzko, J., Inoue, A., Kato, H. E., Robertson, M. J., Nguyen, K. C., Glenn, J. S., Skiniotis, G., and Kobilka, B.

K. (2020) Structure of the neurotensin receptor 1 in complex with beta-arrestin 1. *Nature* **579**, 303–308
45. Wu, F. J., Williams, L. M., Abdul-Ridha, A., Gunatilaka, A., Vaid, T. M., Kocan, M., Whitehead, A. R., Griffin, M. D. W., Bathgate, R. A. D., Scott, D. J., and Gooley, P. R. (2020) Probing the correlation between ligand efficacy and conformational diversity at the alpha1A-adrenoreceptor reveals allosteric coupling of its microswitches. *J. Biol. Chem.* **295**, 7404–7417
46. Liang, Y. L., Belousoff, M. J., Fletcher, M. M., Zhang, X., Khoshouei, M., Deganutti, G., Koole, C., Furness, S. G. B., Miller, L. J., Hay, D. L., Christopoulos, A., Reynolds, C. A., Danev, R., Wootten, D., and Sexton, P. M. (2020) Structure and Dynamics of Adrenomedullin receptors AM1 and AM2 reveal Key mechanisms in the control of receptor Phenotype by receptor activity-Modifying proteins. *ACS Pharmacol. Transl. Sci.* **3**, 263–284
47. Eichel, K., Jullie, D., Barsi-Rhyne, B., Latorraca, N. R., Masureel, M., Sibarita, J. B., Dror, R. O., and von Zastrow, M. (2018) Catalytic activation of beta-arrestin by GPCRs. *Nature* **557**, 381–386
48. Arshavsky, V. Y., and Burns, M. E. (2014) Current understanding of signal amplification in phototransduction. *Cell Logist.* **4**, e29390
49. Tsvetanova, N. G., and von Zastrow, M. (2014) Spatial encoding of cyclic AMP signaling specificity by GPCR endocytosis. *Nat. Chem. Biol.* **10**, 1061–1065
50. Johannessen, L., Remsberg, J., Gaponenko, V., Adams, K. M., Barchi, J. J., Jr., Tarasov, S. G., Jiang, S., and Tarasova, N. I. (2011) Peptide structure stabilization by membrane anchoring and its general applicability to the development of potent cell-permeable inhibitors. *Chembiochem* **12**, 914–921
51. Merriam, L. A., Baran, C. N., Girard, B. M., Hardwick, J. C., May, V., and Parsons, R. L. (2013) Pituitary adenylate cyclase 1 receptor internalization and endosomal signaling mediate the pituitary adenylate cyclase activating polypeptide-induced increase in Guinea pig cardiac neuron excitability. *J. Neurosci.* **33**, 4614–4622
52. Jimenez-Vargas, N. N., Gong, J., Wisdom, M., Jensen, D. D., Latorre, R., Hegron, A., Teng, S., DiCello, J. J., Rajasekhar, P., Veldhuis, N. A., Carbone, S. E., Yu, Y., Lopez-Lopez, C., Jaramillo-Polance, J., Canals, M., *et al.* (2020) Endosomal signaling of delta opioid receptors is an endogenous mechanism and therapeutic target for relief from inflammatory pain. *Proc. Natl. Acad. Sci. U. S. A.* **117**, 15281–15292
53. Cattaruzza, F., Cottrell, G. S., Vaksman, N., and Bunnett, N. W. (2009) Endothelin-converting enzyme 1 promotes re-sensitization of neurokinin 1 receptor-dependent neurogenic inflammation. *Br. J. Pharmacol.* **156**, 730–739
54. Violin, J. D., Zhang, J., Tsien, R. Y., and Newton, A. C. (2003) A genetically encoded fluorescent reporter reveals oscillatory phosphorylation by protein kinase C. *J. Cell Biol.* **161**, 899–909
55. Wachten, S., Masada, N., Ayling, L. J., Ciruela, A., Nikolaev, V. O., Lohse, M. J., and Cooper, D. M. (2010) Distinct pools of cAMP centre on different isoforms of adenylyl cyclase in pituitary-derived GH3B6 cells. *J. Cell Sci.* **123**, 95–106
56. Lan, T. H., Liu, Q., Li, C., Wu, G., and Lambert, N. A. (2012) Sensitive and high resolution localization and tracking of membrane proteins in live cells with BRET. *Traffic* **13**, 1450–1456
57. Jensen, D. D., Godfrey, C. B., Niklas, C., Canals, M., Kocan, M., Poole, D. P., Murphy, J. E., Alemi, F., Cottrell, G. S., Korbmacher, C., Lambert, N. A., Bunnett, N. W., and Corvera, C. U. (2013) The bile acid receptor TGR5 does not interact with beta-arrestins or traffic to endosomes but transmits sustained signals from plasma membrane rafts. *J. Biol. Chem.* **288**, 22942–22960
58. Ayling, L. J., Briddon, S. J., Halls, M. L., Hammond, G. R., Vaca, L., Pacheco, J., Hill, S. J., and Cooper, D. M. (2012) Adenylyl cyclase AC8 directly controls its micro-environment by recruiting the actin cytoskeleton in a cholesterol-rich milieu. *J. Cell Sci.* **125**, 869–886
59. Kilpatrick, L. E., Briddon, S. J., Hill, S. J., and Holliday, N. D. (2010) Quantitative analysis of neuropeptide Y receptor association with beta-arrestin2 measured by bimolecular fluorescence complementation. *Br. J. Pharmacol.* **160**, 892–906
60. Schindelin, J., Arganda-Carreras, I., Frise, E., Kaynig, V., Longair, M., Pietzsch, T., Preibisch, S., Rueden, C., Saalfeld, S., Schmid, B., Tinevez, J. Y., White, D. J., Hartenstein, V., Eliceiri, K., Tomancak, P., *et al.* (2012) Fiji: An open-source platform for biological-image analysis. *Nat. Met.* **9**, 676–682
61. Halls, M. L., Poole, D. P., Ellisdon, A. M., Nowell, C. J., and Canals, M. (2015) Detection and Quantification of intracellular signaling using FRET-based biosensors and high content imaging. *Methods Mol. Biol.* **1335**, 131–161
62. Nowell, C. J., Poole, D. P., and Halls, M. L. (2020) *FRET Analysis - Stack Creator v3.2*, Monash University, Bridges, Melbourne, Australia
63. Zimmermann, M. (1983) Ethical guidelines for investigations of experimental pain in conscious animals. *Pain* **16**, 109–110
64. Alemi, F., Kwon, E., Poole, D. P., Lieu, T., Lyo, V., Cattaruzza, F., Cevikbas, F., Steinhoff, M., Nassini, R., Materazzi, S., Guerrero-Alba, R., Valdez-Morales, E., Cottrell, G. S., Schoonjans, K., Geppetti, P., *et al.* (2013) The TGR5 receptor mediates bile acid-induced itch and analgesia. *J. Clin. Invest.* **123**, 1513–1530

Original research

Agonist that activates the μ-opioid receptor in acidified microenvironments inhibits colitis pain without side effects

Nestor Nivardo Jiménez-Vargas,[1] Yang Yu ,[1] Dane D Jensen,[2,3] Diana Daeun Bok,[3] Matthew Wisdom,[3] Rocco Latorre,[3] Cintya Lopez,[1] Josue O Jaramillo-Polanco,[1] Claudius Degro,[1] Mabel Guzman-Rodriguez,[1] Quentin Tsang,[1] Zachary Snow,[4] Brian L Schmidt,[2] David E Reed,[1] Alan Edward Lomax,[1] Kara Gross Margolis,[4] Christoph Stein,[5] Nigel W Bunnett ,[3,6] Stephen J Vanner[1]

► Additional material is published online only. To view, please visit the journal online (http://dx.doi.org/10.1136/gutjnl-2021-324070).

For numbered affiliations see end of article.

Correspondence to
Professor Nigel W Bunnett, Department of Molecular Pathobiology, New York University College of Dentistry, New York, NY 10010, USA; nwb2@nyu.edu

NNJ-V, YY and DDJ are joint first authors.
NWB and SJV are joint senior authors.

Received 8 January 2021
Revised 15 February 2021
Accepted 9 March 2021

Check for updates

© Author(s) (or their employer(s)) 2021. No commercial re-use. See rights and permissions. Published by BMJ.

To cite: Jiménez-Vargas NN, Yu Y, Jensen DD, *et al*. *Gut* Epub ahead of print: [*please include* Day Month Year]. doi:10.1136/gutjnl-2021-324070

ABSTRACT

Objective The effectiveness of μ-opioid receptor (MOPr) agonists for treatment of visceral pain is compromised by constipation, respiratory depression, sedation and addiction. We investigated whether a fentanyl analogue, (±)-N-(3-fluoro-1-phenethylpiperidine-4-yl)-N-phenyl propionamide (NFEPP), which preferentially activates MOPr in acidified diseased tissues, would inhibit pain in a preclinical model of inflammatory bowel disease (IBD) without side effects in healthy tissues.

Design Antinociceptive actions of NFEPP and fentanyl were compared in control mice and mice with dextran sodium sulfate colitis by measuring visceromotor responses to colorectal distension. Patch clamp and extracellular recordings were used to assess nociceptor activation. Defecation, respiration and locomotion were assessed. Colonic migrating motor complexes were assessed by spatiotemporal mapping of isolated tissue. NFEPP-induced MOPr signalling and trafficking were studied in human embryonic kidney 293 cells.

Results NFEPP inhibited visceromotor responses to colorectal distension in mice with colitis but not in control mice, consistent with acidification of the inflamed colon. Fentanyl inhibited responses in both groups. NFEPP inhibited the excitability of dorsal root ganglion neurons and suppressed mechanical sensitivity of colonic afferent fibres in acidified but not physiological conditions. Whereas fentanyl decreased defecation and caused respiratory depression and hyperactivity in mice with colitis, NFEPP was devoid of these effects. NFEPP did not affect colonic migrating motor complexes at physiological pH. NFEPP preferentially activated MOPr in acidified extracellular conditions to inhibit cAMP formation, recruit β-arrestins and evoke MOPr endocytosis.

Conclusion In a preclinical IBD model, NFEPP preferentially activates MOPr in acidified microenvironments of inflamed tissues to induce antinociception without causing respiratory depression, constipation and hyperactivity.

Significance of this study

What is already known on this subject?

► The use of opioids to manage inflammatory bowel disease pain is restricted by side effects of respiratory depression, constipation, sedation and addiction. The μ-opioid receptor (MOPr) mediates the analgesic and detrimental actions of opioids such as fentanyl. We investigated whether a fentanyl analogue, N-(3-fluoro-1-phenethylpiperidine-4-yl)-N-phenyl propionamide (NFEPP), engineered to preferentially bind to the MOPr under acidic conditions found in diseased tissues could selectively inhibit colitis pain without side effects.

What are the new findings?

► In sharp contrast to fentanyl, which inhibited colonic nociception in healthy mice and mice with acute colitis, NFEPP selectively inhibited nociception in mice with colitis but not healthy controls. NFEPP inhibited activity of colonic nociceptors, but only under acidified conditions. Unlike fentanyl, NFEPP did not induce constipation, respiratory depression or altered locomotion. The acidified extracellular fluid of the inflamed colon allowed NFEPP to engage the MOPr and activate antinociceptive signalling pathways.

How might it impact on clinical practice in the foreseeable future?

► Opioids designed to selectively engage receptors in diseased tissues offer the prospect of treating pain without life threatening side effects mediated by receptors in heathy tissues. Since G protein-coupled receptors such as MOPr are the target of over thirty percent of approved drugs, agonists and antagonists designed to selectively engage receptors in diseased tissues might provide enhanced efficacy and specificity for treatment of widespread disorders.

INTRODUCTION

Opioid receptors (OPrs), members of the large family of G protein-coupled receptors, provide an endogenous mechanism for pain control and are thus targets for the treatment of pain.[1] Opioids

Gut: first published as 10.1136/gutjnl-2021-324070 on 30 March 2021. Downloaded from http://gut.bmj.com/ on September 30, 2021 at New York University, Serials Bobst Library Technical Services Serials. Protected by copyright.

that activate the μ-, ∂- and κ-opioid receptors (MOPr, DOPr) on primary sensory, spinal and supraspinal neurons depress activity and inhibit pain. In the inflamed intestine, opioids from infiltrating immune cells activate MOPr and DOPr on primary sensory neurons and suppress inflammatory bowel disease (IBD) pain.[2 3] Drugs that activate MOPr on neurons of the pain pathway are powerful analgesics.[1] However, the usefulness of opioids for the treatment of pain, including IBD pain, is limited by on-target side effects mediated by OPrs in other neurons. MOPr hyperpolarises neurons of the central nervous system, resulting in diminished respiratory drive and sedation.[1] Opioids can also inhibit peristalsis and electrolyte and fluid secretion in the digestive tract by activating MOPr on enteric and central neurons.[4 5] Whereas the analgesic properties of MOPr agonists diminish with continued use (ie, induce tolerance), on-target side effects such as respiratory depression are more sustained, with life-threatening consequences as escalating doses are required to control pain. The addictive properties of opioids exacerbate these problems. The heavy use of opioids is an independent predictor of mortality in IBD patients.[6] Given these problems, non-opioid analgesics have been identified as targets for visceral pain, including antagonists of pronociceptive G protein-coupled receptors and transient receptor potential ion channels.[7]

Insights into the structure and function of MOPrs have facilitated the development of pharmacological approaches to mitigate the detrimental side effects of opioids.[8] Biased agonists, which stabilise MOPr conformations that favour activation of G protein pathways that might underlie analgesia at the expense of β-arrestin (βARR) pathways that may mediate side effects, could provide analgesia with fewer side effects.[9–13] Some G protein biased MOPr agonists show promise in preclinical and human studies,[11 12 14] which has not always been replicated.[15] The premise that different signalling pathways underlie the beneficial and detrimental actions of MOPr agonists and the promise of biased agonists has been questioned.[16] An alternative approach has been to exploit the acidified extracellular environment of diseased tissues (eg, cancer, inflammation) to minimise the side effects of MOPr agonists. Through molecular modelling of MOPr in an acidified environment, a fluorinated analogue of fentanyl, (±)-N-(3-fluoro-1-phenethylpiperidine-4-yl)-N-phenyl propionamide (NFEPP), with a low pKa was developed and found to preferentially activate MOPr in acidified tissues.[17–20] NFEPP inhibits nociception emanating from acidified, diseased tissues without on-target side effects in healthy tissues. It is not known whether NFEPP suppresses inflammatory pain of the colon without affecting defecation, ventilation or locomotion.

Herein, we compared the actions of NFEPP and fentanyl in a preclinical mouse model of IBD. Our results show that NFEPP preferentially activates MOPr in acidified inflamed colon to inhibit nociception without side effects in healthy tissues. Ligands designed to preferentially activate MOPrs in diseased tissues offer the potential for treatment of visceral pain without life-threatening side effects. The approach presented here may be advantageous compared with G protein-biased ligands because G protein activation is an underlying mechanism of opioid-induced respiratory depression and addiction.[21–23]

MATERIALS AND METHODS

Additional materials and methods are included in online supplemental information.

MOPr agonists

NFEPP has been described.[19] Fentanyl was from Sandoz.

Dextran sodium sulfate-induced colitis

Colitis was induced by the administration of 2.5% dextran sodium sulfate (DSS) in drinking water for 5 days.

Visceromotor response to colorectal distention

A telemetric transmitter was implanted to measure electromyographic activity of external oblique muscles. At 10 days after surgery, mice received DSS in the drinking water or water alone for 5 days and were then switched to water alone for 2 days. Visceromotor responses were assessed day 8 after commencing DSS for NFEPP treatment and day 9 for fentanyl treatment. A catheter was inserted 0.5 cm into the colorectum for distension (20, 40, 60, 80 μL). Visceromotor responses were measured 30 min after vehicle, NFEPP or fentanyl (0.2 mg/kg, s.c.). Compliance of the excised colorectum was measured using a pressure transducer.

Colonic pH measurement

pH of colon segments was measured using the pH indicator SNARF 4 F-5 (and 6) carboxylic acid.

Colonic inflammation

Inflammation was assessed by measurement of myeloperoxidase (MPO) activity and by histological scoring.[24]

Tail flick test

Tail flick latency to noxious heat was recorded.

Defecation

Faecal pellets were counted for 1 hour.

Heart rate, oxygen saturation

A pulse oximeter sensor was used to measure heart rate and oxygen saturation.

Locomotion

Distance travelled, speed and resting time were recorded in an open field test.

Patch clamp recording

The excitability of nociceptors was assessed by measuring rheobase.[25]

Extracellular recording

Extracellular recordings were made from the splanchnic nerve innervating isolated segments of mouse distal colon.[25]

Colonic migrating motor complexes

Spatiotemporal maps along of segments of isolated mouse colon were constructed to assess colonic migrating motor complexes (CMMCs).[26]

cDNAs, transfection

Human embryonic kidney 293 (HEK293) cells were transiently transfected using polyethylenimine.[27]

Bioluminescence resonance energy transfer

cAMP formation, βARR2 recruitment and MOPr trafficking to Rab5a-positive endosomes were measured in HEK293 cells using bioluminescence resonance energy transfer (BRET).[27]

Gut: first published as 10.1136/gutjnl-2021-324070 on 30 March 2021. Downloaded from http://gut.bmj.com/ on September 30, 2021 at New York University, Serials Bobst Library Technical Services Serials. Protected by copyright.

Förster resonance energy transfer

Nuclear extracellular signal regulated kinase (ERK) activity was measured in HEK293 cells expressing the Nuc-EKAR Förster resonance energy transfer (FRET) sensor.[27]

Statistics

Results are expressed as mean±SEM Statistical significance was assessed using Student unpaired t-test with Welch's correction or Mann-Whitney test or one-way or two-way analysis of variance (ANOVA) with Tukey's, Bonferroni's or Dunnett's post hoc test.

RESULTS

NFEPP inhibits visceral nociception only in mice with colitis

An agonist that selectively activates MOPr in diseased tissues might obviate on-target side effects mediated by MOPr in healthy tissues. The fentanyl analogue NFEPP was designed to preferentially activate MOPr in the acidified microenvironment of diseased tissues.[19] To assess whether NFEPP would activate MOPr in the inflamed colon and thereby inhibit colitis-induced pain, we compared the efficacy with which NFEPP and fentanyl inhibit visceral nociception in mice with acute colitis and healthy control mice. Mice were treated with DSS (2.5% drinking water, 5 days, 2 days recovery) to induce acute colitis. Time-matched control mice received normal drinking water. Mice were treated with doses of NFEPP, fentanyl (both 0.2 mg/kg, s.c.) or vehicle (control) based on published work.[19] After 30 min, visceral nociception was examined by measuring visceromotor responses to graded colorectal distension (20, 40, 60, 80 µL). Although NFEPP did not affect the visceromotor responses to graded colorectal distension in healthy control mice (% vehicle at 80 µL: NFEPP 108.6%±32.5%, vehicle 100%, N=7, p=0.999, two-way ANOVA, Bonferroni correction), NFEPP inhibited the visceromotor responses in mice with DSS colitis by 65.2%±2.0% (80 µL) (NFEPP 34.8%±2.0%, vehicle 100%, N=5, p<0.001) (figure 1A–D). In contrast, fentanyl inhibited visceromotor responses to colorectal distension both in control mice by 67.8%±11.1% (80 µL: fentanyl 32.3%±11.1%, vehicle 100%, N=6, p<0.01) (figure 1E) and in mice with DSS colitis by 79.7%±15.5% (80 µL: fentanyl 20.3%±15.5%, vehicle 100%, N=4, p<0.001) (figure 1F). The visceromotor responses to colorectal distension at baseline did not differ significantly between control and colitis mice but trended towards higher values in mice with colitis (area under curve; DSS-colitis 7.19±2.65, control 5.27±2.47, N=5–7, p=0.215, two-way ANOVA) (figure 1G). The production of endogenous opioids in the inflamed colon likely explains the absence of significant hyperalgesia in mice with colitis.[28] Compliance of the colorectum from control and colitis mice was not different (increased volume (µL) DSS-colitis 66.1±8.65, control 61.64±9.73, N=4–5, p=0.736, two-way ANOVA) (figure 1H). The results suggest that NFEPP preferentially activates MOPr on nociceptors innervating the inflamed but not healthy colon to inhibit nociception, whereas fentanyl activates MOPr in healthy and diseased mice.

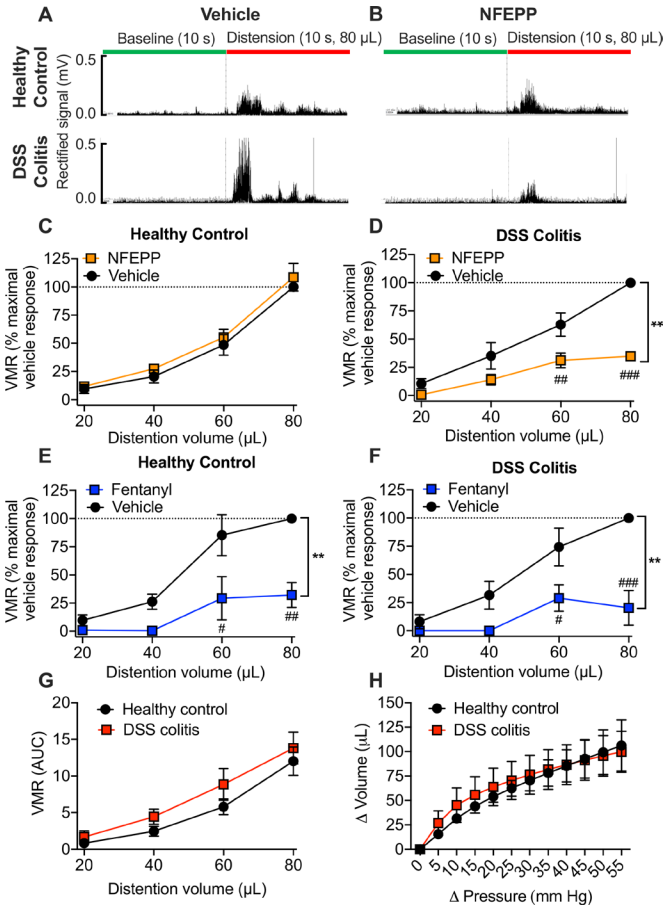


Figure 1 Effects of NFEPP and fentanyl on visceromotor responses to colorectal distension. (A, B) Representative traces showing the effects of vehicle (A) and NFEPP (B) on visceromotor responses to colorectal distension (80 µL) in healthy control and acute DSS colitis mice. (C, D) Effects of vehicle and NFEPP on visceromotor responses to colorectal distension in healthy control mice (C) (N=7, p=0.305) and DSS colitis mice (D) (N=5, p=0.0036). (E, F) Effects of vehicle and fentanyl on visceromotor responses to colorectal distension in healthy control mice (E) (N=6, p=0.0053) and DSS colitis mice (F) (n=4, p=0.0031). Two-way ANOVA, Bonferroni test. (G) Comparison of visceromotor responses to colorectal distension in healthy control (N=7) and DSS colitis (N=5) mice. The area under curve (AUC) of visceromotor responses of control and colitis mice were not significantly different (p=0.215, two-way ANOVA, Bonferroni test. (H) Colorectal compliance in healthy control (N=4) and DSS colitis (N=5) mice. There was no significant difference between control and colitis mice (p=0.736, two-way ANOVA, Bonferroni test). #P<0.05, **##p<0.01, ###p<0.001. In (D–F) # volume distention compared with vehicle, **curve compared with vehicle. ANOVA, analysis of variance; DSS, dextran sodium sulfate; NFEPP, N-(3-fluoro-1-phenethylpiperidine-4-yl)-N-phenyl propionamide; VMR, visceromotor response.

Inflammation acidifies extracellular fluid of the colon

The selectivity of NFEPP depends on its enhanced activity at MOPr in acidified extracellular fluid.[19] To assess whether the inflamed colon is acidified, colon segments from healthy control mice and mice with acute DSS colitis were incubated with the fluorescent pH indicator probe SNARF 4 F-5 (and 6) carboxylic acid, which fluoresces dependent on the protonation state. The inflamed colon (pH 6.71±0.09, N=17) was more acidic (ΔpH 0.33±0.1, p<0.01) than the non-inflamed colon (figure 2A). Colonic MPO activity, an indicator of neutrophil infiltration, was higher in DSS-treated mice (4.08±0.75 U/mg tissue, N=11) than in control mice (0.39±0.13 U/mg tissue, N=11, p<0.001) (figure 2B). Histological examination and measurement of the histological damage score confirmed transmucosal inflammation in the colon of DSS-treated mice (figure 2C,D). Inflammation was more pronounced in the mucosa and submucosa than the muscle layer (figure 2E).

Gut: first published as 10.1136/gutjnl-2021-324070 on 30 March 2021. Downloaded from http://gut.bmj.com/ on September 30, 2021 at New York University, Serials Bobst Library Technical Services Serials. Protected by copyright.

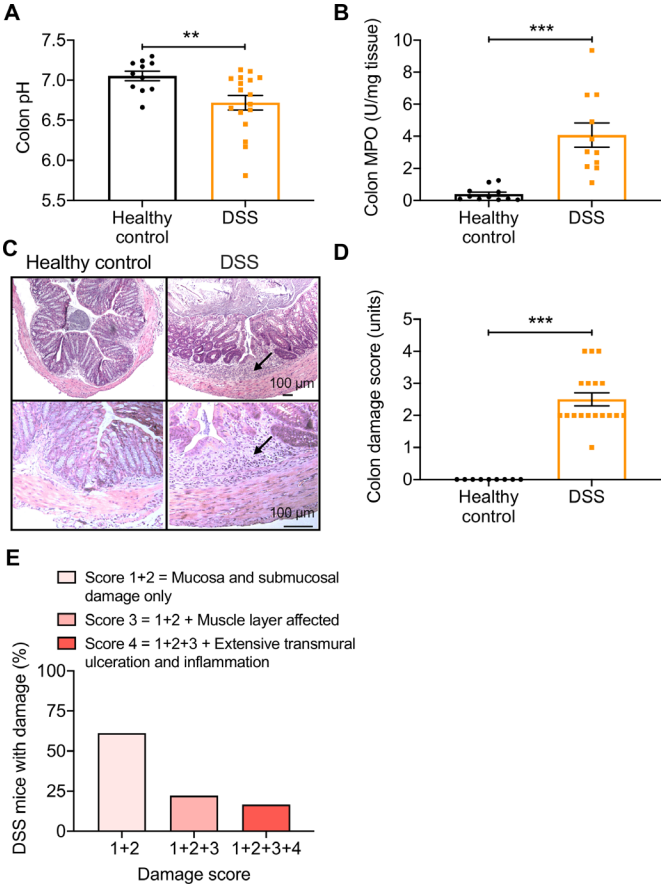


Figure 2 Acidification and inflammation of the colon. (A) pH of extracts of colon from healthy control mice and DSS colitis mice. (B) Myeloperoxidase activity in extracts of colon from healthy control mice and DSS colitis mice. (C–E) Histology (C) and histological damage score (D, E) of the colon from healthy control mice and DSS colitis mice. Arrows in C denote the inflammatory infiltrate in the mucosa of DSS-treated mice. (E) Proportion of specimens with damage score in different layers of colon. N=18 mice. Data points are responses of individual mice. **P<0.01, ***p<0.001. Unpaired Welch's t-test or Mann Whitney test. DSS, dextran sodium sulfate; MPO, myeloperoxidase.

NFEPP does not inhibit somatic thermal nociception, defecation, heart rate, ventilation or locomotion

Conventional agonists activate MOPr in the peripheral and central nervous systems, causing constipation, respiratory depression and sedation.[1 4 5] These on-target side effects limit their usefulness to treatment of IBD pain. We investigated whether NFEPP caused these side effects in healthy control and DSS colitis mice, with the expectation that even defecation might be unaffected in mice with colitis if the pH of the uninflamed musculature is normal. In mice with colitis, NFEPP (0.2 mg/kg, s.c.) did not affect withdrawal responses to noxious heat, assessed by a tail flick assay, whereas fentanyl strongly inhibited the response (p<0.001, figure 3A). These results are in line with the lack of efficacy of NFEPP on visceral nociception in control mice. NFEPP (0.2 or 0.4 mg/kg, s.c.) did not inhibit faecal pellet output in control or colitis mice, whereas fentanyl abolished pellet output in colitis mice (figure 3B,C). NFEPP (0.2 mg/kg, s.c.) did not affect heart rate or blood oxygen saturation in mice with colitis, whereas fentanyl reduced heart rate (ΔBPM 73.33±4.94, N=6, p<0.05 compared with basal) and oxygen saturation (decreased to 85.41%,±1.26, N=6, p<0.05) within 5 min, which returned to basal after 60 min (figure 3D,E). In an open field test of locomotion behaviour, NFEPP did not affect distance travelled, mean speed of travel or resting time (figure 3F–L). In contrast, fentanyl increased distance travelled and speed of travel and decreased resting time as previously shown.[29] These findings suggest that NFEPP does not activate MOPr on peripheral or central neurons of healthy tissues and thus does not cause the typical on-target side effects of fentanyl.

NFEPP preferentially inhibits colonic nociceptors in an acidified extracellular environment

MOPr activates K^+ channels of nociceptors and thereby reduces excitability.[1] Given its pH-dependence, NFEPP might inhibit nociceptors innervating the acidified inflamed colon, without affecting nociceptors in healthy tissues with normal extracellular pH.[17–20] To examine this possibility, we exposed mouse DRG neurons equilibrated at pH 6.5, 6.8 or 7.4 to NFEPP (300 nM), the MOPr agonist DAMGO (100 nM) or vehicle (control) for 15 min (figure 4A). Concentrations were based on published work.[19] Neurons were washed and excitability was assessed by measuring the rheobase (minimum input current required to fire an action potential) of small diameter neurons by patch clamp. NFEPP increased rheobase by 21.32%±8.62% at pH 6.5 and by 29%±8.62% at pH 6.8 when compared with vehicle (p<0.05) but had no effect at pH 7.4 (figure 4B–E). DAMGO increased rheobase by 25.21%±8.07% compared with vehicle (p<0.05) at pH 7.4 (figure 4E) as reported.[25 30] DAMGO had no effect at pH 6.5 (figure 4C). We then examined the duration of NFEPP-mediated inhibition of nociceptor excitability. After measurement of baseline rheobase at pH 7.4, neurons were incubated with NFEPP (300 nM) or vehicle at pH 6.5 for 10 min, and then rapidly switched to agonist-free buffer at pH 7.4. Rheobase was measured at 0, 15 or 30 min after NFEPP or vehicle (figure 4F). At T=0 min, NFEPP increased the rheobase compared with baseline (53.84%±10.5%, p<0.01) and vehicle (36.36%±9.31%, p<0.05) (figure 4F). However, the effect of NFEPP was not sustained at T=15 or T=30 min. When neurons were incubated with NFEPP (300 nM, 15 min) at pH 6.5 and then washed, there was an immediate increase in rheobase (figure 4G). After washing and recovery for 30 min at pH 6.5, the effect of NFEPP was also not sustained.

Although G protein-coupled receptors were once thought to signal exclusively from the plasma membrane, accumulating evidence suggests certain receptors signal from endosomes to control pain transmission.[3 25 27 31–33] Inhibitors of endocytosis blunt the inhibitory actions of DOPr agonists on excitability of DRG neurons, suggesting that endosomal signalling of DOPr underlies the sustained inhibitory effects of certain opioids.[3] However, the clathrin inhibitor PitStop2 did not block the immediate effect (T=0 min) of NFEPP on rheobase at pH 6.5 (figure 4G). Thus, endosomal signalling does not mediate the inhibitory actions of NFEPP-activated MOPr in primary afferent neurons.

To determine whether NFEPP could similarly depress the activation of the peripheral processes of nociceptors that would innervate diseased, acidified tissues, we made extracellular recordings from lumbar splanchnic nerves innervating isolated segments of mouse colon. Nociceptors were characterised by their responsiveness to stimulation of the colon or mesentery with von Frey filaments (VFF) (1 g). Tissues were equilibrated at pH 6.5 or 7.4 (10 min) and basal VFF responses were measured and found to be the same (figure 4H,I). NFEPP (300 nM) or vehicle (control) was superfused into the organ bath for 5 min

Gut: first published as 10.1136/gutjnl-2021-324070 on 30 March 2021. Downloaded from http://gut.bmj.com/ on September 30, 2021 at New York University, Serials Bobst Library Technical Services Serials. Protected by copyright.

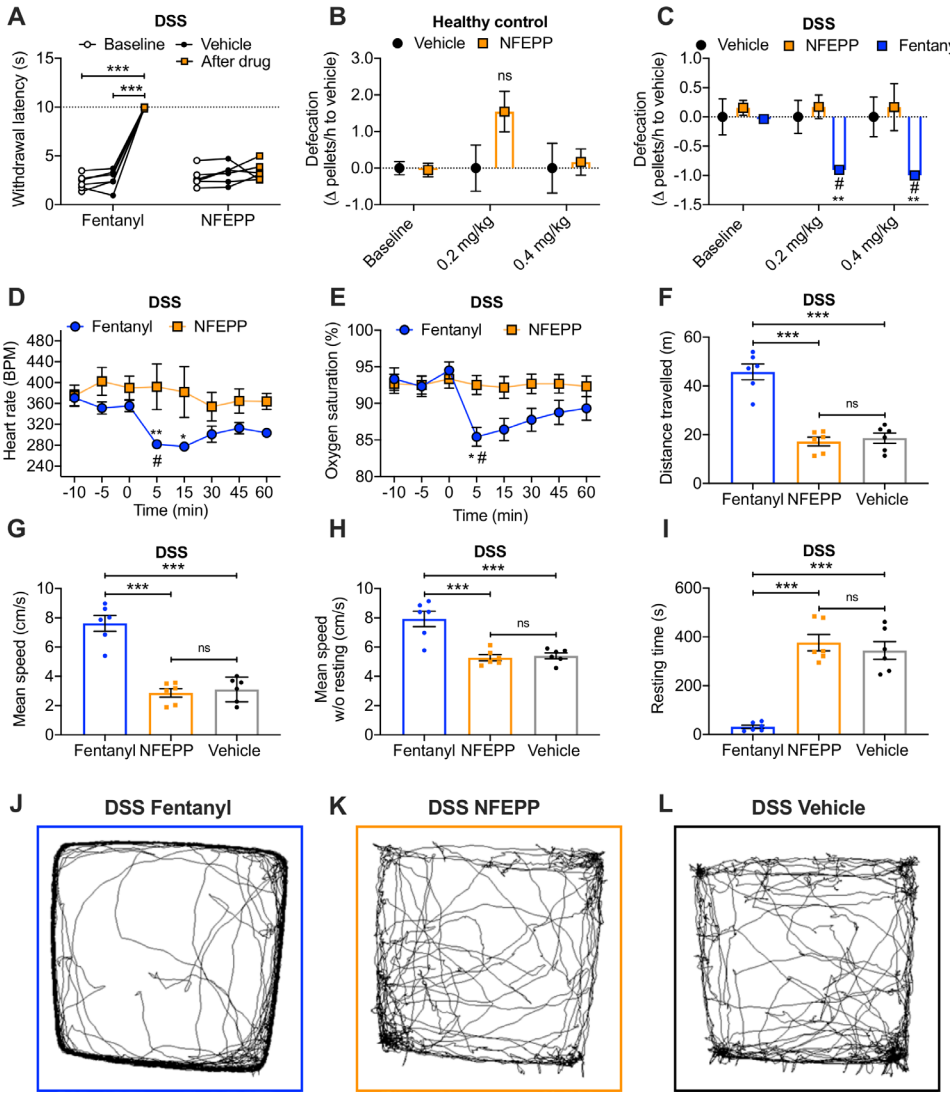


Figure 3 Evaluation of on-target side effects of NFEPP and fentanyl. The effects of NFEPP and fentanyl on withdrawal responses to noxious heat in a tail flick assay (A), N=6 mice per treatment, defecation (B, C), N=6–11 mice per treatment, heart rate (D), N=6 mice per treatment, oxygen saturation (E), N=6 mice per treatment and locomotion (open field test) (F–L), N=6 mice per treatment. (J–L) Are representative travel maps of mice treated with fentanyl, NFEPP or vehicle. Data are from DSS mice with the exception of (B), which is from control mice. Data points are responses of individual mice. #*P<0.05, **p<0.01, ***p<0.001. One-way or two-way ANOVA, Tukey's or Bonferroni's or Dunnett's tests. In C, #compared with vehicle, **fentanyl compared with NFEPP. in D, E, #compared with baseline, *fentanyl compared with NFEPP. ANOVA, analysis of variance; DSS, dextran sodium sulfate; NFEPP, N-(3-fluoro-1-phenethylpiperidine-4-yl)-N-phenyl propionamide; ns, not significant.

and then VFF responses were measured. At pH 6.5, NFEPP attenuated afferent responses to VFF probing compared with basal responses (27.3%±3.5% inhibition, p<0.01) (figure 4H). This effect was reversed after a 15 min washout at pH 7.4 (figure 4H). In contrast, the exposure to NFEPP at pH 7.4 had no effect on afferent mechanical sensitivity (figure 4I). Thus, NFEPP preferentially activates MOPr at the soma and in peripheral processes of nociceptors in acidic environments to transiently depress excitability and mechanical sensitivity.

NFEPP does not alter CMMCs at physiological extracellular pH

Fentanyl and morphine activate MOPr on interneurons of the myenteric plexus, which inhibits release of acetylcholine and nitric oxide and thereby depresses peristaltic contractions of the colon.[4] We made spatiotemporal maps of isolated segments of mouse colon to analyse whether NFEPP would affect the frequency, velocity and length of CMCCs in a pH-dependent manner. Segments of colon were equilibrated in organ baths at extracellular pH 7.4 or 6.8. Spatiotemporal maps were made under basal conditions, in tissues exposed to NFEPP (300 nM), and after NFEPP washout. Under basal conditions, the frequency, velocity and length of CMMCs were not significantly different at pH 7.4 or 6.8 (figure 5A,D,G–I). pH-dependent differences were detected in NFEPP-treated tissues. At pH 7.4, NFEPP had no significant effect on frequency, velocity or length of migrating motor complexes compared with baseline (figure 5B,G–I). These parameters were also unchanged after drug washout (figure 5C,G–I). At pH 6.8 NFEPP abolished migrating motor complexes (figure 5E,G–I). The frequency, velocity and length of migrating motor complexes recovered after drug wash-out (figure 5F,G–I). These findings suggest that NFEPP does not alter colonic peristalsis at physiological pH but may inhibit peristalsis in acidified tissues.

Gut: first published as 10.1136/gutjnl-2021-324070 on 30 March 2021. Downloaded from http://gut.bmj.com/ on September 30, 2021 at New York University, Serials Bobst Library Technical Services Serials. Protected by copyright.

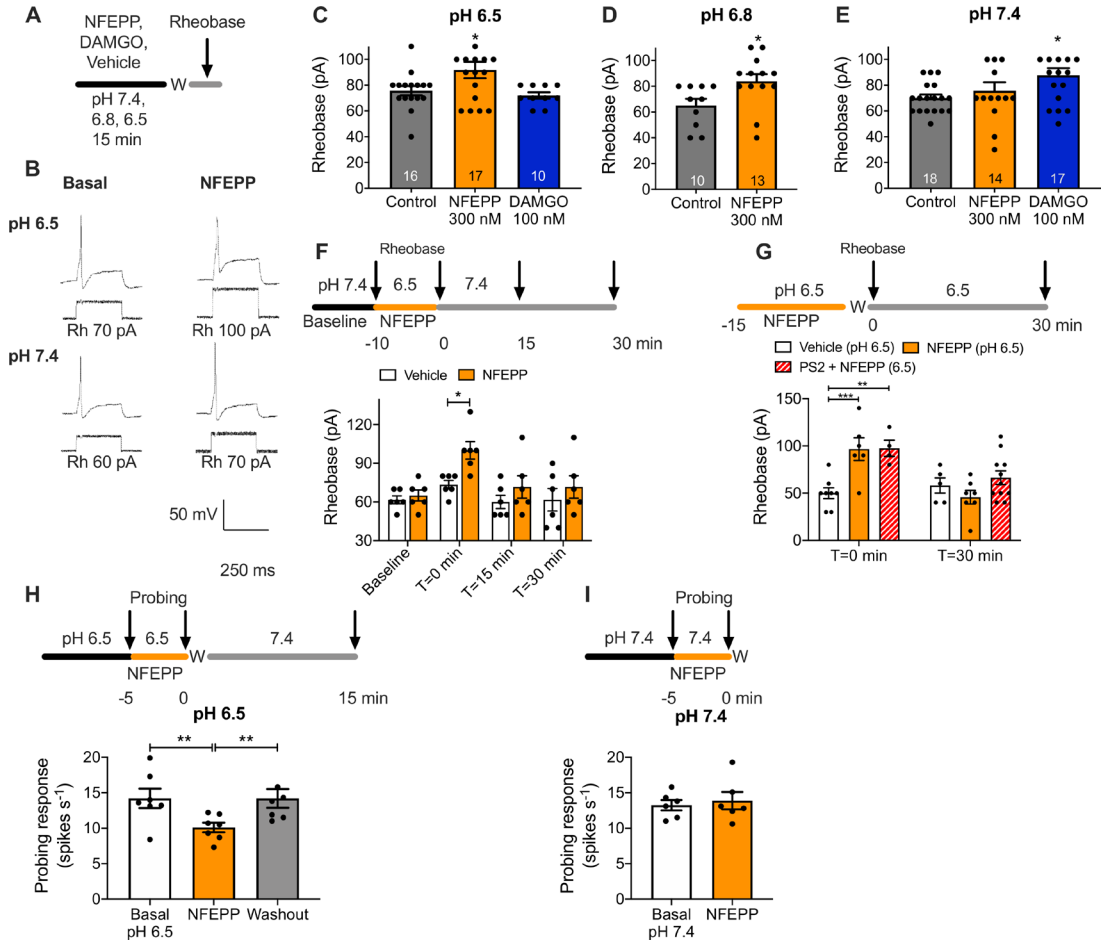


Figure 4 pH-dependent effects of NFEPP on nociceptor excitability. (A–G) Rheobase measurements of excitability of DRG neurons, showing effects of NFEPP and DAMGO at extracellular pH 7.4, 6.8 or 6.5. DRG neurons were preincubated with NFEPP and rheobase (Rh) was measured after washing. (A) protocol. (B) Representative traces under control conditions and after NFEPP at pH 6.5 or pH 7.4. (C–E) effects of NFEPP and DAMGO on rheobase at pH 6.5 (C), 6.8 (D) and 7.4 (E). Data points are responses of individual neurons from n=5–6 mice for each treatment. *P<0.05, 1-way ANOVA, Dunnett's test. (F, G) Duration of NFEPP effects. Neurons were incubated with NFEPP at pH 6.5 and then recovered at pH 7.4 (F) or pH 6.5 (G). Some neurons were treated with PitStop2 (pS2) in G). Data points are responses of individual neurons from N=6–7 mice for each treatment. *P<0.05, **p<0.01, ***p<0.001, two-way ANOVA, Tukey's test. (H, I) Excitability of colonic afferent nociceptors to mechanical stimulation of the mesentery with VFF. Basal responses, effects of NFEPP and recovery of responsiveness on mechano-sensitivity at pH 6.5 (H) and 7.4 (I). Data points are responses of individual receptive fields from n=4 mice. (H) **P<0.01, one-way ANOVA, Bonferroni test. (I) p=0.371, paired t-test. ANOVA, analysis of variance; NFEPP, N-(3-fluoro-1-phenethylpiperidine-4-yl)-N-phenyl propionamide; VFF, von Frey filaments.

NFEPP activates MOPr in an acidified extracellular environment

MOPr couples to $G_{\alpha i}$, which inhibits cAMP formation, and recruits βARRs.[34] We assessed the pH-dependence with which NFEPP might activate these signalling and trafficking pathways. The effects of NFEPP on forskolin-stimulated cAMP generation at extracellular pH 7.4, 6.8 or 6.5 was assessed in HEK293 cells expressing MOPr. NFEPP (300 nM) inhibited cAMP formation at pH 6.5 and 6.8 but not at pH 7.4 for at least 20 min (figure 6A,B). The inhibitory effects of NFEPP at pH 6.5 or 6.8 were comparable to that of the MOPr agonist DAMGO (100 nM) at pH 7.4. Although higher concentrations of NFEPP inhibited cAMP formation at pH 7.4, the effects were less potent and efficacious than at pH 6.5 or 6.8 (figure 6C).

βARRs associate with G protein-coupled receptors to mediate desensitisation, endocytosis and endosomal signalling.[35] To examine the pH-dependence of βARR recruitment to MOPr, we coexpressed in HEK293 cells MOPr tagged with *Rinella* luciferase (MOPr-Rluc8) and βARR2 tagged with yellow fluorescent protein (βARR-YFP). BRET was measured to monitor the proximity between MOPr-Rluc8 and βARR2-YFP. NFEPP (300 nM) increased MOPr-Rluc8/βARR2-YFP BRET at pH 6.5 and 6.8 but not at pH 7.4 (figure 6D,E). To assess pH-dependent MOPr endocytosis, we used BRET to examine the proximity between MOPr-Rluc8 and Rab5a (a resident protein of early endosomes) tagged with Venus (Rab5a-Venus). NFEPP (300 nM) increased MOPr-Rluc8/Rab5a-Venus BRET at pH 6.5 and 6.8, but not at pH 7.4 (figure 6F,G). Thus, NFEPP preferentially activates MOPr under acidic extracellular conditions, leading to inhibition of cAMP formation, recruitment of βARR2 and endocytosis.

Some G protein-coupled receptors, including OPrs, signal in endosomes by G protein-mediated and βARR-mediated mechanisms.[3 25 27 31–33] Receptors in endosomes generate compartmentalised signals that regulate neuronal excitability and pain. For neuropeptide receptors, the acidic microenvironment of the endosome (pH 5.5–6) promotes peptide/receptor dissociation and peptide degradation, which terminate endosomal signalling.[36–40] NFEPP (a non-peptide) might robustly activate MOPr in acidic early endosomes given its pH-dependent

Gut: first published as 10.1136/gutjnl-2021-324070 on 30 March 2021. Downloaded from http://gut.bmj.com/ on September 30, 2021 at New York University, Serials Bobst Library Technical Services Serials. Protected by copyright.

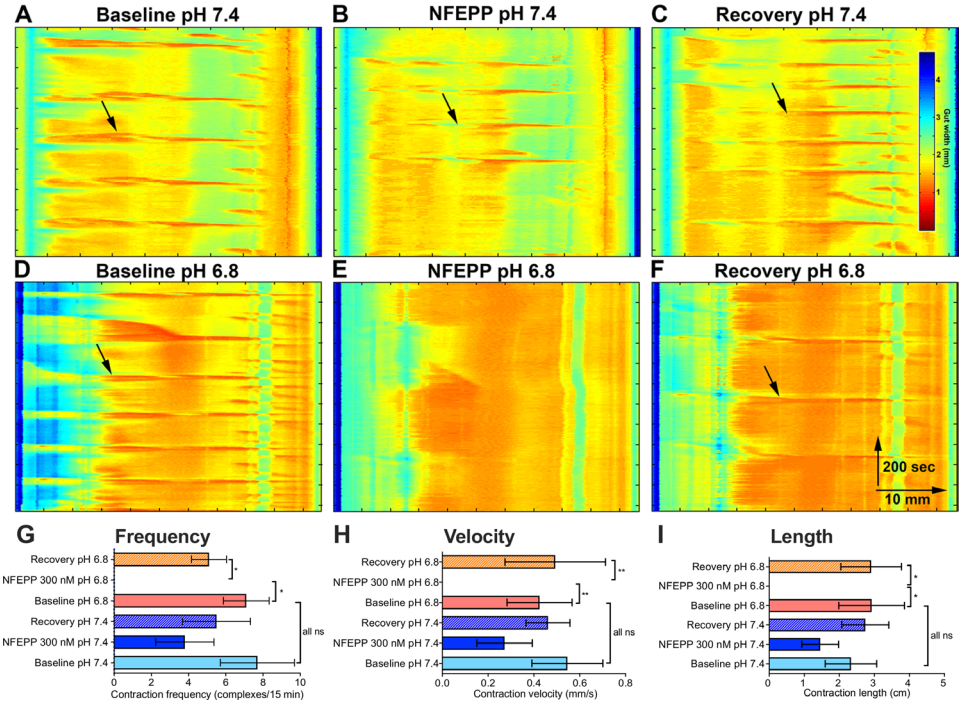


Figure 5 pH-dependent effects of NFEPP on colonic migrating motor complexes. (A–F) Representative spatiotemporal maps of mouse colon at pH 7.4 (A–C) and pH 6.8 (D–F) under baseline conditions (A, D), in the presence of NFEPP 300 nM, (B, D) and after drug wash-out and recovery (C, F). Black arrows indicate sample contractions. (G) Frequency. (H) Velocity. (I) Contraction length. N=6 mice per group. *P<0.05, **p<0.01, Student's unpaired t-tests with Welch's correction were used to compare means. NFEPP, N-(3-fluoro-1-phenethylpiperidine-4-yl)-N-phenyl propionamide; ns, not significant.

properties and presumed resistance to peptidases. To assess endosomal signalling, we expressed in HEK293 cells MOPr and a genetically encoded FRET biosensor for ERK activity in the nucleus (Nuc-EKAR), which is regulated by endosomal receptor signalling.[25 27 33] We measured ERK activity by FRET, which allowed analysis of signalling with high spatial and temporal fidelity. When incubated with cells at pH 6.5 or 6.8, but not at pH 7.4, NFEPP (300 nM) stimulated a sustained activation of nuclear ERK (figure 6H,I). The clathrin inhibitor PitStop2 (30 µM) and the dynamin inhibitor Dyngo4a (50 µM) blocked NFEPP-stimulated nuclear ERK activity (figure 6J,K). The inactive analogues, PitØ and DynØ, had no effect (figure 6J,K). The results suggest that NFEPP-induced MOPr signalling in endosomes activates nuclear ERK.

DISCUSSION

The main finding of our study is that NFEPP, which preferentially activates MOPr in the acidic extracellular environment of diseased tissues, selectively inhibits distension-evoked nociception in the inflamed mouse colon but not in the healthy colon. This finding is consistent with the acidification of the inflamed colon. Under acidic but not physiological conditions, NFEPP also inhibited excitability of nociceptors and suppressed mechanosensitivity of colonic afferent fibres. NFEPP did not affect defecation, ventilation or locomotion in mice with colitis, and did not affect peristaltic contractions of the isolated colon at physiological pH. In line with these findings, NFEPP evoked MOPr $G_{\alpha i}$ signalling, βARR recruitment and endocytosis only under acidic conditions. In contrast, fentanyl inhibited distention-evoked nociception in both the inflamed and healthy colon and induced the expected side effects of a conventional MOPr agonist.

Ischaemia, inflammation and cancer are associated with acidification of the extracellular fluid. During acute and chronic inflammation, the influx of activated immune cells, increased energy expenditure and oxygen use, and accelerated rate of glycolysis result in accumulation of lactic acid, which can acidify extracellular fluid by several pH units.[41] The hypoxic and proliferative zones of solid tumours are also markedly acidified.[42] Extracellular acidification can itself alter the inflammatory response and influence proliferation and metastasis of tumours.[42 43] In the present study, we exploited the acidification of the inflamed colon to increase the selectivity of a MOPr agonist for the treatment of pain, without side effects in healthy tissues. We observed that acute colitis caused a mild acidification of the colon (pH 6.7). pH was measured by incubating the pH indicator probe SNARF 4F-5 (and 6) carboxylic acid with segments of colon in vitro, which might explain the lower-than-expected pH of the uninflamed colon (pH 7.05). Our results support reports of colonic acidosis in patients with ulcerative colitis and Crohn's disease.[44] NFEPP was designed by modelling the docking of fentanyl with MOPr.[19] Since its pKa exceeds 8, fentanyl is protonated and binds to and activates MOPr in healthy (pH 7.4) and inflamed (pH 5–7) tissues. Replacement of hydrogen of fentanyl by fluorine in NFEPP decreased the pKa of NFEPP to 6.8, which resulted in preferential NFEPP activation of MOPr in acidified extracellular fluid (pH 5.5–6.5). We observed that NFEPP more potently activated MOPr at pH 6.5 and 6.8 than at pH 7.4, leading to inhibition of cAMP formation, recruitment of βARR2, and stimulation of MOPr endocytosis.

The ability of fentanyl to interact with MOPr at the pH of both normal and inflamed tissues accounts for its capacity to inhibit mechanically evoked nociception in the non-inflamed and inflamed colon, and explains the side effects of constipation, respiratory depression and altered locomotion that are mediated by MOPr in the peripheral and central nervous systems. The preference of NFEPP for activating MOPr in the acidified

Gut: first published as 10.1136/gutjnl-2021-324070 on 30 March 2021. Downloaded from http://gut.bmj.com/ on September 30, 2021 at New York University, Serials Bobst Library Technical Services Serials. Protected by copyright.

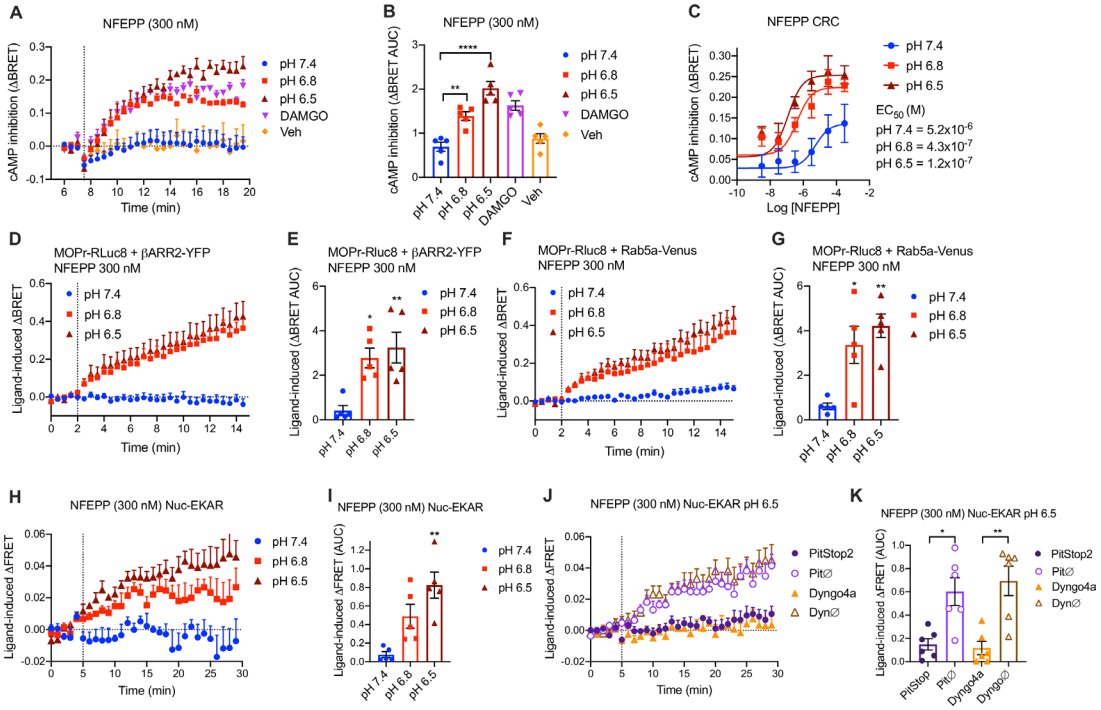


Figure 6 pH-dependent effects of NFEPP on MOPr signalling and endocytosis in HEK293 cells. (A–C) pH-dependency of NFEPP-induced inhibition of forskolin-stimulated formation of cAMP compared with effects of DAMGO at pH 7.4. (A) Time course. (B) Areas under curves (AUC). (C) Concentration-response curve (CRC). (D, E) pH-dependency of NFEPP-induced recruitment of βARR2 to MOPr. (D) Time course. (E) Areas under curves. (F, G) pH-dependency of NFEPP-induced recruitment of MOPr to Rab5a early endosomes. (F) Time course. (G) Areas under curves. (H-K) (H, I) pH-dependency of NFEPP-induced activation of nuclear ERK (Nuc-EKAR). (H) Time course. (I) Areas under curves. (J, K) Effects of PitStop2, Dyngo4a and inactive analogues (PitØ, DynØ) on NFEPP-induced activation of nuclear ERK at pH 6.5. (J) Time course. (K) Areas under curves. Data points are responses of independent experiments. N=5 independent experiments. *P<0.05, **p<0.01, ****p<0.0001, one-way ANOVA, Tukey's test. ANOVA, analysis of variance; ERK, extracellular signal regulated kinase; MOPr, μ-opioid receptor; NFEPP, N-(3-fluoro-1-phenethylpiperidine-4-yl)-N-phenyl propionamide.

extracellular fluid accounts for its selectivity for inhibiting nociception in the inflamed but not non-inflamed colon, and accounts for the lack of observed on-target side effects. We observed that NFEPP decreased the excitability of dorsal root ganglion nociceptors and suppressed mechanically evoked activation of colonic nociceptors in acidic but not physiological conditions. These findings are in line with the capacity of NFEPP to inhibit colonic nociception in mice with colitis. Together, our results suggest that NFEPP selectively activates MOPr at the terminals of nociceptors innervating the inflamed and acidified colonic mucosa. Most experiments in mice compared a single dose of fentanyl and NFEPP. Higher doses of NFEPP may activate MOPr in normal tissues since we observed that NFEPP could activate MOPr expressed in HEK293 cells at normal extracellular pH, although with a reduced potency and efficacy. Further studies are required to examine this possibility.

The effects of NFEPP on colonic motility and defecation deserves further study. Whereas NFEPP did not inhibit defecation in mice with colitis, NFEPP did suppress propulsive contractions of isolated segments of colon at acidic pH. One explanation of the lack of effect of NFEPP on defecation in mice with colitis is that inflammation and thus acidosis is restricted to the mucosa whereas the muscularis externa and myenteric plexus remain at physiological pH. In contrast, in studies of the isolated colon the entire bath and thus all layers were acidified. We observed that the mucosa was the predominant site of DSS-evoked inflammation, which supports the hypothesis that the muscularis externa is not acidified and thus NFEPP does not activate MOPr in myenteric neurons to suppress motility. In addition, MOPr can also regulate defecation by a central mechanism, which would not be activated by NFEPP.[5] A limitation of our experiments is that we were only able to measure pH of the entire colon wall rather than different layers (mucosa, submucosa, muscularis externa), and thus cannot be certain that the pH of the muscularis mucosa is unaffected in mice with DSS colitis. pH-dependent peptide probes, which have been used to localise acidified tumour microenvironments in intact tissues,[42] may enable precise mapping of acidified regions of the inflamed colon. It will also be important to study the effects of NFEPP on defecation in preclinical models of transmural colitis, such as the trinitrobenzene sulphonic acid model, to explore further the potential effects of NFEPP on motility in colitis. Such studies are clinically relevant since whereas ulcerative colitis is largely confined to the mucosa and submucosa, Crohn's disease is transmural. It will be of interest to study the efficacy of NFEPP in preclinical models of chronic colitis and in postinflammatory states that are relevant to irritable bowel syndrome. It will be important to determine if NFEPP, like some other opioids, can predispose the development of toxic megacolon.[45] Whether repeated administration of NFEPP attenuates responsiveness (ie, induces tolerance) remains to be studied. Our results showing that NFEPP selectively inhibits inflammatory pain in the colon are in agreement with other reports of NFEPP selectivity and efficacy for treatment of somatic inflammatory and neuropathic pain, acid-induced abdominal pain, and cancer pain in mice and rats.[18–20 46]

We examined the effects of NFEPP on MOPr signalling and trafficking in HEK293 cells. Our results show that NFEPP activates MOPr at pH 6.5 and 6.8 to inhibit formation of cAMP, recruit βARR2 and stimulate MOPr trafficking to early endosomes

Gut: first published as 10.1136/gutjnl-2021-324070 on 30 March 2021. Downloaded from http://gut.bmj.com/ on September 30, 2021 at New York University, Serials Bobst Library Technical Services Serials. Protected by copyright.

expressing Rab5a. Once viewed as a conduit for receptor trafficking, endosomes are now considered an important site of signal transduction of G protein-coupled receptors that control pain transmission.[3 25 27 31–33] Both MOPr and DOPr can signal from endosomes,[32] and endosomal signalling of DOPr mediates the sustained antinociceptive actions of opioids, including those released from the inflamed colon.[3] The capacity of NFEPP to promote MOPr endocytosis and to engage MOPr at the pH of early endosomes may predispose NFEPP to activate MOPr in endosomes. In support of this possibility, we observed that NFEPP activated ERK in the nucleus, and that inhibitors of clathrin- and dynamin-mediated endocytosis abolished this signal, which thus requires endosomal signalling. DOPr similarly signals from endosomes to activate nuclear ERK.[3] DOPr agonists cause a sustained inhibition of nociceptor excitability, which is suppressed by endocytic inhibitors and thus requires endosomal signalling.[3] In contrast, the inhibitory actions of NFEPP on nociceptor excitability were not sustained despite its ability to activate MOPr in endosomes of HEK293 cells. Other MOPr agonists similarly exert transient inhibitory effects. Together, these findings suggest that NFEPP inhibits nociception primarily be activating MOPr at the plasma membrane of acidified tissues.

Agonists designed to preferentially engage MOPr in diseased tissues offer the potential for effective pain relief without the side effects that are mediated by MOPr in healthy tissues. These drugs would represent a major advance in the treatment of painful digestive diseases, including IBD, irritable bowel syndrome, pancreatitis and pancreatic cancer. Further work is required before NFEPP can be advanced to clinical trials, including toxicology, pharmacokinetic analysis, and studies of efficacy in preclinical models of painful inflammatory and functional diseases of the digestive system. Since G protein-coupled receptors are the single largest target of approved drugs, similar principles might allow the enhanced targeting of other ligands for the treatment of diverse diseases with fewer on-target side effects.

Author affiliations
[1]Gastrointestinal Diseases Research Unit, Kingston General Hospital, Queens University, Kingston, Ontario, Canada
[2]Bluestone Center for Clinical Research, New York University College of Dentistry, New York, New York, USA
[3]Department of Molecular Pathobiology, New York University College of Dentistry, New York, New York, USA
[4]Department of Pediatrics, Columbia University in the City of New York, New York, New York, USA
[5]Department Experimental Anaesthesiology, Charité Campus Benjamin Franklin, Berlin, Germany
[6]Department of Neuroscience and Physiology, Neuroscience Institute, Grossman School of Medicine, New York University, New York, New York, USA

Funding Supported by grants from National Institutes of Health (NS102722, DE026806, DK118971, DE029951, NWB, BLS; RO1NS01554, KGM), Department of Defence (W81XWH1810431, NWB, BLS; PR160365, KGM), Crohn's Colitis Canada (SJV, AEL, DER) and Deutsche Forschungsgemeinschaft (STE 477/19-1, EXC 2046 AA1-1, CS).

Competing interests NWB is a founding scientist of Endosome Therapeutics Inc.

Patient consent for publication Not required.

Ethics approval Queen's University and Columbia University ethics committees approved procedures on C57BL/6 mice (male, 6–8 weeks).

Provenance and peer review Not commissioned; externally peer reviewed.

Data availability statement Data are available on reasonable request. Data are available from the corresponding authors on reasonable request.

Supplemental material This content has been supplied by the author(s). It has not been vetted by BMJ Publishing Group Limited (BMJ) and may not have been peer-reviewed. Any opinions or recommendations discussed are solely those of the author(s) and are not endorsed by BMJ. BMJ disclaims all liability and responsibility arising from any reliance placed on the content. Where the content includes any translated material, BMJ does not warrant the accuracy and reliability of the translations (including but not limited to local regulations, clinical guidelines, terminology, drug names and drug dosages), and is not responsible for any error and/or omissions arising from translation and adaptation or otherwise.

ORCID iDs
Yang Yu http://orcid.org/0000-0001-8388-5825
Nigel W Bunnett http://orcid.org/0000-0003-3367-0644

REFERENCES

1 Corder G, Castro DC, Bruchas MR, *et al*. Endogenous and exogenous opioids in pain. *Annu Rev Neurosci* 2018;41:453–73.
2 Valdez-Morales E, Guerrero-Alba R, Ochoa-Cortes F, *et al*. Release of endogenous opioids during a chronic IBD model suppresses the excitability of colonic DRG neurons. *Neurogastroenterol Motil* 2013;25:39–e4.
3 Jimenez-Vargas NN, Gong J, Wisdom MJ, *et al*. Endosomal signaling of delta opioid receptors is an endogenous mechanism and therapeutic target for relief from inflammatory pain. *Proc Natl Acad Sci U S A* 2020;117:15281–92.
4 Galligan JJ, Sternini C. Insights into the role of opioid receptors in the Gi tract: experimental evidence and therapeutic relevance. *Handb Exp Pharmacol* 2017;239:363–78.
5 Tsuchida D, Fukuda H, Koda K, *et al*. Central effect of mu-opioid agonists on antral motility in conscious rats. *Brain Res* 2004;1024:244–50.
6 Targownik LE, Nugent Z, Singh H, *et al*. The prevalence and predictors of opioid use in inflammatory bowel disease: a population-based analysis. *Am J Gastroenterol* 2014;109:1613–20.
7 Camilleri M. Toward an effective peripheral visceral analgesic: responding to the National opioid crisis. *Am J Physiol Gastrointest Liver Physiol* 2018;314:G637–46.
8 Stein C. New concepts in opioid analgesia. *Expert Opin Investig Drugs* 2018;27:765–75.
9 Bohn LM, Gainetdinov RR, Lin FT, *et al*. Mu-Opioid receptor desensitization by beta-arrestin-2 determines morphine tolerance but not dependence. *Nature* 2000;408:720–3.
10 Bohn LM, Lefkowitz RJ, Gainetdinov RR, *et al*. Enhanced morphine analgesia in mice lacking beta-arrestin 2. *Science* 1999;286:2495–8.
11 Manglik A, Lin H, Aryal DK, *et al*. Structure-Based discovery of opioid analgesics with reduced side effects. *Nature* 2016;537:185–90.
12 Schmid CL, Kennedy NM, Ross NC, *et al*. Bias factor and therapeutic window correlate to predict safer opioid analgesics. *Cell* 2017;171:e13:1165–75.
13 Suomivuori C-M, Latorraca NR, Wingler LM, *et al*. Molecular mechanism of biased signaling in a prototypical G protein-coupled receptor. *Science* 2020;367:881–7.
14 Singla N, Minkowitz HS, Soergel DG, *et al*. A randomized, phase IIb study investigating oliceridine (TRV130), a novel μ-receptor G-protein pathway selective (μ-GPS) modulator, for the management of moderate to severe acute pain following abdominoplasty. *J Pain Res* 2017;10:2413–24.
15 Hill R, Disney A, Conibear A, *et al*. The novel μ-opioid receptor agonist PZM21 depresses respiration and induces tolerance to antinociception. *Br J Pharmacol* 2018;175:2653–61.
16 Servick K. Safety benefits of 'biased' opioids scrutinized. *Science* 2020;367:966.
17 Del Vecchio G, Labuz D, Temp J, *et al*. pK_a of opioid ligands as $_a$ discriminating factor for side effects. *Sci Rep* 2019;9:19344.
18 Rodriguez-Gaztelumendi A, Spahn V, Labuz D, *et al*. Analgesic effects of a novel pH-dependent μ-opioid receptor agonist in models of neuropathic and abdominal pain. *Pain* 2018;159:2277–84.
19 Spahn V, Del Vecchio G, Labuz D, *et al*. A nontoxic pain killer designed by modeling of pathological receptor conformations. *Science* 2017;355:966–9.
20 Spahn V, Del Vecchio G, Rodriguez-Gaztelumendi A, *et al*. Opioid receptor signaling, analgesic and side effects induced by a computationally designed pH-dependent agonist. *Sci Rep* 2018;8:8965.
21 Hill R, Disney A, Conibear A, *et al*. The novel μ-opioid receptor agonist PZM21 depresses respiration and induces tolerance to antinociception. *Br J Pharmacol* 2018;175:2653–61.
22 Kliewer A, Schmiedel F, Sianati S, *et al*. Phosphorylation-Deficient G-protein-biased μ-opioid receptors improve analgesia and diminish tolerance but worsen opioid side effects. *Nat Commun* 2019;10:367.
23 Negus SS, Freeman KB. Abuse potential of biased mu opioid receptor agonists. *Trends Pharmacol Sci* 2018;39:916–9.
24 Wallace JL, Keenan CM. An orally active inhibitor of leukotriene synthesis accelerates healing in a rat model of colitis. *Am J Physiol* 1990;258:G527–34.
25 Jimenez-Vargas NN, Pattison LA, Zhao P, *et al*. Protease-Activated receptor-2 in endosomes signals persistent pain of irritable bowel syndrome. *Proc Natl Acad Sci U S A* 2018;115:E7438–47.
26 Israelyan N, Del Colle A, Li Z, *et al*. Effects of serotonin and slow-release 5-hydroxytryptophan on gastrointestinal motility in a mouse model of depression. *Gastroenterology* 2019;157:507–21.
27 Jensen DD, Lieu T, Halls ML, *et al*. Neurokinin 1 receptor signaling in endosomes mediates sustained nociception and is a viable therapeutic target for prolonged pain

Gut: first published as 10.1136/gutjnl-2021-324070 on 30 March 2021. Downloaded from http://gut.bmj.com/ on September 30, 2021 at New York University, Serials Bobst Library Technical Services Serials. Protected by copyright.

relief. *Sci Transl Med* 2017;9. doi:10.1126/scitranslmed.aal3447. [Epub ahead of print: 31 May 2017].
28 Boué J, Basso L, Cenac N, *et al*. Endogenous regulation of visceral pain via production of opioids by colitogenic CD4(+) T cells in mice. *Gastroenterology* 2014;146:166–75.
29 Varshneya NB, Walentiny DM, Moisa LT, *et al*. Opioid-Like antinociceptive and locomotor effects of emerging fentanyl-related substances. *Neuropharmacology* 2019;151:171–9.
30 Guerrero-Alba R, Valdez-Morales EE, Jiménez-Vargas NN, *et al*. Co-Expression of μ and δ opioid receptors by mouse colonic nociceptors. *Br J Pharmacol* 2018;175:2622–34.
31 Ramírez-García PD, Retamal JS, Shenoy P, *et al*. A pH-responsive nanoparticle targets the neurokinin 1 receptor in endosomes to prevent chronic pain. *Nat Nanotechnol* 2019;14:1150–9.
32 Stoeber M, Jullié D, Lobingier BT, *et al*. A genetically encoded biosensor reveals location bias of opioid drug action. *Neuron* 2018;98:963–76.
33 Yarwood RE, Imlach WL, Lieu T, *et al*. Endosomal signaling of the receptor for calcitonin gene-related peptide mediates pain transmission. *Proc Natl Acad Sci U S A* 2017;114:12309–14.
34 Williams JT, Ingram SL, Henderson G, *et al*. Regulation of μ-opioid receptors: desensitization, phosphorylation, internalization, and tolerance. *Pharmacol Rev* 2013;65:223–54.
35 Peterson YK, Luttrell LM. The diverse roles of arrestin scaffolds in G protein-coupled receptor signaling. *Pharmacol Rev* 2017;69:256–97.
36 Cottrell GS, Padilla BE, Amadesi S, *et al*. Endosomal endothelin-converting enzyme-1: a regulator of beta-arrestin-dependent ERK signaling. *J Biol Chem* 2009;284:22411–25.
37 Gupta A, Fujita W, Gomes I, *et al*. Endothelin-Converting enzyme 2 differentially regulates opioid receptor activity. *Br J Pharmacol* 2015;172:704–19.
38 Jensen DD, Halls ML, Murphy JE, *et al*. Endothelin-Converting enzyme 1 and β-arrestins exert spatiotemporal control of substance P-induced inflammatory signals. *J Biol Chem* 2014;289:20283–94.
39 Padilla BE, Cottrell GS, Roosterman D, *et al*. Endothelin-Converting enzyme-1 regulates endosomal sorting of calcitonin receptor-like receptor and beta-arrestins. *J Cell Biol* 2007;179:981–97.
40 Roosterman D, Cottrell GS, Padilla BE, *et al*. Endothelin-Converting enzyme 1 degrades neuropeptides in endosomes to control receptor recycling. *Proc Natl Acad Sci U S A* 2007;104:11838–43.
41 Erra Díaz F, Dantas E, Geffner J. Unravelling the interplay between extracellular acidosis and immune cells. *Mediators Inflamm* 2018;2018:1–11.
42 Rohani N, Hao L, Alexis MS, *et al*. Acidification of tumor at stromal boundaries drives transcriptome alterations associated with aggressive phenotypes. *Cancer Res* 2019;79:1952–66.
43 Rajamäki K, Nordström T, Nurmi K, *et al*. Extracellular acidosis is a novel danger signal alerting innate immunity via the NLRP3 inflammasome. *J Biol Chem* 2013;288:13410–9.
44 Nugent SG, Kumar D, Rampton DS, *et al*. Intestinal luminal pH in inflammatory bowel disease: possible determinants and implications for therapy with aminosalicylates and other drugs. *Gut* 2001;48:571–7.
45 Katagiri N, Sakai R, Izutsu T, *et al*. Postoperative pain management in patients with ulcerative colitis. *Anesth Prog* 2020;67:158–63.
46 Baamonde A, Menéndez L, González-Rodríguez S, *et al*. A low pKa ligand inhibits cancer-associated pain in mice by activating peripheral mu-opioid receptors. *Sci Rep* 2020;10:18599.

Gut: first published as 10.1136/gutjnl-2021-324070 on 30 March 2021. Downloaded from http://gut.bmj.com/ on September 30, 2021 at New York University, Serials Bobst Library Technical Services Serials. Protected by copyright.

Targeting G protein-coupled receptors for the treatment of chronic pain in the digestive system

Lena Gottesman-Katz,[1,2] Rocco Latorre,[1] Stephen Vanner,[3] Brian L Schmidt,[4] Nigel W Bunnett [1]

[1]Molecular Pathobiology, New York University, New York, New York, USA
[2]Division of Pediatric Gastroenterology, Columbia University Medical Center/New York Presbyterian, New York, New York, USA
[3]Gastrointestinal Diseases Research Unit, Division of Gastroenterology, Queens University, Kingston, Ontario, Canada
[4]Bluestone Center, New York University, New York, New York, USA

Correspondence to
Professor Nigel W Bunnett, Molecular Pathobiology, New York University, New York, NY 10010, USA; nwb2@nyu.edu

Received 23 March 2020
Revised 21 October 2020
Accepted 7 November 2020
Published Online First 3 December 2020

Check for updates

© Author(s) (or their employer(s)) 2021. No commercial re-use. See rights and permissions. Published by BMJ.

To cite: Gottesman-Katz L, Latorre R, Vanner S, *et al*. *Gut* 2021;**70**:970–981.

ABSTRACT

Chronic pain is a hallmark of functional disorders, inflammatory diseases and cancer of the digestive system. The mechanisms that initiate and sustain chronic pain are incompletely understood, and available therapies are inadequate. This review highlights recent advances in the structure and function of pronociceptive and antinociceptive G protein-coupled receptors (GPCRs) that provide insights into the mechanisms and treatment of chronic pain. This knowledge, derived from studies of somatic pain, can guide research into visceral pain. Mediators from injured tissues transiently activate GPCRs at the plasma membrane of neurons, leading to sensitisation of ion channels and acute hyperexcitability and nociception. Sustained agonist release evokes GPCR redistribution to endosomes, where persistent signalling regulates activity of channels and genes that control chronic hyperexcitability and nociception. Endosomally targeted GPCR antagonists provide superior pain relief in preclinical models. Biased agonists stabilise GPCR conformations that favour signalling of beneficial actions at the expense of detrimental side effects. Biased agonists of μ-opioid receptors (MOPrs) can provide analgesia without addiction, respiratory depression and constipation. Opioids that preferentially bind to MOPrs in the acidic microenvironment of diseased tissues produce analgesia without side effects. Allosteric modulators of GPCRs fine-tune actions of endogenous ligands, offering the prospect of refined pain control. GPCR dimers might function as distinct therapeutic targets for nociception. The discovery that GPCRs that control itch also mediate irritant sensation in the colon has revealed new targets. A deeper understanding of GPCR structure and function in different microenvironments offers the potential of developing superior treatments for GI pain.

Key messages

Chronification of pain in the digestive system

- Chronic pain in the digestive system accompanies functional disorders, inflammatory diseases and cancer. It afflicts one quarter of the US population.
- The transition from acute (physiological) to chronic (pathological) pain in the digestive system is a poorly understood and complex process. Chronic hypersensitivity of pain-sensing nerves innervating the digestive system manifests as allodynia and hyperalgesia, hallmarks of chronic abdominal pain.
- There is a dearth of long-term, effective treatment options for chronic pain in the digestive system. The opioid crisis, a leading cause of mortality, highlights the need to understand the aetiology of chronic pain and to develop more effective treatments.

G protein-coupled receptors (GPCRs) are complex and dynamic signalling proteins that control chronic pain

- GPCRs are the largest family of receptors. They regulate most physiological and pathological processes, including pain.
- GPCRs expressed by primary sensory neurons and second-order spinal neurons can stimulate and inhibit pain transmission.
- New knowledge about GPCR structure and function has revealed that GPCRs are complex and dynamic signalling proteins. Once activated, GPCRs translocate to subcellular microdomains and adopt distinct conformations. An understanding of this dynamic behaviour provides insights into how GPCRs control pain and has revealed new opportunities for therapy.

INTRODUCTION

Acute pain is a physiological mechanism of protection that allows the awareness and avoidance of injury. Its importance is illustrated by the severe injuries sustained by individuals with a congenital insensitivity to detect pain.[1] Chronic pain, defined as lasting greater than 3 months, can persist after healing, is often debilitating and afflicts a significant portion of the world's population.[2] Chronic GI pain is a common type of visceral pain that can arise due to multiple underlying aetiologies and, like most chronic pain, is often difficult to treat.[3] The mechanisms that underlie the transition from acute to chronic pain are complex, multifactorial and not fully elucidated. Consequently, there are a dearth of effective treatments for chronic pain. Existing and widely used therapies, including non-steroidal anti-inflammatory drugs and opioids, are often ineffective and have severe and sometimes life-threatening side effects.[4] The large number of deaths attributable to opioid overdoses highlights the need for new treatments.[5] The neuronal pathway of pain transmission from the digestive tract is well established.[6] Primary sensory neurons, with cell bodies within dorsal root ganglia (DRGs), project fibres to the digestive system and dorsal horn of the spinal cord. A subset of these neurons, called nociceptors, detect painful stimuli that are transmitted centrally

Gut: first published as 10.1136/gutjnl-2020-321193 on 3 December 2020. Downloaded from http://gut.bmj.com/ on September 30, 2021 at New York University, Serials Bobst Library Technical Services Serials. Protected by copyright.

Key messages

Insights into the dynamic properties of GPCRs reveals new therapeutic options for chronic pain

- GPCRs are the largest class of drug targets. One-third of Federal Drug Administration-approved drugs target GPCRs.
- The discovery that activated GPCRs internalise and that GPCRs in endosomes can generate persistent signals that contribute to neuronal excitation and pain transmission raises the possibility that GPCRs in endosomes are an appropriate target for treating chronic pain.
- Antagonists of neuropeptide and protease receptors conjugated to transmembrane lipids or encapsulated into nanoparticles target GPCRs in endosomes and provide superior pain relief in preclinical models.
- Biased agonists of GPCRs might stabilise receptor conformations that favour signalling of beneficial pathways. Biased agonists of μ-opioid receptors (MOPrs) have the potential to provide analgesia without addiction, respiratory depression, nausea and constipation.
- Molecular modelling has facilitated the development of opioids that preferentially activate MOPrs in the acid extracellular fluid of diseased tissues (eg, cancer and inflammation). These agonists provide analgesia in preclinical models of pain without side effects.
- By altering the conformation of GPCRs, allosteric modulators can fine-tune the effects of endogenous ligands. Positive allosteric modulators offer the prospect of enhancing the analgesic properties of endogenous opioids for pain control.
- The discovery that GPCR dimers with distinct pharmacological properties may control pain transmission has revealed new therapeutic targets. Drugs that target dimers of MOPrs and δ-opioid receptors have been advanced to treat pain.
- GPCRs expressed by sensory nerves can transmit distinct sensations in different tissues. The discovery that GPCRs that mediate itch in the skin also represent a mechanism of irritant sensation in the colon has led to the identification of new targets for chronic pain in the digestive system.
- Knowledge of the mechanisms and treatment of chronic pain largely derives form studies of somatic pain in preclinical models. There are opportunities to apply this information to chronic pain in the digestive system. Challenges for future research into chronic pain in the digestive system lie in identification of the fundamental processes that control sensitivity of neurons that sense and transmit painful signals in humans.

via second-order neurons in the dorsal horn. Gut afferent nerves synapse at multiple levels in the spinal cord, which accounts for the poorly localised nature of visceral pain.[7]

Multiple mechanisms drive chronic visceral pain, many of which have garnered significant research attention. This review concerns one such mechanism, the role of G protein-coupled receptors (GPCRs) in chronic visceral pain. With almost 850 members in the human genome, GPCRs are the largest and most functionally diverse family of receptors. GPCRs are characterised by seven transmembrane domains, an extracellular amino-terminus and an intracellular carboxyl-terminus. GPCRs can both stimulate and inhibit pain transmission. Pronociceptive GPCRs (eg, substance P (SP) neurokinin-1 receptor (NK_1R)) stimulate signalling molecules (eg, Ca^{2+} and cyclic AMP (cAMP)) that excite neurons of the pain pathway and evoke pain. In contrast, antinociceptive GPCRs (eg, opioid receptors (OPrs)) inhibit these pathways and thereby depress neuronal excitability to provide an endogenous mechanism of pain control. In light of the ubiquitous and vital roles of GPCRs in human physiology and pathology, it is not surprising that they are prime therapeutic targets; one-third of Federal Drug Administration-approved drugs target GPCRs.[8] GPCRs regulate pain transmission at multiple levels and are established and emerging targets for the treatment of chronic pain.[9 10] Table 1 summarises GPCRs that can promote or inhibit chronic pain in the digestive system.

Recent advances in understanding the structure and function of GPCRs have provided new insights into the mechanisms that signal chronic pain and reveal novel opportunities for therapy.[9 10] This review highlights the implications of these advances for understanding the mechanisms that signal chronic pain in the digestive system and discusses how this information might inform the development of more effective pharmacological treatments. Rather than discuss every GPCRs that control pain, the review focuses on select GPCRs and peripheral signalling pathways that illustrate unifying concepts. While some of these concepts have not been examined in the context of GI pain, we discuss how studies of other types of pain can guide future investigations of pain in the digestive system.

SIGNALLING OF CHRONIC PAIN IN THE DIGESTIVE SYSTEM

Functional disorders, inflammatory diseases and cancer are associated with chronic pain in the digestive system. These conditions can be inter-related. Although patients with IBD usually experience acute pain during active disease, a significant subset of patients experience chronic pain during remission, often meeting criteria for IBS.[11] IBS, previously considered a functional chronic pain syndrome without an overt cause, has been linked to sensitisation of colonic afferent neurons after acute inflammation or infection, as in the case of postinflammatory or postinfective IBS.[12] The severe pain of pancreatitis and pancreatic cancer has inflammatory and neuropathic components.[13] Mechanical stress due to obstruction of ducts, mediators from immune cells and damaged acinar cells, and injury of splanchnic nerves contribute to pancreatic pain. Pancreatic cancer cells invade the perineural space, releasing factors that sensitise nerve endings and lead to pain.[14]

Chronic visceral hypersensitivity (CVH) is a hallmark of chronic pain in the digestive system. CVH is caused by sensitisation of nociceptors, lowering the threshold for stimulus-evoked excitation.[6 7] These changes lead to increased pain perception, which manifests as allodynia or hyperalgesia. The pathogenesis underlying the transition from acute pain to CVH is complex and incompletely understood. The sustained release of nociceptive mediators from injured tissues, recurrent inflammation and immune dysregulation, microbial dysbiosis, enteric glial cell influences, decreased antinociceptive mechanisms and epigenetic influences can all lead to sensitisation of ion channels and neuroplastic changes that contribute to CVH (figure 1).[15 16] GPCRs play a major role in many of these processes.

GPCRS AND PAIN IN THE DIGESTIVE SYSTEM

The concept that GPCRs are simple binary switches that couple to a defined set of signalling partners and regulate a single cellular process has been superseded by the realisation that GPCRs are complex and dynamic signalling proteins.[9 10] Thus, GPCRs can adopt different conformations when associated

Gut: first published as 10.1136/gutjnl-2020-321193 on 3 December 2020. Downloaded from http://gut.bmj.com/ on September 30, 2021 at New York University, Serials Bobst Library Technical Services Serials. Protected by copyright.

Table 1 GPCRs implicated in painful digestive diseases

Disease	Receptors	Ligand	Evidence	Reference
Upper GI tract				
Esophagitis	PAR_2	Proteases	In a guinea pig model of esophagitis, mechanical hypersensitivity is mediated by PAR_2 in vagal C-fibres.	81
Oesophageal hypersensitivity	A_{2A}	Adenosine	In a guinea pig model of oesophageal pain, mechanical hypersensitivity is mediated by A_{2A} in vagal C-fibres.	82
Eosinophilic esophagitis	H_1R, H_2R, H_4R	Histamine	H_1R, H_2R and H_4R expression is increased in biopsies of patients with active EoE compared with inactive EoE and controls and H_1R antagonist treatment in vitro decreased cytokine production.	83
Gastritis	PAR_1	Serine proteases	PAR_1 is protective against *Helicobacter pylori* gastritis. Activation decreases release of cytokines important in driving the immune response to *H. pylori*. PAR_1-deficient mice infected with *H. pylori* develop severe gastritis.	84
Pancreatitis and pancreatic cancer	NK_1R	SP	SP and NK_1R mediate nociception, oedema and inflammation in a pancreatitis mouse model.	35
	Calcitonin receptor-like receptor	CGRP	CGRP mediates neurogenic inflammation, vasodilation, oedema and inflammatory cascade in pancreatitis and pancreatic cancer.	13
	Retinoic-induced protein 3	Orphan receptor	Receptor levels are significantly increased in pancreatic ductal cancer cells compared with normal cells and are associated with pancreatic cancer cell growth and migration.	85
Lower GI tract				
IBS	PAR_2	Proteases	PAR_2 mediates persistent neuronal hyperexcitability in mice nociceptors treated with colonic biopsy supernatant obtained from patients with IBS.	22
	H_1R	Histamine	Histamine is upregulated in IBS. Supernatants of patients with IBS exposed to mouse dorsal root ganglion neurons are sensitised via H_1R.	86
	$P2Y_1$, $P2Y_2$	ATP	Receptor expression was increased in rectosigmoid biopsies of diarrhoea-predominant patients with IBS. $P2Y_2$ expression correlated with abdominal pain scores.	87
	Mrgpr	Polyunsaturated fatty acids (PUFAs)	Colonic biopsies from patients with IBS show elevated levels of certain metabolites of PUFAs. PUFAs mediate visceral hypersensitivity and nerve sensitisation in the mouse colon.	79
	5-HT4 receptor	Serotonin	Prucalopride, a highly selective 5-HT4 receptor agonist, is effective for chronic constipation and IBS constipation subtype.	88
IBD	NK_1R	SP	Induction of colitis in mice increases release of SP and evokes NK_1R endocytosis in myenteric neurons.	37
	PAR_2,	Proteases	Acute inflammation leads to increased proteases. PAR_2 mediates colonic hyperalgesia.	89
	MOPr and DOPr	Endogenous opioids	Chronic inflammation upregulates endogenous opioid ligands and receptors.	40
	Kappa OPrs	Endogenous opioids	Asimadoline, a kappa OPr agonist drug, decreases pain in patients with IBS	90
	Adenosine A_3 receptor	Adenosine	A3AR levels are inversely correlated with levels of pro-inflammatory microRNA miR-206 levels. miR-206 is increased while A3AR is decreased in colonic mucosa of patients with active UC.	91
	GPR109A, GPR41, GPR43	Butyrate	Butyrate, a short chain fatty acid produced by certain microbiota, is decreased in IBD and is associated with an increased number of proinflammatory cells in the gut mucosa.	92
	ACE 2, MAS1-R	Angiotensin 1–7	ACE2 and MAS1-R are upregulated in IBD and are associated with anti-inflammatory properties. Antagonising these receptors worsens inflammation.	93
Bile acid diarrhoea	TGR5	Bile acids	TGR5 is activated by luminal bile acids and mediates hypersensitivity and motility.	15
Colorectal cancer	EP4	PGE_2	Through EP4, PGE_2 induces colonic colorectal cancer stem cell expansion and liver metastasis.	94

A_{2A}, adenosine-2A; DOPr, δ-opioid receptor; EoE, eosinophilic esophagitis; EP4, prostaglandin E2 receptor 4; GPCR, G protein-coupled receptor; H_1R, H_2R, H_4R, histamine 1, 2, 4 receptor; MAS1-R, MAS 1 receptor; MOPr, μ-opioid receptor; NK_1R, neurokinin-1 receptor; OPr, opioid receptor; PAR_1, protease-activated receptor-1; PAR_2, protease-activated receptor-2; PGE_2, prostaglandin E_2; SP, substance P.

with different agonists, antagonists or signalling partners, and can redistribute to distinct subcellular microdomains. This conformation and positional dynamism underlies some of the key properties of GPCRs, which depend on subcellular microdomains (eg, compartmentalised signalling and pH dependence), the nature of the ligand (eg, biased agonism and allosteric modulation), the relationship with other receptors (eg, dimerisation) and the specific tissue of action. An

Gut: first published as 10.1136/gutjnl-2020-321193 on 3 December 2020. Downloaded from http://gut.bmj.com/ on September 30, 2021 at New York University, Serials Bobst Library Technical Services Serials. Protected by copyright.

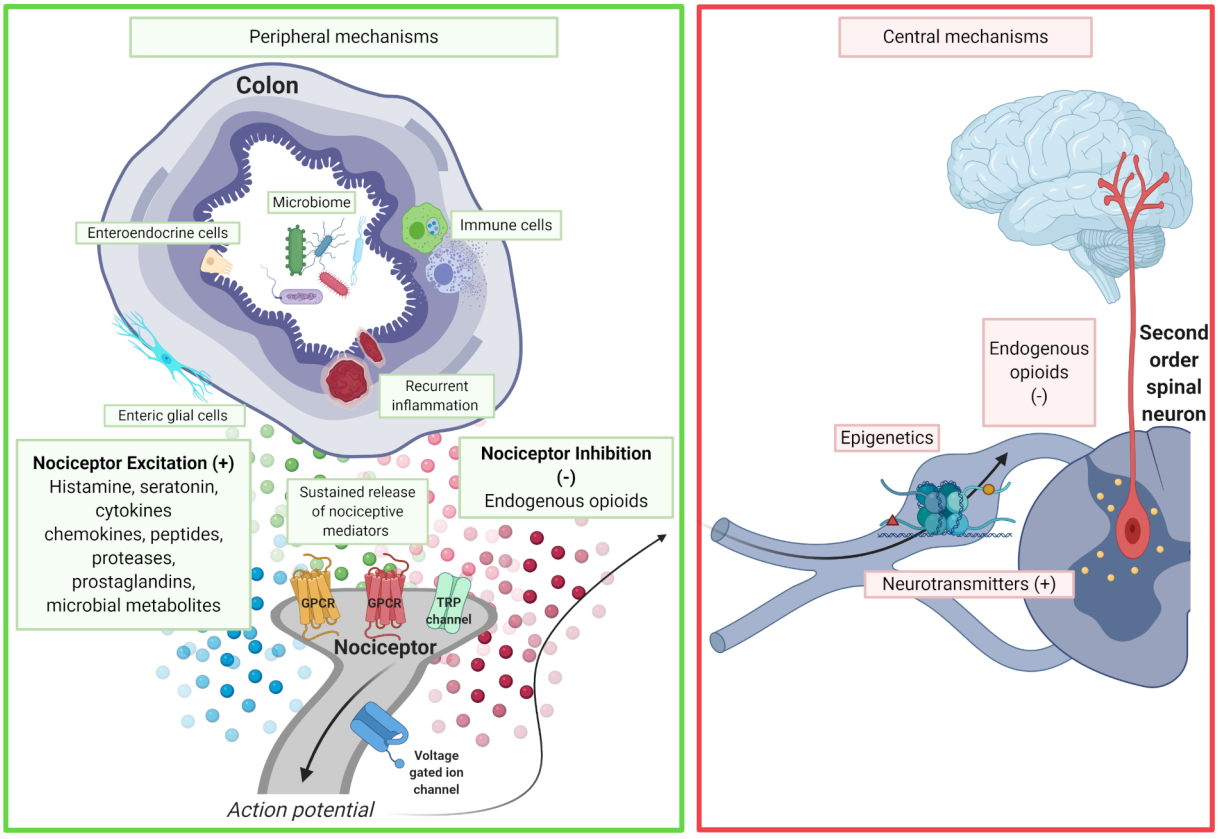


Figure 1 Peripheral and central mechanisms of neuronal sensitisation. Many factors contribute to neuronal sensitisation and chronic visceral pain. Mediators that influence signalling pathways and induce neuronal hypersensitivity in peripheral nociceptors arise from sustained release of nociceptive mediators due to recurrent inflammation, enteric glial cells, immune cells, enteroendocrine cells and microbial dysbiosis. Endogenous opioids suppress neuronal activity. Epigenetic changes within the soma of primary afferent neurons in the dorsal root ganglia contribute to long-term sensitisation. Central mechanisms involve release of excitatory neurotransmitters and decreased inhibitory pathways.

understanding of these complexities, which are discussed further, can provide new information about how GPCRs signal pain and can offer the prospect of developing more selective and effective agonists or antagonists for the treatment of pain.

COMPARTMENTALISED SIGNALLING OF GPCRS

Concept

How can GPCRs that often activate a common set of second messengers and enzymes selectively regulate cellular responses?

The answer may lie in compartmentalised signalling, the capacity of GPCRs to interact with particular signalling partners in defined subcellular microdomains. GPCRs were once considered to function primarily at the plasma membrane, where ligands in the extracellular fluid bind to extracellular and transmembrane domains of receptors and intracellular domains couple to heterotrimeric G proteins. G protein-mediated signalling from the plasma membrane leads to activation of secondary messengers (eg, cAMP, inositol trisphosphate, diacyl glycerol and Ca^{2+}) and subsequent activation of kinases (eg, protein kinase C (PKC), protein kinase A (PKA), phosphorylated extracellular regulated kinase) that phosphorylate and sensitise ligand-gated and voltage-gated ion channels. Ion fluxes depolarise nociceptors and trigger action potentials leading to acute nociception. However, it is now known that GPCR signalling at the plasma membrane can be transient. GPCR kinases phosphorylate activated GPCRs, which serves to increase receptor affinity for β-arrestins (β-ARRs).[17] β-ARRs interdict GPCR association with G proteins and desensitise signalling at the plasma membrane.

Given the fleeting nature of plasma membrane signalling, how can GPCRs generate sustained signals that might underlie long-lasting nociception and neuronal sensitisation?

GPCR signalling in endosomes might provide an answer.[18 19] In addition to desensitisation, β-ARRs mediate endocytosis and intracellular signalling. β-ARRs couple GPCRs to clathrin and adaptor protein-2, which mediate endocytosis of the receptor. Although once considered as a conduit for receptor recycling to the plasma membrane or degradation in lysosomes, endosomes are now considered important sites of GPCR signalling. Endosomal signalling is mediated by both β-ARR-dependent and G protein-dependent processes, which generate sustained intracellular signals via secondary messengers (eg, cAMP) and kinases (eg, PKC and ERK1/2). These pathways can regulate the activity of ion channels and the transcription of genes that underlie persistent neuronal sensitisation (figure 2). Endosomal signalling, as well as sensitisation of ion channels, such as transient receptor potential ion channels, has been shown to play a significant role in driving chronic visceral pain.[20 21] Several GPCRs, some of which have been studied in GI pain, are known to signal from endosomes, including protease-activated receptor-2 (PAR_2),[22] the SP, NK_1R,[23 24] the μ-opioid receptor (MOPr) and δ-opioid receptor (DOPr).[25 26]

Gut: first published as 10.1136/gutjnl-2020-321193 on 3 December 2020. Downloaded from http://gut.bmj.com/ on September 30, 2021 at New York University, Serials Bobst Library Technical Services Serials. Protected by copyright.

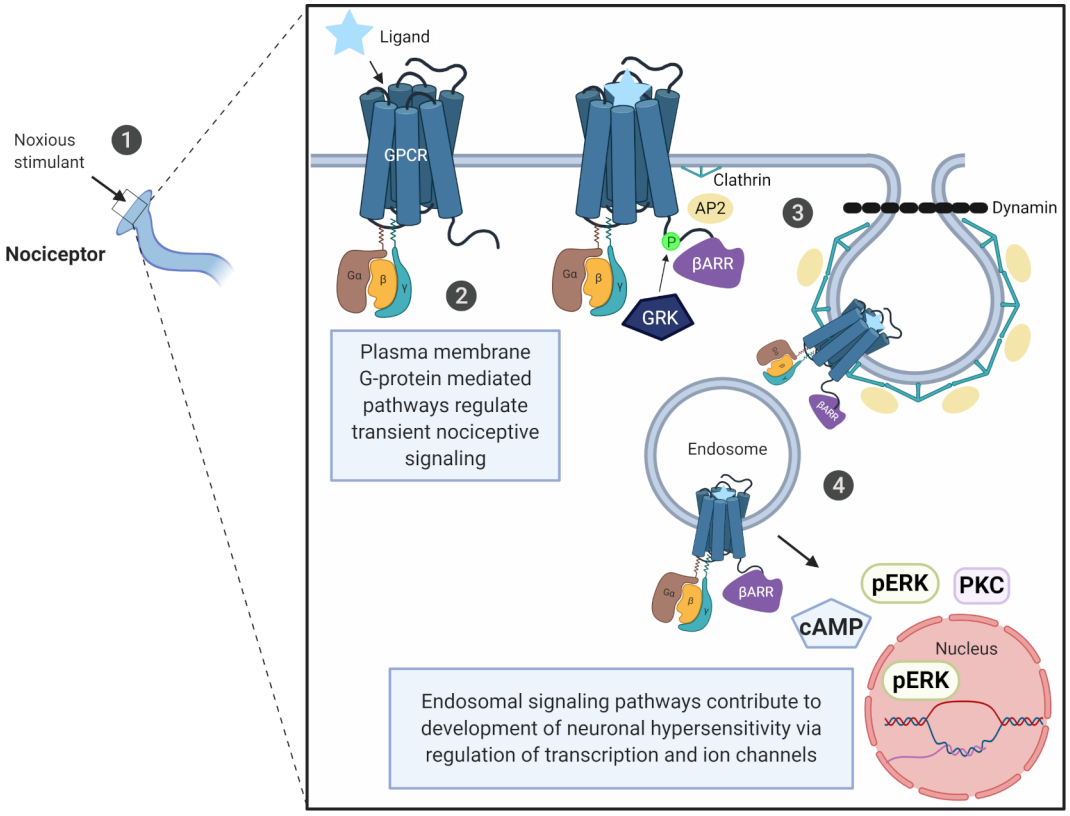


Figure 2 Compartmentalised signalling of GPCRs. Several GPCRs signal nociception from endosomes. (1) Noxious stimuli activate sensory afferents leading to nociceptive transmission; (2) membrane-bound GPCRs couple to heterotrimeric G proteins, which initiate intracellular signalling pathways that contribute to transient nociception; (3) GRKs phosphorylate activated GPCRs and promote the binding of βARRs, which terminate G protein-dependent signalling at the plasma membrane. βARRs facilitate clathrin-mediated receptor endocytosis by linking the GPCR to internalisation machinery. Endocytic proteins include the AP2 complex, which allows clathrin to coat and internalise cargo, and dynamin, which ligates the budding vesicle. (4) GPCRs continue to signal pain from endosomes through both β-ARRs and G-protein-dependent processes, which generate secondary messengers such as cAMP, pERK and PKC. Endosomally derived pathways contribute to sustained nociception and chronic visceral pain via regulation of transcription as well as transcriptionally independent ion channel sensitisation. AP2, adaptor protein-2; βARR, β-arrestin; cAMP, cyclic AMP; GPCR, G protein-coupled receptor; GRK, GPCR kinase; pERK, phosphorylated extracellular regulated kinase; PKC, protein kinase C.

Endosomal signalling of PAR_2

PAR_2 is a GPCR for serine and cysteine proteases, which are activated in disease.[27] PAR_2 is highly expressed in colonocytes, selectively expressed in a subset of primary sensory neurons and has been implicated in the development of visceral hypersensitivity in IBS. In humans, trypsin isoforms from the exocrine pancreas and intestinal epithelial cells, mast cell-derived tryptase and proteases produced by luminal bacteria can cleave within the extracellular amino-terminus of PAR_2, exposing a tethered ligand domain that binds to and activates the cleaved receptor.[28] Trypsin-3, tryptase and PAR_2 are upregulated in biopsies of colonic mucosa from patients with IBS.[29 30] Supernatants from patients with IBS release increased proteases, and injections of these supernatants into colons of awake mice lead to increased visceral hyperalgesia.[31] PAR_2-dependent mechanisms have been suggested to play a significant role in sensitisation of colonic nociceptors and colonic hyperalgesia.[22 27 30] Similarly, in a model of postinfectious IBS in mice induced by the nematode parasite *Trichinella spiralis* elevated protease activity and PAR_2 expression in the colon accompany PAR_2-dependent visceral hypersensitivity.[32]

A recent study suggests that endosomal signalling of PAR_2 underlies sustained hyperexcitability of nociceptors in colonic afferent nerves.[22] Trypsin-activated PAR_2 traffics to endosomes and continues to signal by β-ARR and $G\alpha_q$-mediated mechanisms, leading to activation of ERK in the nucleus and cytosol and activation of PKC in the cytosol. Disruption of clathrin-mediated endocytosis of PAR_2 abrogates the ability of IBS supernatants and trypsin to cause sustained hyperexcitability of nociceptors in neurons. A PAR_2 antagonist conjugated to the transmembrane lipid cholestanol, which preferentially delivers the antagonist to endosomes, also curtails the sustained hyperexcitability of nociceptors.

Compartmentalised signalling of NK_1R

SP belongs to the tachykinin family of neuropeptides that are prominently expressed by primary sensory and enteric neurons.[33] SP interacts with the NK_1R, which is localised to second order spinal neurons, as well as neurons of the myenteric and submucosal nerve plexuses of the intestine.[33 34] NK_1R antagonism or deletion attenuates intestinal and pancreatic nociception and inflammation in preclinical mouse models.[35 36] Nociceptive and proinflammatory stimuli in the intestine, pancreas and skin induce NK_1R endocytosis in spinal and enteric neurons, which is attributable to activation of nociceptors and release of SP.[23 24 34 37 38] The NK_1R continues to signal from endosomes by G-protein-mediated and β-ARR-mediated mechanisms that lead to activation of nuclear ERK as well as cytosolic cAMP and PKC.[24 39] These signals mediate sustained SP-induced excitation

Gut: first published as 10.1136/gutjnl-2020-321193 on 3 December 2020. Downloaded from http://gut.bmj.com/ on September 30, 2021 at New York University, Serials Bobst Library Technical Services Serials. Protected by copyright.

of spinal neurons, gene transcription and somatic nociception. Inhibitors of clathrin-mediated and dynamin-mediated endocytosis and endosomally targeted NK_1R antagonists suppress NK_1R endosomal signalling, neuronal excitation and somatic nociception.[24 39] This provides evidence for a major role of endosomal NK_1R signalling in nociceptive transmission in the spinal cord. Whether NK_1R signalling in endosomes mediates GI pain is unknown but worthy of further investigation in light of the marked redistribution of the NK_1R to endosomes of spinal and enteric neurons in preclinical models of colonic and pancreatic inflammatory pain.[33 34 37 38]

Compartmentalised signalling of MOPr and DOPr

In addition to pronociceptive PAR_2 and NK_1R, antinociceptive GPCRs, exemplified by MOPr and DOPr, can also signal from endosomes to regulate the excitability of neurons in the pain pathway. MOPr and DOPr are expressed by primary sensory neurons and spinal neurons, where agonists depress excitability and thereby dampen nociceptive transmission. Despite their severe detrimental on-target side effects of respiratory depression, constipation and addiction, MOPr agonists, such as morphine, are widely used to treat pain. However, recent studies suggest that peptides and non-peptide opiate drugs can activate OPrs in distinctly different ways. A genetically encoded biosensor derived from a conformation-specific nanobody has been used to detect real-time MOPr and DOPr signalling in subcellular compartments of living neurons.[26] These studies reveal that membrane impermeant opioid peptides initially activate OPrs at the plasma membrane, and that sustained signals then propagate to endosomes coincident with receptor endocytosis. Non-peptide drugs, including morphine, which are membrane permeant distort this normal pattern of plasma membrane and endosomal signalling by rapidly activating internal pools of OPrs in the Golgi apparatus. The functional relevance of this Golgi-directed signalling by opiate drugs for pain control remains to be determined.

Endosomal signalling of DOPr might represent an endogenous mechanism for controlling inflammatory pain in the colon.[25] Chronic colitis is associated with an upregulation of opioids, which derive from infiltrating immune cells and activate DOPr on nociceptors to suppress excitability and nociception.[40] Colonic biopsies from patients with IBD and mice with chronic colitis release opioids that activate the DOPr and suppress the excitability of mouse nociceptors.[25] DOPr agonists that evoke DOPr endocytosis cause long-lasting antinociception, whereas non-internalising DOPr agonists exert only transient inhibitory effects. Inhibitors of clathrin-dependent and dynamin-dependent endocytosis block the sustained actions of opioids from colonic biopsies, supporting a role for endosomal DOPr signalling in sustained suppression of inflammatory pain in humans. Opioids also evoke DOPr endocytosis in enteric neurons, where the role of endosomal signalling remains to be defined.[41]

Therapeutic implications

Efforts to discover drugs that are antagonists or agonists of GPCRs have largely focused on the identification of ligands that interact with receptors at the cell surface. The discovery that GPCRs in subcellular compartments, including endosomes and the Golgi apparatus, can generate sustained signals suggests that intracellular rather than cell surface GPCRs are a more appropriate therapeutic target.[19] Drugs that target GPCRs in endosomes must traverse the plasma and endosomal membranes as well as the cytosol, and be capable of engaging GPCRs in the acidic endosomal microenvironment, where receptors are likely assembled in signalling complexes comprising ligands, GPCRs, G proteins, β-ARRs and kinases. Although GPCR drugs can fail in clinical trials for many reasons, it is possible that the failure of certain drugs for pain control relates to their inability to effectively engage with GPCRs in endosomes. Several strategies have been devised to target GPCRs in endosomes for the treatment of pain (figure 3).

Inhibitors of clathrin, dynamin and β-ARRs block endocytosis of PAR_2 and NK_1R, attenuate endosomal signalling, and prevent sustained activation of primary sensory and spinal neurons (figure 3A). When injected intrathecally, clathrin and dynamin inhibitors and dynamin-1 siRNA suppress NK_1R endocytosis and attenuate nociception in mice and rats.[23] After intraplantar injection, clathrin and dynamin inhibitors attenuate trypsin-evoked and PAR_2-dependent nociception. Endocytosis inhibitors also block PAR_2-dependent sensitisation of colonic nociceptors.[22] Whether these drugs attenuate visceral pain in the GI tract is unknown. Given the widespread roles of clathrin and dynamin in protein trafficking and vesicle formation, side effects may preclude clinical use.

Other approaches to target endosomal GPCRs have focused on drug delivery. Tripartite lipidated probes are composed of three components: cholestanol, which enables membrane insertion; a polyethylene glycol linker; and a GPCR antagonist cargo (figure 3B).[22 39] Tripartite probes insert into the plasma membrane and then accumulate in early endosomes. Tripartite NK_1R antagonists cause long-lasting inhibition of endosomal signalling and attenuate persistent SP-evoked excitation of spinal neurons. A tripartite PAR_2 antagonist accumulates in endosomes of DRG neurons and blocks endosomal signalling of PAR_2. A tripartite PAR_2 antagonist blocks sustained hypersensitivity in DRG nociceptors treated with supernatant of biopsies from patients with IBS.[22] Given these findings, the effects of tripartite antagonists in colonic visceral pain is worthy of further investigation. Despite encouraging preclinical findings, lipid-conjugated antagonists incorporate indiscriminately into membrane of all cells, which may complicate clinical development.

Nanoparticle drug delivery offers the tantalising prospect of selectively delivering antagonists or agonists of GPCRs to endosomes of neurons that sense and transmit pain, which may limit drug dosing, minimise on-target side effects in other cell types and mitigate systemic toxicity. There are multiple methods to target nanoparticles to an area of interest, including based on size, material and charge, and molecular recognition.[42] Stimulus-responsive nanoparticles are designed to release their cargo in response to certain triggers, such as acidity, redox potential and protease activity. Although nanoparticles have primarily been developed for the treatment of cancer,[42] their use has been extended for the treatment of pain.[24 25]

Aprepitant is an NK_1R antagonist that is approved for the treatment of chemotherapy-induced nausea and vomiting but has failed in clinical trials for the treatment of pain.[33] Aprepitant has been incorporated into pH-responsive soft-polymer nanoparticles designed to enter endosomes and disassemble in acidic endosomes, where they release drug cargo (figure 3C).[24] Nanoparticle-encapsulated aprepitant causes sustained inhibition of endosomal NK_1R signalling and attenuates SP-evoked excitation of spinal neurons. Nanoparticle-encapsulated aprepitant provides more efficacious and sustained reversal of somatic inflammatory and neuropathic pain than free aprepitant. Nanoparticle delivery can be further refined by coating nanoparticles with a ligand that promotes targeting to endosomes of nociceptors or spinal neurons. Nanoparticles with both

Gut: first published as 10.1136/gutjnl-2020-321193 on 3 December 2020. Downloaded from http://gut.bmj.com/ on September 30, 2021 at New York University, Serials Bobst Library Technical Services Serials. Protected by copyright.

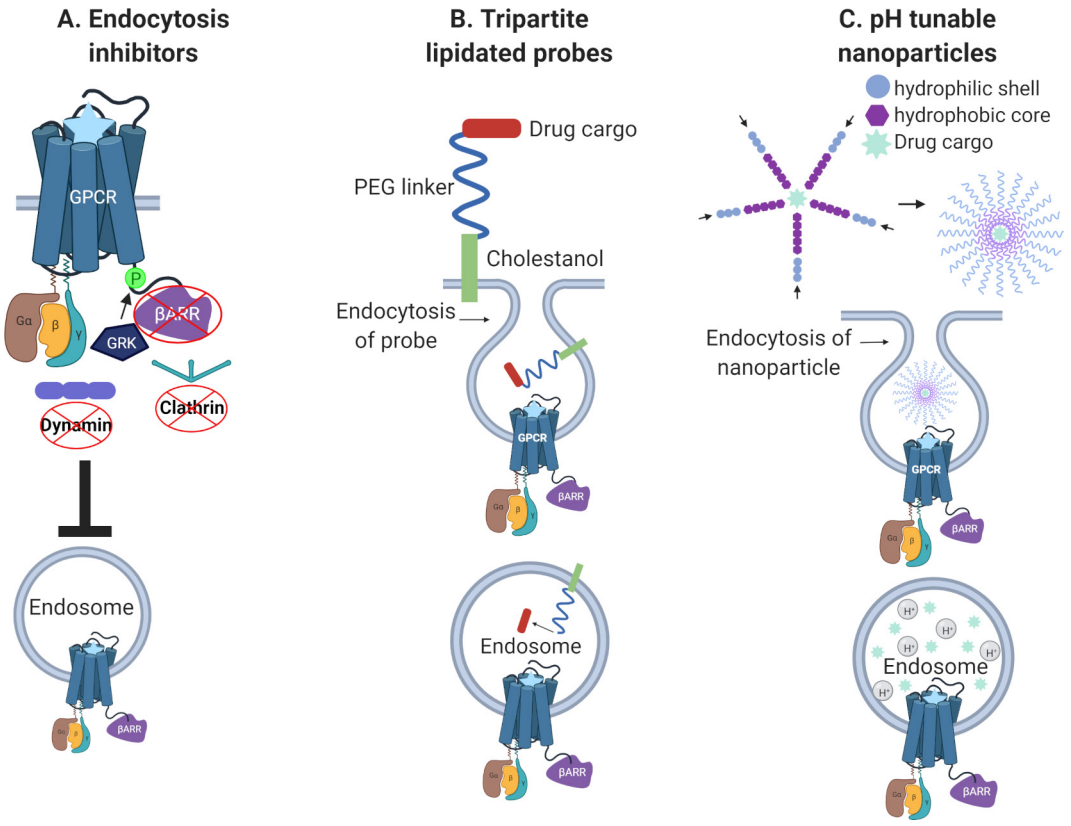


Figure 3 Therapeutic targeting of GPCRs in endosomes. (A) Inhibitors of clathrin, dynamin and βARRs prevent receptor endocytosis and thus inhibit endosomal nociception transmission. (B) Tripartite lipidated probes can deliver GPCR antagonists to endosomes. Tripartite probes are composed of cholestanol, which enables membrane insertion, a polyethylene glycol (PEG) linker and a GPCR antagonist cargo. Tripartite probes insert into the plasma membrane and undergo endocytosis, which delivers the cargo to GPCRs in endosomes. (C.) Nanoparticle drug delivery systems deliver and release therapies to endosomes. pH-dependent nanoparticles are composed of a hydrophobic core and a hydrophilic shell. They self-assemble in an aqueous environment, encapsulating a hydrophobic drug cargo. Nanoparticles undergo endocytosis. In the acidic endosomal environment, protonation of the hydrophobic monomer results in like–like charge repulsion, nanoparticle disassembly and cargo release. βARR, β-arrestin; GPCR, G protein-coupled receptor; GRK, GPCR kinase.

a liposome shell conjugated to the DOPr agonist (DADLE) and a pH-sensitive mesoporous silica core containing DADLE are preferentially endocytosed by DOPr-expressing cells and gradually release cargo in the acidic and reducing endosomal environment.[25] These nanoparticles have sustained antinociceptive effects on primary sensory neurons and colonic afferent neurons from mice. Nanoparticles also offer the capability of incorporating antagonists of several pronociceptive GPCRs into a single particle, which might overcome the redundancy that is inherent in pain transmission pathways.

PH-DEPENDENT ACTIVATION OF GPCRS

Concept

Is it possible to devise strategies that selectively activate GPCRs in diseased tissue and thereby obviate side effects in healthy tissues?

Ligands that activate GPCRs in endosomes must be capable of binding to receptors in an acidic endosomal environment of pH<6.0. The extracellular fluid of diseased tissues (eg, tumours, sites of inflammation and infection) can also become acidified, which might alter ligand–receptor interactions and signalling.[43] The concept of pH-dependent ligand/GPCR interaction and signalling has been exploited for the development of drugs that selectively engage GPCRs in acidified diseased tissues. The MOPr exemplifies the potential usefulness of such an approach. MOPr agonists such as morphine and fentanyl inhibit pain by dampening the excitability of primary sensory and spinal neurons. In a mouse model of IBD, endogenous opioids from infiltrating immune cells activate MOPr on peripheral gut nociceptors to evoke anti-inflammatory and antinociceptive signalling pathways.[40 44] However, the usefulness of MOPr agonists for the treatment of pain is limited by on-target side effects that are mediated by MOPrs in other cell types. These include MOPrs in the enteric nervous system, where activation leads to constipation, and the central nervous system, where MOPr agonists cause respiratory depression, nausea and addiction.

Therapeutic implications

Information about the atomic structure of the MOPr has been used to selectively activate it in diseased tissue.[45 46] Molecular modelling of the effects of extracellular pH on docking of fentanyl to MOPr enabled the design of a fluorinated fentanyl analogue; fluorination enablesthe drug to be preferentially protonated in acidic microenvironments of diseased tissues, which facilitates MOPr binding (figure 4A). This analogue preferentially binds to and activates MOPr in model cells in acidified extracellular fluid and attenuates inflammatory pain without causing addiction, respiratory depression or constipation in preclinical models.

Gut: first published as 10.1136/gutjnl-2020-321193 on 3 December 2020. Downloaded from http://gut.bmj.com/ on September 30, 2021 at New York University, Serials Bobst Library Technical Services Serials. Protected by copyright.

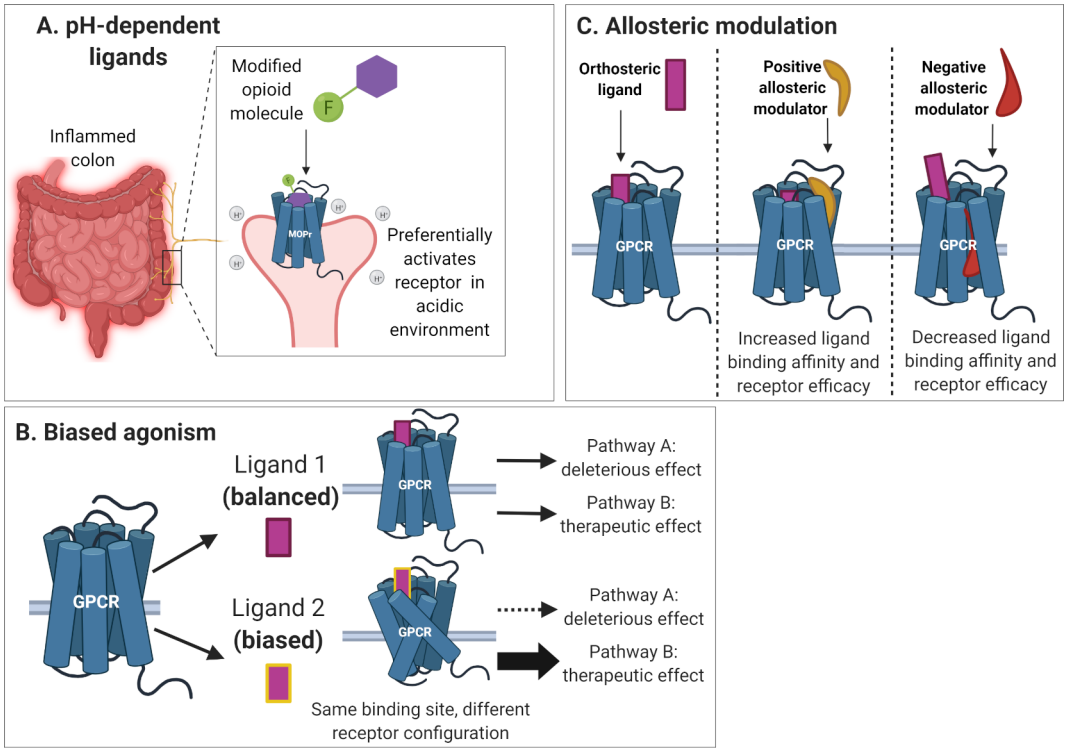


Figure 4 pH-dependent agonism, biased agonism and allosteric modulation of GPCRs. (A) pH-dependent agonism. A fluorinated opioid molecule is modified to selectively bind to GPCRs in acidic extracellular fluid such as at sites of cancer, inflammation and infection. (B) Biased agonism. The process by which different ligands bind to the same GPCR orthosteric site but activate different signalling pathways via stabilisation of specific receptor conformations. As opposed to balanced agonism, whereby the ligand triggers both therapeutic and deleterious pathways, biased agonists are designed to stabilise a specific conformation to favour therapeutic pathways over deleterious pathways. (C) Allosteric modulation. The process by which an effector molecule binds to a region of a GPCR (an allosteric site) that is distinct from that occupied by an endogenous (orthosteric) ligand. Allosteric binding modifies the ability of the endogenous ligand to activate the receptor. Positive allosteric modulators increase the potency of endogenous ligands. Negative allosteric modulators decrease the potency of endogenous ligands. GPCR, G protein-coupled receptor.

These results have far-reaching implications for the development of new opioid treatments that successfully alleviate pain while mitigating unwanted side effects, including abuse potential. Whether such analogues of fentanyl suppress inflammatory pain in the digestive system without causing constipation remains to be determined. Similar approaches might be used to enhance the on-target selectivity of agonists and antagonists of other GPCRs while minimising on-target detrimental actions in healthy tissues.

BIASED AGONISM OF GPCRS

Concept

Can a particular GPCR signalling pathway be preferentially targeted?

Biased agonism refers to the concept that different agonists of the same GPCR can stabilise distinct conformations that might favour signalling by one pathway over another (figure 4B).[47] Recent advances in our understanding of how different proteases activate PAR_2 illustrate the relevance of biased agonism to signalling of pain. In the intestine, proteases that activate PAR_2 arise from multiple sources, including immune cells, microbial cells and pancreatic tissue (figure 5A).[28] As discussed in the aforementioned section on compartmentalised signalling, proteases such as trypsin activate PAR_2 and signal via canonical mechanisms. Cleavage by trypsin induces coupling to $G\alpha_q$ and β-ARRs, which mediate endocytosis and endosomal signalling that are necessary for the sustained sensitisation of colonic sensory nerves during IBS (figure 5B).[22 48] However, endosomal signalling of PAR_2 is not always the mediator of long-term neuronal sensitisation. Other proteases activated in the digestive system during inflammation and cancer, including cathepsin S from macrophages, elastase from neutrophils,and legumain from tumour cells, cleave PAR_2 at unique sites and activate biased signalling pathways that do not lead to receptor endocytosis (figure 5C).[16 22 49 50] Once activated by these proteases, PAR_2 remains at the plasma membrane where it continues to generate pronociceptive signals by mechanisms that entail activation of adenylyl cyclase and PKA, which may phosphorylate and sensitise ion channels. These findings indicate that both endocytosis-dependent as well as endocytosis-independent pathways can contribute to ion channel sensitisation by PAR_2 (figure 5).[16]

Therapeutic implications

The concept of biased agonism is of particular interest for drug development because it may allow the identification of GPCR agonists that activate therapeutically beneficial pathways at the expense of those that invoke deleterious side effects.[9 10 51] There is intense interest in biased agonism of OPrs to mitigate unwanted side effects. The concept of developing biased agonists of MOPr arose from studies of β-ARR2-deficient mice, which implicated β-ARR2 signalling pathways in morphine-evoked respiratory depression and constipation, whereas analgesia was signalled by G protein pathways.[52] These findings spurred efforts to identify biased agonists that evoke MOPr signalling by G proteins but not β-ARR2, some of which have been evaluated in clinical trials.[53 54]

Gut: first published as 10.1136/gutjnl-2020-321193 on 3 December 2020. Downloaded from http://gut.bmj.com/ on September 30, 2021 at New York University, Serials Bobst Library Technical Services Serials. Protected by copyright.

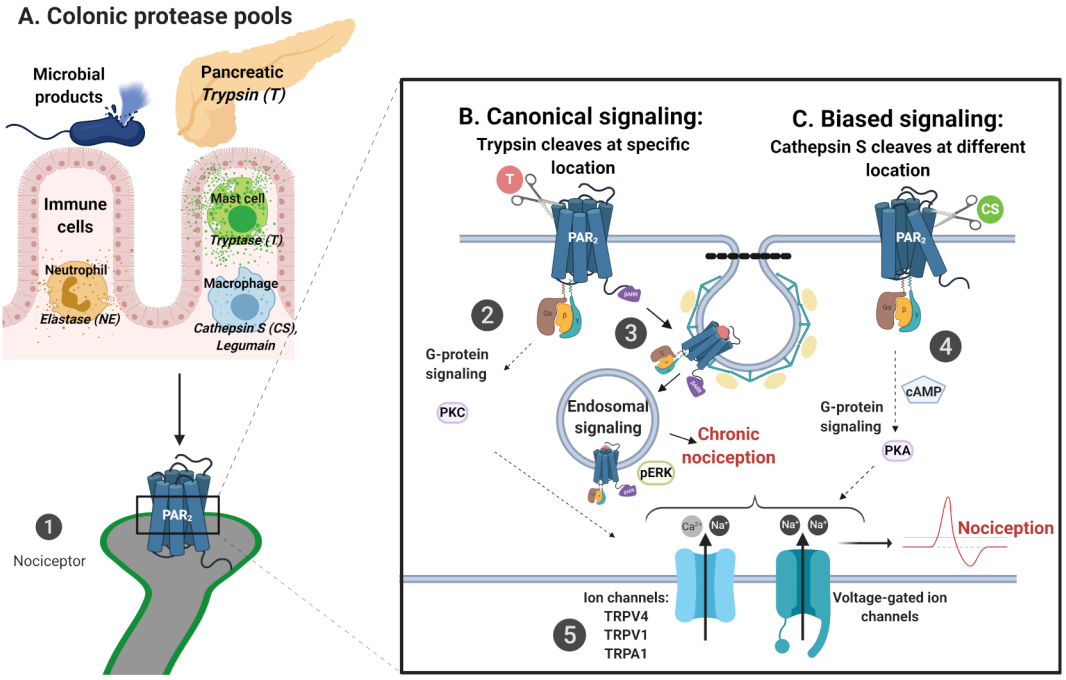


Figure 5 Canonical and biased signalling of PAR_2. (A) Proteases are released from multiple sources including immune cells (ie, T from mast cells, CS and matrix metalloproteinase from granulocytes and NE), exocrine pancreas tissue (ie, trypsin-1/2) and microbial breakdown products. (1) Proteases activate PAR_2 on peripheral nerve endings. (B) Tryptase and trypsin activate canonical signalling, which include (2) G-protein mediated signalling from the plasma membrane, leading to activation of secondary messengers (ie, PKC). (3) Canonical signalling also entails β-ARR-mediated endocytosis of PAR_2 and endosomal signalling by G protein-mediated and β-ARR-mediated processes that activate pERK and mediate persistent hypersensitivity and chronic nociception. (C) Cathepsin S and neutrophil elastase activate biased pathways. They cleave PAR_2 at different sites from tryptase and trypsin, stabilising different receptor conformations and activating biased pathways (4). These include G-protein-mediated signalling from the plasma membrane via cAMP and PKA. They do not induce β-ARR-mediated endocytosis of PAR_2. Secondary messengers activated by both canonical and biased signalling can contribute to sensitisation of ion channels, another mechanism underlying chronic visceral pain (5). Ion movement leads to membrane depolarisation and triggers action potentials leading to nociception. β-ARR, β-arrestin; cAMP, cyclic AMP; CS, cathepsin S; NE, neutrophil elastase; PAR_2, protease-activated receptor-2; pERK, phosphorylated extracellular regulated kinase; PKA, protein kinase A; PKC, protein kinase C; T, tryptase; TRPV, transient receptor potential vanilloid.

TRV130 (oliceridine) is a biased MOPr agonist that activates G protein pathways with minimal β-ARR2 activation. A phase III double-blinded randomised control trial comparing oliceridine, morphine and placebo for treatment of acute postoperative abdominoplasty pain showed that oliceridine provided comparable analgesia to morphine with a favourable side-effect profile, although abuse potential with repeated doses was similar to morphine.[55 56] The Federal Drug Administration declined approval, citing that benefits of analgesia did not outweigh risks compared with morphine. Multiple other biased agonists of MOPr and DOPr have been developed.[55 57–59]

Despite the theoretical benefits of biased agonism, clinical success has been elusive. The sine qua non of biased agonism is that the signalling pathways underlying the therapeutically beneficial versus detrimental actions of GPCR agonists are known and different. However, controversy remains as to whether analgesia and constipation are truly signalled by distinct pathways in human tissues. Indeed, recent reports question the role of β-ARR2-mediated pathways in constipation and respiratory depression. Mice expressing a phosphorylation-defective MOPr mutant that is unable to recruit β-ARR2 show augmented analgesia and decreased tolerance compared with wild-type mice when administered opioids, confirming a role for β-ARR2 in MOPr desensitisation.[60] However, opioid-induced constipation and respiratory depression were maintained. Recent studies have found that opioids induce respiratory depression and constipation to a similar extent in β-ARR2 knockout and wild-type mice.[61] These findings cast doubt on β-ARR2 as a mediator of the side effects of opioid, which may explain the poor efficacy of biased opioids. A pharmacological assessment of MOR-biased ligands such as oliceridine suggests that low intrinsic efficacy (ability for an agonist to trigger a receptor response) compared with morphine, and not biased agonism, may account for the lack of β-ARR2-mediated actions.[62] Thus, although opioids have been developed that preferentially activate certain signalling pathways in model cell lines, controversy about the underlying mechanisms and signalling pathways in human tissues has cast doubt on the importance of biased agonism for drug development. Despite these setbacks, there remains sustained interest in developing biased agonists of GPCRs. Atomic-level molecular modelling has identified GPCR conformations that favour signalling of one pathway over another.[63 64] Such studies might enable the rational design of GPCR-biased agonists.

ALLOSTERIC MODULATION OF GPCRS

Concept

Allosteric modulators are ligands that bind to an allosteric site of a GPCR that is different from that occupied by endogenous ligands, termed the orthosteric site.[65] Allosteric modulators can increase (positive allosteric modulators (PAMs)) or decrease (negative allosteric modulators) the affinity or efficacy of endogenous ligands (figure 4C). Allosteric modulation has been exploited in efforts to develop drugs to treat pain.[10]

Gut: first published as 10.1136/gutjnl-2020-321193 on 3 December 2020. Downloaded from http://gut.bmj.com/ on September 30, 2021 at New York University, Serials Bobst Library Technical Services Serials. Protected by copyright.

Therapeutic implications

By fine-tuning the effects of endogenous analgesics such as opioids, PAMs of OPrs might provide refined control of pain. Allosteric modulators also hold the potential for increased selectivity for GPCR subtypes. Orthosteric sites are evolutionarily conserved so that the same ligand can bind to different GPCR subtypes. In contrast, allosteric sites are typically specific to each GPCR subtype. Thus, allosteric modulators have been attractive drug targets to alter ligand binding on a specific GPCR and enhance receptor subtype specificity.

Multiple allosteric modulators have been developed for the treatment of central nervous system diseases, including Alzheimer's disease and schizophrenia, with limited success.[9] These modulators target muscarinic receptors and increase the affinity of receptor subtypes to acetylcholine. However, despite selectivity for CNS located M_1 muscarinic receptor, PAM MK-7622 caused significant cholinergic side effects, specifically diarrhoea, in peripheral tissues.[66]

There has been considerable interesting in developing allosteric modulators of DOPr and MOPr for the improved treatment of pain.[67 68] While most allosteric modulators have not been tested in preclinical models of GI pain, the focus remains on increasing pain relief while mitigating side effects, including those affecting the GI tract.[67 68] For example, morphine and fentanyl interact with the orthosteric site of MOPr, and allosteric modulation, theoretically, could decrease the dosage needed to achieve analgesia or enhance the effects of endogenous opioids. While MOPr and DOPr PAMs have been developed, clinical testing has not progressed. Nevertheless, the ability to modulate the effects of opioids for the treatment of pain and diarrhoea remains of considerable interest.

GPCR DIMERISATION

Concept

GPCR dimerisation adds to the complexity of GPCRs while offering new avenues for therapeutic design.[69] Despite initial excitement in the concept that different GPCRs might associate to create a receptor with unique physiological roles and pharmacological properties, the concept of GPCR dimerisation remains controversial.[10] It has been challenging to convincingly demonstrate the existence of GPCR dimers in native tissues. The dimerisation of OPrs is a controversial area that has garnered much attention. Early studies provided evidence that MOPr and DOPr signalling is inter-related. Thus, DOPr antagonism or deletion attenuated morphine-evoked tolerance and dependence in mice.[70] Binding low-dose DOPr antagonists increased the potency of MOPr agonists, inviting new therapeutic strategies with bifunctional ligands.[71] Later studies confirmed that they colocalise in certain neuronal populations in both the peripheral and central nervous system and function as heterodimers.[72] However, other studies have disputed these conclusions. Mice expressing fluorescently tagged DOPrs show little coexpression of DOPr and MOPr in primary neurons.[73] Furthermore, where they are coexpressed in interneurons and secondary neurons, there is no evidence for heterodimer formation. Electrophysiological and molecular studies support DOPr and MOPr coexpression by sensory DRG neurons originating in the mouse colon, although heterodimer formation of these receptors remains unclear.[31]

Therapeutic implications

Despite controversy, drugs composed of bifunctional ligands to target both DOPr and MOPr remain an active area of therapeutic research. Eluxadoline is a compound with MOPr agonist and DOPr antagonist activity that demonstrated relief of abdominal pain in patients with IBS-induced diarrhoea without evidence for abuse potential in phase II and III trials.[74] Further investigation regarding the coexpression and interaction of GPCRs in the GI system is needed to understand therapeutic potential.

TISSUE-SPECIFIC OUTCOMES OF GPCR SIGNALLING

Concept

The realisation that GPCRs can convey distinct sensory information in different tissues has led to the identification of new mediators of visceral pain. Studies of GPCRs that mediate itch in the skin, such as mas-related G-protein receptors (Mrgprs) and Takeda GPCR 5 (TGR5), have revealed new roles for irritant sensation and visceral hypersensitivity in the colon.[15] The Mrgpr family of GPCRs are expressed by cutaneous afferent neurons, where they mediate the sensation of itch.[75] Chloroquine, an antimalarial drug, evokes pruritus by activating MrgprA3/MrgprX1 in cutaneous afferent nerves. TGR5, a receptor for secondary bile acids, is also expressed by cutaneous afferents and has been implicated in bile acid-evoked scratching in mice and cholestatic itch.[76 77]

Accumulating evidence suggests that certain Mrgprs and TGR5 are expressed by colonic afferent neurons where they might mediate hypersensitivity and pain, rather than itch. TGR5 is expressed by enteric neurons, where activation by luminal bile acids evokes the peristaltic reflex.[76] Mrgprc11 is expressed on splanchnic and pelvic DRG neurons in mice.[78] Activation with the endogenous ligand, bovine adrenal medulla 8–22, causes visceral hypersensitivity and increased visceromotor responses to colorectal distension. Colonic biopsies from patients with IBS show elevated levels of certain metabolites of polyunsaturated fatty acids compared with healthy controls.[79 80] One metabolite, 5-oxoeicosatetraenoic acid, evokes visceral hypersensitivity and nociceptor activation through the Mrgprd receptor pathway in mice.[79]

Mrgpra3, Mrgprc11 and TGR5 are expressed in DRG neurons innervating the mouse colon and have been implicated in afferent nerve sensitisation associated with IBS pain.[15] Agonists of these receptors sensitise nociceptors innervating isolated segments of mouse colon, which is not seen in receptor knockout mice. Intraluminal administration of these agonists triggers visceral hypersensitivity to colorectal distension. These receptors induce mechanical hypersensitivity through the transient receptor potential ankyrin-1 ion channel, a major mediator of itch.

Therapeutic implications

This irritant-sensing pathway in the colon might represent a visceral representation of the cutaneous itch pathway and could contribute to sensory disturbances accompanying IBS. Thus, antagonists of Mrgprs, TGR5 or downstream channels such as TRPA1, might be considered for the treatment of chronic pain in the digestive system.

CONCLUSIONS AND FUTURE DIRECTIONS

Chronic pain within the digestive tract remains a major unmet medical problem. It accompanies common digestive diseases, is poorly understood and is difficult to treat. Analgesic drugs such as opioids have major GI side effects. Given the importance and complexity of GPCRs in controlling the pathways of CVH, it is not surprising that they have been a focus of drug discovery and development. GPCR-targeted therapies are usually based on observations in preclinical disease models. Few drugs

Gut: first published as 10.1136/gutjnl-2020-321193 on 3 December 2020. Downloaded from http://gut.bmj.com/ on September 30, 2021 at New York University, Serials Bobst Library Technical Services Serials. Protected by copyright.

progress to clinic; of those that do progress, many fail in clinical trials of pain. Reasons for failure might include the inability to generate preclinical models of visceral pain that faithfully replicate human diseases; the challenge of studying visceral pain in animals, the inherent redundancy of pain signalling pathways where multiple receptors and channels participate in important protective pain mechanisms; and the lack of understanding of how receptors and channels regulate pain signalling in relevant human cells.

Despite these challenges, new information about how GPCRs signal nociception holds the potential to develop improved therapies. These include antagonists that selectively target endosomal GPCRs; opioids that preferentially activate OPrs in the acidified extracellular milieu of disease tissues; biased agonists that stabilise OPr conformations that favour signalling of therapeutically desirable pathways but not those that mediate the detrimental actions of opioids; and PAMs that subtly amplify the analgesic properties of endogenous opioids. Many of these approaches have been evaluated for the treatment of somatic pain. Further studies are necessary to test their effectiveness against visceral pain in the digestive system. The opioid crisis, which has highlighted the problem of chronic pain and its treatment, will continue to spur efforts to discover new information about the mechanisms and treatment of chronic pain in the digestive system.

Contributors LGK, RL, SV, BS and NB researched field and wrote the manuscript.

Funding Supported by grants from National Institutes of Health (NS102722, DE026806, DE029951, DK118971; NWB and BLS) and Department of Defense (W81XWH1810431, NWB and BLS).

Competing interests NWB is a founding scientist of Endosome Therapeutics Inc.

Patient and public involvement Patients and/or the public were not involved in the design, conduct, reporting or dissemination plans of this research.

Patient consent for publication Not required.

Provenance and peer review Not commissioned; externally peer reviewed.

ORCID iD

Nigel W Bunnett http://orcid.org/0000-0003-3367-0644

REFERENCES

1 Cox JJ, Reimann F, Nicholas AK, *et al*. An SCN9A channelopathy causes congenital inability to experience pain. *Nature* 2006;444:894–8.
2 Treede R-D, Rief W, Barke A, *et al*. Chronic pain as a symptom or a disease: the IASP classification of chronic pain for the International classification of diseases (ICD-11). *Pain* 2019;160:19–27.
3 Drewes AM, Olesen AE, Farmer AD, *et al*. Gastrointestinal pain. *Nat Rev Dis Primers* 2020;6:1.
4 Hsu ES. Medication overuse in chronic pain. *Curr Pain Headache Rep* 2017;21:2.
5 Hedegaard H, Minino AM, Warner M. Drug overdose deaths in the United States, 1999-2017. *NCHS Data Brief* 2018;329:1–8.
6 Brierley SM, Linden DR. Neuroplasticity and dysfunction after gastrointestinal inflammation. *Nat Rev Gastroenterol Hepatol* 2014;11:611–27.
7 Grundy L, Erickson A, Brierley SM. Visceral pain. *Annu Rev Physiol* 2019;81:261–84.
8 Hauser AS, Attwood MM, Rask-Andersen M, *et al*. Trends in GPCR drug discovery: new agents, targets and indications. *Nat Rev Drug Discov* 2017;16:829–42.
9 Canals M, Poole DP, Veldhuis NA, *et al*. G-Protein-Coupled receptors are dynamic regulators of digestion and targets for digestive diseases. *Gastroenterology* 2019;156:1600–16.
10 Geppetti P, Veldhuis NA, Lieu T, *et al*. G protein-coupled receptors: dynamic machines for signaling pain and itch. *Neuron* 2015;88:635–49.
11 Zielińska A, Sałaga M, Włodarczyk M, *et al*. Focus on current and future management possibilities in inflammatory bowel disease-related chronic pain. *Int J Colorectal Dis* 2019;34:217–27.
12 Balemans D, Mondelaers SU, Cibert-Goton V, *et al*. Evidence for long-term sensitization of the bowel in patients with post-infectious-IBS. *Sci Rep* 2017;7:13606.
13 Vera-Portocarrero L, Westlund KN. Role of neurogenic inflammation in pancreatitis and pancreatic pain. *Neurosignals* 2005;14:158–65.
14 Demir IE, Friess H, Ceyhan GO. Neural plasticity in pancreatitis and pancreatic cancer. *Nat Rev Gastroenterol Hepatol* 2015;12:649–59.
15 Castro J, Harrington AM, Lieu T, *et al*. Activation of pruritogenic TGR5, MrgprA3, and MrgprC11 on colon-innervating afferents induces visceral hypersensitivity. *JCI Insight* 2019;4. doi:10.1172/jci.insight.131712. [Epub ahead of print: 17 Oct 2019].
16 Balemans D, Boeckxstaens GE, Talavera K, *et al*. Transient receptor potential ion channel function in sensory transduction and cellular signaling cascades underlying visceral hypersensitivity. *Am J Physiol Gastrointest Liver Physiol* 2017;312:G635–48.
17 Gurevich VV, Gurevich EV. Gpcr signaling regulation: the role of GRKs and arrestins. *Front Pharmacol* 2019;10:125.
18 Murphy JE, Padilla BE, Hasdemir B, *et al*. Endosomes: a legitimate platform for the signaling train. *Proc Natl Acad Sci U S A* 2009;106:17615–22.
19 Thomsen ARB, Jensen DD, Hicks GA, *et al*. Therapeutic targeting of endosomal G-protein-coupled receptors. *Trends Pharmacol Sci* 2018;39:879–91.
20 Amadesi S, Nie J, Vergnolle N, *et al*. Protease-Activated receptor 2 sensitizes the capsaicin receptor transient receptor potential vanilloid receptor 1 to induce hyperalgesia. *J Neurosci* 2004;24:4300–12.
21 Chen Y, Yang C, Wang ZJ. Proteinase-Activated receptor 2 sensitizes transient receptor potential vanilloid 1, transient receptor potential vanilloid 4, and transient receptor potential ankyrin 1 in paclitaxel-induced neuropathic pain. *Neuroscience* 2011;193:440–51.
22 Jimenez-Vargas NN, Pattison LA, Zhao P, *et al*. Protease-Activated receptor-2 in endosomes signals persistent pain of irritable bowel syndrome. *Proc Natl Acad Sci U S A* 2018;115:E7438–47.
23 Jensen DD, Lieu T, Halls ML, *et al*. Neurokinin 1 receptor signaling in endosomes mediates sustained nociception and is a viable therapeutic target for prolonged pain relief. *Sci Transl Med* 2017;9:eaal3447.
24 Ramírez-García PD, Retamal JS, Shenoy P, *et al*. A pH-responsive nanoparticle targets the neurokinin 1 receptor in endosomes to prevent chronic pain. *Nat Nanotechnol* 2019;14:1150–9.
25 Jimenez-Vargas NN, Gong J, Wisdom MJ, *et al*. Endosomal signaling of delta opioid receptors is an endogenous mechanism and therapeutic target for relief from inflammatory pain. *Proc Natl Acad Sci U S A* 2020;117:15281–92.
26 Stoeber M, Jullié D, Lobingier BT, *et al*. A genetically encoded biosensor reveals location bias of opioid drug action. *Neuron* 2018;98:963–76.
27 Cenac N, Andrews CN, Holzhausen M, *et al*. Role for protease activity in visceral pain in irritable bowel syndrome. *J Clin Invest* 2007;117:636–47.
28 Pontarollo G, Mann A, Brandão I, *et al*. Protease-Activated receptor signaling in intestinal permeability regulation. *Febs J* 2020;287:645–58.
29 Liang W-J, Zhang G, Luo H-S, *et al*. Tryptase and protease-activated receptor 2 expression levels in irritable bowel syndrome. *Gut Liver* 2016;10:382–90.
30 Rolland-Fourcade C, Denadai-Souza A, Cirillo C, *et al*. Epithelial expression and function of trypsin-3 in irritable bowel syndrome. *Gut* 2017;66:1767–78.
31 Guerrero-Alba R, Valdez-Morales EE, Jiménez-Vargas NN, *et al*. Co-Expression of μ and δ opioid receptors by mouse colonic nociceptors. *Br J Pharmacol* 2018;175:2622–34.
32 Du L, Long Y, Kim JJ, *et al*. Protease activated receptor-2 induces immune activation and visceral hypersensitivity in post-infectious irritable bowel syndrome mice. *Dig Dis Sci* 2019;64:729–39.
33 Steinhoff MS, von Mentzer B, Geppetti P, *et al*. Tachykinins and their receptors: contributions to physiological control and the mechanisms of disease. *Physiol Rev* 2014;94:265–301.
34 Pelayo J-C, Veldhuis NA, Eriksson EM, *et al*. Localisation and activation of the neurokinin 1 receptor in the enteric nervous system of the mouse distal colon. *Cell Tissue Res* 2014;356:319–32.
35 Bhatia M, Saluja AK, Hofbauer B, *et al*. Role of substance P and the neurokinin 1 receptor in acute pancreatitis and pancreatitis-associated lung injury. *Proc Natl Acad Sci U S A* 1998;95:4760–5.
36 Pothoulakis C, Castagliuolo I, LaMont JT, *et al*. Cp-96,345, a substance P antagonist, inhibits rat intestinal responses to Clostridium difficile toxin A but not cholera toxin. *Proc Natl Acad Sci U S A* 1994;91:947–51.
37 Poole DP, Lieu T, Pelayo JC, *et al*. Inflammation-Induced abnormalities in the subcellular localization and trafficking of the neurokinin 1 receptor in the enteric nervous system. *Am J Physiol Gastrointest Liver Physiol* 2015;309:G248–59.
38 Wick EC, Hoge SG, Grahn SW, *et al*. Transient receptor potential vanilloid 1, calcitonin gene-related peptide, and substance P mediate nociception in acute pancreatitis. *Am J Physiol Gastrointest Liver Physiol* 2006;290:G959–69.
39 Yarwood RE, Imlach WL, Lieu T, *et al*. Endosomal signaling of the receptor for calcitonin gene-related peptide mediates pain transmission. *Proc Natl Acad Sci U S A* 2017;114:12309–14.
40 Valdez-Morales E, Guerrero-Alba R, Ochoa-Cortes F, *et al*. Release of endogenous opioids during a chronic IBD model suppresses the excitability of colonic DRG neurons. *Neurogastroenterol Motil* 2013;25:39–e4.
41 DiCello JJ, Saito A, Rajasekhar P, *et al*. Inflammation-Associated changes in DOR expression and function in the mouse colon. *Am J Physiol Gastrointest Liver Physiol* 2018;315:G544–59.
42 Morales-Cruz M, Delgado Y, Castillo B, *et al*. Smart targeting to improve cancer therapeutics. *Drug Des Devel Ther* 2019;13:3753–72.
43 Kolosenko I, Avnet S, Baldini N, *et al*. Therapeutic implications of tumor interstitial acidification. *Semin Cancer Biol* 2017;43:119–33.

Gut: first published as 10.1136/gutjnl-2020-321193 on 3 December 2020. Downloaded from http://gut.bmj.com/ on September 30, 2021 at New York University, Serials Bobst Library Technical Services Serials. Protected by copyright.

44 Philippe D, Dubuquoy L, Groux H, *et al*. Anti-Inflammatory properties of the mu opioid receptor support its use in the treatment of colon inflammation. *J Clin Invest* 2003;111:1329–38.
45 Spahn V, Del Vecchio G, Labuz D, *et al*. A nontoxic pain killer designed by modeling of pathological receptor conformations. *Science* 2017;355:966–9.
46 Spahn V, Del Vecchio G, Rodriguez-Gaztelumendi A, *et al*. Opioid receptor signaling, analgesic and side effects induced by a computationally designed pH-dependent agonist. *Sci Rep* 2018;8:8965.
47 Wootten D, Christopoulos A, Marti-Solano M, *et al*. Mechanisms of signalling and biased agonism in G protein-coupled receptors. *Nat Rev Mol Cell Biol* 2018;19:638–53.
48 DeFea KA, Zalevsky J, Thoma MS, *et al*. Beta-Arrestin-Dependent endocytosis of proteinase-activated receptor 2 is required for intracellular targeting of activated ERK1/2. *J Cell Biol* 2000;148:1267–82.
49 Zhao P, Lieu T, Barlow N, *et al*. Cathepsin S causes inflammatory pain via biased agonism of PAR2 and TRPV4. *J Biol Chem* 2014;289:27215–34.
50 Zhao P, Lieu T, Barlow N, *et al*. Neutrophil elastase activates protease-activated receptor-2 (PAR2) and transient receptor potential vanilloid 4 (TRPV4) to cause inflammation and pain. *J Biol Chem* 2015;290:13875–87.
51 Kenakin T. Is the quest for signaling bias worth the effort? *Mol Pharmacol* 2018;93:266–9.
52 Bohn LM, Lefkowitz RJ, Gainetdinov RR, *et al*. Enhanced morphine analgesia in mice lacking beta-arrestin 2. *Science* 1999;286:2495–8.
53 Bohn LM, Raehal KM. Opioid receptor signaling: relevance for gastrointestinal therapy. *Curr Opin Pharmacol* 2006;6:559–63.
54 Raehal KM, Walker JKL, Bohn LM. Morphine side effects in beta-arrestin 2 knockout mice. *J Pharmacol Exp Ther* 2005;314:1195–201.
55 Altarifi AA, David B, Muchhala KH, *et al*. Effects of acute and repeated treatment with the biased mu opioid receptor agonist TRV130 (oliceridine) on measures of antinociception, gastrointestinal function, and abuse liability in rodents. *J Psychopharmacol* 2017;31:730–9.
56 Singla NK, Skobieranda F, Soergel DG, *et al*. APOLLO-2: a randomized, placebo and active-controlled phase III study investigating Oliceridine (TRV130), a G protein-biased ligand at the μ-opioid receptor, for management of moderate to severe acute pain following Abdominoplasty. *Pain Pract* 2019;19:715–31.
57 Azzam AAH, McDonald J, Lambert DG. Hot topics in opioid pharmacology: mixed and biased opioids. *Br J Anaesth* 2019;122:e136–45.
58 Chao P-K, Chang H-F, Chang W-T, *et al*. BPR1M97, a dual mu opioid receptor/nociceptin-orphanin FQ peptide receptor agonist, produces potent antinociceptive effects with safer properties than morphine. *Neuropharmacology* 2020;166:107678.
59 Spahn V, Stein C. Targeting delta opioid receptors for pain treatment: drugs in phase I and II clinical development. *Expert Opin Investig Drugs* 2017;26:155–60.
60 Kliewer A, Schmiedel F, Sianati S, *et al*. Phosphorylation-Deficient G-protein-biased μ-opioid receptors improve analgesia and diminish tolerance but worsen opioid side effects. *Nat Commun* 2019;10:367.
61 Kliewer A, Gillis A, Hill R, *et al*. Morphine-Induced respiratory depression is independent of β-arrestin2 signalling. *Br J Pharmacol* 2020;177:2923–31.
62 Gillis A, Gondin AB, Kliewer A, *et al*. Low intrinsic efficacy for G protein activation can explain the improved side effect profiles of new opioid agonists. *Sci Signal* 2020;13. doi:10.1126/scisignal.aaz3140. [Epub ahead of print: 31 Mar 2020].
63 Suomivuori C-M, Latorraca NR, Wingler LM, *et al*. Molecular mechanism of biased signaling in a prototypical G protein-coupled receptor. *Science* 2020;367:881–7.
64 Wingler LM, Skiba MA, McMahon C, *et al*. Angiotensin and biased analogs induce structurally distinct active conformations within a GPCR. *Science* 2020;367:888–92.
65 Moran SP, Maksymetz J, Conn PJ. Targeting muscarinic acetylcholine receptors for the treatment of psychiatric and neurological disorders. *Trends Pharmacol Sci* 2019;40:1006–20.
66 Voss T, Li J, Cummings J, *et al*. Randomized, controlled, proof-of-concept trial of MK-7622 in Alzheimer's disease. *Alzheimers Dement* 2018;4:173–81.
67 Burford NT, Clark MJ, Wehrman TS, *et al*. Discovery of positive allosteric modulators and silent allosteric modulators of the μ-opioid receptor. *Proc Natl Acad Sci U S A* 2013;110:10830–5.
68 Burford NT, Livingston KE, Canals M, *et al*. Discovery, synthesis, and molecular pharmacology of selective positive allosteric modulators of the δ-opioid receptor. *J Med Chem* 2015;58:4220–9.
69 Faron-Górecka A, Szlachta M, Kolasa M, *et al*. Understanding GPCR dimerization. *Methods Cell Biol* 2019;149:155–78.
70 Zhu Y, King MA, Schuller AG, *et al*. Retention of supraspinal delta-like analgesia and loss of morphine tolerance in delta opioid receptor knockout mice. *Neuron* 1999;24:243–52.
71 Gomes I, Gupta A, Filipovska J, *et al*. A role for heterodimerization of mu and delta opiate receptors in enhancing morphine analgesia. *Proc Natl Acad Sci U S A* 2004;101:5135–9.
72 Gomes I, Jordan BA, Gupta A, *et al*. Heterodimerization of mu and delta opioid receptors: a role in opiate synergy. *J Neurosci* 2000;20:RC110.
73 Scherrer G, Imamachi N, Cao Y-Q, *et al*. Dissociation of the opioid receptor mechanisms that control mechanical and heat pain. *Cell* 2009;137:1148–59.
74 Dove LS, Lembo A, Randall CW, *et al*. Eluxadoline benefits patients with irritable bowel syndrome with diarrhea in a phase 2 study. *Gastroenterology* 2013;145:329–38.
75 Liu Q, Tang Z, Surdenikova L, *et al*. Sensory neuron-specific GPCR Mrgprs are itch receptors mediating chloroquine-induced pruritus. *Cell* 2009;139:1353–65.
76 Alemi F, Poole DP, Chiu J, *et al*. The receptor TGR5 mediates the prokinetic actions of intestinal bile acids and is required for normal defecation in mice. *Gastroenterology* 2013;144:145–54.
77 Lieu T, Jayaweera G, Zhao P, *et al*. The bile acid receptor TGR5 activates the TRPA1 channel to induce itch in mice. *Gastroenterology* 2014;147:1417–28.
78 Van Remoortel S, Ceuleers H, Arora R, *et al*. Mas-Related G protein-coupled receptor C11 (Mrgprc11) induces visceral hypersensitivity in the mouse colon: a novel target in gut nociception? *Neurogastroenterol Motil* 2019;31:e13623.
79 Bautzova T, Hockley JRF, Perez-Berezo T, *et al*. 5-oxoETE triggers nociception in constipation-predominant irritable bowel syndrome through Mas-related G protein-coupled receptor D. *Sci Signal* 2018;11. doi:10.1126/scisignal.aal2171. [Epub ahead of print: 18 12 2018].
80 Cenac N, Bautzova T, Le Faouder P, *et al*. Quantification and potential functions of endogenous agonists of transient receptor potential channels in patients with irritable bowel syndrome. *Gastroenterology* 2015;149:433–44.
81 Yu S, Gao G, Peterson BZ, *et al*. Trpa1 in mast cell activation-induced long-lasting mechanical hypersensitivity of vagal afferent C-fibers in guinea pig esophagus. *Am J Physiol Gastrointest Liver Physiol* 2009;297:G34–42.
82 Brozmanova M, Mazurova L, Ru F, *et al*. Mechanisms of the adenosine A2A receptor-induced sensitization of esophageal C fibers. *Am J Physiol Gastrointest Liver Physiol* 2016;310:G215–23.
83 Merves J, Chandramouleeswaran PM, Benitez AJ, *et al*. Altered esophageal histamine receptor expression in eosinophilic esophagitis (EoE): implications on disease pathogenesis. *PLoS One* 2015;10:e0114831.
84 Chionh Y-T, Ng GZ, Ong L, *et al*. Protease-Activated receptor 1 suppresses Helicobacter pylori gastritis via the inhibition of macrophage cytokine secretion and interferon regulatory factor 5. *Mucosal Immunol* 2015;8:68–79.
85 Zhou H, Telonis AG, Jing Y, *et al*. Gprc5A is a potential oncogene in pancreatic ductal adenocarcinoma cells that is upregulated by gemcitabine with help from HuR. *Cell Death Dis* 2016;7:e2294.
86 Cenac N, Altier C, Motta J-P, *et al*. Potentiation of TRPV4 signalling by histamine and serotonin: an important mechanism for visceral hypersensitivity. *Gut* 2010;59:481–8.
87 Luo Y, Feng C, Wu J, *et al*. P2Y1, P2Y2, and TRPV1 receptors are increased in diarrhea-predominant irritable bowel syndrome and P2Y2 correlates with abdominal pain. *Dig Dis Sci* 2016;61:2878–86.
88 Daniali M, Nikfar S, Abdollahi M. An overview of the efficacy and safety of prucalopride for the treatment of chronic idiopathic constipation. *Expert Opin Pharmacother* 2019;20:2073–80.
89 Cattaruzza F, Lyo V, Jones E, *et al*. Cathepsin S is activated during colitis and causes visceral hyperalgesia by a PAR2-dependent mechanism in mice. *Gastroenterology* 2011;141:1864–74.
90 Delvaux M, Beck A, Jacob J, *et al*. Effect of asimadoline, a kappa opioid agonist, on pain induced by colonic distension in patients with irritable bowel syndrome. *Aliment Pharmacol Ther* 2004;20:237–46.
91 Wu W, He Y, Feng X, *et al*. Microrna-206 is involved in the pathogenesis of ulcerative colitis via regulation of adenosine A3 receptor. *Oncotarget* 2017;8:705–21.
92 Gonçalves P, Araújo JR, Di Santo JP. A cross-talk between Microbiota-Derived short-chain fatty acids and the host mucosal immune system regulates intestinal homeostasis and inflammatory bowel disease. *Inflamm Bowel Dis* 2018;24:558–72.
93 Khajah MA, Fateel MM, Ananthalakshmi KV, *et al*. Anti-Inflammatory action of angiotensin 1-7 in experimental colitis. *PLoS One* 2016;11:e0150861.
94 Wang D, Fu L, Sun H, *et al*. Prostaglandin E2 promotes colorectal cancer stem cell expansion and metastasis in mice. *Gastroenterology* 2015;149:1884–95.

Gut: first published as 10.1136/gutjnl-2020-321193 on 3 December 2020. Downloaded from http://gut.bmj.com/ on September 30, 2021 at New York University, Serials Bobst Library Technical Services Serials. Protected by copyright.

Published OnlineFirst March 26, 2021; DOI: 10.1158/0008-5472.CAN-20-3326

Peripheral Nerve Resident Macrophages and Schwann Cells Mediate Cancer-Induced Pain

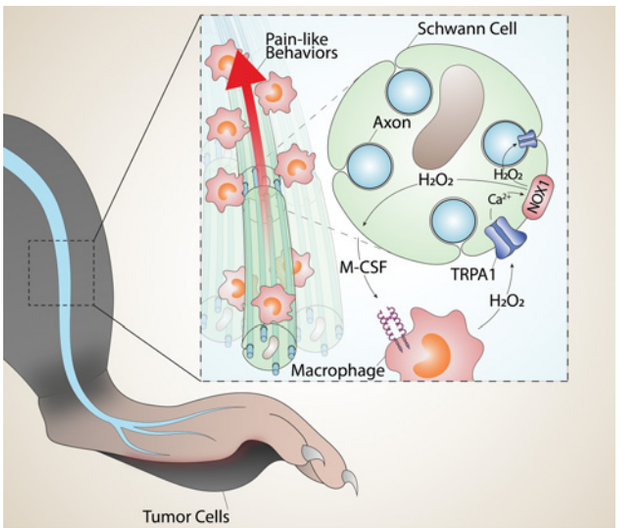
Francesco De Logu[1], Matilde Marini[1], Lorenzo Landini[1], Daniel Souza Monteiro de Araujo[1], Niccolò Bartalucci[2], Gabriela Trevisan[3], Gennaro Bruno[1,4], Martina Marangoni[1], Brian L. Schmidt[5], Nigel W. Bunnett[6], Pierangelo Geppetti[1], and Romina Nassini[1]

ABSTRACT

Although macrophages (MΦ) are known to play a central role in neuropathic pain, their contribution to cancer pain has not been established. Here we report that depletion of sciatic nerve resident MΦs (rMΦ) in mice attenuates mechanical/cold hypersensitivity and spontaneous pain evoked by intraplantar injection of melanoma or lung carcinoma cells. MΦ-colony stimulating factor (M-CSF) was upregulated in the sciatic nerve trunk and mediated cancer-evoked pain via rMΦ expansion, transient receptor potential ankyrin 1 (TRPA1) activation, and oxidative stress. Targeted deletion of *Trpa1* revealed a key role for Schwann cell TRPA1 in sciatic nerve rMΦ expansion and pain-like behaviors. Depletion of rMΦs in a medial portion of the sciatic nerve prevented pain-like behaviors. Collectively, we identified a feed-forward pathway involving M-CSF, rMΦ, oxidative stress, and Schwann cell TRPA1 that operates throughout the nerve trunk to signal cancer-evoked pain.

Significance: Schwann cell TRPA1 sustains cancer pain through release of M-CSF and oxidative stress, which promote the expansion and the proalgesic actions of intraneural macrophages.

Graphical Abstract: http://cancerres.aacrjournals.org/content/canres/81/12/3387/F1.large.jpg.



Sciatic nerve resident macrophages mediate cancer-related pain by producing H_2O_2 that targets Schwann cell TRPA1, which amplifies oxidative stress to sustain M-CSF-dependent macrophage expansion and neuronal pain signals.

Introduction

Pain is a common and devastating symptom of cancer, which afflicts 70% to 90% of patients with cancer and can diminish the quality of life more than the cancer itself (1). However, cancer pain remains incompletely understood and poorly managed, thus representing a major unmet medical need (2). A series of cytokines, chemokines, and their receptors have been proposed to contribute to signal cancer pain (3). These include IL1β, IL6, TNFα, the C-X-C motif chemokine ligand (CXCL) 8 (CXCL8), CXCL13, CXC receptor (CXCR) 4 (CXCR4), and CXCL12/CXCR4. Although some of these cytokines may directly or indirectly attract inflammatory and immune cells, the implication of macrophages (MΦ) in cancer pain remains unknown.

In contrast, the role of MΦs in neuropathic pain associated with nerve injury has been extensively investigated, and distinct MΦ-dependent proalgesic pathways have been identified in the central and peripheral nervous systems (4–11). Recruitment and expansion of proalgesic MΦs can be due to the predominant contribution of the upregulation of chemokine (C-C motif) ligand 2 (CCL2) and its receptor (CCR2; refs. 4–6), or to the release of MΦ-colony stimulating factor (M-CSF; refs. 7–9). Furthermore, peripheral neuropathy can be associated with different MΦ subpopulations (12). Thus, neuropathic pain may be promoted by hematogenous monocytes, which, recruited on demand after neural injury, rapidly invade the damaged peripheral nerves as mature and activated MΦs (5, 6), and by resident MΦs (rMΦ), which are constitutively present inside the *epineurium*, and may undergo a time-dependent expansion when activated by pathologic insults (8, 11).

Transient receptor potential ankyrin 1 (TRPA1), a proalgesic ion channel expressed in a subset of primary sensory neurons (13), is uniquely sensitive to oxidative stress byproducts (14). In a mouse model of trigeminal neuralgia, TRPA1 was proposed to signal

[1]Department of Health Sciences, Clinical Pharmacology Unit, University of Florence, Florence, Italy. [2]Department of Experimental and Clinical Medicine, University of Florence, Florence, Italy. [3]Graduated Program in Pharmacology, Federal University of Santa Maria (UFSM), Avenida Roraima, Santa Maria, Brazil. [4]Division of Pediatric Oncology/Hematology, Meyer University Children's Hospital, Florence, Italy. [5]Department of Oral and Maxillofacial Surgery, Bluestone Center for Clinical Research, New York University College of Dentistry, New York, New York. [6]Department of Molecular Pathobiology, College of Dentistry, Department of Neuroscience and Physiology, and Neuroscience Institute, School of Medicine, New York University, New York.

Note: Supplementary data for this article are available at Cancer Research Online (http://cancerres.aacrjournals.org/).

Corresponding Author: Pierangelo Geppetti, Department of Health Science, University of Florence, Florence, 50134, Italy. E-mail: geppetti@unifi.it

Cancer Res 2021;81:3387–401

doi: 10.1158/0008-5472.CAN-20-3326

©2021 American Association for Cancer Research.

Downloaded from cancerres.aacrjournals.org on September 30, 2021. © 2021 American Association for Cancer Research.

Published OnlineFirst March 26, 2021; DOI: 10.1158/0008-5472.CAN-20-3326

mechanical allodynia elicited by oxidative stress generated by MΦs recruited by CCL2 at the site of nerve injury (5). However, a later study, which used a murine model of partial nerve ligation, clarified that TRPA1 expressed in Schwann cells is interposed between MΦ-evoked oxidative stress and the pain-generating neuronal channel (6). In fact, Schwann cell TRPA1, by eliciting oxidative stress via a Ca^{2+}- and NADPH oxidase 1 (NOX1)-dependent mechanism, initiates an amplification loop, which sustains neuroinflammation and targets neuronal TRPA1 to signal pain (6). We recently reported that genetic deletion or pharmacologic inhibition of TRPA1 attenuated mechanical/cold hypersensitivity and spontaneous nociception in a syngeneic orthotopic model of solid cancer pain induced by inoculation of B16-F10 melanoma cells in the mouse hindpaw (15). However, the mechanism by which TRPA1 mediates mechanical/cold hypersensitivity and spontaneous nociception associated with tumor growth is unknown.

The aim of this study was two-fold. In mouse models of cancer pain, we first explored the implication of MΦs in mechanical/cold hypersensitivity and spontaneous nociception. Then, we investigated the role of Schwann cell TRPA1 in the MΦ-dependent pain-like behaviors. In addition to revealing an essential function of sciatic nerve rMΦs, results obtained after B16-F10 melanoma cell inoculation revealed the role of Schwann cell TRPA1 to release M-CSF, which sustains rMΦ expansion, and to generate the oxidative stress that targets the neuronal TRPA1 to signal pain. Neuroinflammation and mechanical/cold hypersensitivity and spontaneous nociception are maintained by a feed-forward mechanism, which requires the continuous interaction between Schwann cell TRPA1 and expanded rMΦs throughout the entire sciatic nerve trunk. Furthermore, the inoculation of Lewis lung carcinoma (LLC1) cells in the mouse hindpaw evoked mechanical allodynia, which was attenuated by elimination of rMΦ or Schwann cell TRPA1. Thus, M-CSF, rMΦs, oxidative stress, and Schwann cell TRPA1 signal mechanical/cold hypersensitivity and spontaneous nociception in different mouse tumors and may represent potential targets for the treatment of cancer pain.

Materials and Methods

Study design

The group size of $n = 6$ animals for behavioral experiments was determined by sample size estimation using G*Power (v3.1; ref. 16) to detect size effect in a *post hoc* test with type 1 and 2 error rates of 5% and 20%, respectively. Allocation concealment of mice to vehicle (s) or treatment(s) group was performed using a randomization procedure (http://www.randomizer.org/). The assessors were blinded to the identity (genetic background or allocation to treatment group) of the animals. No animals were excluded from experiments.

All experiments and sample collections were carried out according to the European Union (EU) guidelines for animal care procedures and the Italian legislation (DLgs 26/2014) application of the EU Directive 2010/63/EU. All animal studies were approved by Animal Ethics Committee of the University of Florence and the Italian Ministry of Health (permit no. 579/2017-PR). The behavioral studies followed the animal research reporting *in vivo* experiment (ARRIVE) guidelines.

Animals

Adult C57BL/6J (male and female 20–25 g, 5–6 weeks), littermate wild-type (*Trpa1*$^{+/+}$), and TRPA1-deficient (*Trpa1*$^{-/-}$) mice (male, 25–30 g, 6–8 weeks), generated by heterozygotes on a C57BL/6J background (B6.129P-Trpa1$^{tm1Kykw/J}$; RRID:IMSR_JAX:006401, The Jackson Laboratories; ref. 6), were used. To generate mice in which the *Trpa1* gene was conditionally silenced in Schwann cells/oligodendrocytes, homozygous 129S-Trpa1tm2Kykw/J (floxed TRPA1, *Trpa1*$^{fl/fl}$, Stock No: 008649, RRID:IMSR_JAX:008649, The Jackson Laboratories) were crossed with hemizygous B6.Cg-Tg (Plp1-CreERT)3Pop/J mice (*Plp1-Cre*^{ERT}, Stock No: 005975, RRID: IMSR_JAX:005975 Jackson Laboratories), expressing a tamoxifen-inducible Cre in myelinating cells (proteolipid protein myelin 1, Plp1; ref. 6). The progeny (*Plp1-Cre;Trpa1*$^{fl/fl}$) was genotyped by standard PCR for *Trpa1* and *Plp1-Cre*^{ERT} (6). Mice negative for *Plp1-Cre*^{ERT} (*Plp1-Cre*$^{ERT-}$*;Trpa1*$^{fl/fl}$) were used as control. Both positive and negative mice to *Cre*^{ERT} and homozygous for floxed *Trpa1* (*Plp1-Cre*$^{ERT+}$*;Trpa1*$^{fl/fl}$ and *Plp1-Cre*$^{ERT-}$*;Trpa1*$^{fl/fl}$, respectively) were treated with tamoxifen (i.p., 1 mg/100 μL in corn oil, once a day, for 5 consecutive days; ref. 6), resulting in Cre-mediated ablation of *Trpa1* in PLP-expressing Schwann cells/oligodendrocytes. Successful Cre-driven deletion of TRPA1 mRNA was confirmed by RT-qPCR (6). To selectively delete the Trpa1 gene in primary sensory neurons, 129S-Trpa1$^{tm2Kykw/J}$ mice (floxed Trpa1, *Trpa1*$^{fl/fl}$, Stock No.: 008649; Jackson Laboratories), which possess loxP sites on either side of the S5/S6 transmembrane domains of the *Trpa1* gene, were crossed with hemizygous Advillin-Cre male mice (8). The progeny (*Adv-Cre; Trpa1*$^{fl/fl}$) were genotyped by standard PCR for Trpa1 and Advillin-Cre. Mice negative for Advillin-Cre (*Adv-Cre*$^{-}$*;Trpa1*$^{fl/fl}$) were used as control. Successful Advillin-Cre driven deletion of TRPA1 mRNA was confirmed by RT-qPCR. To evaluate the involvement of MΦs, transgenic Macrophage Fas-Induced Apoptosis (MaFIA) mice [C57BL/6-Tg(Csf1r-EGFP-NGFR/FKBP1A/TNFRSF6)2Bck/J, Stock No.: 005070, RRID:IMSR_JAX:005070, The Jackson Laboratories] were used. These transgenic mice express a mutant human FK506 binding protein 1A, 12kDa (FKBP12)-Fas inducible suicide/apoptotic system, driven by the mouse Csf1r promoter conjugated with a GFP, which preferentially binds the B/B dimerizing agent (B/B-HmD, AP20187; Diatech Labline s.r.l.). Treatment of mice with AP20187 induces the dimerization of the suicide protein to activate the cytoplasmic FKBP12-Fas fragments, leading to the apoptosis of transgene-expressing cells and consequent macrophage depletion (17).

At least 1 hour before behavioral experiments, mice were acclimatized to the experimental room and the evaluations were performed between 9:00 am and 5:00 pm. Animals were anesthetized with a mixture of ketamine and xylazine (90 and 3 mg/kg, respectively, i.p.) and euthanized with inhaled CO_2 plus 10% to 50% O_2.

Cancer cell inoculation

Naïve (CRL-6475; RRID:CVCL_0159 ATCC) and GFP expressing B16-F10 murine melanoma and Lewis lung carcinoma (LLC1, CRL-1642, RRID:CVCL_4358 ATCC) cells were cultured in DMEM containing 10% FBS and 1% penicillin-streptomycin (10,000 U/100 μg/mL) at 37 °C with 5% CO_2 in a humidified atmosphere and were used without further authentication. For inoculation, 20 μL of B16-F10 melanoma (2×10^5 cells) or LLC1 (5×10^5 cells) cells were suspended in PBS and injected into the plantar region of the mouse right hindpaw (15, 18). Control groups (sham) were injected with 20 μL of PBS containing B16-F10 melanoma (2×10^5 cells) or LLC1 (5×10^5 cells) cells killed by quickly freezing and thawing them twice without cryoprotection. B16-F10 and LLC1 cell lines are isogenic with the C57BL/6 mouse strain.

Treatment protocols and behavioral assays (mechanical allodynia, cold response, and spontaneous nociception)

See Supplementary Materials and Methods for experimental details.

Downloaded from cancerres.aacrjournals.org on September 30, 2021. © 2021 American Association for Cancer Research.

Published OnlineFirst March 26, 2021; DOI: 10.1158/0008-5472.CAN-20-3326

Cell cultures

Human Schwann cells (HSC, #P10351, Innoprot) were cultured in Schwann cell medium (#P60123, Innoprot) according to the manufacturer's protocol. HSCs used in the study are primary cells. Cells were passaged at 90% confluency and discarded after 20 passages. Approval by the local Ethic committee and written informed consent were obtained by the vendor. All cells were used when received without further authentication. Mouse Schwann cells were isolated from sciatic nerves of C57BL/6J mice. Briefly, the *epineurium* was removed, and nerve explants were divided into 1 mm segments and dissociated enzymatically using collagenase (0.05%) and hyaluronidase (0.1%) in Hank's Balanced Salt Solution (HBSS, 2 hours, 37°C). Cells were collected by centrifugation (800 rpm, 10 minutes, room temperature) and the pellet was resuspended and cultured in DMEM containing: 10% fetal calf serum, 2 mmol/L L-glutamine, 100 U/mL penicillin, 100 mg/mL streptomycin. Three days later, cytosine arabinoside (10 mmol/L) was added to remove fibroblasts. All cells were cultured in an atmosphere of 95% air and 5% CO_2 at 37°C. Cells were used after 15 days of culture.

Sciatic nerve explant culture

See Supplementary Materials and Methods for experimental details.

H_2O_2 assay

See Supplementary Materials and Methods for experimental details.

ELISA assays (multi-analyte, M-CSF, PDL-1)

See Supplementary Materials and Methods for experimental details.

Immunofluorescence

See Supplementary Materials and Methods for experimental details.

Real-Time PCR

See Supplementary Materials and Methods for experimental details.

Statistical analysis

Results are shown as the mean and SEM. The statistical significance of differences between groups was assessed using Student *t* test, one-way or two-way ANOVA followed by Bonferroni *post hoc* where appropriate. Statistical analyses were performed on raw data using Prism 8 (GraphPad Software Inc.). $P < 0.05$ were considered significant.

Results

Neural resident macrophages mediate cancer pain

Intraplantar (i.pl.) inoculation of B16-F10 melanoma cells into the hindpaw of C57BL/6J mice induced a time-dependent increase in paw thickness, mainly due to tumor growth (**Fig. 1A** and **B**). Tumor progression was associated with a parallel increase in mechanical/cold hypersensitivity as well as spontaneous nociception in the ipsilateral paw (**Fig. 1C–E**) and in the number of F4/80$^+$ monocytes and MΦs within the tumor and the adjacent tissue (tMΦs; **Fig. 1F**) and inside the ipsilateral sciatic nerve trunk (rMΦs; **Fig. 1G**). Since no gender differences were observed in cancer growth, mechanical/cold hypersensitivity or spontaneous nociception, male mice were used in subsequent experiments (**Fig. 1B–E**). Control (sham) mice inoculated with dead cells did not develop an increase in paw volume, mechanical/cold hypersensitivity, or spontaneous nociception (**Fig. 1B–E**).

To explore the role of MΦs in cancer-evoked mechanical/cold hypersensitivity and spontaneous nociception, cancer cells were inoculated in MΦ Fas-Induced Apoptosis (MaFIA) transgenic mice. The inoculation of cancer cells in MaFIA mouse hindpaw induced a time-dependent increase in paw thickness, mechanical/cold hypersensitivity, and spontaneous nociception, like those observed in C57BL/6J mice (**Fig. 1H–K**). After inoculation, MaFIA mice received daily injections (day 10–14) of AP20187 (2 mg/kg, i.p.) to induce apoptosis in the entire MΦ population. After AP20187-treatment, MaFIA mice exhibited a marked reduction in the number of GFP$^+$/F4/80$^+$ cells in both the tumor and sciatic nerve (**Fig. 1L**) in mechanical/cold hypersensitivity and spontaneous nociception (**Fig. 1H–K**).

To determine whether tMΦs or rMΦs contribute to cancer-evoked mechanical/cold hypersensitivity and spontaneous nociception, MΦ-depleted tumor-bearing MaFIA mice were inoculated (day 14) in the hindpaw with F4/80$^+$ cells harvested from the peritoneum of naïve C57BL/6J mice to reconstitute the tMΦ population. This intervention, while repopulating F4/80$^+$ cells within the tumor microenvironment, failed to repopulate the number of F4/80$^+$ cells within the sciatic nerve trunk (**Fig. 2A**) and to restore mechanical/cold hypersensitivity and spontaneous nociception (**Fig. 2B–D**). In other experiments, tumor-bearing MaFIA mice received a local injection (60 μg, 6 μL, i.pl.) of AP20187 for 5 consecutive days (day 10–14). This local treatment depleted the tumor GFP$^+$/F4/80$^+$ (tMΦ) cells, but did not diminish the increased sciatic nerve GFP$^+$/F4/80$^+$ (rMΦ) cells (**Fig. 2E**) mechanical/cold hypersensitivity and spontaneous nociception (**Fig. 2F–H**). Although several cellular and humoral factors of the nerve and tumor microenvironment may increase pain signals, our data implicate a major role for rMΦs in mechanical/cold hypersensitivity and spontaneous nociception evoked by cancer in mice.

In a model of neuropathic pain evoked by partial sciatic nerve ligation, we and others have shown that the MΦs responsible for the allodynia quickly accumulate inside the injured sciatic nerve trunk (4, 6, 19, 20). This fast recruitment was eliminated by treatment with liposome-encapsulated clodronate (LCL), which rapidly depletes circulating monocytes (21) and attenuates the number of MΦs recruited at the site of the injury (6). However, in the present model of cancer pain, daily LCL (i.p., 1 day before and day 1–14 after cancer cell inoculation), while markedly reducing tumor F4/80$^+$ cells, did not affect sciatic nerve F4/80$^+$ cells, paw thickness, or mechanical/cold hypersensitivity (Supplementary Figs. S1A–S1C). These findings further support the role of the expanded sciatic nerve rMΦs, but not hematogenous MΦs, which accumulate from the blood stream into the tumor microenvironment, to sustain cancer-evoked allodynia.

M-CSF promotes macrophage expansion and cancer-evoked allodynia

Next, we investigated the mechanisms underlying the rMΦ expansion responsible for cancer-evoked mechanical allodynia. We used a multiplex array to profile chemokines and cytokines in the tumor and sciatic nerve at day 14 after cancer cell inoculation in C57BL/6J mice. Except for IL1α, IL6, IL10, IL12, TGF1β and granulocyte-CSF (G-CSF), which were unchanged in tumor homogenates, the other mediators, including IL1β, IL2, IL4, IL17A, IFNγ, TNFα, CCL2, CCL3, CCL4, M-CSF, and GM-GSF, were increased both in tumor and sciatic nerve homogenates (**Fig. 3A**). Mounting evidence suggests that melanoma cells express the checkpoint inhibitory protein PD-L1 (CD274), which suppresses T-cell function and induces immune tolerance via its cognate receptor, PD-1 (22, 23). We found that PD-L1 levels were increased in the tumor tissue but not in sciatic nerve at day 14 after melanoma cell inoculation in C57BL/6J mice (**Fig. 3B**). Because of the negative result in the sciatic nerve and finding that PD-L1 has been

Downloaded from cancerres.aacrjournals.org on September 30, 2021. © 2021 American Association for Cancer Research.

Published OnlineFirst March 26, 2021; DOI: 10.1158/0008-5472.CAN-20-3326

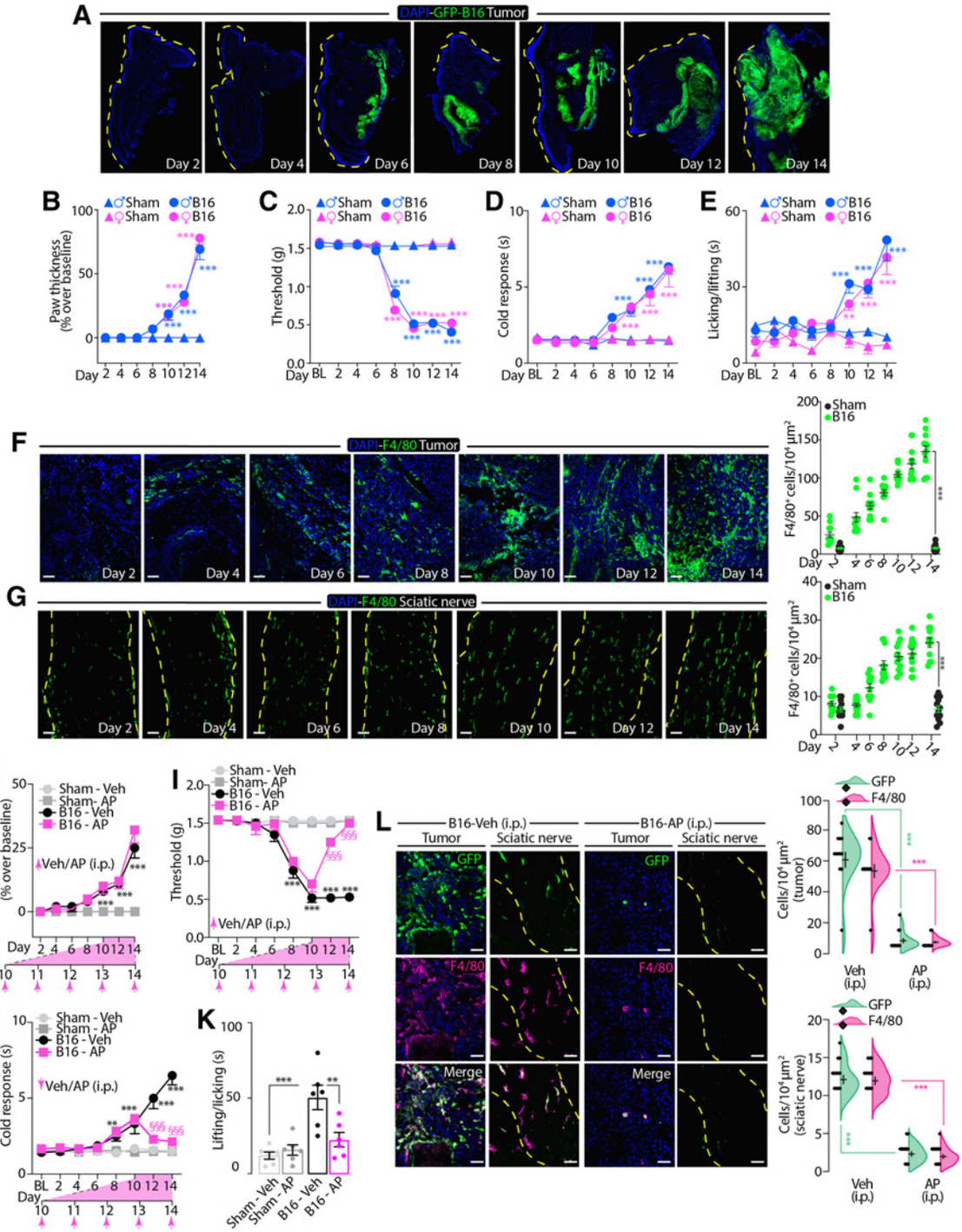


Figure 1.

Mechanical allodynia, cold response, spontaneous nociception, and neuroinflammation induced by B16-F10 melanoma cell inoculation in mouse hindpaw. **A,** Typical whole slide images of the time-dependent expansion of GFP$^+$-B16-F10 melanoma cell after inoculation in C57BL/6J mouse hindpaw. **B–E,** Paw thickness (**B**), mechanical allodynia (**C**), cold response (**D**), and spontaneous nociception (**E**) after B16-F10 melanoma (B16) cell inoculation or sham in male and female C57BL/6J mice. **F** and **G,** Numbers of F4/80$^+$ cells in the tumor (**F**) and sciatic nerve (**G**) after B16 cell inoculation or sham in C57BL/6J mice. **H–L,** Paw thickness (**H**), mechanical allodynia (**I**), cold response (**J**), spontaneous nociception (**K**), typical images and numbers of GFP$^+$ and F4/80$^+$ cell in tumor and sciatic nerve (**L**) after B16 cell inoculation or sham in MaFIA mice treated with AP12087 (AP) or Veh (i.p.). BL, baseline. Pink arrows, time of treatment with Veh/AP. Yellow dashed line delimits hindpaw epidermis (**A**) and *epineurium* (**G** and **L**). Scale bar, 50 µmol/L. $N = 6$ mice. ***, $P < 0.001$ to Sham, Sham-Veh, GFP Veh, F4/80 Veh; §§§, $P < 0.001$ to B16-Veh. Data are presented as mean ± SEM, data points overlaid (**F, G, K,** and **L**). Two-way (**B–J**) and one-way (**K** and **L**) ANOVA and Bonferroni *post hoc* test. **, $P < 0.01$.

Downloaded from cancerres.aacrjournals.org on September 30, 2021. © 2021 American Association for Cancer Research.

Published OnlineFirst March 26, 2021; DOI: 10.1158/0008-5472.CAN-20-3326

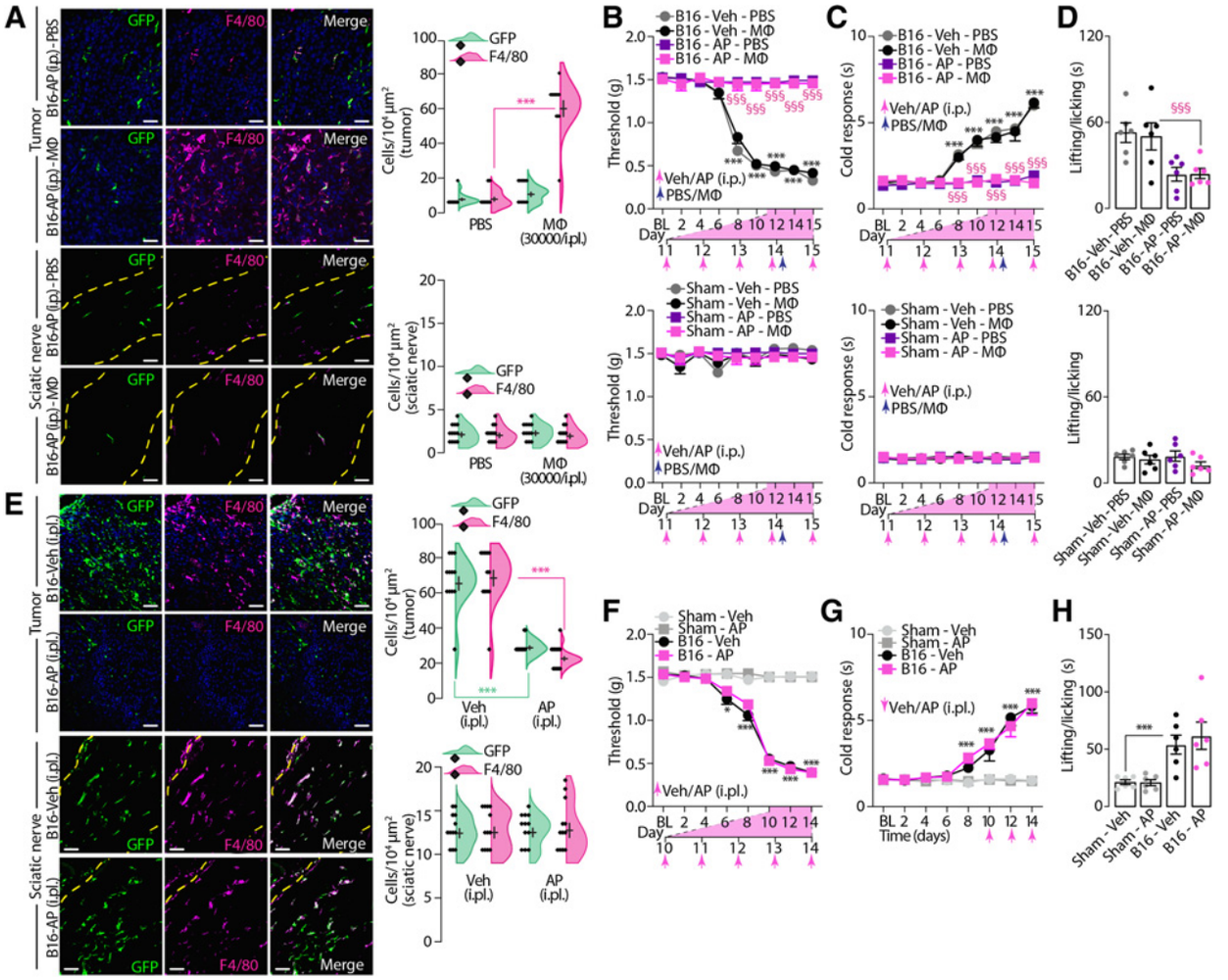


Figure 2.

Resident macrophages are responsible for cancer-evoked mechanical allodynia, cold response, and spontaneous nociception. **A–D,** Typical images and data of GFP$^+$ and F4/80$^+$ cells in the tumor and ipsilateral sciatic nerve (**A**) and mechanical allodynia (**B**), cold response (**C**), and spontaneous nociception (**D**) after B16-F10 melanoma (B16) cell inoculation or sham in MaFIA mice treated with AP12087 (AP) or Veh (i.p.) and inoculated (i.pl., at day 14) with MΦs or PBS. **E–H,** Typical images and data of GFP$^+$ and F4/80$^+$ cells in the tumor and sciatic nerve (**E**) and mechanical allodynia (**F**), cold response (**G**), and spontaneous nociception (**H**) after B16 cell inoculation or sham in MaFIA mice treated with AP or Veh (i.pl.). BL, baseline. Pink arrows, days of treatment; blue arrow, day of MΦ/PBS inoculation. Yellow dashed line delimits the *epineurium*. Scale bar, 50 µmol/L. $N = 6$ mice. *, $P < 0.05$; ***, $P < 0.001$ to F4/80 PBS, F4/80 Veh, GFP Veh, Sham-Veh; §§§, $P < 0.001$ to B16-Veh-MΦ. Data are presented as mean ± SEM, data points overlaid (**A, E, D,** and **H**). Two-way (**B, C, F,** and **G**) and one-way (**A, D, E,** and **H**) ANOVA and Bonferroni *post hoc* test.

shown to inhibit spontaneous pain and allodynia in melanoma-bearing mice (24), this was not further explored.

Among the number of cytokines/chemokines increased in the neuronal and tumor tissue, we first focused on CCL2 because of its prominent role in augmenting MΦ numbers at sites of nerve injury, thereby contributing to neuropathic pain (4, 8). CCL2 blockade favors tumor escape from the primary sites in a mouse model of melanoma (25). However, the contribution of CCL2 in pain evoked by cancer has not been explored. In contrast to the prominent role in MΦ recruitment and allodynia after nerve injury (4–6), CCL2 does not seem to contribute to cancer pain, given that treatment with a neutralizing anti-CCL2 mAb did not affect tumor growth, mechanical/cold hypersensitivity (Supplementary Fig. S2A), or the number of either tMΦs or rMΦs (Supplementary Figs. S2B and S2C).

In addition to CCL2, M-CSF has been shown to mediate both MΦ increase and allodynia in some neuropathic pain models (7–9). In the present model of cancer-evoked pain, we found that M-CSF levels were markedly increased in both tumor and sciatic nerve homogenate at day 14 after B16-F10 melanoma cell inoculation (**Fig. 3C**). Targeting the M-CSF signal with the M-CSF receptor (M-CSFR) antagonist, PLX3397, or a neutralizing anti-M-CSF mAb, which did not affect tumor growth (**Fig. 3D** and **J**), markedly attenuated the number of both tMΦs and rMΦs (**Fig. 3H**, **I**, **N**, and **O**), and mechanical/cold hypersensitivity (**Fig. 3E**, **F**, **K**, and **L**). Accumulation of F4/80$^+$ cells in the sciatic nerve was associated with a robust increase in oxidative stress (H_2O_2), which was reduced by PLX3397 (**Fig. 3G**) or an anti-M-CSF mAb (**Fig. 3M**). Thus, M-CSF mediates cancer-evoked rMΦ expansion and the ensuing allodynia.

Downloaded from cancerres.aacrjournals.org on September 30, 2021. © 2021 American Association for Cancer Research.

Published OnlineFirst March 26, 2021; DOI: 10.1158/0008-5472.CAN-20-3326

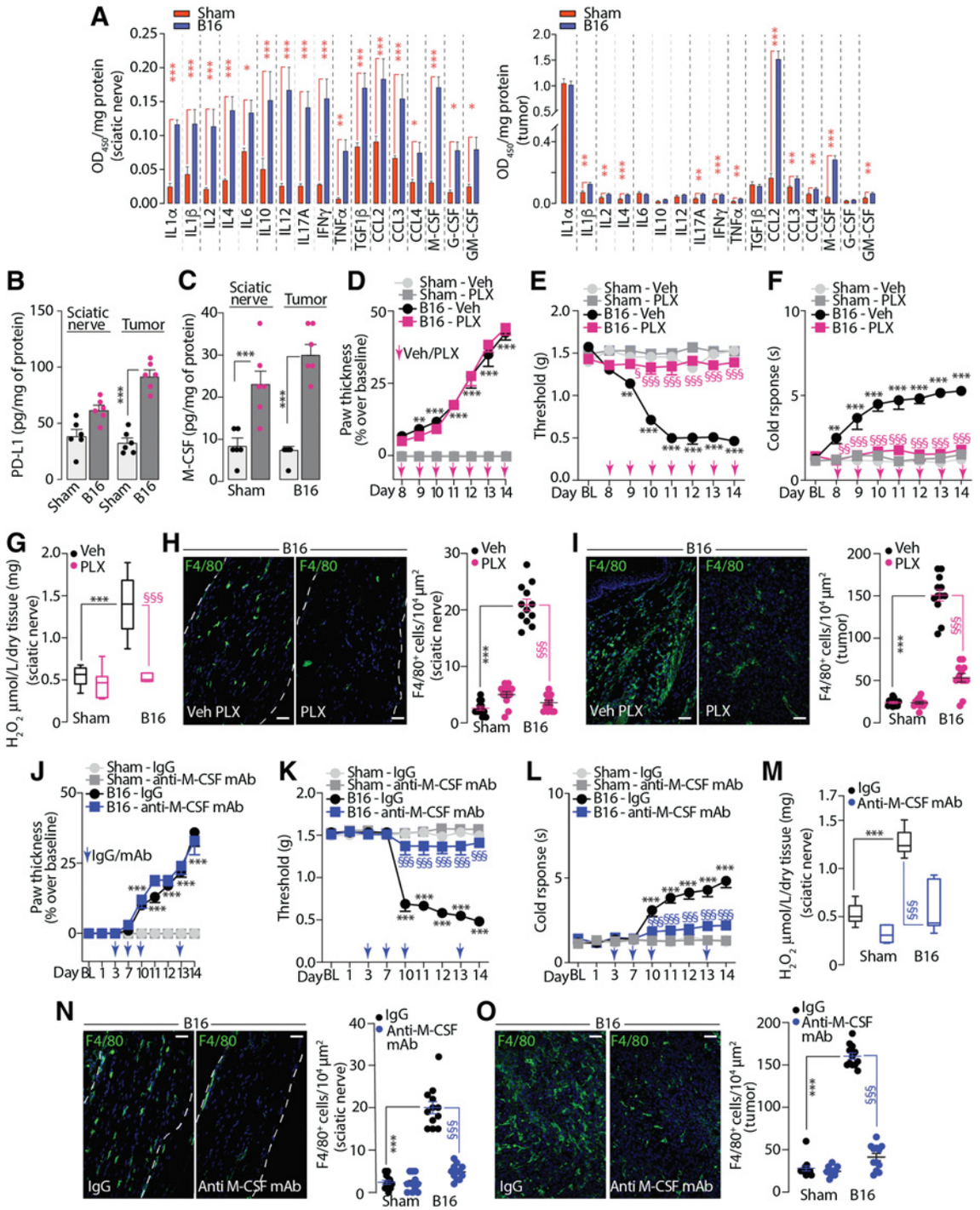


Figure 3.

M-CSF promotes macrophage expansion and cancer-evoked mechanical allodynia and cold response. **A–C,** Cytokines/chemokines array profile (**A**), PD-L1 (**B**), and M-CSF (**C**) content in sciatic nerve and tumor after B16-F10 melanoma (B16) cell inoculation or sham in C57BL/6J mice. **D–I,** Paw thickness (**D**), mechanical allodynia (**E**), cold response (**F**), H_2O_2 content (**G**), and typical images and data of F4/80$^+$ cells in sciatic nerve (**H**) and tumor (**I**) after B16 cell inoculation or sham in C57BL/6J mice after PLX3397 (PLX) or Veh (i.p.). **J–O,** Paw thickness (**J**), mechanical allodynia (**K**), cold response (**L**), H_2O_2 content (**M**), and typical images and data of F4/80$^+$ cell in sciatic nerve (**N**) and tumor (**O**) after B16 cell inoculation or sham in C57BL/6J mice treated with an anti-M-CSF mAb or IgG2B (IgG; i.p.). Assays were performed at day 14 from B16 cell inoculation or sham. BL, baseline. Pink arrows, treatment with PLX/Veh; blue arrow, treatment with anti-M-CSF mAb/IgG. Dashed line delimits the *epineurium.* Scale bar, 50 µmol/L. $N = 6$ mice. *, $P < 0.05$; **, $P < 0.01$; ***, $P < 0.001$ to Sham, Sham-Veh, Sham-IgG; §, $P < 0.05$; §§, $P < 0.01$; §§§, $P < 0.001$ to B16-Veh and B16-IgG. Data are presented as mean ± SEM, data points overlaid (**B, C, H, I, N,** and **O**). **G** and **M**, Box plots 25th and 75th percentile, min and max values, and data points overlaid. Student *t* test (**A–C**); two-way (**D–F** and **J–L**) and one-way (**G, H, I,** and **M–O**) ANOVA and Bonferroni *post hoc* test.

Downloaded from cancerres.aacrjournals.org on September 30, 2021. © 2021 American Association for Cancer Research.

Published OnlineFirst March 26, 2021; DOI: 10.1158/0008-5472.CAN-20-3326

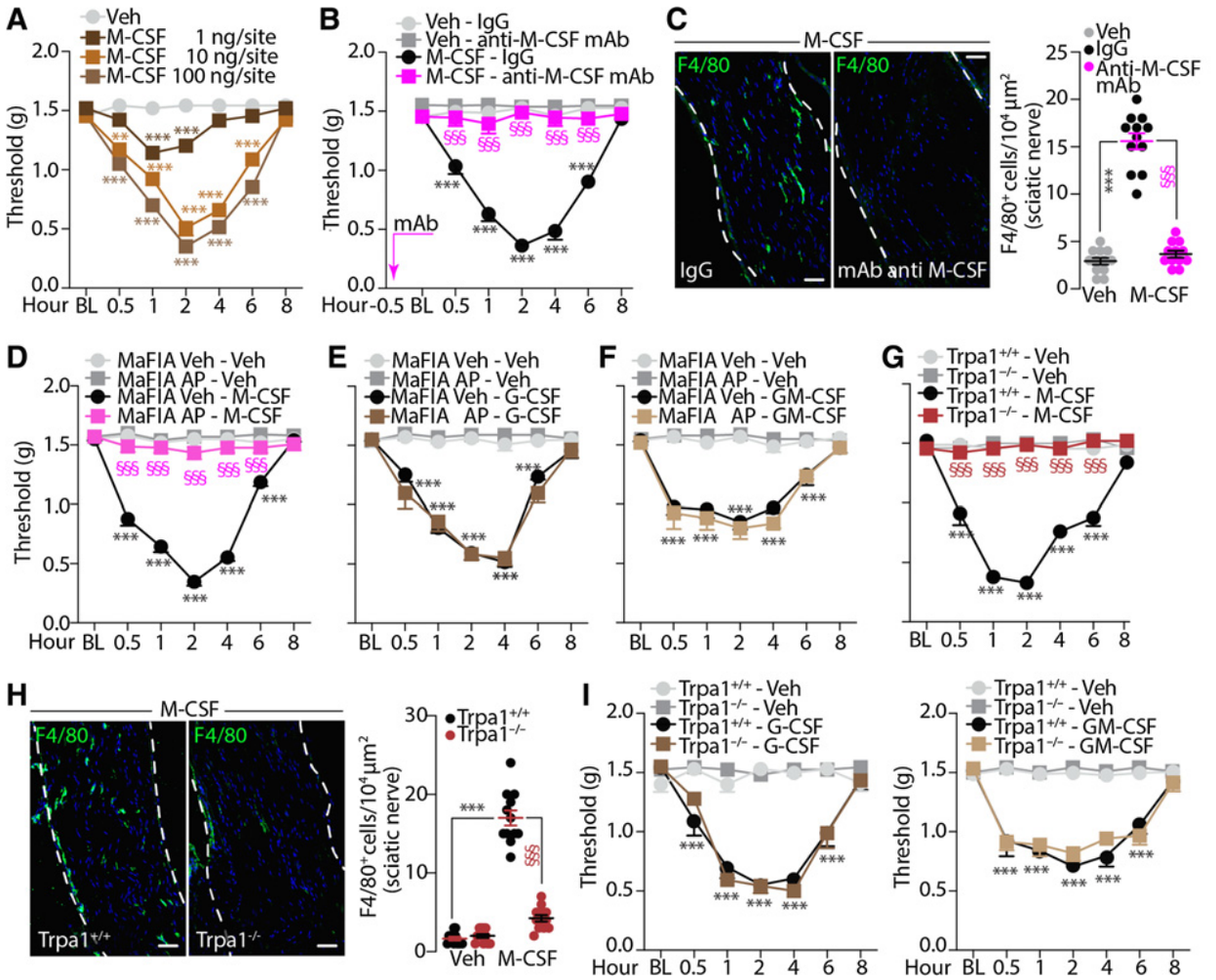


Figure 4.

M-CSF induces allodynia and neuroinflammation via TRPA1. **A** and **B,** Mechanical allodynia in C57BL/6J mice after M-CSF or Veh (i.pl.; **A**) and pretreated with an anti-M-CSF mAb or IgG2B (IgG; i.p.; **B**). **C,** Typical images and data of F4/80$^+$ cell in sciatic nerve of C57BL/6J mice after M-CSF (i.pl.) and pretreated with an anti-M-CSF mAb or IgG (i.p.). **D–F,** Mechanical allodynia induced by M-CSF (**D**), G-CSF (**E**), and GM-CSF (**F**) or Veh (i.pl.) in MaFIA mice treated with AP12087 (AP) or Veh (i.p.). **G** and **H,** Mechanical allodynia (**G**) and typical images and data of F4/80$^+$ cell in sciatic nerve after M-CSF or Veh (i.pl.; **H**) in *Trpa1*$^{+/+}$ and *Trpa1*$^{-/-}$ mice. **I,** Mechanical allodynia after G-CSF, GM-CSF, or Veh (i.pl.) in *Trpa1*$^{+/+}$ and *Trpa1*$^{-/-}$ mice. BL, baseline. Dashed line delimits the *epineurium*. Scale bar, 50 µmol/L. $N = 6$ mice. **, $P < 0.01$; ***, $P < 0.001$ to Veh, Veh-IgG, MaFIA Veh-Veh, *Trpa1*$^{+/+}$-Veh; §§§, $P < 0.001$ to M-CSF-IgG, MaFIA Veh-M-CSF, *Trpa1*$^{+/+}$-M-CSF. Data are presented as mean ± SEM, data points overlaid (**C** and **H**). Two-way (**A, B, D, E, F, G,** and **I**) and one-way (**C** and **H**) ANOVA and Bonferroni *post hoc* test.

M-CSF induces allodynia and neuroinflammation via TRPA1

In addition to M-CSF, the CSF family includes G-CSF and GM-CSF, which were found to regulate tumor–nerve interactions, remodeling of peripheral nerves, and sensitization of damage-sensory neurons in a mouse sarcoma model of bone tumor (26). G-CSF and GM-CSF levels were increased in sciatic nerve trunk homogenates at day 14 after cancer cell inoculation (**Fig. 3A**). However, in contrast to M-CSF, neutralizing anti-G-CSF or anti-GM-CSF mAbs did not affect cancer-evoked mechanical/cold hypersensitivity (Supplementary Figs. S2D and S2E), reinforcing the pivotal role of M-CSF in cancer-induced pain.

We next studied the mechanism by which M-CSF causes mechanical allodynia and neuroinflammation. Local injection of M-CSF (1–100 ng, 20 µL, i.pl.) induced a dose-dependent mechanical allodynia lasting for 6 hours (**Fig. 4A**). Pretreatment with an anti-M-CSF mAb prevented the development of mechanical allodynia and the increase in F4/80$^+$ cells in the ipsilateral sciatic nerve trunk (**Fig. 4B** and **C**). The involvement of MΦs in the M-CSF-induced nociception was shown by using MΦ-depleted MaFIA mice, in which the M-CSF injection failed to induce mechanical allodynia (**Fig. 4D**), whereas G-CSF and GM-CSF still elicited allodynia (**Fig. 4E** and **F**). We previously reported that cancer-evoked allodynia induced by B16-F10 melanoma cell inoculation was absent in *Trpa1*$^{-/-}$ mice (15). To investigate the role of TRPA1 in M-CSF-induced mechanical allodynia and neuroinflammation, M-CSF was injected in *Trpa1*$^{+/+}$ and *Trpa1*$^{-/-}$ mice. In *Trpa1*$^{-/-}$ mice, M-CSF failed to induce mechanical allodynia and F4/80$^+$ cells in the sciatic nerve (**Fig. 4G** and **H**). In contrast, allodynia

Downloaded from cancerres.aacrjournals.org on September 30, 2021. © 2021 American Association for Cancer Research.

Published OnlineFirst March 26, 2021; DOI: 10.1158/0008-5472.CAN-20-3326

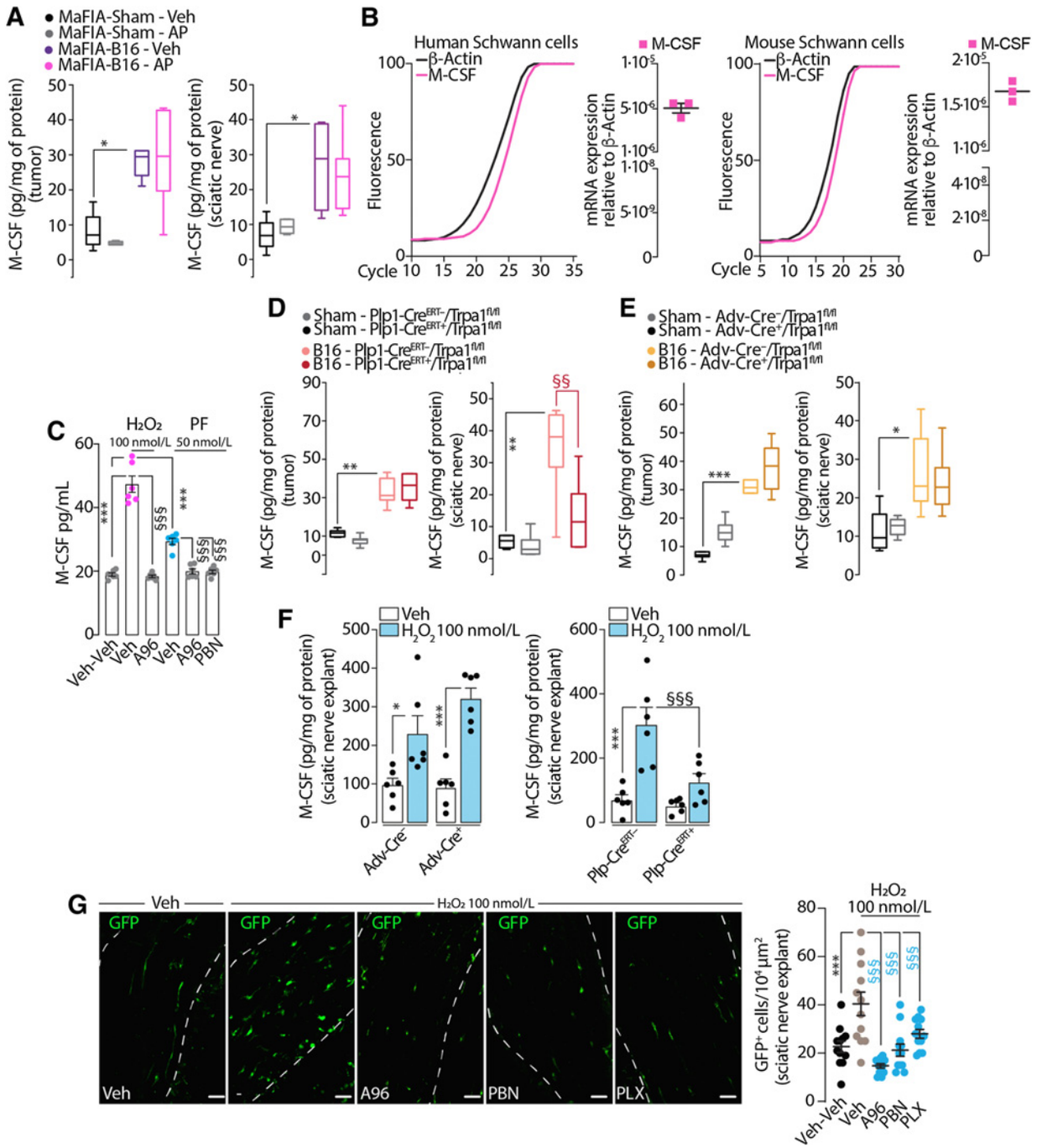


Figure 5.

Schwann cell TRPA1 stimulation releases M-CSF. **A,** M-CSF content in tumor and sciatic nerve after B16-F10 melanoma (B16) cell inoculation or sham in MaFIA mice after AP12087 (AP) or Veh (i.p.). **B,** M-CSF mRNA relative expression in human and mouse Schwann cells. **C,** M-CSF content in human Schwann cells stimulated with H_2O_2, PF-4840154 (PF) or Veh in presence of A967079 (A96), PBN, or Veh. **D** and **E,** M-CSF content in tumor and sciatic nerve at day 14 after B16 cell inoculation or sham in *Plp1-Cre^{ERT-}/$^{ERT+}$/Trpa1$^{fl/fl}$* (**D**) and *Adv-Cre^{-}/Cre^{+}Trpa1$^{fl/fl}$* (**E**). **F,** M-CSF content in sciatic nerve explant from *Plp1-Cre^{ERT-}/$^{ERT+}$/Trpa1$^{fl/fl}$* and *Adv-Cre^{-}/Cre^{+}Trpa1$^{fl/fl}$* mice after H_2O_2 or Veh exposure. **G,** Typical images and data of GFP^{+} cells in sciatic nerve explant from MaFIA mice after H_2O_2 or Veh exposure, in the presence of A96, PBN, PLX or Veh. Dashed line delimits the *epineurium*. Scale bar, 50 µmol/L. $N = 6$ mice (**A, D,** and **E**), $N = 3$ experiments (**B, C, F,** and **G**). *, $P < 0.05$; **, $P < 0.01$; ***, $P < 0.001$ to MaFIA-Sham-Veh, Veh-Veh, Sham-*Plp1-Cre^{ERT-}/Trpa1$^{fl/fl}$*, Sham-*Adv-Cre^{-}/Trpa1$^{fl/fl}$*; §§, $P < 0.01$; §§§, $P < 0.001$ to Veh H_2O_2 and B16-*Plp1-Cre^{ERT-}/Trpa1$^{fl/fl}$*. **A, D,** and **E,** Box plots 25th and 75th percentile, min and max values and data points overlaid. Data are presented as mean ± SEM, data points overlaid (**B, C, F,** and **G**). **A** and **C–G,** One-way ANOVA and Bonferroni *post hoc* test.

Downloaded from cancerres.aacrjournals.org on September 30, 2021. © 2021 American Association for Cancer Research.

Published OnlineFirst March 26, 2021; DOI: 10.1158/0008-5472.CAN-20-3326

evoked by G-CSF and GM-CSF was unaffected by TRPA1 deletion (**Fig. 4I**).

M-CSF from Schwann cells sustains allodynia

As monocytes are known to release M-CSF (27), we tested whether the M-CSF in the paw and sciatic nerve originated from MΦs. M-CSF was measured in the tumor and sciatic nerve from tumor-bearing and MΦ-depleted MaFIA mice. AP12087 treatment, while reducing both tMΦs and rMΦs, left unchanged the M-CSF content in the ipsilateral sciatic nerve and tumor homogenates (**Fig. 5A**). Schwann cells, which ensheath nerve fibers and represent 90% of the nucleated cells of nerve fibers are known to release M-CSF (28, 29). We confirmed that both human and mouse cultured Schwann cells express M-CSF mRNA (**Fig. 5B**). We then explored the mechanism of M-CSF release from Schwann cells. TRPA1 stimulation has been reported to promote oxidative stress (6, 30) and oxidants may release members of the CSF family (31). Exposure of cultured human Schwann cells to the non-reactive (PF-4840154) or reactive (H_2O_2) agonists increased M-CSF levels in the cell supernatant, responses that were attenuated by the TRPA1 antagonist, A967079, and PF-4840154-evoked release of M-CSF was reduced by the antioxidant, phenyl-N-tert-butylnitrone (PBN; **Fig. 5C**). This finding implicates an autocrine pathway that upon Schwann cell TRPA1 activation elicits M-CSF release mediated by ROS generation.

To further explore the contribution of Schwann cell and neuronal TRPA1 in M-CSF release in sciatic nerve, we used *Plp1-Cre^{ERT+};Trpa1$^{fl/fl}$* and *Adv-Cre^{+};Trpa1$^{fl/fl}$* mice, which harbor a selective deletion of TRPA1 in the Schwann cell/oligodendrocyte lineage and in primary sensory neurons, respectively. At day 14 after cancer cell inoculation, M-CSF levels in the ipsilateral sciatic nerve, but not in the tumor, of *Plp1-Cre^{ERT+};Trpa1$^{fl/fl}$* mice, were reduced, whereas in *Adv-Cre^{+};Trpa1$^{fl/fl}$* they were preserved in both the sciatic nerve and tumor, compared with control mice (**Fig. 5D** and **E**). These finding suggest that Schwann cell TRPA1 is a major driver of neuronal M-CSF released in tumor-bearing mice.

To further support the role of Schwann cell TRPA1 in M-CSF release, the cytokine content was measured in the sciatic nerve explant derived from *Plp1-Cre^{ERT+};Trpa1$^{fl/fl}$* and *Adv-Cre^{+};Trpa1$^{fl/fl}$* after exposure to H_2O_2. Upon stimulation, the increase in M-CSF content in nerve explant from control mice was markedly reduced in *Plp1-Cre^{ERT+};Trpa1$^{fl/fl}$*, but unaffected in *Adv-Cre^{+};Trpa1$^{fl/fl}$*, thus supporting the role of TRPA1 Schwann cell in M-CSF release (**Fig. 5F**). In addition, in the sciatic nerve explant culture from naïve MaFIA mice, the exposure to H_2O_2 increased the number of GFP^{+} cells (**Fig. 5G**), an effect that was attenuated by A967079, PBN, and PLX3397 (**Fig. 5G**).

Schwann cell TRPA1 mediates neuroinflammation, which sustains cancer allodynia

TRPA1 is implicated in cancer pain (15). However, the underlying mechanism by which TRPA1 sustains chronic cancer allodynia is unknown. Our results show that cancer pain entails rMΦ expansion in the sciatic nerve and the release of M-CSF, which elicits TRPA1-dependent mechanical allodynia and neuroinflammation. We investigated whether TRPA1 promotes the cancer-evoked neuroinflammation that causes chronic allodynia. B16-F10 melanoma cell inoculation in *Trpa1$^{-/-}$* mice did not induce cancer-evoked mechanical allodynia (**Fig. 6A**). The increased number of rMΦs in *Trpa1$^{+/+}$* mice was markedly reduced in *Trpa1$^{-/-}$* mice (**Fig. 6B**), whereas the number of tMΦs remained equally elevated in both mouse strains (Supplementary Fig. S3A). In addition, we found that the high levels of the oxidative stress marker, H_2O_2, detected in ipsilateral sciatic nerve homogenates of *Trpa1$^{+/+}$* mice, were absent in *Trpa1$^{-/-}$* mice (**Fig. 6C**). In partial contrast with this observation, a single injection (i.p. day 14 after inoculation) of the TRPA1 antagonist A967079, or the antioxidant PBN, transiently and completely reversed mechanical allodynia and the increase in H_2O_2 levels (**Fig. 6D**, **G**, **F**, and **I**), but failed to affect the number of rMΦs (**Fig. 6E** and **H**) and tMΦs (Supplementary Figs. S3B and S3C). Accordingly, a single injection (i.p. 1 hour post-M-CSF) of A967079 and PBN transiently reversed mechanical allodynia (**Fig. 6J**) without decreasing the number of rMΦs (**Fig. 6K**). This observation indicates that a short-term inhibition of the TRPA1 channel or oxidative stress, while efficiently abating allodynia, is not sufficient to attenuate the cellular neuroinflammatory response.

We then investigated the role of Schwann cell TRPA1 in orchestrating mechanical/cold hypersensitivity, spontaneous nociception, and neuroinflammation. After B16-F10 melanoma cell inoculation, *Plp1-Cre^{ERT+}/Trpa1$^{fl/fl}$* mice showed a reduction in mechanical/cold hypersensitivity and spontaneous nociception, as well as in the number of rMΦs (**Fig. 6L–N**) and H_2O_2 levels in the ipsilateral sciatic nerve compared with control mice (**Fig. 6O**). However, the number of tMΦs was unchanged (Supplementary Fig. S3D). In addition, intraplantar injection of B16-F10 melanoma cells significantly increased the expression of ATF3 mRNA (Supplementary Fig. S3E), a marker of nerve injury (32) in DRG neurons ipsilateral to the injected paw, thus suggesting that melanoma can activate an injury response similar to that evoked by axotomy (33). ATF3 mRNA expression in DRGs from *Plp1-Cre^{ERT+}/Trpa1$^{fl/fl}$* was markedly reduced compared with control mice (Supplementary Fig. S3E), further strengthening the contribution of Schwann cell TRPA1 in cancer-evoked neuroinflammation and hypersensitivity.

To investigate the contribution of neuronal TRPA1, we studied *Adv-Cre^{+};Trpa1$^{fl/fl}$*. In these mice, mechanical/cold hypersensitivity and spontaneous nociception were reduced (Supplementary Figs. S3F and S3G), the number of rMΦs (Supplementary Fig. S3H), tMΦs (Supplementary Fig. S3I), and the H_2O_2 levels in the sciatic nerve (Supplementary Fig. S3J) were unaffected. Thus, in contrast to the Schwann cell TRPA1, the channel expressed by nociceptors signals pain, but does not contribute to neuroinflammation.

rMΦs and Schwann cell TRPA1 mediates allodynia in a second cancer pain model

To obtain further evidence on the role of rMΦs and the Schwann cell TRPA1 channel in cancer-related mechanical allodynia, we used a soft tissue tumor/metastasis model induced by intraplantar inoculation of LLC1 cells, which mimics behavioral and functional changes similar to a metastatic bone cancer pain model (34). Inoculation of these cells, but not killed cells, elicited a progressive and rapid cancer growth that was associated to temporarily similar increases in mechanical allodynia (Supplementary Figs. S4A and S4B) and in the number of tMΦs of rMΦs (Supplementary Figs. S4C and S4D) in C57BL/6J mice. No sex differences in cancer growth and mechanical hypersensitivity were observed (Supplementary Figs. S4A and S4B). Thus, also in this case, male mice were used in subsequent experiments. The MΦ role was confirmed by using MaFIA mice, which, after intraplantar inoculation of LCC1 cells, developed a time-dependent increase in paw thickness and mechanical allodynia similar to that observed in C57BL/6J mice (Supplementary Figs. S4E and S4F). However, MaFIA mice receiving daily injections (day 4–8) of AP20187 exhibited a normal cancer

Downloaded from cancerres.aacrjournals.org on September 30, 2021. © 2021 American Association for Cancer Research.

Published OnlineFirst March 26, 2021; DOI: 10.1158/0008-5472.CAN-20-3326

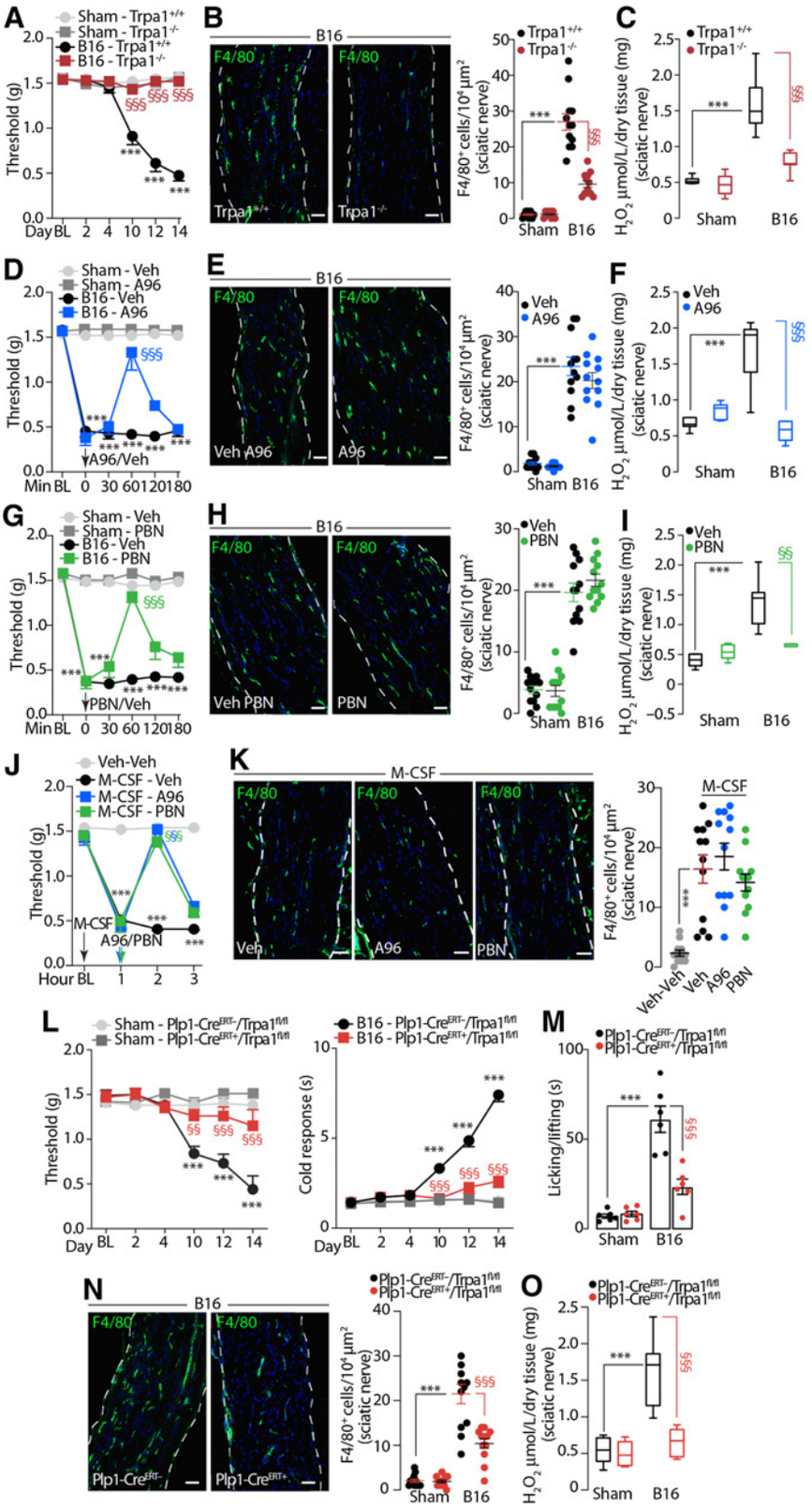


Figure 6.

Schwann cell TRPA1 mediates neuroinflammation and cancer-evoked allodynia. **A–C,** Time-dependent mechanical allodynia (**A**), typical images and data of F4/80$^+$ cells (**B**), and H_2O_2 content in sciatic nerve after B16-F10 melanoma (B16) cell inoculation or sham in *Trpa1*$^{+/+}$ and *Trpa1*$^{-/-}$ mice (**C**). **D–F,** Mechanical allodynia (**D**), typical images and data of F4/80$^+$ cells (**E**), and H_2O_2 content in sciatic nerve in C57BL/6J mice at day 14 after B16 cells inoculation or sham and after A967079 (A96) or Veh (i.p.; **F**). **G–I,** Mechanical allodynia (**G**), typical images and data of F4/80$^+$ cell (**H**), and H_2O_2 content in sciatic nerve in C57BL/6J mice at day 14 after B16 cell inoculation or sham and after PBN or Veh (i.p.; **I**). **J** and **K,** Mechanical allodynia (**J**), and typical images and data of F4/80$^+$ cell in sciatic nerve after M-CSF or Veh (i.pl.) in C57BL/6J mice treated with A96, PBN or Veh (i.p.; **K**). **L** and **M,** Mechanical allodynia and cold response (**L**) and spontaneous nociception after B16 cell inoculation or sham in *Plp1-Cre*$^{ERT-/ERT+}$*/Trpa1*$^{fl/fl}$ (**M**). **N** and **O,** Typical images and data of F4/80$^+$ cells (**N**) and H_2O_2 content in sciatic nerve after B16 cell inoculation or sham in *Plp1-Cre*$^{ERT-/ERT+}$*/Trpa1*$^{fl/fl}$ mice (**O**). BL, baseline. Dashed line delimits the *epineurium*. Scale bar, 50 µmol/L. $N = 6$ mice. ***, $P < 0.001$ to Sham-*Trpa1*$^{+/+}$, Sham-Veh, Veh-Veh, Sham-*Plp1-Cre*$^{ERT-}$*/Trpa1*$^{fl/fl}$; §§, $P < 0.01$; §§§, $P < 0.001$ to B16-*Trpa1*$^{+/+}$, B16-Veh, M-CSF-Veh, B16-*Plp1-Cre*$^{ERT-}$*/Trpa1*$^{fl/fl}$. Data are presented as mean ± SEM, data points overlaid (**B, E, H, K, M,** and **N**). **C, F, I,** and **O,** Box plots 25th and 75th percentile, min and max values and data points overlaid. Two-way (**A, D, G, J,** and **L**) and one-way (**B, C, E, F, H, I, K, M, N,** and **O**) ANOVA and Bonferroni *post hoc* test.

Downloaded from cancerres.aacrjournals.org on September 30, 2021. © 2021 American Association for Cancer Research.

Published OnlineFirst March 26, 2021; DOI: 10.1158/0008-5472.CAN-20-3326

growth (Supplementary Fig. S4E) but a markedly reduced mechanical allodynia (Supplementary Fig. S4F) and GFP$^+$/F4/80$^+$ cells in both the sciatic nerve and tumor (Supplementary Figs. S4G and S4H). Robust evidence of the key role of TRPA1 derived from the observation that *Trpa1*$^{-/-}$ mice inoculated with LLC1 cells showed normal tumor growth (Supplementary Fig. S4I) and increased number of tMΦs (Supplementary Fig. S4L) comparable with *Trpa1*$^{+/+}$ mice. However, in *Trpa1*$^{-/-}$ mice, mechanical allodynia (Supplementary Fig. S4J) and rMΦ expansion (Supplementary Fig. S4K) were remarkably reduced. Similar results were obtained with *Plp1-Cre*$^{ERT+}$/*Trpa1*$^{fl/fl}$ mice, in which mechanical allodynia (Supplementary Fig. S4N) and increase in rMΦ number (Supplementary Fig. S4O), but not increase in paw thickness (Supplementary Fig. S4M) and tMΦ number (Supplementary Fig. S4P), were attenuated as compared with control. Reported data strengthen the hypothesis that rMΦs and Schwann cell TRPA1 are a common mechanism to sustain neuroinflammation and pain in different types of mouse cancer.

The site where resident macrophages mediate allodynia

The importance of dorsal root ganglia (DRG) MΦs in neuropathic pain has been reported previously (11). Thus, the presence of MΦs in DRGs was explored in our model. By quantifying F4/80$^+$ cells, we observed an increase in MΦ number in ipsilateral lumbar (L4–L6) DRGs from MaFIA mice 14 days after melanoma cell inoculation, which, after treatment with systemic AP20187, was slightly, although significantly, decreased by about 30% (Supplementary Fig. S5).

Experiments with MΦ-depleted MaFIA mice highlighted the key role of rMΦs to sustain mechanical/cold hypersensitivity and spontaneous nociception (**Fig. 2**). However, the precise anatomical site where rMΦs mediate allodynia remains unknown. To address this issue, we used MΦ-depleted tumor-bearing MaFIA mice. Mice received AP20187 for 5 days (daily, day 10–14) by perineural injection at three adjacent sites (each at a ∼2 mm distance) of the ipsilateral sciatic nerve trunk (from ∼10 to ∼14 mm from the paw surface; **Fig. 7A**). Perineural treatment elicited a substantial reduction

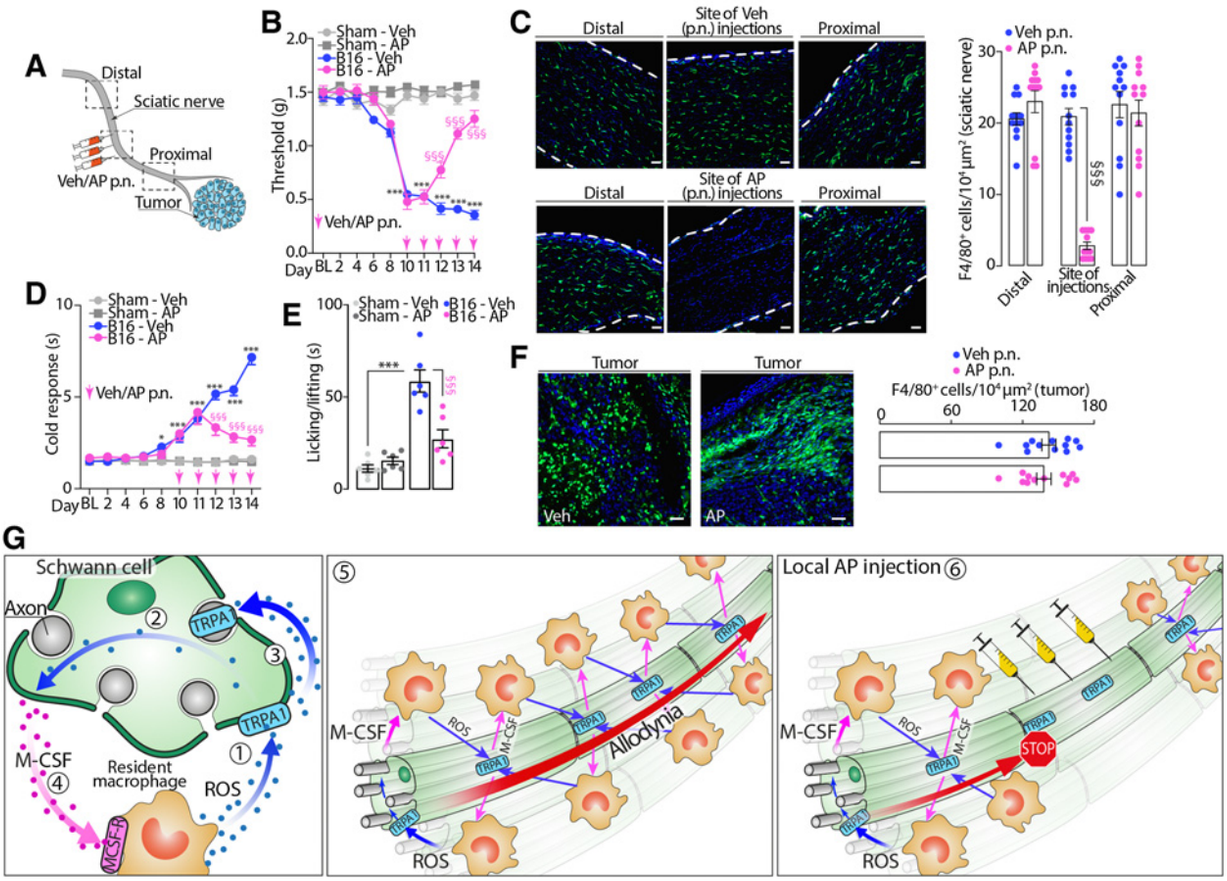


Figure 7.

Segmental resident macrophages depletion switches off cancer-evoked mechanical allodynia, cold response, and spontaneous nociception. **A,** Illustration of three local perineural (p.n.) injections of AP12087 (AP) or Veh in sciatic nerve after B16-F10 melanoma (B16) cell inoculation in MaFIA mice. **B–F,** Mechanical allodynia (**B**), cold response (**D**), and spontaneous nociception (**E**), typical images and data of F4/80$^+$ cell in sciatic nerve (**C**), and tumor (**F**) after B16 cell inoculation or sham in MaFIA mice treated with AP or Veh (p.n.). BL, baseline. Pink arrows, treatment with Veh/AP. Dashed line delimits the *epineurium.* Scale bar, 50 µmol/L. $N = 6$ mice. *, $P < 0.05$; ***, $P < 0.001$ to Sham-Veh; §§§, $P < 0.001$ to B16-Veh. Data are presented as mean ± SEM, data points overlaid (**C, E,** and **F**). Two-way (**B** and **D**) and one-way (**C, E,** and **F**) ANOVA and Bonferroni *post hoc* test. **G,** Illustration of the feed-forward mechanism that sustains cancer pain: (1) expanded sciatic nerve rMΦs by their own oxidative burst target Schwann cell TRPA1; (2) Schwann cell TRPA1 amplifies the oxidative burst; (4) to release M-CSF, which sustains further rMΦ expansion, and (4) to target neuronal TRPA1, which signals allodynia. The paracrine pathway, which entails Schwann cell TRPA1 activation, M-CSF release and signaling and rMΦ expansion, and Schwann cell- and rMΦs-dependent oxidative burst (5) must be present along the entire sciatic nerve to sustain mechanical allodynia, as (6) the disruption of the feed-forward mechanism by segmental depletion of rMΦs switches off the pain-like response.

Downloaded from cancerres.aacrjournals.org on September 30, 2021. © 2021 American Association for Cancer Research.

Published OnlineFirst March 26, 2021; DOI: 10.1158/0008-5472.CAN-20-3326

in mechanical/cold hypersensitivity and spontaneous nociception (**Fig. 7B**, **D**, and **E**) and a marked decrease in the number of GFP^+ cells in the portion corresponding to the sciatic nerve segment that had been treated with AP20187 (**Fig. 7C**). The number of GFP^+ cells in both the distal and proximal portion to that treated with AP20187 was similar in MaFIA mice that received either the dimerizing agent or its vehicle (**Fig. 7C**). The number of GFP^+ cells in the paw (tMΦs) was similar in mice treated with AP20187 or vehicle (**Fig. 7F**). These data indicate that depletion of rMΦs in a limited portion of the ipsilateral sciatic nerve is necessary and sufficient to interrupt the signaling pathway that entails MΦs and Schwann cell interaction to mediate mechanical/cold hypersensitivity and spontaneous nociception.

Discussion

Although pain is a debilitating symptom of cancer and a major medical condition that warrants a better understanding of its underlying mechanism (2), little is known about the role of MΦs in cancer pain. Herein, we reveal the key role of MΦs and, in particular, of rMΦs, in sustaining mechanical/cold hypersensitivity and spontaneous nociception in mouse models of cancer pain. A series of findings support this conclusion. Melanoma B16-F10 cell growth in the mouse hindpaw was associated with a time-dependent and parallel increase in mechanical/cold hypersensitivity and spontaneous nociception and in the number of tMΦs and rMΦs. Depletion of the two MΦ populations by the homodimerizer agent, AP20187, in MaFIA mice abolished the mechanical/cold hypersensitivity and spontaneous nociception. In neuropathic pain models, including partial nerve injury (6, 35), constriction of the infraorbital nerve (5), and diabetic neuropathy (36), clodronate, which depletes circulating monocytes, simultaneously removed MΦs and abated mechanical allodynia. In contrast, in the present cancer pain model, clodronate markedly reduced tMΦs, but affected neither rMΦ expansion nor mechanical/cold hypersensitivity. Additional evidence that cancer-evoked mechanical/cold hypersensitivity and spontaneous nociception is dependent on rMΦs was obtained in MΦ-depleted MaFIA mice, whose tumor microenvironment, but not the nerve bundle, was replenished with peritoneal MΦs from donor mice. In these mice mechanical/cold hypersensitivity and spontaneous nociception were not restored. Conversely, mechanical/cold hypersensitivity and spontaneous nociception were unaffected by local AP20187 treatment in the hindpaw, which depleted tMΦs, but not rMΦs. Thus, mechanical/cold hypersensitivity and spontaneous nociception are elicited by the expansion of rMΦs, whereas tMΦs, which are recruited from the blood circulation, are not relevant. In this respect, the present cancer pain model shows some similarity with certain models of neuropathic pain, such as those produced by the spared nerve injury and the spinal nerve transection, where rMΦs have been identified as the proinflammatory cellular component responsible for allodynia (11, 37). The observation that melanoma cell inoculation increased the staining for the nerve injury biomarker, ATF3 (38), in DRG neurons ipsilateral to the tumor supports the presence of a neuropathic component orchestrated by Schwann cell TRPA1 in the present cancer pain model. Further support is given by the observation of increased MΦs in DRGs, a finding also reported in neuropathic pain models (11). However, as treatment with AP20187 abated mechanical/cold hypersensitivity and spontaneous nociception and only partially reduced DRG MΦs, the role of such a subpopulation in promoting mechanical/cold hypersensitivity and spontaneous nociception appears limited in cancer. Elimination of mechanical allodynia in MΦ-depleted MaFIA mice with LLC1 supports the hypothesis that the role of MΦs in cancer pain is not unique to the B16-F10 melanoma model, but is essential in various types of murine tumors.

The analysis of a proinflammatory cytokine panel in melanoma homogenates showed a pronounced increase in CCL2 and M-CSF levels, whereas a more diffuse augmentation of most cytokines, including CCL2 and M-CSF, was observed in sciatic nerve homogenates. Although an anti-CCL2 mAb did not affect mechanical/cold hypersensitivity, both a M-CSFR antagonist and an anti-M-CSF mAb robustly attenuated mechanical/cold hypersensitivity. Targeting the M-CSF signaling not only reduced mechanical/cold hypersensitivity, but also inhibited neuroinflammation, as after immunologic or pharmacologic blockade of the M-CSF signal both MΦ expansion and increased oxidative stress (H_2O_2 levels) in the sciatic nerve homogenates were attenuated. M-CSF has been shown to induce mechanical allodynia after intrathecal administration (7). We showed that intraplantar M-CSF elicits mechanical allodynia in mice. Although the entire family of CSF chemokines exhibits a similar proalgesic activity (39–41), only M-CSF, and not G-CSF or MG-CSF, produced MΦ-dependent allodynia. Together, these findings support the role of M-CSF in cancer pain and indicate another common feature between the present cancer pain model and certain (8, 9, 11), but not other (4–6), neuropathic pain models where MΦ chemoattraction was driven by CCL2.

We recently reported a major role for TRPA1 in mechanical/cold hypersensitivity and spontaneous nociception induced by melanoma cell inoculation in mice (15). Thus, we hypothesized that TRPA1 is implicated in the rMΦs/M-CSF-mediated pro-allodynic pathway. After confirming that *Trpa1*$^{-/-}$ mice did not develop mechanical hypersensitivity after B16-F10 inoculation, we found that TRPA1 deletion abolished allodynia evoked by (intraplantar) M-CSF, but not by G-CSF or MG-CSF. These results reveal a cause–effect relationship between M-CSF and TRPA1 in pain. Therefore, we investigated how M-CSF elicits TRPA1-dependent allodynia. The inability of M-CSF to evoke allodynia in *Trpa1*$^{-/-}$ mice was associated with failure to expand rMΦs and to increase H_2O_2 levels in the sciatic nerve. Thus, elimination of TRPA1 blunted the neuroinflammatory response evoked by M-CSF. The observation that rMΦ expansion was attenuated by TRPA1 deletion implies that channel activation is required to increase rMΦ number. This finding was unexpected, as MΦs express M-CSFR (42), and therefore, in principle, M-CSF might increase their number by direct activation of its cognate receptor on rMΦs, without the involvement of TRPA1. This apparently contradictory finding was addressed by using multiple tools, including MaFIA mice, cultured human and mouse Schwann cells, and an *ex vivo* sciatic nerve mouse explant culture.

Cancer cells (43), monocytes (27), DRG neurons (11), and Schwann cells (44) can all express and release M-CSF. The increased M-CSF levels evoked by cancer growth were not reduced in either the mouse hindpaw or sciatic nerve in MΦ-depleted MaFIA mice, indicating that MΦs are not involved in cancer-associated secretion of the chemokine. We corroborated the previous findings (44), showing that M-CSF is expressed by either mouse or human Schwann cells in culture. We also showed that the TRPA1 agonist H_2O_2, which is increased in the sciatic nerve of mice with cancer, elicited a TRPA1-dependent release of M-CSF from cultured Schwann cells. Furthermore, in an *ex vivo* sciatic nerve explant culture, rMΦ expansion elicited by H_2O_2 was attenuated by a M-CSFR antagonist, a TRPA1 antagonist, and an antioxidant. As H_2O_2 increases MΦs at sites of injury (6, 45), the inhibitory action of the antioxidant on rMΦ expansion was expected. However, the ability of M-CSFR and TRPA1 antagonists to similarly attenuate rMΦ

Downloaded from cancerres.aacrjournals.org on September 30, 2021. © 2021 American Association for Cancer Research.

Published OnlineFirst March 26, 2021; DOI: 10.1158/0008-5472.CAN-20-3326

expansion and M-CSF release from Schwann cells suggests a feed-forward mechanism, which entails the following steps: oxidative stress from cancer tissue targets Schwann cell TRPA1 to release M-CSF, which elicits rMΦ expansion within the sciatic nerve trunk. Expanded rMΦs, via their own oxidative stress, perpetuate this pathway, which sustains allodynia and spontaneous pain (**Fig. 7G**).

Direct assay of M-CSF in the hindpaw and sciatic nerve provides support to this hypothesis. In mice with a Cre-mediated deletion of *Trpa1* in the Schwann cell/oligodendrocyte lineage (*Plp1-Cre*$^{ERT+}$/*Trpa1*$^{fl/fl}$), cancer-evoked increase in tumor M-CSF was unchanged, whereas a marked reduction in the M-CSF levels was observed in the ipsilateral sciatic nerve. Importantly, M-CSF release elicited by H_2O_2 stimulation was markedly attenuated in the sciatic nerve explant from *Plp1-Cre*$^{ERT+}$/*Trpa1*$^{fl/fl}$ mice. Thus, although M-CSF of the tumor microenvironment does not contribute to the proalgesic rMΦ expansion, the Schwann cell-mediated M-CSF is essential for the cancer-evoked allodynia.

The proalgesic pathways that include glial cell activation, inflammatory cell expansion, and increased proinflammatory mediators in the central and peripheral nervous systems, collectively referred to as neuroinflammation, have been extensively characterized as a major underlying mechanism of neuropathic pain associated with a variety of neuropathologic conditions (4–6, 8, 11, 20). Although several cell types and proalgesic mediators have been proposed, the neuroinflammatory pathways that drive cancer pain remain uncertain (46, 47). Here, we identified the key role of M-CSF, released following Schwann cell TRPA1 activation, in sustaining cancer-evoked rMΦ expansion and the ensuing mechanical/cold hypersensitivity and spontaneous nociception. Supporting evidence derives from the observation that deletion of TRPA1 in Schwann cell/oligodendrocyte lineage attenuates neuroinflammation and mechanical/cold hypersensitivity and spontaneous nociception in the melanoma mouse model of cancer pain. In contrast, deletion of TRPA1 in primary sensory neurons attenuates mechanical allodynia but not neuroinflammation. Thus, we hypothesize that, although neuronal TRPA1 is the final target of the proalgesic signaling pathway, the feed-forward mechanism that encompasses M-CSF, rMΦs oxidative stress, and Schwann cell/TRPA1 is needed to chronically sustain mechanical/cold hypersensitivity and spontaneous nociception (**Fig. 7G**).

A limitation to the translational value of the cancer model used in this study is the relatively low incidence of pain reported in patients with early-stage melanoma (48). However, the rapid cancer growth and prominent inflammatory response of our model may recapitulate the pain reported in metastatic melanoma, where >50% of patients require palliative care and morphine treatment (49–52). The most relevant findings were replicated in another model of cancer pain by using LLC1 cells inoculated in the mouse paw. However, the fact that lung carcinomas usually metastasize to bones (53) and not to skin should be considered an additional limitation of this study. The essential role of rMΦs and Schwann cell TRPA1 in the murine LLC1 model is indicated by the observation that mechanical allodynia and expansion in rMΦs were attenuated in both *Trpa1*$^{-/-}$ and *Plp1-Cre*$^{ERT+}$/*Trpa1*$^{fl/fl}$ mice. The selective elimination of rMΦs in mice with a Cre-mediated Schwann cell deletion of *Trpa1*, associated with eradication of allodynia, supports the crucial role of the Schwann cell channel in orchestrating neuroinflammation and pain not only in melanoma, but also in LLC1 models. Although we identified the macrophage subpopulation implicated in mechanical/cold hypersensitivity and spontaneous nociception, we cannot exclude the contribution of other local autocrine and paracrine factors, which may act upstream or downstream of macrophage expansion to sustain cancer pain.

Two additional findings of our study are difficult to interpret. The first relates to the different effects produced by TRPA1 pharmacologic antagonism versus those elicited by TRPA1 genetic deletion. Although *Trpa1*$^{-/-}$ mice showed a marked attenuation of both mechanical allodynia and neuroinflammation, systemic exposure to a TRPA1 antagonist efficiently abrogated allodynia, but did not affect rMΦ expansion. To explain this apparent contradiction, the different time courses of these interventions should be considered. In fact, *Trpa1*$^{-/-}$ mice harbor a permanent channel deletion, whereas the short half-life of the TRPA1 antagonist, A967079, provides brief channel inhibition. Thus, the transient (a few hours) blockade of the neuronal channel is sufficient to briefly reverse allodynia, but cannot provide the prolonged inhibition (some days) of the Schwann cell TRPA1, which is necessary to attenuate the rMΦ expansion and the ensuing allodynia. This interpretation is further supported by the observation that treatment of MaFIA mice with AP20187, which depletes MΦs for several days, elicits a prolonged attenuation of mechanical/cold hypersensitivity and spontaneous nociception, probably because the rMΦ/Schwann cell TRPA1 feed-forward mechanism is switched off for a prolonged period of time.

The second unsettled finding relates to the anatomical site of action where expanded rMΦs sustain allodynia. In models of MΦ-dependent neuropathic pain, MΦ depletion at the site of nerve injury efficiently attenuated allodynia (5, 6, 37). However, in other models, a series of direct and indirect evidence showed that selective elimination of rMΦs at the site of the damaged nerve did not affect allodynia, which suggested that rMΦ expansion in the DRG was required (11, 35). In the present model of cancer pain, we asked which was the anatomical site where the M-CSF/rMΦ/Schwann cell TRPA1 pathway must operate to sustain allodynia. Because of the technical complications inherent to the elimination of DRG rMΦs, we chose to examine this issue by depleting rMΦs in an anatomically well-identified segment of the sciatic nerve. The observation that a selective rMΦ depletion in a ∼4 mm portion of the sciatic nerve trunk abrogated mechanical/cold hypersensitivity and spontaneous nociception proposes a spatial constraint in the neuroinflammatory mechanism that sustains mechanical/cold hypersensitivity and spontaneous nociception. As rMΦ expansion was unaltered in the proximal and distal untreated segments, the amplification loop consisting of rMΦs and Schwann cell TRPA1 that communicates *via* M-CSF and oxidative stress must function by contiguity throughout the entire sciatic nerve to warrant that the mechanical/cold stimulus applied to the mouse paw is conveyed centrally as an allodynic signal.

The soma of DRG neurons does not participate in the central conduction of action potentials (54). Instead, sensory impulses from peripheral terminals continue directly into the spinal cord and do not depolarize the soma (55). However, the present findings do not exclude the possibility that DRG cells, with the cooperation of surrounding satellite cells and local expanded rMΦs, are implicated in magnifying the sensory impulse that conveys mechanical/cold hypersensitivity and spontaneous nociception. Nevertheless, the present discovery of the role of the neuroinflammatory and proalgesic pathway that entails M-CSF, rMΦs, oxidative stress and Schwann cell TRPA1 in two different types of murine cancer offers novel targets for the identification of better and safer treatments for cancer pain.

Downloaded from cancerres.aacrjournals.org on September 30, 2021. © 2021 American Association for Cancer Research.

Published OnlineFirst March 26, 2021; DOI: 10.1158/0008-5472.CAN-20-3326

Authors' Disclosures

N.W. Bunnett reports grants from NIH and Department of Defense during the conduct of the study, nonfinancial support from Endosome Therapeutics Inc. outside the submitted work, and is a founding scientist of Endosome Therapeutics Inc. P. Geppetti reports grants and personal fees from Eli-Lilly, TEVA, Novartis, Allergan/AbbVie, and grants from Lundbeck outside the submitted work and is a founding scientist of FloNext Srl. R. Nassini is a founding scientist of FloNext Srl. No disclosures were reported by the other authors.

Authors' Contributions

F. De Logu: Conceptualization, data curation, formal analysis, supervision, methodology, writing–original draft, writing–review and editing. **M. Marini:** Data curation, formal analysis, methodology. **L. Landini:** Data curation, formal analysis, methodology. **D. Souza Monteiro de Araujo:** Data curation, formal analysis, methodology. **N. Bartalucci:** Data curation, software, methodology. **G. Trevisan:** Data curation, formal analysis, supervision, writing–review and editing. **G. Bruno:** Data curation, formal analysis, methodology. **M. Marangoni:** Data curation, formal analysis, methodology. **B.L. Schmidt:** Data curation, funding acquisition, writing–original draft, writing–review and editing. **N.W. Bunnett:** Funding acquisition, writing-original draft, writing–review and editing. **P. Geppetti:** Conceptualization, data curation, supervision, funding acquisition, writing–original draft, writing–review and editing. **R. Nassini:** Conceptualization, data curation, formal analysis, supervision, funding acquisition, methodology, writing–original draft, writing–review and editing.

Acknowledgments

We thank D. Preti (University of Ferrara, Ferrara, Italy) for providing A967079. This work was supported by European Research Council (ERC) under the European Union's Horizon 2020 research and innovation programme (Grant Agreement No. 835286; to P. Geppetti), Associazione Italiana per la Ricerca sul Cancro (AIRC, IG2016-ID19247 and IG2020-ID24503) and Fondazione Cassa di Risparmio di Firenze, Italy (to R. Nassini), NIH (NS102722, DE026806, DK118971, DE029951 to N.W. Bunnett and B.L. Schmidt), and Department of Defense (W81XWH1810431 to N.W. Bunnett and B.L. Schmidt).

The costs of publication of this article were defrayed in part by the payment of page charges. This article must therefore be hereby marked *advertisement* in accordance with 18 U.S.C. Section 1734 solely to indicate this fact.

Received October 2, 2020; revised February 13, 2021; accepted March 22, 2021; published first March 26, 2021.

References

1. Breivik H, Cherny N, Collett B, de Conno F, Filbet M, Foubert AJ, et al. Cancer-related pain: a pan-European survey of prevalence, treatment, and patient attitudes. Ann Oncol 2009;20:1420–33.
2. Costantini M, Ripamonti C, Beccaro M, Montella M, Borgia P, Casella C, et al. Prevalence, distress, management, and relief of pain during the last 3 months of cancer patients' life. Results of an Italian mortality follow-back survey. Ann Oncol 2009;20:729–35.
3. Vendrell I, Macedo D, Alho I, Dionísio MR, Costa L. Treatment of cancer pain by targeting cytokines. Mediators Inflamm 2015;2015:984570.
4. Abbadie C, Lindia JA, Cumiskey AM, Peterson LB, Mudgett JS, Bayne EK, et al. Impaired neuropathic pain responses in mice lacking the chemokine receptor CCR2. Proc Natl Acad Sci U S A 2003;100:7947–52.
5. Trevisan G, Benemei S, Materazzi S, De Logu F, De Siena G, Fusi C, et al. TRPA1 mediates trigeminal neuropathic pain in mice downstream of monocytes/macrophages and oxidative stress. Brain 2016;139:1361–77.
6. De Logu F, Nassini R, Materazzi S, Carvalho Goncalves M, Nosi D, Rossi Degl'Innocenti D, et al. Schwann cell TRPA1 mediates neuroinflammation that sustains macrophage-dependent neuropathic pain in mice. Nat Commun 2017;8:1887.
7. Okubo M, Yamanaka H, Kobayashi K, Dai Y, Kanda H, Yagi H, et al. Macrophage-colony stimulating factor derived from injured primary afferent induces proliferation of spinal microglia and neuropathic pain in rats. PLoS One 2016;11:e0153375.
8. Guan Z, Kuhn JA, Wang X, Colquitt B, Solorzano C, Vaman S, et al. Injured sensory neuron-derived CSF1 induces microglial proliferation and DAP12-dependent pain. Nat Neurosci 2016;19:94–101.
9. Lee S, Shi XQ, Fan A, West B, Zhang J. Targeting macrophage and microglia activation with colony stimulating factor 1 receptor inhibitor is an effective strategy to treat injury-triggered neuropathic pain. Mol Pain 2018;14:1744806918764979.
10. Mueller M, Leonhard C, Wacker K, Ringelstein EB, Okabe M, Hickey WF, et al. Macrophage response to peripheral nerve injury: the quantitative contribution of resident and hematogenous macrophages. Lab Invest 2003;83:175–85.
11. Yu X, Liu H, Hamel KA, Morvan MG, Yu S, Leff J, et al. Dorsal root ganglion macrophages contribute to both the initiation and persistence of neuropathic pain. Nat Commun 2020;11:264.
12. Mueller M, Wacker K, Ringelstein EB, Hickey WF, Imai Y, Kiefer R. Rapid response of identified resident endoneurial macrophages to nerve injury. Am J Pathol 2001;159:2187–97.
13. Story GM, Peier AM, Reeve AJ, Eid SR, Mosbacher J, Hricik TR, et al. ANKTM1, a TRP-like channel expressed in nociceptive neurons, is activated by cold temperatures. Cell 2003;112:819–29.
14. Mori Y, Takahashi N, Polat OK, Kurokawa T, Takeda N, Inoue M. Redox-sensitive transient receptor potential channels in oxygen sensing and adaptation. Pflugers Arch 2016;468:85–97.
15. Antoniazzi CTD, Nassini R, Rigo FK, Milioli AM, Bellinaso F, Camponogara C, et al. Transient receptor potential ankyrin 1 (TRPA1) plays a critical role in a mouse model of cancer pain. Int J Cancer 2019;144:355–65.
16. Faul F, Erdfelder E, Lang AG, Buchner A. G*Power. 3: a flexible statistical power analysis program for the social, behavioral, and biomedical sciences. Behav Res Methods 2007;39:175–91.
17. Burnett SH, Kershen EJ, Zhang J, Zeng L, Straley SC, Kaplan AM, et al. Conditional macrophage ablation in transgenic mice expressing a Fas-based suicide gene. J Leukoc Biol 2004;75:612–23.
18. Selvaraj D, Gangadharan V, Michalski CW, Kurejova M, Stösser S, Srivastava K, et al. A Functional role for VEGFR1 expressed in peripheral sensory neurons in cancer pain. Cancer Cell 2015;27:780–96.
19. Kim CF, Moalem-Taylor G. Detailed characterization of neuro-immune responses following neuropathic injury in mice. Brain Res 2011;1405:95–108.
20. Shepherd AJ, Copits BA, Mickle AD, Karlsson P, Kadunganattil S, Haroutounian S, et al. Angiotensin II triggers peripheral macrophage-to-sensory neuron redox crosstalk to elicit pain. J Neurosci 2018;38:7032–57.
21. Gray M, Palispis W, Popovich PG, van Rooijen N, Gupta R. Macrophage depletion alters the blood-nerve barrier without affecting Schwann cell function after neural injury. J Neurosci Res 2007;85:766–77.
22. Sharma P, Allison JP. The future of immune checkpoint therapy. Science 2015;348:56–61.
23. Keir ME, Butte MJ, Freeman GJ, Sharpe AH. PD-1 and its ligands in tolerance and immunity. Annu Rev Immunol 2008;26:677–704.
24. Chen G, Kim YH, Li H, Luo H, Liu DL, Zhang ZJ, et al. PD-L1 inhibits acute and chronic pain by suppressing nociceptive neuron activity via PD-1. Nat Neurosci 2017;20:917–26.
25. Kudo-Saito C, Shirako H, Ohike M, Tsukamoto N, Kawakami Y. CCL2 is critical for immunosuppression to promote cancer metastasis. Clin Exp Metastasis 2013;30:393–405.
26. Schweizerhof M, Stosser S, Kurejova M, Njoo C, Gangadharan V, Agarwal N, et al. Hematopoietic colony-stimulating factors mediate tumor-nerve interactions and bone cancer pain. Nat Med 2009;15:802–7.
27. Oster W, Lindemann A, Mertelsmann R, Herrmann F. Production of macrophage-, granulocyte-, granulocyte-macrophage- and multi-colony-stimulating factor by peripheral blood cells. Eur J Immunol 1989;19:543–7.
28. Groh J, Basu R, Stanley ER, Martini R. Cell-surface and secreted isoforms of CSF-1 exert opposing roles in macrophage-mediated neural damage in Cx32-deficient mice. J Neurosci 2016;36:1890–901.
29. Martini R, Fischer S, Lopez-Vales R, David S. Interactions between Schwann cells and macrophages in injury and inherited demyelinating disease. Glia 2008;56:1566–77.

Downloaded from cancerres.aacrjournals.org on September 30, 2021. © 2021 American Association for Cancer Research.

Published OnlineFirst March 26, 2021; DOI: 10.1158/0008-5472.CAN-20-3326

30. Lin AH, Liu MH, Ko HK, Perng DW, Lee TS, Kou YR. Lung epithelial TRPA1 transduces the extracellular ros into transcriptional regulation of lung inflammation induced by cigarette smoke: the role of influxed Ca^{2+}. Mediators Inflamm 2015;2015:148367.
31. Sturrock A, Mir-Kasimov M, Baker J, Rowley J, Paine R 3rd. Key role of microRNA in the regulation of granulocyte macrophage colony-stimulating factor expression in murine alveolar epithelial cells during oxidative stress. J Biol Chem 2014;289:4095–105.
32. Lindå H, Sköld MK, Ochsmann T. Activating transcription factor 3, a useful marker for regenerative response after nerve root injury. Front Neurol 2011; 2:30.
33. Tsujino H, Kondo E, Fukuoka T, Dai Y, Tokunaga A, Miki K, et al. Activating transcription factor 3 (ATF3) induction by axotomy in sensory and motoneurons: a novel neuronal marker of nerve injury. Mol Cell Neurosci 2000;15:170–82.
34. Constantin CE, Mair N, Sailer CA, Andratsch M, Xu ZZ, Blumer MJ, et al. Endogenous tumor necrosis factor alpha (TNFalpha) requires TNF receptor type 2 to generate heat hyperalgesia in a mouse cancer model. J Neurosci 2008;28: 5072–81.
35. Cobos EJ, Nickerson CA, Gao F, Chandran V, Bravo-Caparros I, Gonzalez-Cano R, et al. Mechanistic differences in neuropathic pain modalities revealed by correlating behavior with global expression profiling. Cell Rep 2018;22:1301–12.
36. Sun JJ, Tang L, Zhao XP, Xu JM, Xiao Y, Li H. Infiltration of blood-derived macrophages contributes to the development of diabetic neuropathy. J Immunol Res 2019;2019:7597382.
37. Peng J, Gu N, Zhou L, BE U, Murugan M, Gan WB, et al. Microglia and monocytes synergistically promote the transition from acute to chronic pain after nerve injury. Nat Commun 2016;7:12029.
38. Gao YJ, Cheng JK, Zeng Q, Xu ZZ, Decosterd I, Xu X, et al. Selective inhibition of JNK with a peptide inhibitor attenuates pain hypersensitivity and tumor growth in a mouse skin cancer pain model. Exp Neurol 2009;219:146–55.
39. Carvalho TT, Borghi SM, Pinho-Ribeiro FA, Mizokami SS, Cunha TM, Ferreira SH, et al. Granulocyte-colony stimulating factor (G-CSF)-induced mechanical hyperalgesia in mice: role for peripheral TNFα, IL-1β and IL-10. Eur J Pharmacol 2015;749:62–72.
40. Zhang F, Wang Y, Liu Y, Han H, Zhang D, Fan X, et al. Transcriptional regulation of voltage-gated sodium channels contributes to GM-CSF-induced pain. J Neurosci 2019;39:5222–33.
41. Nicol LSC, Thornton P, Hatcher JP, Glover CP, Webster CI, Burrell M, et al. Central inhibition of granulocyte-macrophage colony-stimulating factor is analgesic in experimental neuropathic pain. Pain 2018;159:550–9.
42. Van Overmeire E, Stijlemans B, Heymann F, Keirsse J, Morias Y, Elkrim Y, et al. M-CSF and GM-CSF receptor signaling differentially regulate monocyte maturation and macrophage polarization in the tumor microenvironment. Cancer Res 2016;76:35–42.
43. Park J, Lee SE, Hur J, Hong EB, Choi JI, Yang JM, et al. M-CSF from cancer cells induces fatty acid synthase and PPARbeta/delta activation in tumor myeloid cells, leading to tumor progression. Cell Rep 2015;10:1614–25.
44. Trias E, Kovacs M, King PH, Si Y, Kwon Y, Varela V, et al. Schwann cells orchestrate peripheral nerve inflammation through the expression of CSF1, IL-34, and SCF in amyotrophic lateral sclerosis. Glia 2020;68:1165–81.
45. Moreira S, Stramer B, Evans I, Wood W, Martin P. Prioritization of competing damage and developmental signals by migrating macrophages in the *Drosophila* embryo. Curr Biol 2010;20:464–70.
46. Zhu YF, Kwiecien JM, Dabrowski W, Ungard R, Zhu KL, Huizinga JD, et al. Cancer pain and neuropathic pain are associated with A beta sensory neuronal plasticity in dorsal root ganglia and abnormal sprouting in lumbar spinal cord. Mol Pain 2018;14:1744806918810099.
47. Lindsay TH, Jonas BM, Sevcik MA, Kubota K, Halvorson KG, Ghilardi JR, et al. Pancreatic cancer pain and its correlation with changes in tumor vasculature, macrophage infiltration, neuronal innervation, body weight and disease progression. Pain 2005;119:233–46.
48. Negin BP, Riedel E, Oliveria SA, Berwick M, Coit DG, Brady MS. Symptoms and signs of primary melanoma: important indicators of Breslow depth. Cancer 2003; 98:344–8.
49. Leach BC, Kulbersh JS, Day TA, Cook J. Cranial neuropathy as a presenting sign of recurrent aggressive skin cancer. Dermatol Surg 2008;34:483–97.
50. Lehembre S, Carvalho P, Young P, Josset V, Hacpille L, Joly P. [Palliative care management of patients in a Dermatology Department]. Ann Dermatol Venereol 2006;133:967–70.
51. Hashemi M, Stark A, Hugo H, Mehdorn M. Intracranial trigeminal nerve metastasis of a desmoplastic neurotropic melanoma: case report. Cent Eur Neurosurg 2009;70:91–4.
52. Croker J, Burmeister B, Foote M. Neurotropic melanoma: the management of localised disease. J Skin Cancer 2012;2012:706452.
53. Quint LE, Tummala S, Brisson LJ, Francis IR, Krupnick AS, Kazerooni EA, et al. Distribution of distant metastases from newly diagnosed non-small cell lung cancer. Ann Thorac Surg 1996;62:246–50.
54. Devor M. Unexplained peculiarities of the dorsal root ganglion. Pain 1999;S27–35.
55. Marani E, Lakke EAJF. Peripheral nervous system topics. In: Mai JK, Paxinos G, editors. The human nervous system. San Diego: Elsevier Academic Press. p. 82–140.

Downloaded from cancerres.aacrjournals.org on September 30, 2021. © 2021 American Association for Cancer Research.

Published OnlineFirst March 26, 2021; DOI: 10.1158/0008-5472.CAN-20-3326

Cancer Research
The Journal of Cancer Research (1916–1930) | The American Journal of Cancer (1931–1940)

AACR American Association for Cancer Research

Peripheral Nerve Resident Macrophages and Schwann Cells Mediate Cancer-Induced Pain

Francesco De Logu, Matilde Marini, Lorenzo Landini, et al.

Cancer Res 2021;81:3387-3401. Published OnlineFirst March 26, 2021.

Updated version Access the most recent version of this article at: doi:10.1158/0008-5472.CAN-20-3326

Supplementary Material Access the most recent supplemental material at: http://cancerres.aacrjournals.org/content/suppl/2021/03/24/0008-5472.CAN-20-3326.DC1

Visual Overview **A diagrammatic summary of the major findings and biological implications:** http://cancerres.aacrjournals.org/content/81/12/3387/F1.large.jpg

Cited articles This article cites 53 articles, 8 of which you can access for free at: http://cancerres.aacrjournals.org/content/81/12/3387.full#ref-list-1

E-mail alerts Sign up to receive free email-alerts related to this article or journal.

Reprints and Subscriptions To order reprints of this article or to subscribe to the journal, contact the AACR Publications Department at pubs@aacr.org.

Permissions To request permission to re-use all or part of this article, use this link http://cancerres.aacrjournals.org/content/81/12/3387. Click on "Request Permissions" which will take you to the Copyright Clearance Center's (CCC) Rightslink site.

Downloaded from cancerres.aacrjournals.org on September 30, 2021. © 2021 American Association for Cancer Research.

Cellular/Molecular

Granulocyte-Macrophage Colony Stimulating Factor As an Indirect Mediator of Nociceptor Activation and Pain

Damini Tewari,[1] Andrew D. Cook,[2] Ming-Chin Lee,[2] Anne D. Christensen,[2] Andrew Croxford,[3] Burkhard Becher,[3] Daniel Poole,[4] Pradeep Rajasekhar,[4] Nigel Bunnett,[4,5] Julia E. Smith,[6] John A. Hamilton,[2,7] and Stephen B. McMahon[1]

[1]Neurorestoration group, Wolfson Centre for Age-Related Diseases, King's College London, London, SE1 1UL, United Kingdom, [2]University of Melbourne, Department of Medicine at Royal Melbourne Hospital, Parkville, Victoria 3050, Australia, [3]Institute of Experimental Immunology, University of Zurich, Zurich 8057, Switzerland, [4]Monash Institute of Pharmaceutical Sciences, Monash University, Australian Research Council Centre of Excellence in Convergent Bio-Nano Science and Technology, Monash University, Parkville, Victoria 3052, Australia, [5]Columbia University College of Physicians and Surgeons, Columbia University, New York, New York 10032, [6] Adaptive Immunity GSK Medicines Research Centre, Stevenage, Hertfordshire SG1 2NY, United Kingdom, and [7]Australian Institute for Musculoskeletal Science (AIMSS), The University of Melbourne and Western Health, St. Albans, Victoria 3021, Australia

The interaction between the immune system and the nervous system has been at the center of multiple research studies in recent years. Whereas the role played by cytokines as neuronal mediators is no longer contested, the mechanisms by which cytokines modulate pain processing remain to be elucidated. In this study, we have analyzed the involvement of granulocyte-macrophage colony stimulating factor (GM-CSF) in nociceptor activation in male and female mice. Previous studies have suggested GM-CSF might directly activate neurons. However, here we established the absence of a functional GM-CSF receptor in murine nociceptors, and suggest an indirect mechanism of action, via immune cells. We report that GM-CSF applied directly to magnetically purified nociceptors does not induce any transcriptional changes in nociceptive genes. In contrast, conditioned medium from GM-CSF-treated murine macrophages was able to drive nociceptor transcription. We also found that conditioned medium from nociceptors treated with the well established pain mediator, nerve growth factor, could also modify macrophage gene transcription, providing further evidence for a bidirectional crosstalk.

Key words: **chronic pain; GM-CSF; neuroimmune interaction**

Significance Statement

The interaction of the immune system and the nervous system is known to play an important role in the development and maintenance of chronic pain disorders. Elucidating the mechanisms of these interactions is an important step toward understanding, and therefore treating, chronic pain disorders. This study provides evidence for a two-way crosstalk between macrophages and nociceptors in the peripheral nervous system, which may contribute to the sensitization of nociceptors by cytokines in pain development.

Introduction

Chronic pain is a debilitating condition affecting large numbers of people (Phillips, 2009), with the prevalence in Europe estimated to be ~20% (Breivik et al., 2006). More surprising perhaps is that >50% of those suffering do not respond or get effective relief with current treatments (Nicol et al., 2018). Over the last decade, considerable advances have been made toward understanding the neurobiological mechanisms underlying chronic pain, with several promising trials of new classes of drug (Brown et al., 2012; Ford, 2012; Schwertner et al., 2013).

Substantial evidence has been presented to suggest that the interaction between neurons and immune cells can result in pain-related conditions stemming from the activation of nociceptors by immune system mediators (Marchand et al., 2005; Cook et al., 2018; Hore and Denk, 2019). Cytokines are also potent neuromodulators that are capable of activation and sensitization of nociceptors (Moalem and Tracey, 2006; Scholz and Woolf, 2007). One such mediator that we have chosen to investigate in

Received Sept. 16, 2019; revised Jan. 7, 2020; accepted Jan. 14, 2020.

Author contributions: D.T., A.D. Cook, J.E.S., J.A.H., and S.B.M. designed research; D.T., A.D. Cook, M.-C.L., A.D. Christensen, A.C., B.B., D.P., P.R., and N.B. performed research; D.T. analyzed data; D.T., A.D. Cook, J.A.H., and S.B.M. wrote the paper.

This work was supported by the Wellcome trust Senior Investigator Award to S.B.M., GlaxoSmith-Kline, and by Grant 1043147 from the National Health and Medical Research Council of Australia. We thank Dr. Franziska Denk for advice on accessing publicly available RNA-seq data. Julia E. Smith is an employee of GSK.

J.E.S. is an employee and shareholder of GSK. The remaining authors declare no competing financial interests.

Correspondence should be addressed to Damini Tewari at damini.1.tewari@kcl.ac.uk.

https://doi.org/10.1523/JNEUROSCI.2268-19.2020

Copyright © 2020 the authors

this study is granulocyte-macrophage colony stimulating factor (GM-CSF).

GM-CSF has been shown to act as a proinflammatory cytokine (Hamilton, 2008). GM-CSF can enhance antigen presentation and drive macrophages into a proinflammatory phenotype that produces inflammatory cytokines such as TNF, IL-6, IL-1β, and CCL17 (Cook et al., 2004; Fleetwood et al., 2007; Hamilton, 2008; Metcalf, 2008; Achuthan et al., 2016; Wicks and Roberts, 2016). GM-CSF signaling requires the presence of the GM-CSF receptor (CSF2R), a heterodimer made up of a low-affinity ligand binding α chain (CSF2Rα) and the signal transducing β chain (CSF2Rβ) in a ternary complex (Hamilton, 2008; Hansen et al., 2008; Broughton et al., 2016). Downstream signaling of GM-CSF involves the Ras/MAPK pathway as well as the JAK/STAT pathway (Hansen et al., 2008; Broughton et al., 2016).

Within the CNS, GM-CSF has been shown to play a neuroinflammatory role by activating microglia (Parajul et al., 2012; Nicol et al., 2018). The expression of GM-CSFR has also been shown to be increased in infiltrating macrophages and in microglia-like cells in human spinal cord of patients with multiple sclerosis (Donatien et al., 2018). Inhibition of GM-CSF signaling was found to attenuate arthritic pain (Cook et al., 2012). Additionally, silencing GM-CSF and the gene for its receptor resulted in analgesic effects in models of bone cancer and inflammatory pain (Schweizerhof et al., 2009; Cook et al., 2013). Functional studies have shown that injection of GM-CSF into the paw of laboratory animals produces pain-related behavior (Schweizerhof et al., 2009; Achuthan et al., 2016).

However, the pathways and mechanisms behind GM-CSF mediated pain remain elusive (Wicks and Roberts, 2016). There have been claims that the receptor for GM-CSF is expressed in the peripheral nervous system, suggesting that GM-CSF could directly activate nociceptors and thereby drive pain and hyperalgesia (Schweizerhof et al., 2009; Bali et al., 2013). However, multiple recent high-throughput RNA sequencing studies suggest that neurons in the dorsal root ganglion (DRG) express the *CSF2R*α transcript at very low levels but do not express any *CSF2R*β (Thakur et al., 2014; Flegel et al., 2015; Lopes et al., 2017; Zeisel et al., 2018). Because both receptor subunits are needed for GM-CSF signaling, these datasets suggest that any effect of GM-CSF on neurons would have to be indirect, i.e., via another cell type. Many immune cells found in neuronal tissues do express appropriate receptors. Many studies of GM-CSF have to date studied systems containing multiple cell types, making it difficult to identify direct versus indirect effects.

This study addresses this discrepancy and seeks to elucidate the mechanism behind the activation of nociceptors by GM-CSF. It demonstrates that GM-CSF can exert an indirect effect on nociceptors via macrophages. We show that pain-related genes are transcriptionally upregulated by conditioned media from bone marrow-derived macrophages (BMDMs) treated *in vitro* with GM-CSF. Hence, although GM-CSF may be incapable of directly activating nociceptors, it can do so indirectly, and contribute to the algesic effects of GM-CSF.

Materials and Methods

Animals. For most experiments, adult female C57BL/6J mice 6–8 weeks of age, weighing ~20–25 g were ordered from Envigo. The animals were housed with a 12 h light/dark cycle with lights on between 7:00 A.M. and 7:00 P.M. and unrestricted access to food and water. Animals were housed in groups of 4–8 and cared for in accordance to the United Kingdom Animals Scientific Procedures Act (1986).

In some experiments, adult male and female C57BL/6J mice from the Walter and Eliza Hall Institute were used. *Nav1.8*-cre *Csf2rb*$^{fl/fl}$ mice were generated by crossing the *Csf2rb*$^{fl/fl}$ mouse (Croxford et al., 2015) with the *Nav1.8*-cre mouse (gift from J. N. Wood, Institute for Biomedical Research, University College London, London; described by Stirling et al., 2005), i.e., mice with any GM-CSFR expression deleted in Nav1.8^{+} neurons. Where appropriate, experiments were approved by The University of Melbourne Animal Ethics Committee.

Isolation of DRGs and their dissociation by magnetic separation. Adult female C57BL/6J mice were killed with an overdose of pentobarbital and death confirmed by decapitation. The DRG were taken from all vertebral levels as previously described (Malin et al., 2007). DRG were washed in F12 medium and then dissociated by enzymatic digestion, followed by gentle mechanical dissociation (Thakur et al., 2014). The single-cell suspension was exposed to a biotinylated non-neuronal antibody mixture (Miltenyi MACS Neuron Isolation Kit), followed by antibiotin microbeads (Miltenyi MACS Neuron Isolation Kit). Cells were then run through a LD exclusion column and placed in a QuadroMACS separator (Miltenyi Biotec) so that only neuronal cells were eluted (>95% pure neuronal cells generated). Neurons were then plated on Matrigel-coated coverslips and cultured for 48 h (5% CO_2, 95% O_2, at 37°C) in medium with different stimuli as discussed in the following sections on cell culture. For the initial set of experiments, magnetically-activated cell sorting (MACS) nociceptor cultures were prepared in parallel to traditional whole DRG cultures. These were treated for 48 h with either mouse GM-CSF (2 μg/ml; Peprotech) or, as a positive control, mouse 2.5S nerve growth factor (NGF; 10 ng/ml; Alomone Labs).

BMDM isolation and cell culture. Adult female C57BL/6J mice were killed with pentobarbital and death confirmed by decapitation. The lower body was sterilized with 70% ethanol. The skin, muscles and fat surrounding femur, tibia, and fibula were removed, and the bones collected in cold DMEM. The bones were flushed with 5–10 ml of cold PBS and the cells collected, resuspended and plated in DMEM containing 10% FBS, 1% penicillin–streptomycin (Sigma-Aldrich) and macrophage-CSF (M-CSF; CSF-1; PeproTech). Cultures were maintained for 1 week at 37°C (5% CO_2/95% O_2). Once confluent, cells were incubated with non-enzymatic cell dissociation buffer (Millipore) at 37°C for 10 min, scraped carefully and re-plated at a density of 30,000–50,000 cells per well in DMEM containing M-CSF. Twenty-four hours later, the medium was replaced with M-CSF-free medium and cells were treated with either GM-CSF (2 μg/ml) or LPS (100 ng/ml) for 48 h.

Cross stimulation of nociceptor and BMDM cultures. To look for indirect effects of mediators on pure nociceptors and BMDMs, MACS-sorted neurons and BMDMs were cultured for 48 h with either media alone, GM-CSF, or, as a positive control, NGF (for neurons) or LPS (for BMDMs). Forty-eight hours later, fresh cultures of MACS-sorted neurons and BMDMs were plated, as described. Supernatants from the neurons treated for 48 h were added to the fresh BMDM cultures, and similarly supernatants from the BMDMs treated for 48 h were added to the fresh neuron cultures. Supernatants were centrifuged to remove any cells and then 1 ml was added to the respective wells. These were further cultured for 24 h, following which cells were taken for RNA extraction and gene expression analysis.

RNA extraction and TaqMan qPCR array cards. In each of the experiments, cells were lysed and RNA was extracted from cultured whole DRG and MACS-sorted DRG samples using the RNeasy microkit (Qiagen) following the manufacturer's protocol with some minor modifications. RNA integrity was assessed on the Agilent 2100 Bioanalyzer Pico Chip (Agilent). The RNA integrity number (RIN) for each of the samples used was >8. Samples with a RIN of <8 were not used for qPCR analysis. Following RNA extraction, the samples were amplified and reverse transcribed using the Repli-g WTA single-cell amplification kit (Qiagen). The cDNA was used for gene expression analysis by using the TaqMan custom-made microfluidic array cards (ThermoFisher). These custom-made cards were designed in-house and contained primers and probes to detect 45 test genes as well as three housekeeping genes for reference [*18S, GAPDH*, and *Ywhaz* (*B2M* in macrophage card)]. Three types of cards were used in this study. The first card, used to look for differences between whole DRG and MACS-sorted samples, contained probe sets for a

Table 1. Genes probe sets present on qPCR array cards

A		B		C	
Adcyap1	Tac1	Gapdh	Sfpq	Arg1	Il4ra
Atf3	Trpa1	Ywhaz	Scn10a	B2m	Il6
Bdnf	Trpv1	Hbb	Calca	Gapdh	Irf4
Cacna2d1	Gapdh	Fabp7	Hoxb5	Ccl17	Irf5
Calca	Ywhaz	Sox10	Kcnt1	Ccl22	Mertk
Ccl2	Il6st	CCL21b	Scn4a	Ccl24	Mmp9
Nos1	Ccl4	Csf1	Prdm12	Ccr2	Nfkbiz
Vgf	Il6	Il34	Gamt	Ccr6	Nos2
Gal	Il11	Gap43	Prmt8	Cd19	Ppard
Gch1	Stat3	Gal	Ngf	Fcgr1	Pparg
18S	Tnf	18S	Areg	18S	Ptgs2
Ngf	Tlr4	Bdnf	Il6	Chil3	Retnlb
Ngfr	Il1b	Sema6a	Vgf	Cybb	Sbno2
Npy	Ccl3	Npy	Dpysl5	Foxp3	Socs1
Ntrk1	Ccl5	Nts	Jak2	Gata3	Socs2
Ntrk2	Cxcl12	Npy2r	Srrm4	Gata6	Socs3
Ntrk3	Il18	Star	Camk1	Ido1	Sox10
Oprm1	Areg	Adam8	Usp18	Ifng	Stat1
P2rx3	Csf1	Casp3	Ntrk1	Il10	Stat6
P2rx4	Csf3	Atf3	Ucn	Il12a	Tbx21
Il6ra	Csf2ra	Cacna2d1	Jun	Il1b	Dpysl5
Scn10a	Ccl20	P2rx3	Anxa1	Il22	Tgfb2
Scn11a	Il17a	Kcnmb1	Ngfr	Il27	Tnf
Scn9a	Ereg	Dnm3	Tnfsf12	Il4	Nfil3

A, Genes represented on a DRG card. B, Genes represented on an axotomy card. C, Genes represented on a macrophage card.

mixture of neuronal and non-neuronal genes known to be present in the DRG that can be activated by NGF and other mediators. These include genes such as *TRPVI* and *TRPA1*, ion channels widely expressed on neuronal cells known to be involved in nociception (Caterina and Julius, 2001; Bevan et al., 2014; Huang et al., 2017). In addition, the array card contained probe sets for some cytokine and chemokine genes. The second card contained probe sets for genes that are known to be specifically involved in axotomy and pain-related behavior. These included neuropeptides, such as galanin and neuropeptide Y, known for their role in nociception (Kerr et al., 2000; Brothers and Wahlestedt, 2010), proteins such as annexin 1 and ADAM8 known for their role in modulating inflammatory pain (Schlomann et al., 2000; Chen et al., 2014) in addition to other markers associated with pain such as CSF-1, BDNF, and NGF. Finally, the third card contained probe sets for genes that are present in macrophages. They include canonical inflammatory mediators such as IL6, TNF, and CCL17 (Laskin, 2009). The transcripts measured by each card are given in Table 1.

Each cDNA sample was quantified using a Qubit BR ssDNA assay kit and diluted in PCR grade water to a final concentration of 6 ng/μl. This was added to TaqMan Universal 2x Master mix (ThermoFisher) to achieve a final volume of 100 μl. TaqMan array cards were run on a 7900HT Fast Real-Time PCR system (Applied Biosystems) and gene expression calculated using the ddCT method (normalizing each sample to the average of the three housekeeping genes and then to their respective internal controls, usually the unstimulated/untreated samples). Samples with cycling thresholds of 40 in the unstimulated conditions were not included in the analysis.

Measurement of $[Ca^{2+}]_i$ in DRG neuron. Mouse DRG neurons were dissociated from whole DRGs as previously described (Rajasekhar et al., 2015) and plated onto coverslips coated with poly-L-lysine and 100 μg/ml laminin. The DRG neurons were maintained in DMEM containing antibiotic-antimitotic, 10% FBS, and N-1 supplement at 37°C (5% CO_2/95% O_2) for 24 h. The DRG neurons were loaded with Fura-2/AM ester (5 μM, 45 min, 37°C) in calcium assay buffer (10 mM HEPES, 0.5% BSA, 10 mM [SCAP] [SCAP]D[SCAP]-glucose, 2.2 mM $CaCl_2{\cdot}6H_2O$, 2.6 mM KCl, 150 mM NaCl) containing 4 mM probenecid and 0.05% pluronic F127. Cells were washed and incubated in calcium assay buffer for 30 min before imaging. Cells were observed using a Leica DMI-6000B microscope with an HC PLAN APO 0.4 numerical aperture 10× objective and maintained at 37°C. Images were collected at 1 s intervals (excitation: 340 nm/380 nm; emission: 530 nm). Cells were challenged sequentially with vehicle, GM-CSF (200 ng/ml), capsaicin (0.5 μM; TRPV1 agonist). KCl (50 mM) in calcium assay buffer containing probenecid, was applied at the end of the experiment to obtain maximal $[Ca^{2+}]i$.

Results are expressed as the 340/380 nm fluorescence emission ratio, which is proportional to changes in $[Ca^{2+}]i$. Data are presented as $F/F0$, where F is the measured fluorescence intensity and $F0$ is the basal fluorescence. All $F/F0$ values have been subtracted by 1. In each experiment two technical replicates were included with 68–559 neurons recorded in each repeat. The experiment was repeated three times ($n = 3$) with equivalent results. A response was deemed positive if it was ≥10% above baseline. Results were excluded from the analysis if they showed a fluctuating calcium response before addition of GM-CSF or did not show pronounced reversibility (>50%) from the peak response to GM-CSF application and did not respond to KCL addition. This constituted <1% of DRG neurons studied.

Detection of ERK1/2 and STAT5 activation in neurons stimulated with GM-CSF. The dissociated DRG neurons plated onto coverslips, as described above for measurement of $[Ca^{2+}]$ (Rajasekhar et al., 2015), were also used for the detection of ERK1/2 and STAT5 activation following GM-CSF stimulation. Following a 24 h culture in DMEM containing antibiotic-antimitotic, 10% FBS, and N-1 supplement at 37°C (5% CO_2/95% O_2), the neurons were serum-starved overnight (17–18 h) by incubating them in DMEM supplemented with 0.1% (w/v) BSA, 100 U/ml penicillin, 100 mg/ml streptomycin, and 1% (v/v) N1 in a humidified incubator at 37°C (95% O_2, 5% for CO_2). Subsequently, neurons were stimulated for 15 min with PBS, GM-CSF (200 ng/ml) or PMA (2 μM; Sigma-Aldrich). Cells were then washed in ice-cold PBS and fixed in 4% paraformaldehyde in PBS for 20 min at room temperature. After three washes with PBS, cells were blocked and permeabilized by incubating with PBS supplemented with 0.01% Triton-X, 5% heat-inactivated FBS, and 5% goat serum for 60 min. Neurons were washed (3× PBS), then stained overnight with mouse anti-mouse NeuN mAb (clone A60; Millipore) in combination with either rabbit anti-mouse phospho-p44/42 MAPK (Erk1/2) (Thr202/Tyr204) (197G2) mAb (Cell Signaling Technology) or rabbit anti-mouse phospho-STAT5 (Y694) (D47E7) XP mAb (Cell Signaling Technology); all primary antibodies were diluted in PBS with 5% FBS and 0.01% Triton-X. Following washing (3× PBS), neurons were incubated with goat anti-rabbit IgG (H+L) antibody, AlexaFluor 568 conjugate (ThermoFisher) and goat anti-mouse IgG (H+L) antibody, Alexa Fluor488 conjugate (ThermoFisher). Neurons were washed (3× PBS), then stained with DAPI (1 μg/ml, 5 min; EMD Millipore). In all experiments, secondary antibody only and single primary antibody controls were included to check for nonspecific secondary binding and bleed-through of fluorochromes, respectively.

Images were obtained with a Zeiss Axioskop 2 at 10× magnification and captured by a Zeiss AxioCam MRm. Each condition included two technical replicates and five images were taken from each replicate. Quantification of positive cells was performed with ImageJ software. For neurons, only NeuN-positive cells were included in the analysis. To determine when cells were positive a lower threshold for staining intensity in the green channel (AlexaFluor 488) was set based on the PBS-treated control cells. Cells with fluorescence intensities above this threshold were regarded as positive. A mean of positive cells across the 10 images from each condition was calculated. Three separate experiments were performed.

GM-CSF-induced inflammatory pain. Inflammatory pain was induced by a single intraplantar injection (10 μl) of GM-CSF (50 ng/paw; R&D Systems) into the left hind footpad (Achuthan et al., 2016; Cook and Hamilton, 2018).

mBSA/GM-CSF-induced arthritis. Monoarticular arthritis was induced by an intraarticular injection of methylated BSA (mBSA; 100 μg in 10 μl) into the right knee on Day 0, and saline into the left knee, followed by a subcutaneous injection of GM-CSF (600 ng) into the scruff of the neck on Days 0–2, as before (Achuthan et al., 2016; Cook and Hamilton, 2018). Mice were killed (Day 7) and knee joints were removed, fixed, decalcified, and paraffin embedded (Achuthan et al., 2016; Cook and Hamilton, 2018). Frontal sections (7 μm) were stained with H&E and

cellular infiltration, synovitis, pannus formation, cartilage damage, and bone erosions were each scored separately from 0 (normal) to 5 (severe) as described previously (Achuthan et al., 2016; Cook and Hamilton, 2018); these scores were then added to give the total histologic score for each mouse.

Assessment of pain-related behaviors. As an indicator of pain, the differential weight distribution over a 3 s period between the inflamed paw or limb relative to the non-inflamed paw or limb was measured using the incapacitance meter (IITC Life Science). This technique has been validated for measurement of both paw and arthritic knee pain (Achuthan et al., 2016; Cook and Hamilton, 2018). Mice were acclimatized to the incapacitance meter on at least 3 separate days before the commencement of the experiment. Three measurements were taken for each time point and averaged.

Experimental design and statistical analysis. All data are expressed as mean ± SEM, except where stated as median. Statistical analyses were performed using SPSS v23 (IBM). Kruskal–Wallis nonparametric independent samples tests were used for analysis of Figures 1, 3, and 4. The samples were corrected for multiple testing using the Bonferroni correction. For calcium imaging in Figure 2, GM-CSF activation of neurons and histology, a one-way ANOVA was used, and for pain readings, a two-way ANOVA was used, with either a Bonferroni or Tukey *post hoc* test. A p value <0.05 was considered significantly different to the null hypothesis of no difference at the 95% confidence level.

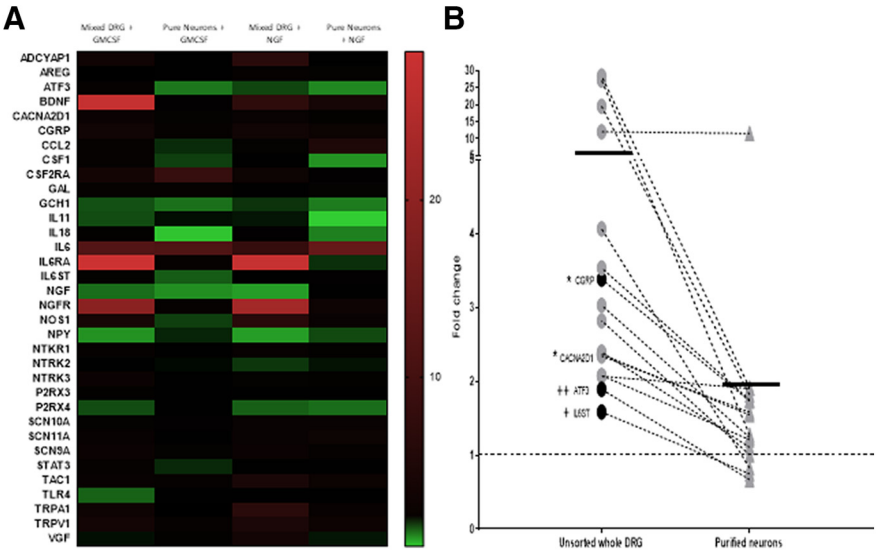


Figure 1. GM-CSF causes dysregulation of genes in mixed DRG cultures but not in purified neuronal cultures. ***A***, Heatmap representing the transcriptional changes in a panel of genes (Table 2) was assessed in mixed DRG cultures and pure MACS sorted neuronal cultures from C57BL/6J mice following treatment with GM-CSF (2 μg/ml) for 48 h and NGF (10 ng/ml). Each column represents average data of $n = 8$ independent experiments. Each individual experiment contained pooled cells from two mice. ***B***, Genes showing a twofold or greater change in expression changes following GM-CSF treatment in unsorted DRG cell cultures as compared with purified neurons. Each dot represents a separate gene which is an average of $n = 8$ experiments. Dotted line represents untreated control. Solid line represents mean of each group. Kruskal–Wallis test was conducted to identify genes that were significantly modulated after treatment with GM-CSF in mixed DRG cultures (highlighted black dots). The results were corrected for multiple comparisons using the Bonferroni correction. None of the genes from purified neuronal cultures reached statistical significance after GM-CSF treatment. *adjusted $p < 0.05$; *genes significantly different from untreated control. +adjusted $p < 0.05$ and ++adjusted $p < 0.01$; +genes significantly different between whole DRG and purified neurons.

Results

The literature around the involvement of GM-CSF in chronic and neuropathic pain remains sparse. However, even within this limited literature there is little consensus on the possible mechanisms behind the actions of GM-CSF in pain. To clarify, we have undertaken a number of experiments, as follows in the next sections.

GM-CSF does not modulate gene expression in purified neurons from mouse DRG

Previous studies have reported that GM-CSF can act directly on nociceptive neurons, and as a result, cause hyperalgesia (Schweizerhof et al., 2009; Parajul et al., 2012). Here, we began by addressing the discrepancy in the literature on the mode of action of GM-CSF by using MACS to enrich for small and medium diameter neurons (which are nearly all nociceptors) from mouse DRG. Thakur et al. (2014) showed that dissociated DRG preparations that are commonly used for analysis actually contain predominantly non-neuronal cells. In contrast, they showed, that following MACS isolation, a culture of 95% pure nociceptors can be produced from adult mouse DRG. Large diameter neurons (>30 μm), which are lost during MACS, are largely non-nociceptive (Dubin and Patapoutian, 2010), and hence their absence is an asset rather than a disadvantage when studying the role of GM-CSF is nociception and peripheral sensitization.

Parallel cultures of cells from adult mouse DRG were set up using either the traditional dissociation technique to prepare the mixed (i.e., unsorted) cultures and purified cultures (i.e., sorted) from adult mouse DRG obtained after MACS. For these sets of experiments, 48 genes that are known to be expressed in the DRG, including some internal housekeeping controls (*GAPDH, 18S* and *YWhAZ*), were developed into a Taqman qPCR array card (Thermofisher). This card was used as a screening tool to help provide an indication toward specific pathways or areas of interest to be investigated further. The list of genes present on the card is provided in Table 1, column A.

Figure 1*A* is a heatmap that shows the gene expression changes in mixed DRG cultures and pure neurons following GM-CSF and NGF treatment in the panel tested. It is evident that GM-CSF had an overall greater impact in mixed cultures as compared with pure neuronal cultures. Only 6% of the genes ($n = 2/34$, namely CSF2RA and IL6) showing a >2-fold average increase in expression level following GM-CSF treatment in the purified neuronal cultures and none of the differences reached statistical significance.

However, when GM-CSF was applied to the mixed DRG cultures, 44% of the genes ($n = 15/34$) showed a twofold or more average increase in gene expression, and four of these were found to reach statistical significance with an average increase in expression of 2.3-fold. Figure 1*B* shows the significantly altered genes (black dots) along with those showing a >2-fold increase in expression. The overall average increase in gene expression in the mixed cultures with GM-CSF stimulation was 3.9-fold, whereas purified cultures following GM-CSF stimulation showed an average of 1.6-fold increase.

As a positive control, we applied NGF instead of GM-CSF to the mixed and purified cultures and found, as expected, a significantly increased expression of 12 and 5 genes, respectively. Fifty percent of the genes showed a twofold or greater average increase in expression in the mixed DRG cultures, whereas ~32% of the genes in purified cultures showed a two-fold or more average increase in expression. The average fold increase of the significant

Table 2. GM-CSF receptor subunit expression in neurons by RNA sequencing[1]

Bulk-sequencing							
	Mouse tissue			Human tissue			
	Thakur et al., 2014; MACS-sorted nociceptors	Lopes et al., 2017; MACS-sorted nociceptors after nerve injury	Lopes et al., 2017; FACS-sorted nociceptors	Flegel et al., 2015; Whole DRG	Ray et al., 2018; Whole DRG	Ray et al., 2019; Human tibial nerve	
Expression Units	FPKM	FPKM	FPKM	FPKM	TPM		TPM
Csf2ra	4	3	2	0	0	CSF2RA	15
Csf2rb	1	0	0	1	1	CSF2RB	6
Calca	912	3987	10287	313	1701	CD40	49
TrpV1	58	154	112	48	73	TRPV1	7
Dnmt3a	4	2	2	5	4	UCHL1	92

Expression values derived from publicly available bulk RNA-sequencing datasets. Data for Csf2ra and Csf2rb are provided along with the following control/comparison genes: *Calca*, which is one of the most highly expressed genes in DRG; *TrpV1*, which is well expressed in nociceptive neurons; *Dnmt3*a, which is very lowly expressed if at all in neurons (Saunders et al., 2018); *Nav1.8*; CD40, a myeloid cell marker; and *Uchl1*, the gene coding for a protein which is highly expressed in nerve fibers,. FPKM, Fragments per kilobase per million mapped reads; TPM, transcripts per million.

Table 3. Single-cell Sequencing of mouse DRG (Zeisel et al; mousebrain.org): Trinarization scores

	Csf2ra	Csf2rb	Calca	TrpV1	Dnmt3a	Nav1.8
Peptidergic (TrpM8), DRG	0.18	0	0.39	2.21	0.36	0
Peptidergic (TrpM8), DRG	0.27	0	0.32	0.67	0.11	0.08
Peptidergic (TrpM8), DRG	0.11	0	4.04	0.31	0.22	0
Peptidergic (PEP1.2), DRG	0.2	0	11.3	3.07	0.1	0.19
Peptidergic (PEP1.3), DRG	0.13	0	43.4	2.68	0.15	1.56
Peptidergic (PEP1.1), DRG	0.19	0	37.3	1.02	0.13	1.16
Peptidergic (PEP1.4), DRG	0.19	0	52.3	3.26	0.32	2.51
Peptidergic (PEP2), DRG	0.12	0	61.6	0.56	0.24	3.38
Neurofilament (NF2/3), DRG	0	0	0.64	0	0.19	0.61
Neurofilament (NF4/5), DRG	0.11	0	0.07	0.05	0.35	0.04
Neurofilament (NF1), DRG	0.08	0	0.07	0	0.13	0.03
Non-peptidergic (TH), DRG	0.18	0	0.17	0.01	0.35	1.08
Non-peptidergic (NP1.1), DRG	0.15	0	6.38	0.06	0.33	3.71
Non-peptidergic (NP1.2), DRG	0.22	0	3.23	0.05	0.27	5.28
Non-peptidergic (NP2.1), DRG	0.24	0	11.1	0.04	0.38	5.47
Non-peptidergic (NP2.2), DRG	0.18	0	34.5	0.73	0.27	4.99
Non-peptidergic (NP3), DRG	0.26	0	0.74	1.95	0.26	4

Expression values derived from publicly available B single-cell RNA-sequencing datasets. Data for Csf2ra and Csf2rb are provided along with the following control/comparison genes: *Calca*, which is one of the most highly expressed genes in DRG; *TrpV1*, which is well expressed in nociceptive neurons; *Dnmt3*a, which is very lowly expressed if at all in neurons (Saunders et al., 2018); *Nav1.8*; CD40, a myeloid cell marker; and *Uchl1*, the gene coding for a protein which is highly expressed in nerve fibers.

genes was 5.8- and 2.5-fold in the mixed and purified cell cultures, respectively (data not shown).

These results suggest that GM-CSF is incapable of driving direct transcriptional changes in neuronal genes in nociceptors. However, changes in neuronal genes in the mixed cultures following GM-CSF treatment indicate that it might be having an indirect effect on nociceptors via satellite cells or other non-neuronal cell types that make up the majority of the cells in the DRG, and indeed in the mixed DRG cultures. To obtain supporting evidence for the proposal that GM-CSF is incapable of directly stimulating nociceptor transcription, we reviewed recent publications that have made use of RNA sequencing to examine gene expression in mouse and human DRG (Tables 2, 3; Thakur et al., 2014; Flegel et al., 2015; Lopes et al., 2017; Ray et al., 2018, 2019; Zeisel et al., 2018). The Table compares the expression of the two GM-CSF receptor chains to several control transcripts: *Calca*, one of the most highly expressed genes in DRG; *TrpV1* and *Nav1.8*, which are well expressed in nociceptive neurons; and Dnmt3a, which is very lowly expressed (Saunders et al., 2018). It is evident the two transcripts coding for the receptor chains of the GM-CSF receptor, namely *CSF2Rα* and *CSF2Rβ*, are expressed at levels below our negative control transcript in the DRG, the *CSF2Rβ* gene, in particular, appears to be undetectable, even by a technique as sensitive as RNA-seq. In whole human tibial nerve, mRNA for both receptors can be detected at higher levels, presumably because of a contribution from non-neuronal cells (Ray et al., 2019).

GM-CSF does not directly activate neurons in vitro and in vivo

To support the above gene expression data, suggesting an indirect effect of GM-CSF on neurons, we monitored some signaling pathways in cultured DRG neurons. We were unable to observe any GM-CSF-stimulated elevation in intracellular Ca^{2+} levels (Fig. 2*A*,*B*) or ERK1/2 phosphorylation (Fig. 2*C*) compared with our positive controls, namely capsaicin and PMA, respectively. We were also unable to detect STAT5 phosphorylation following GM-CSF stimulation in these neurons, unlike in murine macrophages grown from bone marrow cells in GM-CSF (Fleetwood et al., 2007; data not shown).

Table 3 indicates that Nav1.8$^+$ neurons do not express the *Csf2rb* gene and therefore cannot express a functional GM-CSFR. To demonstrate *in vivo* that GM-CSF-induced pain development is not due to GM-CSF receptor signaling via Nav1.8$^+$ neuronal cells (that is, the majority of nociceptors), *Nav1.8*-cre *Csf2rb*$^{fl/fl}$ mice were generated by crossing the *Csf2rb*$^{fl/fl}$ mouse (Croxford et al., 2015) with the *Nav1.8*-cre mouse (Stirling et al., 2005), these mice will lack any functional GM-CSF receptors that may possibility be expressed in Nav1.8$^+$ neurons. GM-CSF-induced inflammatory pain and GM-CSF-induced arthritic pain were then initiated, and pain development measured by a change in weight distribution (using the well validated incapacitance meter method; Achuthan et al., 2016; Cook et al., 2018). Following intraplantar injection of GM-CSF, pain was evident in *Csf2rb*$^{fl/fl}$ control and also in *Nav1.8*-cre *Csf2rb*$^{fl/fl}$ mice (Fig. 2*D*). Similarly, following induction of mBSA/GM-CSF arthritis, similar pain development was evident in WT, *Csf2rb*$^{fl/fl}$ control and *Nav1.8*-cre *Csf2rb*$^{fl/fl}$ mice from Day 3 onward (Fig. 2*E*); all three strains developed a similar degree of arthritis (at Day 7, as judged by histology; Fig. 2*E*). Together, these *in vitro* and *in vivo* data do not support a direct action of GM-CSF on neurons consistent with a lack of GM-CSF receptor gene expression in neurons.

Nociceptor gene expression can be indirectly modulated by GM-CSF stimulated BMDMs

As mentioned, based on these data, we hypothesized that GM-CSF might be having an indirect effect on nociceptors via non-neuronal cells that are present within the DRG and in the

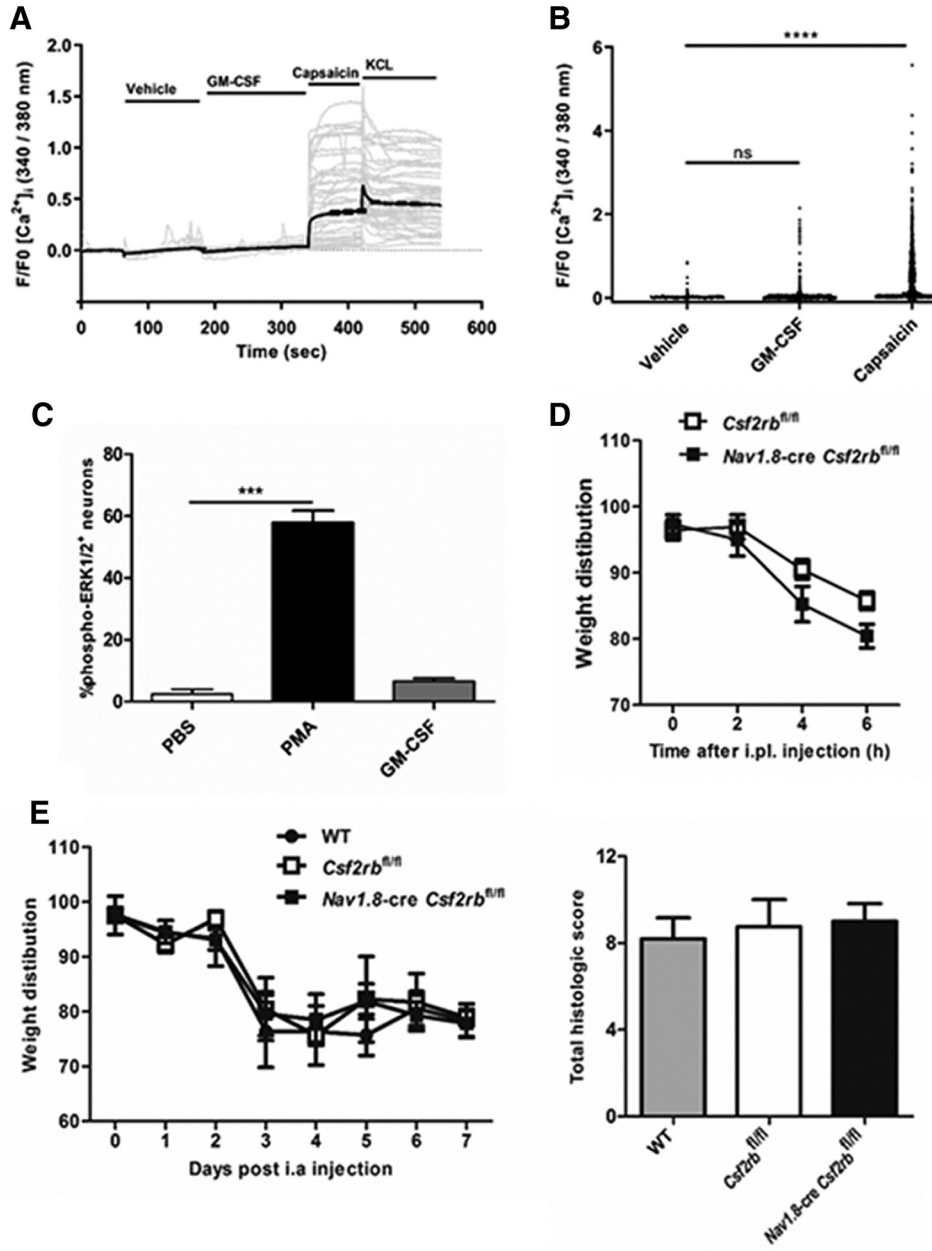


Figure 2. GM-CSF does not directly activate neurons *in vitro* and *in vivo*. ***A***, ***B***, Time course and peak Ca^{2+} responses in mixed DRG cultures in response to vehicle, GM-CSF (200 ng/ml), capsaicin (0.5 μM), and KCl (50 mM; only ***A***), respectively. ***A***, Gray lines, Individual traces from 50 random cells; black lines, mean response; (***B***) $n = 1767$ neurons (pooled data from two independent experiments). ***C***, Percentage of DRG neurons positive for phospho-ERK1/2 following stimulation with PBS, PMA, or GM-CSF (200 ng/ml) for 15 min. Three independent experiments were performed. ***D***, ***E***, Pain development (incapacitance meter, ratio of weight bearing on injected relative to non-injected knee/hindpaw, a value <100 indicates pain) was measured following (***D***) intra-planatar (i.pl.) injection of GM-CSF (20 ng) in *Csf2rb*$^{fl/fl}$ and *Nav1.8*-cre *Csf2rb*$^{fl/fl}$ mice ($n = 5–8$ mice/group); and (***E***) mBSA/GM-CSF arthritis [mBSA intra-articular (i.a.) (Day 0); GM-CSF or saline subcutaneously (Days 0–2)] induction in WT, *Csf2rb*$^{fl/fl}$, and *Nav1.8*-cre *Csf2rb*$^{fl/fl}$ mice ($n = 4–7$ mice/group). Arthritis (histology, Day 7) was also assessed in ***E***. ***C–E***, Data are expressed as mean ± SEM. For ***B*** and ***C***, a one-way ANOVA was used. $^{***}p < 0.001$, $^{****}p < 0.0001$.

periphery at a site of injury. Macrophages are one cell type present in the DRG and known to be responsive to GM-CSF as well as being a potential source of pain mediators (Cook et al., 2018; Hore and Denk, 2019). To look for potential indirect effects of GM-CSF, supernatants from GM-CSF-stimulated BMDM cultures were added to sorted neuronal cultures to test whether these BMDMs are capable of producing mediators that can elicit transcriptional changes in neurons. Because our overall aim was to look at the mechanism of GM-CSF action in pain, a second TaqMan card containing probe sets for genes that are known to be involved in axotomy and pain-related behavior was used (Table 1, column B).

Once again, direct treatment of purified nociceptors with GM-CSF did not cause any significant dysregulation in the genes present on this array card (Fig. 3). Conditioning medium from unstimulated BMDMs had no significant impact on neuronal gene transcription (data not shown). Following treatment with conditioning medium from GM-CSF treated BMDMs, 31% of the genes tested showed twofold or more average increase in gene expression, calculated by normalizing the transcriptional changes to neuronal cultures that received supernatants from unstimulated BMDMs. Six genes were found to be significantly dysregulated following indirect stimulation with GM-CSF. These were *ADAM8* (3-fold increase), *ANXA1* (5-fold increase), *IL6* (3.5-

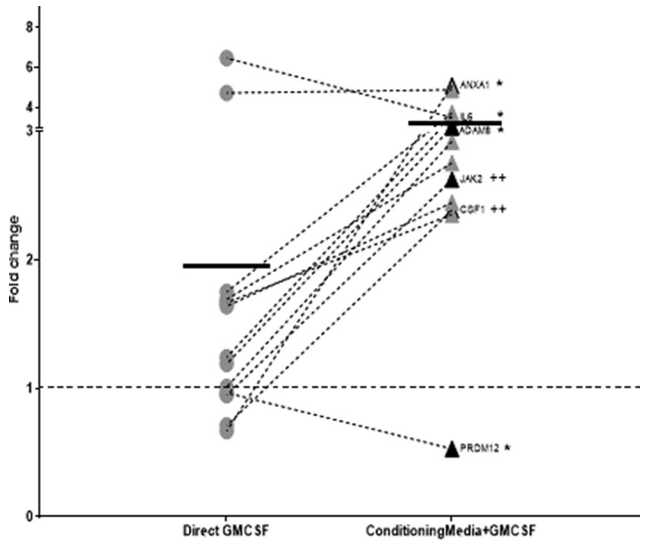


Figure 3. Nociceptor gene expression can be indirectly modulated by conditioning media from GM-CSF stimulated BMDMs. Genes dysregulated by twofold or more from nociceptors that received conditioning medium from GM-CSF (2 μg/ml) treated BMDMs. Each dot represents a separate gene which is an average of $n = 10$ individual experiments. Kruskal–Wallis test was conducted to identify genes that were significantly modulated after treatment with the conditioning medium (highlighted black dots). The results were corrected for multiple comparisons using the Bonferroni correction. None of the genes from purified neuronal cultures that were treated directly with GM-CSF (2 μg/ml) reached statistical significance. Samples with cycling thresholds of 40 in the unstimulated conditions were not included in the analysis. Dotted line represents untreated control. Solid line represents mean of each group. No significant changes were seen with untreated conditioning media control from BMDMs on neuronal cultures. *adjusted $p < 0.05$; *genes significantly different from untreated control. ++adjusted $p < 0.01$; +genes significantly different between direct GM-CSF stimulation and conditioning media with GM-CSF.

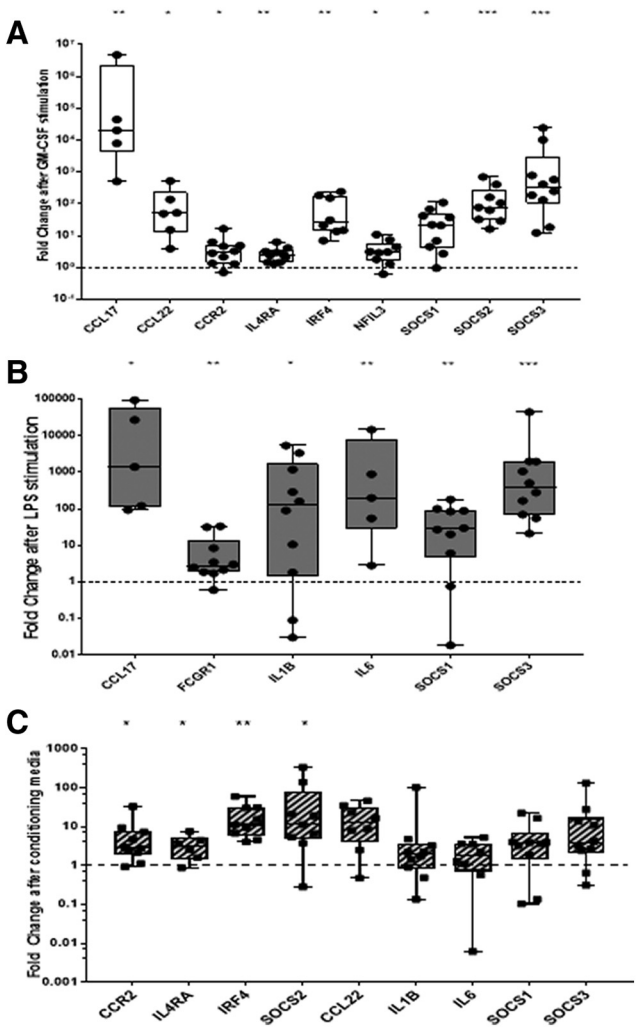


Figure 4. Macrophage gene expression can be indirectly modulated by NGF stimulated nociceptors. BMDMs were treated with (***A***) GM-CSF, (***B***) LPS, and (***C***) conditioning medium from NGF-stimulated nociceptors for 48 h (see Materials and Methods). The fold-change in the expression of dysregulated genes on a macrophage card (Table 1, column C) is depicted on a $\log_{10}$ scale. Only significantly dysregulated genes are depicted in ***A*** and ***B***. Each dot represents a separate experiment ($n = 10$). Kruskal–Wallis test was conducted to identify genes that were significantly modulated after treatment. The results were corrected for multiple comparisons using the Bonferroni correction. Dotted line represents untreated controls where conditioning media from untreated nociceptors was applied to BMDMs. No significant changes were seen in BMDM cultures treated with conditioning medium from untreated nociceptors as a control. Box-and-whisker plots showing maximum to minimum range. Samples with cycling thresholds of 40 in the unstimulated conditions were not included in the analysis. *adjusted $p < 0.05$, **adjusted $p < 0.01$, ***adjusted $p < 0.001$.

fold increase), *PRDM12* (0.5-fold decrease), *CSF-1* (2.4-fold increase), and *JAK2* (2.6-fold increase). In addition to the genes that reached statistical significance, there were several other changes in known pain-related genes, such as *TNFSF12* (3.6-fold increase), *USP18* (5-fold), *GAL* (2.9-fold), *NGF* (2.4-fold), and *NPY* (2.4-fold), which showed increased expression following indirect activation using GM-CSF treated conditioning medium, but which did not reach statistical significance (Fig. 3).

Macrophage gene expression can be indirectly modulated by NGF stimulated nociceptors

We investigated next the possibility of cross talk between stimulated nociceptors and macrophages. Although there is growing evidence to support the view that stimulated immune cells can communicate with neurons (Watkins and Maier, 2002; Marchand et al., 2005; Scholz and Woolf, 2007; Sorge et al., 2015; Hore and Denk, 2019), which is supported by the data in Figure 3, the literature on the ability of stimulated neurons to communicate with immune cells is more limited (McMahon et al., 2015). To examine this possibility, we used a similar strategy to that used in Figure 3 to explore whether nociceptors that had been treated with NGF were capable of producing mediators that could modulate macrophage gene expression. A third TaqMan card containing 48 genes, of which 29 genes are known to be expressed in macrophages at levels which depend on their functional state (Murray et al., 2014) was used (Table 1, column C).

As positive controls, we found that GM-CSF (Fig. 4*A*) and LPS (4*B*) stimulation of BMDMs, as expected, had large impacts on gene transcription. GM-CSF treatment led to 55% of the genes having a twofold or more increase in expression; of these, nine were found to be statistically significant after correcting for multiple testing. They were *Ccl17, Ccl22, Ccr2, Il4ra, Irf4, Nfil3, Socs1, Socs2*, and *Socs3* (Fig. 4*A*). Additionally, cytokine genes such as *Il6, Il1b*, and *Il27* were also found to be upregulated, although without reaching statistical significance. Stimulation of BMDMs with LPS led to 72% of the genes having a twofold or more increase in expression and, of these, six reached statistical significance, namely, *Ccl17, Fcgr1, Il1b, Il6, Socs1*, and *Socs3* (Fig. 4*B*).

Conditioning medium from unstimulated neurons had no impact on BMDM gene transcription (data not shown). Conditioning medium from NGF treated nociceptors caused a twofold or more increase in 69% of the genes. Although only four genes reached statistical significance, namely *CCR2, IL4Ra, IRF4*, and

SOCS2 (Fig. 4*C*). There were several other genes, namely *CCL22, IL1b, IL6, SOCS1*, and *SOCS3*, that showed a trend toward increased expression following treatment with NGF-stimulated conditioning medium (Fig. 4*C*). It should be noted that BMDMs do not express the receptors for NGF (TRKA and p75; e.g., see RNA-seq data by Ostuni et al., 2013; Piccolo et al., 2017; Hill et al., 2018), demonstrating that NGF-stimulated neurons can produce mediators capable of activating macrophages.

Discussion

In this present study we provide evidence that GM-CSF does not directly activate nociceptors but suggest that GM-CSF acts via macrophages to produce mediators that interact with nociceptors. We provide evidence for a bidirectional cross talk between neurons and macrophages.

Previous studies have suggested that GM-CSF can act on and stimulate sensory neurons. Bali et al. (2013) suggested that GM-CSF brought about transcriptional regulation of several pain genes in sensory neurons in a model of cancer pain, an observation replicated by Schweizerhof et al. (2009) and F. Zhang et al. (2019). Donatien et al., 2018 report that GM-CSF can enhance capsaicin-induced calcium influx in DRG neurons, although not directly induce calcium influx. However, these studies did not separate neuronal cells from non-neuronal cells within the DRG and hence it is difficult to attribute these changes specifically to sensory neurons. In contrast, other recent publications (Lopes et al., 2017; Zeisel et al., 2018) making use of RNA-sequencing to look for transcriptional changes in a cell-specific manner have indicated the absence of the GM-CSFRβ chain on nociceptors, indicating alternate mechanisms of action. In this context, a TrkA inhibitor was able to reduce the GM-CSF enhanced capsaicin-induced calcium influx response, suggesting that GM-CSF may be acting indirectly via NGF (Donatien et al., 2018).

Therefore, we looked for changes caused by stimulating purified nociceptors with GM-CSF and found no significant transcriptional changes. Also, even if there was some expression of the GM-CSF receptor on neurons, deleting the Csf2rβ subunit in Nav1.8$^+$ neurons (i.e., most nociceptors) *in vivo* showed no effect on the generation of GM-CSF-driven inflammatory and arthritic pain, suggesting that GM-CSF does not act directly via nociceptors. It has been reported that low and high threshold Aβ fibers respond to GM-CSF (Schweizerhof et al., 2009). Based on our findings, we consider that these responses are possibly indirect although further studies are needed to address this issue. Overall, our results lead us to hypothesize that the reported effects of GM-CSF on DRGs (Schweizerhof et al., 2009; Bali et al., 2013) were predominantly due to the ability of GM-CSF to activate non-neuronal cells associated with nociceptors, likely in the peripheral nerve itself or during myeloid cell infiltration into the DRG. These non-neuronal cells might then indirectly bring about transcriptional changes in nociceptors associated with pain/hyperalgesia.

Macrophages are one of the most commonly studied cell type in the pain field due to their involvement in the pathogenesis of various neuropathies (Lu and Richardson, 1993). H. Zhang et al. (2016) showed that recruitment of macrophages to the DRG was important for inducing and maintaining chemotherapy-induced peripheral neuropathy, an observation in accordance with several other studies showing increased myeloid cells in the DRG following peripheral injury (Fenzi et al., 2001; Hu and McLachlan, 2002; Hu and McLachlan, 2003). Furthermore, Shepherd et al. (2018) showed that the angiotensin II receptor (AT2R) antagonist reduces neuropathic pain by blocking the downstream signaling of AT2R in infiltrating peripheral macrophages, as sensory neurons lack expression of this receptor. Blocking of macrophage activation using TLR antagonists (Jurga et al., 2018) and inhibitors of p38 MAPK/MMP9 (Mika et al., 2007; Hutchinson et al., 2008), PI3K and NF-kB (Popiolek-Barczyk et al., 2015) has analgesic effects in various models of neuropathic pain, consistent with our proposed mechanism of action.

We therefore analyzed whether factors from stimulated macrophages can bring about transcriptional changes in nociceptors that mimic injured or activated nociceptors. We found that supernatants from GM-CSF stimulated macrophages upregulated several neuronal genes, namely *ADAM8, ANXA1, IL6, CSF-1*, and *JAK2*, which are also significantly upregulated following injury (Pei et al., 2011; Chen et al., 2014; Guan et al., 2016; Diaz-delCastillo et al., 2018; Tang et al., 2018). Supernatants from GM-CSF stimulated macrophages were found to significantly downregulate expression of *PRDM12*, an important nociceptor gene (Desiderio et al., 2019). There is evidence to suggest that, following injury, activated monocytes from the spleen and lymph nodes infiltrate into the site of injury as well as the associated DRG (Hu and McLachlan, 2002). It is expected that inflammatory cytokines from these immune cells can then impact the neurons by affecting their firing rates and causing changes in gene expression (Ohtori et al., 2004; Ozaktay et al., 2006).

Of the mediators that were upregulated in our experimental set up, CSF1 was of particular interest from the perspective of nerve injury. The role of microglia in chronic pain is well established, with various proposed mechanisms to drive microglial activation and central sensitization in a variety of pains states (Calvo and Bennett, 2012; Denk et al., 2016; Fernandez-Zafra et al., 2019). It has been demonstrated that peripheral nerve injury induces the production of CSF-1 in neurons, which then recruit spinal cord microglia to proliferate (Guan et al., 2016). The presence of large numbers of activated microglia is responsible for further activation of spinal neurons and maintenance of neuropathic pain through the release of inflammatory and neuropathic mediators (Kawasaki et al., 2008; Zhao et al., 2017). The release of CSF-1 from nociceptors raises the possibility of bidirectional cross talk with nociceptors further recruiting and stimulating macrophages in a positive feedback loop. Therefore, we looked for transcriptional changes in macrophages following treatment with conditioning media from stimulated neurons.

Analysis of macrophages at a site of nerve injury has shown them to be predominantly anti-inflammatory in nature and involved in regeneration and recovery of the nerve (Gaudet et al., 2011; Ydens et al., 2012). Interestingly, macrophages stimulated with supernatants from NGF treated neurons led to an upregulation of cytokine and chemokine receptors (IL4Ra and CCR2) and transcription factors (SOCS2 and IRF4). Because NGF by itself is incapable of directly activating macrophages (Ostuni et al., 2013; Piccolo et al., 2017; Hill et al., 2018), it can be assumed that the transcriptional changes in macrophages were due to mediators being released by these stimulated nociceptors. Furthermore, these transcriptional changes were distinct from those following direct stimulation with LPS or GM-CSF, suggesting a distinct mechanism of action. We found that NGF stimulated nociceptors upregulate the expression of inflammatory mediators and chemokines, such as IL-1β, IL6, and CCL22, which have the potential to activate and recruit macrophages.

Here we, like many others, have used *in vitro* dissociated DRG cultures to study nociceptive processes. However, unlike nearly all previous studies, we use highly purified neurons in the culture.

This allows us to disambiguate direct versus indirect effects of applied agents; a key advantage and main point of this study. The disadvantage being that the cellular properties inevitably change somewhat over time in culture as seen by transcriptional profiling of such cultures (Thakur et al., 2014; Wangzhou et al., 2019; Lopes et al., 2017). Some of the emergent changes suggest that cultured nociceptors take on a "neuropathic" phenotype (Wangzhou et al., 2019) and so one caveat of the current work is that, inevitably, the neurons we studied are not in their native state.

One of the problems we faced during these experiments was the intra-group variability observed in the transcriptional analysis. Variability in transcriptional analysis is a common phenomenon (Raser and O'Shea, 2005; Volfson et al., 2006) since transcription is not a continuous process, but rather a discontinuous one that takes place in "bursts" and "pulses". Hence differences in the expression levels of lowly and highly expressed genes can be observed even in the absence of any stimulus leading to the observed variability (Chubb and Liverpool, 2010). In this study, we have made use of stringent statistical tests to cover the inherent intra-group variability and hence identify transcripts that are genuinely dysregulated because of the treatments.

It is important to note in this context, that although nociceptor transcriptional change is very common in persistent pain states, nociceptors can be activated and sensitized without transcriptional change (Wu et al., 2001; J. M. Zhang and Strong, 2008). But transcriptional change in nociceptors, when it does occur, can lead to changes in the sensitivity and activity of these neurons and is thereby an important regulator of nociceptor function. In the current experiment we looked for acute effects of GM-CSF on calcium signaling in purified nociceptors but did not observe any of these non-transcriptional actions. Others who have seen non-transcriptional effects of GM-CSF on cultured neurons have used mixed cultures containing a variety of cell types which may allow for indirect activation of nociceptors via non-neuronal cells (Schweizerhof et al., 2009; Bali et al., 2013; Donatien et al., 2018). Indeed, in those experiments, the non-transcriptional effects of GM-CSF were blocked by trkA inhibitors, suggesting the release of secondary mediators.

In conclusion, the findings in this study highlight the need to dissect the mechanisms of action of cytokines at a cell-type-specific level, with a view to developing more targeted therapies and interventions to treat pain. Our findings support the concept that immune cells and neurons at the site of nerve injury are engaged in a loop that involves crosstalk between them. More specifically, proinflammatory mediators and cytokines released from GM-CSF stimulated monocytes or macrophages act on neurons, which in turn release neurotransmitters that can further activate these immune cells. The net effect is likely to be peripheral sensitization and consequent chronic pain.

References

Achuthan A, Cook AD, Lee MC, Saleh R, Khiew HW, Chang MW, Louis C, Fleetwood AJ, Lacey DC, Christensen AD, Frye AT, Lam PY, Kusano H, Nomura K, Steiner N, Förster I, Nutt SL, Olshansky M, Turner SJ, Hamilton JA (2016) Granulocyte macrophage colony-stimulating factor induces CCL17 production via IRF4 to mediate inflammation. J Clin Investig 126:3453–3466.

Bali KK, Venkataramani V, Satagopam VP, Gupta P, Schneider R, Kuner R (2013) Transcriptional mechanisms underlying sensitization of peripheral sensory neurons by granulocyte-/granulocyte-macrophage colony stimulating factors. Mol Pain 9:48.

Bevan S, Quallo T, Andersson DA (2014) Trpv1. In Mammalian transient receptor potential (TRP) cation channels, pp 207–245. Berlin; Heidelberg: Springer.

Breivik H, Collett B, Ventafridda V, Cohen R, Gallacher D (2006) Survey of chronic pain in Europe: prevalence, impact on daily life, and treatment. Eur J Pain 10:287–333.

Brothers SP, Wahlestedt C (2010) Therapeutic potential of neuropeptide Y (NPY) receptor ligands. EMBO Mol Med 2:429–439.

Broughton SE, Hercus TR, Nero TL, Dottore M, McClure BJ, Dhagat U, Taing H, Gorman MA, King-Scott J, Lopez AF, Parker MW (2016) Conformational changes in the GM-CSF receptor suggest a molecular mechanism for affinity conversion and receptor signaling. Structure 24:1271–1281.

Brown MT, Murphy FT, Radin DM, Davignon I, Smith MD, West CR (2012) Tanezumab reduces osteoarthritic knee pain: results of a randomized, double-blind, placebo-controlled phase III trial. J Pain 13:790–798.

Calvo M, Bennett DL (2012) The mechanisms of microgliosis and pain following peripheral nerve injury. Exp Neurol 234:271–282.

Caterina MJ, Julius D (2001) The vanilloid receptor: a molecular gateway to the pain pathway. Ann Rev Neurosci 24:487–517.

Chen L, Lv F, Pei L (2014) Annexin 1: a glucocorticoid-inducible protein that modulates inflammatory pain. Eur J Pain 18:338–347.

Chubb JR, Liverpool TB (2010) Bursts and pulses: insights from single cell studies into transcriptional mechanisms. Curr Opin Genet Dev 20: 478–484.

Cook AD, Hamilton JA (2018) Investigational therapies targeting the granulocyte macrophage colony-stimulating factor receptor-α in rheumatoid arthritis: focus on mavrilimumab. Ther Adv Musculoskelet Dis 10:29–38.

Cook AD, Braine EL, Hamilton JA (2004) Stimulus-dependent requirement for granulocyte-macrophage colony-stimulating factor in inflammation. J Immunol 173:4643–4651.

Cook AD, Pobjoy J, Steidl S, Dürr M, Braine EL, Turner AL, Lacey DC, Hamilton JA (2012) Granulocyte-macrophage colony-stimulating factor is a key mediator in experimental osteoarthritis pain and disease development. Arthritis Res Ther 14:R199.

Cook AD, Pobjoy J, Sarros S, Steidl S, Dürr M, Lacey DC, Hamilton JA (2013) Granulocyte-macrophage colony-stimulating factor is a key mediator in inflammatory and arthritic pain. Ann Rheum Dis 72:265–270.

Cook AD, Christensen AD, Tewari D, McMahon SB, Hamilton JA (2018) Immune cytokines and their receptors in inflammatory pain. Trends Immunol 39:240–255.

Croxford AL, Lanzinger M, Hartmann FJ, Schreiner B, Mair F, Pelczar P, Clausen BE, Jung S, Greter M, Becher B (2015) The cytokine GM-CSF drives the inflammatory signature of CCR^{2+} monocytes and licenses autoimmunity. Immunity 43:502–514.

Denk F, Crow M, Didangelos A, Lopes DM, McMahon SB (2016) Persistent alterations in microglial enhancers in a model of chronic pain. Cell Rep 15:1771–1781.

Desiderio S, Vermeiren S, Van Campenhout C, Kricha S, Malki E, Richts S, Fletcher EV, Vanwelden T, Schmidt BZ, Henningfeld KA, Pieler T, Woods CG, Nagy V, Verfaillie C, Bellefroid EJ (2019) Prdm12 directs nociceptive sensory neuron development by regulating the expression of the NGF receptor TrkA. Cell Rep 26:3522–3536.e5.

Diaz-delCastillo M, Woldbye DP, Heegaard AM (2018) Neuropeptide Y and its involvement in chronic pain. Neuroscience 387:162–169.

Donatien P, Anand U, Yiangou Y, Sinisi M, Fox M, MacQuillan A, Quick T, Korchev YE, Anand P (2018) Granulocyte-macrophage colony-stimulating factor receptor expression in clinical pain disorder tissues and role in neuronal sensitization. Pain Rep 3:e676.

Dubin AE, Patapoutian A (2010) Nociceptors: the sensors of the pain pathway. J Clin Investig 120:3760–3772.

Fenzi F, Benedetti MD, Moretto G, Rizzuto N (2001) Glial cell and macrophage reactions in rat spinal ganglion after peripheral nerve lesions: an immunocytochemical and morphometric study. Arch Ital Biol 139:357–365.

Fernandez-Zafra T, Gao T, Jurczak A, Sandor K, Hore Z, Agalave NM, Su J, Estelius J, Lampa, J, Hokfelt T, Wiesenfeld-Hallin Z, Xu X, Denk F, Svensson CI (2019) Exploring the transcriptome of resident spinal microglia after collagen antibody-induced arthritis. Pain 160:224–236.

Fleetwood AJ, Lawrence T, Hamilton JA, Cook AD (2007) Granulocyte-macrophage colony-stimulating factor (CSF) and macrophage CSF-dependent macrophage phenotypes display differences in cytokine profiles and transcription factor activities: implications for CSF blockade in inflammation. J Immunol 178:5245–5252.

Flegel C, Schöbel N, Altmüller J, Becker C, Tannapfel A, Hatt H, Gisselmann

G (2015) RNA-seq analysis of human trigeminal and dorsal root ganglia with a focus on chemoreceptors. PLoS One 10:e0128951.
Ford AP (2012) In pursuit of P2X3 antagonists: novel therapeutics for chronic pain and afferent sensitization. Purinergic Signal 8:3–26.
Gaudet AD, Popovich PG, Ramer MS (2011) Wallerian degeneration: gaining perspective on inflammatory events after peripheral nerve injury. J Neuroinflammation 8:110.
Guan Z, Kuhn JA, Wang X, Colquitt B, Solorzano C, Vaman S, Guan AK, Evans-Reinsch Z, Braz J, Devor M, Abboud-Werner SL, Lanier LL, Lomvardas S, Basbaum AI (2016) Injured sensory neuron-derived CSF1 induces microglial proliferation and DAP12-dependent pain. Nat Neurosci 19:94–101.
Hamilton JA (2008) Colony-stimulating factors in inflammation and autoimmunity. Nat Rev Immunol 8:533–544.
Hansen G, Hercus TR, McClure BJ, Stomski FC, Dottore M, Powell J, Ramshaw H, Woodcock JM, Xu Y, Guthridge M, McKinstry WJ, Lopez AF, Parker MW (2008) The structure of the GM-CSF receptor complex reveals a distinct mode of cytokine receptor activation. Cell 134:496–507.
Hill DA, Lim HW, Kim YH, Ho WY, Foong YH, Nelson VL, Nguyen HCB, Chegireddy K, Kim J, Habertheuer A, Vallabhajosyula P, Kambayashi T, Won KJ, Lazar MA (2018) Distinct macrophage populations direct inflammatory versus physiological changes in adipose tissue. Proc Natl Acad Sci U S A 115:E5096–E5105.
Hore Z, Denk F (2019) Neuroimmune interactions in chronic pain–an interdisciplinary perspective. Brain Behav Immun 79:56–62.
Huang K, Bian D, Jiang B, Zhai Q, Gao N, Wang R (2017) TRPA1 contributed to the neuropathic pain induced by docetaxel treatment. Cell Biochem Funct 35:141–143.
Hu P, McLachlan EM (2002) Macrophage and lymphocyte invasion of dorsal root ganglia after peripheral nerve lesions in the rat. Neuroscience 112:23–38.
Hu P, McLachlan EM (2003) Distinct functional types of macrophage in dorsal root ganglia and spinal nerves proximal to sciatic and spinal nerve transections in the rat. Exp Neurol 184:590–605.
Hutchinson MR, Coats BD, Lewis SS, Zhang Y, Sprunger DB, Rezvani N, Baker EM, Jekich BM, Wieseler JL, Somogyi AA, Martin D, Poole S, Judd CM, Maier SF, Watkins LR (2008) Proinflammatory cytokines oppose opioid-induced acute and chronic analgesia. Brain Behav Immun 22:1178–1189.
Jurga AM, Rojewska E, Makuch W, Mika J (2018) Lipopolysaccharide from rhodobacter sphaeroides (TLR4 antagonist) attenuates hypersensitivity and modulates nociceptive factors. Pharm Biol 56:275–286.
Kawasaki Y, Zhang L, Cheng JK, Ji RR (2008) Cytokine mechanisms of central sensitization: distinct and overlapping role of interleukin-1β, interleukin-6, and tumor necrosis factor-α in regulating synaptic and neuronal activity in the superficial spinal cord. J Neurosci 28:5189–5194.
Kerr BJ, Cafferty WB, Gupta YK, Bacon A, Wynick D, McMahon SB, Thompson SW (2000) Galanin knockout mice reveal nociceptive deficits following peripheral nerve injury. Eur J Neurosci 12:793–802.
Laskin DL (2009) Macrophages and inflammatory mediators in chemical toxicity: a battle of forces. Chem Res Toxicol 22:1376–1385.
Lopes DM, Denk F, McMahon SB (2017) The molecular fingerprint of dorsal root and trigeminal ganglion neurons. Front Mol Neurosci 10:304.
Lu X, Richardson PM (1993) Responses of macrophages in rat dorsal root ganglia following peripheral nerve injury. J Neurocytol 22:334–341.
Malin SA, Davis BM, Molliver DC (2007) Production of dissociated sensory neuron cultures and considerations for their use in studying neuronal function and plasticity. Nat Protoc 2:152–160.
Marchand F, Perretti M, McMahon SB (2005) Role of the immune system in chronic pain. Nat Rev Neurosci 6:521–532.
McMahon SB, La Russa F, Bennett DL (2015) Crosstalk between the nociceptive and immune systems in host defence and disease. Nat Rev Neurosci 16:389–402.
Metcalf D (2008) Hematopoietic cytokines. Blood 111:485–491.
Mika J, Osikowicz M, Makuch W, Przewlocka B (2007) Minocycline and pentoxifylline attenuate allodynia and hyperalgesia and potentiate the effects of morphine in rat and mouse models of neuropathic pain. Eur J Pharmacol 560:142–149.
Moalem G, Tracey DJ (2006) Immune and inflammatory mechanisms in neuropathic pain. Brain Res Rev 51:240–264.
Murray PJ, Allen JE, Biswas SK, Fisher EA, Gilroy DW, Goerdt S, Gordon S, Hamilton JA, Ivashkiv LB, Lawrence T, Locati M, Mantovani A, Martinez FO, Mege JL, Mosser DM, Natoli G, Saeij JP, Schultze JL, Shirey KA, Sica A, et al. (2014) Macrophage activation and polarization: nomenclature and experimental guidelines. Immunity 41:14–20.
Nicol LSC, Thornton P, Hatcher JP, Glover CP, Webster CI, Burrell M, Hammett K, Jones CA, Sleeman MA, Billinton A, Chessell I (2018) Central inhibition of granulocyte-macrophage colony-stimulating factor is analgesic in experimental neuropathic pain. Pain 159:550–559.
Ohtori S, Takahashi K, Moriya H, Myers RR (2004) TNF-α and TNF-α receptor type 1 upregulation in glia and neurons after peripheral nerve injury: studies in murine DRG and spinal cord. Spine 29:1082–1088.
Ostuni R, Piccolo V, Barozzi I, Polletti S, Termanini A, Bonifacio S, Curina A, Prosperini E, Ghisletti S, Natoli G (2013) Latent enhancers activated by stimulation in differentiated cells. Cell 152:157–171.
Özaktay AC, Kallakuri S, Takebayashi T, Cavanaugh JM, Asik I, DeLeo JA, Weinstein JN (2006) Effects of interleukin-1 beta, interleukin-6, and tumor necrosis factor on sensitivity of dorsal root ganglion and peripheral receptive fields in rats. Eur Spine J 15:1529–1537.
Parajul B, Sonobe Y, Kawanokuchi J, Doi Y, Noda M, Takeuchi H, Mizuno T, Suzumura A (2012) GM-CSF increases LPS-induced production of proinflammatory mediators via upregulation of TLR4 and CD14 in murine microglia. J Neuroinflammation 9:268.
Pei L, Zhang J, Zhao F, Su T, Wei H, Tian J, Li M, Shi J (2011) Annexin 1 exerts anti-nociceptive effects after peripheral inflammatory pain through formyl-peptide-receptor-like 1 in rat dorsal root ganglion. Br J Anaesth 107:948–958.
Phillips CJ (2009) The cost and burden of chronic pain. Rev Pain 3:2–5.
Piccolo V, Curina A, Genua M, Ghisletti S, Simonatto M, Sabò A, Amati B, Ostuni R, Natoli G (2017) Opposing macrophage polarization programs show extensive epigenomic and transcriptional cross-talk. Nat Immunol 18:530–540.
Popiolek-Barczyk K, Kolosowska N, Piotrowska A, Makuch W, Rojewska E, Jurga AM, Pilat D, Mika J (2015) Parthenolide relieves pain and promotes M2 microglia/macrophage polarization in rat model of neuropathy. Neural Plast 2015:676473.
Rajasekhar P, Poole DP, Liedtke W, Bunnett NW, Veldhuis NA (2015) P2Y1 receptor activation of the TRPV4 ion channel enhances purinergic signaling in satellite glial cells. J Biol Chem 290:29051–29062.
Raser JM, O'Shea EK (2005) Noise in gene expression: origins, consequences, and control. Science 309:2010–2013.
Ray P, Torck A, Quigley L, Wangzhou A, Neiman M, Rao C, Lam T, Kim JY, Kim TH, Zhang MQ, Dussor G, Price TJ (2018) Comparative transcriptome profiling of the human and mouse dorsal root ganglia: an RNA-seq-based resource for pain and sensory neuroscience research. Pain 159:1325–1345.
Ray PR, Khan J, Wangzhou A, Tavares-Ferreira D, Akopian AN, Dussor G, Price TJ (2019) Transcriptome analysis of the human tibial nerve identifies sexually dimorphic expression of genes involved in pain, inflammation and neuro-immunity. Front Mol Neurosci 12:37.
Saunders J, Hore Z, Gentry C, McMahon S, Denk F (2018) Negative evidence for a functional role of neuronal DNMT3a in persistent pain. Front Mol Neurosci 11:332.
Schlomann U, Rathke-Hartlieb S, Yamamoto S, Jockusch H, Bartsch JW (2000) Tumor necrosis factor α induces a metalloprotease-disintegrin, ADAM8 (CD 156): implications for neuron–glia interactions during neurodegeneration. J Neurosci 20:7964–7971.
Scholz J, Woolf CJ (2007) The neuropathic pain triad: neurons, immune cells and glia. Nat Neurosci 10:1361–1368.
Schweizerhof M, Stösser S, Kurejova M, Njoo C, Gangadharan V, Agarwal N, Schmelz M, Bali KK, Michalski CW, Brugger S, Dickenson A, Simone DA, Kuner R (2009) Hematopoietic colony-stimulating factors mediate tumor-nerve interactions and bone cancer pain. Nat Med 15:802–807.
Schwertner A, Conceição dos Santos CC, Costa GD, Deitos A, de Souza A, de Souza ICC, Torres IL, da Cunha Filho JSL, Caumo W (2013) Efficacy of melatonin in the treatment of endometriosis: a phase II, randomized, double-blind, placebo-controlled trial. Pain 154:874–881.
Shepherd AJ, Mickle AD, Golden JP, Mack MR, Halabi CM, de Kloet AD, Samineni VK, Kim BS, Krause EG, Gereau RW 4th, Mohapatra DP (2018) Macrophage angiotensin II type 2 receptor triggers neuropathic pain. Proc Natl Acad Sci U S A 115:E8057–E8066.
Sorge RE, Mapplebeck JC, Rosen S, Beggs S, Taves S, Alexander JK, Martin LJ, Austin JS, Sotocinal SG, Chen D, Yang M, Shi XQ, Huang H, Pillon NJ, Bilan PJ, Tu Y, Klip A, Ji RR, Zhang J, Salter MW, Mogil JS (2015)

Different immune cells mediate mechanical pain hypersensitivity in male and female mice. Nat Neurosci 18:1081–1083.

Stirling LC, Forlani G, Baker MD, Wood JN, Matthews EA, Dickenson AH, Nassar MA (2005) Nociceptor-specific gene deletion using heterozygous NaV1. 8-cre recombinase mice. Pain 113:27–36.

Tang Y, Liu L, Xu D, Zhang W, Zhang Y, Zhou J, Huang W (2018) Interaction between astrocytic colony stimulating factor and its receptor on microglia mediates central sensitization and behavioral hypersensitivity in chronic post ischemic pain model. Brain Behav Immun 68:248–260.

Thakur M, Crow M, Richards N, Davey GI, Levine E, Kelleher JH, Agley CC, Denk F, Harridge SD, McMahon SB (2014) Defining the nociceptor transcriptome. Front Mol Neurosci 7:87.

Volfson D, Marciniak J, Blake WJ, Ostroff N, Tsimring LS, Hasty J (2006) Origins of extrinsic variability in eukaryotic gene expression. Nature 439:861–864.

Wangzhou A, McIlvried LA, Paige C, Barragan-Iglesias P, Guzman CA, Dussor G, Ray PR, Gereau RW, Price TJ (2019) Transcriptomic analysis of native versus cultured human and mouse dorsal root ganglia focused on pharmacological targets. BioRxiv. doi:10.1101/766865.

Watkins LR, Maier SF (2002) Beyond neurons: evidence that immune and glial cells contribute to pathological pain states. Physiol Rev 82:981–1011.

Wicks IP, Roberts AW (2016) Targeting GM-CSF in inflammatory diseases. Nat Rev Rheumatol 12:37–48.

Wu G, Ringkamp M, Hartke TV, Murinson BB, Campbell JN, Griffin JW, Meyer RA (2001) Early onset of spontaneous activity in uninjured C-fiber nociceptors after injury to neighboring nerve fibers. J Neurosci 21:RC140.

Ydens E, Cauwels A, Asselbergh B, Goethals S, Peeraer L, Lornet G, Almeida-Souza L, Van Ginderachter JA, Timmerman V, Janssens S (2012) Acute injury in the peripheral nervous system triggers an alternative macrophage response. J Neuroinflammation 9:176.

Zeisel A, Hochgerner H, Lönnerberg P, Johnsson A, Memic F, van der Zwan J, Häring M, Braun E, Borm LE, La Manno G, Codeluppi S, Furlan A, Lee K, Skene N, Harris KD, Hjerling-Leffler J, Arenas E, Ernfors P, Marklund U, Linnarsson S (2018) Molecular architecture of the mouse nervous system. Cell 174:999–1014.e22.

Zhang JM, Strong JA (2008) Recent evidence for activity-dependent initiation of sympathetic sprouting and neuropathic pain. Sheng Li Xue Bao 60:617–627.

Zhang F, Wang Y, Liu Y, Han H, Zhang D, Fan X, Du X, Gamper N, Zhang H (2019) Transcriptional regulation of voltage-gated sodium channels contributes to GM-CSF induced pain. J Neurosci 39:5222–5233.

Zhang H, Li Y, de Carvalho-Barbosa M, Kavelaars A, Heijnen CJ, Albrecht PJ, Dougherty PM (2016) Dorsal root ganglion infiltration by macrophages contributes to paclitaxel chemotherapy-induced peripheral neuropathy. J Pain 17:775–786.

Zhao H, Alam A, Chen Q, Eusman MA, Pal A, Eguchi S, Wu L, Ma D (2017) The role of microglia in the pathobiology of neuropathic pain development: what do we know? Br J Anaesth 118:504–516.

Laboratory Investigation (2020) 100:1057–1067
https://doi.org/10.1038/s41374-020-0430-7

ARTICLE

The transient receptor potential vanilloid 4 (TRPV4) ion channel mediates protease activated receptor 1 (PAR1)-induced vascular hyperpermeability

Scott Peng[1,2] · Megan S. Grace[3,4,5] · Arisbel B. Gondin[1,2] · Jeffri S. Retamal[1,2] · Larissa Dill[3] · William Darby[3] · Nigel W. Bunnett[1,2,6] · Fe C. Abogadie[3] · Simona E. Carbone[1,2] · Tara Tigani[1] · Thomas P. Davis[2] · Daniel P. Poole[1,2,7] · Nicholas A. Veldhuis[1,2] · Peter McIntyre[3,8]

Received: 2 January 2020 / Revised: 2 April 2020 / Accepted: 2 April 2020 / Published online: 27 April 2020
© The Author(s), under exclusive licence to United States and Canadian Academy of Pathology 2020

Abstract

Endothelial barrier disruption is a hallmark of tissue injury, edema, and inflammation. Vascular endothelial cells express the G protein-coupled receptor (GPCR) protease acctivated receptor 1 (PAR1) and the ion channel transient receptor potential vanilloid 4 (TRPV4), and these signaling proteins are known to respond to inflammatory conditions and promote edema through remodeling of cell–cell junctions and modulation of endothelial barriers. It has previously been established that signaling initiated by the related protease activated receptor 2 (PAR2) is enhanced by TRPV4 in sensory neurons and that this functional interaction plays a critical role in the development of neurogenic inflammation and nociception. Here, we investigated the PAR1–TRPV4 axis, to determine if TRPV4 plays a similar role in the control of edema mediated by thrombin-induced signaling. Using Evans Blue permeation and retention as an indication of increased vascular permeability in vivo, we showed that TRPV4 contributes to PAR1-induced vascular hyperpermeability in the airways and upper gastrointestinal tract of mice. TRPV4 contributes to sustained PAR1-induced Ca^{2+} signaling in recombinant cell systems and to PAR1-dependent endothelial junction remodeling in vitro. This study supports the role of GPCR–TRP channel functional interactions in inflammatory-associated changes to vascular function and indicates that TRPV4 is a signaling effector for multiple PAR family members.

Introduction

The microvasculature provides important homeostatic functions including the exchange of gas, fluid, and micro- or macro-molecules from the circulation to the interstitial space and surrounding tissues. As the main component of this vascular barrier, endothelial cells regulate blood flow, fluidity, perfusion, as well as vascular permeability. Dysfunction of the endothelium can result in a loss of barrier integrity, prolonged hyperpermeability, and unregulated fluid extravasation, leading to edema and inflammation [1, 2].

Inflammatory signaling in endothelial cells is regulated by a variety of mediators, including the serine proteases

These authors contributed equally: Scott Peng, Megan S. Grace

✉ Daniel P. Poole
Daniel.Poole@monash.edu

✉ Nicholas A. Veldhuis
Nicholas.Veldhuis@monash.edu

[1] Drug Discovery Biology Theme, Monash Institute of Pharmaceutical Sciences, Parkville, VIC 3052, Australia

[2] ARC Centre of Excellence in Convergent Bio-Nano Science & Technology, Monash University, Parkville, VIC 3052, Australia

[3] School of Medical Sciences and Health Innovations Research Institute, RMIT University, Bundoora, VIC 3083, Australia

[4] Department of Physiology, School of Medicine Nursing and Health Sciences, Monash University, Clayton, VIC 3800, Australia

[5] Baker IDI Heart and Diabetes Institute, Melbourne, VIC 3004, Australia

[6] Department of Molecular Pathobiology, New York University, New York, NY 10010, USA

[7] Department of Anatomy & Neuroscience, The University of Melbourne, Parkville, VIC 3010, Australia

[8] The Florey Institute of Neuroscience and Mental Health, Parkville, VIC 3010, Australia

thrombin and trypsin. These proteases can bind and cleave the amino terminal sequence of specific G protein-coupled receptors (GPCRs) known as protease-activated receptors (PARs). This is a unique activation mechanism for GPCRs and once cleaved, the newly exposed N-terminus functions as a tethered ligand that can rapidly engage with, and activate the receptor [3, 4]. Furthermore, the N-terminus of these receptors has also evolved to contain recognition and cleavage sequences for multiple proteases, and cleavage at distinct sites can promote a range of signaling outcomes [5]. Endothelial cells express all four PAR family subtypes (PAR1–PAR4), and these receptors play roles in maintaining vascular homeostasis through promoting adhesion, chemotaxis, coagulation, proliferation, and excretion of cytokines [6]. The proteolytic cleavage of PAR1 by thrombin mediates thrombosis in the coagulation pathway [7]. In addition, PAR1 activation can lead to increased vascular permeability in response to injury and inflammation. This occurs through phosphorylation of myosin light chain proteins, leading to cytoskeletal contraction, junctional remodeling, and disruption of the endothelial barrier [8].

Transient receptor potential (TRP) ion channels are expressed by a variety of cell types including endothelial and smooth muscle cells and contribute to signaling pathways that regulate vasculature processes, by promoting rapid cellular uptake of divalent cations, including Ca^{2+}. The TRP Vanilloid 4 (TRPV4) ion channel, for example, is a polymodal protein that can respond to changes in thermal, chemical, and mechanical stimuli such as shear stress and osmotic pressure [9]. TRPV4 is expressed by endothelial and vascular smooth muscle cells, and regulates vascular tone, cytoskeletal architecture, and junctional remodeling of endothelial barriers [10–12].

GPCRs including PARs can indirectly activate and sensitize TRP channels by upregulating intracellular signaling pathways that lead to increased phosphorylation, to ultimately lower TRP channel activation thresholds. This GPCR–TRP transactivation axis plays a pivotal role in sensory neuron signaling processes to regulate pain, itch, cough, and inflammation [13]. For example, PAR2-mediated sensitization of TRPV4 has been implicated in hyperalgesia [14], inflammation [15], and edema [16]. Given the overlap in downstream signaling pathways mediated by PARs, TRPV4 may also act as a downstream mediator of vascular tone through PAR1-dependent transactivation, either directly, or via the activity of growth factor receptors [17]. Given that PAR1 and TRPV4 both perform critical functions in the vasculature, we investigated whether PAR1–TRPV4 functional interactions are involved in the regulation of endothelial barrier integrity and vascular permeability. Focusing on isolated airway and gastrointestinal (GI) tissues, our data support a role for TRPV4 as a facilitator of PAR1-dependent vascular endothelial barrier permeability.

Experimental procedures

Mice

Wild Type C57Bl/6J, TRPV4$^{-/-}$, and littermate control mice (6–12 weeks) were obtained from Animal Resources Centre (Canning Vale, WA), or were purpose-bred by the Monash Animal Research Platform, Monash University. All animals were maintained in a temperature-controlled environment with a 12 h light/dark cycle and free access to food and water. All animal experiments are reported in accordance with the ARRIVE guidelines [18]. This study was approved by the respective Animal Ethics Committees of RMIT and Monash Institute of Pharmaceutical Sciences.

Reagents

Reagents were obtained from the following suppliers: Evans Blue dye, TFLLR-NH_2, bovine plasma thrombin, tetracycline hydrochloride, poly-L-lysine, and GSK1016790A were purchased from Sigma-Aldrich (Castle Hill, Australia); Fura2-AM was purchased from (ThermoFisher Scientific, Scoresby, Victoria). Vorapaxar (SCH-530348) was purchased from Axon Medchem (Groningen, The Netherlands) and HC067047 was purchased from Tocris Bioscience (Bristol, UK).

Evans Blue extravasation

Mice were anesthetized with a combination of ketamine (100 mg/kg i.p.) and xylazine (10 mg/kg i.p.) and kept on a warming pad throughout the experiment. The skin on the neck was then removed to expose the jugular veins. Substances were administered i.v. by passing the injection needle through the *pectoralis major* muscle to prevent bleeding on withdrawal. Evans Blue dye (20 mg/kg) was administered via the jugular vein 1 min before injection of agonist (0.03–1 mg/kg GSK1016790A or 3 µmol/kg TFLLR) or vehicle (0.9% saline or 1% DMSO in 0.9% saline). The TRPV4-selective antagonist (0.1–10 mg/kg HC067047) was injected i.p. (prepared in 1% DMSO/0.9% saline) 60 min prior to anesthetics, Evans Blue and agonist administration. After 5 min post-agonist injection, the animal was exsanguinated, and the systemic circulation perfused with 0.9% saline to remove all remaining blood and dye. Tissue samples were collected, weighed, and placed immediately in 0.2 ml formamide. The airways were removed *en bloc*, before being separated. Lung parenchyma was removed from the bronchi and intrapulmonary airways

(IPA). Tissues were then incubated in formamide (≥18 h at 37 °C) to facilitate dye extraction. Absorbance of the resulting extracts was determined against standard concentrations of Evans Blue at 620 nm using a CLARIOstar® microplate reader (BMG Labtech, Ortenberg, Germany). Results were expressed as the mass of Evans Blue dye relative to tissue mass (ng/mg of wet weight tissue).

Cell lines

Human Embryonic Kidney 293 (HEK293) cell lines stably expressing wildtype human TRPV4 (hTRPV4) were generated using a tetracycline-inducible system as previously described [15]. Briefly, Flp-In™ T-Rex™ HEK293 cells (ThermoFisher Scientific) were transfected with pcDNA5/FRT/TO containing hTRPV4 (TRPV4-HEK). TRPV4-HEK were grown in Dulbecco's Modified Eagle's Medium (DMEM, ThermoFisher Scientific) containing 10% tetracycline-free fetal bovine serum (FBS), blasticidin (5 µg/ml), and hygromycin (100 µg/ml). Non-transfected control HEK293 cells (NT-HEK) were grown under the same conditions, but without hygromycin. HUVEC were grown in endothelial growth medium (EGM, Lonza) containing 2% FBS.

Intracellular Ca^{2+} assay

TRPV4-HEK and NT-HEK were seeded onto poly-L-lysine (100 µg/ml) coated 96-well plates (60,000 cells/well) and cultured for 48 h. Wildtype and TRPV4 HEK cells were treated with tetracycline (1 µg/ml) for 4 h to induce TRPV4 expression. NT-HEK were treated with the same tetracycline induction conditions. HUVEC were seeded onto non-coated 96-well plates (15,000 cells/well) and cultured for 48 h. Cells were loaded with Fura2-AM ester (2.5 µM) in HBSS containing probenecid (2 mM) and pluronic acid (0.5 µM) (pH 7.4, 37 °C, 45–60 min). Fluorescence was measured at 340/380 nm excitation and 510 nm emission wavelengths using a FlexStation 3 plate reader (Molecular Devices, Sunnyvale, CA) as previously described [19]. Fluorescence was recorded for 15 s prior to compound addition to establish a baseline reading. Agonist and antagonist treatments are indicated in results and data were expressed as the 340/380 nm fluorescence ratio, to determine fluctuations in free intracellular calcium ($[Ca^{2+}]_i$).

Immunofluorescence

Human umbilical vein endothelial cells (HUVEC) were seeded on glass coverslips coated with Matrigel (1:10 dilution, Corning). Once cells formed a confluent monolayer, they were treated as described in the results. Media was then removed and HUVEC were washed with PBS before fixation (4% paraformaldehyde, 15 min). HUVEC were washed (3 × 10 min PBS) then incubated in permeabilization/blocking buffer (5% normal horse serum in PBS containing 0.1% sodium azide and 0.1% saponin) for 1 h at room temperature (RT). Cells were incubated with a polyclonal anti-VE-cadherin antibody (rabbit, #ab33168, Abcam RRID:AB_870662, 1:400) in blocking buffer overnight at 4 °C. Cells were then washed (3× PBS) and incubated with secondary antibody (donkey anti-rabbit Alexa594, 1:500; ThermoFisher) and phalloidin Alexa488 (1:1,000; Abcam) in PBS for 2 h at RT. Nuclei were detected with Hoechst 33342 (1:2,000; ThermoFisher; 10 min at RT). Coverslips were mounted using ProLong Diamond Antifade Mountant (ThermoFisher) and images were captured on a Leica TCS-SP8 confocal system as described [20] using an HC PLAN APO 1.4 NA 63× oil objective. Three regions for each treatment were captured at 16-bit depth and 1024 × 1024-pixel resolution in four independent experiments.

Transwell permeability assay

HUVEC were seeded on non-coated Transwell inserts (6.5 mm diameter, 0.4 µm pore size, Corning, Mulgrave, Victoria) and grown for up to 72 h, until a HUVEC confluent monolayer had been achieved. Cells were then treated with antagonists (as indicated in results) in serum-free cell culture media, followed by co-addition of agonist and FITC-labeled dextran (100 µg/ml, average MW = 70 kDa, Sigma-Aldrich) to the Transwell insert. After 30 min, 100 µL samples from the bottom chamber of the Transwell system were removed and FITC fluorescence was measured (excitation/emission wavelengths 492/520 nm) in a CLARIOstar® microplate reader. Results were expressed as fluorescence intensity normalized to the vehicle control treatment group (0.1% DMSO).

Statistical analysis

A p value of < 0.05 was considered to be significantly different to the null hypothesis of no difference in means at the 95% confidence level. All treatments comparing three or more variables were analyzed using one-way ANOVA with Sidak's multiple comparison tests. Comparisons of two variables were analyzed using an unpaired Student's t test. For cell-based assays, sigmoidal curves were fitted to agonist concentration responses. Due to the higher baseline fluorescence (F_{340}/F_{380} ratio) observed in TRPV4-HEK compared with NT-HEK cells, agonist peaks and coupling analysis were determined based on normalized data by subtracting the baseline fluorescence (average fluorescence from 0–15 s).

Results

Activation of TRPV4-induced vascular hyperpermeability in the airways and upper GI tract

To assess the effect of TRPV4 activation on vascular permeability, we examined the tissue distribution of Evans Blue dye in mice following the administration of the selective TRPV4 agonist GSK1016790A (GSK101). GSK101 elicited dose-dependent extravasation of Evans Blue in the airways (lung parenchyma, bronchi, IPA, and trachea) and upper GI tract (esophagus and stomach) (Fig. 1a). To further confirm that the GSK101-induced vascular hyperpermeability was TRPV4 specific, animals received increasing doses of the TRPV4-selective antagonist HC067047 (HC06; 0.1, 1, or 10 mg/kg) 60 min prior to Evans Blue and a moderate dose of GSK101 (0.1 mg/kg). Comparison of dye retention in these tissues reveals a HC06 dose-dependent reduction in GSK101-induced vascular hyperpermeability (Fig. 1b).

TRPV4 mediates PAR1-induced vascular hyperpermeability in the airways and upper GI tract

We have previously demonstrated that TRPV4 promotes PAR2-dependent signaling and edema [15]. We therefore investigated whether TRPV4 plays a similar role in PAR1-induced hyperpermeability. To confirm that activation of PAR1 leads to vascular hyperpermeability, we administered the PAR1-selective activating peptide TFLLR-NH_2 (TFLLR), using the same mouse model. Relative to the canonical protease thrombin, which activates PAR1 as well as other PARs and extracellular proteins [3], the perfusion of free peptide agonist TFLLR was chosen due to its selectivity for the receptor. TFLLR-treated (3 µmol/kg) mice also exhibited significant Evans Blue retention compared with the vehicle control in the same tissues, as demonstrated by a mean 1.68-fold dye uptake increase in airway tissue, and 2.34-fold increase in upper GI tissue and jejunum (Fig. 2).

To assess a potential role for TRPV4 in PAR1-mediated hyperpermeability, TRPV4 function was blocked either pharmacologically (Fig. 2) or by genetic ablation (Fig. 3). PAR1-induced vascular hyperpermeability in the airways and upper GI tract were reversed by pretreatment with HC06 (10 mg/kg) (Fig. 2). Furthermore, comparable inhibition of TFLLR-induced Evans Blue retention was observed when examined in TRPV4$^{-/-}$ mice (Fig. 3). HC06 alone did not reduce Evans Blue retention relative to the vehicle control, thus indicating that the antagonist reduced vascular hyperpermeability specifically following PAR1 activation. Similarly, there was no basal difference in dye retention in TRPV4$^{-/-}$ mice compared with wild type controls.

TRPV4 promotes sustained Ca^{2+} responses following PAR1 activation

TRPV4 has previously been reported to enhance the duration and magnitude of PAR2-dependent Ca^{2+} signaling in immortalized cells and has also been associated with enhanced edema in an acute model of inflammation [15]. Consistent with this, PAR1-dependent disruption of the endothelial barrier also has the potential to involve rapid changes in free intracellular Ca^{2+} ($[Ca^{2+}]_i$) levels and can be readily investigated in cells co-expressing PAR1 and TRPV4. Utilizing stable TRPV4-HEK cells and non-transfected control HEK cells (NT-HEK) that endogenously express human PAR1, the temporal Ca^{2+} profiles were compared for responses to PAR1 activation with the TFLLR peptide or canonical protease, thrombin (Fig. 4). In control NT-HEK cells, PAR1 stimulation with thrombin (3 U/ml) or TFLLR (30 µM) resulted in a rapid transient $[Ca^{2+}]_i$ mobilization, consistent with activation of $G\alpha_q$-mediated pathways, and returned to basal levels within 40 s post stimulation (Fig. 4a, b). In contrast, the equivalent treatment in TRPV4-HEK cells resulted in a rapid and relatively more sustained elevation in $[Ca^{2+}]_i$. This observation was consistent with the nonlinear regression curves (80 s post stimulation) of Ca^{2+} responses from different TFLLR and thrombin concentrations. The concentration response curves, determined by plotting peak responses, showed no significant difference between the two agonists (Fig. 4c, d), whereas those based on area under the curve (AUC) indicated that TRPV4 promotes a significant increase in sustained Ca^{2+} flux (Fig. 4e, f). Together, these data suggest that TRPV4 activity does not affect the maximum transient Ca^{2+} release from intracellular stores, but does contribute to the global PAR1-mediated Ca^{2+} response in transfected HEK cells.

TRPV4 contributes to PAR1-induced endothelial hyperpermeability in HUVEC

The roles of PAR1 and TRPV4 in Ca^{2+} signaling and permeability were subsequently examined in HUVEC, a well characterized and commonly used cell model system representative of signaling responses in the vasculature. Stimulation of HUVEC with either GSK101 or TFLLR caused a concentration-dependent increase in $[Ca^{2+}]_i$, thus demonstrating that TRPV4 and PAR1 are both endogenously expressed and functional in these cells. The time traces of $[Ca^{2+}]_i$ show that TRPV4 activation resulted in a sustained response, while PAR1 activation resulted in a transient Ca^{2+} response, which is characteristic for $G\alpha_q$ coupled responses (Fig. 5a, c). To determine whether PAR1 sensitizes TRPV4, HUVEC pretreated with TFLLR 15 min prior, were stimulated with GSK101 (Fig. 5a).

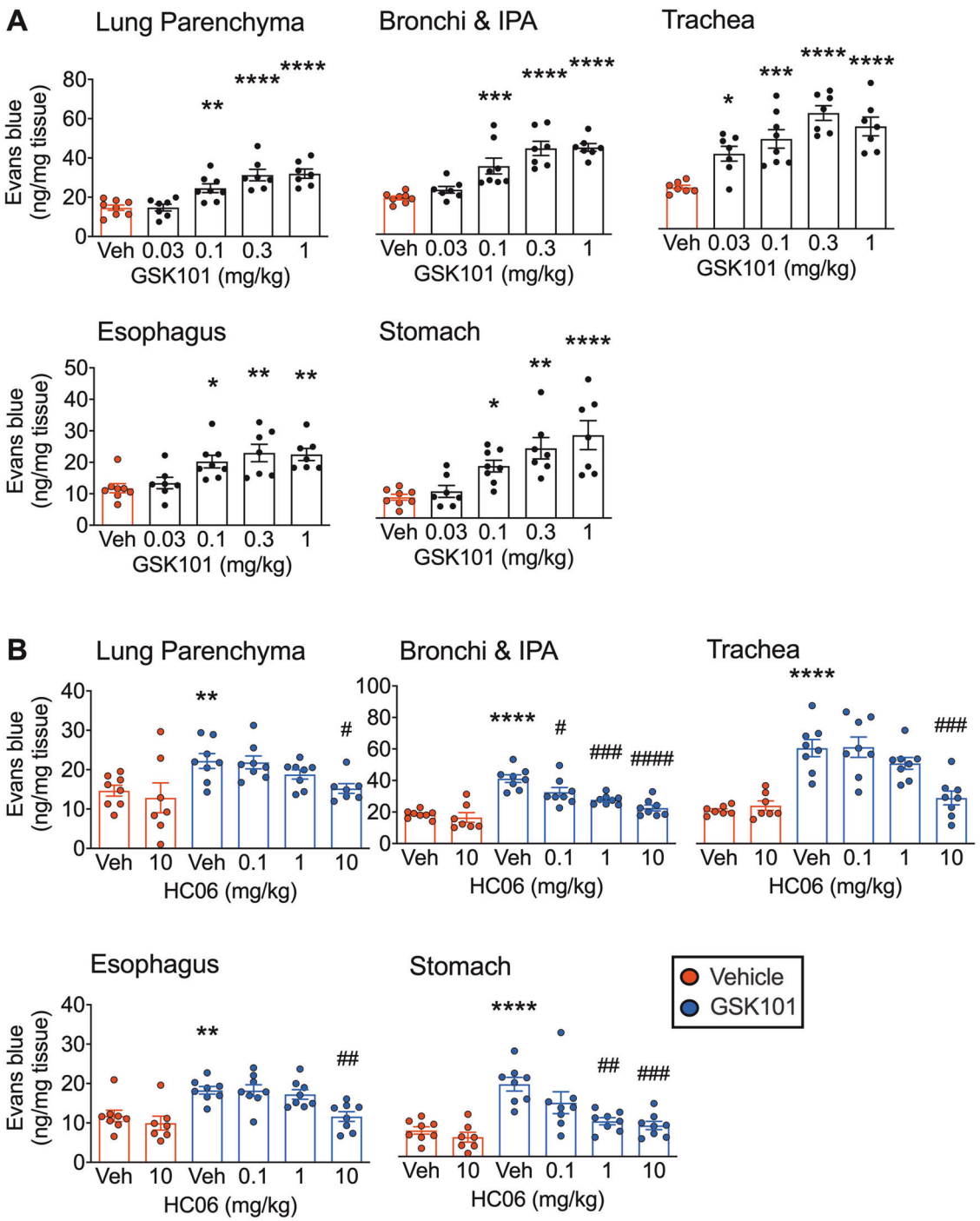


Fig. 1 Role of TRPV4 activity in vascular hyperpermeability in the airways and upper GI tract. a Vascular hyperpermeability assessed by presence of Evans Blue in tissue, following i.v. administration of increasing doses of TRPV4 agonist GSK101, relative to control treatment (Veh, 1% DMSO in 0.9% saline). **b** Inhibition of TRPV4-mediated, GSK101-dependent Evans Blue permeability by co-administration of GSK101 (0.1 mg/kg) with increasing doses of TRPV4 antagonist, HC067047 (HC06, concentrations indicated on *x*-axes), or by co-administration of HC06 (10 mg/kg) with vehicle control. Each data point represents a measurement from the indicated tissue, harvested from an individual animal. Column graphs represent mean ± s.e.m., $n = 7$–9. *, $^{\#}p < 0.05$; **, $^{\#\#}p < 0.01$; ***, $^{\#\#\#}p < 0.001$; ****, $^{\#\#\#\#}p < 0.0001$; one-way ANOVA with Sidak's multiple comparisons test, comparing treatments to Vehicle only control (*) or relative to GSK101 only control (#).

The leftwards shift of the curve was positively associated with TFLLR concentration, suggesting that activation of PAR1 sensitizes TRPV4, particularly at lower GSK101 concentrations (Fig. 5b). To determine the relative contribution of TRPV4 activity to PAR1-mediated responses, cells were pretreated with vehicle, the selective PAR1

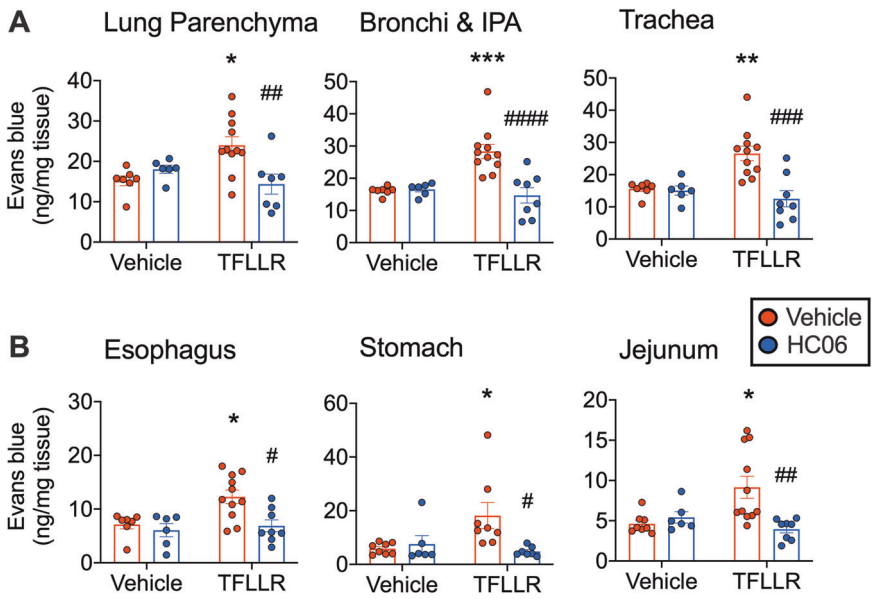


Fig. 2 Effect of TRPV4 pharmacological inhibition on PAR1-induced vascular hyperpermeability. Evans Blue retention measured in regions involved in the airways (**a**) or upper GI tract and jejunum (**b**). Animals were treated with vehicle alone, HC06 (10 mg/kg) with Vehicle (0.9% saline) or HC06 with TFLLR PAR1 agonist peptide (3 µmol/kg). Each data point represents a measurement from an individual animal, column graphs represent mean ± s.e.m., $n = 6$–11. *, $^{\#}p < 0.05$; **, $^{\#\#}p < 0.01$; ***, $^{\#\#\#}p < 0.001$; ****, $^{\#\#\#\#}p < 0.0001$; two-way ANOVA with Sidak's multiple comparisons test; relative to vehicle only control (*) or vehicle + TFLLR treatment (#).

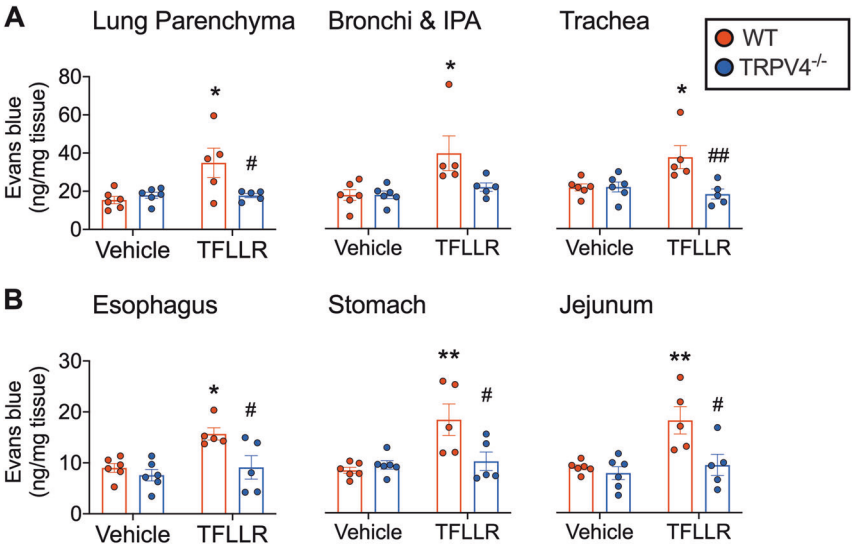


Fig. 3 Effect of TRPV4 genetic ablation on PAR1-induced vascular hyperpermeability. Evans Blue retention measured in regions involved in the airways (**a–c**) or upper GI tract and jejunum (**d–f**). Wildtype or TRPV4$^{-/-}$ mice were treated with vehicle alone or with the PAR1 agonist peptide TFLLR (3 µmol/kg). Each data point represents a measurement from an individual animal, column graphs represent mean ± s.e.m., $n = 5$–6. *, $^{\#}p < 0.05$; **, $^{\#\#}p < 0.01$; two-way ANOVA with Sidak's multiple comparisons test; relative to Vehicle only control (*) or Vehicle + TFLLR treatment (#).

antagonist Vorapaxar, (VPX, 100 nM) or the TRPV4 antagonist HC06 (1 µM), followed by stimulation with increasing concentrations of TFLLR (Fig. 5c). By comparing the total Ca^{2+} response (AUC, 130 s post stimulation), these TFLLR-evoked Ca^{2+} responses in HUVEC were abolished in the presence of VPX, but were unaffected by TRPV4 inhibition (Fig. 5d). Similarly, HC06 did not have a significant effect on the sustained phase of the PAR1-mediated calcium responses (Fig. 5c). It is possible that the differences in TRPV4 contribution to PAR1 signaling in HUVEC and NT-HEK results from variations in receptor quantity or compensatory mechanisms originating from cell type-specific differences.

Evans Blue studies in animals indicated that TRPV4 may be functionally important for promoting PAR1-mediated changes in vascular permeability (Figs. 2, 3). To investigate whether the Ca^{2+} signals match functional responses as well as the influence of PAR1 and TRPV4 on endothelial permeability in vitro, PAR1 and TRPV4-mediated HUVEC permeability was assessed by growing cells to confluence on Transwell® porous membrane inserts followed by measurement of FITC-labeled dextran (fluorescent macromolecule

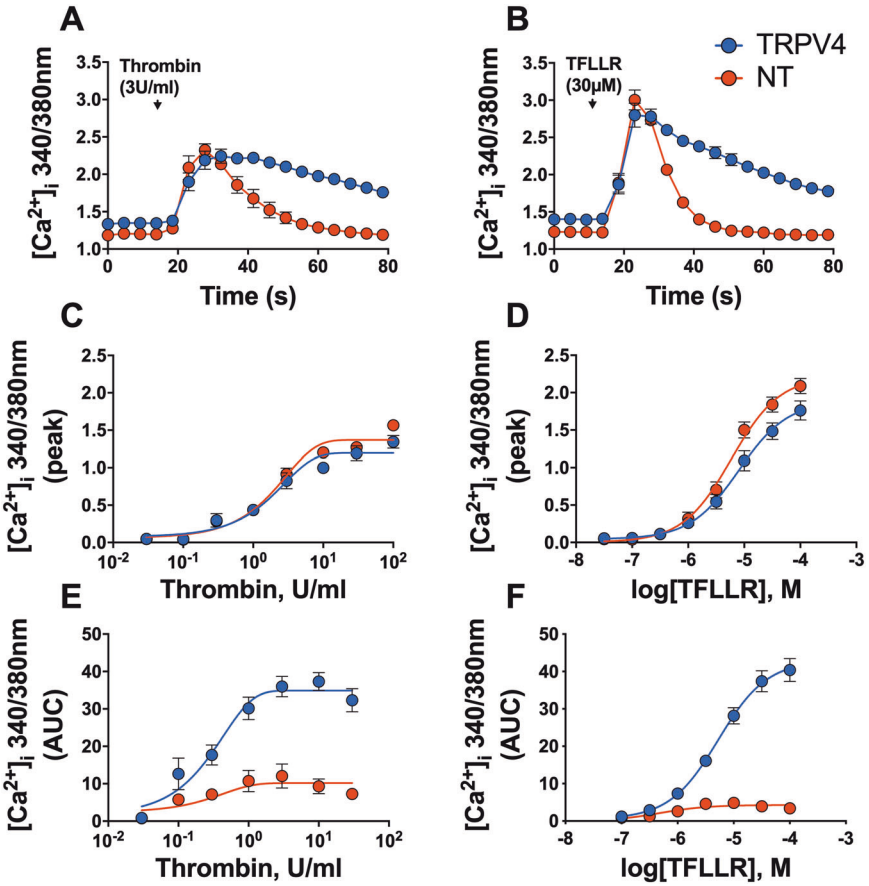


Fig. 4 Contribution of TRPV4 to PAR1-mediated Ca^{2+} mobilization. $[Ca^{2+}]_i$ was measured in NT-HEK (control) or TRPV4-HEK cells, that both endogenously express PAR1. **a, b** Time course of effects of thrombin (3 U/ml) and TFLLR peptide (30 μM) on both cell types. **c, d** Effects of graded concentrations of thrombin and TFLLR on the maximal Ca^{2+} response, to determine the contribution of TRPV4 to PAR1-mediated transient Ca^{2+}-mobilization from intracellular stores. **e, f** Effects of graded concentrations of thrombin and TFLLR on the total Ca^{2+} response (AUC, 60 s post stimulation) to reveal the contribution of TRPV4 to sustained PAR1-mediated Ca^{2+} signaling. Data are presented as mean ± s.e.m., $n = 5–6$.

reporter) transfer from the upper insert to the bottom chamber. Activation of TRPV4 (GSK101, 3 nM) significantly increased permeability of FITC-dextran (100 μg/ml; 70 kDa) across the monolayer relative to vehicle treatment (4.1-fold increase in FITC intensity), thus suggesting that TRPV4 signaling can promote junctional changes in endothelia. To further demonstrate a functional role for TRPV4 in modulating barrier integrity, GSK101-mediated FITC-dextran permeation was abolished in cells pretreated with HC06 (Fig. 5e). PAR1 activation (TFLLR, 10 μM) also increased permeability of FITC-dextran relative to vehicle treatment (4.02-fold increase), and this was blocked by 30 min pretreatment with Vorapaxar (100 nM), a potent PAR1-selective competitive antagonist of TFLLR. To investigate the contribution of TRPV4 in PAR1-mediated permeability, cells were pretreated for 30 min with the TRPV4 antagonist HC06 (1 μM). This resulted in a significant reduction in TFLLR-mediated FITC-dextran permeability (2.6-fold increase relative to vehicle, Fig. 5f). Together, these observations demonstrate that TRPV4 contributes to PAR1-stimulated signaling and vascular permeability, but are not essential for PAR1-mediated Ca^{2+} mobilization. While further studies are required to understand the precise cell signaling pathways involved, these data support a role for Gαq-mediated signaling for PAR1–TRPV4 functional interactions in HEK cells, and Gαq-independent signaling processes to modulate barrier integrity in endothelial cells.

To further support these endothelial monolayer permeability studies, cell–cell junction integrity was also assessed by fluorescence imaging. Cells were treated, fixed and stained to reveal the localization of the endothelial junctional protein VE-cadherin, the actin cytoskeleton, and nucleus. Consistent with previous studies [21], PAR1 activation for 30 min induced a destabilization of cell–cell junctions, shown by elongation of adherens junctions and presence of inter-endothelial gaps, when compared with vehicle treatment. Pretreatment with the TRPV4 antagonist HC06 prevented the TFLLR-induced extension of adherens junctions, but did not prevent the presence of gaps (Fig. 6). Consistent with the FITC-dextran permeability findings (Fig. 5b), TRPV4 inhibition reduces PAR1-mediated junction elongation and destabilization, and therefore supports a role for TRPV4 activity in the modulation of cell–cell junctions. However, the presence of TFLLR-induced inter-endothelial gaps with HC06 pretreatment suggests that PAR1-mediated junctional remodeling is also likely to be driven by TRPV4-independent signaling.

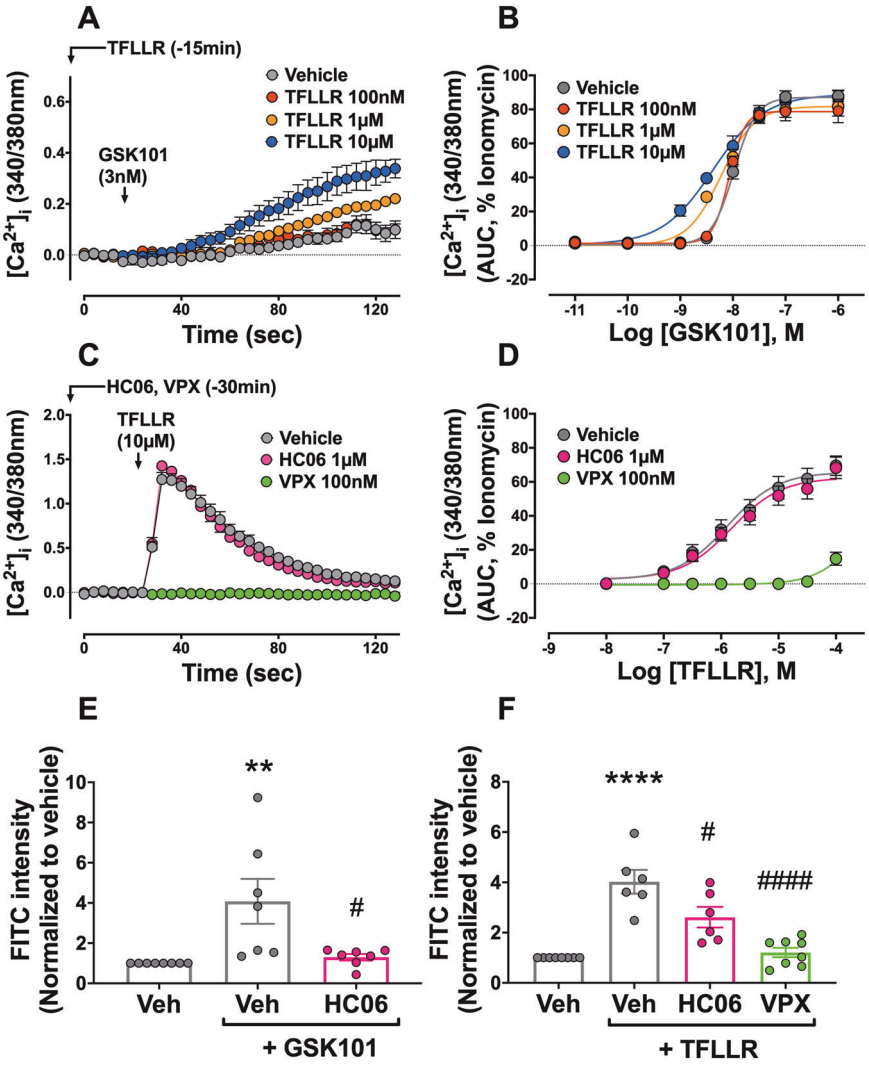


Fig. 5 Contribution of TRPV4 to PAR1-evoked Ca^{2+} signaling and endothelial hyperpermeability in HUVEC. a Time trace of TRPV4 agonist GSK101 (3 nM) pretreated with three different concentrations of PAR1 agonist TFLLR. **b** Effect of graded concentrations of GSK101 (AUC) following pretreatment with TFLLR demonstrated the functional presence of TRPV4 in HUVEC, and indicated that TFLLR induces a leftwards shift in the GSK101 curve. **c** Time trace of TFLLR following pretreatment of cells with the TRPV4 antagonist HC06 or the PAR1 antagonist VPX. **d** Graded concentrations of TFLLR following treatment with vehicle, HC06 or VPX (AUC) confirmed a role for functional TRPV4 and PAR1 in the TFLLR Ca^{2+} response. Calcium signaling data are presented as mean ± s.e.m., $n = 6$–7. To determine the role of TRPV4 and PAR1 in endothelial permeability, the passage of a fluorescent reporter dye (FITC-Dextran) was measured across confluent HUVEC monolayers grown on a porous membrane. **e** Stimulation with vehicle or GSK101 (3 nM, 30 min) was used to confirm a role for TRPV4 activity in HUVEC permeability, which was significantly reduced following pretreatment with HC06. **f** Stimulation with vehicle or TFLLR (10 μM, 30 min) was used to confirm a role for PAR1 in HUVEC permeability. Effect of pretreatment with HC06 (10 μM, 60 min) and VPX (100 nM, 60 min) reveals a role for TRPV4 in the TFLLR-induced hyperpermeability and confirms that TFLLR is mediating effects selectively via PAR1, respectively. Column graphs for permeability data represent mean ± s.e.m., $n = 6$–8. *, $^{\#}p < 0.05$; **$p < 0.01$; ****, $^{\#\#\#\#}p < 0.0001$; one-way ANOVA with Sidak's multiple comparison tests; relative to the vehicle only control (*), vehicle + GSK101 (**e**) or vehicle + TFLLR (**f**) (#).

Discussion

PARs have evolved to respond to extracellular proteases to regulate diverse physiological and pathophysiological processes [4]. As the major receptor for the coagulation protease thrombin, PAR1 has been extensively studied for its role in hemostasis, platelet aggregation and immune cell chemotaxis, and is known to be a dynamic receptor that can initiate downstream signaling by coupling to the $G\alpha_q$, $G\alpha_{12/13}$, and $G\alpha_i$ protein subunits [4, 7, 22]. This diversity of PAR1-mediated signaling outcomes can be further modulated according to proteolytic activity. Specifically, protease-dependent cleavage at different sites within the N-terminus can reveal distinct tethered ligand

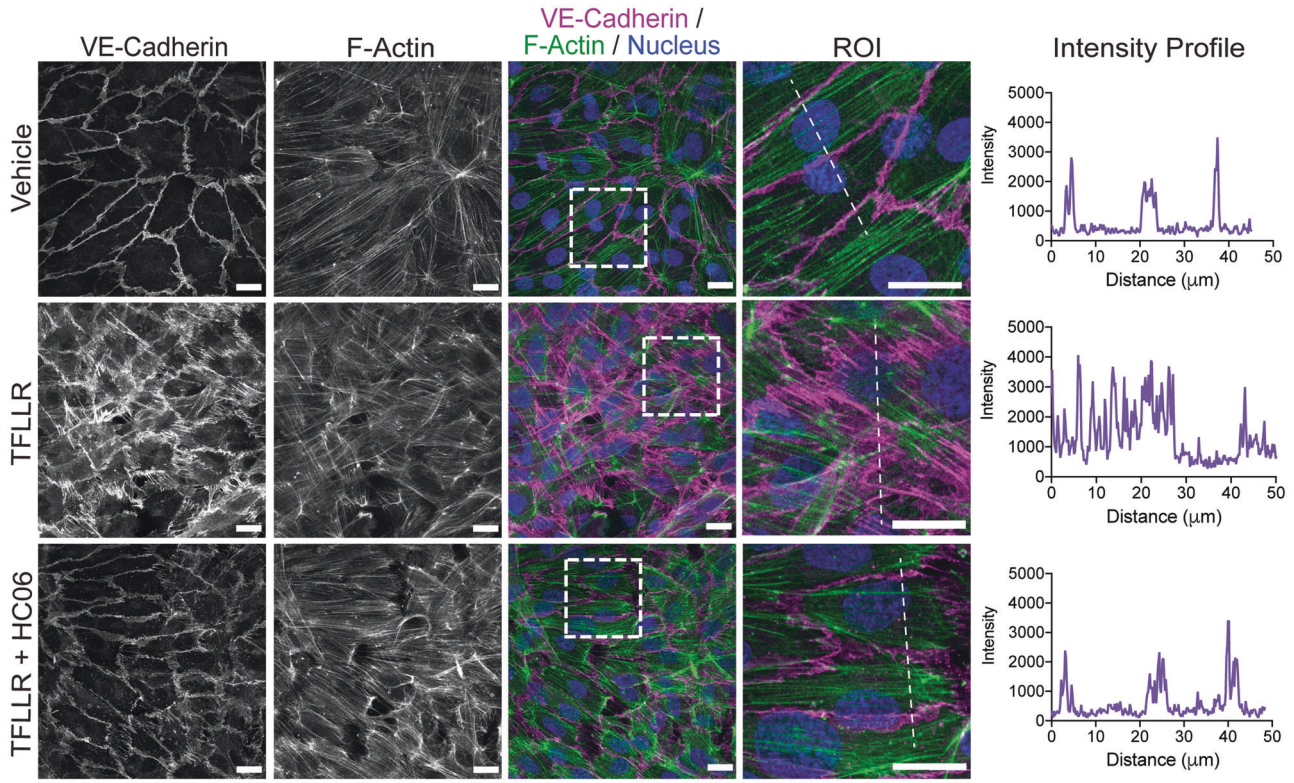


Fig. 6 Role of TRPV4 in PAR1-induced endothelial junctional remodeling. Confluent HUVEC were treated with TFLLR (10 μM) for 30 min after pretreatment with HC06 (1 μM, 1 h), or vehicle control. Cells were stained to reveal the localization of VE-cadherin (magenta), F-actin (green), and the nucleus (blue). Dashed boxes indicate a region of interest enlarged to show the localization and structure of VE-cadherin. Fluorescence intensity profiles correspond to dashed lines in ROI images. Scale bar, 20 μm. The images are representative of three regions from four independent experiments.

sequences, and each of these tethered ligands favors activation of specific signaling processes to achieve unique physiological outcomes [5].

In addition to their well-characterized function in platelet activation, thrombin and PAR1 are known to control endothelial permeability via downstream modulation of junctional proteins that perform essential roles in barrier formations and cytoskeleton dynamics [4, 21]. PAR1 coupling to $G\alpha_{q/11}$ and PLC-mediated release of intracellular calcium stores, for example, is required for the activation of myosin light chain kinase (MLCK), and when combined with $G\alpha_{12/13}$-mediated RhoA activity, this leads to cytoskeletal contraction and post-translational modification of endothelial junction proteins such as VE-cadherin, p120-catenin, and β-catenin [23]. Sustained PAR1 activation promotes transient disruption of these protein complexes, leading to increased endothelial permeability and plasma extravasation.

Functional interactions between GPCRs and TRP channels have previously been explored in a variety of cell settings, and while many PAR1-mediated intracellular signaling networks have been revealed, the potential for PAR1 signaling to utilize TRP channels to achieve edema has not been explored in detail. TRPV4 was proposed to be a downstream effector of PAR1-stimulated signaling pathways due to its known functional interactions with the related receptor PAR2, in inflammatory pathways, and its central role in vascular processes [14–16]. Influx of Ca^{2+} through TRP channels can contribute to, or amplify edema-associated signaling pathways and indirectly modulate MLCK-dependent contraction of smooth muscle cells [24]. In physiological states, TRPV4 responds to mechanical stimuli (e.g., shear stress, membrane stretch) or the release of endogenous arachidonic lipid metabolites, to regulate endothelial homeostasis, vascular tone and endothelial orientation by regulating $[Ca^{2+}]_i$ and nitric oxide synthase activity to promote niric oxide production [9, 25]. TRPV4 has also recently been shown to modulate phosphorylation and trafficking of vascular endothelial growth factor signaling via VEGF receptor-2 [26]. In environments where elevated or chronic TRPV4 activity is likely to occur, TRPV4-mediated increases in $[Ca^{2+}]_i$ cause junctional and cytoskeletal reorganization [12] and previous findings have revealed that sustained activation of TRPV4 by intravenous administration of GSK101 can cause irreversible endothelial barrier disruption and circulatory collapse [27]. Hence,

TRPV4 is proposed to be an important regulator of barrier function and a contributor to pathophysiological conditions where edema is observed and may therefore be a valuable therapeutic target. Indeed, orally active TRPV4 antagonists have previously been shown to effectively reverse pulmonary edema and associated pathologies, induced by high pulmonary venous pressure or myocardial infarction [28–30]. Furthermore, chronic treatment with a TRPV4 inhibitor in animal models did not affect osmoregulation or interfere with the activity of diuretics, which are often used as a therapy to help resolve edema in the clinic [30].

Thrombin and TFLLR-NH_2 have previously been shown to increase vascular permeability in the pulmonary microvasculature, and jejunum of wild-type but not PAR1 knockout mice [31, 32]. To further explore the potential for TRPV4 to function as a downstream effector of thrombin-PAR1-induced edema, we explored Evans Blue uptake and retention in tissues of the airways and upper GI tract and supported these studies with in vitro characterization of endothelia. PAR1 or TRPV4 stimulation resulted in increased Evans Blue permeability in tissues associated with the airways and upper GI tract, as determined by Evans Blue uptake following intravenous administration of PAR1- and TRPV4-selective pharmacological agents, thus suggesting that the observed edema is endothelial-specific, yet may also affect smooth muscle cell layers. The importance of TRPV4-mediated signaling in PAR1-mediated vessel hyperpermeability of the airways and upper GI tract were supported with the use of the selective TRPV4 antagonist HC06 and in $TRPV4^{-/-}$ mice. Together, these data indicate that TRPV4 functions as a component of PAR1-mediated changes in vascular permeability, which is consistent with previous studies demonstrating a role for TRPV4 as a downstream effector of trypsin/PAR2-mediated edema [15].

Comparable TFLLR-stimulated changes in barrier integrity were also observed when measuring permeation of a fluorescent reporter across a porous membrane with a confluent endothelial cell monolayer. Consistent with these findings, thrombin and TFLLR have previously been shown to decrease trans-endothelial electrical resistance in a myosin light chain-dependent manner [33]. It was also noted that the FITC-dextran permeation was more effectively blocked by antagonism of PAR1 relative to pretreatment with a selective TRPV4 antagonist. This role for TRPV4 was also supported by immunofluorescence imaging, where PAR1 activation resulted in junctional remodeling in HUVEC monolayers, yet this destabilization effect was prevented by pharmacological inhibition of TRPV4 activity. VE-cadherin is the main component of adherens junctions between endothelial cells and plays a major role in the regulation of vascular permeability. Cadherins are calcium dependent proteins and the phosphorylation, internalization, and actin-mediated contraction of VE-cadherin are known to modulate permeability in endothelial cells [34–36]. While the mechanisms remain unclear, these data suggest that inhibition of TRPV4 Ca^{2+} influx is not sufficient for preventing PAR1-mediated junction destabilization, but may be necessary for PAR1 to achieve its complete signaling repertoire to promote sustained edema. Further, the observation that HC06 could more effectively prevent Evans Blue permeation and retention in animals suggests that TRPV4 may play additional roles in complex cell systems and indicates the potential for PAR1 signaling to promote TRPV4 activity through additional mechanisms in mice, including through localized production of lipid mediators or mechanical activation that may occur through PAR1-mediated processes [9, 21].

In conclusion, we have demonstrated that TRPV4 functionally contributes to PAR1 signaling in the airways, upper GI tract and endothelial monolayers. The findings of this study suggest that TRPV4 is a signaling effector for multiple PAR family members and while pharmacological inhibition of TRPV4 diminishes PAR1-induced hyperpermeability, it may also contribute to other PAR1-mediated signaling processes that require further investigation.

Acknowledgements The authors thank Dr Wolfgang Liedtke (Duke University) for providing $TRPV4^{-/-}$ mice.

Funding Australian Research Council Centre of Excellence in Convergent Bio-Nano Science and Technology (NWB, TPD), NHMRC Australia 1046860 (PM, NWB), 1083480 (DPP).

Compliance with ethical standards

Conflict of interest The laboratories of NWB, DPP and NAV receive funding from Takeda Pharmaceuticals. The remaining authors declare no conflict of interests.

Publisher's note Springer Nature remains neutral with regard to jurisdictional claims in published maps and institutional affiliations.

References

1. Esper RJ, Nordaby RA, Vilarino JO, Paragano A, Cacharrón JL, Machado RA. Endothelial dysfunction: a comprehensive appraisal. Cardiovasc Diabetol. 2006;5:4.
2. Pober JS, Sessa WC. Evolving functions of endothelial cells in inflammation. Nat Rev Immunol. 2007;7:803–15.
3. Coughlin SR. Thrombin signalling and protease-activated receptors. Nature. 2000;407:258–64.
4. Ossovskaya VS, Bunnett NW. Protease-activated receptors: contribution to physiology and disease. Physiol Rev. 2004;84:579–621.
5. Zhao P, Metcalf M, Bunnett NW. Biased signaling of protease-activated receptors. Front Endocrinol. 2014;5:67.
6. Soh UJ, Dores MR, Chen B, Trejo J. Signal transduction by protease-activated receptors. Br J Pharmacol. 2010;160:191–203.
7. Coughlin SR. Protease-activated receptors in hemostasis, thrombosis and vascular biology. J Thromb Haemost. 2005;3:1800–14.

8. Bogatcheva NV, Garcia JG, Verin AD. Molecular mechanisms of thrombin-induced endothelial cell permeability. Biochemistry. 2002;67:75–84.
9. White JP, Cibelli M, Urban L, Nilius B, McGeown JG, Nagy I. TRPV4: molecular conductor of a diverse orchestra. Physiol Rev. 2016;96:911–73.
10. Filosa JA, Yao X, Rath G. TRPV4 and the regulation of vascular tone. J Cardiovasc Pharmacol. 2013;61:113–9.
11. Mendoza SA, Fang J, Gutterman DD, Wilcox DA, Bubolz AH, Li R, et al. TRPV4-mediated endothelial Ca^{2+} influx and vasodilation in response to shear stress. Am J Physiol Heart Circ Physiol. 2010;298:H466–76.
12. Phuong TTT, Redmon SN, Yarishkin O, Winter JM, Li DY, Krizaj D. Calcium influx through TRPV4 channels modulates the adherens contacts between retinal microvascular endothelial cells. J Physiol. 2017;595:6869–85.
13. Veldhuis NA, Poole DP, Grace M, McIntyre P, Bunnett NW. The G protein-coupled receptor-transient receptor potential channel axis: molecular insights for targeting disorders of sensation and inflammation. Pharmacol Rev. 2015;67:36–73.
14. Grant AD, Cottrell GS, Amadesi S, Trevisani M, Nicoletti P, Materazzi S, et al. Protease-activated receptor 2 sensitizes the transient receptor potential vanilloid 4 ion channel to cause mechanical hyperalgesia in mice. J Physiol. 2007;578(Pt 3):715–33.
15. Poole DP, Amadesi S, Veldhuis NA, Abogadie FC, Lieu T, Darby W, et al. Protease-activated receptor 2 (PAR2) protein and transient receptor potential vanilloid 4 (TRPV4) protein coupling is required for sustained inflammatory signaling. J Biol Chem. 2013;288:5790–802.
16. Zhao P, Lieu T, Barlow N, Sostegni SH, Korbmacher C, et al. Neutrophil elastase activates protease-activated receptor-2 (PAR2) and transient receptor potential vanilloid 4 (TRPV4) to cause inflammation and pain. J Biol Chem. 2015;290:13875–87.
17. Saifeddine M, El-Daly M, Mihara K, Bunnett NW, McIntyre P, Altier C, et al. GPCR-mediated EGF receptor transactivation regulates TRPV4 action in the vasculature. Br J Pharmacol. 2015; 172:2493–506.
18. McGrath JC, Drummond GB, McLachlan EM, Kilkenny C, Wainwright CL. Guidelines for reporting experiments involving animals: the ARRIVE guidelines. Br J Pharmacol. 2010;160:1573–6.
19. Veldhuis NA, Lew MJ, Abogadie FC, Poole DP, Jennings IE, Ivanusic JJ, et al. N-glycosylation determines ionic permeability and desensitization of the TRPV1 capsaicin receptor. J Biol Chem. 2012;287:21765–72.
20. Poole DP, Lieu T, Pelayo JC, Eriksson EM, Veldhuis NA, Bunnett NW. Inflammation-induced abnormalities in the subcellular localization and trafficking of the neurokinin 1 receptor in the enteric nervous system. Am J Physiol Gastrointest Liver Physiol. 2015;309:G248–59.
21. Timmerman I, Heemskerk N, Kroon J, Schaefer A, van Rijssel J, Hoogenboezem M, et al. A local VE-cadherin and Trio-based signaling complex stabilizes endothelial junctions through Rac1. J Cell Sci. 2015;128:3041–54.
22. Alberelli MA, De Candia E. Functional role of protease activated receptors in vascular biology. Vasc Pharmacol. 2014;62:72–81.
23. Thennes T, Mehta D. Heterotrimeric G proteins, focal adhesion kinase, and endothelial barrier function. Microvasc Res. 2012;83: 31–44.
24. Earley S, Brayden JE. Transient receptor potential channels in the vasculature. Physiol Rev. 2015;95:645–90.
25. Earley S, Pauyo T, Drapp R, Tavares MJ, Liedtke W, Brayden JE. TRPV4-dependent dilation of peripheral resistance arteries influences arterial pressure. Am J Physiol Heart Circ Physiol. 2009; 297:H1096–102.
26. Kanugula AK, Adapala RK, Midha P, Cappelli HC, Meszaros JG, Paruchuri S, et al. Novel noncanonical regulation of soluble VEGF/VEGFR2 signaling by mechanosensitive ion channel TRPV4. FASEB J. 2019;33:195–203.
27. Willette RN, Bao W, Nerurkar S, Yue TL, Doe CP, Stankus G, et al. Systemic activation of the transient receptor potential vanilloid subtype 4 channel causes endothelial failure and circulatory collapse: Part 2. J Pharmacol Exp Ther. 2008;326: 443–52.
28. Balakrishna S, Song W, Achanta S, Doran SF, Liu B, Kaelberer MM, et al. TRPV4 inhibition counteracts edema and inflammation and improves pulmonary function and oxygen saturation in chemically induced acute lung injury. Am J Physiol Lung Cell Mol Physiol. 2014;307:16.
29. Huh D, Leslie DC, Matthews BD, Fraser JP, Jurek S, Hamilton GA, et al. A human disease model of drug toxicity-induced pulmonary edema in a lung-on-a-chip microdevice. Sci Transl Med. 2012;4:159ra147.
30. Thorneloe KS, Cheung M, Bao W, Alsaid H, Lenhard S, Jian MY, et al. An orally active TRPV4 channel blocker prevents and resolves pulmonary edema induced by heart failure. Sci Transl Med. 2012;4:159ra148.
31. de Garavilla L, Vergnolle N, Young SH, Ennes H, Steinhoff M, Ossovskaya VS, et al. Agonists of proteinase-activated receptor 1 induce plasma extravasation by a neurogenic mechanism. Br J Pharmacol. 2001;133:975–87.
32. Vogel SM, Gao X, Mehta D, Ye RD, John TA, Andrade-Gordon P, et al. Abrogation of thrombin-induced increase in pulmonary microvascular permeability in PAR-1 knockout mice. Physiol Genomics. 2000;4:137–45.
33. Hirano M, Hirano K. Myosin di-phosphorylation and peripheral actin bundle formation as initial events during endothelial barrier disruption. Sci Rep. 2016;6:20989.
34. Gavard J, Gutkind JS. VEGF controls endothelial-cell permeability by promoting the beta-arrestin-dependent endocytosis of VE-cadherin. Nat Cell Biol. 2006;8:1223–34.
35. Giannotta M, Trani M, Dejana E. VE-cadherin and endothelial adherens junctions: active guardians of vascular integrity. Dev Cell. 2013;26:441–54.
36. Dejana E, Orsenigo F, Lampugnani MG. The role of adherens junctions and VE-cadherin in the control of vascular permeability. J Cell Sci. 2008;121:2115–22.

pubs.acs.org/acschemicalbiology

Articles

Application of a Sulfoxonium Ylide Electrophile to Generate Cathepsin X-Selective Activity-Based Probes

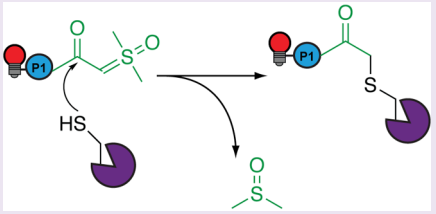
Simon J. Mountford,◆ Bethany M. Anderson,◆ Bangyan Xu, Elean S. V. Tay, Monika Szabo, My-Linh Hoang, Jiayin Diao, Luigi Aurelio, Rhiannon I. Campden, Erik Lindström, Erica K. Sloan, Robin M. Yates, Nigel W. Bunnett, Philip E. Thompson, and Laura E. Edgington-Mitchell*

Cite This: *ACS Chem. Biol.* 2020, 15, 718−727

Read Online

ACCESS | Metrics & More | Article Recommendations | Supporting Information

ABSTRACT: Cathepsin X/Z/P is cysteine cathepsin with unique carboxypeptidase activity. Its expression is associated with cancer and neurodegenerative diseases, although its roles during normal physiology are still poorly understood. Advances in our understanding of its function have been hindered by a lack of available tools that can specifically measure the proteolytic activity of cathepsin X. We present a series of activity-based probes that incorporate a sulfoxonium ylide warhead, which exhibit improved specificity for cathepsin X compared to previously reported probes. We apply these probes to detect cathepsin X activity in cell and tissue lysates, in live cells and in vivo, and to localize active cathepsin X in mouse tissues by microscopy. Finally, we utilize an improved method to generate chloromethylketones, necessary intermediates for synthesis of acyloxymethylketones probes, by way of sulfoxonium ylide intermediates. In conclusion, the probes presented in this study will be valuable for investigating cathepsin X pathophysiology.



INTRODUCTION

Cathepsin X (also referred to as cathepsin Z or P) is a cysteine cathepsin protease that is unique among its family members in that it exhibits strict carboxypeptidase activity. It is one of the most recently discovered cysteine cathepsins, and its functions during health and disease are still incompletely understood. Cathepsin X contributes to adhesion and maturation of macrophages and dendritic cells and suppresses clathrin-dependent phagocytosis through cleavage of profilin.[1,2] Cathepsin X regulates hormone signaling, where its cleavage of bradykinin, kallidin, or angiotensin leads to alterations in specificity toward their cognate receptors and divergent downstream signaling.[3] Cathepsin X is also expressed by neurons, where its cleavage of α-enolase regulates survival and the outgrowth of neurites.[4] Furthermore, cathepsin X expression is enriched in amyloid plaques, where it may have a protective effect against neurodegenerative disorders such as Alzheimer's disease,[5,6] and in the spinal cord during neuropathic pain.[7] Upregulation of cathepsin X mRNA has been reported in pathology-free regions of multiple sclerosis-affected brains,[8] and it has been implicated in the generation of IL-1β[9,10] and in mediating neuroinflammation.[9] It is also upregulated in the microenvironment of breast,[11] pancreatic,[12] prostate,[13] and gastric cancers,[14,15] where it likely promotes tumor invasion. Thus, cathepsin X holds promise as a clinical biomarker and therapeutic target in diverse diseases.

Like most cathepsins, cathepsin X is synthesized as a zymogen that becomes activated in the acidic environment of endolysosomes. Once activated, it may also be negatively regulated by endogenous inhibitors, though likely not cystatin C or stefin A.[16,17] In addition to its proteolytic functions, cathepsin X can also promote integrin-mediated signaling through an Arg-Gly-Asp (RGD) motif in its pro-domain.[12] As a result of these complex modes of post-translational regulation, traditional biochemical methods that survey total protein levels rarely reflect the pool of proteolytically active enzyme. The ability to specifically measure cathepsin X activity in its native environment is therefore required to define its precise proteolytic functions during health and disease.

To this end, efforts have been focused on developing fluorescent activity-based probes (ABPs) for cathepsin X. ABPs are small molecules that contain an electrophilic moiety (warhead), a recognition sequence that confers selectivity, and a fluorophore for detection.[18−20] When active, the protease initiates a nucleophilic attack on the warhead, resulting in the formation of a covalent, irreversible bond. Assessment of probe labeling can then be used to quantify protease activity by SDS-PAGE (in-gel fluorescence), fluorescent microscopy, flow cytometry, or optical imaging of whole tissues or organisms. Importantly, the covalent nature of probe binding allows for target confirmation by immunoprecipitation with specific antibodies or affinity purification followed by proteomic analysis.

Received: November 28, 2019
Accepted: February 5, 2020
Published: February 5, 2020

Downloaded via NEW YORK UNIV on September 30, 2021 at 15:27:27 (UTC).
See https://pubs.acs.org/sharingguidelines for options on how to legitimately share published articles.

ACS Publications

© 2020 American Chemical Society

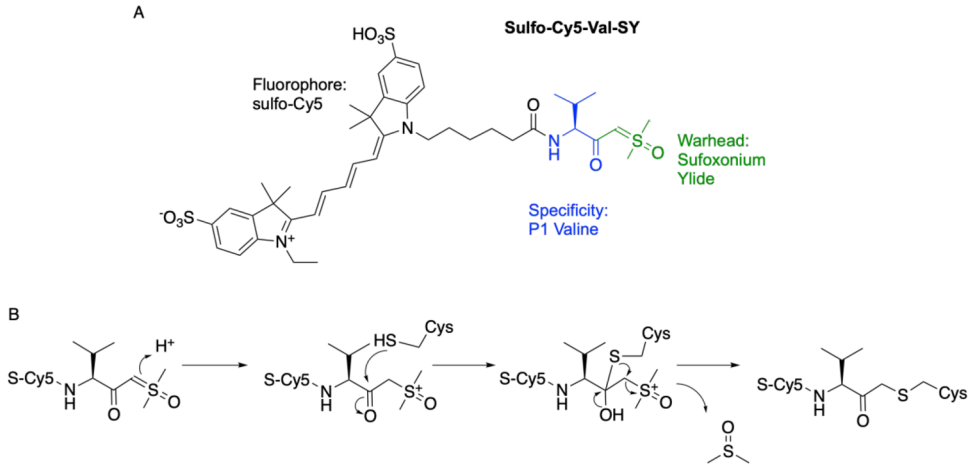
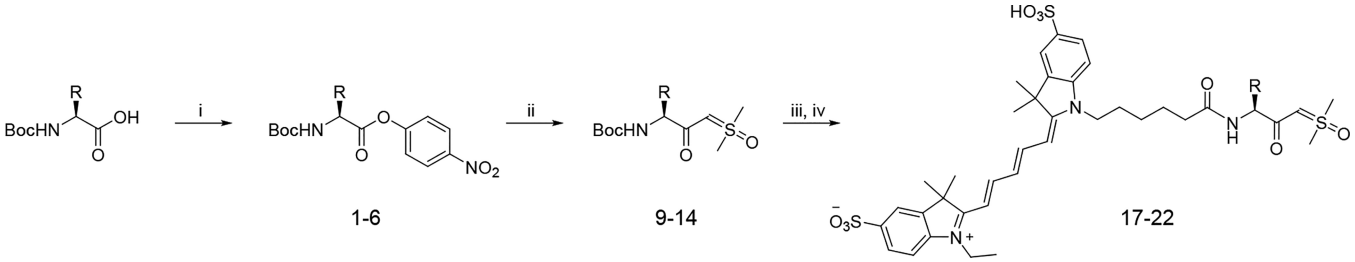


Figure 1. Design of a sulfoxonium ylide-based activity-based probe. (A) Structure of sCy5-Val-SY (**17**) probe. (B) The proposed mechanism by which sCy5-Val-SY binds to an activated cysteine protease.

Scheme 1. Synthesis of sCy5-AA-SY Probes[a]



[a](i) 4-Nitrophenylchloroformate, Et_3N, DMAP, CH_2Cl_2, 0°C, 6 h. (ii) $SOMe_3^+I^-$, KOtBu, THF, reflux, then cool to 0°C and add nitrophenyl ester. (iii) TFA/CH_2Cl_2 (1:1), (iv) sulfo-Cy5, PyClock, DIPEA, DMF, rt, 18 h. The synthetic routes for related compounds Cbz-Lys(sCy5)-SY (**7**, **15**, **23**) and sCy5-Phe-Val-SY (**8**, **16**, **24**) can be found in Scheme S1 and S2, respectively).

Probes with absolute specificity for cathepsin X have not been previously reported. BMV109, a fluorescently quenched ABP with a tetrafluorophenoxymethyl ketone warhead, is a pan-cathepsin probe that targets X, B, S, and L.[21] Because cathepsin X is a similar size as cathepsin B, one of the most abundant and ubiquitously expressed cathepsins, it can be difficult to clearly resolve these two proteases by SDS-PAGE, which precludes accurate quantification by in-gel fluorescence. MGP140 is an epoxide-based probe that exhibits greater specificity for cathepsin X than BMV109 but also potently reacts with cathepsin B.[22] If mice are pretreated with GB11-NH_2, an inhibitor of cathepsin B, S, and L, prior to MGP140 injection, specific labeling of cathepsin X can be achieved. However, this manipulation of the system results in hyper-activation of cathepsin X, possibly a compensatory response due to the loss of cathepsin B activity. Thus, it is crucial to develop probes with improved specificity for cathepsin X to allow for a more detailed investigation of its physiological activity.

Herein, we describe a series of ABPs containing a novel sulfoxonium ylide warhead that exhibit previously unseen selectivity for cathepsin X. We applied these probes to measure cathepsin X activity in lysates and live cells and in live mice. We also used the sulfoxonium ylide as a stepping stone to access chloromethylketones, which are intermediates in the synthesis of acyloxymethylketones (AOMK), warheads commonly used in probes for cathepsins and other cysteine proteases. This new method does not require generation of diazomethanes to access chloromethylketones and is thus a safer alternative to the previously used methods. By comparison to the sulfoxonium ylide probes, AOMK probes bearing identical recognition sequences exhibited unique specificity profiles and low reactivity with cathepsin X. Thus, sulfoxonium ylide probes represent a clear advancement in the tools that are available to study cathepsin X function.

RESULTS AND DISCUSSION

Design and Characterization of a Sulfoxonium Ylide Probe. To explore new potential warheads for cysteine cathepsins, we designed and synthesized an ABP containing a dimethyl sulfoxonium ylide electrophile. This design was initially inspired by a dimethyl sulfonium salt reported to inhibit cathepsin B in 1988 by Shaw.[23] To increase the electrophilicity of this warhead, and thus its reactivity with the catalytic cysteine residue, we modified the dimethyl sulfonium salt to a dimethyl sulfoxonium ylide. We also incorporated a valine residue as the P1 recognition sequence and a sulfo-Cyanine 5 (sCy5) fluorophore to yield our initial probe, sCy5-Val-SY (**17**; Figure 1), synthesized according to Scheme 1.

To determine its reactivity profile, we first incubated sCy5-Val-SY (**17**) with protein lysates prepared from RAW264.7 cells, an immortalized mouse macrophage line that contains high levels of active cysteine cathepsins.[21] Cells were lysed in citrate buffer (pH 5.5) to provide optimal conditions for preserving cathepsin activity, and the probe was added at 1 μM for 20 min. We then resolved the lysates by SDS-PAGE and scanned the gel for sCy5 fluorescence using a flatbed laser scanner. We observed exclusive, concentration- and time-

https://dx.doi.org/10.1021/acschembio.9b00961
ACS Chem. Biol. 2020, 15, 718−727

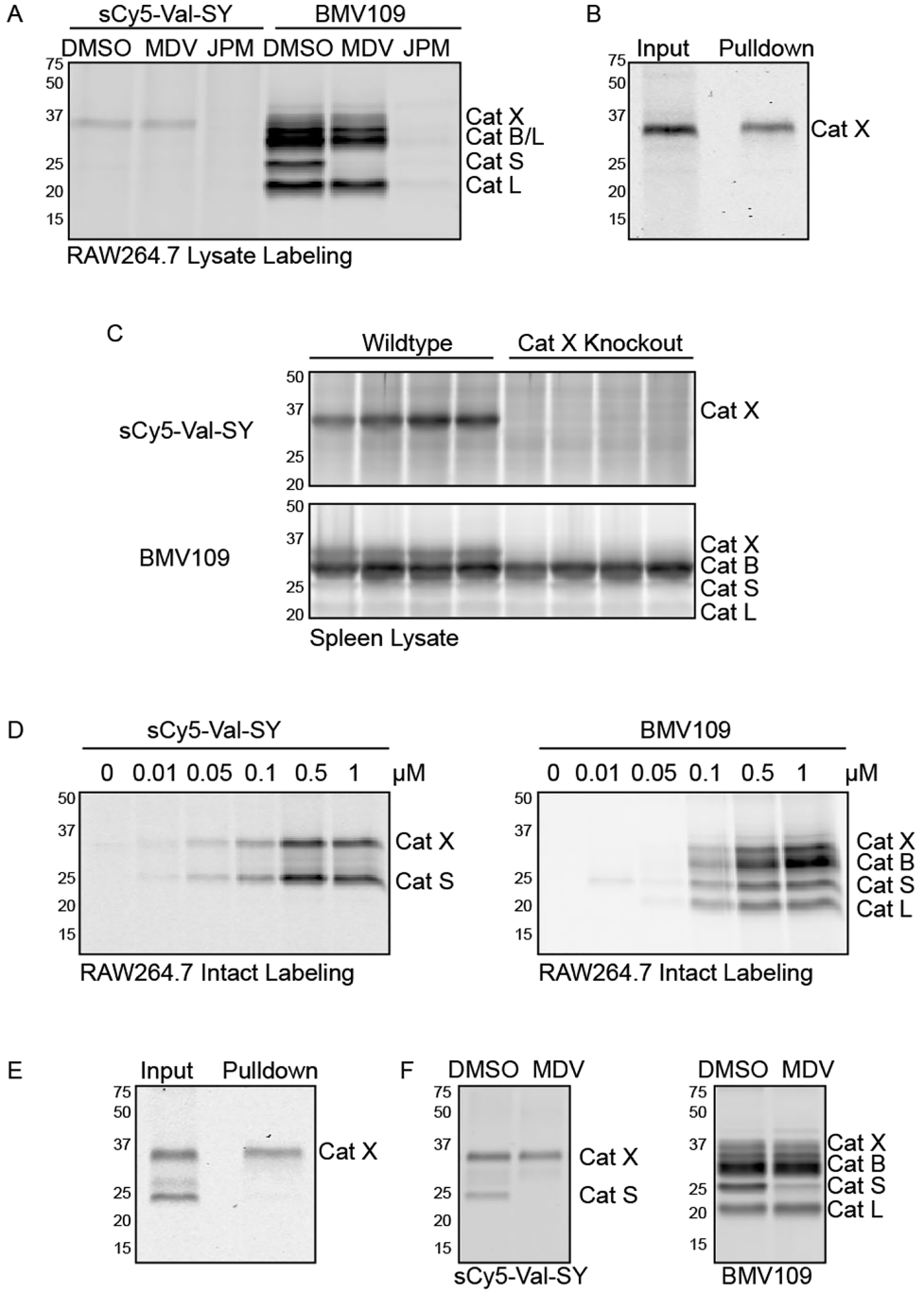


Figure 2. In vitro characterization of sCy5-Val-SY (**17**). (A) Labeling of RAW264.7 lysates with sCy5-Val-SY or BMV109 alone or after pretreatment with 10 μM MDV-590 (cathepsin S inhibitor) or JPM-OEt (pan cysteine cathepsin inhibitor). (B) Immunoprecipitation of sCy5-Val-SY-labeled samples in A with a cathepsin X-specific antibody. (C) Labeling of splenic lysates from wildtype or cathepsin X-deficient mice with sCy5-Val-SY or BMV109. (D) Labeling of living RAW264.7 cells with increasing doses of sCy5-Val-SY or BMV109 for 2 h. (E) Immunoprecipitation of sCy5-Val-SY-labeled samples in D with a cathepsin X-specific antibody. (F) Labeling of living RAW264.7 cells with and without overnight pretreatment with 10 μM MDV-590 with sCy5-Val-SY or BMV109 (1 μM, 2 h). Also refer to Figure S1.

dependent labeling of a ~35-kDa protease (Figures 2A and S1A,B). This labeling was prevented by pretreatment of the lysates with JPM-OEt, a pan-cysteine cathepsin inhibitor, confirming that this protease was a member of the cysteine cathepsin family (Figure 2A). In contrast, MDV-590, a specific inhibitor for cathepsin S,[24] did not compete for sCy5-Val-SY (**17**) binding. We compared the labeling profile to that of BMV109, the pan-cathepsin probe and found that the sCy5-Val-SY (**17**)-labeled protease was the same molecular weight as BMV109-labeled cathepsin X.[21] We confirmed that this protease was indeed cathepsin X by immunoprecipitating sCy5-Val-SY (**17**)-labeled lysates with a cathepsin X-specific antibody (Figure 2B).

Next, we tested the ability of sCy5-Val-SY (**17**) to label cathepsin X in mouse splenic lysates. As we observed in macrophage lysates, the probe exhibited exclusive reactivity with cathepsin X in splenic lysates from wildtype mice, and this labeling was absent in lysates prepared from spleens of

https://dx.doi.org/10.1021/acschembio.9b00961
ACS Chem. Biol. 2020, 15, 718−727

cathepsin X-deficient mice (Figure 2C). By comparison, BMV109 strongly labeled cathepsin B and, to a lesser extent, cathepsin S and L.

Having observed unique specificity of sCy5-Val-SY (**17**) in cell and tissue lysates, we sought to assess the probe's permeability and specificity profile in living RAW264.7 cells. After incubating the probe with live cells for increasing lengths of time (at 1 μM) or with increasing probe concentrations (for 2 h), we analyzed lysates by in-gel fluorescence as above. Here, we observed time- and concentration-dependent labeling of two proteases (Figures 2D and S1C), which we identified as cathepsin X and S by immunoprecipitation (Figure 2E) and competition with MDV-590 (Figure 2F), respectively. We were surprised to see cathepsin S labeling in live cells, given its lack of binding to sCy5-Val-SY (**17**) in cell lysates, where we had confirmed high levels of cathepsin S activity with BMV109. This suggests that the reactivity of cathepsin S with the sulfoxonium ylide is dependent on the labeling conditions. We attempted to explore this by lysing the cells in various buffers that might mimic the endosomal environment of cathepsin S but we were not able to improve the labeling of cathepsin S in lysates (not shown).

Nonetheless, the sulfoxonium ylide probe exhibited clear labeling of cathepsin X in lysates and live cells with considerably improved selectivity compared to BMV109 (Figure 2D,F). To our knowledge, it is the first covalent ABP for cathepsin X that does not also bind to cathepsin B or L. As observed in Figure 2, it is difficult to distinguish cathepsin X labeling from cathepsin B with BMV109 due to the similarity in size of the two proteases. However, sCy5-Val-SY (**17**) allows for clear delineation of cathepsin X activity.

Sulfoxium Ylide Library with Variable P1 Residues. To improve the specificity and potency of the probe for cathepsin X, we generated a small library of sulfoxonium ylide probes by varying the amino acids in the P1 position (Scheme 1, Table 1). In RAW264.7 lysates, probes bearing Ile (**18**), Leu (**19**), Nle (**20**), and Phe (**21**) all showed similar specificity for cathepsin X as sCy5-Val-SY (**17**) with sCy5-Leu-SY (**19**) and sCy5-Nle-SY (**20**) exhibiting a clear improvement in potency (Figure 3A). Cbz-Lys(sCy5)-SY (**23**), in which the sCy5 was attached via the lysine side chain, exhibited a loss of specificity, favoring cathepsin S over X and B. sCy5-Phe-Val-SY (**24**), in which a P2 Phe residue was incorporated, also exhibited a loss of specificity (Figures 3A and S2). The labeling profile of this probe was similar to BMV109, though it showed improved potencies for cathepsin X and S compared to BMV109. A hydrophobic S2 pocket is a feature of virtually all cysteine cathepsins, which may explain the increased affinity of a dipeptide probe for other members of the family.[25]

Table 1. Amino Acids Used in Compounds 1−24 (Scheme 1)

Boc-AA-OH	Boc-AA-ONp	Boc-AA-SY	sCy5-AA-SY
Boc-Val-OH	1	9	17
Boc-Ile-OH	2	10	18
Boc-Leu-OH	3	11	19
Boc-Nle−OH	4	12	20
Boc-Phe-OH	5	13	21
Boc-Trp-OH	6	14	22

In murine kidney lysates, Leu and Nle conferred the most potency and specificity for cathepsin X with Cbz-Lys (**23**), Phe (**21**), and Phe-Val (**24**) yielding broader reactivity and Val (**17**) and Ile (**18**) exhibiting weaker labeling (Figures 3B and S2).

To examine the potency and permeability of the sulfoxinium ylide probe series in living cells, we applied them to RAW264.7 cells for 2 h. Probes bearing Trp (**22**), Val (**17**), Ile (**18**), Leu (**19**), Nle (**20**), and Phe (**21**) labeled cathepsin X and S to similar extents and with similar potency, whereas Cbz-Lys (**23**) exhibited a preference for cathepsin S, and Phe-Val (**24**) labeled B and L in addition to X and S (Figures 3C and S2A,C−G). We confirmed the 25-kDa protease labeled by sCy5-Nle-SY (**20**) to be cathepsin S by competition with two cathepsin S-specific inhibitors, MDV-590 and Z-FL-COCHO (Figure S2B).

We tested the specificity of these probes for cathepsin X in a human breast cancer line known to express very low levels of cathepsin S, MDA-MB-231^{HM}.[26] These cells also allowed us to test whether the probes could bind to human cathepsin X (in addition to mouse cathepsin X shown previously). When we incubated the probes with MDA-MB-231 cells for shorter time periods, we observed very little labeling of cathepsin X (not shown); however, clear labeling was observed after overnight incubation (Figure 3D). This likely reflects differences in the rates of endocytosis between macrophages and tumor cells and suggests that the probes may be taken up directly into the endolysosmal pathway rather than by diffusion through membranes. The sulfoxonium ylide probe series generally shows specific labeling of cathepsin X in these cells with minimal cross-reactivity occurring only at 5 μM. Cbz-Lys(sCy5)-SY (**23**) and especially sCy5-Phe-Val-SY (**24**) exhibited the most cross-reactivity with cathepsin B and L.

In Vivo Characterization of sCy5-Nle-SY. Taking into consideration all of the data from cell and tissue lysates and live mouse and human cells, sCy5-Nle-SY (**20**) emerged as the probe showing the highest potency and selectivity for cathepsin X. Thus, we elected to move forward with this probe for in vivo studies. We injected the probe into mice intravenously, and after 2 h of circulation tissues were harvested, lysed, and analyzed for probe labeling by fluorescent SDS-PAGE. We observed labeling of cathepsin X in liver, kidney, colon, stomach, and spleen (Figure 4A), and this was confirmed by immunoprecipitation with a cathepsin X antibody (Figure 4B). While some labeling of cathepsin S was also observed, the overall specificity profile was clearly improved compared to BMV109, which also strongly labels cathepsin B and L.

It is important to note that, in addition to cathepsin X and S, we also observed the labeling of additional species in vivo at 55 and 15 kDa with sCy5-Nle-SY (**20**). The 55-kDa species was weakly observed when kidney lysates were labeled but not the 15-kDa species. We synthesized a biotinylated Nle-SY probe in attempt to affinity purify these species; however, labeling with this probe was much weaker than the sCy5 probe suggesting that sCy5 contributes in part to selectivity (not shown). Efforts to develop new affinity probes are ongoing.

We then used confocal microscopy to image sCy5-Nle-SY (**20**) fluorescence in kidney cryosections after in vivo probe administration. We observed strong punctate sCy5 fluorescence reminiscent of endolysosomal staining, and this signal largely overlapped with immunoreactive cathepsin X (Figure 5). Thus, we could use sCy5-Nle-SY (**20**) to distinguish active cathepsin X relative to total cathepsin X in tissues after in vivo administration.

https://dx.doi.org/10.1021/acschembio.9b00961
ACS Chem. Biol. 2020, 15, 718−727

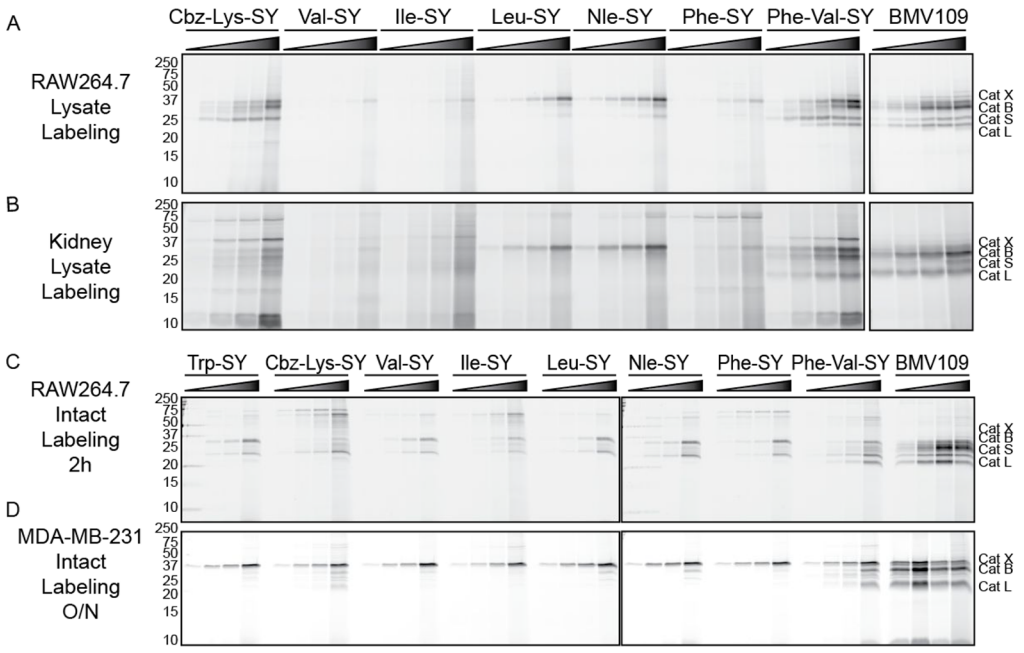


Figure 3. In vitro characterization of a sulfoxonium ylide library in lysates and live cells. Labeling of (A) RAW264.7 lysates (0.01, 0.05, 0.1, 0.5, 1, 5 μM), (B) kidney lysates (0.1, 0.5, 1, 5 μM), (C) live RAW264.7 cells (0.1, 0.5, 1, 5 μM), or (D) live MDA-MB-231^{HM} cells (0.1, 0.5, 1, 5 μM) with the indicated SY probe or BMV109, as analyzed by in-gel fluorescence. Also refer to Figure S2.

Sulfoxonium Ylides as a Route to Acyloxymethylketone Probes. Many of the reported activity-based probes for cysteine proteases incorporate AOMK or phenoxymethylketone (PMK) warheads.[21,27−31] Synthesis of these electrophiles requires generation of chloromethylketone intermediates, a process that has historically been achieved, among other methods, through generation of diazomethane, an extremely explosive yellow gas.[32] To avoid this potentially dangerous reaction, we utilized sulfoxonium ylides as key intermediates to make AOMK derivatives (Scheme 2, Table 2). Previous studies have shown that chiral integrity was maintained after both ylide formation and conversion to the chloromethylketone using these conditions.[33,34]

Using this method, we successfully generated three AOMK probes bearing Nle (**31**), Phe (**32**), and Cbz-Lys (**33**), suggesting that this method could be broadly applied to the synthesis of diverse ABPs. We compared the reactivity of the new AOMK probes with the corresponding sulfoxonium ylide probes in living RAW2647 cells. The AOMK probes were much less potent than the ylide probes, suggesting reduced reactivity. These probes labeled cathepsin B and S but not X (Figure 6A,B), We also compared the labeling profile of sCy5-Nle-SY (**20**) and sCy5-Nle-AOMK (**31**) in RAW264.7 lysates. Here, we could only observe clear labeling of cathepsin B with the AOMK probe at 50 μM, whereas with the SY probe we observed cathepsin X labeling at 0.1 μM (Figure S3A,B). We also treated living RAW264.7 cells overnight, and again 5 μM sCy5-Nle-AOMK labeled cathepsin B and S but minimal cathepsin X (Figure S3C,D).

We compared the serum stability of sCy5-Nle-SY and sCy5-Nle-AOMK probes by preincubating them with fetal calf serum. No loss of activity was observed, compared to untreated probes, suggesting that both probes are stable in serum (Figure S4A). In splenic lysates from wildtype mice, sCy5-Nle-SY (1 μM) clearly labeled cathepsin X and to a lesser extent cathepsin S, but no labeling of cathepsin X was observed in splenic lysates from cathepsin X-deficient mice. As in RAW264.7 lysates, 1 μM sCy5-Nle-AOMK exhibited only weak labeling of cathepsin B splenic lysates, which did not differ between wildtype and cathepsin X-deficient mice (Figure S4B). Finally, we tested sCy5-Nle-AOMK in vivo and analyzed its labeling in tissues. Only weak labeling of cathepsin B and S was observed in the colon but not in other tissues examined (Figure S4C).

CONCLUSIONS

We have designed a new dimethyl sulfoxonium ylide warhead that exhibits unique selectivity toward cysteine cathepsin proteases in cell lysates, live cells, and in mouse and human tissues. Our best probe, sCy5-Nle-SY (**20**), is the most selective probe for cathepsin X to date, showing specificity in cell lysates and cells that express low levels of cathepsin S. While this probe does cross-react with cathepsin S in live macrophages and in vivo, it does not appreciably label cathepsin B or L, which is a clear improvement over the only other covalent probes that target cathepsin X (BMV109, MGP140, DCG-04). The use of sCy5-Nle-SY (**20**) allows for clear measurement of the activity of the cathepsin X by SDS-PAGE, whereas this was difficult with previous probes due to confounding levels of cathepsin B labeling.

Furthermore, we established that the sulfoxonium ylide warhead is stable enough for in vivo detection of cathepsin X activity. While the probe is most reliable in gel-based analyses of tissue lysates, sCy5-Nle-SY (**20**) signal was bright enough to detect by confocal microscopy. In conjunction with cathepsin X-specific antibodies, this method can distinguish active from inactive cathepsin X by cellular imaging and in the future could be applied to advance our understanding of the function of cathepsin X in animal models of disease.

Little is known about the preferred cleavage sequence for cathepsin X and this may be partially due to the difficulties in profiling carboxypeptidases with fluorogenic substrate libraries

https://dx.doi.org/10.1021/acschembio.9b00961
ACS Chem. Biol. 2020, 15, 718−727

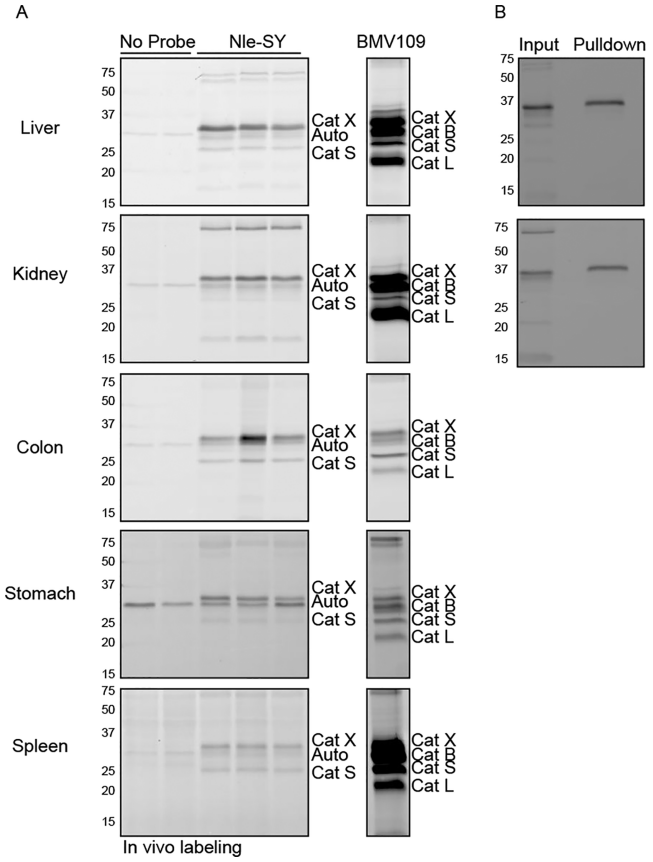


Figure 4. In vivo characterization of sCy5-Nle-SY (20). (A) SDS-PAGE and in-gel fluorescence of tissue lysates prepared from mice that received no probe (NP), sCy5-Nle-SY, or BMV109. BMV109-labeled samples were cut from the same gel and are presented at the same gain setting as the other samples in the corresponding tissue. Gains for each tissue were set individually to display optimal contrast for cathepsin X labeling. An autofluorescent band was observed in the no-probe control (labeled as Auto). (B) Immunoprecipitation of liver and kidney samples from A with a cathepsin X-specific antibody. Also refer to Figure S2.

(i.e., its preference for a free carboxylic acid limits the choice and placement of the fluorophore). A study by Devanathan and colleagues used a fluorogenic substrate library based on the aminobenzoic acid-Phe(4-NO_2) fluorophore-quencher pair to explore the preferred P1 and P2 residues of cathepsin X.[35] In the P1 position, weak reactivity was observed with Met, Phe, Tyr, Thr, Gln, Glu, Lys, and Arg; however, Val, Ile, Leu, and Trp (among others) were not tolerated at all. By contrast, these residues were among the most potent in the P1 position of our sulfoxonium ylide library. In a similar study by Puzer and colleagues, in which aminobenzoic acid and Lys-(dinitrophenol) were used as the fluorophore quencher pair, Leu was well tolerated in the P1 position.[36] In both screens, most residues were well tolerated in the P2 position with the exception of proline. In direct contrast to this, cathepsin X has been shown to cleave natural substrates such as CXCL-12 with proline at the P2 position.[37] Collectively, these studies demonstrate the dependence of probe structure on specificity and warrant the development of larger sulfoxonium ylide libraries with greater diversity of P1, P2, and P3 residues. Given the observed crossreactivity of the current probes with other as yet unknown proteases (e.g., in the kidney), we anticipate that expanding the sulfoxonium ylide library will open the door to selective ABPs for other proteases in addition to cathepsin X.

In conclusion, our new sulfoxonium ylide-based probes will be valuable for understanding the contribution of cathepsin X to normal physiology and disease and for establishing cathepsin X and a drug target and diagnostic marker for cancer and other inflammatory and neurodegenerative diseases.

EXPERIMENTAL SECTION

Synthetic Methods and Key Resources. Detailed synthetic methods and a table summarizing the source of all key reagents (antibodies, chemicals, biochemical assays, cell lines, and mouse strains) can be found within the Supporting Information.

Cell Culture. RAW264.7 or MDA-MB-231^{HM} cells were cultured in DMEM containing 10% fetal bovine serum (v/v) and 1% antibiotic/antimycotic (v/v). RAW264.7 cells were passaged by scraping with a rubber policeman, while MDA-MB-231^{HM} cells were lifted with 0.02% EDTA (w/v) in phosphate-buffered saline (PBS).

Animals. All experiments involving animals were approved by the Monash University Animal Ethics Committee. Male C57BL/6J mice were obtained from the Monash Animal Research Platform and used in accordance with the guidelines at 8−10 weeks of age. Snap-frozen spleens from wildtype and cathepsin X knockout mice, as described in ref 38 were obtained from the University of Calgary and used in accordance with the University of Calgary Animal Care and Use Committee.

Cell Lysate Labeling and SDS-PAGE Analysis. Cells were harvested by scraping, washed once with PBS, and resuspended in lysis buffer containing 50 mM citrate [pH 5.5], 0.5% CHAPS (w/v), 0.1% Triton X-100 (v/v), and 4 mM DTT. Cells were incubated on ice for at least 10 min with intermittent vortexing followed by centrifugation (21×*g* at 4 °C for 5 min). Cleared supernatants were then transferred to a fresh tube and protein concentration was determined by BCA. Total protein (50 μg) was aliquoted into tubes in a final volume of 20 μL lysis buffer. Where indicated, JPM-OEt or MD-590 was added from a 100× DMSO stock and incubated at 37 °C for 20 min prior to probe addition. The indicated concentration of the probe was added from a 100× DMSO stock. Labeling was carried out at 37 °C for 20 min, and the reactions were quenched by the addition of 5× sample buffer (200 mM Tris-Cl [pH 6.8], 8% SDS (w/v), 0.04% bromophenol blue (w/v), 5% β-mercaptoethanol (v/v), and 40% glycerol (v/v)). Samples were then boiled for 5 min and proteins were resolved on a 15% SDS-PAGE gel. The gels were scanned on a Typhoon 5 flatbed laser scanner at 633/670 nm excitation/emission to detect sCy5 fluorescence.

Live Cell Labeling. RAW cells or MDA-MB-231^{HM} cells were plated in 12-well plates. Where indicated, MDV-590, a closely related analogue to the cathepsin S-specific inhibitor MIV-247,[24] Z-FL-COCHO[39] or DMSO (vehicle) was added at 10 μM or 20 μM, respectively, from a 1000× DMSO stock for overnight incubation. When the cell density reached 80%, the indicated probes were added at the indicated concentrations from a 1000× DMSO stock and allowed to incubate for the indicated time. Media was then removed and replaced with PBS. The cells were then scraped and transferred to tubes, and lysis and SDS-PAGE analysis were carried out as above, except skipping the probe addition step.

Serum Stability Test. Probes (5 mM) were diluted 10-fold in fetal calf serum followed by 3 h incubation at 37 °C. Probe-containing serum was then diluted 10-fold in serum-free DMEM, followed by incubation with living RAW265.7 cells for 2 h (5 μM final probe concentration). Serum-free media containing 5 μM probe was used as a control. Cells were then harvested, lysed, and analyzed by in-gel fluorescence as above.

Tissue Analysis. Tissues or biopsies were harvested from healthy mice or patients, respectively, and snap frozen. At the time of analysis, lysis buffer was added at 10× (v/w), and tissues were sonicated on ice. Cleared lysates were labeled with the indicated probe and analyzed as above. For in vivo labeled tissues, mice were first injected

https://dx.doi.org/10.1021/acschembio.9b00961
ACS Chem. Biol. 2020, 15, 718−727

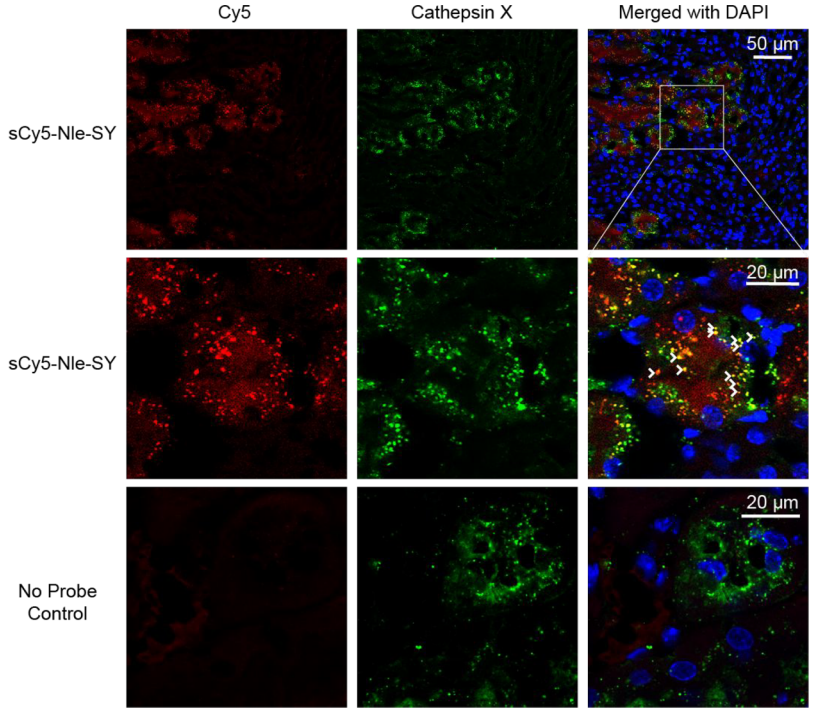
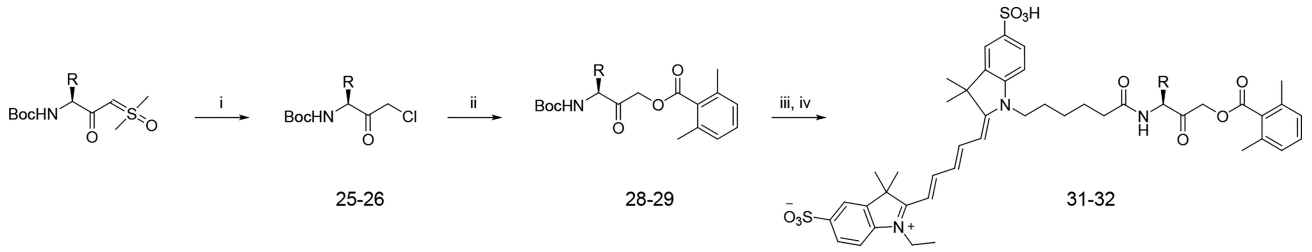


Figure 5. Confocal microscopy of cathepsin X labeling in kidney with sCy5-Nle-SY. Kidney sections from sCy5-Nle-SY-injected mice or no-probe control were analyzed for sCy5 fluorescence (red) or cathepsin X immunoreactivity (green) along with DAPI (blue) to visualize nuclei. The middle row is a zoomed-in image of the top row, as denoted by the white box. White arrowheads point to areas where the probe and immunoreactive cathepsin X are overlaid.

Scheme 2. Synthesis of sCy5-AA-AOMK Probes via a Sulfoxonium Ylide Intermediate[a]



[a](i) 1.15 eq HCl in dioxane, THF, reflux, 4 h. (ii) 2,6-dimethylbenzoic acid, KF, DMF, rt, 18 h. (iii) TFA/CH_2Cl_2 (1:1), (iv) sulfo-Cy5, PyClock, DIPEA, DMF, rt, 18 h. The synthetic route for the related compound Cbz-Lys(sCy5)-AOMK (**27**, **30**, **33**) can be found in Scheme S1.

Table 2. Amino Acids Used in Compounds 25−33 (Scheme 2)

Boc-AA-SY	Boc-AA-CH_2Cl	Boc-AA-AOMK	sCy5-AA-AOMK
Boc-Nle-SY 12	25	28	31
Boc-Phe-SY 13	26	29	32

intravenously via the tail vein with sCy5-Nle-SY, BMV109, or sCy5-Nle-AOMK (50 nmol in 100 μL 10% DMSO/PBS (v/v) or vehicle control). Tissues were harvested after 2 h and analyzed as above except without further probe addition.

Immunoblotting. After detection of in-gel fluorescence, human cancer samples were transferred to a nitrocellulose membrane using the TransBlot system (Bio-Rad). Loading and transfer efficiency were assessed by Ponceau Stain (Sigma). The membrane was then incubated overnight at 4 °C with a goat anticathepsin X antibody (1:1000) in Odyssey Blocking Buffer (LiCor) diluted by 50% in PBS (v/v) containing 0.05% Tween-20 (v/v; PBS-T). After washing the membrane three times with PBS-T, it was incubated with donkey antigoat-IRDYE800 (1:10 000) at rt for 1 h. After washing, binding was detected by scanning the membrane on a Typhoon 5 (IR-long filter).

Immunoprecipitation Assay. Probe-labeled lysate from above (in sample buffer) was divided into input or pulldown (∼50 μg total protein each). The input sample was stored at −20 °C. The pulldown sample was diluted in 500 μL IP buffer (PBS [pH 7.4], 0.5% NP-40 (*v*/*v*), 1 mM EDTA). Goat anticathepsin X antibody (10 μL) was added along with 40 μL slurry of prewashed Protein A/G agarose beads. Samples were rotated overnight at 4 °C. Beads were then washed four times with IP buffer followed by a final wash in 0.9% NaCl (w/v). Beads were then resuspended in 2× sample buffer and boiled. The pulldown supernatants, alongside the input samples, were analyzed by fluorescent SDS-PAGE as above.

Confocal Microscopy. Kidney tissues from mice that received sCy5-Nle-SY (or vehicle control) above were fixed overnight in 4% paraformaldehyde in PBS (w/v) followed by overnight cryoprotection in 30% sucrose (v/v). Tissues were embedded in OCT, frozen on dry ice, and sectioned at 10 μm. Immunostaining for cathepsin X was carried out according to standard protocols. In brief, sections were air-dried, fixed in cold acetone for 10 min, air-dried again, and then rehydrated in PBS. Sections were blocked in PBS containing 3% normal horse serum (v/v) with 0.1% Triton X-100 (v/v). Goat

https://dx.doi.org/10.1021/acschembio.9b00961
ACS Chem. Biol. 2020, 15, 718−727

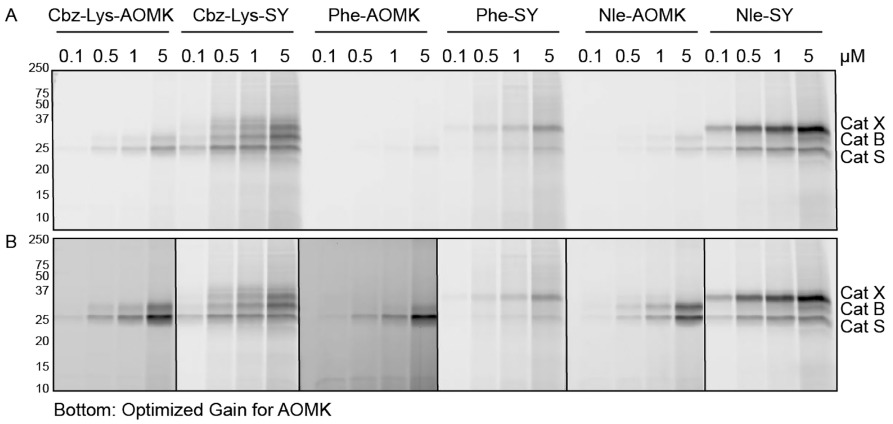


Figure 6. In vitro and in vivo characterization of AOMK and sulfoxonium ylide probes. (A) Labeling of living RAW264.7 cells with the indicated AOMK and SY probes (0.1, 0.5, 1, 5 μM), as analyzed by in-gel fluorescence. In the top panel, gain settings are equal for all samples. In the bottom panel (B), gain settings were individually set to show optimal contrast for the AOMK probes. Also refer to Figures S3 and S4.

anticathepsin X was added at 1:100 in blocking buffer overnight at 4 °C. Sections were then washed, and a secondary antibody, donkey antigoat-AlexaFluor594, was added at 1:500 for 1 h at rt. Sections were stained with DAPI for 5 min, washed, and mounted with ProLong Diamond. Staining was analyzed using a Leica SP8 inverted confocal microscope.

Statistical Analysis. All experiments were performed with at least three biological replicates. Data are reported as means ± SEM. Statistical significance was determined by comparing two groups using a Student's *t* test, and *p* values of less than 0.05 were considered significant.

■ ASSOCIATED CONTENT

Supporting Information

The Supporting Information is available free of charge at https://pubs.acs.org/doi/10.1021/acschembio.9b00961.

Detailed synthetic methods, molecular formula strings and a key resource table, as well as additional synthetic schemes (PDF)

Experimental data (XLS)

■ AUTHOR INFORMATION

Corresponding Author

Laura E. Edgington-Mitchell − *Department of Biochemistry and Molecular Biology, Bio21 Molecular Science and Biotechnology Institute, The University of Melbourne, Parkville, Victoria 3052, Australia; Drug Discovery Biology, Monash Institute of Pharmaceutical Sciences, Monash University, Parkville, Victoria 3052, Australia; Department of Oral and Maxillofacial Surgery, Bluestone Center for Clinical Research, New York University College of Dentistry, New York, New York 10010, United States;* orcid.org/0000-0002-6810-6149; Email: laura.edgingtonmitchell@unimelb.edu.au

Authors

Simon J. Mountford − *Medicinal Chemistry, Monash Institute of Pharmaceutical Sciences, Monash University, Parkville, Victoria 3052, Australia*

Bethany M. Anderson − *Department of Biochemistry and Molecular Biology, Bio21 Molecular Science and Biotechnology Institute, The University of Melbourne, Parkville, Victoria 3052, Australia; Drug Discovery Biology, Monash Institute of Pharmaceutical Sciences, Monash University, Parkville, Victoria 3052, Australia*

Bangyan Xu − *Department of Biochemistry and Molecular Biology, Bio21 Molecular Science and Biotechnology Institute, The University of Melbourne, Parkville, Victoria 3052, Australia*

Elean S. V. Tay − *Department of Biochemistry and Molecular Biology, Bio21 Molecular Science and Biotechnology Institute, The University of Melbourne, Parkville, Victoria 3052, Australia*

Monika Szabo − *Medicinal Chemistry, Monash Institute of Pharmaceutical Sciences, Monash University, Parkville, Victoria 3052, Australia*

My-Linh Hoang − *Medicinal Chemistry, Monash Institute of Pharmaceutical Sciences, Monash University, Parkville, Victoria 3052, Australia*

Jiayin Diao − *Drug Discovery Biology, Monash Institute of Pharmaceutical Sciences, Monash University, Parkville, Victoria 3052, Australia*

Luigi Aurelio − *Medicinal Chemistry, Monash Institute of Pharmaceutical Sciences, Monash University, Parkville, Victoria 3052, Australia*

Rhiannon I. Campden − *Snyder Institute for Chronic Disease and Department of Biochemistry and Molecular Biology, University of Calgary, Calgary, Alberta T2N 1N4, Canada*

Erik Lindström − *Medivir AB, Huddinge 141 22, Sweden*

Erica K. Sloan − *Drug Discovery Biology, Monash Institute of Pharmaceutical Sciences, Monash University, Parkville, Victoria 3052, Australia*

Robin M. Yates − *Snyder Institute for Chronic Disease and Department of Biochemistry and Molecular Biology, University of Calgary, Calgary, Alberta T2N 1N4, Canada*

Nigel W. Bunnett − *Drug Discovery Biology, Monash Institute of Pharmaceutical Sciences, Monash University, Parkville, Victoria 3052, Australia; Department of Craniofacial Biology, New York University College of Dentistry, New York, New York 10010, United States; Department of Pharmacology and Experimental Therapeutics, The University of Melbourne, Parkville, Victoria 3052, Australia*

Philip E. Thompson − *Medicinal Chemistry, Monash Institute of Pharmaceutical Sciences, Monash University, Parkville, Victoria 3052, Australia;* orcid.org/0000-0002-5910-7625

Complete contact information is available at: https://pubs.acs.org/10.1021/acschembio.9b00961

Author Contributions

◆S.J.M. and B.M.A. contributed equally to this work.

https://dx.doi.org/10.1021/acschembio.9b00961
ACS Chem. Biol. 2020, 15, 718−727

Author Contributions

LEM conceived study, planned all experiments, analyzed data, wrote manuscript, and contributed funding. SJM, MLH, MS, and LA synthesized the compounds included in the study. SJM completed the compound characterization and contributed to the writing of the manuscript. BMA, BX, ESVT, MLH, and JD executed the experiments and collected data. RIC and RMY contributed cathepsin X knockout tissues for the study. EKS provided MDA-MB-231^{HM} cells. EL provided cathepsin S inhibitor. PT contributed intellectually and supervised the compound synthesis. NB contributed funds for the work.

Notes

The authors declare the following competing financial interest(s): N.W.B. is a founding scientist of Endosome Therapeutics Inc. Research in N.W.B.'s laboratory is supported in part by Takeda Pharmaceuticals, Inc.

■ ACKNOWLEDGMENTS

We thank C. Nowell for maintaining the imaging facilities at the Monash Institute of Pharmaceutical Sciences. MDA-MB-231^{HM} cells were a kind gift from Z. Ou, Fudan University, Shanghai Cancer Center. L.E.M. was supported by an Early Career Fellowship from the National Health and Medical Research Council of Australia (NHMRC, GNT1091636), a Grimwade Fellowship funded by the Russell and Mab Grimwade Miegunyah Fund at the University of Melbourne, a DECRA Fellowship from the Australian Research Council (ARC, DE180100418), and by seed grants from Monash University. N.W.B. was supported by grants from the National Institutes of Health (NS102722, DE026806, DK118971) and the United States Department of Defense (W81XWH1810431).

■ ABBREVIATIONS

ABP, activity-based probe
SY, sulfoxonium ylide
AOMK, acyloxymethylketone
PMK, phenoxymethylketone

■ REFERENCES

(1) Obermajer, N., Švajger, U., Bogyo, M., Jeras, M., and Kos, J. (2008) Maturation of Dendritic Cells Depends on Proteolytic Cleavage by Cathepsin X. *J. Leukocyte Biol. 84*, 1306−1315.
(2) Pečar Fonović, U., and Kos, J. (2015) Cathepsin X Cleaves Profilin 1 C-Terminal Tyr139 and Influences Clathrin-Mediated Endocytosis. *PLoS One 10*, e0137217.
(3) Nägler, D. K., Kraus, S., Feierler, J., Mentele, R., Lottspeich, F., Jochum, M., and Faussner, A. (2010) A Cysteine-Type Carboxypeptidase, Cathepsin X, Generates Peptide Receptor Agonists. *Int. Immunopharmacol. 10*, 134−139.
(4) Obermajer, N., Doljak, B., Jamnik, P., Fonović, U. P., and Kos, J. (2009) Cathepsin X Cleaves the C-Terminal Dipeptide of Alpha- and Gamma-Enolase and Impairs Survival and Neuritogenesis of Neuronal Cells. *Int. J. Biochem. Cell Biol. 41*, 1685−1696.
(5) Wendt, W., Zhu, X.-R., Lübbert, H., and Stichel, C. C. (2007) Differential Expression of Cathepsin X in Aging and Pathological Central Nervous System of Mice. *Exp. Neurol. 204*, 525−540.
(6) Hafner, A., Glavan, G., Obermajer, N., Živin, M., Schliebs, R., and Kos, J. (2013) Neuroprotective Role of Γ-Enolase in Microglia in a Mouse Model of Alzheimer's Disease Is Regulated by Cathepsin X. *Aging Cell 12*, 604−614.
(7) Leichsenring, A., Bäcker, I., Wendt, W., Andriske, M., Schmitz, B., Stichel, C. C., and Lübbert, H. (2008) Differential Expression of Cathepsin S and X in the Spinal Cord of a Rat Neuropathic Pain Model. *BMC Neurosci. 9*, 80−13.
(8) Huynh, J. L., Garg, P., Thin, T. H., Yoo, S., Dutta, R., Trapp, B. D., Haroutunian, V., Zhu, J., Donovan, M. J., Sharp, A. J., and Casaccia, P. (2014) Epigenome-Wide Differences in Pathology-Free Regions of Multiple Sclerosis−Affected Brains. *Nat. Neurosci. 17*, 121−130.
(9) Allan, E. R. O., Campden, R. I., Ewanchuk, B. W., Tailor, P., Balce, D. R., McKenna, N. T., Greene, C. J., Warren, A. L., Reinheckel, T., and Yates, R. M. (2017) A Role for Cathepsin Z in Neuroinflammation Provides Mechanistic Support for an Epigenetic Risk Factor in Multiple Sclerosis. *J. Neuroinflammation 14*, 103.
(10) Orlowski, G. M., Colbert, J. D., Sharma, S., Bogyo, M., Robertson, S. A., and Rock, K. L. (2015) Multiple Cathepsins Promote Pro−IL-1β Synthesis and NLRP3-Mediated IL-1β Activation. *J. Immunol. 195*, 1685−1697.
(11) Edgington-Mitchell, L. E., Rautela, J., Duivenvoorden, H. M., Jayatilleke, K. M., van der Linden, W. A., Verdoes, M., Bogyo, M., and Parker, B. S. (2015) Cysteine Cathepsin Activity Suppresses Osteoclastogenesis of Myeloid-Derived Suppressor Cells in Breast Cancer. *Oncotarget 6*, 27008−27022.
(12) Akkari, L., Gocheva, V., Kester, J. C., Hunter, K. E., Quick, M. L., Sevenich, L., Wang, H.-W., Peters, C., Tang, L. H., Klimstra, D. S., Reinheckel, T., and Joyce, J. A. (2014) Distinct Functions of Macrophage-Derived and Cancer Cell-Derived Cathepsin Z Combine to Promote Tumor Malignancy via Interactions with the Extracellular Matrix. *Genes Dev. 28*, 2134−2150.
(13) Nägler, D. K., Krüger, S., Kellner, A., Ziomek, E., Ménard, R., Buhtz, P., Krams, M., Roessner, A., and Kellner, U. (2004) Up-Regulation of Cathepsin X in Prostate Cancer and Prostatic Intraepithelial Neoplasia. *Prostate 60*, 109−119.
(14) Bernhardt, A., Kuester, D., Roessner, A., Reinheckel, T., and Krueger, S. (2010) Cathepsin X-Deficient Gastric Epithelial Cells in Co-Culture with Macrophages: Characterization of cytokine response and migration capability after Helicobacter pylori infection. *J. Biol. Chem. 285*, 33691−33700.
(15) Krueger, S., Kalinski, T., Hundertmark, T., Wex, T., Küster, D., Peitz, U., Ebert, M., Nägler, D. K., Kellner, U., Malfertheiner, P., Naumann, M., Röcken, C., and Roessner, A. (2005) Up-Regulation of Cathepsin X inHelicobacter Pylori Gastritis and Gastric Cancer. *J. Pathol. 207*, 32−42.
(16) Nägler, D. K., Zhang, R., Tam, W., Sulea, T., Purisima, E. O., and Ménard, R. (1999) Human Cathepsin X: a Cysteine Protease with Unique Carboxypeptidase Activity. *Biochemistry 38*, 12648−12654.
(17) Duivenvoorden, H. M., Rautela, J., Edgington-Mitchell, L. E., Spurling, A., Greening, D. W., Nowell, C. J., Molloy, T. J., Robbins, E., Brockwell, N. K., Lee, C. S., Chen, M., Holliday, A., Selinger, C. I., Hu, M., Britt, K. L., Stroud, D. A., Bogyo, M., Möller, A., Polyak, K., Sloane, B. F., O'Toole, S. A., and Parker, B. S. (2017) Myoepithelial Cell-Specific Expression of Stefin a as a Suppressor of Early Breast Cancer Invasion. *J. Pathol. 243*, 496−509.
(18) Edgington, L. E., Verdoes, M., and Bogyo, M. (2011) Functional Imaging of Proteases: Recent Advances in the Design and Application of Substrate-Based and Activity-Based Probes. *Curr. Opin. Chem. Biol. 15*, 798−805.
(19) Edgington, L. E., and Bogyo, M. (2013) In Vivo Imaging and Biochemical Characterization of Protease Function Using Fluorescent Activity-Based Probes. *Curr. Protoc. Chem. Biol. 5*, 25−44.
(20) Sanman, L. E., and Bogyo, M. (2014) Activity-Based Profiling of Proteases. *Annu. Rev. Biochem. 83*, 249−273.
(21) Verdoes, M., Oresic Bender, K., Segal, E., van der Linden, W. A., Syed, S., Withana, N. P., Sanman, L. E., and Bogyo, M. (2013) Improved Quenched Fluorescent Probe for Imaging of Cysteine Cathepsin Activity. *J. Am. Chem. Soc. 135*, 14726−14730.
(22) Paulick, M. G., and Bogyo, M. (2011) Development of Activity-Based Probes for Cathepsin X. *ACS Chem. Biol. 6*, 563−572.
(23) Shaw, E. (1988) Peptidyl Sulfonium Salts. a New Class of Protease Inhibitors. *J. Biol. Chem. 263*, 2768−2772.

https://dx.doi.org/10.1021/acschembio.9b00961
ACS Chem. Biol. 2020, 15, 718−727

(24) Hewitt, E., Pitcher, T., Rizoska, B., Tunblad, K., Henderson, I., Sahlberg, B. L., Grabowska, U., Classon, B., Edenius, C., Malcangio, M., and Lindstrom, E. (2016) Selective Cathepsin S Inhibition with MIV-247 Attenuates Mechanical Allodynia and Enhances the Antiallodynic Effects of Gabapentin and Pregabalin in a Mouse Model of Neuropathic Pain. *J. Pharmacol. Exp. Ther. 358*, 387−396.
(25) Turk, V., Stoka, V., Vasiljeva, O., Renko, M., Sun, T., Turk, B., and Turk, D. (2012) Cysteine Cathepsins: From Structure, Function and Regulation to New Frontiers. *Biochim. Biophys. Acta, Proteins Proteomics 1824*, 68−88.
(26) Chang, X.-Z., Li, D.-Q., Hou, Y.-F., Wu, J., Lu, J.-S., Di, G.-H., Jin, W., Ou, Z.-L., Shen, Z.-Z., and Shao, Z.-M. (2008) Identification of the Functional Role of AF1Q in the Progression of Breast Cancer. *Breast Cancer Res. Treat. 111*, 65−78.
(27) Edgington, L. E., van Raam, B. J., Verdoes, M., Wierschem, C., Salvesen, G. S., and Bogyo, M. (2012) An Optimized Activity-Based Probe for the Study of Caspase-6 Activation. *Chem. Biol. 19*, 340−352.
(28) Edgington, L. E., Verdoes, M., Ortega, A., Withana, N. P., Lee, J., Syed, S., Bachmann, M. H., Blum, G., and Bogyo, M. (2013) Functional Imaging of Legumain in Cancer Using a New Quenched Activity-Based Probe. *J. Am. Chem. Soc. 135*, 174−182.
(29) Edgington, L. E., Berger, A. B., Blum, G., Albrow, V. E., Paulick, M. G., Lineberry, N., and Bogyo, M. (2009) Noninvasive Optical Imaging of Apoptosis by Caspase-Targeted Activity-Based Probes. *Nat. Med. 15*, 967−973.
(30) Verdoes, M., Edgington, L. E., Scheeren, F. A., Leyva, M., Blum, G., Weiskopf, K., Bachmann, M. H., Ellman, J. A., and Bogyo, M. (2012) A Nonpeptidic Cathepsin S Activity-Based Probe for Noninvasive Optical Imaging of Tumor-Associated Macrophages. *Chem. Biol. 19*, 619−628.
(31) Oresic Bender, K., Ofori, L., van der Linden, W. A., Mock, E. D., Datta, G. K., Chowdhury, S., Li, H., Segal, E., Sanchez Lopez, M., Ellman, J. A., Figdor, C. G., Bogyo, M., and Verdoes, M. (2015) Design of a Highly Selective Quenched Activity-Based Probe and Its Application in Dual Color Imaging Studies of Cathepsin S Activity Localization. *J. Am. Chem. Soc. 137*, 4771−4777.
(32) Pace, V., Castoldi, L., and Pregnolato, M. (2013) α-Amino-α'-Halomethylketones: Synthetic Methodologies and Pharmaceutical Applications as Serine and Cysteine Protease Inhibitors. *Mini-Rev. Med. Chem. 13*, 988−996.
(33) Wang, D., Schwinden, M. D., Radesca, L., Patel, B., Kronenthal, D., Huang, M.-H., and Nugent, W. A. (2004) One-Carbon Chain Extension of Esters to α-chloroketones: A Safer Route without Diazomethane. *J. Org. Chem. 69*, 1629−1633.
(34) Wang, D., and Nugent, W. A. (2007) Synthesis of anti-α-amino epoxide by one carbon homologation of an α-amino ester: (2S,3S)-1,2-epoxy-3-(Boc-amino)-4-phenylbutane. *Org. Syntheses 84*, 58−67.
(35) Devanathan, G., Turnbull, J. L., Ziomek, E., Purisima, E. O., Ménard, R., and Sulea, T. (2005) Carboxy-Monopeptidase Substrate Specificity of Human Cathepsin X. *Biochem. Biophys. Res. Commun. 329*, 445−452.
(36) Puzer, L., Cotrin, S. S., Cezari, M. H. S., Hirata, I. Y., Juliano, M. A., Stefe, I., Turk, D., Turk, B., Juliano, L., and Carmona, A. K. (2005) Recombinant Human Cathepsin X Is a Carboxymonopeptidase Only: a Comparison with Cathepsins B and L. *Biol. Chem. 386*, 2321−2325.
(37) Staudt, N. D., Aicher, W. K., Kalbacher, H., Stevanovic, S., Carmona, A. K., Bogyo, M., and Klein, G. (2010) Cathepsin X Is Secreted by Human Osteoblasts, Digests CXCL-12 and Impairs Adhesion of Hematopoietic Stem and Progenitor Cells to Osteoblasts. *Haematologica 95*, 1452−1460.
(38) Sevenich, L., Schurigt, U., Sachse, K., Gajda, M., Werner, F., Muller, S., Vasiljeva, O., Schwinde, A., Klemm, N., Deussing, J., Peters, C., and Reinheckel, T. (2010) Synergistic Antitumor Effects of Combined Cathepsin B and Cathepsin Z Deficiencies on Breast Cancer Progression and Metastasis in Mice. *Proc. Natl. Acad. Sci. U. S. A. 107*, 2497−2502.
(39) Walker, B., Lynas, J. F., Meighan, M. A., and Brömme, D. (2000) Evaluation of Dipeptide A-Keto-B-Aldehydes as New Inhibitors of Cathepsin S. *Biochem. Biophys. Res. Commun. 275*, 401−405.

https://dx.doi.org/10.1021/acschembio.9b00961
ACS Chem. Biol. 2020, 15, 718−727

Endosomal signaling of delta opioid receptors is an endogenous mechanism and therapeutic target for relief from inflammatory pain

Nestor N. Jimenez-Vargas[a], Jing Gong[b], Matthew J. Wisdom[c], Dane D. Jensen[c,d], Rocco Latorre[c], Alan Hegron[c], Shavonne Teng[c], Jesse J. DiCello[e], Pradeep Rajasekhar[e], Nicholas A. Veldhuis[e,f], Simona E. Carbone[e], Yang Yu[a], Cintya Lopez-Lopez[a], Josue Jaramillo-Polanco[a], Meritxell Canals[g], David E. Reed[a], Alan E. Lomax[a], Brian L. Schmidt[d], Kam W. Leong[b], Stephen J. Vanner[a], Michelle L. Halls[e,1], Nigel W. Bunnett[c,1], and Daniel P. Poole[e,f,1]

[a]Gastrointestinal Diseases Research Unit, Division of Gastroenterology, Queen's University, Kingston, ON, Canada K7L 2V7; [b]Department of Biomedical Engineering, Fu Foundation School of Engineering and Applied Science, Columbia University, New York, NY 10032; [c]Department of Molecular Pathobiology, New York University College of Dentistry, New York, NY 10010; [d]Bluestone Center for Clinical Research, New York University College of Dentistry, New York, NY 10010; [e]Drug Discovery Biology, Monash Institute of Pharmaceutical Sciences, Monash University, Parkville, VIC 3052, Australia; [f]Australian Research Council Centre of Excellence in Convergent Bio-Nano Science and Technology, Monash University, Parkville, VIC 3052, Australia; and [g]Centre for Membrane Proteins and Receptors and Division of Physiology, Pharmacology, and Neuroscience, School of Life Sciences, Queen's Medical Centre, University of Nottingham, NG7 2RD Nottingham, United Kingdom

Edited by Robert J. Lefkowitz, Howard Hughes Medical Institute and Duke University Medical Center, Durham, NC, and approved May 18, 2020 (received for review January 9, 2020)

Whether G protein-coupled receptors signal from endosomes to control important pathophysiological processes and are therapeutic targets is uncertain. We report that opioids from the inflamed colon activate δ-opioid receptors (DOPr) in endosomes of nociceptors. Biopsy samples of inflamed colonic mucosa from patients and mice with colitis released opioids that activated DOPr on nociceptors to cause a sustained decrease in excitability. DOPr agonists inhibited mechanically sensitive colonic nociceptors. DOPr endocytosis and endosomal signaling by protein kinase C (PKC) and extracellular signal-regulated kinase (ERK) pathways mediated the sustained inhibitory actions of endogenous opioids and DOPr agonists. DOPr agonists stimulated the recruitment of $G\alpha_{i/o}$ and β-arrestin1/2 to endosomes. Analysis of compartmentalized signaling revealed a requirement of DOPr endocytosis for activation of PKC at the plasma membrane and in the cytosol and ERK in the nucleus. We explored a nanoparticle delivery strategy to evaluate whether endosomal DOPr might be a therapeutic target for pain. The DOPr agonist DADLE was coupled to a liposome shell for targeting DOPr-positive nociceptors and incorporated into a mesoporous silica core for release in the acidic and reducing endosomal environment. Nanoparticles activated DOPr at the plasma membrane, were preferentially endocytosed by DOPr-expressing cells, and were delivered to DOPr-positive early endosomes. Nanoparticles caused a long-lasting activation of DOPr in endosomes, which provided sustained inhibition of nociceptor excitability and relief from inflammatory pain. Conversely, nanoparticles containing a DOPr antagonist abolished the sustained inhibitory effects of DADLE. Thus, DOPr in endosomes is an endogenous mechanism and a therapeutic target for relief from chronic inflammatory pain.

pain | inflammation | G protein-coupled receptors | signaling | nanomedicine

G protein-coupled receptors (GPCRs) control essential pathophysiological processes. One-third of Food and Drug Administration-approved drugs target GPCRs (1). GPCRs at the plasma membrane detect extracellular ligands and couple to heterotrimeric G proteins. Plasma membrane signaling is rapidly terminated. GPCR kinases phosphorylate activated GPCRs, which increases the affinity for β-arrestins (βARRs) (2). βARRs uncouple GPCRs from G proteins and desensitize signaling, and also couple GPCRs to the clathrin endocytic machinery (3). βARRs also recruit GPCRs, G proteins, and mitogen-activated protein kinases to endosomes (4, 5). Endosomes are an important site of continued GPCR signaling (6–8).

GPCRs control multiple steps of pain transmission (9). Endosomal signaling of protease-activated receptor-2 in primary sensory neurons and of neurokinin 1 receptor (NK_1R) and calcitonin-like receptor (CLR) in second-order neurons mediates neuronal excitation and pain transmission (10–13). The δ-, μ- and κ-opioid receptors (DOPr, MOPr, and KOPr) inhibit excitation of primary sensory, spinal, and supraspinal neurons and thereby induce analgesia (14). In patients with inflammatory bowel disease (IBD), infiltrating lymphocytes release opioids that activate opioid receptors on nociceptors to suppress excitability, providing an endogenous system of pain control (15–19). It is not known whether opioid receptors at the plasma

Significance

G protein-coupled receptors are considered to function principally at the cell surface. We present evidence that the δ-opioid receptor (DOPr) signals from endosomes to cause a sustained inhibition of pain. Opioids from the inflamed human and mouse colon, along with selective agonists that evoked DOPr internalization, inhibited the excitability of nociceptors by a mechanism requiring DOPr endocytosis. DOPr in endosomes generated a subset of signals in subcellular compartments that inhibited neuronal excitability. A DOPr agonist that was encapsulated into nanoparticles designed to selectively activate DOPr in endosomes of nociceptors caused a long-lasting inhibition of neuronal excitability and pain. Our results support the hypothesis that endosomal signaling of DOPr is an endogenous mechanism and therapeutic target for relief from inflammatory pain.

Author contributions: N.N.J.-V., J.G., D.D.J., R.L., A.H., J.J.D., P.R., N.A.V., S.E.C., Y.Y., C.L.-L., J.J.-P., M.C., D.E.R., A.E.L., B.L.S., K.W.L., S.J.V., M.L.H., N.W.B., and D.P.P. designed research; N.N.J.-V., J.G., M.J.W., D.D.J., R.L., A.H., S.T., J.J.D., P.R., N.A.V., S.E.C., Y.Y., C.L.-L., J.J.-P., D.E.R., and A.E.L. performed research; N.N.J.-V., J.G., M.J.W., D.D.J., R.L., A.H., J.J.D., P.R., N.A.V., S.E.C., Y.Y., C.L.-L., J.J.-P., M.C., D.E.R., A.E.L., B.L.S., K.W.L., S.J.V., M.L.H., N.W.B., and D.P.P. analyzed data; and N.N.J.-V., A.H., B.L.S., K.W.L., S.J.V., M.L.H., N.W.B., and D.P.P. wrote the paper.

Competing interest statement: N.W.B. is a founding scientist of Endosome Therapeutics Inc. Research in the laboratories of N.A.V., N.W.B., and D.P.P. is funded in part by Takeda Pharmaceuticals International.

This article is a PNAS Direct Submission.

Published under the PNAS license.

[1]To whom correspondence may be addressed. Email: michelle.halls@monash.edu, nwb2@nyu.edu, or daniel.poole@monash.edu.

This article contains supporting information online at https://www.pnas.org/lookup/suppl/doi:10.1073/pnas.2000500117/-/DCSupplemental.

First published June 16, 2020.

membrane or in endosomes mediate this endogenous analgesic pathway and are the optimal target for treatment of inflammatory pain.

Here we investigated the hypothesis that opioids from the inflamed colon activate DOPr in endosomes of nociceptors to evoke signals that cause long-lasting inhibition of excitability and analgesia, and that DOPr in endosomes is a superior therapeutic target for inflammatory pain.

Results

DOPr Inhibits Inflammatory Pain. We investigated whether opioids from the inflamed colon activate opioid receptors on nociceptors and decrease excitability. Segments of colon from healthy control (HC) mice and from mice with colitis induced by chronic administration of dextran sulfate sodium (cDSS) were incubated in culture medium for 24 h to allow opioid release into the supernatant (16–18). Mouse dorsal root ganglia (DRG) neurons were exposed to HC or cDSS supernatant for 60 min and then washed (Fig. 1*A*).

To assess sustained changes in excitability, the rheobase (minimum input current required to fire an action potential) of small-diameter neurons was measured by patch-clamp recordings at 30 min after washing (T = 30 min) (11). The rheobase of neurons exposed to cDSS supernatant was 29 ± 6% higher than that of neurons exposed to HC supernatant ($P < 0.05$), consistent with decreased excitability (Fig. 1 *A* and *B*). To examine whether these findings translate to IBD, supernatants were obtained from colonic biopsy specimens from HC patients and patients with chronic ulcerative colitis (cUC). The rheobase of neurons exposed to cUC supernatant was 62 ± 16% higher than that of neurons exposed to HC supernatant ($P < 0.01$) (Fig. 1 *C* and *D*). Preincubation of neurons with the DOPr antagonist SDM25N (100 nM, 60 min) abolished the sustained effects of cDSS supernatant on rheobase, whereas the MOPr antagonist CTOP (100 nM, 60 min) had no effect (Fig. 1 *E* and *F*). Neither SDM25N nor CTOP affected the rheobase of neurons exposed to mouse HC supernatant (Fig. 1*F*). Thus, opioids from the inflamed colon cause a DOPr-mediated inhibition of nociceptors.

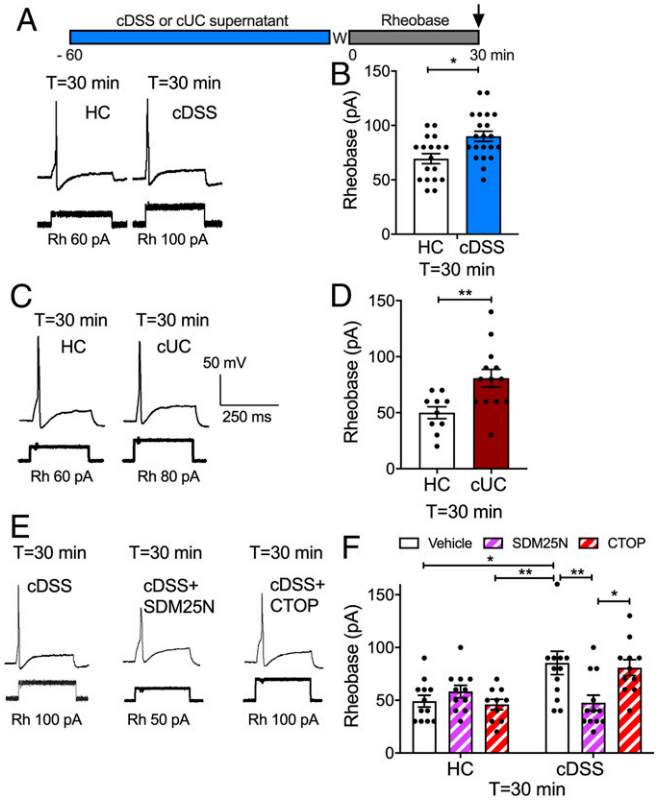


Fig. 1. Endogenous opioids and nociceptor excitability. Mouse DRG neurons were preincubated with supernatant from biopsies of HC, cDSS, or cUC colon and washed (W), and rheobase (Rh) was measured at 30 min after washing. Representative traces (*A*, *C*, and *E*) and pooled results (*B*, *D*, and *F*) of effects of supernatants from mouse (*A*, *B*, *E*, and *F*) and human (*C* and *D*) colonic biopsies. (*E* and *F*) Effects of antagonists of DOPr (SDM25N) or MOPr (CTOP) on responses to HC or cDSS supernatants. Data points indicate the number of studied neurons from $n = 12$ to 16 mice in *B*, 6 mice in *D*, and 8 mice in *F* for each treatment (mean ± SEM). $^*P < 0.05$, $^{**}P < 0.001$, two-way ANOVA with Tukey's post hoc test.

Endosomal DOPr Inhibits Nociceptor Excitability. To determine whether DOPr undergoes clathrin- and dynamin-mediated endocytosis in nociceptors, we isolated DRG neurons from knockin mice expressing DOPr fused to enhanced green fluorescent protein (DOPr-eGFP) (20). In vehicle-treated neurons, DOPr-eGFP was detected at the plasma membrane and in vesicles of the soma and neurites (Fig. 2*A*). The DOPr agonist DADLE (1 μM, 30 min) induced depletion of DOPr-eGFP from the plasma membrane and redistribution to endosomes. Dyngo4a (Dy4; 30 μM), which inhibits dynamin (21), and PitStop2 (PS2; 15 μM), which inhibits clathrin-mediated endocytosis (22), prevented DADLE-evoked endocytosis of DOPr-eGFP, as confirmed by quantification of plasma membrane and cytosolic DOPr-eGFP (Fig. 2*B*).

To examine the contribution of DOPr endocytosis to the inhibitory effects of endogenous opioids, we pretreated neurons with Dy4 or PS2 and then challenged them with cDSS, cUC, or HC supernatant. Neurons were washed, and rheobase was measured after 30 min. Dy4 and PS2 prevented the sustained increase in rheobase of neurons exposed to cDSS and cUC supernatants (Fig. 2 *C* and *D*). Inactive forms of Dy4 and PS2 do not affect the rheobase of nociceptors (11).

We similarly examined the contribution of endocytosis to the effects of DOPr- and MOPr-selective agonists on neuronal excitability. We exposed nociceptors to DOPr-selective agonists, including DADLE and SNC80 (10 nM, 15 min), which evoke βARR recruitment and DOPr endocytosis, and a 10-fold higher concentration of ARM390 (100 nM, 15 min), a weakly internalizing agonist (23) (Fig. 2*E*). Neurons were washed, and rheobase was measured immediately (T = 0 min) or 30 min (T = 30 min) after washing. DADLE and SNC80 caused both immediate (T = 0 min) and sustained (T = 30 min) increases in rheobase (Fig. 2 *E* and *F*). ARM390 increased rheobase at T = 0 min but not at T = 30 min (Fig. 2*G*). PS2 abolished the effects of DADLE and SNC80, but not of ARM390. The MOPr agonist DAMGO caused an immediate increase in rheobase that was not sustained and was inhibited by PS2 (Fig. 2*H*).

GPCRs in endosomes can activate protein kinase C (PKC) and extracellular signal-regulated kinases (ERKs), which control nociceptor excitability (11). To examine the role of these kinases in the sustained inhibitory actions of DOPr, we preincubated neurons with GF109203X (1 μM, 30 min), which inhibits PKC (24), or with PD98059 (50 μM, 30 min), which inhibits MEK1 (25). GF109203X and PD98059 abolished the sustained increase in rheobase (T = 30 min) to DADLE (Fig. 2 *I* and *J*).

To compare the chronic actions of DOPr agonists, neurons were incubated overnight with DADLE (100 nM) or ARM390 (300 nM). Neurons were washed, and rheobase was measured (Fig. 2*K*). DADLE caused both immediate (T = 0 min) and sustained (T = 30 min) increases in rheobase. PS2 blocked both phases (Fig. 2*K*). ARM390 caused an immediate increase (T = 0 min), but not a sustained (T = 30 min) increase, in rheobase, which was unaffected by PS2 (Fig. 2*L*). Thus, opioids from the inflamed colon and agonists that evoke DOPr endocytosis cause a sustained decrease in excitability of nociceptors that requires PKC and ERK signaling.

Endosomal DOPr Inhibits Colonic Afferent Activity. To assess whether endosomal DOPr signaling in the peripheral projections of colonic nociceptors mediates the inhibitory actions of opioids, we made extracellular recordings from lumbar splanchnic nerves innervating isolated segments of mouse distal colon (11). Nociceptors were identified by probing the colon or mesentery with von Frey filaments (VFF). Basal responses (1 g VFF, 100%) of each unit to repeated

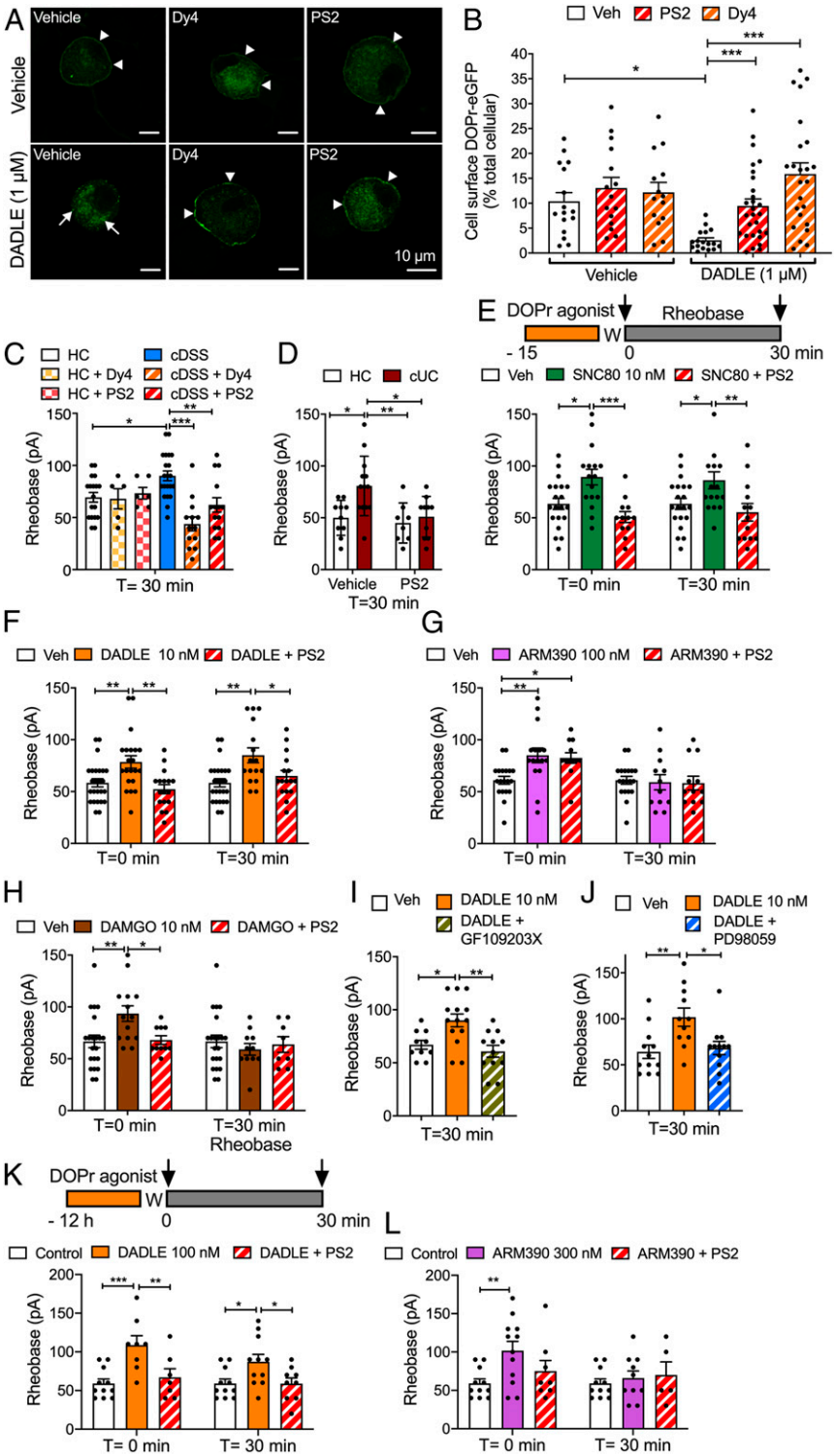


Fig. 2. Endosomal DOPr signaling and nociceptor excitability. (*A* and *B*) Endocytosis of DOPr-eGFP in DRG neurons from DOPr-eGFP mice. Neurons were incubated with vehicle (Veh) or DADLE (1 μM, 30 min), and DOPr-eGFP was localized by immunofluorescence. Neurons were preincubated with vehicle, Dy4, or PS2. (*A*) Representative images from four independent experiments. Arrowheads denote plasma membrane; arrows, endosomal DOPr-eGFP. (*B*) Quantification of the proportion of total cellular DOPr-eGFP at the plasma membrane. Data points indicate the number of studied neurons (N). $*P < 0.05$, $***P < 0.001$, two-way ANOVA with Tukey's post hoc test. (*C–L*) Rheobase of mouse DRG neurons at 0 or 30 min after exposure to supernatant or DOPr agonists and washing. (*C* and *D*) Supernatant from cDSS, cUC, or HC biopsy specimens. (*E–J*) Neurons were incubated with the following agonists for 15 min and washed (W), and rheobase was measured at 0 or 30 min after washing: DOPr agonists SNC80 (*E*, 10 nM, internalizing), DADLE (*F*, 10 nM, internalizing) or ARM390 (*G*, 100 nM, weakly internalizing), and MOPr agonist DAMGO (*H*, 10 nM). In *C–H*, neurons were preincubated with Dy4, PS2, or vehicle. In *I* and *J*, neurons were preincubated with PKC inhibitor GF10923X or MEK1 inhibitor PD98059 before DADLE. (*K* and *L*) Neurons were incubated with the following agonists overnight and washed, and rheobase was measured at 0 or 30 min after washing: DADLE (*K*, 100 nM, internalizing) or ARM390 (*L*, 300 nM, weakly internalizing). Data points indicate the number of studied neurons from 12 to 16 mice in *C*, 6 mice in *D*, 10 to 15 mice in *E–J*, and 6 mice in *K* and *L* for each treatment (mean ± SEM). $*P < 0.05$, $**P < 0.01$, $***P < 0.001$, one-way or two-way ANOVA with Tukey's post hoc test.

stimulation (three times for 3 s) were recorded (Fig. 3*A*). Agonists of DOPr (SNC80 and ARM390) or MOPr (DAMGO) (all 100 nM) were superfused into the organ bath for 15 min. Tissues were washed, and responses to VFF probing were reassessed every 15 min for 1 h. Compared with basal responses, DAMGO and ARM390 transiently inhibited the activity of colonic nociceptors, whereas SNC80 had a persistent inhibitory effect (Fig. 3 *B* and *C*). DAMGO maximally inhibited activity after 15 min of perfusion (i.e., 0 min, 53 ± 10% inhibition). ARM390 (weakly internalizing) inhibited activity only at 0 min (29 ± 4% inhibition). SNC80 (strongly internalizing) maximally inhibited activity at 30 min (33 ± 9% inhibition), which persisted for 60 min. PS2 (50 μM, 15 min) prevented the sustained inhibitory action of SNC80 (Fig. 3*D*). Thus, DOPr endosomal signaling within the peripheral projections of colonic nociceptors may induce a sustained inhibition of mechanical sensitivity.

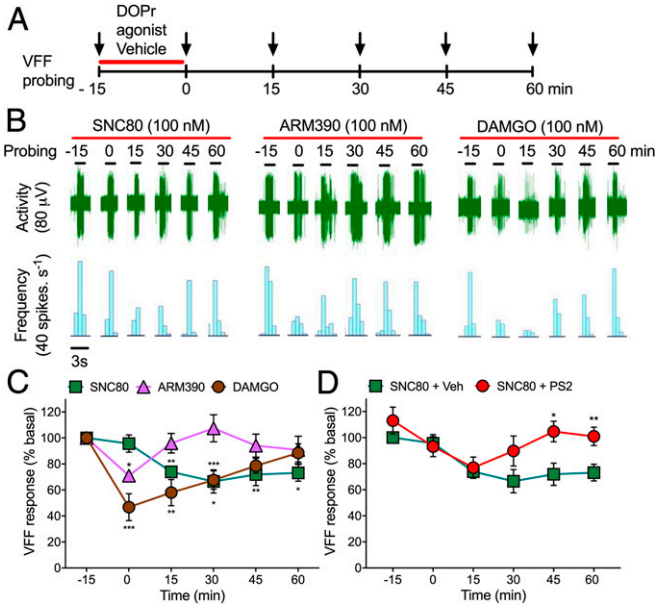


Fig. 3. MOPr and DOPr inhibition of colonic nociceptors. (*A*) Experimental protocol to examine MOPr and DOPr regulation of responses of colonic nociceptors to VFF probing. (*B*) Representative responses to agonists of DOPr (SNC80 and ARM390, 100 nM) and MOPr (DAMGO, 100 nM). (*C* and *D*) Time course of responses. In *D*, tissue was preincubated with PS2 or vehicle (Veh) before SNC80. $n = 5$ mice for each treatment. Data are mean ± SEM. $*P < 0.05$, $**P < 0.01$, $***P < 0.001$, two-way ANOVA with Tukey's post hoc test.

DOPr Agonist Differentially Activate G Proteins, Recruit βARRs, and Stimulate Endocytosis. We characterized the differential effects of DOPr agonists on receptor signaling and trafficking using bioluminescence resonance energy transfer (BRET) (26). HEK293 cells were transiently transfected with Gα-Rluc8 subtypes plus Gγ2-Venus, Gβ1, and DOPr. Gα-Rluc8/Gγ2-Venus BRET was measured to assess G protein dissociation (activation). SNC80, DADLE, and ARM390 (100 nM) decreased $G\alpha_{i1}$-Rluc8/Gγ2-Venus and $G\alpha_o$-Rluc8/Gγ2-Venus BRET, indicative of $G\alpha_{i/o}$ and Gβγ activation (*SI Appendix*, Fig. S1 *A* and *B*). SNC80, DADLE, and ARM390 had no effect on $G\alpha_s$-Rluc8/Gγ2-Venus BRET or $G\alpha_q$-Rluc8/Gα-Rluc8 BRET (*SI Appendix*, Fig. S1 *C* and *D*). SNC80, DADLE, and ARM390 decreased $G\alpha_{i1,2,3,o}$-Rluc8/Gγ2-Venus BRET with similar efficacy and an order of potency of DADLE > SNC80 > ARM390 (*SI Appendix*, Fig. S1 *E–G*).

To investigate βARR recruitment, HEK293 cells were transfected with DOPr-Rluc and βARR1/2-YFP. SNC80 and DADLE, but not ARM390 (all 100 nM), increased DOPr-Rluc/βARR1/2-YFP BRET (*SI Appendix*, Fig. S1 *H* and *I*). ARM390 increased BRET only at high concentrations (>1 µM). The order of potency for βARR recruitment was DADLE > SNC80 > ARM390 (*SI Appendix*, Fig. S1 *J* and *K*).

Thus, SNC80, DADLE, and ARM390 induce DOPr coupling to $G\alpha_{i/o}$, and SNC80 and DADLE, but not ARM390, stimulate DOPr coupling to βARR1/2. These results are consistent with the capacity of SNC80, but not of ARM390, to promote DOPr-eGFP phosphorylation, which is required for βARR recruitment (27).

To assess DOPr trafficking, we measured bystander BRET between DOPr-Rluc and Venus-tagged proteins resident of the plasma membrane (HRas-Venus, lipid rich; KRas-Venus, non–lipid-rich) and endosomes (Rab5a, early; Rab7a, late; Rab11a, recycling) (26). SNC80 and DADLE (100 nM) decreased BRET between DOPr-Rluc, HRas-Venus, and KRas-Venus (*SI Appendix*, Fig. S1 *L* and *M*). These changes were mirrored by an increase in BRET between DOPr-Rluc and Rab5a-Venus (*SI Appendix*, Fig. S1*N*). SNC80 stimulated BRET between DOPr-Rluc and Rab7a-Venus (*SI Appendix*, Fig. S1*O*). ARM390 (100 nM) did not affect BRET between DOPr and plasma membrane or endosomal proteins. SNC80, DADLE, or ARM390 did not affect BRET between DOPr-Rluc and Rab11a-Venus (*SI Appendix*, Fig. S1*P*). Thus, SNC80 and DADLE cause DOPr internalization to early endosomes, whereas ARM390 does not. Internalized DOPr traffics to degradatory pathways in neurons (28).

DOPr Agonists Differentially Activate G Proteins and βARRs at the Plasma Membrane and in Endosomes. To assess activation of G proteins at the plasma membrane and in endosomes of HEK293 cells, we measured enhanced bystander (eb) BRET between mini-G proteins (Rluc8-m$G\alpha_{si/o/s/sq}$) (29, 30) and *Renilla* (R) GFP-CAAX (prenylation CAAX box of KRas) (31) for plasma membrane activation or tandem (td) RGFP-Rab5a for early endosome activation. Whereas Gα proteins associate with Gβγ subunits and GPCRs in the plasma membrane, mini-Gα proteins are N-terminally truncated and freely diffuse throughout the cytoplasm. Mini-Gα proteins can translocate to active GPCRs at the plasma membrane or in organelles. Mini-$G\alpha_{si}$ and $G\alpha_{sq}$ proteins were developed by mutating $mG\alpha_s$ residues to equivalent $G\alpha_q$ and $G\alpha_i$ residues. Recruitment of βARRs was assessed by measuring ebBRET between Rluc8-βARR1 (32) or Rluc2-βARR2 (31) and RGFP-CAAX or tdRGFP-Rab5a. Rab5a was localized to endosomes (*SI Appendix*, Fig. S2*A*). SNC80, DADLE, and ARM390 (100 nM) increased Rluc8-m$G\alpha_{si/o}$/RGFP-CAAX ebBRET (*SI Appendix*, Fig. S2 *B–E*) but did not affect Rluc8-m$G\alpha_{s/sq}$/RGFP-CAAX ebBRET (*SI Appendix*, Fig. S2 *F* and *G*). SNC80 and DADLE, but not ARM390, increased Rluc8-βARR1 or Rluc2-βARR2/RGFP-CAAX ebBRET (*SI Appendix*, Fig. S2 *H–K*). SNC80 and DADLE, but not ARM390, increased Rluc8-m$G\alpha_{si/o}$/tdRGFP-Rab5a ebBRET (*SI Appendix*, Fig. S2 *L–O*). These agonists did not affect Rluc8-m$G\alpha_{s/sq}$/tdRGFP-Rab5a ebBRET (*SI Appendix*, Fig. S2 *P* and *Q*). SNC80 and DADLE, but not ARM390, increased Rluc8-βARR1 or Rluc2-βARR2/tdRGFP-Rab5a ebBRET (*SI Appendix*, Fig. S2 *R–U*). Pertussis toxin blunted βARR recruitment to the plasma membrane (*SI Appendix*, Fig. S2 *H–K*) and endosomes (*SI Appendix*, Fig. S2 *R–U*), indicating involvement of $G\alpha_{i/o}$ signaling.

The foregoing results suggest that SNC80, DADLE, and ARM390 activate $G\alpha_{i/o}$ at the plasma membrane. Only agonists that strongly internalize DOPr (SNC80 and DADLE) activate $G\alpha_{i/o}$ in endosomes and recruit βARR1/2 to the plasma membrane and endosomes.

Endosomal DOPr Activates a Subset of Compartmentalized Signals. To examine DOPr signaling in subcellular compartments, we expressed DOPr and Förster resonance energy transfer (FRET) biosensors targeted to the plasma membrane, cytosol, or nucleus in HEK293 cells (10, 33). FRET biosensors included pmCKAR (plasma membrane PKC), cytoCKAR (cytosolic PKC), cytoEKAR (cytosolic ERK), and nucEKAR (nuclear ERK) (Fig. 4). To probe the link between endocytosis and compartmentalized signaling, we compared the effects of strongly internalizing (SNC80 and DADLE) and weakly internalizing (ARM390) DOPr agonists and used inhibitors of clathrin and dynamin.

SNC80 and DADLE (100 nM) stimulated a sustained increase in plasma membrane and cytosolic PKC activity (Fig. 4 *A–C*). ARM390 (100 nM) did not affect plasma membrane or cytosolic PKC activity. All three agonists stimulated a sustained increase in cytosolic ERK activity (Fig. 4 *D* and *F*). SNC80 and DADLE, but not ARM390, caused sustained activation of nuclear ERK (Fig. 4 *E* and *F*). These results suggest that DOPr signals from endosomes to activate plasma membrane and cytosolic PKC and nuclear ERK.

To assess the importance of endocytosis for compartmentalized signaling, we expressed wild-type (WT) dynamin or K44E dominant negative mutant dynamin (K44E dynamin) (34), or treated cells with PS2 or the inactive analog PS2 inactive. In control experiments with WT dynamin and PS2 inactive, SNC80 and DADLE induced rapid and sustained increases in PKC activity at the plasma membrane and in the cytosol (Fig. 5 *A–F*). Dynamin K44E and PS2 abolished SNC80 and DADLE stimulation of PKC at the plasma membrane and in the cytosol (Fig. 5 *A–F* and *SI Appendix*, Fig. S3 *A* and *B*). SNC80 and DADLE induced a gradual and sustained increase in

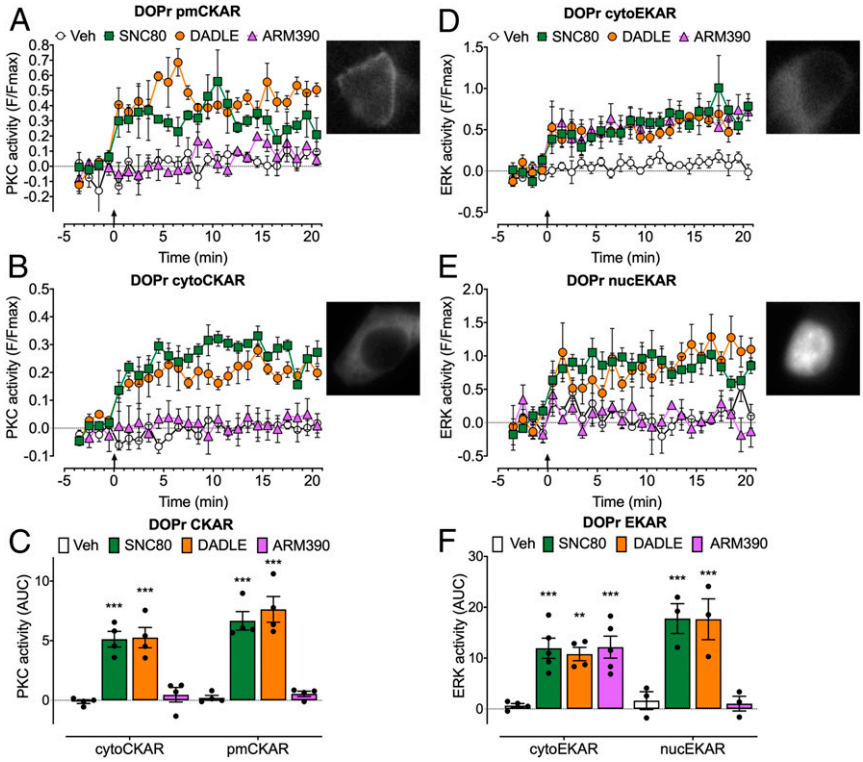


Fig. 4. DOPr-mediated PKC and ERK signaling in subcellular compartments of HEK293 cells. FRET biosensors for pmCKAR and cytoCKAR or cytoEKAR and nucEKAR were coexpressed with DOPr. *Insets* show cellular localization of FRET biosensors. Agonists (all 100 nM) or vehicle (Veh) were administered at the arrows. (*A* and *B*) Time course of plasma membrane (*A*) and cytosolic (*B*) PKC. (*C*) Integrated responses of plasma membrane and cytosolic PKC over 20 min (area under the curve [AUC]). (*D* and *E*) Time course of activation of cytosolic (*D*) and nuclear (*E*) ERK. (*F*) Integrated responses of cytosolic and nuclear ERK over 20 min (AUC). Data points show results of individual experiments. $n = 4$ (*A*–*C*), $n = 5$ cytoEKAR, $n = 3$ nucEKAR (*D*–*F*) independent experiments. Data are mean ± SEM. $^{**}P < 0.01$, $^{***}P < 0.001$ ligand to vehicle, one-way ANOVA with Tukey's post hoc test.

ERK activity in the cytosol and nucleus (Fig. 5 *G*–*L*). Dynamin K44E and PS2 did not affect SNC80- and DADLE-induced cytosolic ERK activity but abolished SNC80- and DADLE-induced nuclear ERK activity (Fig. 5 *G*–*L* and *SI Appendix*, Fig. S3 *C* and *D*). The contribution of βARR1/2 to signaling was examined by siRNA knockdown (10, 26). βARR1/2 siRNA, but not scrambled siRNA (control), inhibited SNC80-induced activation of nuclear, but not cytosolic, ERK (Fig. 5 *M*–*O*).

To evaluate DOPr compartmentalized signaling in nociceptors, we expressed FRET biosensors in DRG neurons from DOPr-eGFP mice. SNC80 and DADLE stimulated sustained activation of PKC at the plasma membrane and in the cytosol (Fig. 6 *A*–*C*) and of ERK in the cytosol and nucleus (Fig. 6 *D*–*F*). ARM390 stimulated a sustained activation of cytosolic ERK but did not affect plasma membrane PKC or nuclear ERK activity. Dy4 abolished SNC80-stimulated activation of nuclear ERK, whereas cytosolic ERK activity was unaffected (Fig. 6 *G*–*J*). These results suggest that DOPr endocytosis in HEK293 cells and primary nociceptors mediates activation of plasma membrane and cytosolic PKC and nuclear ERK, but not of cytosolic ERK.

Nanoparticle-Encapsulated Agonists Target Endosomal DOPr. The realization that endosomal DOPr signaling mediates the inhibitory actions of opioids on nociceptor excitability suggests that agonists that activate DOPr in endosomes might provide effective relief from inflammatory pain. Nanoparticles can be used to deliver an NK_1R antagonist into endosomes of spinal neurons, where acidification triggers nanoparticle disassembly and antagonist release, leading to sustained antinociception (12). We incorporated DADLE into mesoporous silica nanoparticles (MSNs) designed to dissolve and release cargo in the acidic and reducing endosomal environment (35, 36) (Fig. 7*A*). For selective targeting of DOPr-expressing neurons, we cloaked MSNs with PEGylated liposome covalently linked to DADLE.

Empty nanoparticles (LipoMSN), DADLE-coated nanoparticles (DADLE-LipoMSN), and nanoparticles with a DADLE coat and core (DADLE-LipoMSN-DADLE) were spherical with a hydrodynamic diameter of 140 to 210 nM, a surface charge of +28 to 36 mV, and a polydispersity index of 0.24 to 0.27 (Fig. 7 *B* and *C*). The loading efficiency of DADLE into the MSN core was 57 ± 6%. To examine MSN disassembly and cargo release, MSNs loaded with DADLE-Alexa647 (MSN-DADLE-Alexa647) were incubated in buffers at pH 7.2 or 5.2 or with or without 10 mM glutathione to mimic the acidic and reducing conditions of endosomes. The release of DADLE-Alexa647 into buffer was faster and more complete at pH 5.2 and in the presence of glutathione, and it continued for 24 h (Fig. 7 *D* and *E*).

To determine whether a DADLE-Lipo shell could facilitate selective uptake by DOPr-expressing cells, MSNs loaded with Alexa Fluor 647 and coated with DADLE-Lipo were incubated with untransfected HEK293 cells or HEK-DOPr cells for 2 h. The number of cells containing Alexa647 was determined by flow cytometry. DADLE-LipoMSN-Alexa647 was internalized into 66 ± 7% of HEK-DOPr cells, compared with 22 ± 1% of untransfected HEK293 cells ($P < 0.05$, t test), indicating preferential delivery to cells expressing DOPr (Fig. 7*F*). Dy4 and PS2, but not inactive analogs, inhibited DADLE-LipoMSN-Alexa647 uptake by HEK-DOPr cells, consistent with clathrin- and dynamin-mediated endocytosis (Fig. 7*G*).

To determine whether nanoparticles target DOPr in endosomes, HEK-HA-DOPr cells expressing Rab5a-GFP were incubated with HA antibodies to label surface DOPr. Cells were incubated with DADLE-LipoMSN-Alexa647 (20 μM DADLE, 200 μg/mL LipoMSN) and imaged by confocal microscopy. DADLE-LipoMSN-Alexa647 accumulated at the plasma membrane, stimulated endocytosis of HA-DOPr, and colocalized with HA-DOPr in early endosomes at 30 min (Fig. 7*H* and

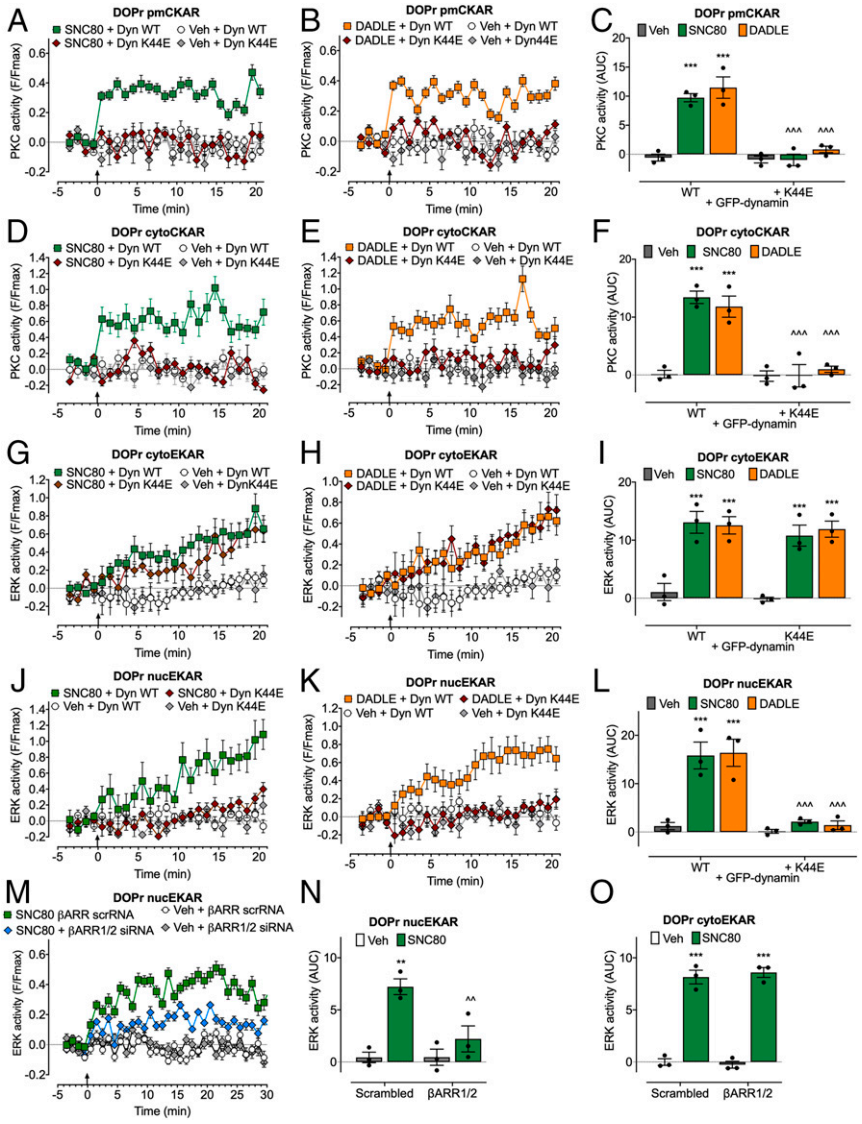


Fig. 5. Endosomal DOPr-mediated PKC and ERK signaling in subcellular compartments of HEK293 cells. FRET biosensors for pmCKAR and cytoCKAR or cytoEKAR and nucEKAR were coexpressed with DOPr and either dynamin WT (Dyn WT) or dominant negative dynamin K44E (Dyn K44E) (*A*–*L*) or with βARR1+2 siRNA or scrambled (scr) siRNA (control) (*M*–*O*). Agonists (all 100 nM) or vehicle (Veh) were administered at the arrows. (*A*–*C*) Plasma membrane PKC activity. (*D*–*F*) Cytosolic PKC activity. (*G*–*I* and *O*) Cytosolic ERK activity. (*J*–*N*) Nuclear ERK activity. (*A*, *B*, *D*, *E*, *G*, *H*, *J*, *K*, and *M*) Time course of responses. (*C*, *F*, *I*, *L*, *N*, and *O*) Integrated responses over 20 or 30 min (AUC). Data points show results of individual experiments. $n = 3$ independent experiments. Data are mean ± SEM. $^{**}P < 0.01$, $^{***}P < 0.001$ ligand to vehicle; $^{\wedge\wedge}P < 0.01$, $^{\wedge\wedge\wedge}P < 0.001$ inhibitors to control; two-way ANOVA with Tukey's post hoc test.

SI Appendix, Fig. S4*A*). Live cell imaging, which avoided the loss of nanoparticle fluorescence during immunostaining, revealed DADLE-LipoMSN-Alexa647 binding to the plasma membrane and uptake into Rab5a-GFP endosomes within 30 min (Movie S1). Control LipoMSN-Alexa647, lacking the DADLE targeting group, showed diminished uptake (Movie S2).

We examined whether DADLE nanoparticles activate DOPr signaling at the plasma membrane (inhibition of cAMP, βARR1 recruitment) and in endosomes (nuclear ERK). Compared with Lipo-MSN or vehicle, DADLE (100 nM), DADLE-LipoMSN (20 μM DADLE), and DADLE-LipoMSN-DADLE (20 μM DADLE) inhibited forskolin (10 μM)-stimulated formation of cAMP in HEK-DOPr cells but not in untransfected HEK293 cells (Fig. 7*I* and *SI Appendix*, Fig. S4 *B* and *C*). DADLE and DADLE-LipoMSN-DADLE increased DOPr-Rluc8/βARR1-YFP BRET (Fig. 7*J* and *SI Appendix*, Fig. S4*D*). DADLE, DADLE-LipoMSN, and DADLE-LipoMSN-DADLE activated nuclear ERK, which was particularly sustained for DADLE-LipoMSN and DADLE-LipoMSN-DADLE (Fig. 7*K* and *SI Appendix*, Fig. S4*E*). These results suggest that DADLE coupled to the liposome shell can activate DOPr at the plasma membrane and stimulate DOPr endocytosis. DADLE released from the MSN core in endosomes might activate DOPr to stimulate nuclear ERK activity.

Primary cultures of DRG neurons from DOPr-eGFP knockin mice were studied to assess nanoparticle targeting and uptake into neurons. Neurons were incubated with DADLE, LipoMSN-Alexa647 (control), or DADLE-LipoMSN-Alexa647 (1 μM, 60 min, 37 °C) and fixed. GFP and the neuronal marker Hu were localized by immunofluorescence. DADLE evoked endocytosis of DOPr-eGFP in neurons (*SI Appendix*, Fig. S5*A*). LipoMSN-Alexa647 was detected at the surface of some neurons but did not promote DOPr-eGFP endocytosis (Fig. 8*A*). DADLE-LipoMSN-Alexa647 evoked DOPr-eGFP internalization and colocalized in endosomes with DOPr-eGFP.

A Nanoparticle-Encapsulated DOPr Agonist Provides Long-Lasting Antinociception. To assess antinociception, DRG neurons were incubated with DADLE, DADLE-LipoMSN, or DADLE-LipoMSN-DADLE (100 nM DADLE) for 30 min and washed, and then rheobase was

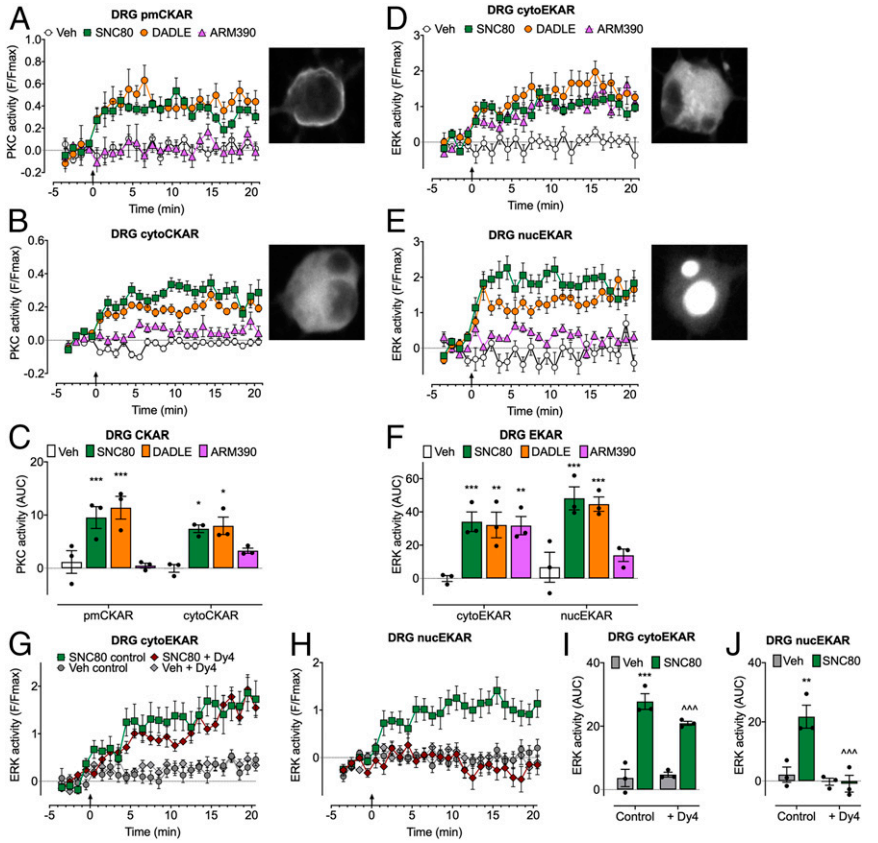


Fig. 6. Endosomal DOPr-mediated PKC and ERK signaling in subcellular compartments of DRG neurons. FRET biosensors for pmCKAR and cytoCKAR or cytoEKAR and nucEKAR were expressed in DRG neurons from DOPr-eGFP mice. *Insets* show localization of FRET biosensors. Agonists (all 100 nM) or vehicle (Veh) were administered at arrow. (*A* and *B*) Time course of plasma membrane (*A*) and cytosolic (*B*) PKC. (*C*) Effects of agonist treatments on PKC over 20 min (AUC). (*D* and *E*) Time course of cytosolic ERK (*D*) and nuclear ERK (*E*). (*F*) Effects of agonists on ERK activity over 20 min (AUC). (*G* and *H*) Time course of effects of dynamin inhibitor (Dy4) on cytosolic (*G*) and nuclear (*H*) ERK activity. (*I* and *J*) Effects of Dy4 treatments on ERK over 20 min (AUC). Data points show results of individual experiments. $n = 3$ independent experiments. Data are mean ± SEM. $^{*}P < 0.05$, $^{**}P < 0.01$, $^{***}P < 0.001$ ligand to vehicle; $^{\wedge\wedge\wedge}P < 0.001$ inhibitor to control; one-way ANOVA with Tukey's post hoc test.

measured at 0, 90, 120, or 180 min after washing. DADLE and DADLE-LipoMSN increased rheobase only at 0 min (Fig. 8 *B* and *C*). DADLE-LipoMSN-DADLE increased rheobase at 0, 90, and 120 min (26 ± 6% at 120 min). PS2 prevented the sustained inhibitory actions of DADLE-LipoMSN-DADLE (Fig. 8 *B* and *C*).

To assess the activity of peripheral colonic nociceptors, extracellular recordings were made from colonic afferents. DADLE-LipoMSN-DADLE (100 nM DADLE) was superfused into the organ bath for 30 min. Responses to VFF probing were assessed at 60 min and 120 min after washing. DADLE-LipoMSN-DADLE inhibited the activity of colonic nociceptors for at least 120 min (54 ± 13% inhibition) (Fig. 8*D*). PS2 prevented the sustained inhibitory action of DADLE-LipoMSN-DADLE.

To assess inflammatory nociception, complete Freund's adjuvant (CFA) was administered to mice by intraplantar injection, and withdrawal responses to stimulation of the plantar surface of the ipsilateral paw with VFFs were measured after 48 h. When administered by intrathecal injection to target DOPr on the central projections of nociceptors and on spinal neurons, DADLE (100 nM, 5 μL) had a moderate and transient antinociceptive action, whereas DADLE-LipoMSN-DADLE (100 nM DADLE, 5 μL) had a strong antinociceptive action that was sustained for 6 h (Fig. 8*E*). LipoMSN (1 μg/mL, 5 μL) had no effect. Nanoparticles did not affect withdrawal responses of the contralateral paw (*SI Appendix*, Fig. S5*B*). Thus, neuronal-targeted stimulus-responsive nanoparticles provide long-lasting antinociception.

A Nanoparticle-Encapsulated DOPr Antagonist Prevents the Sustained Antinociceptive Actions of DOPr. To provide evidence that DOPr endosomal signaling underlies sustained inhibition of neuronal excitability, we encapsulated the DOPr antagonist SDM25N into nanoparticles with a liposome shell (LipoMSN-SDM25N). LipoMSN-SDM25N had a hydrodynamic diameter of 176.5 ± 0.6 nm, a surface charge of +32 ± 3 mV, and a polydispersity index of 0.15 ± 0.02. SDM25N loading efficiency was 73.5 ± 0.8%. To assess the uptake of nanoparticles lacking the DADLE targeting group, LipoMSN-Alexa647 nanoparticles were incubated with HEK293 cells (0 to 4 h, 37 °C). After 120 min, LipoMSN-Alexa647 was detected in Rab5a-positive early endosomes (Fig. 8*F*). LipoMSN-Alexa647 was internalized in 67.7 ± 1.3% of HEK293 cells after 120 min, as assessed by flow cytometry (Fig. 8*G*). To determine whether an endosomally targeted DOPr antagonist can block nociception, DRG neurons were incubated with LipoMSN-SDM25N (100 nM SDM25N, 100 μg/mL LipoMSN) or LipoMSN (100 μg/mL, control) (120 min, 37 °C) (Fig. 8*H*), then washed, incubated with DADLE (10 nM, 15 min) and washed again. Rheobase was measured at 0 and 30 min after washing. In LipoMSN-treated neurons, DADLE increased rheobase at 0 min (53.44 ± 17.1%) and 30 min (55.56 ± 10.07%) compared with control. LipoMSN-SDM25N had no effect on the rheobase at 0 min (52.18 ± 13.78%) but abolished the inhibitory effect of DADLE at 30 min. These results support the hypothesis that DOPr signals from endosomes to cause persistent antinociception.

Discussion

Our results support the hypothesis that DOPr in endosomes is as a key component of an endogenous mechanism of pain control, and

that endosomal DOPr is a viable therapeutic target for chronic inflammatory pain.

Antinociceptive Signaling of Endosomal DOPr. Several observations suggest that DOPr signaling in endosomes mediates the sustained antinociceptive actions of endogenous opioids and certain DOPr-selective agonists (*SI Appendix*, Fig. S6). Biopsy specimens of inflamed human and mouse colon released opioids that caused a sustained inhibition of the excitability of nociceptors, as revealed by increased rheobase. These effects are attributable to DOPr, because a selective antagonist prevented inhibition. Colitis evokes endocytosis of DOPr-eGFP in myenteric neurons, consistent with opioid release and DOPr activation (37). Our findings support reports of an opioid-mediated mechanism of antinociception in inflamed colon (15–19). DOPr agonists that stimulated robust receptor endocytosis (DADLE and SNC80) caused a persistent inhibition of nociceptor excitability, whereas a weakly internalizing DOPr agonist (ARM390) had only a transient inhibitory action. Inhibitors of clathrin and dynamin prevented agonist-evoked endocytosis of DOPr-eGFP in nociceptors and blocked the sustained inhibitory actions of endogenous opioids and internalizing DOPr agonists.

These results support a role for endosomal signaling of DOPr in regulating sustained excitability of the soma, which was examined by patch clamp recordings. Similar mechanisms may control the excitability of nerve endings in the colon, since SNC80 caused a long-lasting inhibition of mechanically sensitive nociceptors, whereas weakly internalizing ARM390 did not. A clathrin inhibitor blocked the effects of SNC80, which require endosomal signaling. DOPr endocytosis has also been linked to analgesic tolerance (23, 27, 38, 39). A DOPr antagonist (SDM25N) incorporated into nanoparticles designed to deliver and release cargo in endosomes prevented the sustained inhibitory actions of DADLE on nociceptor excitability. These findings suggest that DADLE continues to activate DOPr in endosomes to inhibit nociception.

Our results do not exclude a role for plasma membrane signaling of DOPr in antinociception. Inhibitors of endocytosis and nanoparticle-encapsulated SDM25N did not affect the short-term inhibitory effects of DOPr agonists on excitability. Thus, DOPr signaling at the plasma membrane and in endosomes mediates antinociception, but with different time courses.

Our results reveal spatial and temporal differences in the way in which DOPr and MOPr regulate the excitability of nociceptors. A MOPr antagonist did not prevent the inhibitory actions of colonic supernatants on neuronal excitability, suggesting that MOPr does not contribute antinociception during colitis. Although the MOPr agonist DAMGO transiently decreased the excitability of DRG neurons and colonic afferents, these effects were not sustained. A clathrin inhibitor prevented the transient inhibitory actions of DAMGO, which likely require endosomal signaling of MOPr. These results are in agreement with studies in which a conformationally selective nanobody was used to detect activated MOPr in subcellular compartments (40).

Biophysical approaches were used to examine DOPr trafficking and signaling in HEK-DOPr cells and nociceptors, with consistent results. All DOPr agonists (DADLE, SNC80, and ARM390) activated $G\alpha_{i/o}$ with similar efficacy. Only strongly internalizing agonists (DADLE and SNC80) potently recruited βARR1/2 and stimulated DOPr depletion from the plasma membrane and accumulation and retention in early endosomes. The results confirm reported differences in the ability of DADLE, SNC80, and ARM390 to promote DOPr internalization (23). These differences are attributable to GRK-induced DOPr phosphorylation; SNC80 induces DOPr phosphorylation at Ser^{363}, whereas ARM390 does not (27).

The use of FRET biosensors targeted to the plasma membrane, cytosol, or nucleus revealed that DOPr endocytosis is necessary for a subset of signals in subcellular compartments. Our results suggest that DOPr signaling from the plasma membrane activates ERK in the cytosol, whereas DOPr signaling in endosomes activates PKC at the plasma membrane and in the cytosol and activates ERK in the nucleus but not in the cytosol. Support for these conclusions derives from the observation that internalizing agonists alone activated plasma membrane and cytosolic PKC and nuclear ERK. Inhibitors of clathrin- and dynamin-mediated endocytosis, dominant negative dynamin, and βARR1/2 knockdown selectively suppressed these signals. Other GPCRs also signal from endosomes to regulate subsets of compartmentalized signals (10, 11, 13). Inhibitors of PKC and MEK1 prevented the sustained inhibitory actions of DADLE on neuronal excitability, providing a link between endosomal DOPr signaling and antinociception. PKC is a critical regulator of DOPr-mediated signaling and antinociception (41). DOPr endocytosis is also required for ERK activation and trafficking to perinuclear and nuclear locations (42).

$G\alpha_{i/o}$ and βARRs may mediate endosomal DOPr signaling, since internalizing, but not weakly internalizing, DOPr agonists stimulated the recruitment of mini-$G\alpha_{i/o}$ and βARR1/2 to early endosomes, as determined by BRET. βARR1/2 knockdown inhibited SNC80-stimulated nuclear ERK activation, possibly due to inhibition of DOPr endocytosis and endosomal signaling. Further studies are needed to determine the contribution of βARRs and $G\alpha_{i/o}$ to endosomal DOPr signaling.

Therapeutic Targeting of Endosomal DOPr. The realization that GPCRs can signal from endosomes to mediate pain has revealed endosomal GPCRs as a viable therapeutic target (8). Conjugation to transmembrane lipids or encapsulation into pH-tunable nanoparticles delivers antagonists of pronociceptive GPCRs to endosomes (10–13). Endosomally targeted antagonists preferentially inhibit endosomal signaling and provide enhanced antinociception compared with conventional antagonists. The present study shows that endosomally targeted agonists of antinociceptive GPCRs also provide long-lasting pain relief. DADLE-LipoMSN-DADLE inhibited nociceptor excitability for at least 3 h after washout, in contrast to the transient inhibitory action of free DADLE. DADLE-LipoMSN-DADLE caused a long-lasting inhibition of mechanically evoked activation of colonic nociceptors and effectively reversed inflammatory nociception. One component of the enhanced antinociceptive properties of nanoparticles might relate to the selective delivery of primary sensory neurons to endosomes. Targeted delivery to DOPr-expressing neurons was accomplished by cloaking MSNs with PEGylated liposomes covalently linked to DADLE. DADLE-LipoMSNs retained the ability to activate DOPr in HEK-DOPr cells, as assessed by inhibition of cAMP, recruitment of βARR1, stimulation of DOPr endocytosis, and activation of nuclear ERK (*SI Appendix*, Fig. S6). Uptake of DADLE-LipoMSNs by HEK-DOPr cells was threefold greater than that by untransfected HEK cells, suggesting preferential targeting. DADLE-LipoMSNs entered cells by clathrin-mediated endocytosis and were delivered to DOPr-positive early endosomes. Another component of enhanced antinociception could be the sustained activation of DOPr in endosomes, which was attained by incorporating DADLE into the MSN core. DADLE release was accelerated in the acidic and reducing endosomal environment and continued for 24 h. The finding that a clathrin inhibitor abrogated the antinociceptive actions of DADLE-LipoMSN-DADLE indicates a requirement for nanoparticle endocytosis.

More direct evidence for a role of endosomal DOPr in antinociception was provided by incorporating the DOPr antagonist SDM25N into nanoparticles. When preincubated with neurons to allow for endosomal accumulation, followed by extensive washing to remove extracellular antagonist, LipoMSN-SDM25N prevented the sustained inhibitory actions of DADLE on nociceptor excitability, supporting endosomal signaling. The immediate inhibitory actions of DADLE were unaffected and likely arose from plasma membrane DOPr.

Incorporation into nanoparticles can enhance the stability and delivery of drugs, thereby improving efficacy (43–45). Stimulus-responsive nanoparticles deliver combinations of chemotherapeutics to tumors, where increased vascular permeability and extracellular acidification promote delivery and cargo release (46, 47). Although nanoparticles are often endocytosed, endosomal disruption is necessary for drug delivery to cytosolic and nuclear targets, which can compromise efficacy (48). The discovery of GPCRs in endosomes as therapeutic targets provides an opportunity to use nanoparticles to deliver treatments for pain (8). Our results

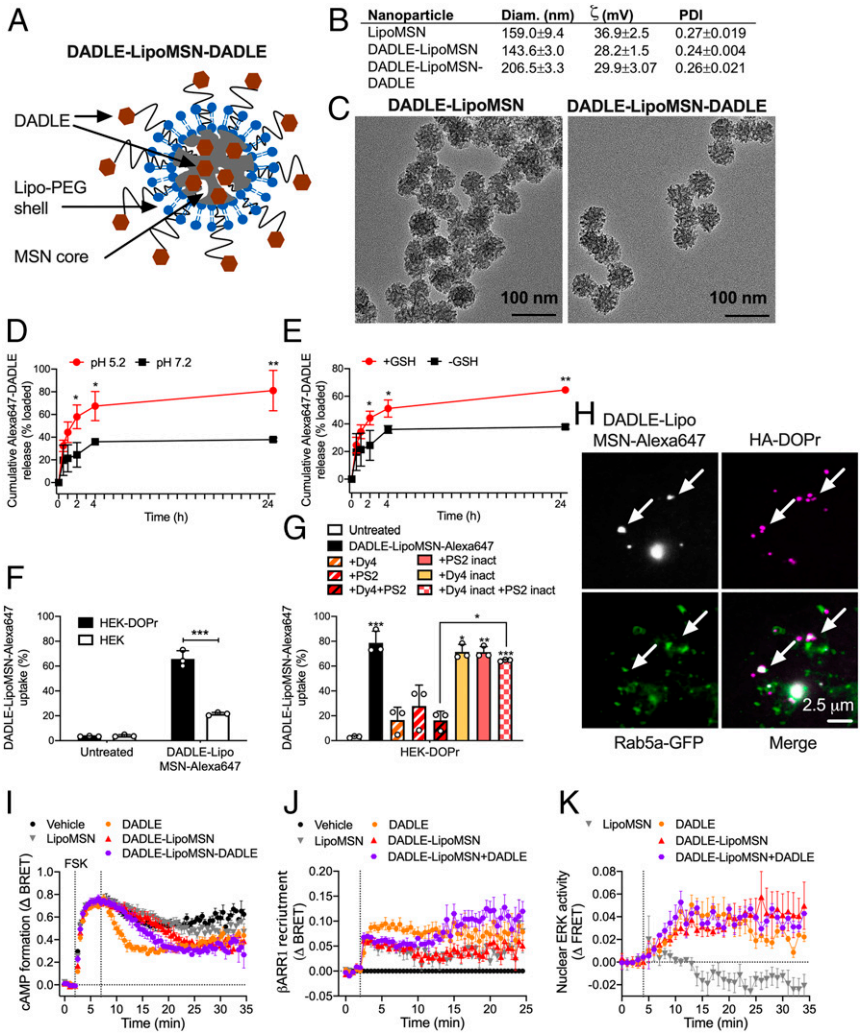


Fig. 7. Characterization of nanoparticles. (*A*) Structure of DADLE-LipoMSN-DADLE. (*B*) Physical properties of nanoparticles. $n = 4$ experiments. (*C*) Transmission electron micrographs of DADLE-LipoMSN and DADLE-LipoMSN-DADLE. Representative images, $n = 3$ independent experiments. (*D* and *E*) Time course of in vitro release of DADLE-Alexa647 from MSN-DADLE-Alexa647 at graded pH (*D*) and glutathione concentrations (*E*). $n = 3$ independent experiments. $^*P < 0.05$, $^{**}P < 0.01$, *t* test with Holm–Sidak correction. (*F* and *G*) Uptake of DADLE-LipoMSN-DADLE-Alexa647 into HEK293 control and HEK-DOPr cells determined by flow cytometry. (*F*) Uptake into HEK293 control and HEK-DOPr cells after 2 h. $^{***}P < 0.001$, *t* test with Holm–Sidak correction. (*G*) Effects of inhibitors of clathrin and dynamin and inactive analogs on uptake into HEK-DOPr cells after 2 h. $n = 3$ independent experiments. $^*P < 0.05$, $^{**}P < 0.01$, $^{***}P < 0.001$ compared with untreated cells, one-way ANOVA with Tukey's post hoc test. (*H*) Uptake of DADLE-LipoMSN-DADLE-Alexa647 into HEK-HA-DOPr cells after 30 min. Arrows show colocalization of DADLE-LipoMSN-DADLE-Alexa647 with DOPr in Rab5a-positive early endosomes. Representative images from four independent experiments. (*I–K*) Effects of DADLE (100 nM), DADLE-LipoMSN (20 μM), and DADLE-LipoMSN-DADLE (20 μM) on forskolin (FSK; 10 μM)-stimulated cAMP formation (*I*), βARR1 recruitment (*J*), and activation of nuclear ERK (*K*). $n = 5$ independent experiments. All results are mean ± SEM.

demonstrate the feasibility of using nanoparticles to target nociceptors with consequent reductions in dose. Nanoparticles might allow the simultaneous delivery to endosomes of agonists or antagonists of several endosomal GPCRs involved in pain. Since multiple GPCRs control pain transmission (9), the ability to target multiple receptors in pain-transmitting neurons for prolonged periods might provide effective and long-lasting antinociception.

Nanoparticle-encapsulated GPCR ligands may have utility beyond the treatment of pain. GPCRs control many pathophysiological processes and are the targets of more than one-third of Food and Drug Administration-approved drugs (1). Many GPCRs internalize when activated and likely continue to signal from endosomes. The use of stimulus-responsive nanoparticles for delivery of drugs to endosomes of targeted cells might enhance efficacy with reduced doses and fewer side effects.

Limitations. This study has several limitations. We cannot exclude a possible role for plasma membrane signaling even in the sustained inhibitory actions of opioids. The relative contributions of plasma membrane and endosomal signaling likely depend on the nature and concentration of the ligand and the time at which nociception is assessed. The differential effects of DOPr agonists that strongly (SNC80 and DADLE) or weakly (ARM390) promote endocytosis support a role for endosomal DOPr signaling for sustained antinociception. ARM390 is a partial agonist for βARR recruitment, which may explain its inability to cause long-lasting antinociception. We were unable to determine whether DOPr endosomal signaling involves G proteins and βARRs, which mediate endosomal signaling of other GPCRs (4, 5, 10, 11, 49, 50). Although dynamin and clathrin inhibitors blocked a subset of DOPr signals and inhibited sustained antinociception, these inhibitors also have nonspecific actions (51). Dominant negative dynamin and βARR knockdown replicated some effects of endocytosis inhibitors but could affect other functions as well. We cannot exclude the possibility that DOPr signals from intracellular compartments other than endosomes, since MOPr can signal from different compartments depending on the membrane

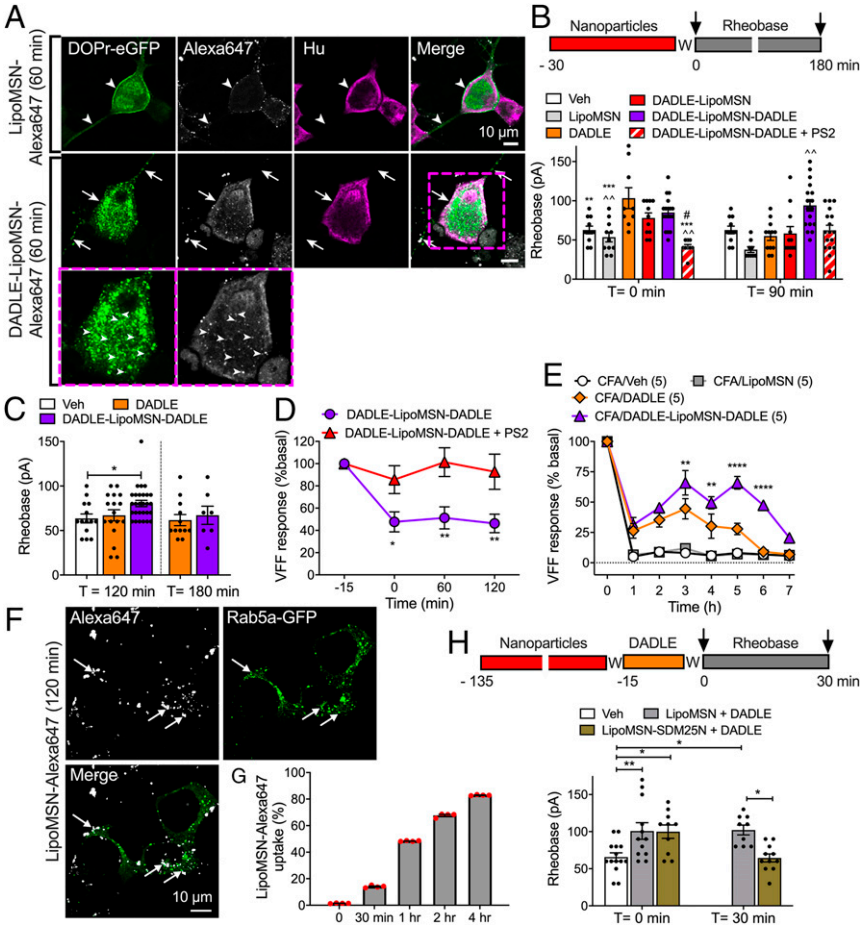


Fig. 8. Effects of nanoparticle-encapsulated DOPr ligands on nociceptors. (*A*) Uptake of LipoMSN-Alexa647 (control) or DADLE-LipoMSN-Alexa647 into primary cultures of DRG neurons from DOPr-eGFP mice. Neurons were incubated with nanoparticles for 60 min. Representative images from two experiments, from four mice. (*B* and *C*) Rheobase of mouse DRG neurons at 0, 90, 120, or 180 min after exposure to DADLE, DADLE-LipoMSN-DADLE, DADLE-LipoMSN (all 100 nM), LipoMSN (control), or vehicle (control) and washing. Some neurons were exposed to PS2 and DADLE-LipoMSN-DADLE. Data points indicate the number of studied neurons from $n = 6$ to 12 mice in *B* and *C* for each treatment. Compared with *DADLE, ^DADLE-LipoMSN-DADLE, and #DADLE-LipoMSN; $*^{\#}P < 0.05$, $**^{\wedge\wedge}P < 0.01$, $***P < 0.001$, one-way (*B*) or two-way (*C*) ANOVA with Tukey's post hoc test. (*D*) Colonic afferent activity at 0, 60, or 120 min after exposure of tissues to DADLE-LipoMSN-DADLE (100 nM). Some preparations were exposed to PS2 and DADLE-LipoMSN-DADLE. $n = 5$ mice per group. $*P < 0.05$, $**P < 0.01$, two-way (*) ANOVA with Sidak's post hoc test. (*E*) Ipsilateral paw withdrawal responses in mice. DADLE, DADLE-LipoMSN-DADLE (both 100 nM DADLE), LipoMSN, or vehicle (Veh) was injected intrathecally at 48 h after intraplantar CFA. $n = 5$ mice per group. $**P < 0.01$, $****P < 0.0001$ DADLE compared with DADLE-LipoMSN-DADLE, two-way ANOVA with Tukey's multiple comparison post hoc test. (*F*) Uptake of LipoMSN-Alexa647 into endosomes of HEK293 cells expressing Rab5a-GFP after 120 min. (*G*) Time course of uptake of LipoMSN-Alexa647 into HEK293 cells. $n = 3$ independent experiments. (*H*) Rheobase of mouse DRG neurons. Neurons were incubated with LipoMSN-SDM25N (100 nM) or LipoMSN (control) for 120 min, washed (W), incubated with DADLE (10 nM, 15 min), and washed again. Rheobase was measured at 0 or 30 min after washing. Data points indicate the number of studied neurons from four mice for each treatment. $*P < 0.05$, $**P < 0.01$, two-way ANOVA with Tukey's post hoc test. All results are mean ± SEM.

permeability of the agonist (40). Although our results show that PKC and ERK mediate the inhibitory actions of endosomal DOPr on nociceptor excitability, the targets of these kinases and how they inhibit nociception remain to be defined. Toxicologic analysis of nanoparticle constituents, pharmacokinetic studies of nanoparticle cargo, and pharmacodynamic studies in preclinical models of pain will be necessary before this approach can be advanced to patients.

Materials and Methods

Animal Subjects. Institutional Ethics Committees approved the mouse studies.

Human Subjects. The Queen's University Human Ethics Committee approved the human studies. Patients undergoing colonoscopy for routine clinical care gave informed consent for biopsy specimens of the mucosa to be obtained from the descending colon during colonoscopy and for their data to be recorded for research purposes. Biopsy specimens of mucosa were collected from the descending colon of three patients with active cUC and three healthy control patients. Disease severity was evaluated using the endoscopy component of the Mayo Clinic score for ulcerative colitis (*SI Appendix*, Table S1).

Colon Supernatants. Mice were treated for three cycles with 2% DSS in drinking water to induce chronic colitis or with water (control). Segments of whole colon were incubated in medium (24 h) to obtain supernatants (16–18). Biopsy specimens of colonic mucosa from cUC patients and controls (*SI Appendix*, Table S1) were incubated in medium to obtain supernatants (11, 52).

Patch Clamp Recording. Patch clamp recordings were made from mouse DRG neurons (11, 16, 18, 52). Neurons were preincubated for 60 min with supernatants and then washed. Neurons were stimulated for 15 min with DADLE (10 nM), SNC80 (10 nM), ARM390 (100 nM), DAMGO (10 nM), or vehicle (control) and then washed. Neurons were also incubated overnight (12 to 16 h) with DADLE (100 nM) or ARM390 (300 nM) and then washed. In some experiments, neurons were preincubated for 30 min with SDM25N (100 nM), CTOP (100 nM), Dy4 (30 μM), PS2 (15 μM), GF109203X (1 μM), PD98059 (50 μM), or vehicle. Rheobase was measured after agonist treatment and washing.

Extracellular Recording. Extracellular recordings were made from the lumbar splanchnic nerve innervating isolated mouse distal colon (11, 53, 54). SNC80, ARM390, or DAMGO (all 100 nM) was superfused into the organ bath for 15 min. In some studies, colon was preincubated for 15 min with PS2 (50 μM) before SNC80.

cDNAs, Cell Culture, and Transfection. Details are provided in *SI Appendix, Materials and Methods*.

Dissociation of DRG Neurons. DRG neurons were dispersed from DOPr-eGFP mice (55).

BRET Assays. BRET was measured in HEK293 cells (10, 26).

FRET Assays. FRET was measured in HEK293 cells and DRG neurons from DOPr-eGFP mice (10, 55). After FRET imaging, DOPr-eGFP was localized by immunofluorescence. FRET was measured in neurons expressing DOPr-eGFP.

DOPr-eGFP Trafficking. DRG neurons from DOPr-eGFP mice were exposed to vehicle, DADLE (1 μM), DADLE-LipoMSN-Alexa647 (1 μM DADLE), or LipoMSN-Alexa647 (10 μg/mL LipoMSN) (30 or 60 min, 37 °C). In some experiments, neurons were preincubated with Dy4 (30 μM) or PS2 (15 μM) (30 min). DOPr-eGFP in neurons was localized by immunofluorescence.

Preparation and Physicochemical Characterization of Nanoparticles. Details are provided in *SI Appendix, Materials and Methods*.

Cellular Targeting of LipoMSNs. HEK293-HA-DOPr or untransfected cells were incubated with DADLE-LipoMSN-Alexa647 or LipoMSN-Alexa647 (40 μg/mL). Uptake of nanoparticles was quantified by flow cytometry. In some experiments, cells were preincubated with Dy4, PS2, or inactive analogs (10 μg/mL, 30 min). For imaging studies, cells were transduced with Rab5a-GFP. After 24 h, cells were preincubated with rat anti-HA. Cells were washed and incubated with DADLE-LipoMSN-Alexa647 or LipoMSN-Alexa647 (20 μM DADLE, 200 μg/mL LipoMSN). HA-DOPr was localized by immunofluorescence. In some experiments, LipoMSN-Alexa647 uptake was examined by live cell imaging.

LipoMSNs and DOPr Signaling. Details are provided in *SI Appendix, Materials and Methods*.

LipoMSNs and Electrophysiology. Rheobase was measured at 0 to 180 min after exposure to DADLE or SDM25N nanoparticles and washing. Colonic afferent responses were assessed at 0 to 120 min after exposure to nanoparticles and washing.

LipoMSNs and Inflammatory Pain. The investigator was blinded to the treatments. Mice were assigned at random to treatments and acclimatized. CFA (0.5 mg/mL) was administered by intraplantar injection (10 μL) into the left hindpaw. DADLE (100 nM), DADLE-LipoMSN-DADLE (100 nM DADLE, 0.8 μg/mL LipoMSN), LipoMSN (1 μg/mL LipoMSN, control), or vehicle (control) was injected intrathecally (5 μL) at 48 h after CFA. Paw withdrawal to VFF was determined (10, 12).

Statistics. Results were analyzed and graphs prepared using Prism 8. Results are expressed as mean ± SEM. Statistical significance was assessed using *t* tests or one-way or two-way ANOVA with Tukey's or Sidak's post hoc test (*SI Appendix*, Table S2).

Data Availability. All of the data and protocols are provided in the main text or the *SI Appendix*.

ACKNOWLEDGMENTS. We thank Lih En Tiah for technical support and Dr. Malvin Janal for statistical support. The tdRGFP-Rab5a plasmid was designed and validated by Christian LeGouill and Lucas Tabajara Parreiras e Silva from the laboratory of Dr. Michel Bouvier. RGFP-CAAX and β-arrestin2-Rluc2 were provided by the Bouvier laboratory. This work was supported by grants from the NIH (NS102722, DE026806, and DK118971 to B.L.S. and N.W.B.), Department of Defense (W81XWH1810431, to B.L.S. and N.W.B.), Crohn's Colitis Canada (D.E.R., A.E.L., and S.J.V.), National Health and Medical Research Council (63303, 1049682, 1031886, 1049730, 1121029, and 1083480 to M.C., M.L.H., N.W.B., and D.P.P.), and Australian Research Council Centre of Excellence in Convergent Bio-Nano Science and Technology (N.W.B.).

1. A. S. Hauser, M. M. Attwood, M. Rask-Andersen, H. B. Schiöth, D. E. Gloriam, Trends in GPCR drug discovery: New agents, targets and indications. *Nat. Rev. Drug Discov.* **16**, 829–842 (2017).
2. K. E. Komolov, J. L. Benovic, G protein-coupled receptor kinases: Past, present and future. *Cell. Signal.* **41**, 17–24 (2018).
3. Y. K. Peterson, L. M. Luttrell, The diverse roles of arrestin scaffolds in G protein-coupled receptor signaling. *Pharmacol. Rev.* **69**, 256–297 (2017).
4. K. A. DeFea *et al*., The proliferative and antiapoptotic effects of substance P are facilitated by formation of a beta-arrestin-dependent scaffolding complex. *Proc. Natl. Acad. Sci. U.S.A.* **97**, 11086–11091 (2000).
5. K. A. DeFea *et al*., Beta-arrestin-dependent endocytosis of proteinase-activated receptor 2 is required for intracellular targeting of activated ERK1/2. *J. Cell Biol.* **148**, 1267–1281 (2000).
6. R. Irannejad, M. von Zastrow, GPCR signaling along the endocytic pathway. *Curr. Opin. Cell Biol.* **27**, 109–116 (2014).
7. J. E. Murphy, B. E. Padilla, B. Hasdemir, G. S. Cottrell, N. W. Bunnett, Endosomes: A legitimate platform for the signaling train. *Proc. Natl. Acad. Sci. U.S.A.* **106**, 17615–17622 (2009).
8. A. R. B. Thomsen, D. D. Jensen, G. A. Hicks, N. W. Bunnett, Therapeutic targeting of endosomal G protein-coupled receptors. *Trends Pharmacol. Sci.* **39**, 879–891 (2018).
9. P. Geppetti, N. A. Veldhuis, T. Lieu, N. W. Bunnett, G. Protein-Coupled Receptors, G protein-coupled receptors: Dynamic machines for signaling pain and itch. *Neuron* **88**, 635–649 (2015).
10. D. D. Jensen *et al*., Neurokinin 1 receptor signaling in endosomes mediates sustained nociception and is a viable therapeutic target for prolonged pain relief. *Sci. Transl. Med.* **9**, eaal3447 (2017).
11. N. N. Jimenez-Vargas *et al*., Protease-activated receptor-2 in endosomes signals persistent pain of irritable bowel syndrome. *Proc. Natl. Acad. Sci. U.S.A.* **115**, E7438–E7447 (2018).
12. P. D. Ramírez-García *et al*., A pH-responsive nanoparticle targets the neurokinin 1 receptor in endosomes to prevent chronic pain. *Nat. Nanotechnol.* **14**, 1150–1159 (2019).
13. R. E. Yarwood *et al*., Endosomal signaling of the receptor for calcitonin gene-related peptide mediates pain transmission. *Proc. Natl. Acad. Sci. U.S.A.* **114**, 12309–12314 (2017).
14. G. Corder, D. C. Castro, M. R. Bruchas, G. Scherrer, Endogenous and exogenous opioids in pain. *Annu. Rev. Neurosci.* **41**, 453–473 (2018).
15. J. Boué *et al*., Endogenous regulation of visceral pain via production of opioids by colitogenic CD4(+) T cells in mice. *Gastroenterology* **146**, 166–175 (2014).
16. R. Guerrero-Alba *et al*., Co-expression of μ and δ opioid receptors by mouse colonic nociceptors. *Br. J. Pharmacol.* **175**, 2622–2634 (2018).
17. R. Guerrero-Alba *et al*., Stress activates pronociceptive endogenous opioid signalling in DRG neurons during chronic colitis. *Gut* **66**, 2121–2131 (2017).
18. E. Valdez-Morales *et al*., Release of endogenous opioids during a chronic IBD model suppresses the excitability of colonic DRG neurons. *Neurogastroenterol. Motil.* **25**, 39–46.e4 (2013).
19. M. Verma-Gandhu *et al*., $CD4^+$ T-cell modulation of visceral nociception in mice. *Gastroenterology* **130**, 1721–1728 (2006).
20. G. Scherrer *et al*., Knockin mice expressing fluorescent delta-opioid receptors uncover G protein-coupled receptor dynamics in vivo. *Proc. Natl. Acad. Sci. U.S.A.* **103**, 9691–9696 (2006).
21. M. J. Robertson, F. M. Deane, P. J. Robinson, A. McCluskey, Synthesis of dynole 34-2, dynole 2-24 and dyngo 4a for investigating dynamin GTPase. *Nat. Protoc.* **9**, 851–870 (2014).
22. M. J. Robertson *et al*., Synthesis of the Pitstop family of clathrin inhibitors. *Nat. Protoc.* **9**, 1592–1606 (2014).
23. A. A. Pradhan *et al*., Agonist-specific recruitment of arrestin isoforms differentially modify delta opioid receptor function. *J. Neurosci.* **36**, 3541–3551 (2016).
24. D. Toullec *et al*., The bisindolylmaleimide GF 109203X is a potent and selective inhibitor of protein kinase C. *J. Biol. Chem.* **266**, 15771–15781 (1991).
25. D. T. Dudley, L. Pang, S. J. Decker, A. J. Bridges, A. R. Saltiel, A synthetic inhibitor of the mitogen-activated protein kinase cascade. *Proc. Natl. Acad. Sci. U.S.A.* **92**, 7686–7689 (1995).
26. D. D. Jensen *et al*., Endothelin-converting enzyme 1 and β-arrestins exert spatiotemporal control of substance P-induced inflammatory signals. *J. Biol. Chem.* **289**, 20283–20294 (2014).
27. A. A. Pradhan *et al*., In vivo delta opioid receptor internalization controls behavioral effects of agonists. *PLoS One* **4**, e5425 (2009).

28. D. P. Poole *et al*., Localization and regulation of fluorescently labeled delta opioid receptor, expressed in enteric neurons of mice. *Gastroenterology* **141**, 982–991.e18 (2011).
29. Q. Wan *et al*., Mini G protein probes for active G protein-coupled receptors (GPCRs) in live cells. *J. Biol. Chem.* **293**, 7466–7473 (2018).
30. R. Nehmé *et al*., Mini-G proteins: Novel tools for studying GPCRs in their active conformation. *PLoS One* **12**, e0175642 (2017).
31. Y. Namkung *et al*., Monitoring G protein-coupled receptor and β-arrestin trafficking in live cells using enhanced bystander BRET. *Nat. Commun.* **7**, 12178 (2016).
32. P. Donthamsetti, J. R. Quejada, J. A. Javitch, V. V. Gurevich, N. A. Lambert, Using bioluminescence resonance energy transfer (BRET) to characterize agonist-induced arrestin recruitment to modified and unmodified G protein-coupled receptors. *Curr. Protoc. Pharmacol.* **70**, 2 14 11–12 14 14 (2015).
33. M. L. Halls, M. Canals, Genetically encoded FRET biosensors to illuminate compartmentalised GPCR signalling. *Trends Pharmacol. Sci.* **39**, 148–157 (2018).
34. J. S. Herskovits, C. C. Burgess, R. A. Obar, R. B. Vallee, Effects of mutant rat dynamin on endocytosis. *J. Cell Biol.* **122**, 565–578 (1993).
35. C. Pinese *et al*., Sustained delivery of siRNA/mesoporous silica nanoparticle complexes from nanofiber scaffolds for long-term gene silencing. *Acta Biomater.* **76**, 164–177 (2018).
36. D. Shao *et al*., Bioinspired diselenide-bridged mesoporous silica nanoparticles for dual-responsive protein delivery. *Adv. Mater.*, e1801198 (2018).
37. J. J. DiCello *et al*., Inflammation-associated changes in DOR expression and function in the mouse colon. *Am. J. Physiol. Gastrointest. Liver Physiol.* **315**, G544–G559 (2018).
38. C. M. Cahill, S. V. Holdridge, A. Morinville, Trafficking of delta-opioid receptors and other G-protein-coupled receptors: Implications for pain and analgesia. *Trends Pharmacol. Sci.* **28**, 23–31 (2007).
39. A. A. Pradhan *et al*., Ligand-directed trafficking of the δ-opioid receptor in vivo: Two paths toward analgesic tolerance. *J. Neurosci.* **30**, 16459–16468 (2010).
40. M. Stoeber *et al*., A genetically encoded biosensor reveals location bias of opioid drug action. *Neuron* **98**, 963–976.e5 (2018).
41. M. Narita, H. Mizoguchi, J. P. Kampine, L. F. Tseng, Role of protein kinase C in desensitization of spinal delta-opioid-mediated antinociception in the mouse. *Br. J. Pharmacol.* **118**, 1829–1835 (1996).
42. E. G. Ignatova, M. M. Belcheva, L. M. Bohn, M. C. Neuman, C. J. Coscia, Requirement of receptor internalization for opioid stimulation of mitogen-activated protein kinase: Biochemical and immunofluorescence confocal microscopic evidence. *J. Neurosci.* **19**, 56–63 (1999).
43. W. H. De Jong, P. J. Borm, Drug delivery and nanoparticles: Applications and hazards. *Int. J. Nanomedicine* **3**, 133–149 (2008).
44. O. C. Farokhzad, R. Langer, Impact of nanotechnology on drug delivery. *ACS Nano* **3**, 16–20 (2009).
45. K. E. Uhrich, S. M. Cannizzaro, R. S. Langer, K. M. Shakesheff, Polymeric systems for controlled drug release. *Chem. Rev.* **99**, 3181–3198 (1999).
46. H. Maeda, J. Wu, T. Sawa, Y. Matsumura, K. Hori, Tumor vascular permeability and the EPR effect in macromolecular therapeutics: A review. *J. Control. Release* **65**, 271–284 (2000).
47. G. K. Such, Y. Yan, A. P. Johnston, S. T. Gunawan, F. Caruso, Interfacing materials science and biology for drug carrier design. *Adv. Mater.* **27**, 2278–2297 (2015).
48. C. E. Nelson *et al*., Balancing cationic and hydrophobic content of PEGylated siRNA polyplexes enhances endosome escape, stability, blood circulation time, and bioactivity in vivo. *ACS Nano* **7**, 8870–8880 (2013).
49. D. Calebiro *et al*., Persistent cAMP-signals triggered by internalized G-protein-coupled receptors. *PLoS Biol.* **7**, e1000172 (2009).
50. R. Irannejad *et al*., Conformational biosensors reveal GPCR signalling from endosomes. *Nature* **495**, 534–538 (2013).
51. R. J. Park *et al*., Dynamin triple knockout cells reveal off target effects of commonly used dynamin inhibitors. *J. Cell Sci.* **126**, 5305–5312 (2013).
52. E. E. Valdez-Morales *et al*., Sensitization of peripheral sensory nerves by mediators from colonic biopsies of diarrhea-predominant irritable bowel syndrome patients: A role for PAR2. *Am. J. Gastroenterol.* **108**, 1634–1643 (2013).
53. S. M. Brierley, R. C. Jones, 3rd, G. F. Gebhart, L. A. Blackshaw, Splanchnic and pelvic mechanosensory afferents signal different qualities of colonic stimuli in mice. *Gastroenterology* **127**, 166–178 (2004).
54. P. A. Hughes *et al*., Post-inflammatory colonic afferent sensitisation: Different subtypes, different pathways and different time courses. *Gut* **58**, 1333–1341 (2009).
55. M. L. Halls, D. P. Poole, A. M. Ellisdon, C. J. Nowell, M. Canals, Detection and quantification of intracellular signaling using FRET-based biosensors and high content imaging. *Methods Mol. Biol.* **1335**, 131–161 (2015).